The Role Of The Parkinson's Disease-Related Protein LRRK2 In Autophagy And Calcium Signalling In Cellular Models

Thesis

School of Life, Health and Chemical Sciences

The role of the Parkinson's disease-related protein LRRK2 in autophagy and calcium signalling in cellular models

Sonia Azeggagh, BSc, MSc

A Thesis submission to The Open University

for the degree of Doctor of Philosophy

October 2020

Declaration

I declare that the work presented in this thesis is my own original work and does not contain any material submitted for a degree, diploma or any other qualification at the Open University or any other University. Contributions made by other researchers are fully acknowledged in relevant parts of the thesis.

Abstract

Parkinson's disease (PD) is the second most common neurodegenerative disease worldwide, affecting 3% of individuals of >75 years of age. The disease is relentless and incurable, and the need to understand its causes and develop new treatments is overwhelming. Mutations in the *LRRK2* gene are the most common cause of familial PD, and strongly influence the risk of sporadic PD. This study investigates the impact of LRRK2 enzymatic activities and LRRK2 pathogenic and protective variants on autophagy and calcium signalling to gain insight into the early impairments involved in PD pathogenesis. To this end, the initial approach was to develop isogenically matched cell lines using the CRISPR/Cas9 gene-editing technique, which was unsuccessful. Alternative strategies to study LRRK2 were therefore pursued. The LRRK2 kinase and GTPase activities were modulated with pharmacological inhibitors, and the effects of *LRRK2* mutations were investigated by transfection of wild-type and mutant LRRK2 constructs. Autophagy assays combined the quantification of GFP-LC3 punctae and endogenous WIPI2 punctae numbers using fluorescence and electron microscopy, whilst intracellular calcium signals were measured using ratiometric Fura-2 imaging following treatment with ATP, CPA or ionomycin. Overall, this project revealed a cell-type specific action of LRRK2 in autophagy, where LRRK2 appears to be pro-autophagic and involved in a kinase and GTPase activity-dependent manner in the early stages of this process in HEK293 GFP-LC3 cells, whilst data from RAW264.7 macrophages do not support a role for Lrrk2 in autophagy. Calcium-related findings indicated that Lrrk2 is involved in the regulation of IP_3-R mediated calcium signals in WT RAW264.7 macrophages and suggest that this role for Lrrk2 may be as a scaffolding protein. The data also indicated that the function of LRRK2 in autophagy induction in HEK293 GFP-LC3 cells is unlikely to require intracellular calcium, and LRRK2 was not found to participate in the regulation of lysosomal calcium storage in either cell line. Additional findings revealed that the calcium indicators Fura-2 and Cal-590, as well as BAPTA and the BAPTA analogues di-bromo-BAPTA and di-fluoro-BAPTA, displayed significant off-target effects on autophagy, and indicated that BAPTA is an unsuitable tool to explore the involvement of calcium signals in autophagy. Taken together, this study yields new and important data about the role of LRRK2 kinase and GTPase activities in the early stages of autophagy, and sheds light on the relevance of LRRK2 to the regulation of intracellular calcium signalling.

Acknowledgments and dedications

This thesis is the result of several years of hard work, and would not have been possible without the help and support of the following people.

First, I would like to thank my supervisors Dr Daniel Berwick, Dr Martin Bootman and Dr Kerry Murphy for their support throughout my PhD. In particular, I would like to express my sincere appreciation to Dan, who guided and encouraged me, helped me improve my critical thinking skills, and whose insight and expertise was invaluable. Thank you for helping me become a better researcher. I would like to also thank Cheryl Hawkes for her help, wisdom and our interesting discussions.

I would like to thank Guarantors of Brain for supporting my attendance to an incredible Society for Neuroscience Conference with a travel grant, as well as The Open University for funding this project and this opportunity to make my first steps in academia.

I would like to recognise the invaluable assistance and knowledge provided by the OU lab support staff Julia, Brett, George and Eduardo, and the EM Suite staff, Igor and Radka. I would also like to thank Jen, for her help with anything I needed, but also for being such a joy to be around, as well as Priya and Dee for their precious help.

My time during this PhD would not have been the same without other students with whom I shared fun moments and thought-provoking conversations. In particular, I would like to thank Edu, Ester, Alexandra, Shereen, Laura, and Iwona for their friendship, their support, but especially for being the best friends/colleagues I could have asked for during this life-changing experience. We have made wonderful memories together, and hopefully, more are yet to come.

I would like to extend my thanks to other students, including visiting students, who also did their part in making this environment friendly, fun and interesting: Maëva, Juan, Naiara, Sarai, Emily B, Emily C, Maurine, Marta, Ellie, Morgane, Lewis, Salah, Conor, Marcelle, Pelumi, Stephen, Tala… to name “a few”.

I would like to thank my incredible and dearest friends Namya and Linda, both amazing doctors, for their constant support and motivation that helped me through highs and lows. Thank you for believing in me. I will always be grateful that our paths crossed all those years ago. No matter the distance, our friendship continues to grow. Thanks to my other long-time friends in France, whom I always looked forward to meet when I travelled back home.

Above all, I would like to give my biggest thanks to my family. It goes without saying that this thesis could not have been written without the strong support of my family throughout these challenging years. As a family, we are always together, no matter the distance. You truly inspire me to be the best version of myself and do better. To my incredible sisters Lyna, Sabina and Lilia, I am proud of you and the women you are, and seeing you thrive warms my heart.
This thesis is especially dedicated to my wonderful mother, a true force of nature, my role model.

Lastly, I am forever indebted to James, who has helped me in innumerable ways. I am grateful for all his encouragements, his unconditional love and support, and for getting me through these last few years. You are amazing.

"*Many people say that it is the intellect which makes a great scientist. They are wrong: it is character.*"
Albert Einstein.

"*It does not matter how slowly you go as long as you do not stop.*"
Confucius.

Conference items and publications

Publications

- Berwick Daniel C.; Heaton George R.; Azeggagh Sonia; Harvey Kirsten. (2019) **LRRK2 Biology from structure to dysfunction: research progresses, but the themes remain the same.** *Molecular neurodegeneration*, 14, article no. 49. doi: 10.1186/s13024-019-0344-2

- Azeggagh Sonia. (2017) **Rewriting DNA: An introduction to genome editing**. Explainer article published on The Open University Open Learn website. Used by the BBC/OU co-production team to directly support "Tomorrow's World". doi: 10.13140/RG.2.2.15807.51360

- Azeggagh Sonia. (2017) **Targeted genome editing: Introducing the CRISPR/Cas9 system**. Explainer article published on The Open University Open Learn website. Used by the BBC/OU co-production team to directly support "Tomorrow's World". doi: 10.13140/RG.2.2.29229.28642

Conference items

- Azeggagh Sonia; Berwick Daniel C.; Bootman M.; Murphy K. P. S. J.; Allman Sarah A. (2018) **The combined use of pathogenic and protective variants as a tool to explore the role of LRRK2 in autophagy and calcium signalling,** Poster, Program No. 655.04. 2018 Neuroscience Meeting Planner. San Diego, CA: Society for Neuroscience. Online

- Azeggagh Sonia; Adan Abdullahi; Needs Sarah; Murphy K. P. S. J.; Allman Sarah A.; Berwick Daniel C. (2017**). A comprehensive "Disease-in-a-Dish" approach to Parkinson's Disease,** Poster in: *British Neuroscience Association - 2017 Festival of Neuroscience*, 10-13 Apr 2017, Birmingham, United Kingdom.

Table of Contents

List of Figures

List of Tables

List of abbreviations

Abbreviation	Full Name
3'-UTR	three prime untranslated region of a mRNA
3-MA	3-methyladenine
6-OHDA	6-hydroxydopamine
ALK	anaplastic lymphoma kinase
AMBRA1	Activating molecule in BECN1-regulated autophagy protein 1
AMP	Adenosine monophosphate
AMPK	Adenosine monophosphate-activated protein kinase
ANK	Ankyrin-like
APC	Adenomatous polyposis coli (Wnt pathway)
ARM	Armadillo
ATG	Autophagy related protein (usually followed by a number)
ATP	Adenosine triphosphate
ATPase	Adenosine triphosphate hydrolase
BafA1	Bafilomycin A1
BAG5	Bcl-2-Associated Athanogene 5
BAPTA-AM	1,2-bis-(o-aminophenoxy)-ethane-N,N,N',N'- tetra acetoxymethyl ester
BAPTA-DB	5,5'-Dibromo-1,2-bis(2-aminophenoxy)ethane-N,N,N',N'-tetraacetic acid
BAPTA-FF	5,5'-Difluoro-1,2-bis(2-aminophenoxy)ethane-N,N,N',N'-tetraacetic acid
Bcl-2	B-cell lymphoma 2
Ca^{2+}	Calcium ion
cADPR	Cyclic ADP ribose
Cal-590-AM	Cal-590 acetoxymethyl ester
CaMKK-β	Calcium/calmodulin dependent protein kinase β
CICR	Calcium-induced calcium release
CK1α	Casein kinase 1 α
CPA	Cyclopiazonic acid
CRISPR/Cas9	Clustered regularly interspaced short palindromic repeats/CRISPR-associated gene 9
CSF	Cerebrospinal fluid
CZC-25146	LRRK2 kinase inhibitor
DAPK1	Death-associated protein kinase 1
DFCP1	Double FYVE domain-containing protein 1
DMSO	Dimethyl sulfoxide
DN	Dopaminergic neuron
DNA	Deoxyribonucleic acid

DSB	Double-stranded break
DVL	Dishevelled
ER	Endoplasmic reticulum
ERK	Extracellular signal-regulated kinases, also called MAPK
FLT3	D835Y oncogenic variant of fms like tyrosine kinase 3 (also known as CD35)
FIP200	Focal adhesion kinase family-interacting protein
Fura-2-AM	Fura-2 acetoxymethyl ester
GAK	Cyclin G associated kinase
GBA	Glucocerebrosidase
GECI	Genetically encoded calcium indicator
GFP	Green fluorescent protein
GFP-LC3	Green fluorescent protein-Microtubule-associated protein 1 light chain 3
GNE-9605	LRRK2 kinase inhibitor
GS	G2019S, *LRRK2* mutation (pathogenic)
GSK2578215A	LRRK2 kinase inhibitor
GSK3-β	Glycogen synthase kinase-3 beta
GTP	Guanosine triphosphate
GTPase	Guanosine triphosphate hydrolase
H^+	Hydrogen ion
HDR	High-fidelity repair mechanism
HEK	Human embryonic kidney
IκB	Inhibitor of nuclear factor kappa B (NF-κB)
IP_3	Inositol 1,4,5-trisphosphate
IP_3-R	Inositol 1,4,5-trisphosphate receptor
iPSCs	Induced-pluripotent stem cells
JIP4	c-Jun N-terminal kinase (JNK)–interacting protein 4
KD	Knockdown
KI	Knock-in
KO	Knockout
LB	Lewy bodies
LC	Locus coeruleus
LC3	Microtubule-associated protein 1 light chain 3
LC3-I	Microtubule-associated protein 1 light chain 3, soluble
LC3-II	Microtubule-associated protein 1 light chain 3, lipidated
LIR	LC3 interaction region
LRP6	Low-density lipoprotein receptor-related protein 6
LRR	Leucine-rich repeat
LRRK1	Leucine-rich repeats kinase 1, paralog of LRRK2

LRRK2	Leucine-rich repeats kinase 2
LRRK2-IN-1	LRRK2 kinase inhibitor
MAMs	Mitochondria-associated ER membranes
MAPK	Mitogen-activated protein kinase, also called ERK
MAPKKK-like	Mitogen-activated protein kinase kinase kinase, or MAP3K
MASL-1	Malignant fibrous histiocytoma amplified sequences with leucine-rich tandem repeats 1
MEK	Mitogen-activated protein kinase kinase, or MAP2K
miR-205	Micro RNA molecule 205, tumour suppressor
MLi-2	LRRK2 kinase inhibitor
MPTP	1-methyl-4-phenyl-1,2,3,6-tetra-hydropyridine
MRI	Magnetic resonance imaging
MST	STE20-like protein kinases
mTOR	Mammalian (or mechanistic) target of rapamycin
mTORC1/C2	Mammalian (or mechanistic) target of rapamycin complex 1 or 2
Na^+	Sodium ion
NAADP	Nicotinic acid adenine dinucleotide phosphate
NFAT	Nuclear factor of activated T-cells
NF-κB	Nuclear Factor Kappa B
NHEJ	Non-homologous end-joining repair mechanism
NMDA	N-Methyl-d-aspartate
NOD2	Nucleotide-binding oligomerization domain-containing protein 2
NRON	Non-coding repressor of NFAT
p62	Ubiquitin-binding protein
PARK2	Gene encoding for Parkin
PAS	Phagophore assembly site
PCP	Planar cell polarity pathway (non-canonical Wnt pathway)
PD	Parkinson's disease
PE	Phosphatidylethanolamine
PF-06447475	LRRK2 kinase inhibitor
PI	Phosphatidylinositol
PI(3,5)P_2	Phosphatidylinositol 3,5-bisphosphate
PI3K	Phosphoinositide 3-kinase
PI3K class III CI	Phosphoinositide 3-kinase complex 1
PI3P	Phosphatidylinositol 3-phosphate
PINK1	PTEN-induced kinase 1
PP242	Torkinib, mTORC1 & mTORC2 inhibitor
PRAS40	Proline-rich Akt substrate of 40 kDa, subunit of mTORC1 complex
Rab GTPase	Ras-associated binding protein Guanosine triphosphate hydrolase

RAW264.7	Mouse macrophages
RNA	Ribonucleic acid
ReN VM	Human neural progenitor ventral mesencephalon
RFP	Red fluorescent protein
RG	R1441G, *LRRK2* mutation (pathogenic)
RH	R1398H, *LRRK2* mutation (protective variant)
RHEB GTPase	Ras homolog enriched in brain GTP-binding protein hydrolase
RIPK2	Receptor Interacting Serine/Threonine Kinase 2
RPTOR	Regulatory-associated protein of mTOR, subunit of mTORC1 complex
RocCOR	Ras of complex proteins-C-terminal of Roc
ROS	Reactive oxygen species
RyR	Ryanodine receptor
SERCA	Sarcoplasmic/endoplasmic reticulum calcium ATPase
SH-SY5Y	Human neuroblastoma
smMLCK	smooth muscle myosin light chain kinase (also known as MYLK1)
SN	Substantia nigra
SOCE	Store-operated calcium entry
SQSTM1/p62	Sequestosome 1/ubiquitin-binding protein 62
STE20	Sterile 20 family of serine/threonine kinases
TAK1-TAB1	fusion of transforming growth factor-β1-activated kinase-1 with its activator, TAK1-binding protein 1
TEM	Transmission Electron Microscopy
TFEB	Transcription factor EB
TPC	Two-pore channel
TRPML	Transient receptor potential mucolipins channel
TSC1/2 complex	Tuberous sclerosis proteins 1 (hamartin) and 2 (tuberin) complex
ULK1	Unc-51-like kinase 1 / Unc-51-like kinase 1 complex 1
UPS	Ubiquitin proteasome system
UV	Ultraviolet
VDAC	Voltage-dependent anion channel
VGCC	Voltage-operated/gated calcium channels
VPS15	Phosphoinositide-3-kinase regulatory subunit 4, or PIK3R4
VPS34	Phosphatidylinositol 3-kinase catalytic subunit type 3, or PIK3C3
VPS35	Vacuolar protein sorting-associated protein 35
WIPI2	WD-repeat-interacting phosphoinositide protein 2
Wnt	Wingless-related integration site, family of proteins
WT	Wild type

1

Introduction

1.1 Parkinson's disease

Parkinson's disease is the second most common neurodegenerative disease worldwide, affecting up to 10 million individuals typically over the age of 60, with a lifetime risk estimated around 2%[1–3]. Initially described by James Parkinson in 1817 as a "shaking palsy"[4], PD remains incurable 200 years later.

1.1.1 Symptoms and treatments

PD is characterized by debilitating motor symptoms due to the degeneration of dopaminergic neurons, which leads to a depletion of the neurotransmitter dopamine. Individuals with PD typically present clinical features such as resting tremor, muscle rigidity, posture instability and bradykinesia[4,5]. However, PD is not limited to motor dysfunction[6,7] (Table 1.1). Several neuronal networks are affected in PD, and patients also suffer from psychiatric and dysautonomic symptoms[7,8]. These non-motor symptoms can occur more than 10 years prior to the onset of the motor symptoms and the diagnosis.

Since the world's population is ageing, it is becoming increasingly important to unravel the mystery surrounding the causes of the disease, and to develop new treatments. At this time, no disease-modifying treatments are available. Thus, for all patients with PD, current treatments are only able to alleviate symptoms, with a focus on improvement in motor and non-motor symptoms[5,7–12] (Table 1.2).

Importantly, pharmacological treatments for motor symptoms are generally based on re-establishing dopamine signalling (Table 1.2) by mimicking the effect of dopamine (e.g., dopamine precursor L-DOPA, dopamine agonist ropinirole), increasing dopamine levels (e.g., promoting dopamine synthesis with

amantadine or NMDA Receptors antagonist), or inhibiting dopamine metabolism (e.g., monoamine oxidase-B inhibitors). To address non-motor symptoms, approaches typically used in other conditions or in the general population can be considered[5,7–12], such as antidepressants. Interestingly, some non-motor symptoms also respond to motor symptoms treatments[5,7–12], including depression or anxiety which can be improved by Quetiapine (a dopamine-related approach), or cognitive impairments which could be improved by monoamine oxidase-B inhibitors. Although individual approaches to treat PD are heterogenous, PD patients generally use a carefully selected combination of medications providing benefits on both motor and non-motor symptoms.

However, these therapies have little to no effect on slowing disease progression, and can have side effects such as impulse control disorders[5,7–12]. Additional non-pharmacological strategies are also explored, such as exercise and physiotherapy, but further study is required to establish their disease-modifying abilities[12]. Furthermore, deep brain stimulation, which involves a transcranial surgery and implantation of electrodes, can be used in patients presenting medication-resistant or worsening symptoms[12]. Although its mechanisms are not fully understood, this approach is based on the stimulation of the sub-thalamic nucleus or globus pallidus interna, which ultimately relieves repression of the thalamus, often resulting in the reduction of motor-symptoms such as dyskinesia.

Table 1.1: Most common Parkinson's disease symptoms.

This table summarises the most common motor and non-motor symptoms reported in PD patients[4–7].

Motor symptoms	Non-motor symptoms
Resting tremor	Autonomic dysfunction (constipation, bladder dysfunction, blood pressure changes)
Muscle rigidity	Impaired olfaction
Posture instability	Sleep disruption, insomnia
Bradykinesia	Psychiatric disturbances (depression, anxiety, psychosis)
	Cognitive dysfunction, dementia
	Fatigue

Table 1.2: Current treatments for Parkinson's disease.

This table summarises the most commonly used PD treatments that target motor dysfunction by re-establishing the physiological dopamine pathway, and non-motor symptoms with approaches used in the non-PD population. Some non-motor symptoms also respond to treatments for motor symptoms[5,7–12].

Target	Strategy	Treatment(s)
Motor symptoms (loss of dopaminergic neurons and striatal dopamine depletion)	Dopamine Replacement	Dopamine precursor (e.g., L-DOPA), dopamine agonists (e.g., ropinirole)
	Inhibition of dopamine degradation	Monoamine oxidase-B inhibitors (e.g., rasagiline), catecholamine-O-methyltransferase inhibitors (e.g., entacapone)
	Glutamatergic activity decrease (promote dopamine synthesis) and other neurotransmitters	Amantadine, NMDA receptors antagonist, cholinesterase inhibitors
	Surgical Intervention	e.g., Deep Brain Stimulation
	Non-pharmacological approaches	Exercise, rehabilitative therapy, physiotherapy
Non-motor symptoms	Approaches used in the general population	Psychiatric symptoms (e.g., depression, anxiety, psychosis): dopamine-related (Quetiapine), antidepressants, serotonin and norepinephrine reuptake inhibitors, cholinesterase inhibitors
		Cognitive impairments: cholinesterase inhibitors, monoamine oxidase-B inhibitors

The following sections will briefly review disease pathology, known causes of PD and the strengths and weaknesses of the current experimental models used to model PD.

1.1.2 Pathology and hallmarks

1.1.2.1 Degeneration of dopaminergic neurons

The central pathognomonic feature of PD is the degeneration of dopaminergic neurons of the *substantia nigra pars compacta*[5], although other brain regions are affected. The substantia nigra is located in the midbrain and is a part of the basal ganglia, which is essential for several brain functions, especially voluntary movement control[13–18].

Dopaminergic neurons of the substantia nigra have a characteristic pigmentation, due to the presence of a dark pigment called neuromelanin. It is the loss of these neurons, which is distinguishable at the gross anatomical level by the loss of pigmentation (Figure 1.1), that causes the classical movement disorder. Interestingly, motor symptoms only appear after at least 50% of the dopaminergic neurons and 80% of the dopamine have been lost[19], which may explain why non-motor symptoms can precede motor dysfunction by many years[7,9]. This highlights the significance of understanding the biological mechanisms upstream of cell death.

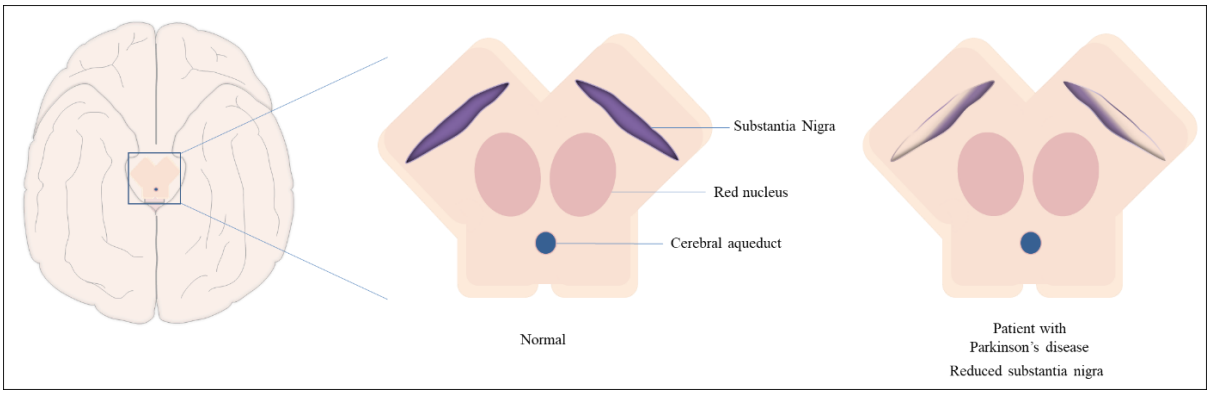

Figure 1.1: The substantia nigra in Parkinson's disease

Schematic representation of the location of the substantia nigra in the midbrain in a PD patient and a healthy subject, showing the degeneration of dopaminergic neurons of the substantia nigra pars compacta in the patient.

1.1.2.2 Lewy bodies

Additionally to the loss of dopaminergic neurons, the second PD hallmark is the presence of Lewy bodies in post-mortem brains[20]. Lewy bodies are large eosinophilic neuronal cytoplasmic inclusions containing aggregates of misfolded proteins, in particular α-synuclein and ubiquitin. The presence of α-synuclein in Lewy bodies allows the classification of PD as a synucleinopathy[21].

Consistent with an important role in PD pathology, Lewy bodies are predominantly found in the substantia nigra, but are also found in other brain regions affected in PD. Although the mechanisms are unclear, the α-synuclein pathology is thought to spread to connected regions in a prion-like manner[22] (discussed further in Section 1.6.1.3). It is presumed that this spreading of Lewy bodies pathology is central to disease progression, although it remains controversial whether Lewy bodies are themselves neurotoxic or whether their formation is part of a neuroprotective response[23]. However, findings argue that Lewy bodies are unlikely to be a key factor in PD pathogenesis since the extent of post-mortem Lewy bodies pathology correlates poorly with the extent of cell death, disease progression and clinical symptoms[24,25].

1.1.2.3 α-synuclein pathology

Although the involvement of Lewy bodies in the pathogenesis of PD is debated, the involvement of α-synuclein is not. α-synuclein is a highly expressed neuronal protein generally enriched in presynaptic nerve terminals. The normal physiological role of α-synuclein is not fully understood, but it is considered to be a membrane-binding protein that plays a role in vesicular trafficking at pre-synaptic termini where it may regulate synaptic transmission[26,27].

Numerous studies have described the pathogenic role of misfolded α-synuclein accumulation and aggregates, while PD genetics has identified strong linkage between *SNCA*, the gene encoding α-synuclein, and PD[28]. Furthermore, misfolded α-synuclein accumulation appears to be the ultimate

pathological agent common in all causes of PD, since it occurs in almost all PD patients, irrespective of whether the patient is considered to have idiopathic PD or PD due to genetic mutations.

α-synuclein can be present in several states. Whilst soluble α-synuclein proteins natively exist as monomers, α-synuclein molecules form multimers at membranes. The formation of oligomers in a pathological environment is generally believed to be neurotoxic, aggregating in fibrils and ultimately in intraneuronal deposits (i.e. Lewy bodies)[27,29]. However, there is no consensus regarding which is the toxic form of α-synuclein, a problem that hinders the discovery of potential therapeutics targeting α-synuclein[30,31].

As such, it is likely that the α-synuclein pathology occurs early in PD pathogenesis, which starts before the onset of PD, and that it drives the progression of the disease. Although the mechanisms are poorly understood, it is thought that α-synuclein pathology mediates the impairment of fundamental cellular processes[27], such as the autophagic pathway, thereby causing further accumulation of α-synuclein and eventually leading to neuronal loss. Therefore, it is relevant to investigate these potential upstream pathological mechanisms that occur prior to the accumulation of α-synuclein.

While research has been prolific in other aspects of PD, the upstream mechanisms initiating PD are not fully deciphered, although impairments in several cellular processes have been proposed[26,32–37]. These impairments may act together to promote and trigger neurodegeneration by rendering dopaminergic neurons more vulnerable to cellular insults and cell death, but can also result from neurodegeneration. Impairments include defects in protein degradation pathways, mitochondrial dysfunction, synaptic and axonal defects, neuroinflammation and deregulated calcium signalling. Their role in the mechanisms underlying cellular dysfunction in PD and the involvement of PD-trigger factors will be discussed later in this Chapter, in Section 1.6.1.

1.1.3 Aetiology

Although PD is mostly sporadic and considered an idiopathic disease with unknown aetiology, several potential causes have been described for the neurodegeneration observed in PD. These risks factors include ageing, genetic factors and environmental factors, culminating in mitochondrial dysfunction, neuroinflammation and oxidative stress[32,33,38]. Importantly, PD is considered a multifactorial disease, and it is likely that the interplay of all these risk factors, whether environmental or intrinsic, worsen the cellular dysfunction and trigger PD pathology (Figure 1.2).

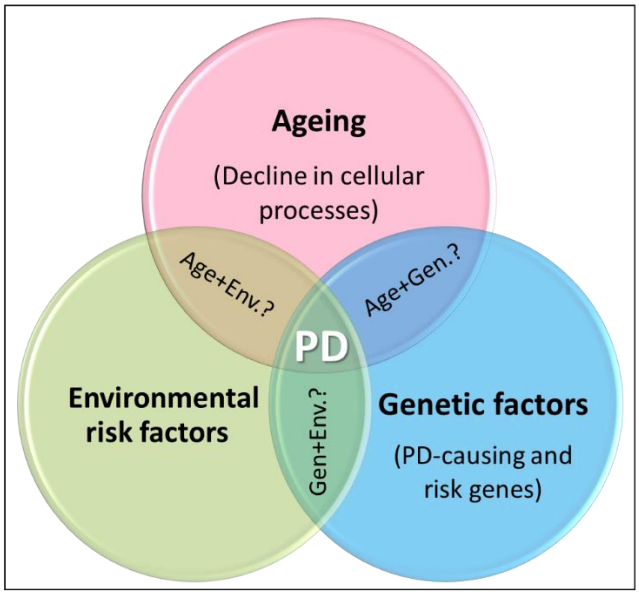

Figure 1.2: Parkinson's disease is a multifactorial disorder.

The potential interplay between the intrinsic and extrinsic risk factors in PD is thought to induce and aggravate cellular dysfunction and trigger Parkinson's disease (PD) pathology.

1.1.3.1 Ageing

The most important predisposition factor for PD is age[31], with an onset of motor symptoms at a mean age of 60. In fact, the motor symptoms of PD are attributable to changes within dopaminergic neurons from the substantia nigra with advancing age. It should be noted that early-onset (and in some cases juvenile) PD exists[39–41], but these individuals account for a very small proportion of cases – the vast majority of PD is late-onset (referred to as late-onset PD)[42]. Early onset forms of PD, which tend to be genetic in nature, are discussed briefly in Section 1.1.3.3.

Ageing is a normal physiological process that induces functional changes at the level of the organism but also at the cellular level. These functional changes are associated with a decline in fundamental processes maintaining cellular homeostasis. As such, cellular ageing is due to the accumulation of damage occurring over time due to the deregulation or failure of several essential mechanisms, including defects in macromolecule clearance, i.e. autophagic machinery, impaired proteostasis, dysfunctional mitochondria and oxidative stress, toxicity handling with antioxidants, DNA damage, and inflammatory senescence[43–46]. These age-related factors ultimately lead to cellular dyshomeostasis and participate in the development of age-related diseases, in particular neurodegeneration. The general opinion supports this age-associated decline of physiological processes in the enhanced vulnerability of dopaminergic neurons to cytotoxicity and cell death.

1.1.3.2 Environmental factors

The vast majority of PD cases are sporadic, therefore environmental factors likely influence the onset of most cases either directly or by interacting with predisposing factors such as less penetrant PD risk genes[47].

Established environmental risk factors for PD include chronic exposure to certain toxic compounds, most notably pesticides[48–52] such as organophosphates[53], which are generally associated with farm activities or occupational exposure. This follows the discovery that the neurotoxins 6-hydroxydopamine[54,55] and 1-methyl-4-phenyl-1,2,3,6-tetra-hydropyridine (MPTP)[55,56], similar to the herbicide paraquat[57,58], cause the loss of dopaminergic neurons and chronic parkinsonism[59]. These compounds act through mitochondrial dysfunction and enhanced oxidative stress. Rotenone, another pesticide, can also lead to PD[60–62] through similar mechanisms.

Although the mechanisms are still unclear, numerous studies have described an additional range of compounds[52,63–67] that can induce PD, such as metals, chemicals used in industry or even air pollution. On the other hand, certain factors such as coffee and tea consumption[68], tobacco[50] and ibuprofen[52] potentially lower the risk for developing PD. PD has also been linked to head trauma[69], and an increased

risk of developing PD was found in patients with several inflammatory disorders or infections, such as tuberculosis[70] or inflammatory bowel disease[71].

1.1.3.3 Genetic factors

Most importantly in the context of this project, there is increasing evidence that genetic factors play a critical role in an individual's lifetime risk of developing PD[72–74]. About 10% of cases have a clear hereditary origin, either due to dominant or recessive mutations. These monogenic forms of PD are referred to as familial PD, and at least 9 have been reported to date[75] (Table 1.3). However, genome-wide association studies indicate that when combined with additional genetic risk factors, the genome of an individual accounts for a far greater proportion of their total PD risk than traditionally assumed[74,76,77]. Substantial work has thus focused on the genetic causes of PD.

The first gene linked to PD was *SNCA*[78], followed by *PARK2*, *PINK1* and *DJ-1*[41,79,80] in juvenile or early-onset autosomal recessive inherited PD. Interestingly, the proteins encoded by *PARK2*, *PINK1* and *DJ-1* are involved in mitochondrial homeostasis, in particular mitophagy[81], which is the selective degradation of mitochondria via autophagy. As such, genetic studies of rare early-onset PD have been incredibly informative, supporting mitochondrial dysfunction as a key event in PD pathogenesis[81,82], and also established the critical pathogenicity of α-synuclein aggregation[83].

The most common genetic risk factors for late-onset PD are disease-causing mutations affecting the *LRRK2* and *GBA* genes[42,84]. Since these mutations tend not to be highly penetrant, they may have to be combined with other genetic or environmental factors to trigger PD. In contrast to early-onset PD, genetics studies of late-onset PD have been less fruitful. Indeed, while it is now accepted that pathways deregulated by most PD-causing genes converge to α-synuclein accumulation downstream, the upstream events remain poorly understood. Nevertheless, all these PD-causing genes are involved in or regulate the autophagic pathway, supporting its importance in neurodegeneration and PD pathogenesis.

Table 1.3: Main dominant and recessive PD-causing mutations and overview of the associated pathology.

This table summarises the current knowledge on PD causing mutations[75,85]. SN: substantia nigra, DN: dopaminergic neurons, LB: Lewy bodies, LC: locus coeruleus.

Inheritance	Phenotype	Gene	Protein	Function	Mutations	Neuropathology
Autosomal Dominant PD	Severe Parkinsonism Early-Onset PD	***SNCA***	α-synuclein	Likely involved in neurotransmitter release at pre-synaptic terminals and vesicles dynamic	missense, duplications and triplications A53T, 130P, E46K, H50Q, G51D	- Main component of LB present in cortex and brain stem - Overexpression of α-synuclein - Loss of DN in the SN and LC
	Classical PD	***LRRK2***	Leucine Rich Repeat Kinase 2	- Signalling pathways - Cytoskeleton dynamic - Mitochondrial function - ER/Golgi - Vesicle trafficking - Autophagy and endolysosomal pathways	missense, R1441C/G/H, R1441S, Y1699C G2019S, I2020T, I2012T, R1628P, G2385R, N1437H/S	- Loss of DN in SN - Presence or not of LB in brain stem - Neurofibrillary tangles
		VPS35	Vacuolar Protein Sorting	Component of the retromer complex	D620N	Undetermined
		EIF4G1	Eukaryotic translation initiation factor	Component of the translation initiation complex	R1205H	Lewy bodies disease
		GBA	β-gluco-cerebro-sidase	Lysosomal enzyme	L44P risk factor	Typical LB
Autosomal Recessive PD	Early-Onset PD (Juvenile)	**Parkin (*PARK2*)**	E3 Ubiquitin Ligase	- Target proteins for ubiquitination - Mitochondrial function	Indels, duplications, nonsense and missense mutations	- Presence or not of LB - Loss of DN in the SN - Neurofibrillary tangles
		PINK1	PTEN-Induced Putative Kinase 1	Mitochondrial ser/thr kinase		
		DJ-1 (*PARK7*)	Deglycase	Redox-sensitive chaperone and protease	Missense mutations	Undetermined
		ATP13A2	5 P-type ATPase	Lysosomal ATPase	Loss of function mutations	Kufor-Rakeb syndrome (levodopa-responsive PD)

1.1.4 Biomarkers for Parkinson's disease

Due to the long latency between the start of the neurodegeneration process and the manifestation of motor symptoms, PD cannot be diagnosed in its early stages, which in turn makes early therapeutic intervention impossible. Thus, the identification of reproducible and objective biomarkers of early-stage PD is a crucial area of research.

PD is divided into several stages that are defined prior to the clinical diagnosis of PD[86,87] (Figure 1.3). The preclinical stage is defined as the time when neurodegeneration is ongoing but without any symptoms, with certain non-motor symptoms occurring during the subsequent prodromal stage. Research has therefore been focused on biomarkers for early diagnosis during these stages, in various areas[86,87]. For instance, potential prodromal markers include non-motor symptoms, genetic and epigenetic markers, or fluid biomarkers (Figure 1.3). Importantly, the PD biomarkers that have been proposed require the use of a combination of several markers to be reliable, which implies that further studies are required. Aside from PD diagnosis, biomarkers for PD could also help predict the risk of PD, monitor PD progression and severity, help in therapeutic interventions, and distinguish PD from other form of parkinsonism and synucleinopathies[86,87].

However, despite progress in understanding PD pathophysiology, the complexity of PD aetiology makes the discovery of biomarkers challenging[86,87]. An additional factor is the clinical heterogeneity in PD, which manifests at each stage. Moreover, the lack of standardisation and generalisation in biomarker studies constitutes another drawback. Findings vary between studies due to gender-related differences, sample size or methods. As such, the available biomarkers still lack specificity for the detection of prodromal stage, establishing diagnosis, or predict PD, and potential biomarkers still need to be validated in clinical studies. Research is ongoing, and validated biomarkers are avidly awaited[86,87].

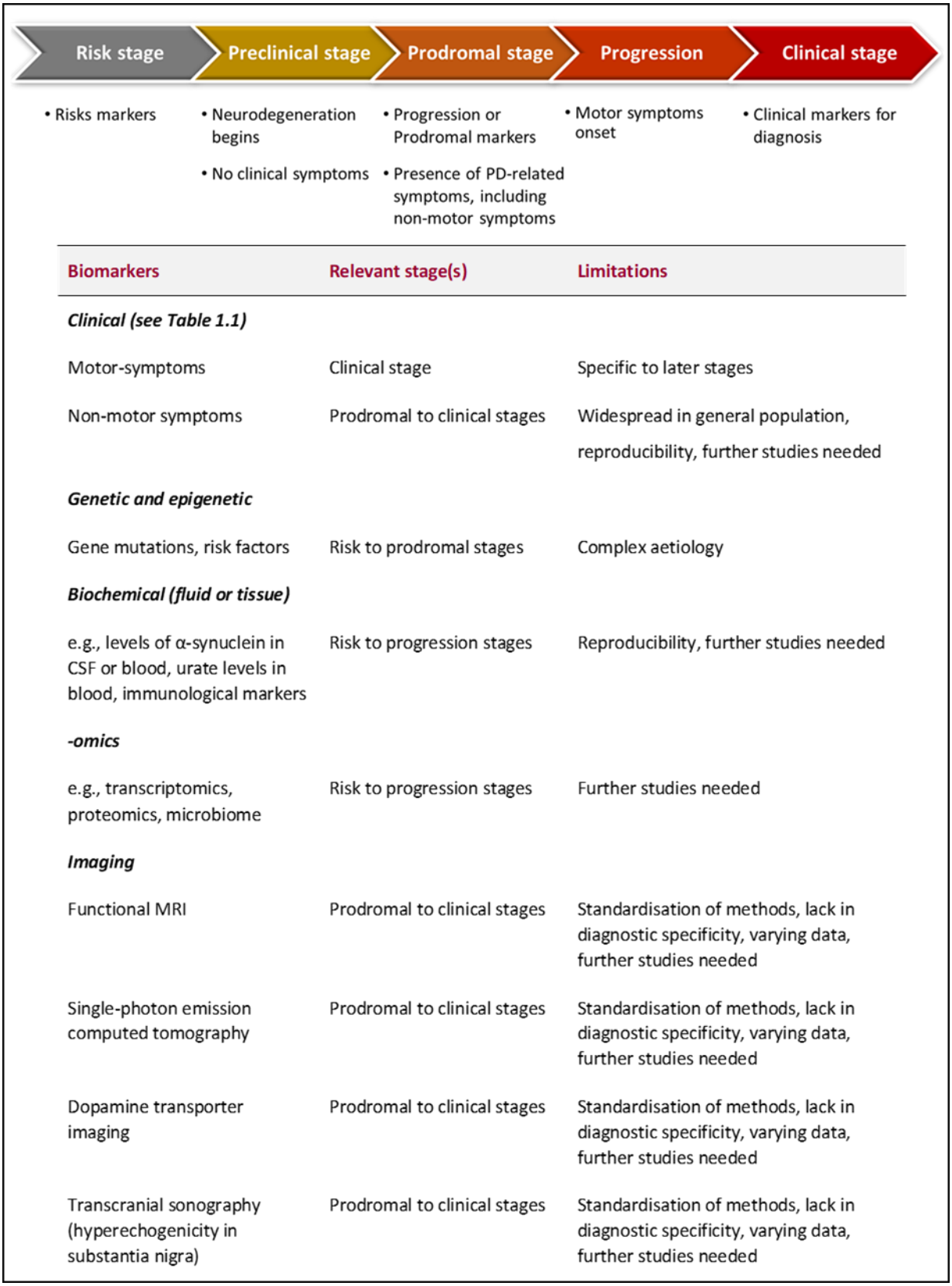

Biomarkers	Relevant stage(s)	Limitations
Clinical (see Table 1.1)		
Motor-symptoms	Clinical stage	Specific to later stages
Non-motor symptoms	Prodromal to clinical stages	Widespread in general population, reproducibility, further studies needed
Genetic and epigenetic		
Gene mutations, risk factors	Risk to prodromal stages	Complex aetiology
Biochemical (fluid or tissue)		
e.g., levels of α-synuclein in CSF or blood, urate levels in blood, immunological markers	Risk to progression stages	Reproducibility, further studies needed
-omics		
e.g., transcriptomics, proteomics, microbiome	Risk to progression stages	Further studies needed
Imaging		
Functional MRI	Prodromal to clinical stages	Standardisation of methods, lack in diagnostic specificity, varying data, further studies needed
Single-photon emission computed tomography	Prodromal to clinical stages	Standardisation of methods, lack in diagnostic specificity, varying data, further studies needed
Dopamine transporter imaging	Prodromal to clinical stages	Standardisation of methods, lack in diagnostic specificity, varying data, further studies needed
Transcranial sonography (hyperechogenicity in substantia nigra)	Prodromal to clinical stages	Standardisation of methods, lack in diagnostic specificity, varying data, further studies needed

Figure 1.3: Brief overview of disease stages and biomarker research in Parkinson's disease.

Parkinson's disease is divided into several stages. Neurodegeneration begins during the preclinical stage but without symptoms. PD-related symptoms appear during the prodromal stage, but the diagnosis is usually only possible when the clinical stage is reached. Biomarkers could be used to predict the risks, detect the preclinical stage, provide clues on disease progression, or help with diagnosis. At this time, no specific and reliable biomarker exists for these purposes, but research is ongoing[86,87].

It is worth mentioning that imaging studies are promising tools to complement clinical observations in PD[86,87] (Figure 1.3). Indeed, depletion of dopamine results in functional connectivity changes and abnormalities across the whole brain. Several techniques, such as functional MRI, transcranial sonography or single-photon emission computed tomography can be used to detect structural and functional changes in the brain[86,87]. For instance, loss of dopaminergic neurons leads to reduced dopamine uptake and dopamine transporter density, which is a key imaging biomarker for PD diagnosis, even prior to the onset of motor symptoms. However, these techniques also have drawbacks that limit their use to detect PD biomarkers, including the need for methods standardisation and lack in diagnostic specificity, since these techniques do not necessarily allow for the monitoring of disease progression or the distinction between PD and other synucleinopathies[86,87]. As such, this area merits further exploration.

1.1.5 Model systems to study the aetiology of PD

PD clinical phenotypes are heterogenous, and the underlying pathophysiology is not well understood. Although motor and non-motor symptoms are clinically assessed, the associated brain pathology can only be detected through examination of post-mortem tissues, which are fairly rare and limited. As such, experimental models replicating the diverse aspects of PD have proven to be crucial tools to extend the knowledge of the mechanisms underlying PD pathology and pathogenesis, and develop new treatment strategies.

1.1.5.1 Animal models of PD

In principle, animal models should allow PD to be studied under physiologically relevant *in vivo* conditions, replicating the clinical and pathological characteristics of the disease observed in patients. Typically, current animal models of PD can be divided into two main categories: neurotoxin models and genetic models[55,88,89] (Appendix 1).

Neurotoxin models are usually used to model sporadic PD using environmental or synthetic neurotoxins to reproduce the main defects found in PD. Various models have been developed, such as exposure to MPTP, 6-OHDA, paraquat or rotenone[55,88–90]. Toxin-based rodent models of PD significantly replicate, to some extent, a number of key features in PD[89]. Generally, these models exhibit a rapid loss of dopaminergic neurons of the substantia nigra, accompanied with motor deficits and behavioural impairments, but lack formation of Lewy bodies[89–91]. Usually, the neurodegeneration correlates with the motor deficits, and these models reflect the late stages of PD[60]. Such models have been essential for investigating dopaminergic loss and motor symptoms, and are useful as an initial mean to screen drugs and potential treatment for PD symptoms[91]. However, neurotoxin models are not suitable for the development of preventative treatments, or to elucidate the molecular mechanisms that cause dopaminergic loss in the first place.

The identification of PD-related genes offered an alternative to neurotoxin-based PD models and led to the development of genetic PD models[88,92]. These animals include transgenic and viral vector-mediated models based on the overexpression of familial PD-related gene mutations[60,91,92]. In contrast to toxin-based models, genetic models should replicate the early stages of PD pathology[60]. These models have proven useful for the study of autosomal recessive early onset forms of PD (e.g. *PINK1* and *Parkin)*, where knockout mice display clear nigrostriatal impairments that are consistent with a pre-PD phenotype[93,94]. However, for late onset autosomal dominant forms of familial PD, these models have not provided conclusive outcomes. Many genetic models have little or no phenotype, while those that do develop motor symptoms fail to fully recapitulate the pathophysiology of the disease[88,91]. In the case of Lrrk2, transgenic mouse and rat models have generally failed in reproducing all PD hallmarks, and *Lrrk2* knockout mice do not exhibit neuropathological features[88,90,91,95]. These findings appear discouraging in the context of PD, but it should be acknowledged that *Lrrk2* knockout animals have at least been useful for uncovering the basic role of Lrrk2, not least evidence of a role for Lrrk2 in the autophagic pathway[88,90,91,95], and also providing evidence that loss of Lrrk2 function causes age-related kidney and

lung pathology in several mouse and rat models, which may have implications for the long-term use of LRRK2 inhibitors in patients.

In summary, animal models of PD have contributed to the understanding of the disease but have important limitations[91]. Furthermore, inconsistency in findings reinforce the need for the standardisation of current PD models and procedures. It may be the case that the short lifespans of rodents are simply insufficient for the development of a late-onset human disease. But even where more convincing phenotypes are present, these animal PD models rarely allow the comparison of different causes of PD in parallel, due to the financial and practical difficulties of housing multiple strains. Therefore, there is a great need for alternative models.

1.1.5.2 Cell models of PD

In contrast to animal models, cellular models are promising tools for studying the early molecular events underlying PD[96,97]. Indeed, cellular models permit multiple mutations to be studied in parallel by using transient transfection of wildtype and mutant proteins. Most advances in understanding the function of PD-associated proteins and in the mechanisms underlying PD pathology have come from these types of study. In addition, it is possible to combine the use of toxins with genetic mutations, which might help determine the contribution of environmental and genetic factors.

A number of cell lines are frequently used in neurodegenerative disease research, depending on the type of experiment and aims[90,96,98] (Appendix 2). Although cellular models of PD based on neuronal tumour cell lines have provided insights into cellular impairments, the mechanisms responsible for PD are not always investigated in dopaminergic neurons, the most affected cell type[96]. This is debatable, since several neuronal cell types are affected in PD, which suggests that investigating the molecular basis of PD in neuronal cells other than dopaminergic neurons might also help expand the understanding of the disease.

Cellular models have several advantages compared to animal models[96,98]. Aside from reduced financial and practical difficulties, the use of pharmacological agents or genetic intervention are easier, and they allow multiple experiments to be performed at the same time. As such, cellular models do not replicate all features of PD, but allow the experimenter to explore the mechanisms responsible for a specific event in a short amount of time and robustly.

However, cellular models are limited by non-physiological protein expression levels, and also by the unrepresentative nature of transformed cell lines that do not replicate neurons *in vivo*[96,98]. Furthermore, in many cases the cell lines are not of human origin but primary cell lines obtained from animal models[96,98]. Thus, results obtained in cell models have to be validated in more relevant systems[96]. To overcome the limitations of species and physiological relevance, induced pluripotent stem cells (iPSCs), which are derived from patient tissue[99,100] are becoming popular *in vitro* models. However, iPSCs also carry epigenetic modifications associated with the tissue from which they were derived, which limits their ability to accurately model a physiological cell type[101]. In addition, the use of iPSCs cells depends on ethical approval, and they are less cost-efficient than immortalised cell lines.

1.2 Leucine-rich repeat kinase 2

Mutations in the *LRRK2* gene (*PARK8*) encoding the leucine-rich repeat kinase 2 protein (LRRK2), also known as dardarin, are the most common cause of familial late-onset PD and also strongly influence the risk of sporadic PD[76,102–105]. Importantly, pathogenic *LRRK2* mutations induce phenotypes that are clinically indistinguishable from idiopathic PD, including age of onset, symptoms, and patterns of neurodegeneration of nigrostriatal dopaminergic neurons and Lewy bodies accumulation[25,102,106,107]. In addition, genome-wide association studies have also identified *LRRK2* risk variants[108,109]. These observations suggest that LRRK2 is likely to be a central element in understanding both idiopathic and familial PD aetiology.

Since the discovery of its involvement in PD in 2004, the complexity of LRRK2 has challenged the field of PD with regards to determining its precise role in the pathogenesis of the disease, but also its normal physiological role. Nevertheless, since LRRK2 is involved in various cellular functions that will be detailed in the following sections, it is thought that *LRRK2* mutations lead to PD through several potential mechanisms.

1.2.1 LRRK2 protein and PD-causing mutations

LRRK2 is a large 2527 amino acid protein belonging to the ROCO family of GTPases (which also comprises death-associated protein kinase 1 or DAPK1, malignant fibrous histiocytoma amplified sequences with leucine-rich tandem repeats 1 or MASL-1, and LRRK1), that contains multiple functional domains[110–112]. The structure of LRRK2 is depicted in Figure 1.4. Interestingly, these include four protein-protein interaction domains and domains conferring both a serine-threonine kinase activity (MAPKKK-like) and a GTPase activity (RocCOR domain). This complex structure implies both an enzymatic role and a scaffolding role for LRRK2 in signal transduction[112–117]. In addition, protein-protein interactions have also been reported to occur at the level of the RocCOR domain and amino-acids located between the ANK and LRR domains, most notably with microtubules[115] and 14-3-3 proteins[118,119].

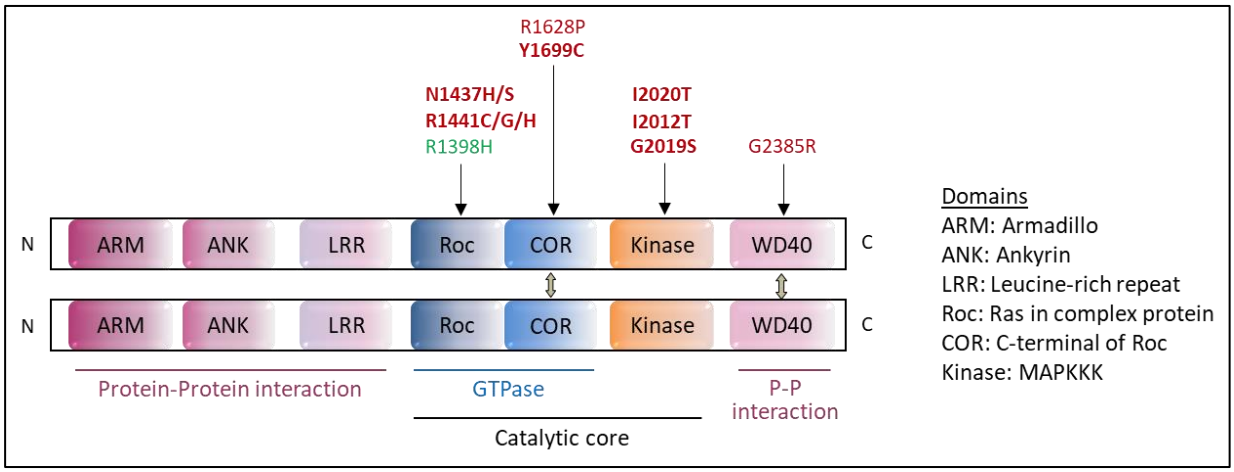

Figure 1.4: LRRK2 structure and mutations

LRRK2 is a homodimer belonging to the ROCO family of GTPases. LRRK2 contains multiple domains: protein-protein interaction domains ARM (armadillo), ANK (Ankyrin-like), LRR (leucine rich repeat) and WD40 (all in pink); a serine-threonine kinase domain (in orange); and a Roc (Ras of complex proteins)-COR (C-terminal of Roc) tandem domain conferring GTPase activity (in blue). The arrows indicate the putative intramolecular interactions. The locations of the pathogenic mutations are indicated in bold red; the risk variants are indicated in red; and the protective variant is indicated in green.

LRRK2 is ubiquitously expressed and can either be cytoplasmic or found on organelle membranes, such as lysosomes or mitochondria[118,120–122]. Typically, LRRK2 exists as both homodimers and monomers in cells, regulating LRRK2 subcellular location and function[112,123]. Indeed, monomers are generally cytosolic, whilst dimers are predominantly located on membranes with a higher kinase activity[124–126].

Numerous PD-causing mutations have been identified within *LRRK2* (Table 1.3). Since these mutations are autosomal dominant, the assumption is that they cause a toxic gain of function[127,128], although this cannot be proven definitively until the normal physiological role of LRRK2 is established. Interestingly, most of the disease-causing mutations cause amino acid substitutions within the catalytic core of LRRK2[112,126]. This suggests that the modulation of LRRK2 enzymatic activities influences PD pathogenesis. However, although several *LRRK2* mutations have been studied in detail, few shared effects have been reported. For example the G2019S *LRRK2* kinase domain mutation, which is the most common pathogenic *LRRK2* mutation followed by R1441C/G/H[72,130], increases LRRK2 kinase activity *in vitro*, yet other pathogenic mutations do not appear to do this[131–133]. Conversely, mutations in the GTPase domains decrease the GTPase activity of LRRK2, but this enzymatic activity is unaffected by G2019S.

Combining multiple studies reporting on these PD-associated *LRRK2* mutations, it is now commonly accepted that they are associated with increased phosphorylation of LRRK2 kinase substrates and reduced GTPase activity and/or increased GTP-binding[103,132–139]. In fact, it has been shown that LRRK2 kinase activity is the major actor in mediating LRRK2 toxicity and pathogenicity in PD[132,140–142], and is involved in various cellular mechanisms impaired in PD such as the autophagy-lysosomal pathway, vesicular trafficking, inflammation, and neurite outgrowth[143,144].

1.2.2 LRRK2 biochemistry

LRRK2 is involved in several cellular mechanisms and pathways, but its physiological role seems complex and is still under debate. The current known role of LRRK2 kinase and GTPase activities in LRRK2 function is detailed below.

1.2.2.1 LRRK2 kinase activity

Despite extensive research efforts, few widely accepted LRRK2 kinase substrates have been reported, with the best-defined substrate being LRRK2 itself. LRRK2 is capable of autophosphorylation, which is reported to regulate its kinase activity via phosphorylation of the kinase activation loop structure[145,146]. Autophosphorylation of the GTPase domain has also an impact on the kinase activity[147,148], and might influence the subcellular location of LRRK2 through protein-protein interactions. Importantly, reports have shown that pathogenic LRRK2 mutants display an elevated autophosphorylation at S1292[147], a site located in the LRR domain. The role of S1292 autophosphorylation is not known, but this phosphorylation site is likely to be a reliable biomarker to assess LRRK2 kinase activity *in vivo.*

Nonetheless, a group of Rab small GTPases have now become established as *bona fide* LRRK2 substrates[136]. Importantly, Rab proteins can have different subcellular localisations and are involved in a variety of cell biological processes[149–151], including synaptic vesicle recycling, vesicular trafficking and the autophagy-lysosomal pathway. Rab phosphorylation may therefore provide a mechanistic insight into

the function of LRRK2 in these processes[122,152–154]. In particular, studies have focussed on Rab8a and Rab10 as substrates of LRRK2, with Rab29 (Rab7L1) also described as a putative upstream activator of LRRK2 in addition to being its substrate[155]. Of note, *RAB29* is also a PD-risk gene[76]. Importantly, LRRK2 phosphorylation of Rab proteins is enhanced by all PD-causing *LRRK2* variants tested[136]. Consistently, phosphorylation of Rab proteins by LRRK2 results in the accumulation of Rab proteins at membranes and impairs their function[136,156,157], which in turn impairs the autophagic and endolysosomal pathways[158–160]. As is outlined later in this Chapter, these processes are of central importance to PD, so Rab phosphorylation may be a key pathological mechanism of *LRRK2* mutations.

1.2.2.2 LRRK2 GTPase

The number of pathogenic mutations located in the LRRK2 GTPase domain support an important role for LRRK2 GTPase activity in LRRK2 pathogenicity[161]. These pathogenic RocCOR *LRRK2* mutations, such as R1441G, are associated with weaker GTPase activity and/or increased affinity for GTP, both of which lead to a greater proportion of LRRK2 existing in a GTP-bound state. Interestingly, the PD-protective variant R1398H appears to have opposite effects[108].

Recent work has suggested that pathogenic *LRRK2* RocCOR domain mutations impair the equilibrium between the monomeric and dimeric forms of LRRK2, which may in turn impact upon LRRK2 kinase activity. In particular, in the model described in recent reviews[112,162], recruitment of monomeric LRRK2 at Golgi membranes by Rab29 proteins promotes its phosphorylation, dimerization and activation, i.e. kinase activity and GTP hydrolysis[137,155,163]. As such, Rab29 regulates LRRK2 subcellular location and promotes the phosphorylation of other Rab substrates in a Rab29-LRRK2-Rab axis[112]. Pathogenic mutations, such as R1441C/G/H, might prevent a return to the cytosolic inactive GDP-bound monomeric form of LRRK2, thereby stabilising GTP-bound/or nucleotide-free LRRK2 dimers. This has the effect of increasing LRRK2 kinase activity and extending its presence on intracellular membranes, thus leading to elevated substrate phosphorylation. This suggests a role for LRRK2 GTPase activity as a regulator of

LRRK2 kinase activity, which is consistent with previous studies suggesting a complex functional relationship between these enzymatic activities[112,164].

1.2.2.3 Upstream regulation of LRRK2

To expand on Rab29, the upstream regulation of LRRK2 by Rab29 mentioned in the previous section has also revealed a potential inhibitory feedback loop regulating Rab29 activity. As a LRRK2 substrate, phosphorylation of Rab29 has been shown to prevent its effect on LRRK2 kinase activity[155,163]. Therefore, the already important relationship between LRRK2 and Rab proteins appears to have more levels of complexity.

Aside from LRRK2 autophosphorylation and dimerization, other factors regulate LRRK2-mediated signalling, highlighting the complex regulation of LRRK2. In particular, studies have shown that LRRK2 can undergo regulatory phosphorylations by other kinases. For example, expression of LRRK2 is increased in immune cells upon their activation[165,166], and is associated with an increased LRRK2 phosphorylation by kinases from the IκB family[167]. In addition, the serine/threonine kinase CK1α has been reported to phosphorylate LRRK2 at locations between the ANK and LRR domains. These heterophosphorylation events modulate the protein-protein interactions of LRRK2, most notably binding of LRRK2 with 14-3-3 proteins, which are known to have a large interactome and various effects depending on the target protein and cellular process[168]. Binding of 14-3-3 proteins to LRRK2 has been suggested to promote the monomeric form of LRRK2, maybe inactive, thereby regulating both its subcellular localisation and activity[118,169,170]. Interestingly, pathogenic *LRRK2* mutations have been reported to disrupt the LRRK2-14-3-3 interaction, which support its potential relevance in PD[118,119,169,171].

1.2.3 Development of LRRK2 inhibitors

The upregulation of LRRK2 kinase activity is believed to be the major factor in mediating the pathogenic effects of PD-causing *LRRK2* mutations[132,140–142]. In fact, LRRK2 kinase activity, as judged by S1292 autophosphorylation and Rab10 phosphorylation, is also enhanced in patients with idiopathic PD, irrespective of the presence or not of *LRRK2* mutations[172]. Given that kinases are common pharmaceutical targets, these observations indicate that LRRK2 kinase activity is a potential druggable target, creating a new opportunity for the development of disease-modifying therapies. Consequently, efforts have supported the development of pharmacological LRRK2 kinase inhibitors to reduce LRRK2 kinase activity and reverse LRRK2-mediated impairments. Towards this end, a number of small-molecule inhibitors for LRRK2 kinase activity have been generated[134,139,164,173,174].

1.2.3.1 LRRK2 kinase inhibitors

The earliest compounds tested for LRRK2 kinase inhibition were non-selective, broad-spectrum or "pan" kinase inhibitors, which, despite their effect in cellular models and rodents, displayed a low potency, relatively high off-target activity, and pharmacokinetic limitations[134,143]. This prevented their clinical application and stimulated the discovery of more efficient compounds.

Thus, several generations of pharmacological inhibitors have been developed since, improving their potency, selectivity, affinity, permeability and pharmacokinetics[134,143,164]. However, although the so-called "first generation" inhibitors (such as LRKK2-IN-1) were more efficient than early compounds, they presented off-target effects and were not permeable through the blood-brain barrier, limiting their use *in vivo*. Indeed, the ability of compounds to cross the blood-brain barrier is one of the most critical "barriers" in the development of therapeutic compounds for PD. Second generation LRRK2 kinase inhibitors (including GSK2578215A, GNE-9605 and PF-06447475, which were used in the present study and will be further detailed in Chapter 4) display an improved bioavailability and permeability; however, they also display significant off-target effects[134,143,164]. Importantly, these LRRK2 inhibitors are derived

from inhibitors targeting other kinases, so off-target effects can, to some extent, be expected. Thus, further improvements were required. The development of potent and selective LRRK2 inhibitors was continued with the latest third generation small molecule LRRK2 kinase inhibitors (such as MLi-2), which have shown significant advantages, such as improved selectivity, brain permeability, bioavailability and safety compared to the previous generations of inhibitors[134,143,164].

First and second generation LRRK2 kinase inhibitors have proven their utility *in vitro*. Cellular studies using LRRK2 inhibitors have enabled researchers to determine whether an effect of LRRK2 is dependent on LRRK2 kinase activity, in either a physiological or a pathological context. As such, their participation in understanding the role of LRRK2 in autophagy will be detailed in Section 1.6.2.3.

Although findings supporting the neuroprotective effect of LRRK2 inhibitors are accumulating[164,175,176], the development of disease-modifying agents for PD has proven to be challenging, and important limitations still need to be addressed. Indeed, the potential toxicity of LRRK2 inhibitors raises concerns. Preclinical studies have shown deleterious effects of LRRK2 kinase inhibitors in several animal models, including in the lungs and kidney of animal models, and safety studies have not been able to rule-out toxic long-term effects yet[134,139,164,174].

In addition, prior to using the LRRK2 kinase inhibitors as therapeutic agents, precise and reliable biomarkers and assays for measuring LRRK2 kinase inhibition are still needed in order to provide indisputable evidence that LRRK2 inhibitors are efficacious in patients. Some potential candidate biomarkers are the LRRK2 substrates Rab proteins or the autophosphorylation site S1292, as mentioned in the Section 1.2.2.1. This area is still under investigation.

Nevertheless, the development of small molecules to block LRRK2 kinase activity has advanced to an extent that the most promising compounds are used in preclinical models, but are also the subjects of clinical trials that have shown encouraging results, with human trials currently in process[134,139]. Over the last few years, the use of LRRK2 kinase inhibitors has also greatly improved knowledge regarding LRRK2 biology and the effects of *LRRK2* pathogenic mutations on LRRK2 catalytic activities. Nonetheless, there

are still gaps in the precise role of LRRK2, which will be key to successfully using LRRK2 activity-modifying drugs as PD therapeutic agents.

1.2.3.2 LRRK2 GTPase inhibitors

Although most efforts have been focused towards the development of LRRK2 kinase inhibitors, the LRRK2 GTPase domain is also an interesting drug target for therapeutic intervention. Indeed, in line with the findings described in Section 1.2.2.2, decreasing the proportion of LRRK2 existing in a GTP-bound state would reduce LRRK2 kinase activity and would likely be neuroprotective. Therefore, selective and blood-brain barrier-permeable LRRK2 GTPase inhibitors (in particular, GTP-binding inhibitors) may represent an additional option to explore beyond kinase inhibition. Surprisingly though, research on LRRK2 GTPase inhibitors has not been prolific and very few research groups have actively taken that route and developed GTPase inhibitors. To date, one group has developed LRRK2 GTPase inhibitors, including compound 68 and its analogue FX2149[177–179]. Interestingly, since the structure of the LRRK2 GTPase domain has been shown to differ from other small GTPases, these inhibitors theoretically only target LRRK2[177]. Both compounds are potent and selective LRRK2 GTPase inhibitors *in vitro*, but FX2149 has the advantage compared to compound 68 of having an improved blood-brain barrier permeability, thereby improving its application *in vivo*. 68 and FX2149 are both able to reduce LRRK2 GTP binding, but the compounds also reduce LRRK2 kinase activity *in vitro*, with a neuroprotective effect in presence of pathogenic LRRK2 mutants *in vivo* and *in vitro*[177–179].

However, the field around LRRK2 GTPase inhibitors is in its early stages. Thus, similar to LRRK2 kinase inhibitors, LRRK2 GTPase inhibitors also need to be tested further to rule out potential toxic side-effects in animal models.

1.2.4 Overview of LRRK2 function in cells

Although little is widely agreed about its role, LRRK2 has been implicated in various cellular processes and signalling pathways[112,180,181]. These processes, which include mitochondrial function, microtubule dynamics, autophagy, vesicle trafficking, lysosomal biology and Wnt signalling (Figure 1.5), are summarised in this Section. The role of LRRK2 in autophagy and calcium signalling will be discussed in greater detail later in this Chapter (Section 1.6.2). Importantly, despite the importance and relevance of the catalytic activities of LRRK2 to its function, current evidence suggests that overall LRRK2 may mainly act as a scaffold protein[180,182], and not necessarily through its enzymatic activities.

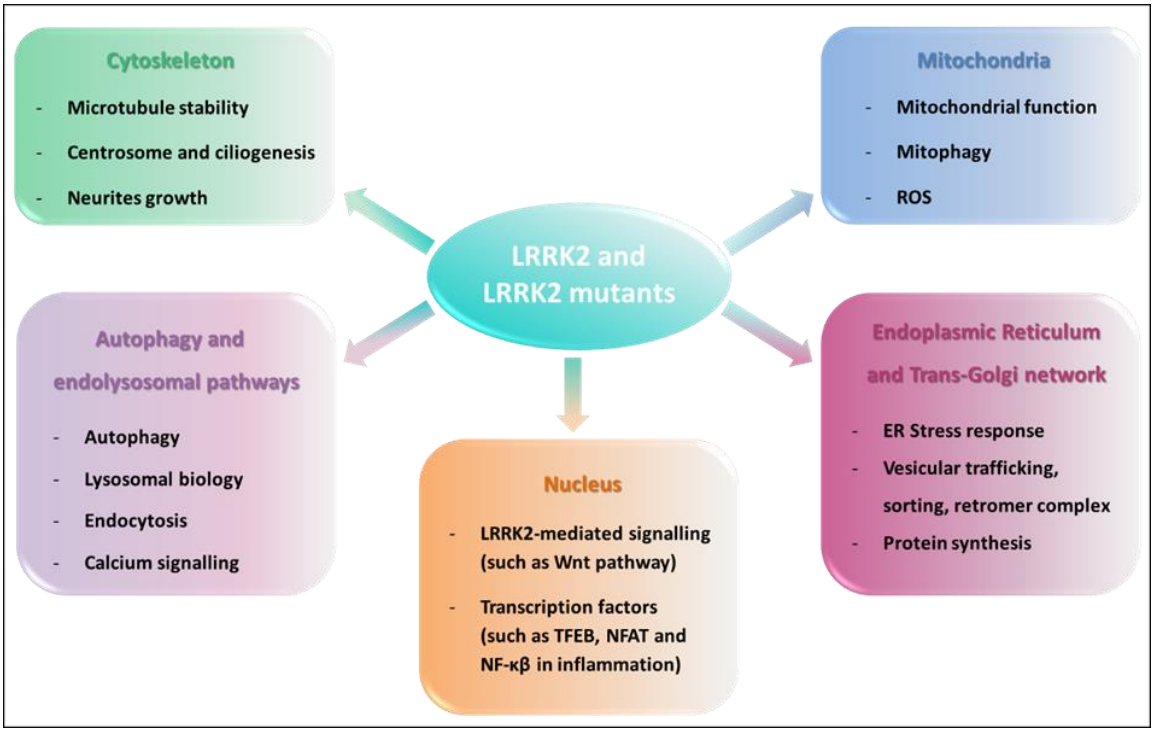

Figure 1.5: Cellular processes regulated by LRRK2 and affected by LRRK2 mutants

As described in the main text, LRRK2 is involved in the regulation of several biological processes, some of which are intertwined. Rab proteins are involved in several of these processes and potentially mediate some effects of LRRK2.

1.2.4.1 Wnt signalling pathways

One of the suggested LRRK2-mediated signalling mechanisms are the Wnt signalling pathways, where LRRK2 mainly acts as a scaffold protein[180,182] as part of a signalling complex[128,183,184]. LRRK2 interacts through protein-protein interactions with several proteins involved in the activated canonical Wnt

signalling pathway, such as dishevelled phosphoproteins, the serine/threonine kinase GSK3β, and the co-receptor LRP6, where LRRK2 promotes the signalling activity via translocation of β-catenin in the nucleus. However, LRRK2 is thought to inhibit the canonical Wnt signalling under basal conditions, where LRRK2 acts as a scaffold within the β-catenin destruction complex with APC, Axin and GSK3β to induce the phosphorylation of β-catenin proteins and facilitates their proteasomal degradation[128]. Consistently, LRRK2 may promote the antagonistic non-canonical Wnt, or PCP, pathway[185], indicating a dual role for LRRK2[128,183].

Importantly, PD-causing mutations throughout *LRRK2* have been reported to inhibit canonical Wnt signalling[125,126,180]. This observation is particularly interesting since it adds to growing lines of evidence suggesting that the canonical Wnt signalling pathway is involved in early PD pathogenesis[186,187]. This includes the key role of Wnt signalling in dopaminergic neuronal development[188], whilst many other PD-related genes, not just LRRK2, are linked to the Wnt signalling pathway[187]. Strengthening the connection further, a *LRRK2* protective variant R1398H appears to have opposite effects to *LRRK2* PD-causing mutations in assays of Wnt signalling activity[108]. This implies that the impairment of Wnt signalling may have an essential role in the neurodegeneration resulting from *LRRK2* mutations in PD[116,189] and could be targeted for therapeutic use.

1.2.4.2 Microtubules

A large body of evidence support a role for LRRK2 in microtubule stability in several cellular mechanisms requiring the microtubular scaffold[190]. In fact, LRRK2 can bind dynamic microtubules structures[115,191]. As such, the interaction of LRRK2 with microtubules is thought to be one of the explanations for the role of LRRK2 expression in neurites, where pathogenic *LRRK2* mutations have been shown to enhance the repressing effect of LRRK2 on neurite outgrowth[190,191]. Similarly, LRRK2 also interacts with the actin cytoskeleton which is thought to participate in the effects of LRRK2 on axonal growth[191,192].

Given the fact that microtubule function is essential in maintaining cellular homeostasis, the impairment

of microtubule function caused by pathogenic LRRK2 mutants has an obvious negative impact on the transport of organelles and vesicles, which may in turn alter cellular processes such as autophagy or mitochondrial trafficking[191]. In addition, interaction of LRRK2 with Rab proteins, in particular Rab8a and Rab10, has been shown to be involved in the regulation of two other microtubular structures, cilia and centrosomes, where studies showed that several pathogenic *LRRK2* mutations impaired ciliogenesis[156,193] and induced centrosomal defects[194,195].

Reports have identified another role for LRRK2 as a scaffold involving microtubules. The axonal microtubule-associated protein Tau is known for its role in the pathology of Alzheimer's disease and in Frontotemporal dementia with Parkinsonism[196], where Tau hyperphosphorylation disrupts microtubule stability and leads to neurofibrillary tangles[197]. Interestingly, PD cellular and animal studies, as well as post-mortem studies, have shown that pathogenic *LRRK2* mutations can also lead to Tau pathology[198–202]. The mechanism by which LRRK2 causes Tau pathology is not yet known, but it could potentially be by facilitating the activation of GSK3β, a known Tau kinase[181,200,201], which would be analogous to the reported role of LRRK2 as a β-catenin repressor in Wnt signalling. As such, one of the roles of LRRK2 in neurodegeneration might be as a scaffold protein regulating GSK3β activity in various contexts.

1.2.4.3 Mitochondrial function

The role of LRRK2 and the impact of pathogenic *LRRK2* mutations on mitochondrial function are unclear, but hypotheses have emerged. One possibility is that LRRK2 is involved in mitochondrial trafficking and mitophagy via the outer mitochondrial membrane protein Miro, since pathogenic mutations impair the physical interaction of LRRK2 with Miro and deregulate mitophagy[188,202]. On the other hand, pathogenic LRRK2 mutants might impair the neuroprotective anti-oxidant mechanisms[206,207], leading to an increase in reactive oxygen species (ROS). In addition, pathogenic LRRK2 mutants have been shown to influence the vulnerability of dopaminergic neurons towards MPTP and oxidative stress, in animal models and humans[208–210]. Impaired mitochondrial homeostasis, especially via deregulation of mitophagy, eventually leads to reduced ATP generation, accumulation of damaged mitochondria, and elevated oxidative stress,

which ultimately results in the neurodegeneration of dopaminergic neurons (for further details on the selective loss of dopaminergic neurons and the mechanisms, see Section 1.6.1).

1.2.4.4 Endoplasmic Reticulum homeostasis and Trans-Golgi network

The protective Endoplasmic Reticulum (ER) stress response, also called the unfolded-protein stress response, occurs when misfolded proteins accumulate within the ER lumen, with the aim of increasing the production of chaperones and decreasing protein translation[211]. Interestingly, several studies have shown that this process is elevated in PD and suggest that LRRK2 may participate by being involved in the expression of chaperones[212,213]. Furthermore, LRRK2 has been described to mediate ER vesicle release and the transport of ER-derived vesicles to the Golgi apparatus[112], another organelle with which LRRK2 has been implicated.

Evidence of a role for LRRK2 at the Golgi apparatus started with screenings for LRRK2 interacting-proteins that identified BAG5 and GAK, both of which were already linked to PD[112]. These proteins, in complex with LRRK2 and Rab29, are believed to localise on vesicular membranes of the trans-Golgi network, where they promote the clearance of trans-Golgi network-derived vesicles via autophagy. Interestingly, all pathogenic *LRRK2* mutations tested were reported to enhance this mechanism, supporting a role for LRRK2 enzymatic activities in the clearance of the Golgi apparatus as a component of a four-part complex. In addition, LRRK2 and Rab29 may be involved in the function of the retromer complex, regulating the sorting of endosomes for recycling towards the trans-Golgi network or for degradation in lysosomes, since data support a role for retromer dysfunction and Rab29 in the phenotype associated with LRRK2 mutants[152].

1.2.4.5 Lysosomal homeostasis

Recent findings have described lysosomes as important organelles in PD, and have even proposed that PD could be a lysosomal disease[214]. In the context of LRRK2-PD, pathogenic *LRRK2* mutations have been

reported to alter lysosomal structure and function in several cell types, including astrocytes[120,215,216]. In addition, Tong and colleagues reported an accumulation of lysosomal damage with age in kidneys of LRRK2 knockout mice[217], which is particularly interesting since LRRK2 is highly expressed in kidneys. However, how LRRK2 affects lysosomal homeostasis remains unclear.

Importantly, data linking LRRK2 to the lysosomal damage response have recently emerged, and may provide part of an answer. Eguchi and colleagues first revealed the involvement of LRRK2 in the regulation of the overload stress-induced lysosomal response[218]. Indeed, Rab29 promotes the translocation of LRRK2 to stressed lysosomes, which in turn recruits and activates Rab8a and Rab10. This promotes both lysosomal secretion/exocytosis of non-degraded cargo, and a reduction of lysosomal enlargement. In addition, Herbst and colleagues showed that LRRK2 is involved in the regulation of endolysosomal homeostasis in RAW264.7 macrophages[219], especially by promoting membrane repair via the recruitment of Rab8A and other effectors on damaged endolysosomes, otherwise targeted for degradation (via lysophagy). This was supported by observations from macrophages from PD patients carrying pathogenic *LRRK2* gain-of-function mutations (G2019S and R1441G), in which damaged endolysosomes accumulated. As such, these findings suggest that overactivation of LRRK2 signalling might reduce autophagy in PD patients.

Finally, a recent study further supports the connection between LRRK2 and lysosomal membrane damage, where LRRK2 appears to govern lysosomal tubulation in a newly discovered process that might be relevant to PD[220]. The authors showed that, upon lysosomal membrane permeabilization, the LRRK2-dependent phosphorylation and activation of Rab35 and Rab10 at lysosomal membranes promotes the subsequent recruitment of the motor adaptor protein c-Jun N-terminal kinase (JNK)–interacting protein 4 (JIP4). Consequently, JIP4 stimulates the formation of tubules to release vesicles from lysosomes, likely to communicate with other lysosomes.

1.2.4.6 Neurotransmission

Increasing evidence support an additional role for LRRK2 in neurotransmission, in particular at the presynaptic level[221]. Although not in total agreement on whether LRRK2 has a positive or negative impact, studies have shown a role for LRRK2 in synaptic vesicle trafficking and in neurotransmitter release[117,222–226]. Fascinatingly, LRRK2 appears to act positively via its kinase activity[227,228], and negatively as a scaffold[225]. Therefore, changes affecting either LRRK2 kinase activity or its ability to interact with proteins might disrupt neurotransmission. In addition, reports have shown that LRRK2 may be involved in the activation, degradation and recycling of dopamine receptors in post-synaptic compartments[223,229,230]. Importantly, these observations are also consistent with a role for LRRK2 in the endo-lysosomal system, which further support its role in autophagy (detailed further in Section 1.6.2.2.2).

1.2.4.7 Immune cells and inflammation

In addition to roles in ubiquitous cell biological processes and those specific to neurons, LRRK2 has also been linked to immune cells[112]. Indeed, there is growing evidence that inflammation, both in the central nervous system and systemic, is involved in PD pathomechanisms. Importantly, LRRK2 is highly expressed in immune cells, and this expression is increased further upon pro-inflammatory cues[165,166]. In addition, LRRK2 has been functionally associated to inflammation-related pathways[231], including autophagy, phagocytosis and cytokine release. Thus, it is likely that LRRK2 has a significant role in immune cells and inflammation[232,233].

This is fascinating, since inflammatory disorders have been reported as a PD risk[70,71], whilst genome-wide association studies have implicated *LRRK2* polymorphisms in the pathogenesis of several chronic inflammatory conditions[112], including leprosy[234], Crohn's disease[109] and tuberculosis[235]. Interestingly, these apparently unrelated inflammatory diseases share similarities. For instance, tuberculosis and leprosy are due to similar mycobacterial infections. In addition, genome-wide association studies have

linked a number of *bona fide* inflammatory genes to all three conditions, such as NOD2 and RIPK2[112,236], and have revealed similarities between their genetic risks. As such, these conditions might plausibly share similar pathomechanisms. By contrast, PD has little in common with these inflammatory diseases, the only link being LRRK2. Of note, since leprosy and tuberculosis are not common in countries where PD is most researched, it is possible that other links have not been identified yet. Nevertheless, whilst LRRK2 mutations alone cause PD, all three inflammatory conditions are linked to LRRK2 as risk variants, and not to PD-causing LRRK2 mutants. This is consistent with other causal factors triggering these inflammatory diseases. Importantly, these findings indicate that LRRK2 is likely to be involved in different pathomechanisms in PD compared to these inflammatory conditions.

Returning to the subject of the role of LRRK2 in immune cells, a common view speculates that pathological LRRK2 activity in microglia – immune cells of the brain – may contribute to neuronal dysfunction. In line with this hypothesis, a number of reports have associated LRRK2 with inflammation, and pathogenic LRRK2 mutants have been associated with impaired inflammatory responses[165,166,237–239]. In particular, LRRK2 mutations alter the activation of the transcription factors NF-kB and NFAT[237,239–241], which are also relevant in neurodegeneration[242]. Indeed, NFAT signalling is relevant to both neuronal development and innate immune responses. LRRK2 has been shown to stabilise the NRON RNA-protein complex through its scaffolding ability, which facilitates the phosphorylation of NFAT, thereby preventing its translocation to the nucleus and inhibiting NFAT signalling[241]. In addition, studies in microglia report that LRRK2 promotes neuroinflammation through the NF-kB signalling[237,243,244].

1.3 Autophagy

The findings described so far suggest that the process of autophagy might be essential in PD pathology. Autophagy and its regulation will be described in the next sections.

1.3.1 Role of autophagy in cells

Autophagy, deriving from the Greek words for "self-eating", is a mechanism for survival and normal homeostasis at both the organismal and cellular levels, that is conserved from yeast to mammals[245]. Autophagy has a critical role in various processes, in particular maintaining cell homeostasis by promoting lysosomal degradation of undesirable cargos, such as damaged or old organelles, long-lived proteins, aggregates and macromolecules, which might otherwise become toxic if accumulated. The main purpose of autophagy is cytoprotective and to deliver nutrients for cellular functions from the recycling of the resulting breakdown products. For example, free amino acids and fatty acids are reused for *de novo* protein synthesis[246]. However, if cells are damaged beyond repair, pathways such as apoptosis are activated to eliminate damaged cells. As such, cellular homeostasis is maintained through continuous degradation and synthesis[247]. Of note, the ubiquitin proteasome system (UPS) is the other main degradative pathway, which only involves protein degradation.

Autophagy is an adaptive cellular process that occurs constitutively at basal levels, but can also be stimulated in response to exposure to cellular stress such as nutrient starvation, growth factors depletion, hypoxia, mitochondrial depolarisation, misfolded proteins or damaged organelles. This is also true in immune cells, where autophagy is activated against pathogens and bacteria[248]. Due to its vital function as a homeostatic regulator, disruption of any stages of the autophagic pathway can result in autophagy impairment and the build-up of autophagic vesicles and cargo, which is implicated in several human pathologies including certain cancers, metabolic syndromes, infectious diseases, liver diseases, myopathies, ageing and neurodegenerative disorders including PD[22,249–252].

1.3.2 Types of autophagy

Generally, three types of autophagy are distinguished based on how the cargo is delivered to lysosomes: macroautophagy, chaperone-mediated autophagy and microautophagy. Microautophagy is a mechanism through which cytoplasmic material is directly sequestered into lysosomes for degradation[253]. Chaperone-mediated autophagy is a selective process responsible for the clearance of soluble proteins containing a specific motif recognised and targeted to the lysosome by chaperones[254]. Finally, macroautophagy is a mechanism through which cytosolic material is targeted for degradation by sequestration into double-membraned vesicles called autophagosomes, that ultimately fuse with lysosomes[255]. Importantly, macroautophagy enables the clearance of larger material that cannot be degraded via the two other autophagy types[256].

This Section (and study) focuses on macroautophagy, hereafter referred to as autophagy, of which the early steps have been extensively studied, and the later steps are poorly understood. Commonly, autophagy is described as non-selective ("in bulk") towards its substrates. In contrast, selective autophagy is the degradation of a specific ubiquitinylated target, including organelles, such as mitochondria (mitophagy) or aggregate-prone proteins (aggrephagy)[257,258], and involves adaptor proteins promoting the degradation of the cargo[259].

1.3.3 Mechanisms of the autophagic pathway

An overview of the autophagic pathway is depicted in Figure 1.6, and summarised in this Section.

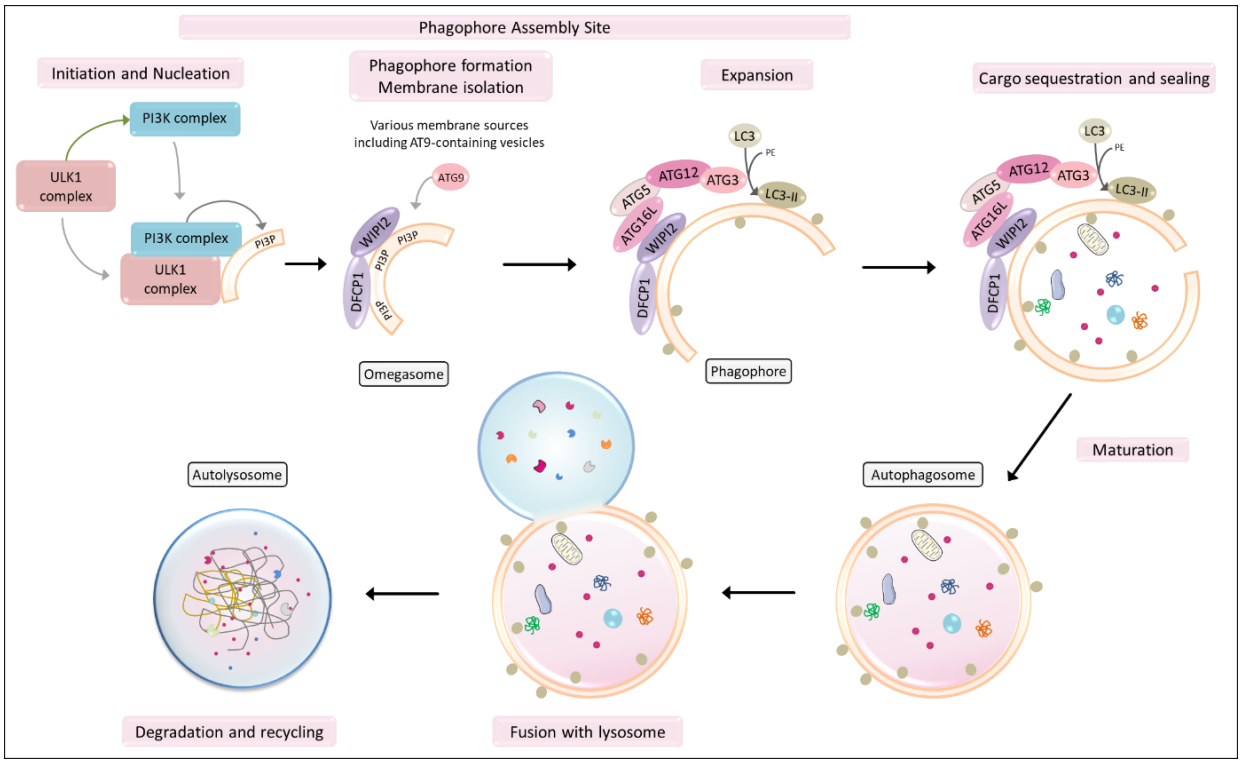

Figure 1.6: Overview of the autophagic pathway in mammalian cells

A schematic depicting the general process and machinery of autophagy is shown. Autophagy is a multistep process that can be divided into 7 steps: (1) initiation and nucleation (2) phagophore formation and membrane isolation (omegasome) (3) expansion of the phagophore membrane (4) cargo sequestration (bulk or selective) and sealing of the membrane (5) maturation of the autophagosome (6) fusion with lysosome and formation of autolysosomes (7) degradation, recycling of content and lysosome reformation. These steps are regulated by multiple ATG proteins assembled in sequentially recruited complexes, which relocate to a specific membranous subcellular location named the phagophore assembly site. Following autophagy induction, the ULK1-initiation complex is activated, which recruits and activates the PI3K nucleation complex. PI3K produces PI3P from phosphatidylinositol on the isolated membrane and recruits the effectors DFCP1 and WIPI2. The scaffolds WIPI2 and DFCP1 recruit ubiquitin-like conjugation systems, including ATG5-ATG12-ATG16L (and other ATGs that have been omitted for simplicity, see Figure 1.7 for more details), which promote the binding of LC3-I proteins to phosphatidylethanolamine, converting LC3-I to an anchored form LC3-II. In parallel, the ULK1 complex promotes the recruitment of ATG9 and ATG9-containing vesicles/membranes to deliver membrane material (originating from different sources), and form the phagophore, a cup-shaped structure. Cellular components targeted for their bulk-degradation get encapsulated in the phagophore, or alternatively, cargo receptors and adaptors recognise ubiquitinated organelles or macromolecules targeted for degradation. LC3-II facilitates this process by interacting with LIR motifs present on receptors. The phagophore membrane then seals into a double membraned vesicle named autophagosome. The maturation step is poorly understood; while ATG proteins are progressively removed, autophagosomes are transported towards acidic lysosomes, and the machinery responsible for lysosomal delivery, tethering and fusion is recruited (omitted for simplicity). Following fusion with lysosomes, the cargo is degraded in autolysosomes by proteolytic and hydrolytic enzymes. The degraded components are then recycled to the cytosol or directly to other organelles, and lysosomes reform.

Autophagy induction results in the recruitment of autophagy related proteins (ATGs), which regulate all steps of the autophagic process. These proteins relocate to a specific membranous subcellular location named the phagophore assembly site (PAS). ATGs are organised into functional complexes, defined by their interactions and function, which cooperate with each other. One of the first complexes involved in initiation of autophagy is the ULK1 complex, which contains the serine/threonine kinase ULK1 (Unc-51-

like kinase 1), FIP200 (focal adhesion kinase family-interacting protein), ATG13 and ATG101. However, the mechanisms involved in the recruitment of ULK1 to the PAS are not well understood.

Activation of the ULK1 complex allows for the subsequent recruitment and activation of other complexes necessary for the induction of autophagy[260,261] (Figure 1.6), such as PI3K class III complex I[262], which comprises VPS34 (vacuolar protein sorting 34; a lipid kinase that is the catalytic subunit of the complex), Beclin1, VPS15 and ATG14. This complex produces PI3P (phosphatidylinositol 3-phosphate) by the phosphorylation of PI (phosphatidylinositol) on the isolated membrane at the nucleation site to form the omegasome (Figure 1.6). PI3K complex is also essential to recruit and bind the PI3P effectors DFCP1 (double FYVE domain-containing protein 1) and WIPI proteins (WD-repeat-interacting phosphoinositide protein), in particular WIPI2.

WIPI2 and DFCP1 next act as scaffolds and recruit ubiquitin-like conjugation systems that participate in the binding of the family of proteins comprising LC3 (microtubule-associated protein 1-light chain 3) and GABARAPs (γ-aminobutyric acid receptor-associated proteins) to phosphatidylethanolamine on the isolation membrane[263] (pre-autophagosomal structure) (Figure 1.6). This process enables the conversion of LC3-I from a diffuse form into an anchored and lipidated form LC3-II[261,264]. In parallel, the ULK1 complex regulates the recruitment of ATG9, the only transmembrane ATG protein, and ATG9-containing vesicles are one of the sources providing membrane material (i.e., lipid bilayers). Although the exact origin of the membrane material supplied is not well understood, different membrane sources are thought to participate, including the plasma membrane, mitochondria, ER, recycling endosomes and Golgi complex[261].

These steps are necessary for the formation and expansion of the phagophore[265–267], a sphere-like membranous shape. Cellular components targeted for bulk degradation get encapsulated in the phagophore (Figure 1.6). Alternatively, cargo receptors and adaptors, such as SQSTM1/p62[268], recognise ubiquitinated organelles or macromolecules targeted for degradation via selective autophagy[269]. This process is facilitated by LC3-II anchored at the phagophore membrane which interacts with LIR regions

present on cargo receptors[270]. The phagophore membrane then seals into a double-membraned vesicle named autophagosome.

The mechanisms involved in the maturation of the autophagosomes and their regulation are coordinated, but poorly characterised. Whilst the ATGs proteins are gradually removed from the autophagosomal membrane (Figure 1.6), LC3-II contributes to the transport of autophagosomes on microtubules towards the acidic lysosomes, and the machinery mediating lysosomal delivery, tethering and fusion is recruited[271–276]. The fusion of autophagosomes with lysosomes forms autolysosomes, where the cargo is degraded by the luminal proteolytic and hydrolytic enzymes supplied by the lysosomes[277]. Autophagic flux is defined as this dynamic cargo clearance, from the formation of the phagophore to the delivery of the cargo to the lysosome, and is essentially the amount of autophagic clearance.

The steps following cargo degradation are poorly understood, but the current view suggests an efflux of the amino acids and other components to be recycled, either into the cytosol via transporters, or into other organelles via membrane-membrane contacts, and a reformation of lysosomes from autolysosomes through budding-off[278,279].

1.3.4 Regulation of autophagy by mTORC1

Autophagy is a dynamic process tightly controlled by various factors, including the availability and activity of ATGs, and regulatory kinases. Importantly, in addition to their degradative function, lysosomes are also involved in nutrient sensing and signal transduction[275], and impaired lysosomal function results in defects in cargo clearance and accumulation of autophagosomes[280].

ATG proteins are the molecular mediators essential for all steps of the autophagic process. The ULK1 and PI3K complexes, as well as ATG9, are essential for autophagy initiation. Deletion or inhibition of these factors impairs phagophore formation and leads to the accumulation of autophagic substrates, which is thought to underlie several pathological states, including neurodegeneration[257,281–283]. As depicted in

Figure 1.7, ATG proteins are also regulated through phosphorylation. For example, if the subunits of the ULK1 complex have not been phosphorylated, the ULK1 complex remains inactive and cannot activate the PI3K complex or promote LC3 lipidation, which prevents the initiation of autophagy.

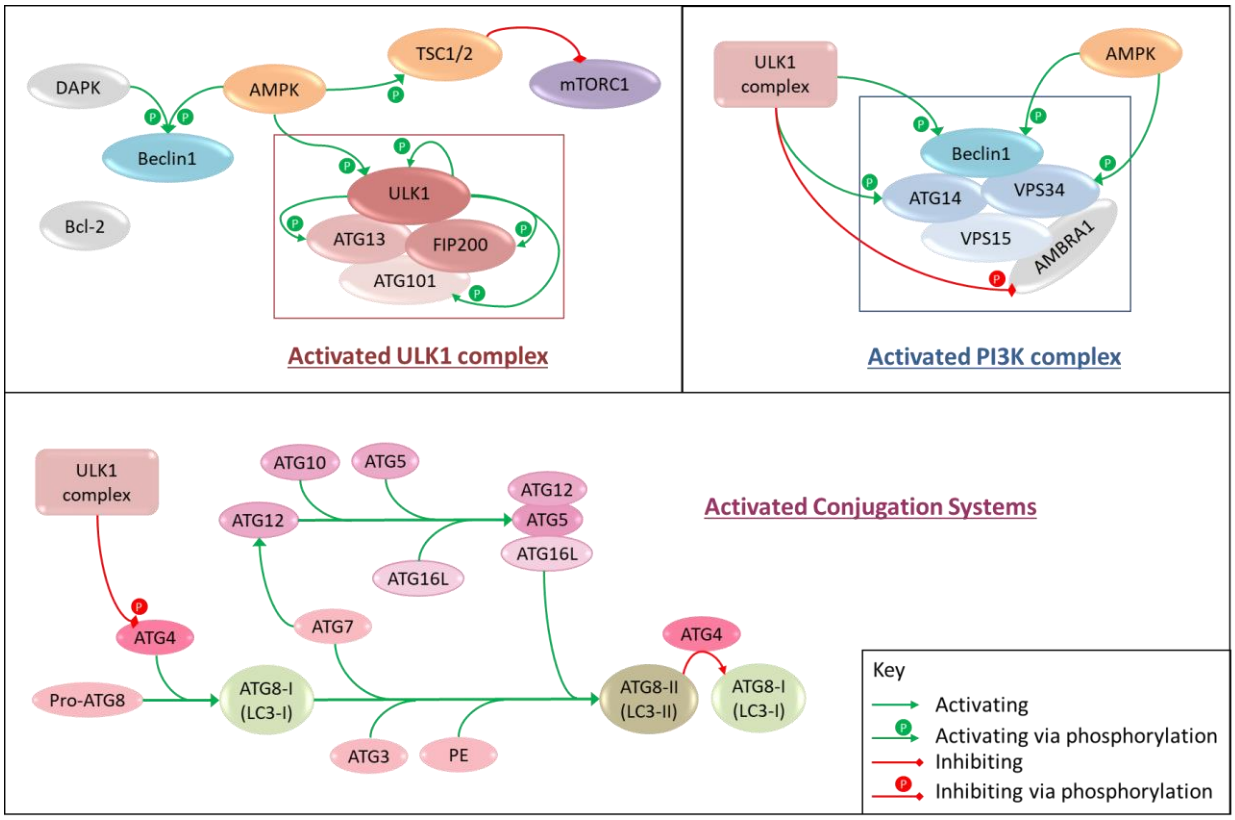

Figure 1.7: Events involved in the activation of the ATG complexes initiating autophagy

A series of phosphorylation events affecting the core ATG proteins occur to initiate autophagy. (**ULK1 and PI3K complexes**) Upon nutrient starvation, mTORC1 dissociates from the ULK1 complex and is inhibited, notably via the activation of the TSC1/2 complex by AMPK. Inhibition of mTORC1 leads to dephosphorylation of ULK1 at the mTORC1 repressor site. AMPK also activates ULK1 directly, and ULK1 autophosphorylates (Thr180). Activated ULK1 subsequently phosphorylates ATG13 (Ser318), FIP200 and ATG101 which activates the ULK1 complex. Beclin1, part of the PI3K complex, is activated by AMPK (Ser90/94 or Ser93/96) and DAPK1 (Thr119), which leads to the release of Beclin1 from Bcl2. The ULK1 complex then phosphorylates the subunits of the PI3K complex, Beclin1 (Ser14), ATG14 (Ser29) and VPS34 (Ser249), necessary for autophagy induction, but also AMBRA1 (S465/635) which releases the PI3K complex that was tethered to the cytoskeleton, allowing its relocation to the phagophore assembly site. VPS34 is also phosphorylated and activated by AMPK. (**The ubiquitin-like conjugation systems**) The ATG12 conjugation system comprises ATG12, activated by ATG7 and bound to ATG5, which is attached to ATG16L via ATG10. The ATG12-ATG5-ATG16L is then recruited to the phagophore assembly site by the effectors WIPI2 and DFCP1 recruited by the activated PI3K complex. Pro-ATG8 (LC3 or GABARAP) is cleaved by the protease ATG4 to form LC3-I. The ATG12-ATG5-ATG16L then promote the conjugation of LC3-I to phosphatidylethanolamine via ATG3 and ATG7, to form LC3-II on the phagophore membrane. Of note, ATG4 can convert LC3-II back to LC3-I, as a control mechanism. Similarly, the ULK1 complex can inhibit ATG4.

One of the most studied upstream mechanisms regulating autophagy is the mTOR (mammalian target of rapamycin) pathway. mTOR itself is a conserved serine-threonine kinase that exists as part of two distinct complexes, mTORC1 and mTORC2, each of which contains different subunits and have different functions. mTORC2 is mostly involved in cell survival and cytoskeletal organisation and is influenced by growth factors. On the other hand, mTORC1 is a key negative regulator of autophagy, which promotes biosynthesis and cellular growth[284–286].

Upstream signals sensing the cellular energy state control the activation of mTORC1 through phosphorylation/dephosphorylation events[287,288] to coordinate cell growth and homeostasis[289]. As depicted in Figure 1.8 , growth factor deprivation, nutrient depletion and low energy levels are well-established autophagy inducers, and the regulation of autophagy by mTORC1 is mediated by ATG proteins. Under nutrient-rich conditions, activated mTORC1 relocates to lysosomes[290] and suppresses autophagy by phosphorylation-dependent inactivation of ULK1 and PI3K complexes[263,291,292]. In addition, mTORC1 prevents the expression of autophagy-related and lysosomal biogenesis-related genes through the phosphorylation of the key regulator TFEB, a transcription factor[293–296]. In contrast, energy deprivation (low levels of ATP, glucose or amino acids deprivation) leads to the activation of several upstream molecules including AMPK (AMP-activated protein kinase), which inhibits mTORC1 and activates ULK1[297], and ultimately induces autophagy (Figure 1.7 and Figure 1.8). Importantly, AMPK can also activate autophagy via the ULK1 complex in an mTORC1-independent manner[298,299], in response to increased AMP levels corresponding to a loss of energy.

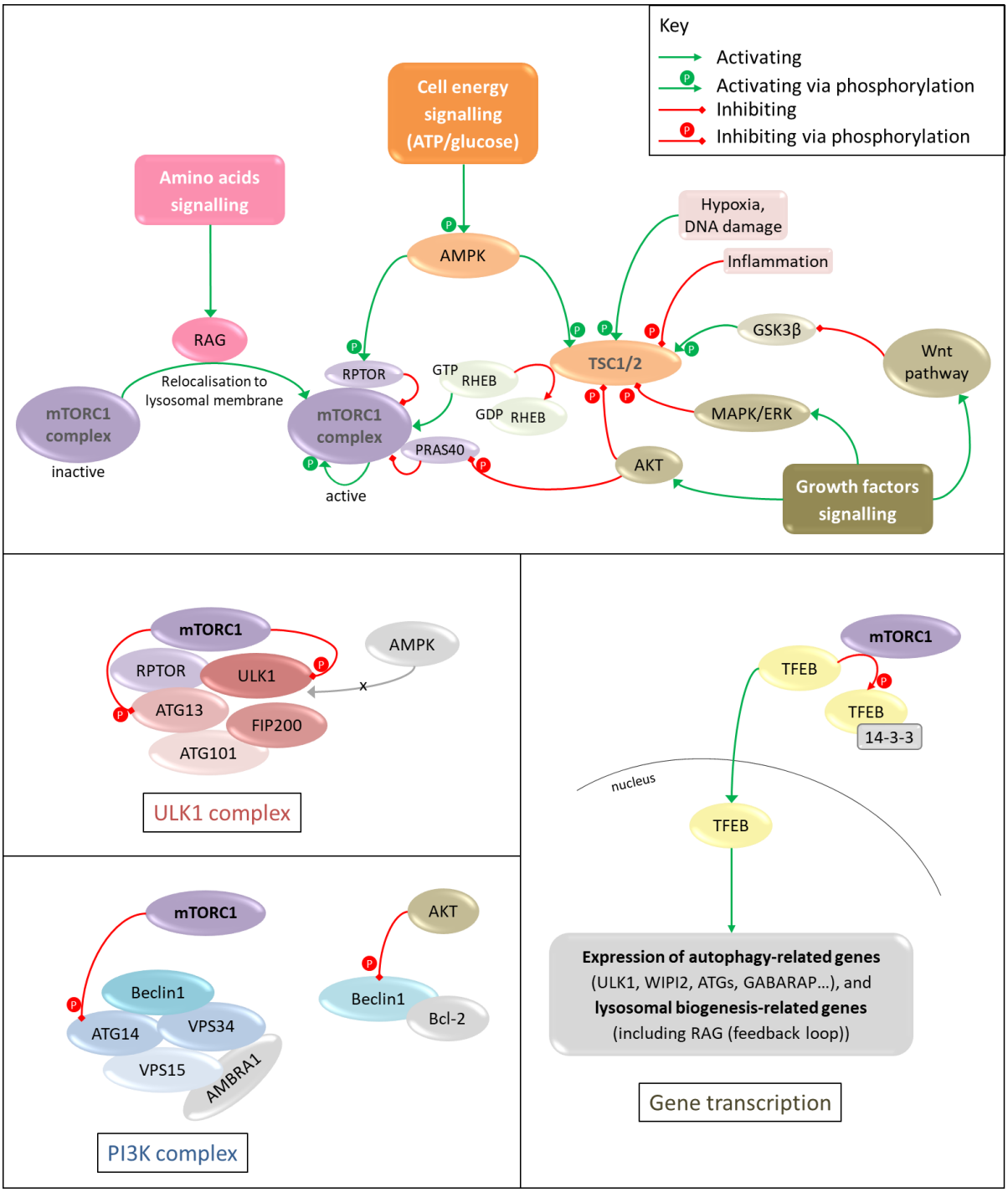

Figure 1.8: Brief overview of upstream regulation of mTORC1 and mTORC1-dependent regulation of autophagy initiation

(**Top section**) Upstream signals sensing the cellular energy state control the activation of mTORC1 through phosphorylation/dephosphorylation events. Growth factor deprivation, nutrient depletion, low energy levels, hypoxia or DNA damage lead to the activation of several effectors that ultimately inhibit mTORC1 through the activation of TSC1/2 complex and promote autophagy. In contrast, mTORC1 is activated in nutrient-rich conditions or inflammation, through inhibition of the TSC1/2 complex which cannot inactivate the GTPase RHEB, repressing autophagy. In response to amino acid signalling, RAG GTPases are activated and induce the relocalisation of mTORC1 to lysosomal membranes. Amino acid depletion inactivates RAG GTPases, and AMPK activation inactivates mTORC1 and blocks its translocation. AMPK also inactivates mTORC1 via activation of the TSC1/2 complex. (RPTOR and PRAS40: subunits of ULK1 complex) (**Bottom sections**) In nutrient-rich conditions, mTORC1 binds to the ULK1 complex via RPTOR, and phosphorylates ULK1 (Ser757/637) and ATG13 to inactivate the complex and prevent interaction with AMPK, thereby repressing autophagy. In parallel, mTORC1 phosphorylates ATG14 to prevent the activation of the class III PI3K complex, tethered to the cytoskeleton via AMBRA1. Bcl2 associates with Beclin1 to repress autophagy, and Beclin1 is also phosphorylated by AKT. mTORC1 also prevents the expression of autophagy- and lysosome-related genes by phosphorylating TFEB (Ser142) and promoting its association to 14-3-3 proteins and retention in the cytosol.

1.3.5 Autophagy in the brain

1.3.5.1 Role of basal autophagy in neurons

Autophagy is essential for maintaining homeostasis and survival in neurons. Since neurons are polarised cells, the soma, dendrites and axons are described as cellular compartments in which autophagy is spatially regulated. As such, the early steps of the autophagic pathway can occur in axonal terminals, and the clearance of the autophagic cargo in the soma[300]. Beyond the maintenance of cellular homeostasis, constitutive autophagy is also essential for neuronal synapse development, activity and plasticity[301,302], and contributes to the regulation of presynaptic function in dopaminergic neurons[303,304]. Basal autophagy also participates in axonal and dendritic plasticity and development[305]. The degradation of myelin in Schwann cells in cases of nerve injury also depends on autophagy in the peripheral nervous system[306,307].

The importance of autophagy in neuronal health has been evidenced by mouse genetic studies in models where inhibition of autophagy and deletion of ATG genes, in the absence of other known neurodegeneration-causing factors, are sufficient to result in impaired axonal structure and development, accumulation of cytoplasmic protein inclusions, motor impairments and neurodegeneration[257,282,283,308]. The data also suggest that there is a differential response to age-related autophagy failure from neuronal cell types depending on their vulnerability to toxic protein aggregation[309,310].

1.3.5.2 Autophagy and ageing

Neurons rely on quality control pathways as pro-survival mechanisms. Ageing is accompanied with a decline in these processes, and a reduced expression of ATGs genes (including Beclin1) in the brain, which are required for the proper functioning of autophagy[311]. In particular, the efficiency of both the autophagic pathway and lysosomal proteolytic activity have been shown to deteriorate with age[43,142,312–316], leading to a build-up of autophagic vesicles. This greatly contributes to the accumulation of damaged

or dysfunctional organelles, such as mitochondria and lysosomes, and other toxic macromolecules, such as aggregate-prone α-synuclein[317–320], characteristic of neurodegenerative disorders. Of note, accumulation of protein aggregates can also directly impair autophagy, resulting in further build-up[321]. These phenomena are particularly deleterious for neurons since they are post-mitotic cells required for the entire life of the organism, where mitosis is not able to help in the handling and dilution of waste material[312].

These data strongly suggest that improving the function of the autophagic pathway in the ageing brain might delay age-associated dysfunction[43], and will provide essential tools to improve health and longevity. In fact, current work is focused on restoring autophagy homeostasis to improve age-related diseases in model organisms[322,323], and pharmacological treatment for enhancing autophagy has been shown to ameliorate disease or increase longevity in various animal models, whilst inhibiting autophagy has been shown to accelerate the ageing process[98,324,325].

As such, the interplay between abnormal autophagy and ageing may speed up neurodegeneration in the context of PD[326,327]. In line with this hypothesis, impairments in the autophagic machinery have been found to contribute to the toxicity of aggregate-prone proteins in neurons and are a major feature in PD[98,322,326,327]. The role of autophagy in PD will be explored further in Section 1.6.

1.3.6 Microscopy methods to measure autophagy in cells

Since autophagy is a dynamic and multi-step process, it can be challenging to measure, especially in *in vivo* systems and humans. Importantly, there are different approaches to measure autophagy in cell models using microscopy techniques which have been extensively reviewed[328,329].

One approach is to monitor autophagy in cells that lack some key ATG proteins (i.e. loss of function) to investigate their physiological role, which has been widely used and revealed the spatiotemporal dynamics of the autophagic pathway[260,281]. However, this requires the comparison of models depleted in ATGs involved at different stages of the process, since some ATGs might have other cellular

functions[330]. Another frequent approach is to monitor autophagic flux by measuring the degradation of autophagic substrates[328,331]. Finally, specific markers can be used to directly monitor and quantify autophagic structures in a particular experimental set-up. In this section, widely used microscopy methods available to study autophagy *in vitro* are briefly discussed.

1.3.6.1 Autophagy modulators

Importantly, induction of the autophagic process can be modulated in an *in vitro* experimental setting. Typically, starvation of cells by deprivation of amino acids and growth factors from the extracellular medium is a potent physiological inducer of autophagy[328,329]. In addition, autophagic flux can be assessed by the selective modulation of specific stages of autophagy using pharmacological compounds. Essentially, inducers or inhibitors of upstream or downstream steps in the autophagic process can help understand their regulation. Therefore, innovative studies should combine the use of autophagy inducers with inhibitors.

Autophagy can be induced by direct inhibition of mTORC1 using compounds such as rapamycin or PP242, as described in more detail in Chapter 4, Section 4.2. Conversely, autophagy induction can be repressed through inhibition of the PI3K complex using 3-methyladenine[332]. A caveat associated with the use of 3-methyladenine is that long treatments can also induce autophagy[332]. In contrast, lysosomal inhibitors such as Bafilomycin A1 or Chloroquine, which respectively suppress lysosomal activity and impair the fusion of autophagosomes with lysosomes[333,334], block autophagosomal clearance and cause the accumulation of autophagosomes. In the context of neurodegeneration models, the recent autophagy activators Trehalose and Nilotinib have been shown to act via AMPK[335,336].

1.3.6.2 Transmission electron microscopy

Transmission electron microscopy was the first widely used method in autophagy research[328,329,337]. This technique is the only tool adapted to study ultrastructures within fixed cells with a subcellular resolution in the nanometre range. Consequently, electron microscopy has been used in numerous studies to identify autophagic structures and to establish their presence, luminal content, number, and morphology in their cellular environment[329,337]. In particular, the morphological details of autophagosome formation were obtained using cells lacking some of the ATG proteins[281].

Morphologically, autophagosomes typically appear as double-membraned structures with a clear separation between the membranes[328]. In contrast, autolysosomes are single-membraned structures. Therefore, the successive morphological changes occurring throughout the autophagic pathway can be observed. For instance, sequestrated organelles (such as mitochondria) generally appear electron-dense within autophagic structures, and can be observed at various stages of degradation, initially recognisable but becoming amorphous at later stages[328].

Importantly, transmission electron microscopy assays combining the use of autophagy modulators and multiple time points can provide crucial information on autophagy and autophagic flux, even on fixed cells. Commonly, the analysis of images obtained with electron microscopy is used to reveal an accumulation of a specific type of autophagic vesicle (e.g. autophagosomes or autolysosomes), or any potential changes in the appearance of autophagic structures that might occur due to the experimental conditions[328]. However, electron microscopy-based assays are generally complicated, time-consuming and not the most suitable method to quantitatively investigate the dynamic events of autophagy. One limitation of this technique is associated with the risk of misinterpreting the type of autophagic structures[338,339]. In part as an answer to some of these limitations, fluorescent-based assays have been developed using specific fluorescent autophagic markers.

1.3.6.3 Fluorescence microscopy

Fluorescence microscopy is another potent tool widely employed for studying autophagy in cells[328,340,341]. Compared to transmission electron microscopy, this approach has the essential advantage that it enables the investigation of autophagy in live cells, allowing the autophagic process to be followed in real-time. As such, fluorescence microscopy-based assays can be used to investigate the formation and processing of autophagosomes using fluorescent markers.

A commonly used marker is LC3 tagged with the green fluorescent protein (GFP)[328]. Stable cell lines in which GFP-LC3 is expressed can be valuable tools to study autophagy. Since LC3 proteins are present on autophagic vesicles throughout the autophagic pathway, GFP-LC3 can be used to visualise all autophagic vesicles. GFP-LC3 that has been recruited to autophagic vesicles appears as bright punctate structures and as such, quantification (i.e., counting) of the number of GFP-LC3 punctae in a cell corresponds to the number of autophagic vesicles, and can be used to monitor basal autophagy levels, as well as changes in autophagy levels under given experimental conditions.

Other ATG proteins such as ULK1, WIPI2 or ATG5, can also be used as autophagy markers when combined with a fluorescent protein[328]. However, in contrast to LC3, most ATGs are rapidly recycled and are removed from the phagophore membrane prior to the maturation into autophagosome. Thus, they are only present on the outer membrane of early autophagic structures. As such, the expected caveat is that only isolation membranes and phagophores on which ATGs are still attached can be observed, and therefore only proximal events can be studied. Thus, fluorescence microscopy assays designed to monitor autophagy at a specific stage should use the correct autophagy marker to be able to observe autophagosomes at later stages of the autophagic pathway.

Another method to visualise autophagy in living cells is to use LC3 tagged with both GFP and red fluorescent protein (RFP)[328]. This tandem-reporter allows early and late autophagic vesicles to be distinguished from each other by taking advantage of the different sensitivity to pH of these fluorescent proteins. Whilst RFP-GFP-LC3 emits both red and green fluorescence in autophagosomes, GFP

fluorescence is quenched in acidic compartments, so mature autophagosomes and autolysosomes appear only as red punctae. This system enables the observation of the autophagic flux and induction of autophagy concomitantly.

Of note, the use of recombinant fluorescently tagged ATGs (including LC3) in transient transfection experiments might not represent the best technique, since transfections can lead to cellular stress and upregulated autophagy, but also due to possible artifacts caused by excessive and/or variable overexpression levels. In this case, stable cell lines expressing fluorescently tagged ATGs at a consistent lower level are preferable. An alternative possibility to detect ATG proteins is the use of immunofluorescence assays, where fixed cells are incubated with antibodies targeting specifically the endogenous ATG protein of interest. This technique also enables the combined use of several autophagic markers, such as WIPI2 and LC3, although this can also be done in live cells using ATGs tagged with different coloured fluorescent proteins. Furthermore, the dynamic monitoring of autophagic substrates and their rate of degradation, such as the cytosolic protein lactate dehydrogenase, is an additional method to analyse the autophagic flux[342,343].

Fluorescence microscopy is the main method used throughout Chapter 4 in the present study.

1.4 Calcium signalling

The spatiotemporal orchestration of calcium signals and calcium storage in intracellular organelles regulate both cellular homeostasis and apoptosis[344–346]. The role of calcium in cells is briefly described below.

1.4.1 Calcium as a messenger in cells

Since its identification as a signalling messenger in 1883[347], extensive research has delineated the role of calcium as one of the most important intracellular messengers for signal transduction. Through dynamic intracellular signalling events, calcium signals are involved in the regulation of numerous cellular functions, including cell growth, neuronal excitability, neurotransmitter release, proliferation, cell death, muscle contraction, endocrine secretion, oocyte fertilisation and gene expression[348–352], if not all cellular pathways.

Calcium can be sequestered and stored in organelles. Essentially, the regulation of calcium signalling is based on the capacity of these organelles to release and subsequently re-uptake calcium following a cell stimulation[348,353,354]. Calcium is continuously transferred between cellular compartments (or stores) and the cytosol, and calcium levels and fluxes at both basal levels and in response to stimuli are tightly regulated in a spatiotemporal manner[349]. These coordinated calcium fluxes occur via calcium-permeable channels, and involve calcium-mobilising messengers or effectors, calcium-binding proteins and transporter proteins[354]. This machinery is also involved in maintaining the calcium gradient between the extracellular and intracellular spaces. Indeed, cells at rest maintain a low cytosolic calcium concentration of around 100 nM[349], which can increase to 1 µM in response to stimuli. In contrast, extracellular calcium levels can reach 1-2 mM[355], which creates a marked gradient. Changes in the concentration of cytosolic calcium can result from calcium release from intracellular stores, or calcium influx from the plasma membrane[348].

Aside from controlling the generation and folding of *de novo* synthesised proteins, the endoplasmic reticulum (ER) is also the largest and best characterised mobilizable intracellular source of calcium, establishing the cytosolic calcium signals[353,356]. In stark contrast to cytosolic calcium concentration, calcium stored in the ER ranges between 100 to 800 µM[355]. Calcium is also stored at concentrations greater than that of the cytosol in mitochondria, Golgi apparatus and endolysosomal compartments. In the lumen of all these organelles, calcium can exist as free ions or is buffered by specific calcium buffer proteins and calcium-binding proteins, which can have other functions within these compartments[348,354].

Various stimuli can evoke different calcium signals, involving different effector proteins depending on the cell response. These stimuli can be for example neurotransmitters, hormones, growth factors, membrane depolarisation, osmotic changes, but also physical stimuli such as changes in membrane curvature[352,357]. Cells can decode specific calcium signals into specific outputs and downstream pathways, and information is contained in the spatiotemporal and amplitude release of calcium oscillatory signalling. What makes calcium a potent messenger is its capacity to modulate the function, or conformation, of transducers that will carry out the downstream effects. Upon stimulation, transient and localised cytosolic calcium signals are induced through generation of intracellular second messengers and activation of calcium channels[351], leading to an increase in cytosolic calcium levels via the release of calcium from intracellular stores or entry from the extracellular space across the plasma membrane[358].

1.4.2 Channels and mechanisms

Calcium fluxes occur through channels present on the plasma membrane and on internal calcium stores. The dynamics of calcium signalling can be divided in a few steps[349].

First, cells are exposed to a stimulus, which triggers the rapid release of calcium from intracellular stores via generation of diffusible second intracellular messengers, which results in store-depletion. The most common intracellular second messengers are calcium itself, IP_3 (inositol 1,4,5-trisphosphate), cADPR (cyclic ADP ribose), and NAADP (nicotinic acid adenine dinucleotide phosphate)[351]. Calcium release from

the ER store is triggered by IP_3-receptor (IP_3-R) and ryanodine receptor (RyR) channels, which are activated upon binding of IP_3 and cADPR respectively[359,360]. Furthermore, calcium itself can regulate the activity of the IP_3-receptor; low levels of calcium can stimulate the IP_3-receptor, whilst higher concentrations are inhibitory. For example, binding of a growth factor ligand to its receptor on the membrane surface leads to the generation of IP_3. IP_3 then activates the release of calcium from the ER and increases global cytosolic calcium levels. Upon entry into the cytoplasm, calcium binds cytosolic buffer proteins, such as calbindin, but also proteins transducing the effect of calcium called calcium-effector proteins, such as calmodulin. These proteins allow the activation of downstream calcium-sensitive cellular mechanisms[361].

Secondly, this transient elevation in cytosolic calcium levels and store-depletion, in turn, induce a calcium influx from the extracellular space via store-operated calcium entry (SOCE)[362–364], which is also involved in the replenishment of intracellular stores. Voltage-operated/gated calcium channels (VGCC) present on the plasma membrane of excitable cells (such as neurons) also participate in the calcium influx.

Upon termination of the signal, various actors participate in the quick removal of excess cytosolic calcium to reinstate basal calcium levels. Sarco-endoplasmic reticulum ATPase (SERCA) pumps transport calcium into the ER to replenish the store[365] in an energy-dependent manner[366]. In contrast, calcium ATPase pumps and Na^+/Ca^{2+} exchangers present on the plasma membrane extrude the calcium towards the extracellular space[367].

1.4.2.1 ER and mitochondria

Although one of the main roles of mitochondria in cells is the production of ATP (i.e., energy), mitochondria are also important calcium stores. Importantly, calcium signalling contributes to the maintenance of mitochondrial homeostasis[368,369], and is involved in the regulation of mitochondrial dynamics, trafficking, and activity[370,371]. This organelle can uptake calcium from the cytoplasm via the

voltage-dependent anion channel (VDAC) and the mitochondrial uniporter complex, present on the outer and inner mitochondrial membrane respectively, and release calcium via Na^+/Ca^{2+} exchangers.

Mitochondria also have an important role in calcium buffering (i.e., sequestration of calcium) following the increase in cytosolic calcium levels. Indeed, mitochondria can uptake and provide calcium from/to the ER via cyclical exchange[372]. This interplay occurs in close-contact sites called mitochondria-associated ER membranes (MAMs), and is essential in mitochondrial homeostasis and calcium homeostasis[368,369,372,373]. This interplay is also involved in regulating important cell mechanisms such as lipid synthesis, autophagy, apoptosis, ROS-induced cell stress, ER-stress, mitochondrial morphology and mobility[374–379]. These processes can lead to calcium overload in mitochondria, decreased ATP production and result in mitochondrial dysfunction. Consequently, these defects induce autophagy and ultimately lead to cell death[359,372]. As a pro-survival mechanism, damaged or dysfunctional mitochondria can be degraded via a selective type of autophagy named mitophagy[380].

1.4.2.2 Lysosomes

Acidic organelles, and more specifically the endolysosomal system, have emerged as important intracellular calcium stores[381–383]. This system is involved in numerous cellular functions such as protein transport, signal transduction, autophagy and endolysosomal trafficking[275,384]. However, the calcium signalling function of the endolysosomal system is controversial[385] and not well understood, but its pathophysiological relevance is becoming increasingly clear[386,387].

Lysosomes are acidic vesicles containing several types of hydrolytic enzymes and acidic hydrolases. As degradative organelles, lysosomes are known for their role in clearance of macromolecules and organelles, with both autophagy and endocytosis culminating in lysosomes. However, lysosomes are also involved in signal transduction, energy metabolism and secretion[275]. In particular, lysosomes are important calcium stores[388,389] and calcium is essential for lysosomal homeostasis[381,386,390]. Both lysosomal degradative functions and fusion events are regulated by local calcium release, and there is evidence of a close relationship between calcium channels and lysosomal pH[391–393].

In light of the relevance of lysosomal calcium to both cellular calcium signalling and autophagy, the mechanisms of lysosomal calcium release and uptake are addressed specifically in the next sections.

1.4.2.2.1 Lysosomal calcium release

Lysosomal calcium release has important implications for intracellular calcium signalling[275]. Typically, lysosomal calcium concentrations are similar to that of the ER, around 600 µM[394], although more calcium can be released from the ER given its larger total volume in cells. Similar to the ER, a range of calcium channels are responsible for the release or uptake of calcium in lysosomes. Although IP_3-receptors and RyRs have been found on acidic organelles[395], another potent endogenous calcium-mobilising agent has been shown to be the major regulator of calcium release from these stores, namely NAADP (nicotinic acid adenine dinucleotide phosphate)[381,396]. Two families of calcium-permeable channels, TPCs (two-pore channels) and TRPMLs (transient receptor potential mucolipins channels), have been described as lysosomal calcium channels with a pH-dependent activation, but also as the intracellular source of NAADP-induced calcium signals from lysosomes and endosomes[381,386,397].

Interestingly, NAADP appears to bind TPCs indirectly, through yet unknown small proteins, to regulate TPC activity[381,398,399]. TPC isoforms have been shown to have distinct functions, and TPC2 is mostly present on lysosomes[397,400,401]. Other studies suggest that aside from calcium permeability[402], TPCs might be Na^+- or H^+-selective channels[403,404], and can also be gated by the phospholipid PI(3,5)P_2 (phosphatidylinositol 3,5-bisphosphate)[404]. Although TPCs regulation remains controversial[405], a comprehensive review concluded that these channels are regulated by both NAADP and PI(3,5)P_2[406].

Similar to TPCs, TRPMLs channels are potentially targeted by NAADP and PI(3,5) P_2[386,407,408]. However, their regulation and permeability remain poorly understood. It has been suggested that local release of calcium via TRPML1 is essential in fusion events within the endolysosomal system, but also in lysosomal exocytosis and autophagy[408–410]. Of note, TRPML1 has been reported to co-immunoprecipitate with TPCs[411]. Consistently, mutations in TPC2 or TRPML1 can result in lysosomal storage disorders[409,412].

1.4.2.2.2 Lysosomal calcium uptake

In contrast to the ER, there is a very limited knowledge about calcium uptake in lysosomes. The current hypothesis suggests that lysosomal calcium uptake is pH-dependent[386,413], occurs through calcium-ATPase pumps or exchangers, and is mediated by ER calcium and IP_3-receptors[414–416]. This hypothesis is supported by the existence of membrane contact sites between the ER and lysosomes[417,418], and by the reported close proximity of TPCs to ER regions enriched in IP_3-Rs and RyRs[416,419,420]. In addition, ER-lysosomal contact sites have been described as NAADP "trigger zones"[417,421], where a calcium-regulated functional coupling exists. In principle, NAADP induces a local calcium release from lysosomes, which is then enhanced by a secondary calcium-induced calcium release (CICR) from the ER. As mentioned above, calcium is a second messenger itself, and modulates the ER calcium channels to create a global "wave" of calcium in cells[422]. Studies also showed that it is a two-way coupling between the two organelles, where calcium released by the ER is buffered by lysosomes[422–425].

1.4.3 Chemical indicators to measure calcium

Monitoring the amplitude and spatiotemporal changes in calcium levels, whether it might be in the cytosol or in organelles, is challenging. Nonetheless, a number of techniques are available, the choice of which depends on their suitability for a cell type and their feasibility.

Although various physiological ways to trigger calcium signals have been described in the previous sections, it is worth mentioning that intracellular calcium signals can also be induced with extracellular soluble calcium-mobilising molecules. For example, cells can be stimulated with natural agonists that lead to IP_3 production, such as exogenous ATP[426,427]. If the goal is to block or induce a specific process, other molecules can also be used such as cyclopiazonic acid (CPA), which induces the depletion of the ER calcium content and inhibits the SERCA pumps, thereby preventing the refilling of the ER[427,428].

A commonly used approach to measure intracellular calcium concentrations is electrophysiology[429], a highly sensitive technique that is able to measure calcium signals and dynamics over time using

microelectrodes via patch-clamp. However, electrophysiology has several drawbacks; it requires specific skills, and is far from being time-efficient or high-throughput since only one cell at a time can be analysed.

Alternative approaches are available, such as membrane-permeant fluorescent calcium probes with a high selectivity for calcium. Tsien and colleagues were the first to develop calcium indicators based on the structure of the calcium chelator BAPTA (1,2-bis(O-aminophenoxy)ethane-N,N,N',N'-tetra- acetic acid), which couples a fluorophore and a calcium chelator, and allows the study of calcium homeostasis[430]. The principle of this method is relatively simple and relies on the fluorescence intensity changes of the calcium indicator depending on the calcium concentration, especially upon binding or release of calcium molecules. A variety of calcium indicators are available[431].

Chemical indicators are subdivided into single-wavelength indicators, which exhibit a brighter fluorescence intensity change that is calcium-dependent, and double-wavelength indicators, which exhibit a variation in the excitation or emission wavelengths following calcium binding[432]. The latter offers the opportunity to monitor calcium in a ratiometric and quantitative manner, which means that the dynamic range is improved and that it can account for uneven indicator loading in cells, leakage and progressive loss of signal. Fura-2 is one of the most common used double-wavelength calcium indicators, and will be detailed further in Chapter 2 Section 2.5.1.2.

In the case of Fura-2[432], while the emission spectrum remains unchanged, the excitation wavelength undergoes a shift from around 380 to 340 nm subsequent to calcium binding. The ratio of fluorescence that is emitted at these two excitation wavelengths 340/380 provides a quantitative measure of the concentration of calcium. However, since excitation of Fura-2 is achieved using UV wavelengths, the caveat associated with this approach is that measurements are performed while the excitation and emission wavelength are alternated, which can potentially limit time resolution. Another limitation is that both BAPTA and calcium indicator dyes have been shown to have potential significant off-target effects[433] which can have various cellular outcomes and lead to misinterpretations. Nonetheless, calcium indicators have become one of the chosen methods as a result of their wide dynamic range, fluorescence intensity and stability.

1.5 Calcium as an autophagy regulator

Amino acid depletion, a common autophagy inducer, has been found to trigger an increase in cytosolic calcium levels in various cell types[434]. As such, calcium signalling is an additional mechanism that regulates autophagy. Studies have shown that calcium is involved in autophagosome formation and maturation[435,436], but also in the fusion events at later stages and in lysosomal reformation[390]. Consistently, autophagic impairments have been shown following the use of calcium-mobilising agents[437,438]. The mechanisms underlying the effect of increased cytosolic calcium on the autophagic pathway are not yet fully understood, but involve different calcium sources and several downstream effectors[434,437,439].

It has been reported that calcium signalling has a dual regulatory role on autophagy and can both promote or supress autophagy[368,434,437,438]. These opposite effects may depend on the energetic state of the cell, the levels of intraluminal calcium, or the spatiotemporal characteristics of calcium signals[440]. As such, calcium may act as an energetic sensor and suppress autophagy under normal growth conditions, whilst promoting a pro-survival autophagy in conditions of stress. Generally, studies show that increased cytosolic calcium levels facilitate autophagy, whereas IP_3-R-mediated release of calcium commonly inhibits autophagy[441]. Figure 1.9 represents some of the known mechanisms through which calcium regulates autophagy, which are described in the next sections.

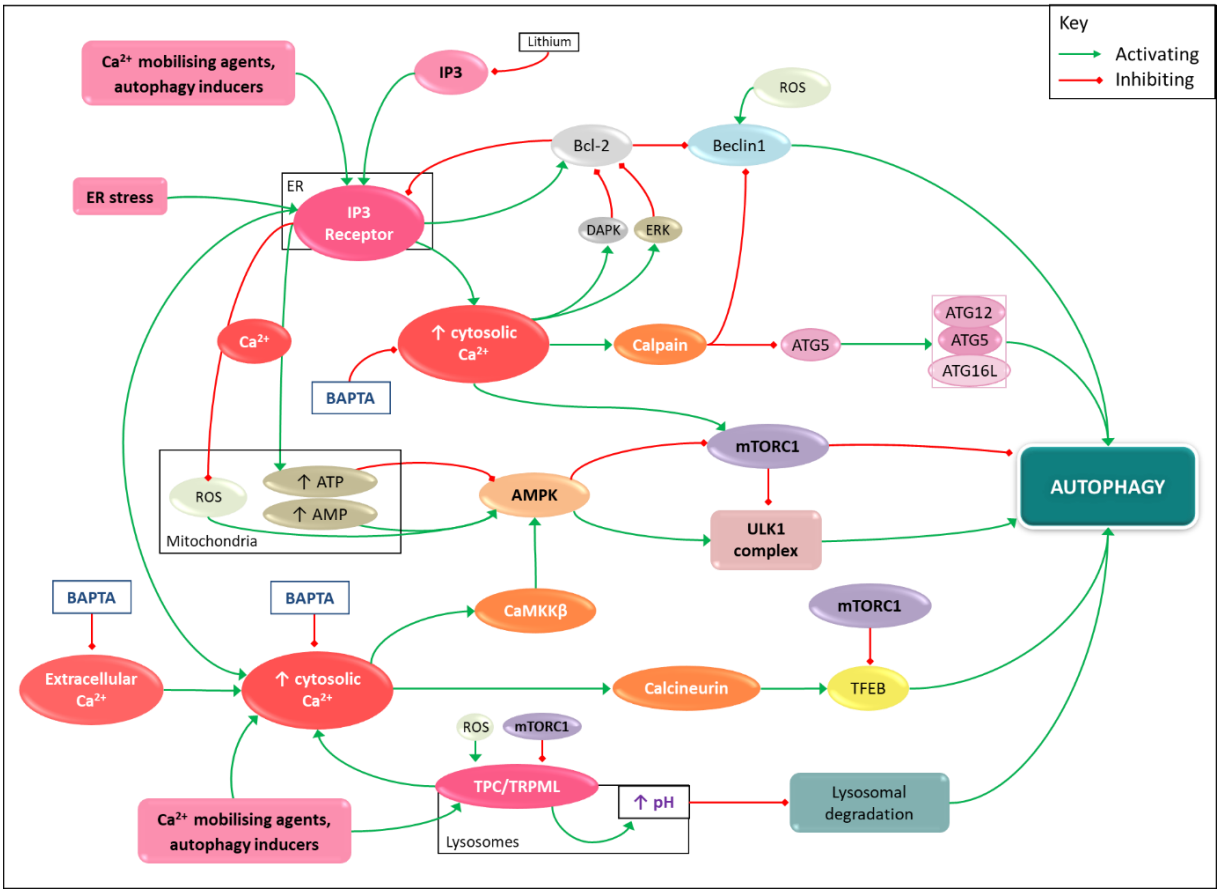

Figure 1.9: Calcium-dependent regulation of autophagy

(**Positive regulation of autophagy**) Multiple factors can lead to a rise in cytosolic calcium levels by stimulating IP3-R-mediated calcium release from the ER and lysosomal calcium release, triggering autophagy through several mechanisms. These include calcium mobilising agents that promote calcium release or prevent calcium buffering in organelles, ER stressors, or autophagy inducers. Elevated cytosolic calcium levels activate CaMKKβ which stimulates the inhibition of mTORC1 via the phosphorylation and activation of AMPK. Increased cytosolic calcium also activates DAPK, which phosphorylates the PI3K complex subunit Beclin1, and the ERK pathway, which phosphorylates Bcl-2, thereby mediating the dissociation of Beclin1 from Bcl-2 and promoting the initiation of autophagy. Calcium is required for lysosomal function and lysosomal fusion events. Calcium release from TRPML1-3 contributes to the rise in cytosolic calcium levels, either directly and locally, or globally through the calcium-induced calcium release from the ER. Elevated cytosolic calcium leads to the activation of the phosphatase calcineurin, which dephosphorylates TFEB, a transcription factor anchored to 14-3-3 proteins following phosphorylation by mTORC1, which promotes its nuclear translocation and the expression of genes associated with autophagy and lysosomal biogenesis. A potential feedback loop to control autophagy involves mTORC1 which can phosphorylate and inhibit TRPML1, and the TRPML1-calcium release-mediated activation of mTORC1. The disruption of the elevation of cytosolic calcium levels by the calcium chelator BAPTA abolishes autophagy induction. (**Negative regulation of autophagy**) Increased levels of the second messenger IP_3 and subsequent IP_3-mediated calcium release from the ER prevent autophagy. Consistently, lithium treatment triggers autophagy by reducing IP_3 levels. High cytosolic calcium levels participate in the generation of ATP in mitochondria which buffers calcium. High levels of ATP prevent the activation of AMPK and inhibit autophagy, whereas high levels of AMP promote AMPK activation and consequent mTORC1 inhibition and ULK1 complex activation, triggering autophagy. Mitochondria also produce ROS, which can activate AMPK and induce TRPML1-mediated calcium release to promote autophagy. As opposed to the role of DAPK, IP_3-R may act as a scaffold and suppress autophagy by reducing the release of Beclin1 from Bcl-2 and therefore facilitating its sequestration. In addition, Bcl2 can prevent IP_3-R mediated calcium release, thereby blocking autophagy. Another key autophagy-repressor mechanism involves calpains, activated by ER-mediated increased cytosolic calcium, which can cleave Beclin1, and also ATG5 to prevent the formation of the ATG12-ATG5-ATG16L conjugation complex. Additionally, calpains are involved in the degradation of plasma membrane calcium channels, thereby leading to excess cytosolic calcium and autophagy inhibition (not represented for simplicity). However, calpain activation has also been shown to be necessary for autophagy. TPC2-mediated calcium release can promote autophagy, since mTORC1 inhibits TPC2 in normal conditions, but TPC2 can also lead to an alkalinisation of lysosomes, impairing lysosomal function and preventing the formation of autolysosomes, thereby blocking the autophagic pathway. ER RyRs (not represented) can also inhibit autophagy by impairing lysosomal degradation.

1.5.1 Perspective on the contradictory roles of calcium

These seemingly opposite functions for cytosolic calcium on autophagy need to be considered more comprehensively, using the ER for example. On one hand, ER dysfunction and ER stress can impair luminal calcium levels, which triggers the unfolded protein response[442], a pro-survival mechanism that acts to re-establish ER homeostasis. On the other hand, both calcium depletion and excess calcium in the ER can lead to ER stress. Furthermore, calcium release due to ER stress can also stimulate autophagy as a pro-survival process[443], likely through the calmodulin-dependent protein kinase kinase-β (CaMKKβ)-dependent activation of AMPK[437] or via the activation of the calcium-regulated death associated protein kinase (DAPK)[444] (Figure 1.9).

1.5.2 Positive regulation of autophagy by intracellular calcium

1.5.2.1 CaMKKβ/AMPK pathway

The rise in cytosolic calcium levels following ER calcium release through IP_3-R can stimulate autophagy[368]. One example is via the activation of CaMKKβ[434,437]. CaMKKβ promotes the induction of autophagy via the phosphorylation and activation of AMPK, which inhibits mTORC1 (Figure 1.9). Elevation of cytosolic calcium upon treatment with calcium mobilising agents or SERCA inhibitors has been shown to activate CaMKKβ and autophagy; in contrast, reduced cytosolic calcium prevents the initiation of autophagy[426,434,445]. Moreover, resveratrol promoted autophagic clearance of aggregated proteins in neuronal cells via this pathway[426]. This calcium/CaMKK-β/AMPK pathway therefore links autophagy, mTORC1 and calcium signals. As such, this pathway might be involved in the mTORC1-dependent activation of autophagy, since it was reported to rely on IP_3-R-mediated calcium release[446,447]. As opposed to its role as an autophagy inhibitor through Beclin1 sequestration, Bcl2 has been proposed to contribute to the activation of CaMKKβ and autophagy[437].

1.5.2.2 *Effects of calcium chelators*

In line with findings indicating that autophagy is activated as a result of increased cytosolic calcium levels, studies have also shown that mechanisms that limited the increase in cytosolic calcium also limited autophagy induction (Figure 1.9). Indeed, it is established that the chelation of cytosolic calcium suppresses autophagy induction[434,435,448]. Cytosolic calcium signals are commonly chelated by loading cells with BAPTA, a high-affinity cell permeable calcium-buffering agent that has been widely used in studies of the autophagic pathway to test the involvement of calcium in a cellular process. In many reports associating a repressive effect of BAPTA on autophagy[449], BAPTA has invariably provided evidence that raised cytosolic calcium levels are essential in the induction of autophagy, although the precise effectors and calcium sources are still debated. In fact, BAPTA has been shown to suppress not only autophagy following treatment with calcium mobilising agents, but also in basal conditions and in response to common autophagy inducers such as mTORC1 inhibition, starvation or amino acid depletion[424,425,436–438]. In addition, BAPTA-mediated chelation of calcium in the lumen of acidic stores also prevented membrane fusion, further supporting an essential role for this source of calcium and its dynamics in autophagy[394,450].

1.5.2.3 *Calcineurin and TRPML1*

Calcium is involved in the regulation of various stages of the autophagic pathway, and is in particular required for lysosomal function and lysosomal fusion events[386]. Since lysosomes are vital actors in the autophagic pathway, it is not surprising that lysosomal calcium is involved in its regulation.

In contrast to TPC2, which will be detailed below, calcium release from the lysosomal channel TRPML1 and TRPML3 has recently been reported to promote autophagy, with the modulation of the expression of these channels regulating autophagy in response to various stimuli[451]. Alternatively, upon nutrient starvation, local calcium release through TRPML1, either directly or indirectly by inducing an increase in global cytosolic calcium levels[452] (CICR), leads to the activation of calcineurin (a calcium-dependent

phosphatase). In turn, calcineurin dephosphorylates TFEB and thereby promotes its nuclear translocation and the expression of genes associated with autophagy and lysosomal biogenesis[453,454] (Figure 1.8 and Figure 1.9). In addition, TRPML1 has recently been described as a redox status sensor, since ROS stimulation can induce calcineurin activation via TRPML1-mediated calcium release[455,456].

However, there is an ambiguous relationship between mTORC1 and TRPML1. On one hand, activated mTORC1 can directly inhibit TRPML1 activity by phosphorylation in normal conditions[412]. On the other hand, mTORC1 was found to be activated by TRPML1-calcium release[457], involving the association of mTORC1 with calmodulin, and TRPML1 knockdown blocked mTORC1 activity. Potentially, this mechanism might work as a feedback loop to control autophagy.

1.5.3 Negative regulation of autophagy

1.5.3.1 The IP_3-R pathway

Interestingly, several reports propose that calcium negatively regulates autophagy via IP_3, in an mTORC1-independent manner[368,458–461].The IP_3-R has been described as a key regulator of autophagy via IP_3-mediated calcium release from the ER[462]. Both the blockage with pharmacological compounds and knockdown of IP_3-R induce autophagy[460,463], suggesting that IP_3-dependent calcium release from the ER and subsequent elevation of cytosolic calcium levels prevent autophagy. Consistent with these observations, whilst IP_3 accumulation blocks autophagy in starvation conditions, decreased IP_3 levels through treatment with lithium has been shown to enhance autophagy[438].

1.5.3.1.1 Beclin1, Bcl-2

Recent studies have implicated an inhibitory role for IP_3-R on autophagy that is independent of calcium release, by acting as a scaffold for the regulation of Beclin1[464]. As such, IP_3-R facilitates the formation of the sequestration complex Bcl2-Beclin1 by preventing the release of Beclin1[440,461] (Figure 1.9). Since Beclin1 is essential in the induction of autophagy and formation of the phagophore as part of the PI3K

complex, this mechanism limits the availability of Beclin1 and ultimately blocks autophagy (Figure 1.8). Furthermore, IP_3-R can be modulated by Bcl2[460].

1.5.3.1.2 Calpains

An additional key autophagy-repressor mechanism involves calpains, cytosolic calcium-sensitive proteases that are activated upon increased cytosolic calcium levels and involved in development and apoptosis[465,466]. In regards to autophagy, the constitutive cleavage of ATG5, which forms a complex with ATG12, is mediated by the calcium-dependent activation of calpain and inhibits the initiation of autophagy[459] (Figure 1.7 and Figure 1.9). Accordingly, reduced cytosolic calcium levels prevented the calpain-mediated degradation of ATG5 and induced autophagy. Of note, apoptosis can be triggered by the translocation of cleaved ATG5 to mitochondria[467]. In addition to ATG5, calpain can also impair autophagy by mediating the cleavage of Beclin1 in conditions of increased cytosolic calcium[468]. Furthermore, the calpain-dependent degradation of calcium channels located at the plasma membrane, involved in the removal of cytosolic calcium towards the extracellular space, leads to excess cytosolic calcium and inhibits autophagy[469].

Whilst several studies indicate that calpain can inhibit autophagy, other studies have found that calpain activation is necessary for autophagy[470], at both early (autophagosome formation) and late stages (lysosomal degradation). In the context of neurodegeneration, this dual role of calpain in the regulation of autophagy could be comparable to the function of autophagy itself, which has been shown to have both protective and harmful roles during different stages of neurodegeneration[471–473].

1.5.3.2 RyRs

As opposed to IP_3-R, the role of RyRs in the calcium-dependent regulation of autophagy has not been the focus of many studies. A potential role for RyRs has been reported in a study where inhibition of RyRs prevented autophagy alterations and promoted survival in a mouse model of neuropathic Gaucher disease[474]. Additionally, in neuronal hippocampal stem cells, RyRs were involved in autophagic cell

death[475]. Recently, Vervliet and colleagues showed that RyR-mediated calcium release is involved in the repression of autophagy in cell lines and primary neurons, especially impairing autolysosomal fusion events[476]. Indeed, an mTORC1-independent increase of autophagic flux was observed following inhibition of RyRs[476]. Thus, both IP_3-R and RyRs can have inhibitory effects on autophagy, and whilst the effects of IP_3-R-mediated calcium release appear to impact the induction of autophagy, the effects of RyRs seem to be more distal and at the level of lysosomal degradation.

1.5.3.3 TPC2 channels

In contrast with TRPML1, calcium release mediated by TPC2 has been identified as a negative regulator of autophagy[392,477]. Specifically, calcium-release from TPC2 is thought to lead to the alkalinisation of lysosomes (i.e. elevation of lysosomal pH), thereby preventing the formation of autolysosomes[392] (Figure 1.9). In line with this, studies have shown that autophagosomes accumulate following overexpression of TPC2, confirmed by the further accumulation resulting from TPC2 activation by NAADP, and by the opposite effect observed using the NAADP-mediated calcium release antagonist Ned19[477,478]. However, other studies have shown impaired lysosomal pH when TPC2 was dysfunctional, resulting in impaired autophagy[393]. These data suggest a tight regulation of TPC2-dependent lysosomal pH.

Conversely, TPCs and mTORC1 have been reported to co-immunoprecipitate, with mTORC1 inhibiting TPCs in normal conditions[479]. Upon nutrient deprivation and low ATP concentration, conditions associated with activated autophagy, this inhibition is relieved and TPCs are activated.

1.5.4 Limitations of the current studies implicating calcium in autophagy

Although some mechanisms promoting or repressing autophagy are well described and accepted in the field, overall, modulation of calcium signalling in cells has yielded inconsistent results. Caution needs to be taken when interpreting data obtained while modulating cellular calcium signals, since physiological

signals are generally spatially and temporally controlled, brief, transient and oscillatory events that fit with their physiological function.

Indeed, this is problematic for two reasons. First, the compounds used can have other effects not intended by the experimenter, for example a long treatment with SERCA inhibitors (such as thapsigargin) or calcium mobilising agents (such as ionomycin or ATP) induce a sustained cytosolic calcium increase, thereby depleting intracellular calcium stores and triggering cellular stress[449]. As a result, the autophagic pathway could potentially be activated as a pro-survival mechanism, and not as a result of elevation of cytosolic calcium levels. Secondly, although BAPTA has been repeatedly shown to prevent autophagy, the involvement of calcium signals in a cellular process has often been assessed depending on the activation or repression of that process in the presence of calcium chelators, and not combined with monitoring changes in calcium signals following chelation. In addition, BAPTA has been shown to have significant off-target effects independently of calcium (detailed in [433]).

These observations imply that more work needs to be done to support the data resulting from the use of BAPTA and calcium ionophores. Regardless, the precise role of calcium in the regulation of autophagy is currently being extensively studied.

1.6 Central role of Autophagy and Calcium signalling in PD

1.6.1 Molecular mechanisms underlying cellular dysfunction in PD

Despite years of research to understand the molecular basis of neurodegeneration in PD, the underlying mechanisms leading to the selective neurodegeneration of dopaminergic neurons are still under debate. However, it is commonly accepted that PD is not only due to the progression of α-synuclein pathology, but to a combination of several cellular events acting together to impair the homeostatic balance. The general hypothesis suggests that dopaminergic neurons are particularly vulnerable to oxidative damage and cell death, due to an impairment of degradative processes. The next sections will expand upon potential explanations related to the intracellular setting of these neurons that have been proposed in the literature (Figure 1.10).

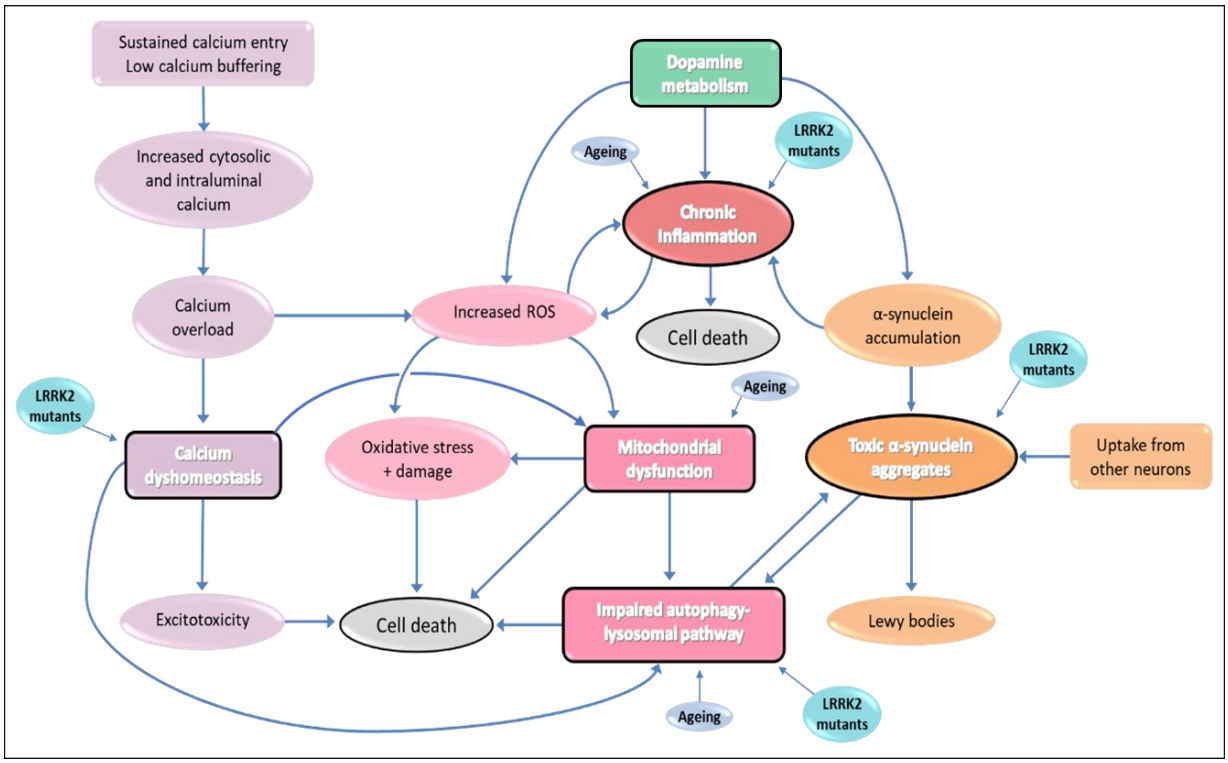

Figure 1.10: Mechanisms underlying cellular dysfunction in Parkinson's disease

The physiological activity of dopaminergic neurons causes high levels of oxidative stress. Dopamine metabolism, mitochondrial dysfunction, calcium dyshomeostasis and neuroinflammation contribute to the increase of ROS and the subsequent impairment of the autophagic pathway, resulting in the vulnerability of dopaminergic neurons to cell death. In the context of Parkinson's disease, pathogenic LRRK2 mutants promote the accumulation of α-synuclein, deregulations in calcium handling, and autophagy defects. Pathogenic LRRK2 mutants and α-synuclein accumulation also participate in microglial activation. Importantly, all these processes are also affected by ageing. The combination of an age-related decline in these cellular processes and cellular insults caused by pathogenic LRRK2 mutants, is thought to accelerate neurodegeneration and cause Parkinson's disease pathology.

1.6.1.1 *Oxidative stress*

PD is a neurodegenerative disease that has been described as an "enhanced" ageing process[480–482], and as mentioned in Section 1.1.3.1, ageing is a major risk factor for PD. One of the age-related factors that leads to the progression of cellular ageing is oxidative stress, in particular reactive oxygen species (ROS)[483,484]. ROS are a by-product of oxidative phosphorylation occurring in the mitochondria to generate ATP[483,485]. The controlled production of ROS is involved in several cellular processes[486], such as growth and apoptosis[487]. Elevated ROS levels lead to oxidative stress which is harmful for cells and can cause permanent oxidative damage to cellular components such as genomic and mitochondrial DNA, proteins and lipids, and impairs several cellular pathways[487–492].

Oxidative stress has been shown to significantly contribute to PD pathogenesis and neurodegeneration[32,33,490,492–494]. This is supported by evidence from the substantia nigra of PD patients showing high level of oxidative damage[33]. A variety of vital mechanisms believed to be involved in PD pathogenesis are thought to induce oxidative stress, including dopamine metabolism, mitochondrial dysfunction, calcium homeostasis and neuroinflammation[37,315,495], which are also processes affected by ageing (Figure 1.10). Their dysfunction in turn impacts other cellular processes[32,494,496,497], such as the autophagy-lysosomal pathways, which are crucial in the clearance of toxic α-synuclein oligomers. Their role will be detailed in the sections below.

1.6.1.2 *Neurotransmission and mitochondrial dysfunction*

Importantly, the structure and physiological function of dopaminergic neurons are both thought to cause high levels of oxidative stress, resulting in their vulnerability in PD. Structurally, dopaminergic neurons from the substantia nigra are characterised by high connectivity and a branched axonal network, implying a high number of transmitter release sites[37,495]. The maintenance of such connectivity likely relies on cellular degradative pathways to prevent the accumulation of waste material due to the high metabolic activity[498].

In addition to their burst firing activity, these neurons have an autonomous pacemaking activity, required to maintain the levels of dopamine in the striatum[499–501]. This activity is accompanied by large variations in calcium flux, promoting the generation of energy[36,502–505]. Indeed, intracellular calcium levels are tightly controlled and essential for the survival of these neurons. However, since cytosolic calcium buffering is low[506,507], this type of electrical activity leads to elevated cytosolic calcium levels and mitochondrial calcium overload (Figure 1.10). Because dopaminergic neurons rely on mitochondrial activity due to their high metabolic demands, ROS generation is elevated. Over time, these neurons become vulnerable to excitotoxicity, and calcium dyshomeostasis results in mitochondrial dysfunction[36,37,508–512], which further increases oxidative stress[316]. Eventually, if damaged mitochondria are not removed via mitophagy, they become permeable and release their content, leading to apoptosis[513,514]. Compromised autophagy and mitophagy with age[315] contribute to these phenomena[484,485,515,516].

In addition, given that calcium signalling has an established role in most cellular mechanisms, calcium is potentially involved in PD in other ways. For example, impaired calcium signalling can participate in the deregulation of autophagy (Figure 1.10). Furthermore, loss of calcium homeostasis can be predicted to affect other intracellular stores such as the ER and lysosomes, in particular through the interactions at MAM and between ER/lysosomes sites[422,517]. Although the mechanisms need to be elucidated to be proven with confidence, these interactions likely support a ripple effect, with dysfunction affecting one organelle which in turn induces defects in another, thereby contributing to neuronal dysfunction and neurodegeneration.

Since mitochondria-generated ROS are also involved in the up-regulation of autophagy[516,518–521], it is not surprising that mitochondrial dysfunction and oxidative stress, in turn, disrupt autophagy-lysosomal pathways and α-synuclein turnover[494,496,522]. Interestingly, enhanced autophagy has been shown to be neuroprotective by reducing the production of ROS in dopaminergic neurons[523]. Similarly, it has been shown that reducing the size of arborisation also reduced oxidative stress in these neurons[37].

Of note, α-synuclein is believed to play a role in synaptic transmission and is present at synaptic vesicle release sites[26]. Another direct consequence of their extensive branching and high number of release sites, dopaminergic neurons require a higher expression of α-synuclein, which potentially contributes to increased α-synuclein aggregates over time. Furthermore, α-synuclein also participates in the elevation of cytosolic calcium through calcium influx[524,525]. This further supports the cross-talk between different actors which all contribute to the degeneration of dopaminergic neurons.

Taken together, a large body of evidence from animal and cellular models and post-mortem analyses on PD patients[1,54,57,61,498,500,517–526] supports an important role for calcium dyshomeostasis, mitochondrial dysfunction and impaired autophagy in dopaminergic neurons in the pathology of PD.

1.6.1.3 Autophagy and α-synuclein spread

Whilst autophagy is initially a neuroprotective process, defective autophagy has been associated with accelerated neurodegeneration and PD[323,536,537]. For instance, evidence suggests that autophagy is repressed in PD brains, with an elevation of mTORC1 signalling and a reduced expression of essential ATG proteins and transcription factors (such as TFEB)[538,539].

Importantly, there is a causative link between impaired autophagic machinery and accumulation of toxic α-synuclein aggregates. Indeed, α-synuclein is a substrate of autophagy, in particular chaperone-mediated autophagy[540–542], but is also targeted for degradation by aggrephagy[258,543,544]. Therefore, a common view suggests that a defective autophagic machinery in PD results in the neurotoxic accumulation of α-synuclein aggregates, which further disrupts the autophagy-lysosomal pathway[321,539,540,545]. Thus, α-synuclein aggregates may contribute to their own accumulation as well as to the accumulation of other proteins, eventually leading to neurodegeneration (Figure 1.10). However, this view is challenged by the hypothesis that the build-up of toxic misfolded proteins leads to the impairment of the autophagic machinery in the first place[321,545,546].

Another reason why research has focused on the autophagic pathway in PD is that it is thought to be the means by which α-synuclein oligomers spread between neurons[547–550]. The general hypothesis is that a "cell-to-cell spread" occurs from the vesicular release of toxic α-synuclein aggregates into the extracellular compartment, from where these aggregates are uptaken by other neuronal cells[551]. Then, the pathology progresses in a prion-like manner, where α-synuclein aggregates induce further protein misfolding and cytotoxicity. Therefore, autophagic and lysosomal impairments within a neuron may not only lead to PD pathology in that cell, but also participate in its progression to other neurons. However, the exact mechanisms are still unknown and debated. Interestingly, this process has also been described as a compensatory mechanism aiming at removing toxic material that cannot be degraded[552].

Importantly, calcium signalling has already been implicated in the autophagic degradation of aggregate-prone proteins in neuronal cells, suggesting that abnormal calcium signalling may inhibit autophagy. In particular, it has been reported that mTOR-independent clearance of aggregated proteins via autophagy is activated following calpain inhibition[458].

1.6.1.4 Dopamine metabolism

Consistent with the detrimental changes associated with sustained electrical activity and calcium dyshomeostasis, dopamine metabolism itself can be toxic and contributes to the selective sensitivity of dopaminergic neurons to oxidative stress[522,553,554]. In fact, although dopamine is stored in vesicles, accumulated and unstable cytosolic dopamine becomes oxidised and converted to quinones, which are reactive species. This is accompanied by the generation of toxic ROS (Figure 1.10). Therefore, dopamine catabolism eventually results in high levels of ROS and mitochondrial dysfunction, which promotes cellular stress[555]. As such, both their transmission activity and dopamine metabolism, i.e., their own phenotype, makes dopaminergic neurons more vulnerable to cell death.

An interesting interplay in dopaminergic neurons might occur between dopamine and α-synuclein. Indeed, quinones are involved in the conversion of monomeric α-synuclein into its toxic oligomeric form[556]. This can block the degradation of α-synuclein[497] and contribute to its accumulation. In addition,

cytosolic α-synuclein has been shown to induce the release of dopamine stored in secretory vesicles in the cytosol[557], which further promotes the formation of dopamine-quinones, and α-synuclein accumulation.

1.6.1.5 Neuroinflammation

Importantly, mitochondrial dysfunction is closely related to neuroinflammation[558–560]. The involvement of microglial cells and neuroinflammatory pathways in PD is now widely recognised[561], with neuropathological and biochemical evidence from PD patients providing strong evidence of uncontrolled activation of microglia. In support of this is the finding that microglial cells are present at a high density in the substantia nigra[562], but also by the discovery that LRRK2 and α-synuclein are involved in pro-inflammatory responses[563].

Oxidative stress consequent to dopamine oxidation leads to the formation of neuromelanin[564], which accumulates with age. The loss of this pigment in PD is thought to be the result of neuroinflammation[564], which might both contribute to and be a result of neurodegeneration. Although the role of neuromelanin is not well understood, studies propose that, at first, neuromelanin has a protective effect, and activates microglial cells. However, neuronal death and further release of neuromelanin both lead to chronic inflammation[564–566]. As such, neuromelanin participates in a vicious cycle creating a deleterious neuroinflammation contributing to further neurodegeneration and PD pathogenesis over time[512,567,568].

As well as neuromelanin, neuronal death is accompanied by the release of α-synuclein oligomer aggregates, which activate microglia[569,570]. This means that, in addition to the autophagic pathway, α-synuclein-mediated toxicity and PD progression is amplified through microglial activation and neuroinflammation[571] (Figure 1.10). α-synuclein-dependent activation of microglia might also occur following internalisation of α-synuclein monomers, originating from the cleavage of α-synuclein mediated by calpain, which is activated by increased cytosolic calcium[572,573].

1.6.1.6 LRRK2-associated pathology

The perturbation of the processes outlined above promote the perpetuation of a vicious cycle leading to neurodegeneration. These neurons are thus inherently vulnerable to cell death. It is therefore clear that any genetic or external factor that might provide the toxic input necessary to aggravate the defects in any of the processes mentioned above is likely to lead to dopaminergic neuron dysfunction, α-synuclein pathology and PD[574]. Pathogenic *LRRK2* mutations are such PD-trigger factors, and since LRRK2 interacts with several downstream partners and is involved in a plethora of cellular processes, these cellular processes might all be generally deregulated by *LRRK2* mutations (Figure 1.10). Furthermore, LRRK2 might have a different role depending on the cell type or cellular environment[180], suggesting that the toxicity associated with *LRRK2* PD-causing mutations might be more important in vulnerable dopaminergic neurons. As such, neurons carrying *LRRK2* mutations are predisposed to be more sensitive to cellular and external stress factors.

Strong evidence of a close relationship between LRRK2 and α-synuclein is emerging, suggesting that LRRK2 might act upstream of α-synuclein[575–578]. Indeed, LRRK2 and α-synuclein have been reported to endogenously interact in brain tissue from PD patients and in cell models, and to co-localise in some, but not all, Lewy bodies[575–577,579]. Loss of LRRK2 also induced defects in degradation pathways and accumulation of α-synuclein in aged mice[217]. Recent studies in mouse and human models of LRRK2 G2019S described increased neurodegeneration and α-synuclein aggregation, linked to an augmented neuroinflammation state[580–582].

Interestingly, it has been shown that ROS can activate LRRK2 and increase the phosphorylation of its substrate Rab10 in absence of pathogenic mutations[172], suggesting that oxidative stress might upregulate LRRK2 kinase activity. Thus, in the context of cellular oxidative stress in dopaminergic neurons, pathogenic LRRK2 mutants may further enhance LRRK2 kinase activity, promoting their toxic effects.

With regard to neuroinflammation, loss of LRRK2 in microglial cells caused an increased internalisation of monomeric α-synuclein through Rab5-positive endosomes[583]. In addition, one of the aggrephagy-receptors targeting α-synuclein is p62[544,584], and since LRRK2 kinase-dependent p62 phosphorylation is reported to increase neurotoxicity[585,586], pathogenic LRRK2 mutants may enhance this effect. These data support a role for PD-causing *LRRK2* mutations in the spreading of α-synuclein pathology. Furthermore, α-synuclein is also thought to be required for the toxic effects of LRRK2 mutants[578], acting either by promoting the accumulation and misfolding of LRRK2, or synergistically with LRRK2 by inducing defects in proteostasis and other cellular mechanisms, leading to cellular dysfunction. As such, the interaction between these two proteins has yet to be fully characterised, although a plausible mechanism is via vesicular trafficking, since both LRRK2 and α-synuclein are linked to this process.

Returning to the subject of intracellular calcium, there is evidence for a broad regulatory role for LRRK2 in calcium signalling. Impaired mitochondrial and ER calcium signalling has been observed in neuronal models expressing pathogenic LRRK2 mutants[587–590], with various downstream effects such as neurite degeneration. In addition to its role in cytosolic calcium buffering[590], LRRK2 has been shown to modulate plasma membrane calcium channels. Indeed, LRRK2 can stimulate the activity of the Na^+/Ca^{2+} exchanger[591], and overexpression of LRRK2 WT and mutants has been shown to increase the activity of VGCC in a kinase-dependent manner[228,590]. These data suggest that pathogenic LRRK2 mutants may affect cellular calcium homeostasis, and since calcium signalling is involved in most cellular processes, LRRK2 may at least in part operate through impaired calcium signalling to induce cellular defects. For example, LRRK2 is involved in lysosomal calcium homeostasis[391], which, if deregulated, would be expected to impair lysosomal degradation and autophagy (Figure 1.10).

In summary, this body of evidence points towards a particular effect of PD-causing *LRRK2* mutations on autophagy and calcium signalling.

1.6.2 LRRK2-mediated regulation of autophagy

The effects of LRRK2 mutants reported on the autophagy-lysosomal pathway strongly support the involvement of LRRK2 in the regulation of this pathway[122,142,154,218,592]. Nonetheless, the role for LRRK2 remains elusive. *In vitro* studies carried out in numerous cell lines describe opposite impacts of LRRK2 activity. For example, the knockdown of LRRK2 has been reported to either have no effect[120,593], to increase[122], or inhibit autophagy[233]. Overexpression of wildtype LRRK2 results in increased autophagy in some cases[120,154,479,594], but reduced autophagy[391] or no effects[141] in others. Similarly, previous work described that *LRRK2* pathogenic mutants G2019S and R1441G lead to increased[120,479,594–597] or decreased autophagy[122,391,593,598,599]. *In vivo* studies have also been inconsistent, describing differential variations in the autophagy-lysosomal pathway depending on the model used[142], such as transgenic mice that are knocked-out for *Lrrk2*, express LRRK2 mutants, or knocked-down for Lrrk2.

These contradictory results can in principle be explained by numerous variables in protocols used, such as the model, the method to monitor autophagy, or the expression levels of LRRK2.

Nonetheless, when taken together, evidence of the participation of LRRK2 and pathogenic *LRRK2* mutations in the autophagic and/or lysosomal impairments found in PD are accumulating, but further work is necessary to define the seemingly complex role of LRRK2 in these processes. Several cellular processes have been proposed, which are summarised below and in Figure 1.11.

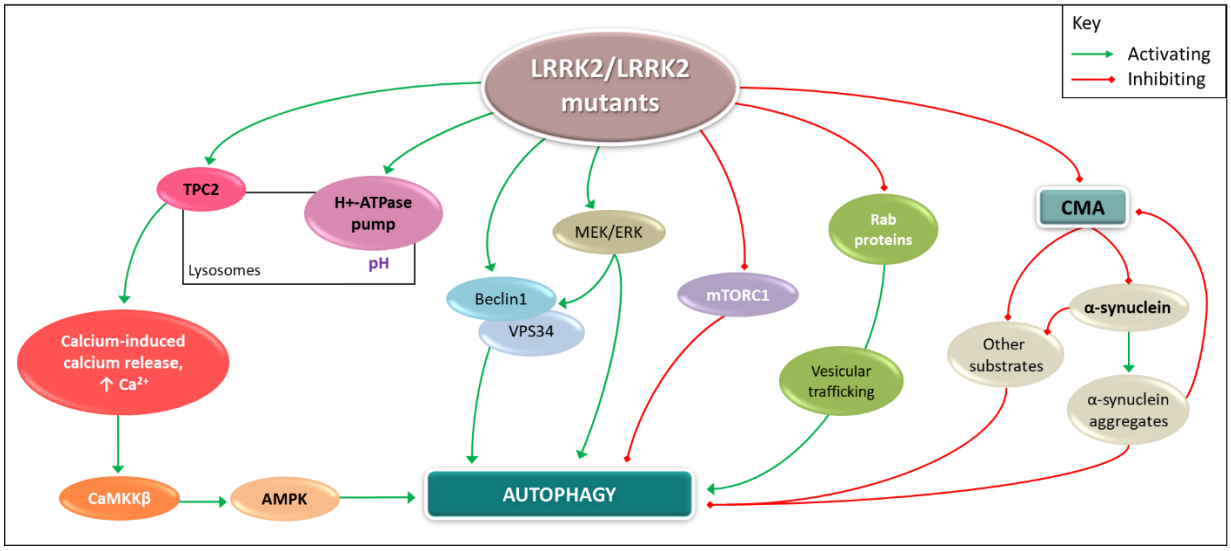

Figure 1.11: Potential pathways through which LRRK2 contributes to the regulation of autophagy in the context of PD.

LRRK2 potentially operates through different pathways to regulate autophagy depending on the cell type. Evidence suggests that LRRK2 may promote autophagy in a LRRK2 kinase-dependent but mTORC1-independent manner, by inducing TPC2-dependent lysosomal calcium release, amplified by the calcium-induced calcium release from the ER, and activation of the CaMMKβ/AMPK pathway. This pathway is deregulated in the presence of *LRRK2* pathogenic mutants, which can induce defects in lysosomal morphology and calcium handling. Alternatively, LRRK2-mediated elevation of autophagy may be mTOR-dependent. LRRK2 is also involved in the regulation of lysosomal pH via interaction with the v-H^+-ATPase pump, which can be impaired by *LRRK2* pathogenic mutants. In addition, LRRK2 might regulate autophagy either via the MEK/ERK pathway directly, or via the VPS34/Beclin1 complex (PI3K complex). Furthermore, LRRK2 may be involved in the regulation of autophagy through vesicular trafficking via Rab proteins, and LRRK2 mutants impair their normal function. LRRK2 and α-synuclein are both chaperone-mediated autophagy substrates, and both pathogenic LRRK2 mutants and toxic forms of α-synuclein are poorly degraded via this mechanism, and in turn inhibit it, thereby promoting the accumulation of α-synuclein and other chaperone-mediated autophagy substrates, which in turn impair autophagy.

1.6.2.1 LRRK2 calcium-dependent regulation of autophagy

1.6.2.1.1 CaMMKβ/AMPK pathway

As described in Section 1.5 and Figure 1.9, it is widely accepted that cytosolic calcium levels are involved in the regulation of autophagy[449]. Since this process is deregulated in LRRK2-PD, it is not unexpected that calcium signalling might mediate some aspects of LRRK2 cytotoxicity. Evidence of functional cross-talk between LRRK2, autophagy and calcium homeostasis has recently been revealed[216,479,600,601]. Indeed, LRRK2 may act through the CaMKKβ/AMPK pathway to increase autophagy in a manner independent of mTOR, but dependent on LRRK2 kinase activity. These data support a model where LRRK2 interacts with TPC2 and triggers the TPC2-dependent calcium release from lysosomes, which is then amplified by the calcium-induced calcium release from the ER (Figure 1.11). This elevation of cytosolic calcium then

promotes the CaMKKβ/AMPK-dependent activation of autophagy. This model is supported by evidence indicating that NAADP reproduces the effects of LRRK2 overexpression or G2019S pathogenic mutation, with inhibition of TPC2 preventing these effects. In addition, the use of a calcium chelating agent or the depletion of ER calcium stores also blocked these effects, supporting the involvement of calcium signals in the regulation of autophagy by LRRK2[216,479,600,601]. Importantly, these authors reported consistent results in various cell lines tested, including dopaminergic neurons.

1.6.2.1.2 Lysosomal pH

Consistent with the role of calcium in lysosomal function mentioned in the previous sections, decreased lysosomal calcium concentration results in increased luminal pH, which impairs lysosomal function and causes autophagy defects, leading to α-synuclein accumulation in PD[142]. A recent investigation into lysosomal activity in neurons showed that LRRK2 is involved in the regulation of lysosomal acidity, through interaction with the v-H^+-ATPase membrane proton pump. This pump maintains a low lysosomal pH essential for the activity of hydrolytic enzymes within the lysosomal lumen[391]. Overexpression of the pathogenic LRRK2 mutant R1441C blocked this interaction and increased lysosomal pH in primary neurons, whilst wild-type LRRK2 and G2019S did not alter this interaction but impaired autophagy as well. Interestingly, the deleterious effect of R1441C was LRRK2 kinase-independent. These findings corroborate the importance of lysosomal homeostasis in PD and the significance of LRRK2 in lysosomal biology.

Of note, other studies support the LRRK2-mediated regulation of lysosomal calcium homeostasis through TPC2. Both cytosolic calcium chelation and TPC2 inhibition restored the marked lysosomal morphology and calcium deregulations observed in fibroblasts from LRRK2 G2019S patients[216]. Furthermore, LRRK2 and TPC2 are reported to co-immunoprecipitate, suggesting that TPCs are LRRK2 targets[479]. It is possible that the interaction between LRRK2 and TPC2 is direct, or indirect, perhaps through one or more Rab family small GTPases.

Thus, pathogenic *LRRK2* mutations appear to be involved in both morphological and functional lysosomal defects, which might explain their widespread effects on the autophagy-lysosomal pathway.

1.6.2.2 Calcium-independent regulation of autophagy by LRRK2

1.6.2.2.1 Modulation of core autophagic machinery

As depicted in Figure 1.8 and Figure 1.9, the MEK/ERK pathway participates in the regulation of autophagy via Beclin1 (Figure 1.11). In particular, studies showed that inhibition of MAPK signalling was sufficient to reverse the effects of the LRRK2 G2019S pathogenic mutant, such as neurite shortening[141] and increased autophagy[595], whilst inhibition of the mTOR-dependent activation of autophagy via PI3K did not prevent these effects[141,595]. In line with these findings, others reported that LRRK2-mediated effects on autophagy were mTOR and ULK1 independent in neuroglioma cells, but Beclin1 and VPS35-dependent[593].

However, other studies present conflicting results. For example, a recent study reported that LRRK2 can phosphorylate ULK1, which suggests that LRRK2 can also regulate autophagy via ULK1[602]. In addition, Schapansky and colleagues showed that the LRRK2-mediated elevation of autophagy was mTOR-dependent in RAW264.7 macrophages and murine microglial cells[233]. A caveat in this comparison is that LRRK2 is highly expressed in immune cells[165,166,238,239], where it might play a distinct role. These observations suggest that LRRK2 potentially operates through a different pathway to regulate autophagy depending on the cell type, which might be relevant to the physiological function of LRRK2 or involved in LRRK2 pathogenicity.

1.6.2.2.2 Vesicular trafficking and Rab GTPases

Studies in animals and *in vitro* models place LRRK2 at the interconnection of autophagy and the endo-lysosomal pathway, supporting a role for LRRK2 in vesicular trafficking, in both non-neuronal and neuronal cells[122,142,154,218,592,603]. For example, LRRK2 can localise at vesicular structures and lysosomes[122,604], and the LRRK2 G2019S pathogenic mutant has been associated with defects in

endocytosis in dopaminergic neurons derived from iPS cells[605]. Several reports have also described impeded endocytosis at synapses when LRRK2 was either genetically depleted or overexpressed, but also in the presence of the LRRK2 R1441C mutant, which is associated with α-synuclein accumulation[227,606–609]. In support of this is evidence that Endophilin A, which regulates membrane curvature and vesicle release, can be phosphorylated by LRRK2[610].

Although the role of LRRK2 in vesicular dynamics is not fully elucidated, the recent connection to Rab GTPases provides insights into a functional mechanism[136]. As mentioned in Section 1.2.2.1, a number of Rab GTPases are LRRK2 kinase substrates. Around 70 Rab GTPases are found in human cells, and these proteins localise to distinct membranous compartments, including the Golgi apparatus and endosomes. Rab GTPases act as regulators of perhaps all forms of intracellular membrane trafficking events, including the directionality and specificity of vesicular trafficking pathways. Thus, Rab GTPases control diverse cellular functions, including the organisation and transport of vesicles in the autophagic pathway. To carry out their functions, membrane-associated Rab GTPases recruit effector proteins to create functional membrane domains, linking them to the cytoskeleton and permitting transport, but also allowing membrane fusion with acceptor membranes. In addition, Rab proteins regulate each other in cascades, as is the case in the Rab29-LRRK2-Rab proteins axis. Therefore, any alteration in the function of Rab proteins will directly impact vesicular trafficking and impair the mechanisms regulated by these proteins, especially autophagy[152,156,158,160,218,611,612].

The link between Rab proteins and LRRK2 may therefore provide at least part of an answer for the autophagy and lysosomal defects associated with LRRK2 mutants[136,158]. Current data indicate that LRRK2 can directly phosphorylate certain Rab GTPases, with pathogenic LRRK2 mutants causing elevated Rab phosphorylation, which interferes with their proper functioning[136], blocking their ability to regulate trafficking events, and resulting in their accumulation at membranes. This in turn impairs the autophagic pathway[158–160], and dysfunctional Rab proteins are sufficient to cause neurodegeneration of dopaminergic neurons[613]. Therefore, the detrimental effects of LRRK2 and PD-causing LRRK2 mutants on

autophagy might be mediated by the interference with vesicle transport machinery through aberrant Rab protein phosphorylation (Figure 1.11).

Supporting this connection further, to expand on the role of LRRK2 and Rab29 mentioned in Section 1.2.2, pathogenic LRRK2 mutants appear to be associated with retromer complex dysfunction, which might in turn impair lysosomal function. Fascinatingly, the retromer is a multiprotein complex which contains VPS35; mutations in the *VPS35* gene are also known to cause PD[152,614]. As such, LRRK2 is thought to regulate VPS35 function in the recycling of components from the endosomal system to the trans-Golgi network[112].

1.6.2.2.3 Chaperone-mediated autophagy

Chaperone-mediated autophagy participates in the first line of defence against protein aggregation by promoting the degradation of damaged or misfolded soluble proteins. In the case where a "non-conventional" substrate (e.g., a pathogenic form of a substrate) abnormally interacts with chaperone-mediated autophagy components, this substrate fails to enter into lysosomes, and instead accumulates at the lysosomal surface where it can form into oligomeric structures. These oligomers impair proteostasis and the chaperone-mediated autophagy pathway dynamics, as well as the degradation of other substrates, thereby disrupting this mechanism further. Consequently, this toxic effect can impact upon autophagy, for example by affecting lysosomal biogenesis. As such, defective chaperone-mediated autophagy has been associated with PD. Indeed, similar to α-synuclein[615], LRRK2 is a substrate of chaperone-mediated autophagy[120], but the mutant forms appear to be poorly degraded by this system. Both toxic forms of α-synuclein and mutant forms of LRRK2 appear to inhibit chaperone-mediated autophagy (Figure 1.11), enhancing the toxicity and accumulation of α-synuclein and other substrates[120,497,540,575]. When taken with data on the role of LRRK2 and α-synuclein in the deregulation of autophagy, these observations support a model where PD-causing *LRRK2* mutations promote the deleterious effects of toxic α-synuclein and vice-versa.

1.6.2.3 Effects of LRRK2 inhibition on the autophagic pathway in cells

Studies investigating the effect of the LRRK2 kinase inhibitors on autophagy, in particular *in vitro*, are limited and the outcomes are inconsistent and often contradictory[142,164]. These studies used various inhibitors, including GSK2578215A and PF-06447475 which were used in the present study and will be detailed in Chapter 4. Some of the findings have already been described throughout this Chapter, but they will be further detailed here.

One of the first autophagy studies to use LRRK2 inhibitors was performed in H4 neuroglioma cells, and showed that the LRRK2 inhibitors GSK2578215A, LRRK2-IN-1 and CZC-25146, targeting endogenous LRRK2, led to increased autophagy in an mTOR-independent but Beclin1- or ULK1-dependant manner[593,598,616], with similar effects observed in SHSY5Y neuroblastoma cells and HEK293 cells. In another study[617], GSK2578215A treatment led to increased levels of LC3-II and lower levels of p62 in bone marrow derived macrophages, which is consistent with the induction of autophagy described by Manzoni et al[598]. These findings support a role for LRRK2 kinase activity in the regulation of autophagy induction in these cell lines, and suggest that blocking LRRK2 kinase activity would have a neuroprotective effect by promoting autophagy and reducing cell death. Consistently, LRRK2-IN-1 and CZC-25146 reduced the accumulation of α-synuclein and reversed the lysosomal impairments in primary cortical neurons from LRRK2 G2019S knock-in mice[175], and GSK2578215A and LRRK2-IN-1 reversed the PINK1/Parkin-dependent mitophagy defects caused by the G2019S mutation[176].

Conversely, LRRK2-IN-1 and GSK2578215A led to impaired autophagy in microglial and monocyte cells[233], suggesting a different role for LRRK2 kinase activity in autophagy in these cell lines. In addition, GSK2578215A has been shown to induce cytotoxicity and alter the autophagic flux by preventing the degradation steps, but also leads to a protective autophagy response as mitophagy was stimulated in SHSY5Y cells[618]. Overall, although the data suggest a consistent autophagy-stimulating effect of LRRK2 kinase inhibition in most cell lines, this is not always the case.

Another LRRK2 inhibitor, PF-06447475, induced neuroprotective effects in an *in vitro* model of PD (human nerve-like differentiated cells treated with rotenone), since this compound prevented the apoptotic signals caused by oxidative stress and phosphorylation of LRRK2 at S935 induced by rotenone treatment[619]. Furthermore, the LRRK2 G2019S mutation caused neurotoxicity by increasing the accumulation of α-synuclein inclusions in rat dopaminergic neurons[581], but the use of MLi-2 and PF-06447475 inhibitors rescued this phenotype[164]. Treatment with PF-06447475 *in vivo* alleviated the increased inflammation and dopaminergic neurodegeneration due to the overexpression of α-synuclein in LRRK2 G2019S transgenic rats, and was neuroprotective in WT transgenic rats[164].

Regarding the *LRRK2* RocCOR mutations, LRRK2 kinase inhibitors have been described to reverse the effect of RocCOR mutations on LRRK2 substrate phosphorylation[112]. However, these compounds are reported to *reproduce* other effects of pathogenic mutations, such as enhanced microtubule association[620], disrupted Wnt signalling[116,128] and LRRK2 GTP binding[620,621], which is clearly a concern.

In summary, the use of LRRK2 kinase inhibitors can help gain insight into LRRK2 function, but with regards to the role of LRRK2 in autophagy, these compounds have yielded opposite findings. Although these contradictory results might in principle be explained by variations in protocols and models used, or by differences in the expression levels of LRRK2, the type of inhibitor used might also provide at least part of an explanation. Indeed, whilst some of these findings were obtained using second generation (such as GSK2578215A, GNE-9605 and PF-06447475) and third generation (MLi-2) LRRK2 kinase inhibitors[139], other studies used first generation LRRK2 inhibitors (LRRK2-IN-1 and CZC-25146), for which important off-target effects have been described[139,143,622].

Of note, there is little published research on the LRRK2 GTPases inhibitors mentioned in Section 1.2.3.2. The papers that described the discovery and efficiency of compound 68 and FX2149[177,178] also report that treatment with these GTPase inhibitors was protective against pathogenic LRRK2 mutants-induced neurodegeneration. Recently, the same group[623] showed that 24 hours treatment with either 68 or FX2149 promoted LRRK2 ubiquitination, aggregation, and contributed to an aggresome response (formation of Lewy bodies-like inclusions), which is thought to represent a cellular mechanism of self-

protection to sequestrate toxic proteins. Although the authors only mentioned it briefly, we can speculate that these findings might potentially result from prolonged autophagy inhibition, which could have led to the aggresome response.

1.7 Working hypothesis and Aims

1.7.1 Rationale and hypothesis

Understanding the pathogenesis of PD is key for the selection of therapeutic candidates that act during the early stages of the disease to prevent or, at least, slow down the progression of the disease. Since LRRK2 has been implicated in both familial and idiopathic PD, the mechanisms underlying the pathology mediated by pathogenic LRRK2 mutants has been the focus of extensive research. The findings discussed in this Chapter reinforce the hypothesis of LRRK2 being a central element to understanding PD aetiology, but also highlight the conflict in the literature, which points to a need to study *LRRK2* mutations in a new, relevant model.

As discussed, how pathological *LRRK2* mutations eventually lead to neurodegeneration remains controversial. However, common processes seem to stand out, in particular the autophagic pathway and lysosomal biology. Pathogenic *LRRK2* mutations impairing autophagy might not only account for the accumulation of α-synuclein, but also the accumulation of dysfunctional mitochondria and elevated ROS seen in PD, thereby participating in Lewy bodies formation and neurodegeneration.

Alternatively, it is plausible that pathogenic *LRRK2* mutations alter cellular calcium homeostasis during the early stages in the development of PD-associated pathology, impacting downstream mechanisms such as the calcium-mediated autophagy-lysosomal processes. Given the close relationship between LRRK2, autophagy and calcium signalling detailed throughout this Chapter, understanding the role of LRRK2 in the regulation of calcium signalling and in autophagy can be expected to provide insight into the early impairments involved in PD pathogenesis. Targeting the autophagy-lysosomal pathway is therefore an interesting approach to prevent neurodegeneration in LRRK2-PD.

1.7.2 Objective and aims

The primary objective of this project is to develop new cellular models to investigate the role of LRRK2 in the regulation of autophagy and calcium signalling. In the following sections this objective is further described as two explicit aims:

- The development of isogenically matched cell lines containing pathogenic and protective *LRRK2* mutations.
- The use of these cells and pharmacological tools to study the requirements for LRRK2 and LRRK2 enzymatic activities in autophagy and calcium signalling.

1.7.2.1 Isogenic cell lines to compare LRRK2 mutations

PD-causing and PD-protective *LRRK2* mutations will be introduced into ReN VM cells, which are neuronal stem cells, using the CRISPR/Cas9 gene-editing technique (detailed in Chapter 3). These cell lines will be human, will express mutant protein at endogenous levels, and can be differentiated into dopaminergic neurons. Most importantly, the cells lines will be isogenic, which means they will be genetically identical except for the presence of a mutation. This method will allow the different *LRRK2* mutations to be studied in parallel, such that common pathological changes that are absent from wild-type cells can be identified.

The *LRRK2* mutations intended to be made are (depicted in Figure 1.12):

- Two pathogenic mutations; G2019S, which is located in the kinase domain and causes a gain of kinase function; and R1441G, which is located in the GTPase domain and causes a loss of GTPase function.
- A protective mutation, R1398H, which is located in the GTPase domain and results in a gain of GTPase function.

Importantly, opposite effects in cell lines carrying the protective R1398H variant compared to the cell

lines carrying the G2019S and R1441G mutations can likely be expected, making R1398H cells powerful controls for subsequent experiments.

In parallel CRISPR/Cas9 will be used to introduce a sequence encoding a FLAG epitope tag into the translational start site of *LRRK2,* causing an N-terminal FLAG-tag to be added to endogenous LRRK2. This will allow improved immunological detection of wild type LRRK2 protein, facilitating subsequent studies.

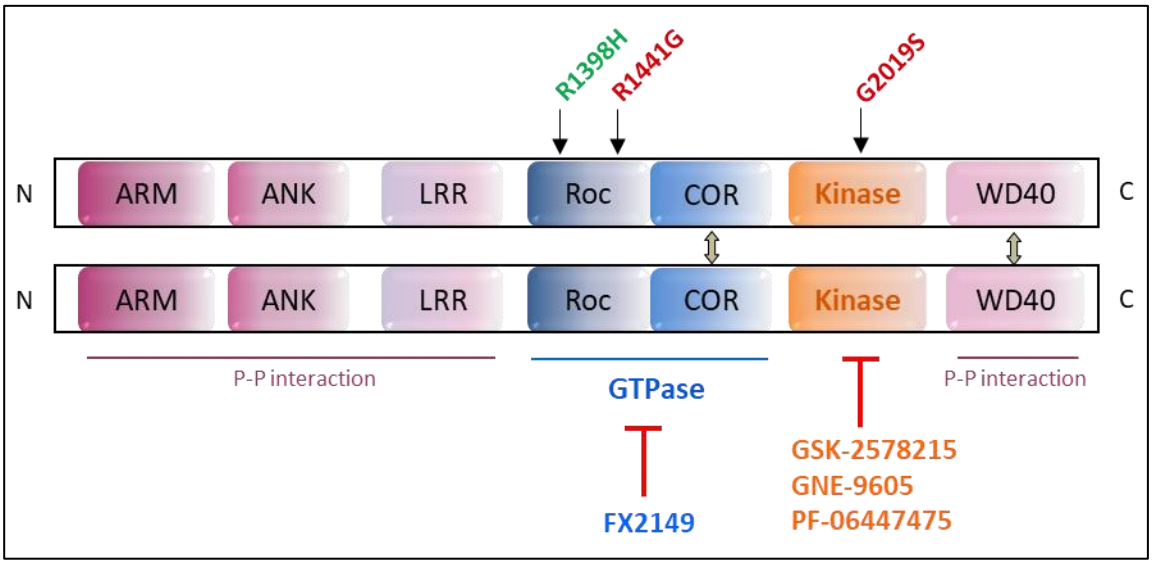

Figure 1.12: *LRRK2* mutations and LRRK2 inhibitors used in this study.

The pathogenic (R1441G and G2019S) and protective (R1398H) *LRRK2* mutations focused on in the present study are represented. The name of the LRRK2 kinase inhibitors (in orange) and the LRRK2 GTPase inhibitor (in blue) are also depicted.

1.7.2.2 Investigation into the role of LRRK2 enzymatic activities in autophagy and calcium signalling

Since numerous PD mutations occur in the kinase and in the RocCOR domains, both LRRK2 kinase and GTPase activities are instrumental to understanding LRRK2 toxicity mechanisms. However, GTPase inhibitors have sparked less interest than the multitude of kinase inhibitors developed. Therefore, the second aim of this work is to assess the requirement for both the LRRK2 kinase and GTPase activities in the effects of LRRK2 and LRRK2 mutants on autophagy and calcium signalling. To do so, experiments using LRRK2 mutants mentioned in the previous section will be combined with experiments using LRRK2 kinase and GTPase inhibitors (Figure 1.12) to create a tailored set of assays to monitor autophagy and measure calcium signals.

2

Materials and Methods

2.1 Materials

All the reagents and chemicals used are listed in the Tables below or in the relevant Section. Plasticware was from Greiner bio-one or Fisher Scientific.

Table 2.1: List of solutions, chemicals and kits used, with their supplier and catalogue number.
The name of the item and its acronym or abbreviation used in the text are shown.

Item/Kits	Supplier	Catalogue number
6X DNA Loading Dye 1ml	Thermo Scientific	R0611
Agarose	Fisher Scientific	BP1356-500
Ampicillin	Sigma Aldrich (Merck)	A9393-5G
DH5α Competent Cells (Subcloning Efficiency)	Invitrogen	11541505
DH5α Competent Cells (MAX Efficiency™)	Invitrogen	11563117
Dimethyl sulfoxide DMSO	Fisher Scientific	BP231-100
Gel DNA extraction kit	Macherey-Nagel	740609.50
Gel DNA extraction Kit Qiaquick	Qiagen	28706
Gel DNA extraction kit (Monarch)	New England Biolabs	T1020G
Gene Ruler DNA Ladder 100bp	Thermo Scientific	SM0241
Genomic DNA extraction kit	Sigma Aldrich	G1N70
Invitrogen™ Molecular Probes™ ProLong™ Gold Antifade Mountant	ThemoFisher	P36931
Kanamycin	Sigma Aldrich (Merck)	60615-5G
LB Agar (Miller)	Fisher Scientific	BP9723-500
Luria-Bertani Broth (Miller) – LB medium	MERCK	VM309985436

Maxi prep plasmid extraction kit	Qiagen	12263
Midori Green Advance DNA Stain	GeneFlow	S6-0022
Paraformaldehyde	Fisher Scientific	C192/13
Phosphate buffer saline, PBS, Tablets	Fisher Scientific	11510546
Polymerase Kapa HiFi kit	Kapa Biosystem	KK2502
Polymerase Kit Phusion	Thermo Scientific	F530S
Polymerase kit Robust KAPA2G	Kapa Biosystem	KK5702
Proteinase K	Zymo Research	D3001-2-B
Silica Bead DNA Gel Extraction kit	Thermo Scientific	K0513
Tris Acetate EDTA TAE Buffer 50X	Fisher Scientific	BP132-500
Trypsin-EDTA 1X	Gibco, Life-Technologies	25200-056

Table 2.2: List of technical equipment used with their supplier and catalogue number.

Item	Description	Supplier/Cat. number
Electrophoresis tools	Tank, powerpack	BioRad
G:BOX	Gel Imaging doc system	Syngen
Microscope	Leica DMI6000	Leica
PCR machine	C1000 thermal cycler and icycler	BioRad
Tali® cellular analysis slides	Tali®	T10794
Tali™	Image-based cytometer	Thermo Fisher
NanoDrop™ One	Microvolume UV-Vis spectrophotometer	Thermo Scientific

2.2 General Methods

For further details on reagents, kits and chemical mentioned in this Section, refer to Table 2.1 and Table 2.2.

2.2.1 General cell culture conditions

The cell culture reagents are listed in Table 2.3 and the cell lines used are summarised in Table 2.4.

Table 2.3: List of cell culture reagents, with their supplier and catalogue number.

The name of the item and its acronym or abbreviation used in the text are shown.

Item	Supplier	Catalogue number
Accutase	Merck Millipore	SCR005
B27 Supplement	Invitrogen	12587010
BioCoat Poly-D-Lysine	Fisher Scientific	11503550
Dulbecco's Modified Eagle Medium	Gibco, Life-Technologies	11330-032
Epidermal Growth Factor (EGF)	Merck Millipore	GF144
Foetal Bovine Serum (FBS)	Gibco, Life-Technologies	11550356
basic Fibroblast Growth Factor (b-FGF)	Merck Millipore	GF003
Fisherbrand™ Borosilicate Glass Circle Coverslips	Fisher Scientific	12313138
G418 sulfate (Geneticin)	Cambridge Bioscience	CAY13200-5G
Gentamycin	Fisher Scientific	11500506
Hank's Buffer Saline Solution, HBSS	Gibco, Life-Technologies	14170-088
Heparin sodium salt	Merck Millipore	375095-100KU
jetPEI® DNA transfection reagent	Polyplus	101-01N
Laminin	Fisher Scientific	10152421
Penicillin (10,000 units/mL) - Streptomycin (10,000µg/mL)	Gibco, Life-Technologies	15140-122

Table 2.4: Cell lines used in this project, with their respective origin.

Abbreviation	Origin	Purchased	Use as a model for PD research
HEK293	Human embryonic kidney cells	ECACC 12022001	Easily transfectable cell line, frequently used in neurode-generative disease research.
HEK293T	Human embryonic kidney cells	ECACC 12022001	Easily transfectable cell line, derivative of the HEK293 cells, contains the SV40 T-antigen, frequently used in neurode-generative disease research.
HEK293-GFP-LC3	Human embryonic kidney cells	Created in house by Dr Tala Chehab	Derivative of the HEK293 cells, stably transfected to express GFP-LC3
SH-SY5Y	Human neuroblastoma	ECACC 94030304	Possesses many characteristics of dopaminergic neurons, can be differentiated into a functionally mature neuronal phenotype[624].
ReN VM	Human neural progenitor ventral mesencephalon	Merck Millipore	Can differentiate into neurons or glial cells[625], comes from the midbrain region where there is dopaminergic cells loss.
WT RAW 264.7	Mouse macrophages	Supplied by Dr Kirsten Harvey, UCL. ATCC SC-6003	Produced in collaboration with the Michael J. Fox Foundation. Tool to study the neuro-inflammatory process in LRRK2-associated Parkinson's disease.
Lrrk2 KO RAW 264.7	Mouse macrophages	Supplied by Dr Kirsten Harvey, UCL. ATCC SC-6004	

Cells were cultured according to standard mammalian tissue culture protocols and sterile techniques:

• HEK293 cells, HEK293T cells, HEK293 GFP-LC3 cells, SHSY5Y cells, and RAW 264.7 macrophages (both wildtype and Lrrk2 KO) were grown in DMEM/F12 complemented with 10% (v/v) Foetal Bovine Serum (FBS) and 1% (v/v) Penicillin-Streptomycin, in a standard cell incubator in a humidified atmosphere with 5% CO2 at 37°C. This cell culture medium is referred to as "Complete DMEM" in the following Sections in this Chapter.

• HEK293 GFP-LC3 cells required continual selection in geneticin (the integrated GFP-LC3 expression cassette having a neomycin resistance gene). Thus, these cells were cultured with the addition of Geneticin 400 µg/ml to the Complete DMEM and this medium is referred to as "GFP DMEM" in the following Sections in this chapter.

• ReN VM cells were grown on laminin-coated plasticware in DMEM/F12 complemented with B27 (2% (v/v) of final volume), gentamycin (50 µg/ml final), heparin sodium sulfate (10 U/ml final), FGF-b (20 ng/ml final) and EGF (20 ng/ml), and referred to as "Growth Medium". Laminin coating was performed a day prior to seeding cells, by incubating plasticware in 20 µg/ml laminin solution diluted in DMEM/F12 media (covering the entire surface) for 4 hours in a cell incubator, followed by one wash with DMEM/F12, and left with fresh DMEM/F12 in a cell incubator until use.

2.2.1.1 Growth of cells

Cells were cultured in 75 cm² flasks and passaged when they reached 70-80% confluency, in order to maintain a sub-confluence. In the majority of cases, this required cells to be passaged every 2-3 days (cell medium changed every 2 days for ReN VM cells) and usually split in a ratio of 1:10 (1:8 for ReN VM cells). To split the cells, the medium surrounding the cells was removed, cells were washed once with 10 ml of prewarmed Hank's Buffer Saline Solution HBSS (or phosphate-buffered saline for ReN VM cells) and incubated with 1 ml of pre-warmed Trypsin-EDTA for 3 minutes (or 5 ml of Accutase for 5 minutes at 37°C for ReN VM cells) to allow cells to dissociate from the surface of the flask or plate.

For routine passaging or for setting up experiments where the cell number did not need to be specified, cells were resuspended in 10 ml of their respective fresh cell culture medium and plated into new cell culture plasticware at an appropriate concentration. ReN VM cells were transferred to a 15 ml tube for an additional centrifugation step for 5 minutes at 8784 rcf (9000 rpm, Rotanta 460 R benchtop centrifuge, Hettich Instruments). The supernatant was removed, cells were resuspended in 10 ml of Growth Medium and plated onto new laminin-coated cell culture plasticware.

When needed, cells in suspension were counted with a haemocytometer, the total number of cells per ml being 10 000 multiplied by the number of cells in a 1 mm^2 square of the grid. Cells were then resuspended in their respective cell culture medium at the desired density.

Cells (except ReN VM cells) required for imaging purposes were seeded onto freshly poly-D-lysine-coated 16 mm glass coverslips in 12-well plates. Poly-D-lysine coating was performed by incubating coverslips in 50 µg/ml poly-D-lysine solution (dissolved in phosphate-buffered saline) for 2 hours at room temperature, followed by two washes with autoclaved water, allowing the coverslips to air dry prior to seeding the cells.

2.2.1.2 Cryopreservation and recovery

- Cryopreservation

For long-term storage, cultured cells at confluency were first washed once with 5 ml of prewarmed HBSS (or PBS for ReN VM cells) and incubated with 1 ml of Trypsin-EDTA for 3 minutes (or 5 ml of Accutase for 5 minutes at 37°C for ReN VM cells) to allow cells to dissociate from the surface of the flask. Cells were then resuspended in 9 ml of HBSS (or PBS) and centrifuged for 5 minutes at 10844 rcf (10000 rpm, Rotanta 460 R benchtop centrifuge, Hettich Instruments) to remove the Trypsin-EDTA (or Accutase) and obtain a cell pellet. Once the supernatant was removed, the cell pellet was resuspended in freezing medium (50% (v/v) respective cell culture medium, 40% (v/v) FBS, 10% (v/v) DMSO, or containing 80% (v/v) Growth Medium and 20% (v/v) DMSO for ReN VM cells) before being transferred into 1.5 ml

cryovial aliquots. The cryovials were then placed in isopropanol-filled freezing containers (Nalgene®) overnight in a -80°C freezer. Cryovials were then moved to a cryopreservation container and kept in liquid nitrogen.

- Recovery

Frozen cells were recovered by thawing a cryovial in a warm water bath at 37°C. Cells were transferred to a T25cm² flask and resuspended in 6 ml of warm cell culture medium before being placed at 37°C. ReN VM cells were transferred to a 15 ml tube for an additional centrifugation for 5 minutes at 8784 rcf (9000 rpm, Rotanta 460 R benchtop centrifuge, Hettich Instruments). The supernatant was removed, and cells resuspended in 1 ml of DMEM/F12 and transferred to a laminin-coated flask containing 5 ml of Growth Medium.

Once the cells had adhered to the flask (usually 24 hours later), the cell culture medium was replaced by fresh cell culture medium to remove the DMSO that was present in the freezing medium, and allowed to grow at 37°C. Once the cells reached 70-80% confluence, they were washed once with 5 ml of prewarmed HBSS (or PBS for ReN VM cells) and incubated with 1 ml of Trypsin-EDTA for 3 minutes (or 3 ml of Accutase for 3 minutes at 37°C for ReN VM cells) to allow cells to dissociate from the surface of the flask. Cells were then resuspended in 15 ml of fresh cell culture medium and transferred into a new T75 cm² flask and placed at 37°C. ReN VM cells were transferred to a 15 ml tube for an additional centrifugation for 5 minutes at 8784 rcf (9000 rpm, Rotanta 460 R benchtop centrifuge, Hettich Instruments). The supernatant was removed, and cells resuspended in 10 ml of Growth Medium and transferred to a laminin-coated T75 cm² flask containing 5 ml of Growth Medium.

2.2.2 Molecular biology

2.2.2.1 Transformation of E. coli

Chemically competent DH5α bacteria cells were transformed with plasmid DNA using a heat shock method described below.

Prior to transformation of bacteria, LB media was prepared using 25 g of LB broth diluted in 1 litre of ultrapure water and autoclaved, while in parallel 1.2% (w/v) agar plates were prepared with 37 g of LB agar powder diluted in 1 litre of autoclaved purite water. LB media and agar plates were complemented with the relevant antibiotic for selection as appropriate (ampicillin or kanamycin at 100 µg/ml).

For the transformation, competent cells were taken from storage at -80°C and thawed on ice. 50 µl of cells were added to a sterile tube to which 1 µl of plasmid DNA was added (usually ≈100 ng). The competent cell and DNA mixture was incubated on ice for 20 minutes, and then heat shocked at 42°C for 45 seconds and returned on ice for 2 minutes. 250 µl of LB media (without antibiotics) was added to the mixture, and the transformation tube was placed at 37°C in an orbital shaker for 45 minutes for the recovery step. 200 µl of the transformation mixture was then spread onto agar plates near a Bunsen burner and incubated overnight at 37°C.

Single colonies were picked from agar plates using a plastic pipette tip, and used to inoculate 200 ml of LB media complemented with the relevant antibiotic for the selection of bacteria. The colonies were grown overnight at 37°C in an orbital shaker. The LB media with the bacteria (bacteria culture) was then collected in 50 ml tubes.

2.2.2.2 Glycerol stock preparation

To create glycerol stocks of bacteria containing a plasmid of interest that can be stored for future use, 500 µl of bacterial culture, obtained following the steps detailed in Section 2.2.2.1, was added to a cryovial containing 500 µl of 50% (v/v) glycerol (diluted in ultrapure water), and stored at -80°C.

2.2.2.3 Plasmid DNA preparation

Plasmid DNA was obtained from bacterial cultures following two procedures:

- Transformed bacterial strains containing the relevant plasmids were taken from glycerol stock cryovials previously made (Section 2.2.2.2) using a plastic pipette tip to inoculate 200 ml of LB media complemented with the relevant antibiotic for selection (ampicillin or kanamycin at 100 µg/ml). Liquid cultures of bacteria were grown at 37°C in an orbital shaker for 16-24 hours to express the plasmid of interest.
- Alternatively, the DNA was extracted (as described below) directly from the bacteria culture obtained in Section 2.2.2.1.

Plasmid DNA was then isolated from bacterial cultures using the Qiagen Maxiprep plasmid purification kit according to the manufacturer protocol (Table 2.1). Plasmid DNA concentration was assessed using a NanoDrop™ spectrophotometer, and the DNA stored at -20°C.

2.1.1 Statistical analysis

Autophagy and calcium signalling data were analysed using GraphPad Prism 7.05 Software (La Jolla, US). The Shapiro-Wilk normality test was used to assess the normal distribution of the data and confirmed with Q-Q plot. The data was analysed using One-way ANOVA or Two-way ANOVA with the data grouped by experiment, with Tukey or Dunnett's post hoc tests used as appropriate (indicated in the Figure legends). Grouping by experiment was included as part of the experimental design to account for anticipated variations between repeats, since autophagy and calcium signalling are fundamental homeostatic mechanisms that can be influenced by variations in the state of the cells, for example the confluency or the passage number.

2.3 Chapter 3 – CRISPR/Cas9-related methods

2.3.1 Creation of LRRK2 CRISPR/Cas9 plasmid constructs

The CRISPR/Cas9 reagents were designed previous to this current work by Dr Daniel Berwick and a visiting student, Abdullahi Adan. All CRISPR/Cas9 plasmids were derived from the Zhang Lab CRISPR plasmid pSpCas9(BB)-2A-GFP (PX458) available from Addgene626 (plasmid # 48138). CRISPR/Cas9 plasmids encode a Cas9 enzyme co-expressed with a specifically designed gRNA (sgRNA for "single guide" RNA) to induce a double-strand break at a relevant DNA cut site (Table 2.5). gRNAs were designed according to the recommendation of the Addgene website and tested through the CRISPR design tool available from the Zhang Lab (http://crispr.mit.edu:8079/). Sequences were searched against the human genome to minimize off targeting using the NCBI BLAST tool (https://blast.ncbi.nlm.nih.gov/Blast.cgi). Two different gRNA were designed for each genomic location targeted (A and B). A plasmid map is depicted in Appendix 3. Cas9 is under the control of a constitutive chicken beta-actin promoter and the gRNA is under the control of a U6 promoter. CRISPR plasmids also contain a Green Fluorescent Protein gene (GFP) reporter, to identify cells expressing the plasmids.

Table 2.5: CRISPR plasmids used for the transient transfections.
For each mutation site, the two plasmids (A and B) designed to test their specificity are shown.

LRRK2 Mutation	Plasmid	sgRNA and PAM Sequence
N-terminal FLAG-tag or Start codon deletion	Start A	GCATGAACGTCCGCTGCTCA [GGG]
	Start B	GAGGGCGGCGGGTTGGAAGC [AGG]
R1398H	RH A	TTTTTAATCTTTCAAACGAC [AGG]
	RH B	TAATCTTTATTTAGGTCGTG [AGG]
R1441G	RG A	GGGAAGAAGAAGCGCGAGCC [TGG]
	RG B	GATTCTCGTTGGCACACATT [TGG]
G2019S	GS A	GTCAGCAATCTTTGCAATGA [TGG]
	GS B	GCTCAGTACTGCTGTAGAAT [TGG]

2.3.2 Transfection of CRISPR plasmids

CRISPR/Cas9 plasmids were delivered into cells by transient transfection. HEK293T cells were seeded in 6-well plates with a density of ≈5x10^4 cells per well in 1 ml of Complete DMEM. 24 hours after seeding, the cell medium was replaced with 1 ml of fresh medium. Previous results from the Berwick team suggested that co-transfection with the pUC18 cloning plasmid as carrier DNA improved the uptake of the plasmid of interest and improved transfection efficiency. Therefore, cells were then co-transfected with one of eight CRISPR plasmids (Start A, Start B, RH A, RH B, RG A, RG B, GS A, or GS B) (Table 2.5) and pUC18 at a 1:1 weight ratio (3 µg DNA in total, 1.5 µg each) using the JetPei® DNA transfection reagent following the manufacturer procedure. After 48-72 hours, the cell medium was replaced with fresh Complete DMEM and the transfection efficiency was assessed as described in Section 2.3.3.

2.3.3 Calculation of transfection efficiency

Since the CRISPR plasmids express GFP, transfection efficiency was assessed by counting cells and comparing the number of fluorescent transfected cells to the total number of cells. This was either done using a fluorescence microscope or via the use of a Tali™ image-based benchtop cytometer device. For counting by fluorescence microscopy (see 2.4.6.1 for details on the fluorescence microscope), representative images of fields of cells were taken under green and bright field channels and the numbers of green cells and total cells were counted by eye by the experimenter. For counting using the Tali™ device, which is a more objective method, 25 µl of cells in suspension needed to be added to disposable cellular analysis chamber slides. Transfected cells were therefore dissociated using 200 µl of pre-warmed Trypsin-EDTA for 3 minutes and resuspended in 1 ml of Complete DMEM.

The background was measured with a sample of untransfected, non-fluorescent cells to set the threshold to detect green fluorescence. The correct size for the cells was also gated so that debris or aggregates were not included in the quantification. 13 images of different fields were taken in each condition, and the total number of cells and the total number of green cells were automatically counted. A percentage

representing the number of green cells among the total number of cells was obtained, indicating the transfection efficiency.

2.3.4 PCR reactions

PCR reactions were performed to amplify the region of interest following the manufacturers' protocols using a Kapa HiFi kit, a Robust or a Phusion kit, in a volume of 25 µl on a thermal cycler.

2.3.4.1 Primer optimisation

The PCR method was used to amplify the region of interest using PCR primers spanning the different mutation sites, i.e., with a complementary sequence to each relevant DNA region of interest within *LRRK2*, which were designed by Dr Daniel Berwick (Table 2.6). The PCR conditions for each pair of primers were first determined with HEK293T, SH-SY5Y or ReN VM genomic DNA to assess whether they work in each cell line or needed to be redesigned. Cell pellets were obtained from these cell lines using the dissociation and centrifugation method described in Section 2.2. Genomic DNA from HEK293T, SHSY5Y and ReN VM cells was extracted using the Sigma Aldrich gDNA extraction kit (Table 2.1). The various PCR conditions tested are summarised in Appendix 4.

Table 2.6: PCR primers used.

Mutation name	Forward	Reverse	Dilution from stock solution
START codon (START)	CTGCCTCCTTCCTC ATAAACAG	GTAAGGAGGGGG AGAAAGTTTG	1:10 to 10 µM
R1398H (RH)	TTGCCTCCAGAAT GGAGAAG	TGAAGAGCCAAG GCTTCATG	
R1441G (RG)	AGGCATGAAGAT GGGAAAGG	CTTTGCGTTGCTT CTCATCAG	
G2019S (GS)	CTTTAAGGGACAA AGTGAGCAC	TGGTTATCCATCC TGAAGATAG	

2.3.4.2 *Assessment of DNA cutting in transfected cell lines*

After transfection with CRISPR plasmids (Section 2.3.2), a heterogenous population of cells was obtained. Within this population of cells, it was necessary to determine whether a mutation had been created at the desired genomic location. To do so, PCRs were performed. First, transfected cells were detached and resuspended in Complete DMEM as described in the previous sections, before cell suspensions were centrifuged for 5 minutes at 10844 rcf (10000 rpm, Rotanta 460 R benchtop centrifuge, Hettich Instruments) to obtain pellets. Genomic DNA was then extracted using the Sigma Aldrich gDNA Extraction Kit (Table 2.1) following the manufacturer protocol. PCR were performed using this genomic DNA and the PCR primers detailed in Table 2.6.

2.3.4.3 *Electrophoresis*

PCR amplification products were separated using agarose gel electrophoresis at 1% (w/v) agarose. Gels were prepared with 1.5 g of agarose dissolved in 150 ml TAE 1X buffer and boiled. 10 µl of Midori green was then added to the cooled down solution. The solution was then poured and allowed to set. Samples were loaded with 5 µl of a 6X loading dye, and the band size was estimated with a standard 100 base pair DNA ladder. Electrophoresis was performed at a constant voltage of 150 V for around 1 hour. The DNA was visualised and the gel imaged using the Syngen Gel Box with UV light. If the PCR was successful, a band at 400 base pairs should be seen.

2.3.4.4 *Gel extraction*

The relevant PCR products were excised from the gel using a scalpel over a UV transilluminator to visualise the DNA. DNA was then extracted and purified using a DNA gel extraction kit (three were tested, see Table 2.1) in accordance with the manufacturer protocol. DNA concentration was finally assessed using a NanoDrop™ spectrophotometer, and samples were prepared for sequencing as detailed below.

2.3.5 Sequencing of genomic DNA

Genotyping of cell lines was performed by sequencing of the targeted genomic region, to determine if Cas9 effectively cut at the anticipated site. 15 ng of DNA template was used with 3.2 pmol of the relevant primer and diluted with water to a final volume of 30 µl, according to the instructions of the sequencing service. Samples were then sent to MRC PPU DNA Sequencing and Services (University of Dundee, UK). The sequencing process provides chromatograms representing the detailed DNA sequence with peaks corresponding to the base located at each position.

With regard to CRISPR/Cas9-transfected cells, the chromatograms of a mixed population of mutated and unmutated cells should display a discordant signal from the mutation site onwards.

2.3.6 Growth of transfected cells

The goal is to establish homogenous stable cell lines containing mutations within the *LRRK2* gene. To do so, it is essential to derive clonal cell lines from the initial mixed population and determine if the clones are carrying the desired mutation. Following the transfection step described in Section 2.3.2, the transfection efficiency was determined as detailed in Section 2.3.3. When the transfection efficiency was high enough, a portion of the mixed population of cells was prepared for genotyping via genomic DNA sequencing (see Section 2.3.4.2 for genomic DNA extraction and Section 2.3.5 for details on sequencing), while the remainder of the cells were plated in new 6 well plates. Clonal cell lines were only expanded further if the sequencing results indicated that successfully mutated cells may be present within the original mixed population.

The limiting dilution method aims at isolating each individual cell and plating them at a very low density, thereby allowing for isolated colonies to be obtained. Transfected cells were detached using 500 µl of pre-warmed Trypsin-EDTA for 3 minutes and resuspended in 1 ml of Complete DMEM, and then were diluted in Complete DMEM at a concentration that can be expected to yield an average of 0.5 cells per well into 96-well plates. After plating in this manner, cells were allowed to grow for a minimum of 7 days

prior to identifying wells with a single monoclonal colony. These colonies were allowed to expand until confluent, then cells were detached using 10 µl of pre-warmed Trypsin-EDTA for 2 minutes, transferred to 12 well plates and then to 6 well-plates with Complete DMEM, allowed to grow in between transfer until there were sufficient cells per well to be passaged. A portion of cells from a given clonal cell line (1-2 wells) was then prepared for genotyping; cells were detached using 500 µl of pre-warmed Trypsin-EDTA for 3 minutes and resuspended in 1 ml of Complete DMEM, centrifuged for 5 minutes at 10844 rcf (10000 rpm, Rotanta 460 R benchtop centrifuge, Hettich Instruments) to obtain a pellet, and genomic DNA was extracted using the Sigma Aldrich gDNA extraction kit (Table 2.1) in accordance with the manufacturer protocol. PCRs using the PCR primers detailed in Table 2.6 followed by DNA sequencing were performed to verify that CRISPR/Cas9 cut at the anticipated site.

2.4 Chapter 4 – Autophagy-related methods

The reagents used in Autophagy assays are listed in Table 2.7 below.

Table 2.7: List of supplementary autophagy assay-related reagents, with their supplier and catalogue number.
The name of the item and its acronym or abbreviation used in the text are shown.

Reagent	Supplier	Catalogue number
AlamarBlue™ Cell Viability Reagent	Thermo Fisher	DAL1025
GSK2578215A (LRRK2 kinase inhibitor)	Insightbio	HY-13237-S
GNE-9605 (LRRK2 kinase inhibitor)	Insightbio	HY-12282-S
PF-06447475 (LRRK2 kinase inhibitor)	Insightbio	HY-12477-S
FX2149 (LRRK2 GTPase inhibitor)	Synthesised in house*	
PP242 (Torkinib)	Insightbio	HY-10474
Bafilomycin A1 (BafA1)	LC Labs	B-1080
Ivermectin (IVM)	Sigma Aldrich (Merck)	I8898
* FX2149 was kindly synthesised in house for us by Dr Sarah Allman, following the procedure described in reference n°[177].		

2.4.1 Cell viability assay

The LRRK2 inhibitors were tested for cytotoxicity in HEK293 GFP-LC3 cells and RAW264.7 macrophages using the Alamar Blue Cell viability reagent. Cells were seeded onto a 96 well plate 24 hours prior to the experiment in Complete DMEM (RAW264.7 cells) or GFP DMEM (HEK293 GFP-LC3 cells). Cells were incubated with the different LRRK2 inhibitors (all at 1 µM) or DMSO (at an equivalent 1:1000 dilution) in 90 µl of fresh cell culture medium for 17 hours, which is a longer incubation time than used in other experiments. 10 µl of Alamar Blue dye (AB) was then added to each well to make a total volume of 100 µl. After 4 hours of incubation in a cell culture incubator, the absorbance in each well was measured at

570 nm on a BMG Labtech FLUOstar OPTIMA plate reader, and the data was exported as Excel files and analysed.

Importantly, three control reactions were performed in parallel with the LRRK2 inhibitor- or DMSO-treated cells. These were:

- Condition A, a positive control in which the AB had been autoclaved prior to the experiment so that it was entirely in a reduced form.
- Condition B, a "blank" constituted of untreated cells in cell culture medium without AB, to measure the background. The values obtained for Condition B were subtracted from all the experimental conditions to account for absorbance at 570 nm that was not associated with the AB.
- An untreated condition, to determine if the addition of DMSO itself had any effects on cell viability.

After subtracting the background values as measured in Condition B from all other samples, values were normalised to the DMSO condition to obtain the percentage of reduction of Alamar Blue, which corresponds to the relative viability of cells subjected to each treatment compared to those treated with the vehicle DMSO. For each condition, 3 replicates were used in each 3 repeats of the experiment.

2.4.2 Cell culture and treatments

For general cell culture protocols, see Section 2.2.1. An overview of the different protocols used in Chapter 4 can be seen in Figure 2.1, detailed below.

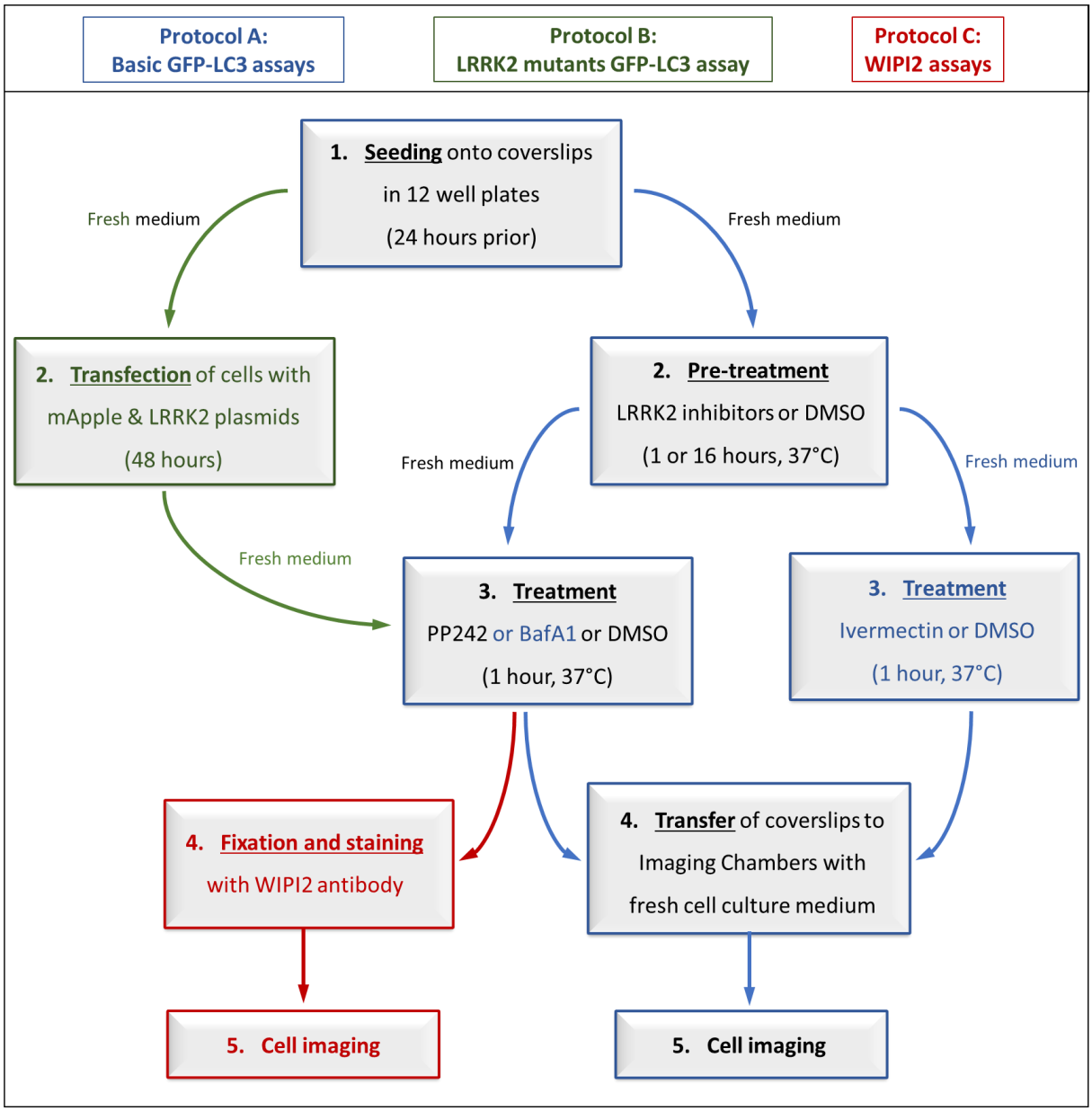

Figure 2.1: Overview of the protocols used in the autophagy assays performed in the Chapter 4.

The general experimental design used in Chapter 4 can be divided into 5 steps, with variations depending on the experiment. Protocol A refers to experiments where GFP-LC3 punctae were quantified from HEK293 GFP-LC3 cells. Protocol B refers to experiment where the GFP-LC3 punctae were quantified from HEK293 GFP-LC3 cells expressing the LRRK2 mutant constructs. Protocol C refers to experiments where endogenous WIPI2 punctae were quantified from fixed HEK293 GFP-LC3 cells or RAW264.7 macrophages. The black text represents the steps in common between the protocols. Each protocol is detailed in Section 2.4.2.

2.4.2.1 Protocol A – GFP-LC3 assay in HEK293 GFP-LC3 treated with LRRK2 inhibitors

This protocol refers to experiments where GFP-LC3 punctae were quantified in HEK293 GFP-LC3 cells using live-imaging microscopy.

Step 1 – Cells were cultured in 1 ml of cell culture medium on 16 mm poly-D-lysine-coated glass coverslips in 12 well plates and allowed to grow in a cell culture incubator. 24-48 hours after seeding, the cell medium was replaced with 1 ml of fresh GFP DMEM.

Step 2 – Cells were pre-treated with the LRRK2 kinase inhibitors GSK2578215A, GNE-9605 or PF-06447475 (at 1 µM), or the LRRK2 GTPase inhibitor FX2149 (at 100 nM or 1 µM) or the vehicle DMSO (at an equivalent 1:1000 dilution), for a duration of 1 hour or 16 hours at 37°C.

Step 3 – Following this pre-treatment, the cell medium was replaced with 1 ml of fresh GFP DMEM. Cells were then treated with different autophagy modulators depending on the experiment, such as PP242 (2 µM) for 1 hour (induces autophagy), BafA1 (0.1 µM) for 1 hour (inhibits the last stages of autophagy), or Ivermectin (15 µM) for 2 hours (induces mitophagy), or the vehicle DMSO (at an equivalent 1:1000 dilution) at 37°C.

Step 4 & 5 – At the end of the treatment, the coverslips were transferred into circular imaging chambers adapted for the stage of the Leica DMI6000 fluorescence microscope with 1 ml of fresh GFP DMEM and images were acquired. Importantly, cells were maintained in complete culture medium for the total duration of all live-imaging autophagy assays. The measurement of autophagy is detailed in Section 2.4.6.

2.4.2.2 Protocol B – GFP-LC3 assay in HEK293 GFP-LC3 overexpressing LRRK2 mutants

This protocol refers to live-imaging experiments where GFP-LC3 punctae were quantified in HEK293 GFP-LC3 cells transiently transfected with LRRK2 mutant constructs.

Step 1 – common with **Protocol A.**

Step 2 – Cells were then transfected with the LRRK2 mutants. For more details on the transfection procedure, see Section 2.4.3. 48 hours after transfection, the cell medium was replaced with fresh GFP DMEM.

Step 3 to 5 – common with **Protocol A**, except that cells were only treated with PP242 (2 µM) or the vehicle DMSO (at an equivalent 1:1000 dilution) for 1 hour at 37°C.

2.4.2.3 Protocol C – WIPI2 punctae assays in HEK293 GFP-LC3 cells and RAW264.7 macrophages

This protocol refers to experiments where endogenous WIPI2 punctae were quantified in fixed HEK293 GFP-LC3 cells or RAW264.7 macrophages stained with an antibody against WIPI2.

Steps 1 to 3 – common with **Protocol A**, except that HEK293 GFP-LC3 cells or RAW264.7 macrophages were only treated with PP242 (2 µM) or the vehicle DMSO (at an equivalent 1:1000 dilution) for 1 hour at 37°C.

Step 4 – At the end of the treatment, cells were fixed and stained using an antibody against endogenous WIPI2. For further details on the immunocytochemistry procedure, see Section 2.4.4.

Step 5 – Slides were observed on the fluorescence microscope (see 2.4.6.1 for details on the fluorescence microscope).

2.4.3 Transfection of LRRK2 mutants

HEK293 GFP-LC3 cells were seeded onto poly-D-lysine coated coverslips in 12-well plates. 24-48 hours after seeding, the cell medium was replaced with 1 ml of fresh GFP DMEM. Cells were then co-transfected with an mApple plasmid and one of five myc-tagged LRRK2 constructs (wild-type, R1398H, R1441G, G2019S and the R1398H/R1441G double mutant) (Table 2.8) at a 70:30 by weight ratio of LRRK2 plasmid to mApple plasmid (1 µg of DNA in total) using the JetPei® DNA transfection reagent following the manufacturer procedure. After 48 hours, the cell medium was replaced with fresh GFP DMEM, and the cells were treated according to the experimental conditions detailed in Section 2.4.2 and in Section 2.5.2.

Table 2.8: Plasmids used with *LRRK2* mutations in this project.

LRRK2 missense mutations proven to segregate with PD are listed, alongside their status as a protective or pathogenic mutation. The location of the corresponding amino acid substitution within LRRK2 protein is shown together with a brief explanation.

Mutation	Pathogenicity	Location within LRRK2	Reason selected for this project
R1398H	Protective	Roc domain	Protective variant; has decreased GTPase function
R1441G	Pathogenic	Roc domain	A particularly penetrant pathogenic mutant; has increased GTPase function
G2019S	Pathogenic	Kinase domain	Most common pathogenic mutation; has increased kinase activity
Wild-type			Control of mutant effect
Empty Vector			Control of overexpression

2.4.4 Immunocytochemistry

Immunocytochemistry experiments were performed to (1) assess the co-transfection of the marker mApple with myc-tagged LRRK2 plasmids in HEK293 GFP-LC3 cells; and (2) detect and visualise endogenous WIPI2 punctae in HEK293 GFP-LC3 cells and in WT and Lrrk2 KO RAW264.7 macrophages. All the steps were performed at room temperature.

Following the transfection method described in Section 2.4.3 and the treatments described in Section 2.4.2, cells were fixed with paraformaldehyde (4% (v/v) in PBS) for 5 minutes in a fume hood and subjected to two 5 minutes washes in PBS. Cells were then permeabilised with 0.1% (v/v) Triton X-100 in PBS for 10 minutes and washed twice with PBS for 5 minutes. Non-specific epitopes were then blocked with an incubation with 10% (w/v) BSA in PBS for 30 minutes. Cells were then incubated with the relevant primary antibody at 1/200 dilution (mouse anti-myc, or mouse anti-WIPI2) in the presence of 2% (w/v) BSA in PBS for 2 hours (Table 2.9). Cells were washed twice with PBS for 5 minutes, then incubated with the relevant secondary antibody at 1/600 dilution (anti-mouse conjugated with the red fluorophore Alexa 568 or the far-red fluorophore Alexa 633) in the presence of 2% (w/v) BSA in PBS for 45 minutes in the dark, since the secondary antibodies are sensitive to light. Cells were washed 3 times with PBS for

5 minutes, and the coverslips were mounted on glass slides with 10 µl of DAPI-containing ProLong™ Gold Antifade Mountant and left in the dark overnight to set. The coverslips were then sealed to the slide with clear nail polish, and stored at 4°C.

Table 2.9: List of antibodies used in immunocytochemistry assays, with their supplier and catalogue number.

Item	Supplier	Catalogue number
Antibody Alexa 568, secondary Goat Anti-mouse	Thermo Fisher	A-11031
Antibody Alexa 633, secondary Goat Anti-mouse	Thermo Fisher	A-21052
Antibody anti-WIPI2, mouse	Bio-Rad	MCA5780GA
Antibody anti-myc, mouse	Cell Signalling Technology	2276S

2.4.5 Determination of use of mApple as marker for expression of LRRK2 mutants

The use of mApple as a reliable live-cell marker for cells co-transfected with LRRK2 constructs was determined using the frequency with which these constructs co-express when transfected together. In order to detect exogenous LRRK2 following the transfection method described in Section 2.4.3, cells were subsequently fixed and stained with an antibody against the myc-tag of the LRRK2 constructs using the immunocytochemistry method described in Section 2.4.4, and co-transfection was determined by fluorescence microscopy.

The proportion of transfected cells expressing one or both type of plasmids (Figure 4.21 A) was obtained using this formula:

$$\frac{\text{(number of cells expressing LRRK2 and/or mApple)}}{\text{(the total number of transfected cells)}} \times 100$$

The proportion of labelled cells that co-express LRRK2 (Figure 4.21 B) was obtained using this formula:

$$\frac{\text{(number of cells co-expressing LRRK2 and mApple)}}{\text{(number of cells co-expressing LRRK2 and mApple)} + \text{(number of cells expressing mApple only)}} \times 100$$

2.4.6 Monitoring Autophagy

2.4.6.1 GFP-LC3 assays

GFP-LC3 assays were performed following the protocols described in Section 2.4.2. HEK293 GFP-LC3 cells stably express GFP-tagged LC3 and therefore in the absence of treatment to induce autophagy appear green due to the diffuse distribution of this protein. This diffuse GFP-LC3 distribution represents the LC3 molecules that are not associated with autophagic vesicles. By contrast, brighter green fluorescent spots represent autophagic vesicles that contain GFP-LC3, referred to as GFP-LC3 punctae. Thus, autophagy can be quantified using the number of GFP-LC3 punctae per cell.

- Following **Protocol A** described in Section 2.4.2.1, the number of GFP-LC3 punctae per cell was quantified using the Image J manual counter from fluorescence images captured using a 12-bit DFC360 FX digital camera on a Leica DMI6000 light microscope. GFP was excited at 450-490 nm and emitted at 500-550 nm, and the 63x oil immersion objective was used to allow for the resolution of individual punctae. For each condition the mean number (± SEM) of GFP-LC3 punctae per cell was calculated, using 50 cells per condition in n=3 experimental repeats in PP242 and BafA1 assays, and using 30 cells per condition in n=4 experimental repeats in Ivermectin assays. Cells that appeared to undergo apoptosis or morphological changes were excluded from the analysis.
- In regards to **Protocol B** detailed in Section 2.4.2.2, the procedure is similar to the one described above. However, since the red fluorescent protein mApple is used as a proxy to identify LRRK2-overexpressing cells, GFP-LC3 punctae were quantified only in cells that expressed mApple. As such, these cells appeared red when excited at 541-551 nm and emitted at 565-605 nm. For each condition, the mean number (± SEM) of GFP-LC3 punctae per cell was calculated, using 50 cells per condition in n=4 experimental repeats.

2.4.6.2 WIPI2 assays

Endogenous WIPI2 assays were performed following the protocol described in Section 2.4.2.3. HEK293 GFP-LC3 and RAW264.7 macrophages (WT and Lrrk2 KO) were subjected to the immune staining protocol described in Section 2.4.4 with an antibody against WIPI2 molecules and an Alexa 568 conjugated secondary antibody (Table 2.9). As such, WIPI2 molecules appeared red when excited at 541-551 nm and emitted at 565-605 nm. Cells appeared red due to the diffuse WIPI2 distribution representing the WIPI2 molecules that are not associated with autophagic vesicles. By contrast, brighter red punctae represented autophagic vesicles that contain WIPI2.

Thus, autophagy was measured using the quantification of WIPI2 punctae per cell using the same method and set-up as described in Section 2.4.6.1. For each condition the mean number (± SEM) of WIPI2 punctae per cell was calculated, using 30 cells per condition in n= 4 experimental repeats in HEK293 GFP-LC3 and in n= 3 experimental repeats in RAW264.7 macrophages.

Three categories of punctae were quantified within HEK293 GFP-LC3 cells to allow a direct comparison to be made: WIPI2 positive punctae, GFP-LC3 positive punctae and WIPI2 and GFP-LC3 double-positive punctae. To specifically assess the effect of the LRRK2 inhibitors on the number of PP242-induced punctae (the three categories), the percentage of inhibition attained by each LRRK2 inhibitor was calculated as follows. First, for each inhibitor, DMSO values were subtracted from the corresponding PP242 values (for each repeat) so that the obtained numbers represent only the punctae specifically induced by PP242. Then, these values were expressed as a percentage of the number of punctae induced by PP242 in the absence of inhibitor treatment (i.e., as a percentage of “PP242+DMSO”). The extent to which each LRRK2 inhibitor affected the PP242-induced increase in the three categories of punctae, i.e., “percentage of inhibition”, was calculated by subtracting the above values from 100.

2.4.7 Electron microscopy assay

Transmission electron microscopy was used to study the effects of LRRK2 inhibitors on the number of vacuoles in HEK293 GFP-LC3 cells and the effects of loss of LRRK2 in RAW264.7 macrophages. The reagents used in transmission electron microscopy assays are listed in Table 2.10 below.

Table 2.10: List of supplementary electron microscopy-related reagents, with their supplier and catalogue number.

The name of the item and its acronym or abbreviation used in the text are shown.

Reagent	Supplier	Catalogue number
Epon resin (Epoxy embedding medium) – a mixture of 4 components: Agar 100 DDSA MNA BDMA	Agar Scientific	 AGR1043 AGR1051 AGR1081 AGR1062
Glutaraldehyde	Agar Scientific	n/a
Osmium tetroxide	Agar Scientific	AGR1015
Pioloform-coated copper grids	Made in house by experienced lab support team	
Pioloform powder	Agar Scientific	AGR1275
Potassium Ferrocyanide, $K_4Fe(CN)_6*3H_2O$	Fisher Scientific	10216460
Reynolds lead citrate	Delta Microscopies	11300
Uranyl Acetate	Agar Scientific	AGR1260A

2.4.7.1 Cell culture

Step 1 and 2 – common to **Protocol A** (2.4.2.1).

Step 3 – common to **Protocol A**, with the exception that in parallel to HEK293 GFP-LC3 cells, RAW264.7 macrophages WT or Lrrk2 KO were treated with PP242 (2 µM) or the vehicle DMSO (at an equivalent 1:1000 dilution) in Complete DMEM for 1 hour at 37°C.

Step 4 – At the end of the treatment, the cell medium was replaced with 1 ml of fresh GFP DMEM (HEK293 GFP-LC3 cells) or Complete DMEM (macrophages), and cells were dissociated from the plasticware using a cell scraper and transferred to sterile tubes.

Step 5 – Cells were then centrifuged for 5 minutes at 10844 rcf (10000 rpm, Rotanta 460 R benchtop centrifuge, Hettich Instruments) to obtain cell pellets. Once the supernatant was removed, cell pellets were fixed in 2.5% (v/v) glutaraldehyde fixative in 0.1 M phosphate buffer (prepared with Na_2HPO_4 at 10 mM and KH_2PO_4 at 1.8 mM) overnight at 4 °C.

2.4.7.2 Sample processing for transmission electron microscopy

The samples were processed by Dr Igor Kraev and Dr Radka Gromnicova at The Open University Electron Microscopy Facility. The processing included post-fixation, dehydration, and embedding in resin. The following steps were performed at room temperature, and the pellets were centrifuged at 370 rcf (2000 rpm, Jencons-PLS Spectrafuge 24D Microcentrifuge) (day 1) or 1130 rcf (3500 rpm, Jencons-PLS Spectrafuge 24D Microcentrifuge) (day 2) in between each step. On day 1, cells were incubated in a 1:1 (v/v) solution of osmium tetroxide (2%) and potassium ferrocyanide (4%) in 0.1 M phosphate buffer (prepared with Na_2HPO_4 at 10 mM and KH_2PO_4 at 1.8 mM) for 1 hour as a post-fixation to enhance membrane labelling. Cells were then washed three times in 0.1 M phosphate buffer. Cells were then dehydrated in a series of ethanol solutions as follows: 30% ethanol for 5 minutes, 50% for 5 minutes, 70% for 10 minutes, 100% for 10 minutes twice, and cells were dehydrated further using molecular sieves (crystalline metal aluminosilicates, which is a material with pores that helps reduce the amount of water in the ethanol to its minimum) in 100% ethanol for 10 minutes. Cells were then dehydrated further in 100% acetone twice for 10 minutes. The pellets were then incubated with a mixture of 100% acetone and Epon resin in a 1:1 ratio overnight. On day 2, cells were infiltrated with Epon resin for 2 hours with two changes. Cells were then embedded in fresh Epon resin and formed blocks were polymerised at 60°C for 48 hours. The blocks were micro-sectioned at 80 nm thickness with a diamond knife (Diatome). The

Sections were mounted onto pioloform-coated copper grids and counter-stained in an aqueous solution of 3.5% (v/v) uranyl acetate and Reynolds lead citrate.

2.4.7.3 Imaging and analysis

The grids were imaged on a transmission electron microscope JEM 1010 (Jeol, Japan) at an acceleration voltage of 80 kV. The images were captured using an XR40 camera (Advance microscopy techniques; AMT, Woburn, MA, USA) and the software AMT Image Capture Engine (AMT, Woburn, MA, USA) with a low magnification (2500-3000x).

For each condition the mean number (± SEM) of vacuoles per cell was calculated using the cell counter plug-in within ImageJ, and the values were obtained from a minimum of 5 images using >100 cells in n= 3 experimental repeats. First, the number of cells that were entirely visible within the area of each image were counted (Figure 4.23, labelled with a blue number 1). Second, vacuoles of any size that were present in the counted cells were quantified (labelled with a red number 2). The mean total number of vacuoles per cell in each condition was then calculated from these two values.

2.5 Chapter 5 – Calcium signal recording-related methods

The reagents used in Calcium assays are listed in Table 2.11 below.

Table 2.11: List of supplementary calcium signalling assay-related reagents, with their supplier and catalogue number.

Reagent	Supplier	Catalogue number
3-Methyladenine	Sigma Aldrich	M9281
ATP, Adenosine 5'-triphosphate disodium salt hydrate	Sigma Aldrich (Merck)	A7699
BAPTA-AM	AAT Bioquest	21001
Cal-590™ AM, Molecular Probes™, cell permeant	AAT Bioquest	20511
Cyclopiazonic acid	HelloBio	HB1117
Dibromo-BAPTA-AM	EFLabs	No longer available from this supplier
Difluoro-BAPTA-AM	EFLabs	
Fura-2 AM, Molecular Probes™, cell permeant	Fisher Scientific	11524766
Ionomycin free acid	HelloBio	HB1002
Pluronic acid F-127	Thermo Fisher	P-3000MP

2.5.1 Preparation for calcium imaging

2.5.1.1 Imaging buffer

The solution of imaging buffer was prepared with ultrapure water, 121 mM NaCl, 5.4 mM KCl, 0.8 mM $MgCl_2$, 6 mM $NaHCO_3$, and 25 mM HEPES (pH 7.4 verified with a pH-meter and a solution of NaOH). Prior to performing each experiment, this solution was completed with 5.5 mM D-glucose and 1.8 mM $CaCl_2$ and referred to as "imaging buffer". When required, the addition of $CaCl_2$ was omitted and the solution was referred to as "calcium-free imaging buffer".

2.5.1.2 Calcium indicator

The fluorescence calcium indicator Fura-2AM, which is excitable with UV light, was chosen to measure intracellular calcium in this study. Upon calcium binding, Fura-2 presents a shift in excitation from around 380 nm to around 340 nm, and emits at 510 nm. This feature allows for a ratiometric measure of calcium signals, which accounts for uneven indicator loading in cells, and progressive loss of signal. The AM-form of Fura-2 is not initially calcium-sensitive, but this modification permits entry into cells. Upon entry in the cells however, the AM ester group is processed by esterases, and Fura-2 becomes calcium-sensitive.

Stock solutions of Fura-2-AM were made at 2 mM in DMSO containing 20% (w/v) pluronic acid (facilitates the solubilisation of Fura-2-AM) and aliquots were kept at -20°C. On the day of the experiment, Fura-2 loading solution was prepared with 2 µM Fura-2-AM diluted in 1 ml of imaging buffer per imaging chamber (i.e., per coverslip) and protected from light. For further details on calcium indicator loading in cells, see Section 2.5.2. When necessary (see Section 2.6.3), the calcium dye Cal-590-AM was also used and prepared similarly to Fura-2-AM.

2.5.2 Cell culture and treatments

For general cell culture protocols, see Section 2.2.1. An overview of the different protocols can be seen in Figure 2.2, where the diagram represents different protocols used in Chapter 5, detailed below.

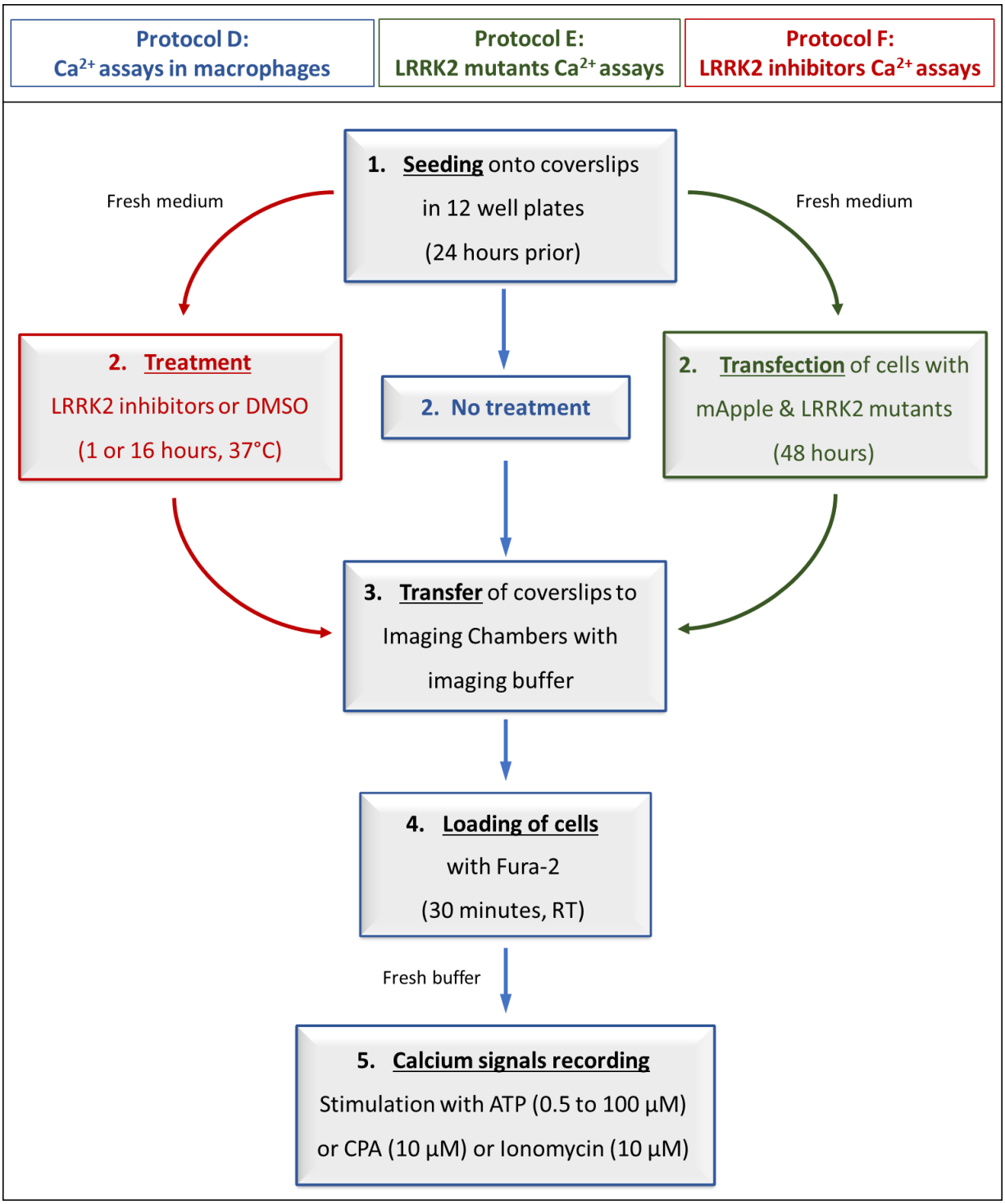

Figure 2.2: Overview of the protocols used in calcium signalling assays performed in the Chapter 5.

The general experimental design used in the Chapter 5 can be divided into 5 steps, with variations depending on the experiment. Protocol D refers to experiments where calcium signals were recorded from RAW264.7 macrophages. Protocol E refers to experiments where calcium signals were recorded from HEK293 GFP-LC3 cells expressing the LRRK2 mutant constructs. Protocol F refers to experiments where calcium signals were recorded from HEK293 GFP-LC3 cells or RAW264.7 macrophages treated with LRRK2 inhibitors. The black text represents the steps in common between the protocols. Each protocol is detailed in Section 2.5.2.

2.5.2.1 Protocol D: calcium response patterns in RAW264.7 macrophages

This protocol refers to the experiments where calcium signals were recorded from RAW264.7 macrophages, following stimulation with ATP, a natural agonist of P2Y receptors which leads to the production of IP_3 and IP_3-R-mediated calcium release, to characterise the calcium response pattern (**Assays nº1** and **nº2**, Section 2.5.3.1). This protocol also applies to the control experiment verifying the effects of CPA (**Assay nº3**, Section 2.5.3.1).

Step 1 – Cells were cultured in 1 ml of Complete DMEM on 16 mm poly-D-lysine-coated glass coverslips in 12 well plates and allowed to grow in a cell culture incubator. 24-48 hours after seeding, the cell medium was replaced with 1 ml of fresh Complete DMEM.

Step 2 – The macrophage cells were not treated.

Step 3 – The coverslips were then transferred into circular imaging chambers, adapted for the stage of the Leica DMI6000 fluorescence microscope, with 1 ml of imaging buffer.

Step 4 – The buffer was removed and cells were then loaded with Fura-2 (2 µM diluted in 1 ml of imaging buffer) for 30 minutes at room temperature protected from light. This solution was then aspirated and replaced with 1 ml of fresh imaging buffer for 30 minutes to allow for the de-esterification of the calcium indicator.

Step 5 – Imaging chambers were then placed on the stage of the microscope and calcium signals were recorded; the procedure is detailed in Section 2.5.3.

2.5.2.2 Protocol E: calcium responses in HEK293 GFP-LC3 cells expressing LRRK2 mutants

This protocol refers to the experiments where calcium signals were recorded in HEK293 GFP-LC3 cells expressing the LRRK2 mutant constructs following stimulation with ATP, CPA (a compound that blocks the SERCA pumps, prevents ER calcium replenishment, and leads to a gradual elevation of cytosolic calcium due to natural leakage from the ER), or Ionomycin (a membrane permeant calcium ionophore

which binds calcium ions and facilitates their transport across the membrane of acidic stores). (**Assays nº4** and **nº5**, Section 2.5.3.2)

Step 1, 3, 4 and 5 – common with **Protocol D**.

Step 2 – Cells were then transfected with LRRK2 mutants following the procedure described in Section 2.4.3. 48 hours after transfection, the cell medium was replaced with fresh GFP DMEM.

2.5.2.3 Protocol F: effect of LRRK2 inhibition on calcium responses

- This protocol refers to experiments where calcium signals were recorded from HEK293 GFP-LC3 cells or RAW264.7 macrophages treated with LRRK2 inhibitors following stimulation with calcium agonists (ATP, CPA, Ionomycin). (**Assays nº6** and **nº7**, Section 2.5.3.3)

Step 1, 3, 4 and 5 – common with **Protocol D**.

Step 2 – HEK293 GFP-LC3 cells or RAW264.7 macrophages were treated with the LRRK2 kinase inhibitors GSK2578215A, GNE-9605 or PF-06447475 (at 1 μM), or the LRRK2 GTPase inhibitor FX2149 (at 100 nM or 1 μM) or the vehicle DMSO (at an equivalent 1:1000 dilution), for a duration of 1 hour or 16 hours at 37°C. Following this treatment, the cell medium was replaced with 1 ml of fresh GFP DMEM (HEK293 GFP-LC3 cells) or Complete DMEM (RAW264.7 macrophages).

- This **Protocol F** was also used in a control experiment to verify that DMSO had no effects on calcium release (Assay nº8, Section 2.5.3.3).

Step 1, 3, 4 and 5 – common with **Protocol D**.

Step 2 – WT RAW264.7 macrophages were treated with DMSO (at an equivalent 1:1000 dilution) for 1 hour at 37°C. Following this treatment, the cell medium was replaced with 1 ml of fresh Complete DMEM.

2.5.3 Calcium signal recordings

Calcium signals were recorded using a 12-bit DFC360 FX digital camera on the Leica DMI6000 light microscope with the 63x oil immersion objective or the 20x objective. Fura-2 was excited at 340 nm and 387 nm wavelengths and emitted at 510 nm, and the ratio was measured. For each calcium signal recording a field of cells on the coverslip was selected based on a healthy appearance and even indicator loading. 20 regions of interest (ROIs) minimum were selected in each area (see Figure legends), and the background was automatically subtracted with the microscope software background formula using a 'background area' selected on the image. To make the change of solutions easier when necessary, a vacuum aspirator was set up on the stage of the microscope. The data were then exported as an Excel file, and used in Microsoft Excel and the GraphPad Prism software to plot the graphs and calculate different parameters (detailed in Section 2.5.4).

2.5.3.1 Protocol D: calcium responses pattern in RAW264.7 macrophages

This protocol was used in three separate assays:

- **Assay nº1**: **use of ATP at 100 µM** (Section 5.2.2.1). Basal calcium signals or spontaneous activity were recorded for 5 minutes. Then, the imaging buffer was aspirated and cells were stimulated with 100 µM ATP (IP_3-generating agonist) diluted in imaging buffer, until termination of the signals. The recording was paused, cells were washed 4-8 times with imaging buffer and allowed to rest in imaging buffer for 10 minutes. The recording was resumed for 1 minute to obtain a baseline, then the imaging buffer was aspirated and cells were stimulated again with 100 µM ATP diluted in imaging buffer, until termination of the signal. These steps were repeated one more time, and the recording was ended. The recordings were then processed as described in Section 2.5.4.
- **Assay nº2**: **use of a range of ATP concentrations** (0.5 µM to 100 µM) (Section 5.2.2.2). The protocol is similar to the one described above for **Assay nº1**, except that cells were stimulated a total of four times, with an increasing concentration of ATP diluted in imaging buffer: 0.5 µM, 1 µM, 10 µM and

100 µM, with the same periods of wash and rest in between each stimulation.

- **Assay nº3**: **control experiment to verify the effect of CPA** (Section 5.5.4). Calcium signals were recorded using the same steps as **Assay nº1** described above, except that cells were stimulated a total of three times, with 0.01% (v/v) DMSO, 10 µM CPA (specific and reversible inhibitor of SERCA/ATPase pumps that empties ER calcium), and 10 µM ATP all diluted in calcium-free buffer, with the same periods of wash and rest in between each stimulation.

2.5.3.2 Protocol E: calcium responses in HEK293 GFP-LC3 cells expressing LRRK2 mutants

This protocol was used in two separate assays:

- **Assay nº4**: **use of ATP to measure global calcium signals** (Section 5.7.1). Calcium signals were recorded using the same steps as **Assay nº1** described above, except that the basal levels were recorded for 1 minute in HEK293 GFP-LC3 cells, and cells were stimulated twice with ATP at 10 µM diluted in imaging buffer, with the same periods of wash and rest in between each stimulation.
- **Assay nº5**: **use of CPA and Ionomycin to measure lysosomal calcium signals** (Section 5.7.2). Calcium signals were recorded using the same steps as **Assay nº1**, except for the following differences. The basal levels were recorded for 1 minute in HEK293 GFP-LC3. Then, the imaging buffer was aspirated, and cells were stimulated with 10 µM CPA diluted in calcium-free buffer. Upon termination of the signal, the calcium-free buffer was aspirated, and the cells were stimulated with 10 µM CPA and 10 µM Ionomycin (mobilises calcium from acidic stores) diluted in calcium-free buffer, without periods of wash and rest in between each stimulation.

2.5.3.3 Protocol F: effect of LRRK2 inhibition on calcium responses

This protocol was used in two separate assays and one additional control assay:

- **Assay nº6**: **use of ATP to measure global calcium signals in HEK293 GFP-LC3 cells** (Section 5.4) **and RAW264.7 macrophages** (Section 5.3.2). Calcium signals were recorded using the same steps as

Assay nº4.

- **Assay nº7**: **use of CPA and Ionomycin to measure lysosomal calcium signals in HEK293 GFP-LC3 cells** (Section 5.6) **and RAW264.7 macrophages** (Section 5.5). Calcium signals were recorded using the same steps as **Assay nº5**.
- **Assay nº8**: **control experiment to verify that DMSO (vehicle of LRRK2 inhibitors) has no effect on calcium signals** in RAW264.7 macrophages (Section 5.3.1). Calcium signals were recorded using the same steps as **Assay nº1** described above, except that cells were stimulated a total of three times, with an increasing concentration of ATP diluted in imaging buffer: 2 µM, 10 µM and 100 µM, with the same periods of wash and rest in between each stimulation.

2.5.4 Processing of recordings and parameters analysed

- Processing of the recordings

Each intracellular calcium release generates a trace. For each recording, at least 20 cells were selected, and single-cell calcium traces recorded individually. The data was exported as an Excel file, and Microsoft Excel was used to average the data (except for the spontaneous activity) and obtain one representative value per time-point (refer to Figure 5.2 for illustration). As such, for each peak, the data are the mean (± SEM) of n= 3 to 8 experimental repeats (see Figure legends for specific details), the value of each repeat representing an average of the values obtained from 20 cells. GraphPad Prism software was used in addition to Microsoft Excel to plot the graphs, and different parameters of these traces were measured in all the calcium experiments performed to help assess any changes in calcium signals due to the experimental conditions. The calculations are detailed below.

- Baseline

The baseline calcium levels for each peak were calculated using an average of the fluorescence values recorded for 5 minutes (in RAW264.7 macrophages) or 1 minute (in HEK293 GFP-LC3 cells) prior to any stimulation. This parameter provides the resting levels of calcium.

- Spontaneous activity (refer to Figure 5.1)

To assess the average spontaneous activity within the 5 minutes of recording (in RAW264.7 macrophages only, as the HEK293 GFP-LC3 cells did not display spontaneous calcium release), individual calcium traces from each cell were plotted on Prism, as depicted in Figure 2.3 and Figure 5.1. A peak corresponds to a release of calcium, and the response had to be 10% above the baseline to be considered a peak. The number of peaks per cell were counted and averaged to obtain the rate of spontaneous peaks per minute (Figure 5.1). This 10% threshold is the standard number routinely used in Dr Martin Bootman's lab. Nonetheless, analysis of the mean, standard deviation and range for a period of baseline recording and a period of peak recording that were sampled (Figure 2.3) showed that a 10% threshold is a stringent way of distinguishing a calcium peak from the baseline. As shown in Figure 2.3 in bold red, the 10% change in baseline (0.326) exceeds the range of baseline deviations (0.276-0.316), which is also the case for the peak-related range of the data (0.321-0.682).

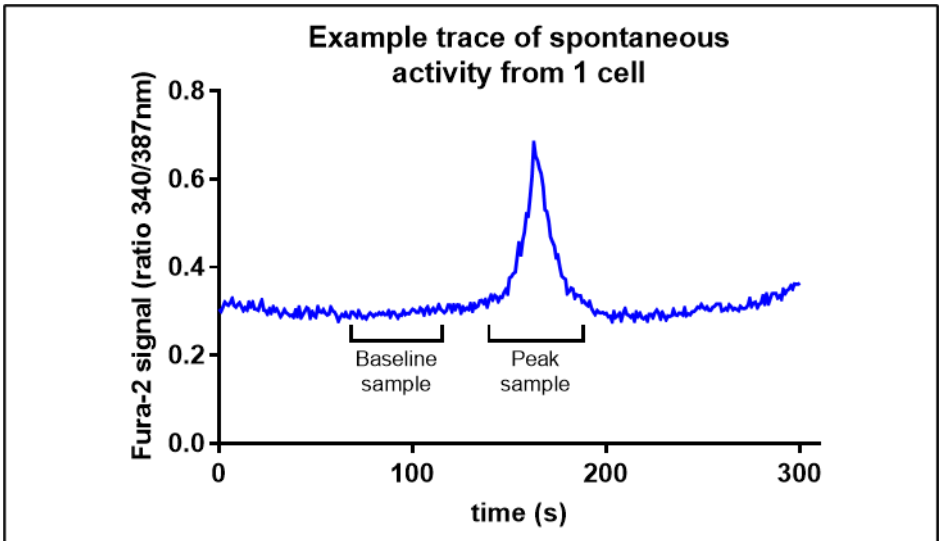

Sample	Mean	Standard deviation (SD)	Range of the data	Range of baseline deviations (mean ± 3*SD)	10% change in mean baseline
Baseline	0.297	0.006718	0.283 - 0.315	**0.276 - 0.316**	**0.326**
Peak	0.430	0.10213	**0.321 - 0.682**		

Figure 2.3: Determination of the threshold allowing the distinction between 'baseline' and 'peak'

Top panel: RAW264.7 WT macrophages were loaded with Fura-2 AM (2 µM) in imaging buffer and the calcium signals were recorded for 5 minutes to measure the spontaneous release of calcium. The trace represents the individual calcium signals and peak from 1 region of interest (ROI) corresponding to 1 individual cell. An example of a baseline sample and of a peak sample are shown in black. Bottom panel: A period of baseline recording and a period of peak recording were sampled, and several parameters were calculated. The relevant values supporting the use of a 10% threshold are indicated in bold red.

- Amplitude (refer to Figure 5.3)

The amplitude of an agonist-evoked calcium response was obtained by subtracting the lowest fluorescence value (Ymin, baseline) from the highest fluorescence value (Ymax) for each averaged peak, and was used as a measure of the rate of the calcium release.

- Area Under the Curve (AUC) (refer to Figure 5.3)

The area under the curve was obtained for each averaged peak with the tool “Total Peak Area” using GraphPad Prism and the baselines calculated beforehand. This area was used as a measure of the total amount of calcium released.

- Decay τ (refer to Figure 5.3)

The decay data was obtained for each peak using the “full width of the peak at half maximum response” method. For each averaged calcium trace, the formula Ymin + (Ymax-Ymin)/2 provided a fluorescence value, and a line corresponding to this value was added to the plot. This allowed the determination of two X values at the two intersections of the peak with the line (X1 and X2). The decay τ was then obtained by subtracting the X1 value from the X2 value. This value represents the time necessary for the termination of the signal and return to baseline.

2.6 Experiments to assess the effects of BAPTA, BAPTA analogues and BAPTA-based calcium indicators

For general cell culture protocols, see Section 2.2.1. An overview of the different protocols can be seen in Figure 2.4, detailed below.

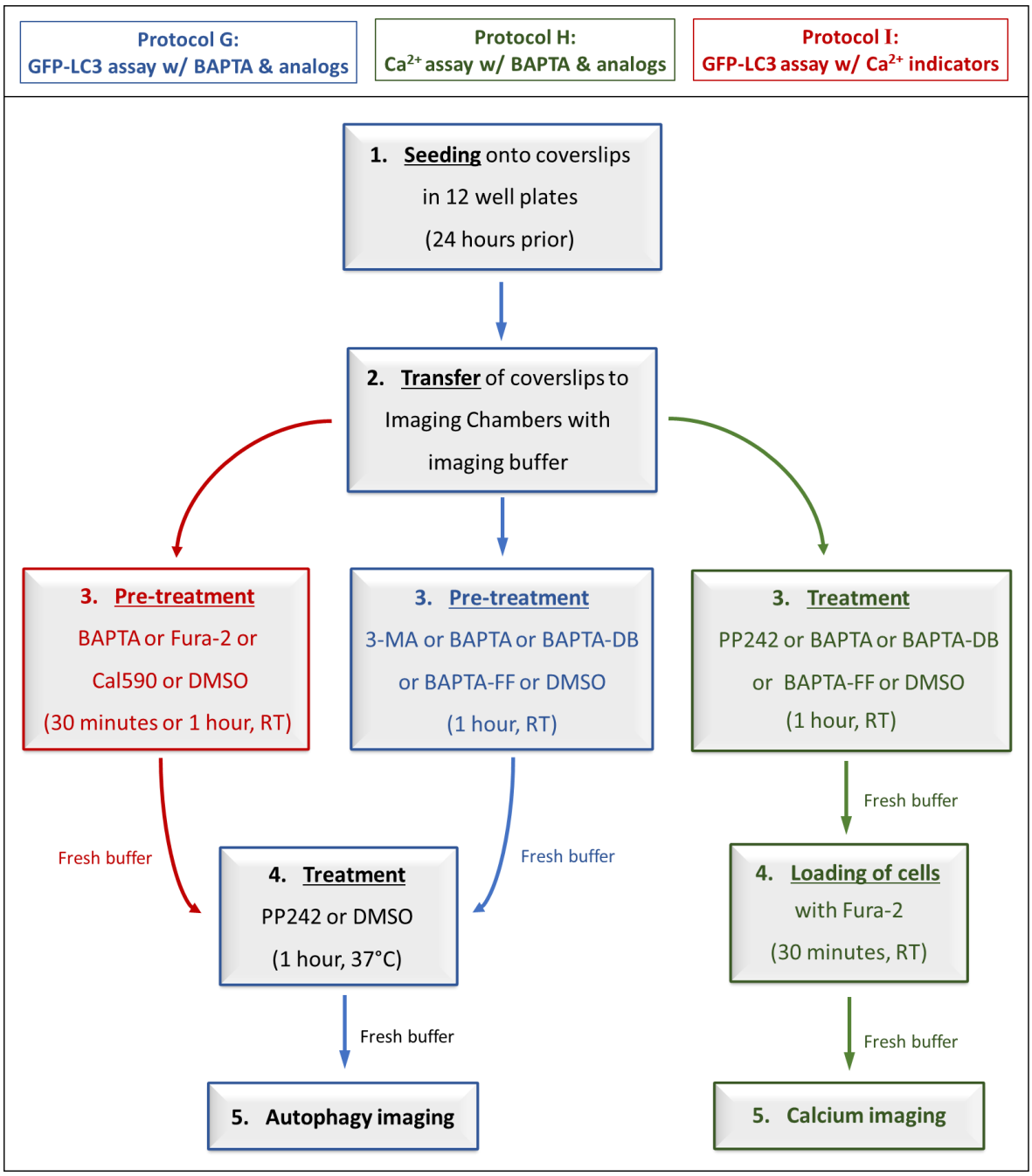

Figure 2.4: Overview of the supplementary protocols used in Chapter 5.

The general experimental design used in Section 5.8 of Chapter 5 can be divided into 5 steps, with variations depending on the experiment. Protocol G refers to experiments where GFP-LC3 punctae were quantified from HEK293 GFP-LC3 cells treated with BAPTA and its analogues. Protocol H refers to experiments where calcium signals were recorded from HEK293 GFP-LC3 cells treated with BAPTA and its analogues. Protocol I refers to experiments where GFP-LC3 punctae were quantified from HEK293 GFP-LC3 cells treated with calcium indicators. The black text represents the steps in common between the protocols. Each protocol is detailed in Section 2.6.

2.6.1 Protocol G: effects of BAPTA and BAPTA analogues on PP242-induced autophagy

This protocol refers to the experiments where GFP-LC3 punctae were quantified from HEK293 GFP-LC3 cells treated with BAPTA and its analogues.

Step 1 – HEK293 GFP-LC3 cells were cultured in 1 ml of GFP DMEM on 16 mm poly-D-lysine-coated glass coverslips in 12 well plates and allowed to grow in a cell culture incubator. 24-48 hours after seeding, the cell medium was replaced with 1 ml of fresh GFP DMEM.

Step 2 – Then the coverslips were transferred into circular imaging chambers adapted for the stage of the Leica DMI6000 fluorescence microscope with 1 ml of imaging buffer.

Step 3 – Cells were then pre-treated with different compounds: 3-MA (5 mM) (used as a control for the blocking of autophagy) or BAPTA (10 µM) or Dibromo-BAPTA (10 µM) or Difluoro-BAPTA (10 µM) or the vehicle DMSO (at an equivalent 1:1000 dilution) for 1 hour at room temperature. Following this pre-treatment, the buffer was aspirated and replaced with 1 ml of fresh imaging buffer.

Step 4 – Cells were then treated with PP242 (2 µM) or the vehicle DMSO (at an equivalent 1:1000 dilution) for 1 hour at 37°C.

Step 5 – At the end of the treatment, the buffer was aspirated and replaced with 1 ml of fresh imaging buffer and the imaging chambers were then placed on the stage of the microscope. GFP-LC3 punctae were quantified as described in Section 2.4.6, using 30 cells per condition.

2.6.2 Protocol H: effects of BAPTA and BAPTA analogues on calcium signals

This protocol refers to experiments where calcium signals were recorded from HEK293 GFP-LC3 cells treated with BAPTA and BAPTA analogues, following stimulation with ATP (IP_3-generating agonist).

Step 1 & 2 – common with **Protocol G**.

Step 3 – Cells were then pre-treated with different compounds: BAPTA (10 µM), or Dibromo-BAPTA (10 µM) or Difluoro-BAPTA (10 µM) or DMSO (at an equivalent 1:1000 dilution) or PP242 (2 µM) for 1 hour at room temperature.

Step 4 – common to **Protocol D**.

Step 5 – Imaging chambers were then placed on the stage of the microscope and calcium signals were recorded; basal calcium signals were recorded for 1 minute, then the imaging buffer was aspirated and cells were stimulated with 100 µM ATP diluted in imaging buffer, until termination of the signals. The technical details of the procedure are detailed in Section 2.5.3. and the parameters measured (AUC and amplitude) are detailed in Section 2.5.4.

2.6.3 Protocol I: effects of calcium indicators on autophagy

This protocol refers to the experiments where GFP-LC3 punctae were quantified from HEK293 GFP-LC3 cells treated with calcium indicators using live-imaging microscopy.

Step 1, 2, 4 and 5 – common with **Protocol G**.

Step 3 – Cells were then pre-treated with different compounds: BAPTA (10 µM), Fura-2 (at 2 µM or 10 µM), Cal-590 (at 2µM or 10 µM) or DMSO (at an equivalent 1:1000 dilution) for 30 minutes or for 1 hour at room temperature. Cal-590-AM is a red-shifted fluorescent calcium indicator used here alongside Fura-2, to assess the potential effects of two different calcium indicators on autophagy, since they both possess a structure similar to that of BAPTA.

3

Creation of isogenic cell lines using CRISPR/Cas9

3.1 Introduction

Parkinson's disease genetics has the potential to uncover different aspects of PD aetiology by helping identify altered processes caused by individual mutations. It is proposed that LRRK2 is involved in a process central to early PD aetiology, and, by extension, the investigation of *LRRK2* mutations to uncover common effects will help to understand the molecular basis of PD pathogenesis. Given that animal models of *LRRK2* and conventional over-expression based *in vitro* systems have had limited success in identifying the mechanisms by which *LRRK2* mutations trigger PD, alternative experimental models are required, where multiple *LRRK2* mutations can be investigated in parallel.

Thus, the primary aim of this project that is detailed in the current Chapter is to develop new cellular models to investigate the effects of *LRRK2* mutations. To do so, efforts were made to use the CRISPR/Cas9 gene-editing technique to introduce PD-causing and PD protective *LRRK2* mutations into cells. This technique is described in Section 3.1.3.2.

The cell line of choice is ReN VM, immortalised human neural stem cells with a stable 46 X,Y karyotype that are derived from the ventral midbrain, the major region of dopaminergic cell loss in PD[625]. In principle, genetically modified ReN VM cells will express mutant LRRK2 protein at endogenous levels, and will be isogenic, a feature that will allow the different cell lines to be compared directly. Ultimately, the cell lines can be differentiated into physiologically representative dopaminergic neurons and used to compare the different *LRRK2* mutations in cellular assays relevant to PD, such that a commonly

deregulated pathway that is likely to cause the pathogenic accumulation of α-synuclein and PD can be identified. Nonetheless, most of the experiments described in this Chapter were first performed in another cell line, HEK293T cells, a commonly used cell line in PD research, since this human cell line is a more tractable system for initial proof-of-principle experiments.

The mutations chosen to be made are G2019S and R1441G, which cause a gain of kinase function and a loss of GTPase function, respectively, and R1398H, which is a PD-protective variant in which GTPase activity is increased (Figure 1.12). Additionally, a further cell line in which a sequence encoding an N-terminal FLAG-tag will be added in-frame to *LRRK2* was planned, with the objective of facilitating the detection of endogenous LRRK2 in subsequent studies. Note that in much of this Chapter, the CRISPR/Cas9 reagents involved in engineering PD-related mutations are named according to the mutation site and abbreviated to GS (G2019S), RG (R1441G) and RH (R1398H). The reagents used to generate cells carrying the FLAG-tag are referred to as START, since they are designed to target the start codon of *LRRK2*.

The following Sections will detail the CRISPR/Cas9 technique, as well as the phenotypes expected in the engineered cell lines.

3.1.1 Limitations of the ReN VM model to study PD

ReN VM cells were chosen for this study since they are a practical and physiologically relevant choice to explore the causes of PD. Nonetheless there are constraints with this system and it is essential that they are established in advance. The most obvious weakness is that a homogenous cell line cannot replicate the variety of different cell types present in the human brain (i.e., there are no glia or astrocytes). PD is fundamentally a disease of dopaminergic neurons, but it is possible that disease phenotypes will require interactions with other cell types, especially microglial cells.

A second drawback is that cell models have a relatively short lifespan compared to those of the human brain, or even the neurons of the rodent models that often fail to develop PD. As such, there is little time

for pathological changes associated with PD to occur. However, the focus of this work is on the earliest stages of PD. Furthermore, data from other studies indicate that this approach is likely to work, since disease-relevant phenotypes have been found in neurons differentiated from patient-derived iPSCs[599].

Therefore, the creation of these cell lines could potentially be a new and reliable human model of PD to study the molecular interactions relevant to Parkinson's disease[627].

3.1.2 Expected phenotype of LRRK2 mutant cells

Reports have shown that iPSCs from *LRRK2* PD patients differentiated into dopaminergic neurons present morphological changes compared to control cell lines, notably a decrease in the number of neurites and impaired autophagy[599,628]. These observations are consistent with data from other experimental systems[105], so it is possible to make cautious predictions about the expected PD-related phenotypes in the engineered cell lines. Differentiated ReN VM cells carrying pathogenic *LRRK2* mutations would be expected to display altered neurite arborisation and axon growth, as well as impairments in the morphology and function of organelles involved in the autophagy-lysosomal systems. Finally, with extended time in culture, PD-causing *LRRK2* mutations would also be predicted to cause increased levels of α-synuclein.

Importantly, the R1398H mutation could provide a unique insight into LRRK2 function in PD since it is a PD-protective variant. Indeed, it is plausible that R1398H will cause opposite effects to the pathogenic G2019S and R1441G mutations. R1398H therefore has the potential to be a strong control for any experiment using pathogenic LRRK2 variants. In line with this, the R1398H variant induced enhanced axon growth when transfected into rat primary cortical neurons, the opposite phenotype to cells transfected in parallel with the R1441G mutant[108].

3.1.3 Genome editing to create modified cell lines

The following two Sections provide a brief overview of the CRISPR/Cas9 technology used in this project, and the science underlying it.

3.1.3.1 DNA repair mechanisms

DNA is constantly subjected to insults from the environment, for instance exposure to UV radiation or tobacco smoke[629], but also spontaneous insults from endogenous sources such as metabolism by-products including ROS, or DNA replication errors[629]. Such damage challenges genome integrity, and can cause mismatched bases and base incorporation errors, as well as structural deformations and lesions in the double-helix, in particular double-strand breaks.

There are a number of DNA repair mechanisms that detect and repair various types of damage to genomic DNA[629]. In regards to double-stranded breaks in the DNA backbone, there are two major DNA damage repair mechanisms[630]. The most commonly used, or "default", mechanism is called non-homologous end joining repair (NHEJ). NHEJ promotes the religation of the two ends, but is an error-prone process. Small insertions or deletions are often produced, which can lead to the disruption (i.e., knockout) of genes (Figure 3.1). The second repair mechanism, homology directed repair (HDR), occurs at a lower frequency, predominantly in dividing cells, but is a high-fidelity process. In HDR, a homologous DNA sequence that spans the site of DNA damage is used as a template to restore the original DNA sequence through homologous recombination[630] (Figure 3.1).

In the last decades, it has become possible to modify genomic loci with genome editing[631]. Genome editing techniques involve the use of programmable synthetic nucleases that act as molecular scissors to create double-strand breaks at a specific DNA locus, and then take advantage of the DNA repair mechanisms to introduce targeted mutations. Genome editing has already been used in a variety of cell types including iPSCs[632,633], and will be explained further in the next section.

3.1.3.2 Genome editing and CRISPR/Cas9

The creation of isogenic cell lines requires a fine-tuned genome editing technique. Various genome editing techniques have been developed, including zinc-finger nucleases (ZFNs) and transcription activator-like effector nucleases (TALENs)[631,634,635]. The technique of choice in the present study is CRISPR/Cas9, which stands for clustered regularly interspaced short palindromic repeats (CRISPR)-Cas9 (CRISPR associated gene 9). CRISPR/Cas9 is more accurate, cheaper and quicker than the previous methods[634].

CRISPR/Cas9 was originally described as an immune system in bacteria[636]. The bacterial genome contains short DNA repeats separated with "spacers" that are sequences derived from viral DNA integrated after an infection. Cas genes, coding endonucleases, are positioned close to the repeats. This mechanism of immunological memory allows bacteria to detect and destroy viruses quickly and provide resistance to infection. Transcribed RNA from the spacers form complexes with Cas proteins and these complexes hunt for matching viral DNA sequence to inactivate the virus.

CRISPR/Cas9 is used as a genome editing tool by supplying the Cas9 protein with a synthesised RNA molecule that is homologous to the genomic region of interest, such that the Cas9 protein makes a double-stranded break at the desired location[626,637,638] (Figure 3.1). This synthesized RNA is referred to as a guide RNA (gRNA). In the CRISPR/Cas9 system used in this study, gRNAs are cloned into the same expression plasmid used to express Cas9, such that the gRNA and Cas9 protein can be produced by a single vector (a plasmid map of pSpCas9(BB)-2A-GFP is included in Appendix 3).

Transfection of such a plasmid into cells can be expected to induce DNA damage that will be repaired by NHEJ, leading to insertion or deletion mutations, and potentially gene knockout. Alternatively, these plasmids can be co-transfected with a single-stranded DNA molecule with a sequence that is complementary to the regions spanning the site of DNA damage, such that repair is carried out by HDR. By incorporating a limited number of nucleotide differences between this DNA molecule and the

genomic region being targeted, specific mutations can be introduced. These two approaches are represented in Figure 3.1.

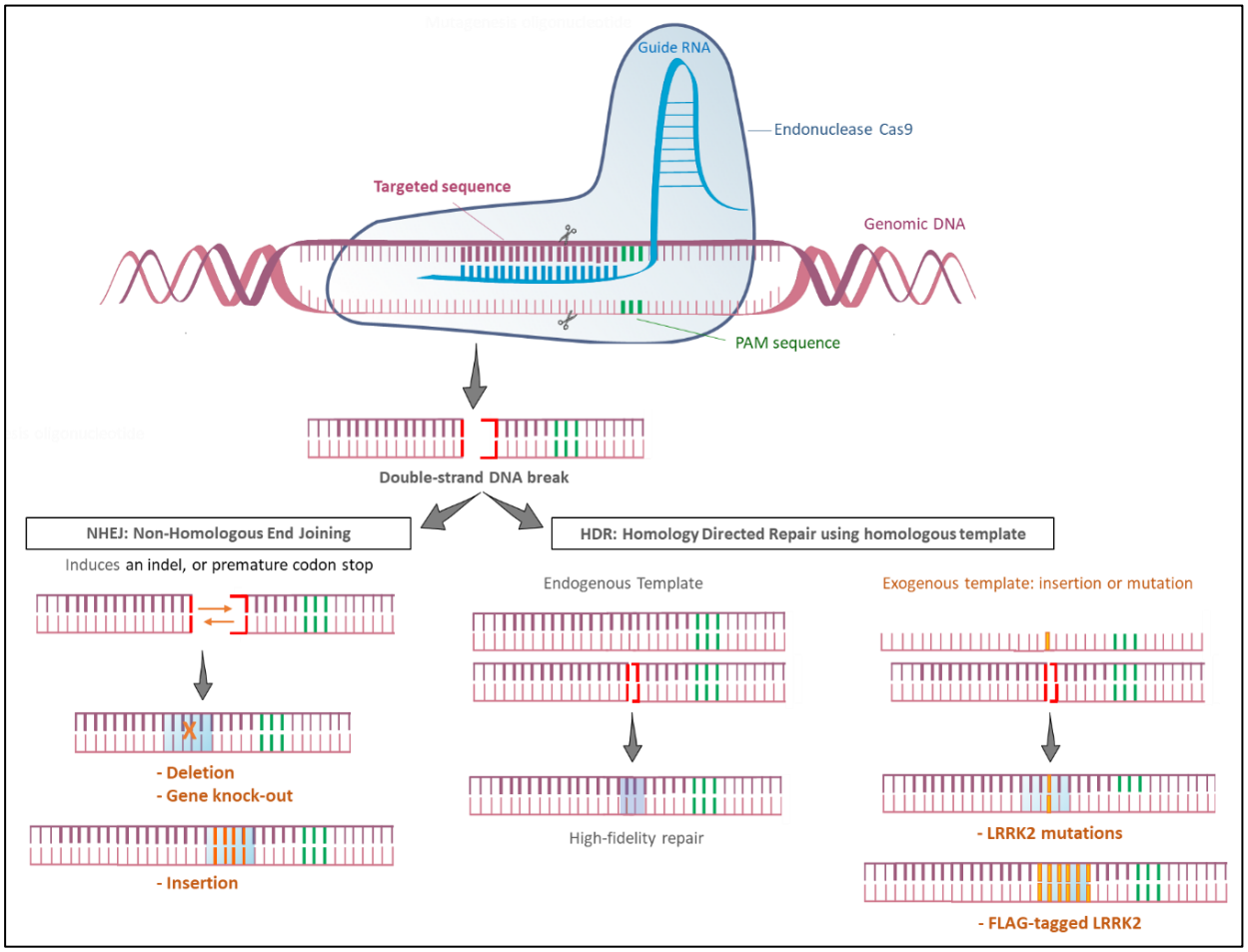

Figure 3.1: Genome editing with CRISPR/Cas9 and DNA repair mechanisms

The CRISPR/Cas9 technology combines the endonuclease Cas9 with a designed non-coding RNAs. Cas9 is guided by an RNA scaffold containing a 20nt sequence complementary to the targeted sequence. The target sequence must be immediately upstream of a protospacer adjacent motif (PAM). Cas9 creates a double-strand break in the genomic DNA at the specified location. The damaged strands can either be repaired by a default DNA-repair mechanism (NHEJ) or via a high-fidelity mechanism. NHEJ (non-homologous end joining repair) ligates the two ends together, sometimes correctly but often incorrectly, introducing insertions or deletions, which are liable to corrupt the gene causing loss-of-function (knockout) or frameshifts. The alternative, HDR (homology directed repair), is a high-fidelity mechanism and uses a homologous DNA molecule as a repair template to restore the original DNA sequence through homologous recombination. Standard repair by HDR is depicted in the middle. However (on the right), providing an artificial template containing a mutation will allow the introduction of this mutation into the repaired sequence. Here, in the context of LRRK2, *LRRK2* mutations can be introduced which will produce LRRK2 mutant proteins, or a FLAG sequence that will produce FLAG-tagged LRRK2 proteins.

In the following Sections, the efforts made to establish optimal conditions to generate cell lines carrying *LRRK2* mutations will be discussed, as well as the methods to evaluate the efficiency of genome editing using CRISPR/Cas9 plasmids.

3.2 Overview of the experimental strategy used in this project

Ultimately, the goal of the work in this Chapter is to produce ReN VM cells containing the described mutations within *LRRK2.* However, this was not expected to be easy to achieve, so the project was broken down into several steps, as outlined in Figure 3.2.

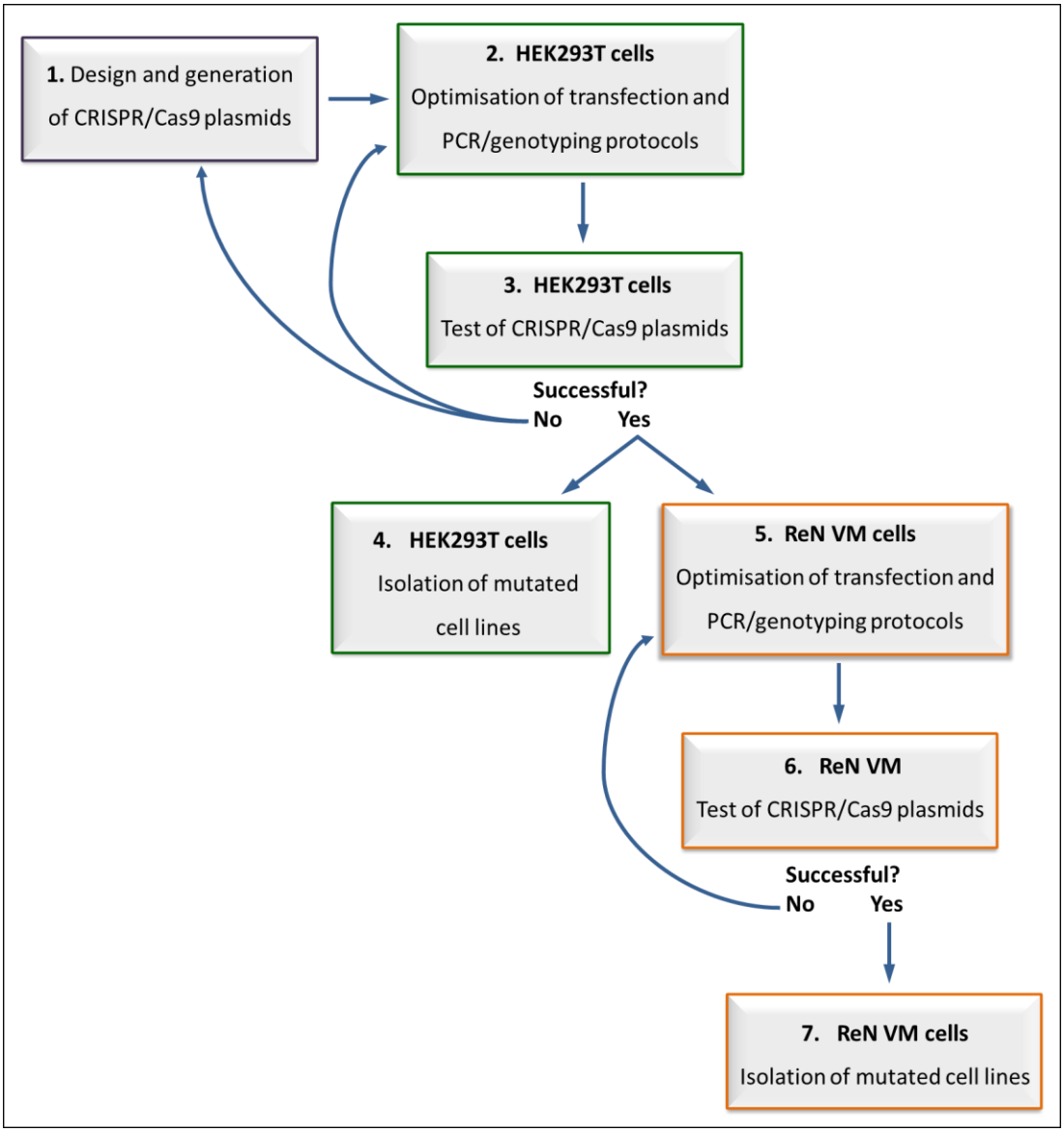

Figure 3.2: Overview of the workflow employed in the creation of genome edited ReN VM cells

As depicted in the Figure, the workflow was designed so that following the design and generation of the CRISPRS/Cas9 plasmids (Figure 3.2, step 1), but before combining them with synthetic oligonucleotides to introduce specific mutations in Ren VM cells, the CRISPR/Cas9 plasmids would first be tested to ensure that they are able to efficiently cause DNA damage at the correct DNA loci.

However, since neural stem cells are typically hard to transfect, it was considered judicious to perform these experiments in a more easily transfectable cell line. Thus, the initial experiments that are detailed in the next Sections of this Chapter were designed to be performed in HEK293T cells. Importantly, this work includes optimisation steps (both to the cell transfection and genotyping PCR protocols), so that the CRISPR/Cas9 plasmids would have the greatest chance of working and so that any resulting mutations could be efficiently identified (Figure 3.2 step 2).

Following this optimisation phase, the next step was designed to determine whether the transfected cells, or at least a significant portion, have been edited. To do so, genomic DNA from transfected HEK293T cells would be analysed using a genotyping PCR followed by DNA sequencing method (Figure 3.2 step 3). In the case where editing is validated, the mutated HEK293T cells could be isolated and allowed to undergo clonal expansion (Figure 3.2 step 4). Although the principal objective of this project is to create genome edited ReN VM cells, HEK293T cells containing germline *LRRK2* mutations would still be useful experimental tools in their own right. Should these test experiments fail, further optimisation could be performed prior to subsequent attempts to use the CRISPR/Cas9 plasmids, or alternatively, new plasmids targeting different sequences within *LRRK2* could be designed and synthesised.

Should the CRISPR/Cas9 plasmids work in HEK293T cells, the next step would be to transfer work to ReN VM cells. Since it cannot be assumed that the optimal transfection and PCR conditions in this cell line will be identical to those in HEK293T cells, analogous optimisation experiments would first be performed (Figure 3.2, step 5). Once these have been established, the CRISPR/Cas9 reagents would then be combined with the mutagenesis oligonucleotides in order to introduce *LRRK2* mutations into ReN VM cells (Figure 3.2 step 6), with successful mutagenesis identified by the same PCR and DNA sequencing approach. At this point, cells containing the desired mutations could be isolated and allowed to undergo clonal expansion (Figure 3.2 step 7), prior to storage for subsequent experimentation.

3.3 Results

3.3.1 Transfection of CRISPR/Cas9 plasmids into cells

CRISPR/Cas9 technology is more likely to be successful if plasmids are introduced into cells with a high efficiency transfection, and a transfection efficiency of 60 to 80% can be expected in HEK293T cells. Two CRISPR/Cas9 plasmids, containing the START (FLAG-tag) or the GS (G2019S) mutations, were thus co-transfected with the empty pUC18 plasmid (as carrier DNA) in initial transfection experiments in HEK293T cells. These initial experimental conditions were based on parameters used by others in the laboratory to successfully introduce *NGLY1* mutations into HEK293T cells using this same CRISPR/Cas9 system (Sarah Needs, Daniel Berwick and Sarah Allman, personal communication). The cells were observed under the fluorescence microscope after a period of two days, and the transfection efficiencies determined (see Chapter 2 Section 2.3.3 for more details on the method).

Surprisingly, transfection efficiencies were not as high as expected (Figure 3.3), and groups of detached cells were noticed (images not shown). In addition, cells appeared confluent in some conditions, whereas a lower number of cells was observed in other wells. Interestingly, more cells appeared green in the latter.

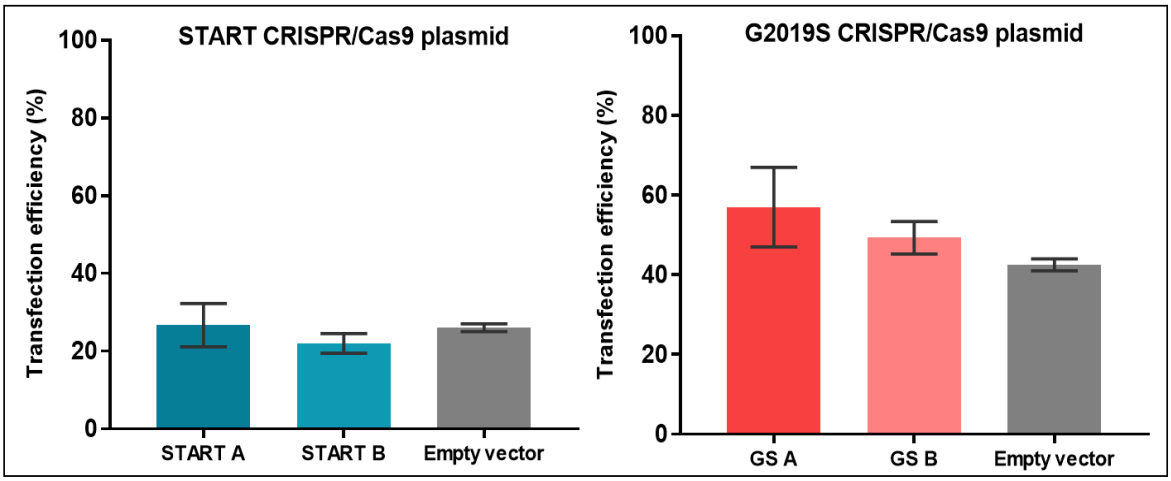

Figure 3.3: Initial transfection efficiencies of START and GS CRISPR/Cas9 plasmids in HEK293T cells.

HEK293T cells were co-transfected with an empty plasmid pUC18 and with CRISPR/Cas9 plasmids containing the START (FLAG-tag) or the GS (G2019S) mutation and co-expressing GFP. Cells were observed by fluorescence microscopy two days after transfection and 2-3 representative images from the same well were captured under the green and the bright field channels. The percentage is the number of green cells compared to the total number of cells in the field, multiplied by 100, which indicates the transfection efficiency. The values are the mean percentages (± SEM) obtained in each condition, n=3.

Since the transfection efficiencies were low, the next step was to investigate whether a smaller number of cells (i.e., lower cell concentration) provided a better transfection efficiency and fewer detached cells. To do so, different numbers of cells were seeded in each well to determine the variation of transfection efficiency according to the cell concentration in comparison to the seeding of 200 000 cells per well that was recommended by the jetPEI manufacturer protocol. Cells were co-transfected with the empty plasmid pUC18 and with the CRISPR/Cas9 plasmid containing the START (FLAG-tag) mutation co-expressing GFP, and the transfection efficiencies were then quantified two days after (Figure 3.4).

Under these conditions, although decreasing the number of cells did not improve the transfection efficiency in this experiment (Figure 3.4), fewer detached cells were observed at the lower cell concentrations (images not shown). Therefore, it was decided to seed approximately 50 000 cells for future experiments.

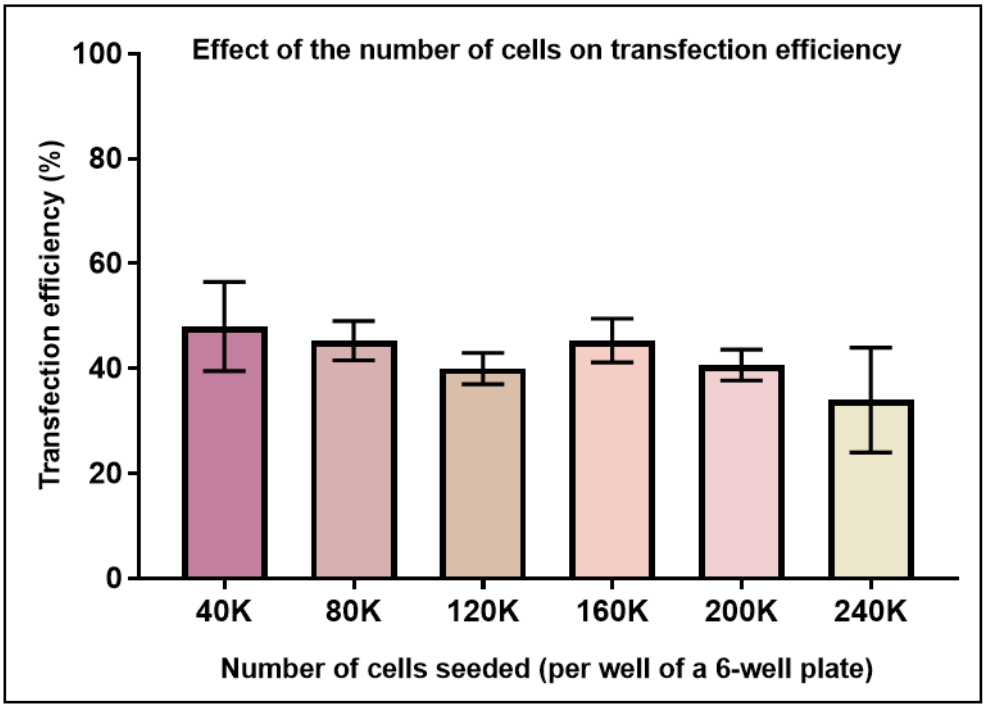

Figure 3.4: Transfection efficiencies in HEK293T cells seeded at different concentration.

Cells were co-transfected with an empty pUC18 plasmid and with the CRISPR/Cas9 plasmid containing the START (FLAG-tag) mutation co-expressing GFP to determine the variation of transfection efficiency according to the cell concentration. Cells were observed by fluorescence microscopy two days after transfection. The values are the mean (± SEM) percentages obtained from 2-3 images captured from the same well under the green and the bright field channels. An average of 178 cells were counted in each image in each condition. The percentage is the number of green cells compared to the total amount of cells in the field of n=1 experiment, which indicates the transfection efficiency. Fewer floating cells were observed with the lower cell concentrations (images not shown) compared to the higher concentrations.

In addition to reducing the number of cells, two important changes were made for the next experiments. Firstly, the method to count cells was shifted from an experimenter-eye based count to the use of a TALI™ cytometer to evaluate transfection efficiency. This allowed a more precise and unbiased estimation (see Chapter 2 Section 2.3.3 for more details). Secondly, the transfection conditions recommended by the manufacturer were further adapted by increasing the transfection period from two days to three, since this would allow increased time for GFP expression. All CRISPR/Cas9 plasmids were tested under these conditions, and the transfection efficiencies are shown in Figure 3.5.

Albeit with the caveat that a different method of quantification was performed, the combination of a lower number of cells and three days of transfection improved the results (Figure 3.5) as transfection efficiencies were in a range of 60 to 80%, confirming that these conditions worked better. As such, the adapted transfection parameters allowed the expected transfection efficiencies to be met.

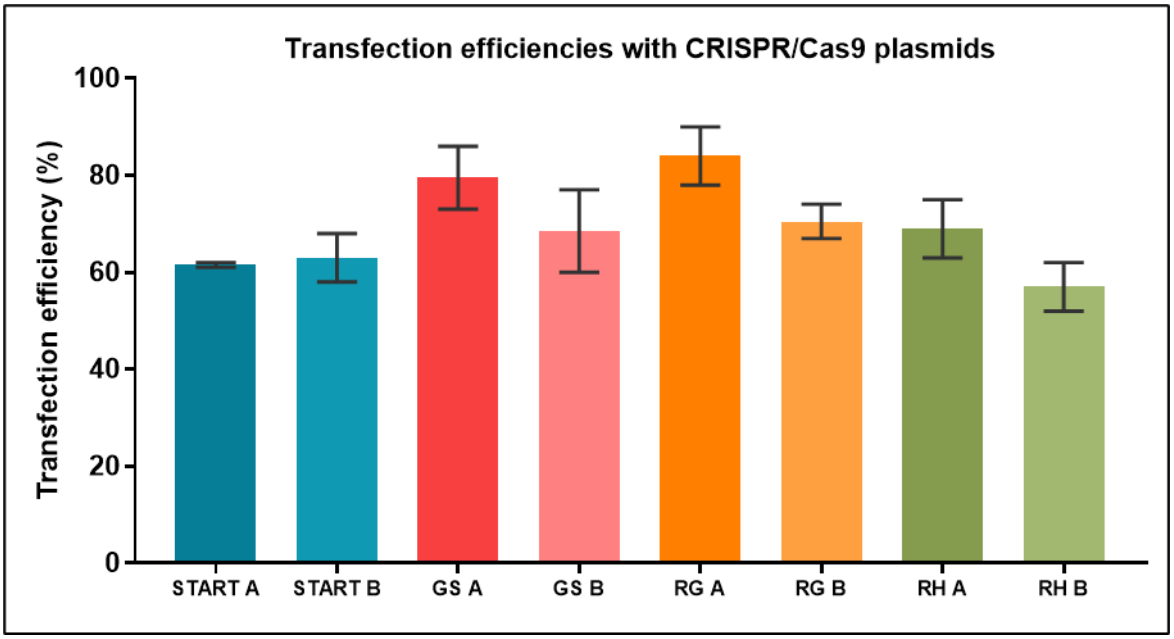

Figure 3.5: Improved transfection with 50 000 cells seeded and a transfection period of three days.

HEK293T cells were co-transfected with an empty plasmid pUC18 and with CRISPR/Cas9 plasmids containing the START (FLAG-tag), GS (G2019S), RG (R1441G), or the RH (R1398H) mutations (both the A and B plasmids) and co-expressing GFP. Cells were observed using the Tali™ cytometer device 3 days after transfection and images were captured with green and bright field channels. For each condition, 13 images were taken, and the data correspond to the average (± SEM) of n=2 repeats. The percentage is the number of green cells compared to the total number of cells in the field, which indicates the transfection efficiency.

3.3.2 Genotyping PCR assays

Successful transfection of CRISPR/Cas9 plasmids into HEK293T cells is likely to produce a heterogeneous population containing a variety of different insertion and deletion mutations at the cut site (deletions of different length and insertions of different lengths and base sequence), whilst even a highly successful transfection can be expected to leave some unmutated *LRRK2*. In principle, the PCR and sequencing method allows for the verification of the presence or absence of mutations in the region of interest, thereby indicating whether the CRISPR/Cas9 plasmids were efficiently able to cause DNA damage at the correct DNA loci.

As such, four sets of genotyping primers were designed by Dr Daniel Berwick, each possessing a complementary sequence to regions either side of each DNA region of interest within *LRRK2,* corresponding to the START, G2019S, R1441G and R1398H mutations. However, before this could be achieved, the PCR conditions for each pair of primers were first optimised using genomic DNA from untransfected HEK293T cells, to assess whether the primers are able to amplify the correct sequence surrounding the mutation sites.

3.3.2.1 Initial PCR assays

To determine the PCR conditions and test the sets of genotyping primers, PCRs were performed using genomic DNA from untransfected cells. If the PCR is successful and the primers work, each primer pair should produce a band of approximately 400 base pairs that should be observable on an agarose gel. Preliminary data obtained in the lab indicated that the four sets of primers were efficient in PCRs using genomic DNA from SHSY5Y cells at an annealing temperature of 60°C using HiFi polymerase (Kapa Biosystem). Therefore, the initial PCR assays were performed under the same conditions. However, the results were inconclusive (Figure 3.6), since various non-specific bands were obtained for each set of primers. This highlighted the need to optimise the PCR parameters for the four sets of primers to increase their specificity.

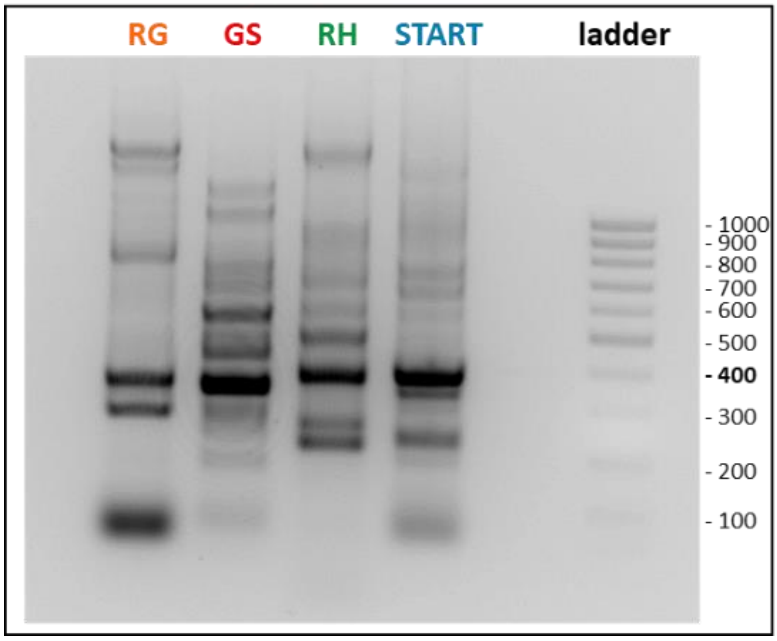

Figure 3.6: Initial experiment to reproduce preliminary data.

Representative agarose gel electrophoresis results of PCR products analysis. The PCR was performed using the HiFi polymerase with the four sets of primers (START: FLAG-tag, GS: G2019S, RG: R1441G, and RH: R1398H, as indicated on top of each lane) with SH-SY5Y genomic DNA. The temperature of the annealing step of the PCR program was set at 60°C. Similar to the preliminary result obtained in the lab, non-specific bands were also obtained.

3.3.2.2 Optimisation of the PCR assay

To optimise the genotyping PCRs, different conditions were tested, in which one or several parameters were modified; all the different PCR programs tested are summarised in Appendix 4. Notably, many different annealing temperatures were tested. The efforts to establish optimal PCR conditions are detailed in the following sections.

3.3.2.2.1 Decreasing the elongation step did not improve PCR results

Since the primary goal was to eliminate the non-specific bands, one of the first parameters modified was the elongation step. In theory, decreasing the time allowed for the elongation step of the PCR could improve the results by preventing the amplification of larger non-specific PCR products. As such, the duration of the elongation step was reduced from 30 seconds to 15 seconds. However, as depicted in Figure 3.7, this modification was not found to improve the results and non-specific bands were still obtained.

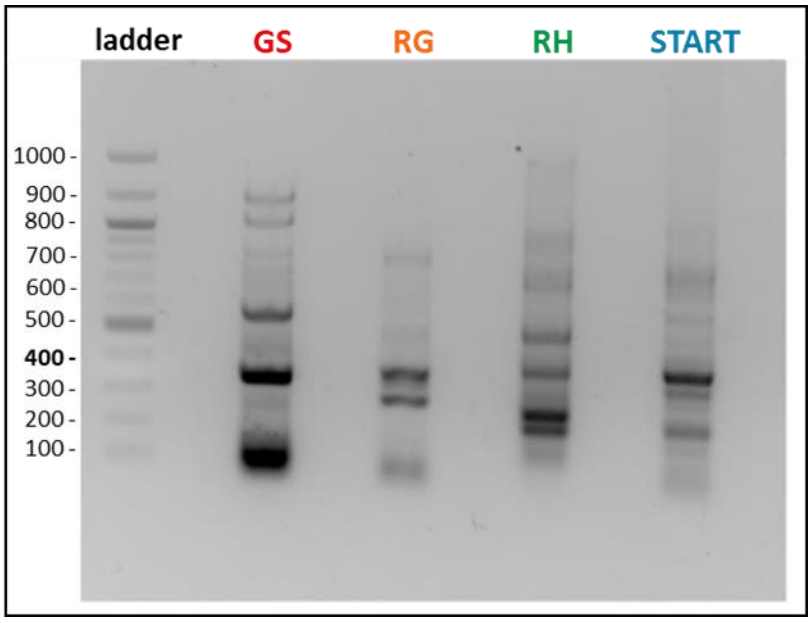

Figure 3.7: Decreasing the duration of the elongation step did not reduce non-specific bands.

Representative agarose gel electrophoresis results of PCR products analysis. The PCR was performed using the HiFi polymerase with the four sets of primers (START: FLAG-tag, GS: G2019S, RG: R1441G, and RH: R1398H, as indicated on top of each lane) with SH-SY5Y genomic DNA. The elongation step of the PCR program was set at 72°C for 15 seconds. Similar to the previous result, non-specific bands were also obtained.

For consistency with experiments optimising CRISPR/Cas9 transfections in HEK293T cells, HEK293T genomic DNA was used to optimise the PCRs parameters from this point forward. Additionally, it was also decided to focus on the START primers. Furthermore, to address the possibility that the primers may have degraded, replacement primers were purchased. Aside from testing different PCR parameters, other ways to improve the PCR outcomes were explored, and are detailed in the sections below.

3.3.2.2.2 Boiling genomic DNA but not adding DMSO improves PCR results

As the PCR results obtained were poorly reproducible, another supposition involved the proteinase K used in the genomic DNA extraction kit, which might degrade the DNA polymerase during the PCR. To solve this potential issue, genomic DNA samples extracted from HEK293T were boiled at 95°C for 10 minutes (in a dry bath heating block) to denature any residual proteinase K, prior to being used in PCR assays.

In addition, the use of DMSO was also considered. Typically, DMSO is a compound that can be added to the PCR mix when the target sequence is located in a GC-rich region to bind DNA and induce a

conformation change which helps primer annealing. As such, the presence of this compound in PCR reactions was also tested.

In this experiment, both the addition of a 95°C denaturation step and the presence of DMSO in the PCR mixtures were tested. PCRs were performed using the HiFi polymerase with the START primers using HEK293T genomic DNA that was either boiled beforehand or left untreated, and in presence or absence of DMSO (5% (v/v) of total volume). Perhaps surprisingly, PCR products were visible when no DMSO was included, but not when PCRs were performed in the presence of this compound, indicating that DMSO is inhibitory to these reactions (Figure 3.8). However, boiling the genomic DNA samples was clearly beneficial, since, in reactions performed without DMSO, there was more PCR product produced from genomic DNA samples that had been boiled beforehand (Figure 3.8). These results thus indicate that DMSO did not improve the PCR results, whereas boiling the genomic DNA prior to adding it to the PCR mix was beneficial. Nevertheless, genotyping PCRs continued to be poorly reproducible, indicating that additional optimisation of the PCR conditions was required.

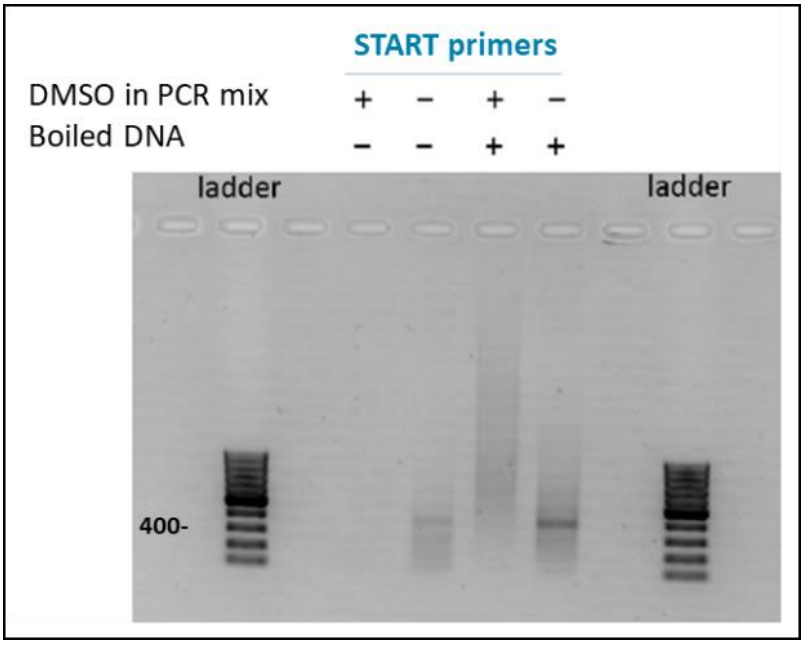

Figure 3.8: Boiling the genomic DNA and omitting DMSO improve the PCR reaction

Representative agarose gel electrophoresis results of PCR products analysis. The PCR was performed using the HiFi polymerase with the START primers (START: FLAG-tag) using HEK293T genomic DNA. As indicated on top of each lane, the genomic DNA was boiled (at 95°C for 10 minutes) or not prior to being added to the PCR mix, and DMSO (5% (v/v) of total volume) was added to or omitted from the PCR mix. Bands at 400 base pairs can only be seen when DMSO was omitted from the reaction mixture, but this PCR product is markedly fainter when using genomic DNA that was not boiled.

3.3.2.2.3 Phusion polymerase appears to improve PCR results

Given that the genotyping PCR reactions needed further optimisation, the next step was to investigate the polymerase enzyme. Therefore, two other polymerases, Phusion (Thermo Scientific) and Robust (Kapa Biosystem), were used alongside the HiFi polymerase in experiments using the START primer set and two genomic DNA samples from HEK293T cells.

Reflecting the previous poor reproducibility, no band was observed when the HiFi polymerase was used (Figure 3.9 A). However, the electrophoresis gels obtained suggested that the Phusion polymerase provided better results than the two other polymerases, since a band at the expected size was observed with both genomic DNA samples. A confirmation experiment just comparing Robust and Phusion provided a similar result (Figure 3.9 B). Therefore, the Phusion polymerase was used from this point forward.

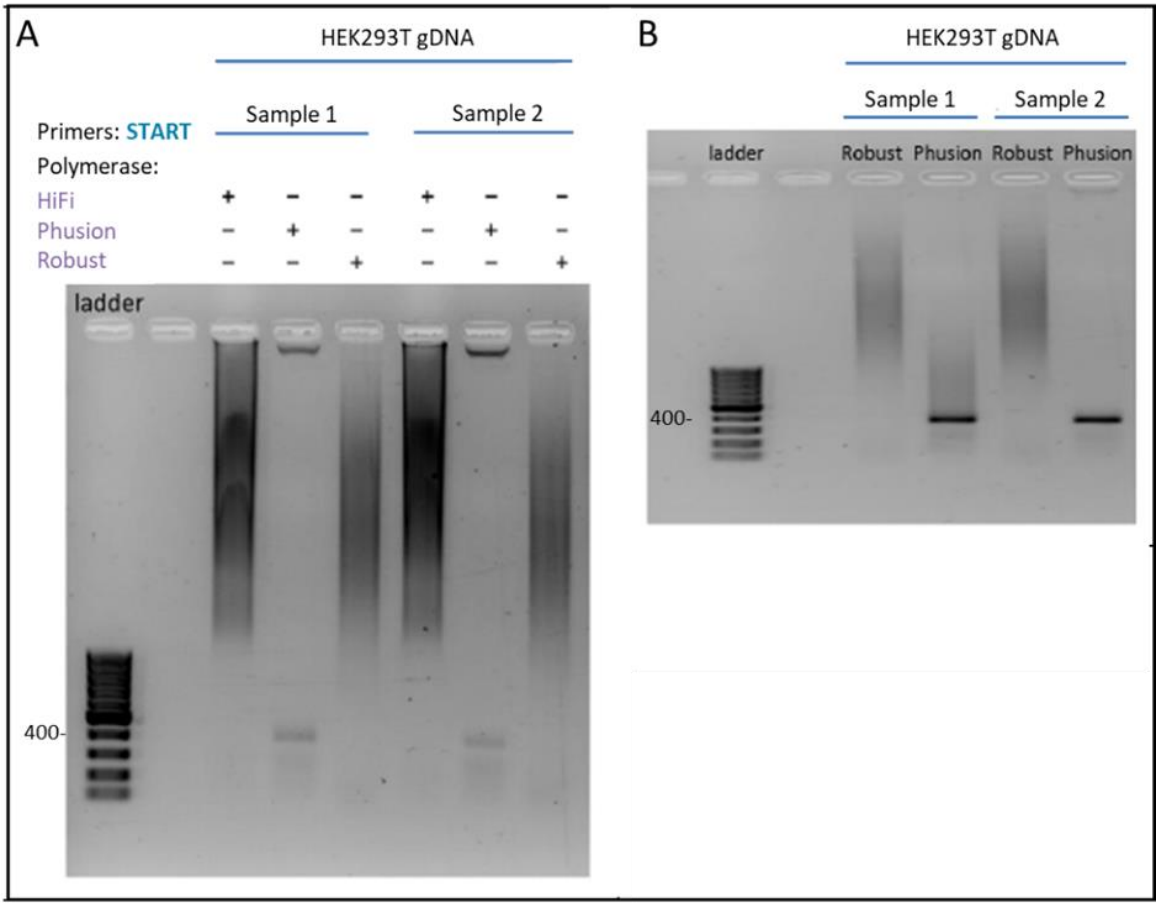

Figure 3.9: Phusion polymerase provided better results with the START primers than Kapa HiFi polymerase

Representative agarose gel electrophoresis results. PCR was performed using three different polymerases (HiFi, Phusion, and Robust, as indicated on top of each lane) with the START primers set (START: FLAG-tag) using two genomic DNA samples from HEK293T cells. A) Comparison of the three polymerases. B) Comparison between Robust and Phusion. In both panels, a band at 400 base pairs was observed only when the Phusion polymerase was used for the PCR.

3.3.2.2.4 Final optimisation

The previous PCR-related results described in this Chapter indicated that the addition of a DNA-boiling step and the use of the Phusion polymerase improved the PCR results using the START primers. Thus, the annealing temperature was then optimised for the other three sets of primers using the same parameters. In these conditions and using HEK293T genomic DNA, the RH and RG primers worked effectively at an annealing temperature of 60°C (Figure 3.10). However, exact conditions under which the GS and START primers worked reliably in every experiment were not found. Nevertheless, the GS primers appeared to work best at an annealing temperature of 60°C, and the START primers at an annealing temperature of 66°C (Figure 3.10).

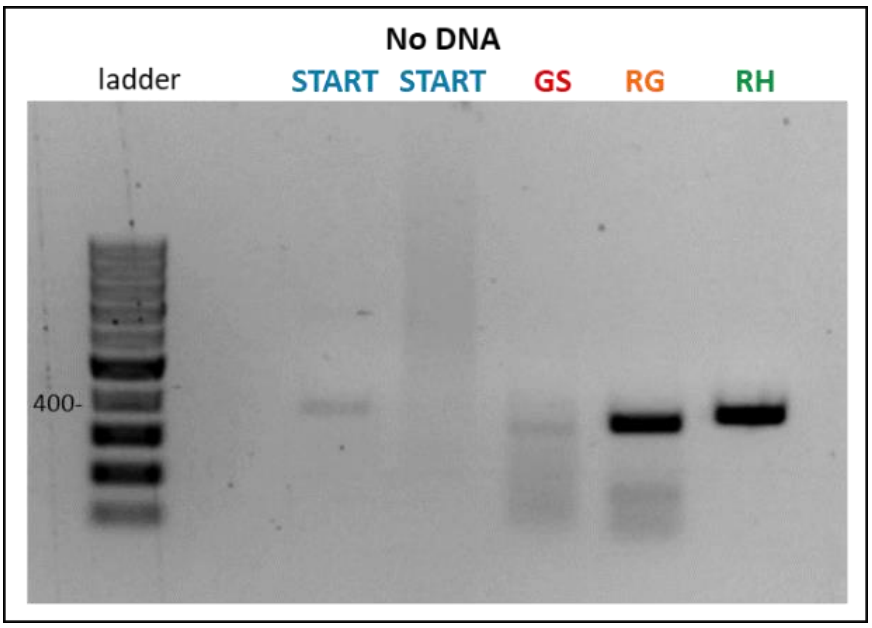

Figure 3.10: Representative gel obtained after a PCR with genomic DNA from HEK293T cells.

Representative agarose gel electrophoresis results of PCR products analysis. The PCR was performed using the Phusion polymerase with the four sets of primers (START: FLAG-tag, GS: G2019S, RG: R1441G, and RH: R1398H, as indicated on top of each lane) with HEK293T genomic DNA. The temperature of the annealing step of the PCR program was set at 66°C (for START primers) or 60°C (for GS, RG and RH primers). "no DNA START" is a negative control where the PCR was performed using the START set of primers without genomic DNA sample. Bands can be observed for each set of primers; the primers GS, RG and RH work with a 60°C annealing temperature, and START with a 66°C annealing temperature.

Given that the four sets of primers and the CRISPR/Cas9 reagents appeared to work in HEK293T cells in these optimised conditions, albeit to varying degrees, the primers were then tested in PCRs with genomic DNA extracted from ReN VM cells, to determine whether they are able to amplify the correct sequence

surrounding the mutation sites in the ReN VM cell type or whether they needed to be redesigned. Since three out of the four sets of primers appeared to work at an annealing temperature of 60°C with HEK293T DNA, all four primer pairs were tested at this temperature in initial experiments with ReN VM DNA.

Consistent with the results obtained in Figure 3.10, Figure 3.11 shows that all four sets of primers worked at an annealing temperature of 60°C, as bands at the expected base pair size could be observed. This indicated that the primers are also efficient in this specific cell type and do not need to be redesigned, but also that no further PCR optimisation appeared to be needed.

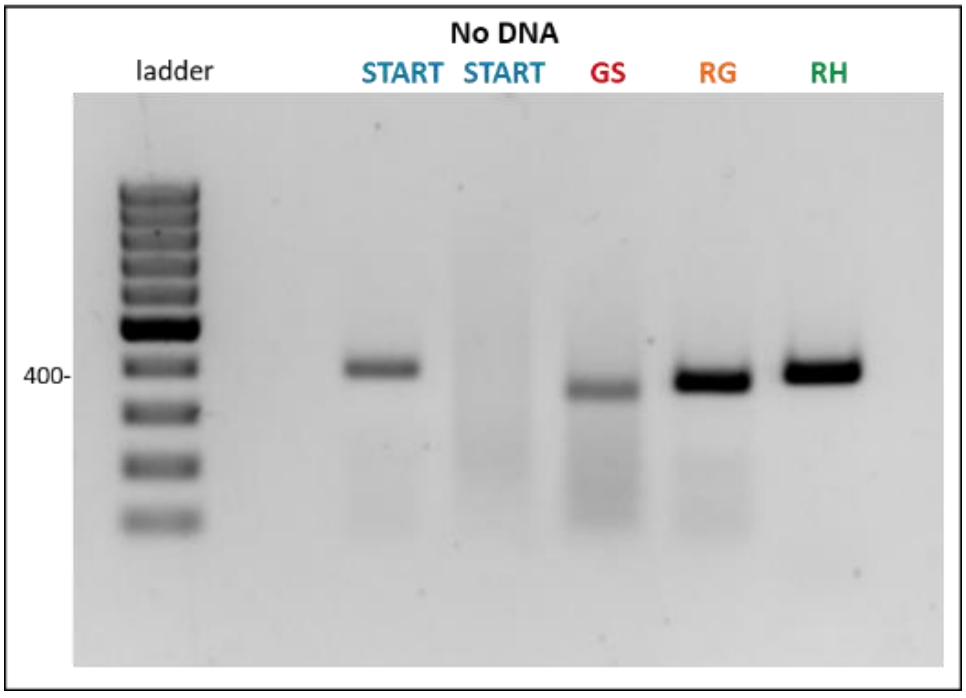

Figure 3.11: Representative gel obtained after a PCR with genomic DNA from ReN VM cells.

Representative agarose gel electrophoresis results of PCR product analysis. The PCR was performed using the Phusion polymerase with the four sets of primers (START: FLAG-tag, GS: G2019S, RG: R1441G, and RH: R1398H, as indicated on top of each lane) with ReN VM genomic DNA. The temperature of the annealing step of the PCR program was set at 60°C. "no DNA START" is a negative control where the PCR was performed using the START set of primers without genomic DNA sample. Bands can be observed for each set of primers, and the four sets of primers work with a 60°C annealing temperature.

3.3.3 Testing of CRISPR/Cas9 plasmids in HEK293T cells

Following this optimisation phase, the next step was to assess the efficiency of genome cutting caused by each CRISPR/Cas9 plasmid in HEK293T cells. To this end, genomic DNA extracted from transfected cells was used in PCR assays, and the PCR amplification products were then analysed by sequencing, which provides chromatograms that allow for the detection of any disruption in the DNA sequence.

Surprisingly, for all eight of the CRISPR/Cas9 plasmids, none of the chromatograms displayed a discordant signal that would be consistent with DNA damage causing insertions or deletions, as summarised in Table 3.1 and depicted in representative chromatograms in Figure 3.12 and Figure 3.13. However, the sequencing reads were not of sufficient quality to be usable in some cases (Table 3.1, START B and G2019S B). These results indicate that despite reaching transfection efficiencies that maximise the chance of the CRISPR/Cas9 plasmids working, none of the cells appeared to have been mutated.

Table 3.1: Summary of the testing of the CRISPR/Cas9 plasmids in HEK293T cells.

Mutation type	Plasmid	Transfection efficiency (on average)	Sequencing trials	Chromatograms	
START (FLAG-tag)	A	61%	9 trials	No cut, readable sequence across the putative cut site	Figure 3.12
	B	68%	8 trials	None of the reads were of sufficient quality to be usable	-
G2019S	A	86%	7 trials	No cut, readable sequence across the putative cut site	Figure 3.12
	B	77%	5 trials	None of the reads were of sufficient quality to be usable	-
R1441G	A	84%	5 trials	No cut, readable sequence across the putative cut site	Figure 3.13
	B	70%	5 trials		-
R1398H	A	75%	5 trials		Figure 3.13
	B	62%	3 trials		-

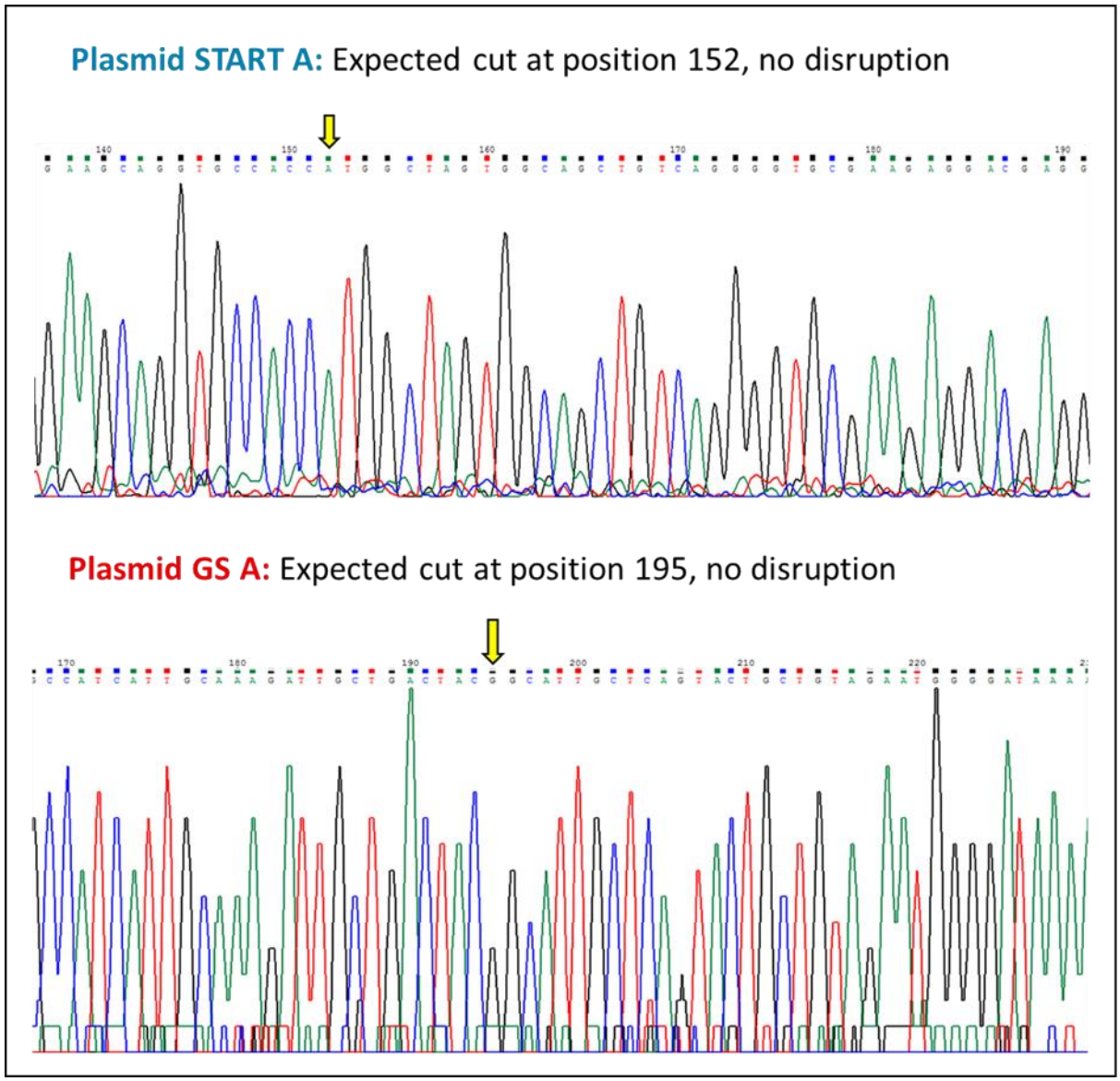

Figure 3.12: Representative chromatograms from sequencing of the genomic DNA of HEK293T cells transfected with CRISPR/Cas9 plasmids showing the absence genomic mutations in *LRRK2*

Image shows the sequence of genomic DNA from transfected cells at the predicted cut site, which is indicated with a yellow arrow.

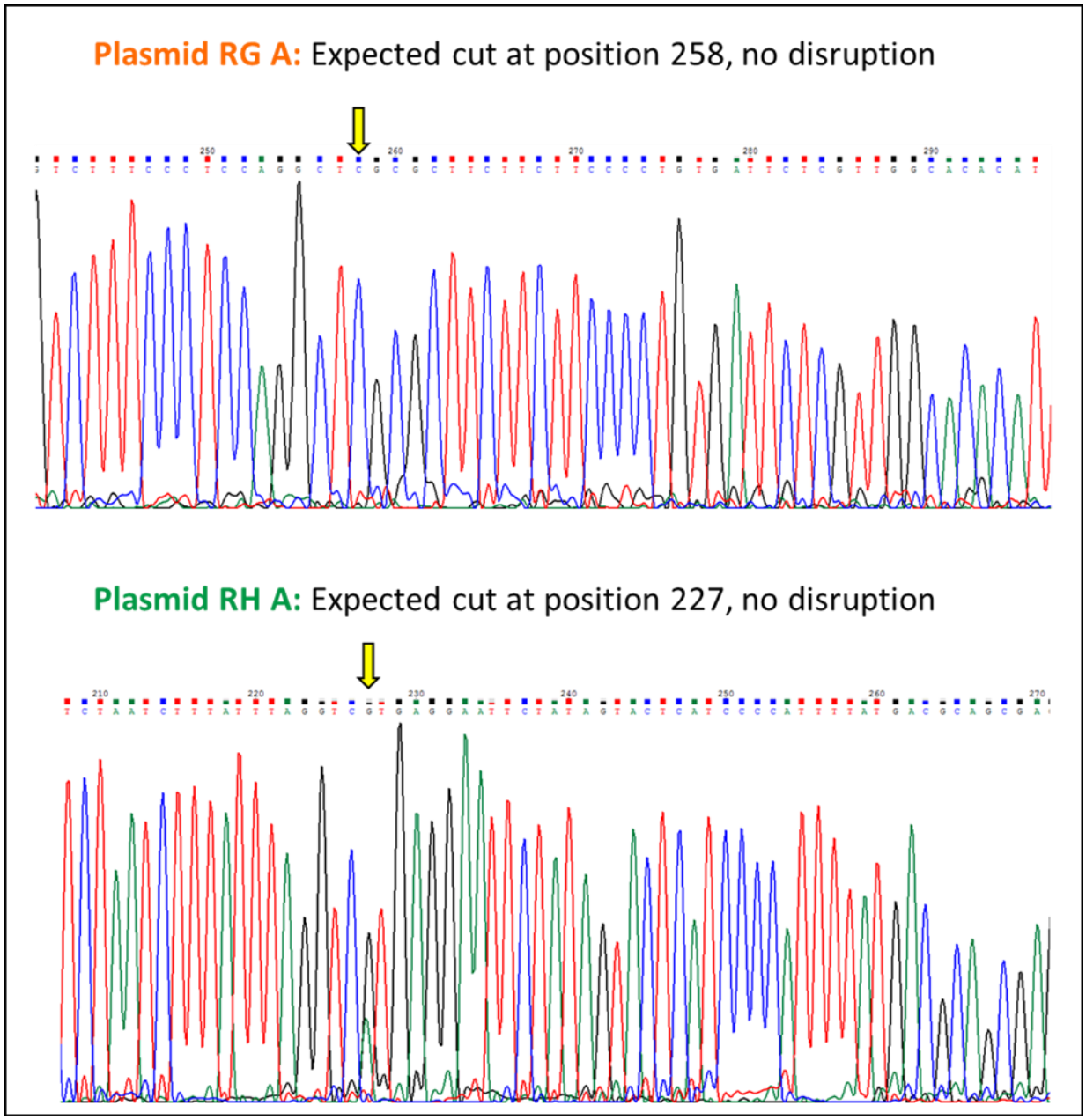

Figure 3.13: Figure 3.12 continued

Image shows the sequence of genomic DNA from transfected cells at the predicted cut site, which is indicated with a yellow arrow.

Thus, despite numerous attempts following thorough optimisation, none of the CRISPR/Cas9 plasmids showed any evidence of being able to elicit double-stranded DNA breaks in *LRRK2* in HEK293T cells. Given the time constraints of a PhD, it was decided to move the project to studying LRRK2 in autophagy and calcium signalling using conventional transient transfection and pharmacological inhibition, rather than designing new CRISPR reagents and risking more lost time.

3.4 Discussion

This Chapter describes the strategy and steps towards creating new human cellular models using CRISPR/Cas9 technology, with the aim of uncovering the role of LRRK2 in PD pathogenesis by comparing the effects of *LRRK2* mutations in isogenic wild-type and mutant cells.

In particular, this Chapter presented the optimisation and testing of CRISPR reagents used to induce genome editing in cell lines, especially the efficacy of delivery of the CRISPR/Cas9 plasmids into cells and the measure of their efficiency using PCR and DNA sequencing. A discussion of the results and an outline of possible future plans related to this work are described below.

3.4.1 Transfection optimisation

In view of the fact that the first transfections performed in HEK293T cells were not meeting the expected efficiency of 60-80%, the conditions recommended by the manufacturer were adapted by decreasing the number of cells and increasing the time of transfection to three days which improved transfection efficiencies to 60-80% (Figure 3.5). Although there was still some variability in transfection efficiency, this limitation was manageable, as transfection efficiency could be determined within three days, so experiments with low efficiency could be aborted and repeated quickly.

3.4.2 PCR optimisation

Optimisation of PCR conditions required multiple trials. Modifying the length of the elongation step, the number of cycles, or adding DMSO to the PCR mix did not ameliorate the results. However, results were improved by boiling genomic DNA samples after extraction to denature residual proteinase K, and by switching to Phusion polymerase (Figure 3.8 and Figure 3.9). The best PCR protocols were n°9 and n°11 (Appendix 4). In these conditions, all the sets of primers worked at an annealing temperature of 60°C in ReN VM cells, and the START primers worked at an annealing temperature of 66°C and the GS, RG and RH primers at 60°C in HEK293T cells. This discrepancy for the START primers suggests a cell-type

specificity, for example that the sequence or chromosomal structure targeted by the START genotyping primers might be slightly different between the cell types.

Importantly also, the primers did not need to be redesigned as the four sets of primers worked in all three cell types, HEK293T (Figure 3.10), SH-SY5Y (data not shown) and ReN VM (Figure 3.11). Furthermore, sequencing of PCR products generated from untransfected cells (data not shown) confirmed that all the products were correct, and that there was no difference between the genomic sequences in our cell lines compared to the reference sequence to which the CRISPR/Cas9 plasmid guide RNAs were designed. Thus, the issues with PCR optimisation seemed resolved.

3.4.3 Testing CRISPR/Cas9 plasmids in HEK293T cells

The strategy presented in this Chapter has been successful in the lab before to introduce a mutation in the *NGLY1* gene (Sarah Needs, Sarah Allman and Daniel Berwick, personal communication). Nevertheless, all the attempts to use the CRISPR plasmids to cause DNA damage to the *LRRK2* gene in HEK293T cells were unsuccessful. The sequencing results showed no evidence of successful genetic editing in these HEK293T cells (Figure 3.12, Figure 3.13, Table 3.1). A possibility might be that there is only a very low rate of mutation, as to be hardly detectable, although it is also possible that the Cas9 endonuclease just did not cut the DNA. In either scenario, the data suggest difficulties for the Cas9/sgRNA complex to access *LRRK2* to introduce a mutation. This topic will be discussed further in Chapter 6. Additional optimisation of the methods is possible, for example, since GFP was used as a proxy for transfected cells, FACS sorting could be used to select transfected cells and enrich the samples for cells more likely to have been mutated. Nonetheless, given the number of trials attempted, a more realistic next step would be to re-design the sgRNAs.

The work in this Chapter was beset by technical issues in regards to transfection and detection of genome editing. One of the issues encountered was that PCRs with genomic DNA from transfected cells could not be performed reproducibly. This may have been due to the genomic DNA obtained from transfected cells, which may not have been of sufficient quality for PCR and sequencing analysis in some cases. In

addition, the low amount of DNA obtained after gel extraction was also an issue, although various kits were tested, which might explain the obtention of poor-quality reads for PCR products from PCRs using genomic DNA from cells transfected with the START B and G2019S B plasmids. To assess DNA damage and genome editing, an alternative technique to the PCR/sequencing method used in the present study which could have been used is the Surveyor Assay[639]. This technique is based on an endonuclease that recognises a DNA mismatch, and can therefore assess the presence of mutations (insertions/deletions).

3.5 Conclusions

Using the CRISPR/Cas9 technique, the goal was to study the impact of *LRRK2* mutations on cellular pathways. The findings presented in this Chapter show that this technique was unsuccessful in the present study, and isogenic cell lines carrying *LRRK2* mutations to be studied in parallel could not be created.

Because of this, an alternative approach based on the use of LRRK2 enzymatic inhibition and transient overexpression of wild-type and mutant forms of LRRK2 was pursued for the assays exploring the role of LRRK2 in autophagy and calcium signalling that are the focus of Chapter 4 and Chapter 5.

4

Investigations into the role of LRRK2 in autophagy

4.1 Introduction

As mentioned previously (Chapter 1, Section 1.6.2), evidence that LRRK2 plays an important and complex role in the autophagic pathway is accumulating, but whether LRRK2 acts as a positive or negative regulator is controversial. This is due to the existence of a wide range of models, protein expression levels, and protocols used, which together lead to a high variability in the experimental outcomes[142]. There is little doubt that LRRK2 and autophagy are intertwined, but with seemingly cell-type specific effects on the early and late steps of autophagy.

Although the role of LRRK2 in autophagy is not clearly established yet, it is possible to hypothesise that pathogenic *LRRK2* mutations might ultimately lead to neurodegeneration via deregulated autophagy. LRRK2 mutants might impair this process, resulting in the defective clearance of α-synuclein. Since age is the major risk factor for PD, it is worth mentioning that aging leads to impairments in the autophagy-lysosomal pathway[142]. Thus, aging might participate alongside *LRRK2* mutations in preventing α-synuclein clearance through defective autophagy[640].

Various techniques have been used to study, modulate and monitor autophagy and autophagic flux since the middle of the 20th century[328]. The work in this Chapter is largely based around a widespread technique to investigate the formation and processing of autophagosomes, namely the use of cells expressing LC3 proteins tagged with GFP (GFP-LC3). The use of GFP-LC3 allows the visualisation of autophagic vesicles in both living and fixed cells, but in living cells autophagy can also be followed in real-time. LC3 proteins are cytosolic, but are recruited to nascent autophagic vesicles (phagophores) and

remain present on autophagic vesicles throughout the autophagic process. Thus, when viewed on a fluorescent microscope, GFP-tagged LC3 molecules can be seen as both a diffuse staining corresponding to cytosolic protein, and also as bright punctae of a diameter ≤ 1.5 µm that correspond to autophagic vesicles. Quantification of the number of GFP-LC3 punctae per cell can then be used to determine the relative levels of autophagy at any given time, for example basally or following treatment to induce autophagy. The limitation with this technique is that an increased number of GFP-LC3 punctae can reflect either an increase in autophagy or a blockage of the final steps of autophagy causing an accumulation of autophagic vesicles, or a combination of both factors. Thus, well designed GFP-LC3 studies combine the use of specific autophagy inducers, such as PP242, with agents that block the fusion of autophagic vesicles with lysosomes, in particular Bafilomycin A1.

The current chapter investigates the impact of LRRK2 enzymatic activities and LRRK2 pathogenic and protective variants on the autophagic pathway with the aim of gaining insight into the involvement of LRRK2 in this process and in particular, the steps at which it acts. To do so, the LRRK2 kinase and GTPase activities were modulated with pharmacological inhibitors, and the effects of *LRRK2* mutations were investigated by transfection of wild-type and mutant LRRK2 constructs.

Three cell lines were used for the experiments described in this Chapter. The majority of experiments were performed in HEK293 GFP-LC3 cells, since their expression of GFP-LC3 facilitates measurements of autophagy. In addition, HEK293 GFP-LC3 are easily transfectable which means that LRRK2 mutants can be tested by transient transfection. The other two cell lines used were wildtype RAW264.7 macrophages and isogenically matched Lrrk2-knockout RAW264.7 macrophages (referred to as WT macrophages and Lrrk2 KO macrophages, respectively). These paired cell lines were investigated in parallel to assess the impact of the loss of Lrrk2 on autophagy.

4.2 Verification of the experimental conditions for quantifying GFP-LC3 punctae

Prior to using HEK293 GFP-LC3 cells for more detailed experimentation, it was first considered necessary to ensure that changes in the number of GFP-LC3 punctae could be robustly induced and quantified in our system.

To this end, published work using this cell line was consulted, which indicated that one-hour treatment with PP242 at a concentration of 2 μM in normal nutrient-rich media (10% (v/v) FBS) would likely be sufficient for inducing GFP-LC3 punctae. PP242 (also known as Torkinib) is a potent inhibitor of the two mTOR complexes mTORC1 and mTORC2[641]. Since mTORC1 is a negative regulator of autophagy, treatment of cells with PP242 relieves this repression of autophagy, thereby triggering an increase in autophagic vesicle production.

As can be seen in Figure 4.1, PP242 treatment elicited a marked increase in the number of GFP-LC3 punctae compared to DMSO-treated cells. Consequently, these conditions were used in subsequent studies. Confirming their suitability for the study of autophagy in this cell line, when averaged across all experiments presented in this Chapter, HEK293 GFP-LC3 cells had a mean number of 20 GFP-LC3 punctae per cell following treatment, compared to 5 punctae per cell without treatment (i.e., basally).

The conditions chosen for the assay are therefore appropriate to obtain robust differences between the number of GFP-LC3 punctae and allow the distinction between basal and induced autophagy (see Chapter 2 for details on quantification methods).

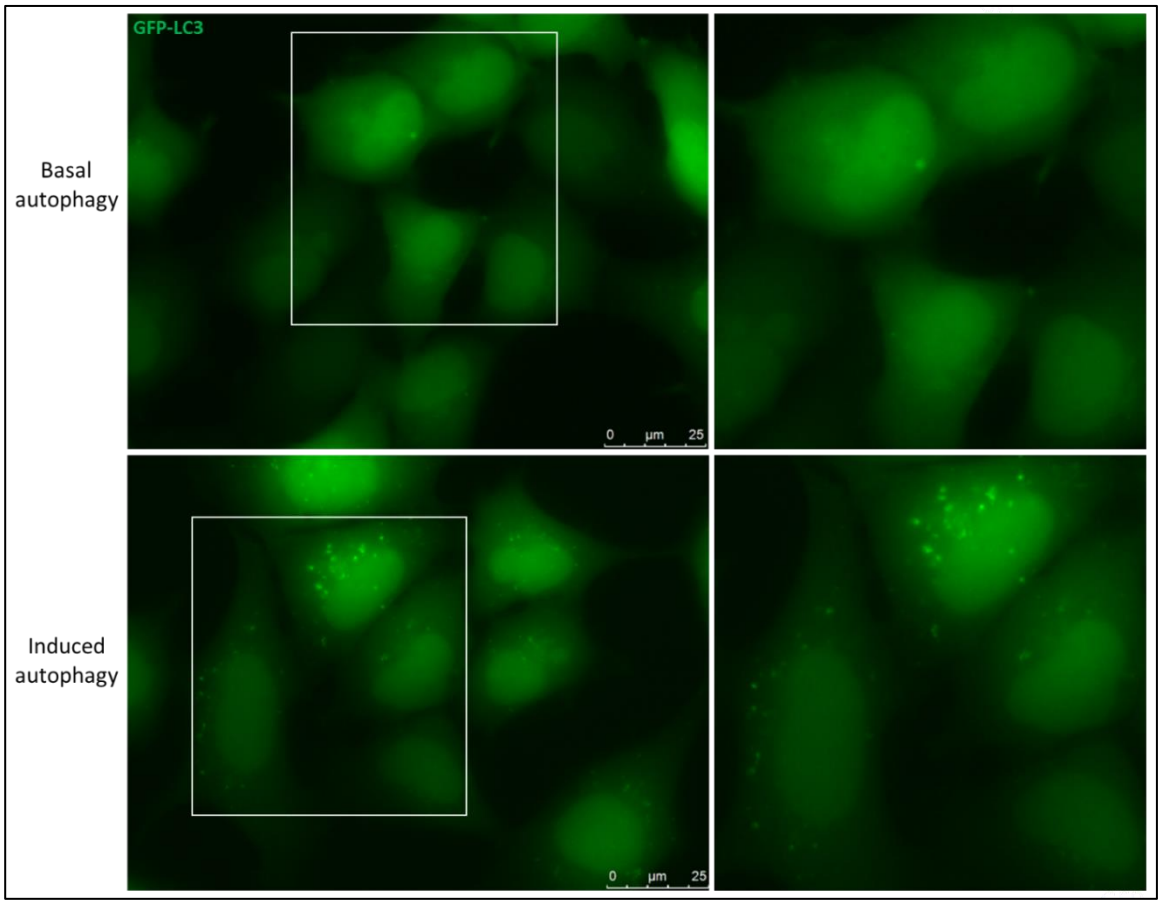

Figure 4.1: Representative images of GFP-LC3 punctae in HEK293 GFP-LC3 cells.

The HEK293 GFP-LC3 cells stably express GFP-LC3 and appear green due to the diffuse distribution of this protein. The diffuse GFP-LC3 distribution represents GPF-LC3 molecules that are not associated with autophagic vesicles. By contrast, the brighter green punctae represent autophagic vesicles. A higher number of punctae are visible in the autophagy-induced condition (PP242 2 µM, 1 hour) compared to unstimulated cells (DMSO, 1:1000 equivalent dilution) with a basal level of autophagy. Images on the left are original images acquired at 63x magnification. Images on the right are enlargements of the indicated areas within the original.

4.3 Effects of LRRK2 inhibitors on autophagy in HEK293 GFP-LC3 cells

Having established conditions to induce autophagy in HEK293 GFP-LC3 cells, the effects of LRRK2 kinase and GTPase inhibitors on basal and PP242-induced autophagy in HEK293 GFP-LC3 cells were explored.

4.3.1 LRRK2 inhibitors used in this thesis

The three different kinase inhibitors and the GTPase inhibitor used are shown in Figure 4.2. Although the three kinase inhibitors are mechanistically similar, their structures are different, so it can be assumed that they will have different off-target activities. Additionally, Hatcher and colleagues[174] have categorised these three kinase inhibitors differently based on their chemistry, i.e. GSK2578215A is an arylbenzamide, GNE-9605 is an aminopyrimidine, and PF-06447475 is a pyrrolopyrimidine. Thus, when combined with the use of a GTPase inhibitor that is both structurally and mechanistically distinct, any effects that are common to all four molecules are almost certainly the consequence of direct targeting of LRRK2.

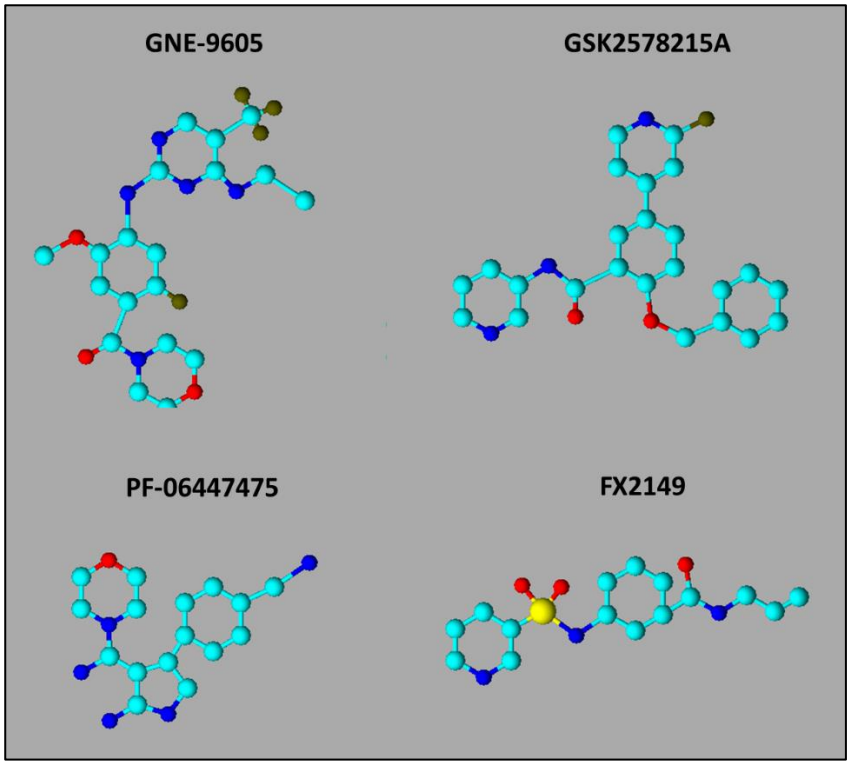

Figure 4.2: Structure of the LRRK2 inhibitors used in this study.

The three LRRK2 kinase inhibitors are GSK2578215A, GNE-9605 and PF-06447475, and the GTPase inhibitor is FX2149. The colours of the atoms represent: cyan: carbon, red: oxygen, blue: nitrogen, yellow: sulfur and olive: fluorine. The sources of the structures are the original papers for each inhibitor (GSK2578215A[642], GNE-9605[643], PF-06447475[644] and FX2149[177]). The structures were made using ChemSketch and ACD/3D Viewer freeware (ACD Labs).

Importantly, this assumption is supported empirically by these drugs' respective *in vitro* kinome analyses. In the case of GSK2578215A[642], kinome analysis reported three kinases as likely off-targets; smooth muscle myosin light chain kinase (smMLCK; also known as MYLK1) was the only kinase in a panel of 131 kinases found to display decreased enzymatic activity, whereas anaplastic lymphoma kinase (ALK) and the D835Y oncogenic variant of fms like tyrosine kinase 3 (FLT3; also known as CD35) were the only hits from a 460 enzyme kinase-binding screen. Showing a similar degree of selectivity, GNE-9605, whose structure has been described as different from most of the LRRK2 inhibitors that were reported at the time of discovery (presumably including GSK2578215A), was found to inhibit the enzymatic activity of just one of 178 other kinases, TAK1-TAB1[643]. TAK1-TAB1 is an artificial constitutively active variant made by fusing transforming growth factor-β1-activated kinase-1 (TAK1; also known as MAP3K7) with its activator, TAK1-binding protein 1 (TAB1)[645]. PF-06447475 appears to be less specific, with the same Ambit kinase-binding screen technology[646] used for GSK2578215A identifying a number of STE20 family kinases as potential targets, in particular 3 MST kinases[644]. There are some important caveats when comparing these studies, including the different assays and concentrations of inhibitor used, and the fact that all experiments were *in vitro* and do not assess kinase inhibition in living cells. In addition, none of these studies covered every one of the 518 human kinases[647], with kinase panels often inflated by including multiple variants of the same enzyme. Nonetheless, the data indicate that each compound is relatively selective, and also support the idea that each is likely to have a different profile of off-target activity, with a common off-target shared by all three relatively unlikely.

With regard to the GTPase inhibitor FX2149, this compound is described as being LRRK2-specific and synthesised based on the crystal structure of the LRRK2 GTPase domain[177]. Importantly, the vast majority of other human kinases do not contain GTPase domains, and the LRRK2 kinase domain is also distinct in structure from those of small GTPases, which would make an indirect effect on kinase activity via small GTPase inhibition in cells less likely. Nonetheless, FX2149 has not been subjected to comparable kinase analyses as those described for the aforementioned LRRK2 kinase inhibitors, so the kinase selectivity of this compound remains unsupported by evidence. Of note however, FX2149 has been shown to not alter

LRRK1 GTP-binding nor kinase activity[177]. This is an important observation in the context of the work in this thesis, since none of the kinase inhibitors studies mentioned above appeared to have explored the potential for these compounds to affect the protein most closely related to LRRK2.

Following published literature, the three LRRK2 kinase inhibitors GSK2578215A, GNE-9605 and PF-06447475 were used at 1 µM. The GTPase inhibitor FX2149[179], which was synthesised at The Open University by Dr Sarah Allman (University of Reading), has reportedly a greater potency than the kinase inhibitors. Thus, it was considered judicious in initial experiments to use this compound at the lower concentration of 100 nM, but also at 1 µM for consistency with the other compounds.

4.3.2 Cell viability assay

Prior to using the inhibitors in assays of autophagy, their potential cytotoxicity was assessed in our system. For this purpose, the effects of the compounds were measured with an established and widely used approach, the Alamar Blue cell viability assay. The Alamar Blue Assay is based on the redox properties of the indicator dye resazurin (henceforth called AB) that changes colour upon metabolic activity. AB is blue and non-fluorescent in its initial oxidised form but pink and fluorescent when reduced. Viable, growing cells maintain a reducing environment due to respiration, whereas inhibition of growth creates an oxidised environment. The fluorescence or absorbance of AB can thus be measured using a plate reader, to reveal changes in the metabolic activity and viability of cultured cells.

HEK293 GFP-LC3 cells were incubated with LRRK2 inhibitors for 17 hours, which corresponded to the longest inhibitor treatment used in autophagy assays (a 16 hours overnight pre-treatment, followed by a further one-hour treatment with PP242 or DMSO). Following the addition of AB, absorbance was measured after 4 hours of incubation at 37°C. The presence of the inhibitors did not alter the reduction of AB compared to DMSO, indicating that the inhibitors displayed no significant toxicity when applied at 1 µM for 17 hours (Figure 4.3). As such, these treatment conditions can be used to study autophagy in HEK293 GFP-LC3 cells without confounding cytotoxic effects.

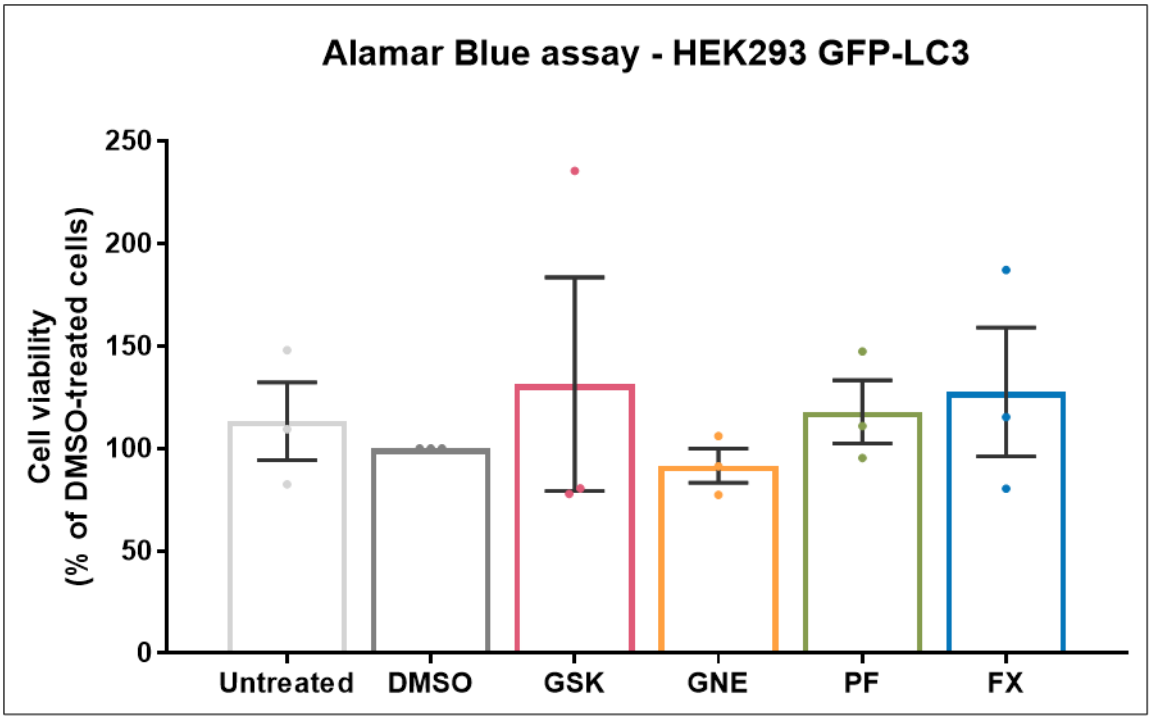

Figure 4.3: The LRRK2 inhibitors did not show cytotoxicity in HEK293 GFP-LC3 cells using Alamar Blue assay.

HEK293 GFP-LC3 cells were incubated overnight (17 hours) with the four LRRK2 inhibitors (GSK2578215A: GSK; GNE-9605: GNE; PF-06447475: PF; FX2149: FX; all at 1 µM) or DMSO (at an equivalent 1:1000 dilution). The absorbance was measured at 570 nm after 4 hours of incubation in a cell culture incubator. The background (negative control) was subtracted from the values, and the data was normalised to the DMSO values to obtain the percentage of reduction of AB, which corresponds to the viability of the cells. For each condition, 3 replicates were used per experiment. n=3 repeats (triplicates/repeat), One-way ANOVA (with grouping by experimental repeat), Geisser-Greenhouse's correction, non-significant. Treatment effect: F(1.103, 2.207)=0.6591; p=0.5107.

4.3.3 LRRK2 inhibition does not affect basal GFP-LC3 punctae levels in HEK293 GFP-LC3 cells

The effect of overnight LRRK2 inhibition on basal levels of autophagy was tested (Figure 4.4). Importantly, neither the LRRK2 kinase inhibitors (1 µM) nor the GTPase inhibitor (100 nM or 1 µM) induced significant changes in the number of GFP-LC3 punctae compared to the control. Although the overall mean for GNE-9605 treated cells is noticeably higher, this was caused by a single outlier experiment and the difference did not approach statistical significance in post-hoc analysis (p= 0.69).

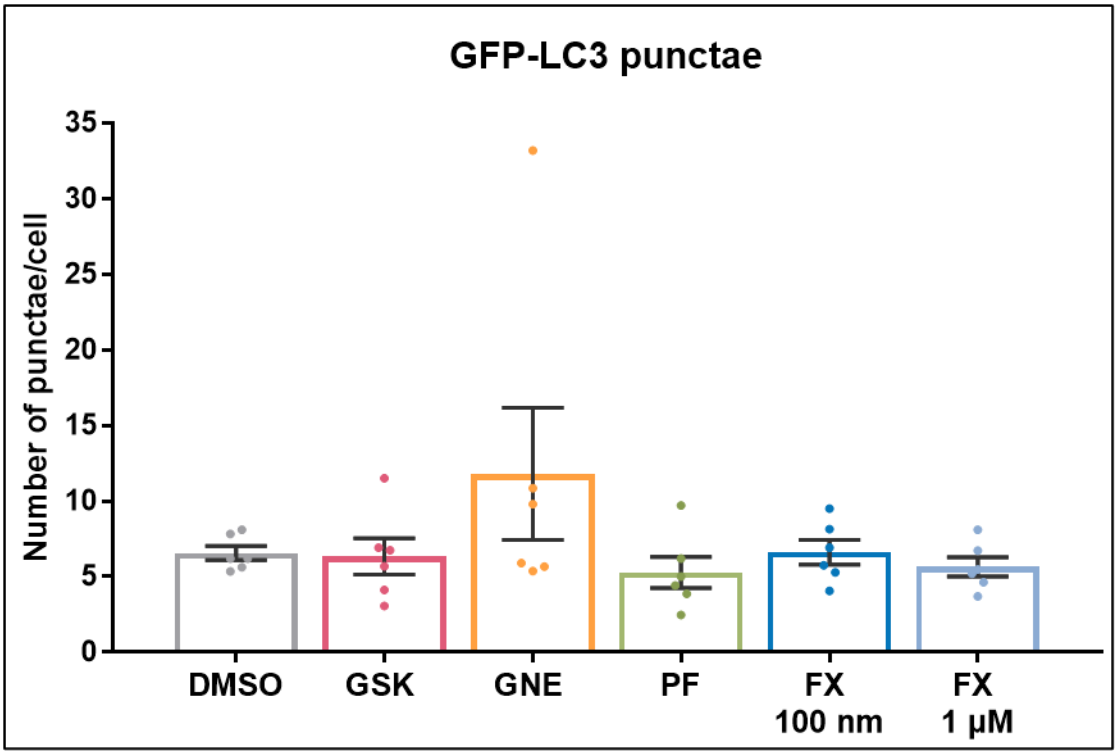

Figure 4.4: No effect of 16 hours LRRK2 inhibition on basal GFP-LC3 punctae levels in HEK293 GFP-LC3 cells.

HEK293 GFP-LC3 cells were treated with LRRK2 kinase inhibitors (GSK2578215A: GSK; GNE-9605: GNE; PF-06447475: PF; all at 1 µM) or a GTPase inhibitor (FX2149: FX, 100 nM and 1 µM) for 16 hours. For each condition, the mean number (± SEM) of GFP-LC3 punctae per cell was calculated, using 50 cells per condition. n=6 repeats (1 coverslip/repeat). One-way ANOVA (with grouping by experimental repeat), Geisser-Greenhouse's correction, non-significant. Treatment effect: F(1.058, 5.291)=1.434; p=0.28.

4.3.4 LRRK2 inhibition prevents the PP242-induced increase of GFP-LC3 punctae in HEK293 GFP-LC3 cells

Since no effects of LRRK2 inhibitors were found on basal autophagy, the next step was to investigate whether these compounds might affect autophagy under conditions where the numbers of autophagic vesicles are elevated. As mentioned in the introduction to this Chapter, an increase in the number of autophagic vesicles can originate from two distinct mechanisms: an induction of autophagy, i.e. increasing the amount of autophagy beyond its basal levels; or from a blockage in basal autophagy at its later stages, which causes an accumulation of autophagosomes without affecting the rate at which they are produced[329]. Nonetheless, these mechanisms can be distinguished experimentally with the use of PP242 and Bafilomycin A1 (BafA1)[334,648]. As mentioned, PP242 relieves mTORC1-mediated repression of autophagy, and thus causes an increase in autophagic vesicle number by inducing autophagy. By

contrast, BafA1 is an inhibitor of lysosomal v-H^+-ATPases that has the effect of preventing lysosomal acidification, which in turn prevents both the formation of autolysosomes and the fusion between autophagosomes and lysosomes, leading to an impairment in the clearance of autophagic vesicles.

Consistent with the pilot experiment shown in Figure 4.1, one-hour treatment with PP242 at 2 µM induced a marked increase in the number of GFP-LC3 punctae (Figure 4.5). Surprisingly however, 16 hours pre-treatment with the LRRK2 kinase (1 µM) and GTPase (100 nM or 1 µM) inhibitors completely abolished this increase. Thus, whilst LRRK2 kinase and GTPase activities do not appear to be involved in basal autophagy in HEK293 GFP-LC3 cells, these enzymatic activities may be a requirement for autophagy induced by mTORC1 inhibition in this cell line.

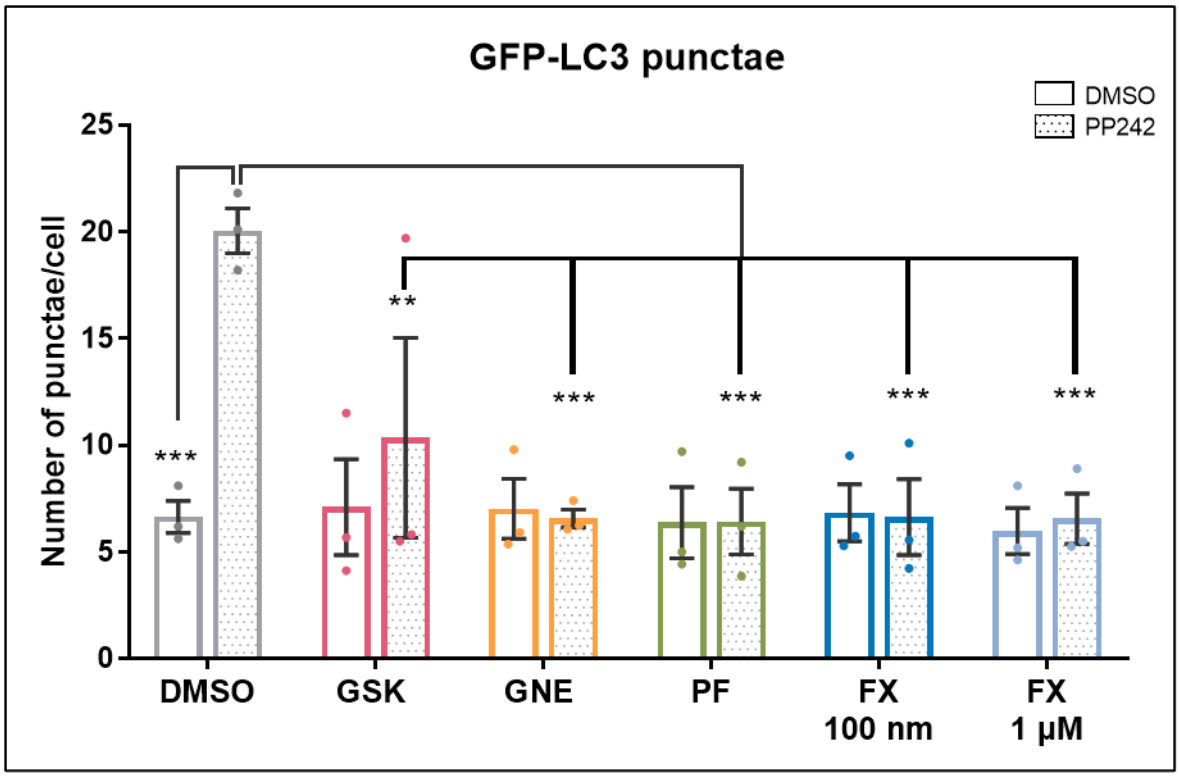

Figure 4.5: 16 hours LRRK2 inhibition prevented the PP242-induced increase in GFP-LC3 punctae number in HEK293 GFP-LC3 cells.

HEK293 GFP-LC3 cells were pre-treated with LRRK2 kinase inhibitors (GSK2578215A: GSK; GNE-9605: GNE; PF-06447475: PF; all at 1 µM) or a GTPase inhibitor (FX2149: FX, 100 nM and 1 µM) or DMSO (1:1000 equivalent dilution) for 16 hours, and treated with PP242 (2 µM) or DMSO (1:1000 equivalent dilution) for 1 hour. For each condition, the mean number (± SEM) of GFP-LC3 punctae per cell was calculated, using 50 cells per condition. n=3 repeats (1 coverslip/repeat). Two-way ANOVA (with grouping by experimental repeat), Tukey post-hoc test. PP242 treatment effect: $F(1, 2)=1295$; $p=0.0008$, inhibitors effect: $F(5, 10)=5.457$; $p=0.01$, interaction: $F(5, 10)=12.43P=0.0005$. On graph: $p<0.001$ (***), $p<0.01$ (**).

4.3.5 LRRK2 inhibition does not prevent BafA1-induced accumulation of GFP-LC3 punctae in HEK293 GFP-LC3 cells

The previous results indicate that LRRK2 inhibitors have no effect on basal autophagy but suppress the PP242-induced increase in GFP-LC3 punctae number, which is consistent with the involvement of LRRK2 in the induction of autophagy in HEK293 GFP-LC3 cells. To support this, the effect of these compounds was tested on the increase in GFP-LC3 punctae number resulting from treatment with BafA1 (0.1 µM, 1 hour) (Figure 4.6).

Consistent with published data, BafA1 induced an increase of GFP-LC3 punctae in control cells (Figure 4.6 and Figure 4.7). However, in contrast to PP242 treatment, a similar increase can be observed in HEK293 GFP-LC3 cells that were pre-treated overnight with each of the four LRRK2 inhibitors (Figure 4.7). These data thus indicate that LRRK2 kinase and GTPase activities are unlikely to be involved in the later stages of autophagy in these cells.

The results presented in Figure 4.7 also indicate that overnight treatment with LRRK2 kinase or GTPase inhibitors does not appear to place an upper limit on total GFP-LC3 punctae production within the range observed in this experiment (i.e., up to approximately 40 punctae per cell). Importantly, the numbers of GFP-LC3 punctae per cell elicited by PP242 treatment were within this range (up to approximately 20 puncta per cell; Figure 4.5). These results give confidence that the reduction in PP242-induced autophagy elicited by these compounds is likely caused by a specific impairment in autophagy induction, and is not the consequence of a general restriction in the number of GFP-LC3 punctae that the cells are able to form.

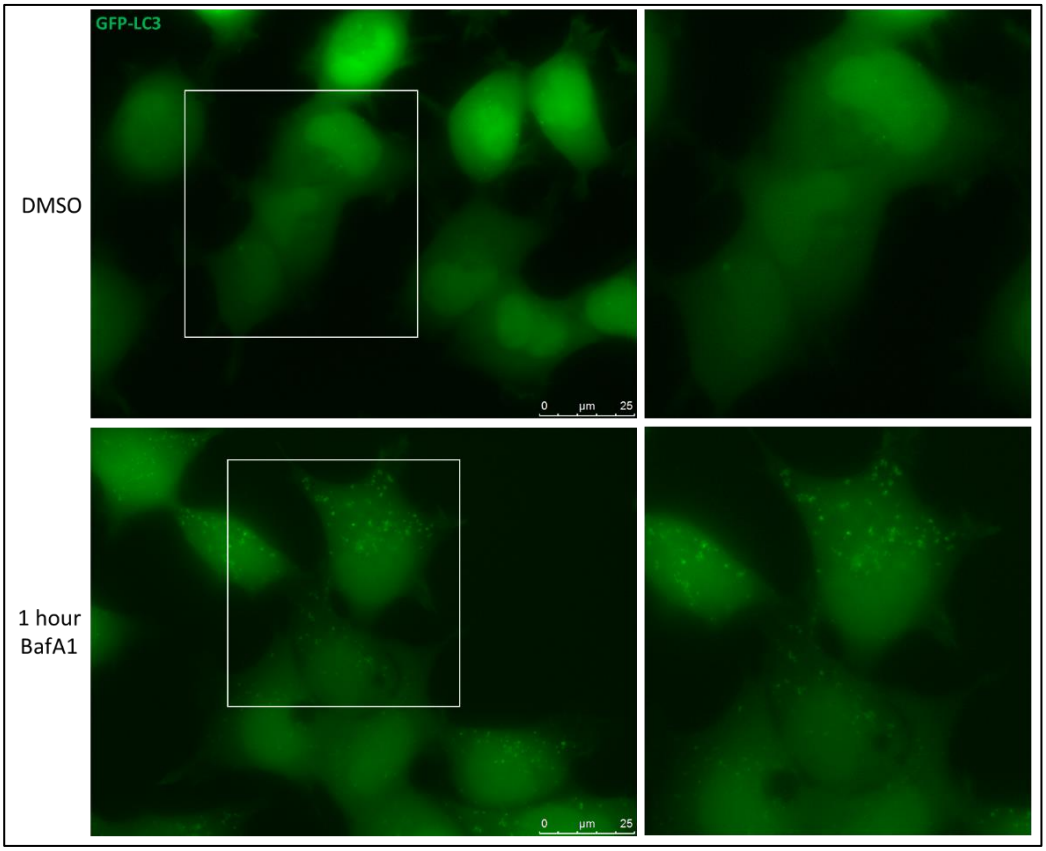

Figure 4.6: Representative images of GFP-LC3 punctae in BafA1-treated HEK293 GFP-LC3 cells
Representative images of cells treated with DMSO or 0.1 µM BafA1 for 1 hour. Images on the left are original images acquired at 63x magnification. Images on the right are enlargements of the indicated areas within the original images.

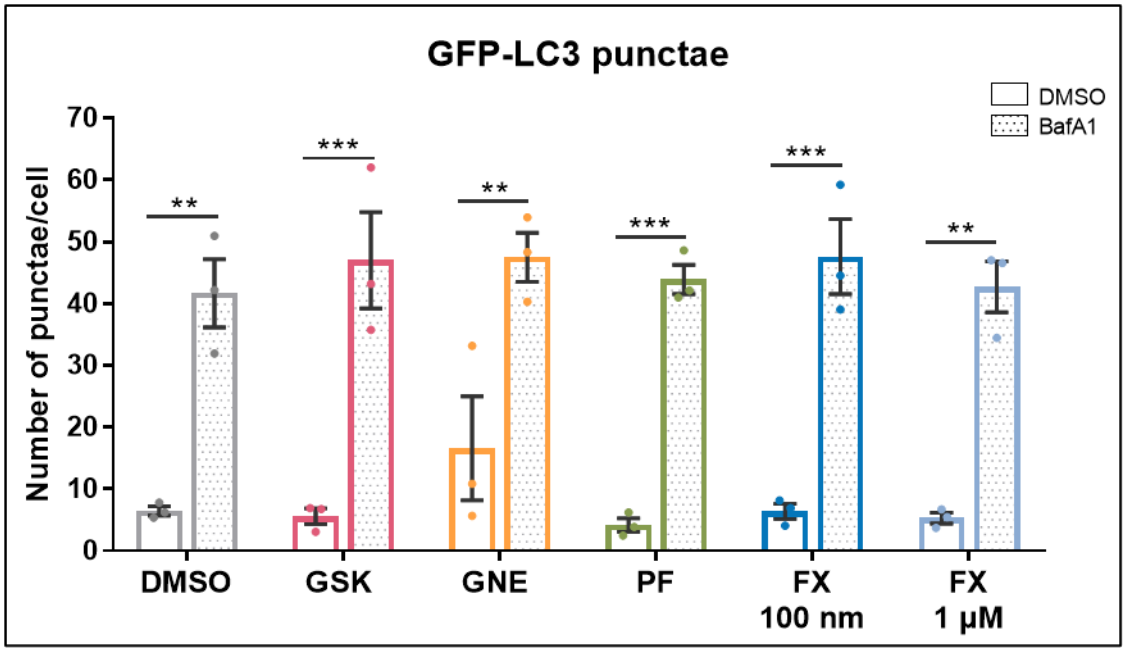

Figure 4.7: No effect of 16 hours LRRK2 inhibition on BafA1-induced GFP-LC3 punctae levels in HEK293 GFP-LC3 cells.
HEK293 GFP-LC3 cells were pre-treated with LRRK2 kinase inhibitors (GSK2578215A: GSK; GNE-9605: GNE; PF-06447475: PF; all at 1 µM) or a GTPase inhibitor (FX2149: FX, 100 nM and 1 µM) or DMSO (1:1000 equivalent dilution) for 16 hours followed by treatment with BafA1 (0.1 µM) or DMSO (1:1000 equivalent dilution) for 1 hour. For each condition, the mean number (± SEM) of GFP-LC3 punctae per cell was calculated, using 50 cells per condition. n=3 repeats (1 coverslip/repeat). Two-way ANOVA (with grouping by experimental repeat), Tukey post-hoc test. BafA1 treatment effect: $F(1, 2)=64.76$; $p=0.015$, inhibitors effect: $F(5, 10)=1.593$; $p=0.25$, interaction: $F(5, 10)=0.5837$; $p=0.71$. On graph: $p<0.001$ (***), $p<0.01$ (**).

4.3.6 Acute LRRK2 inhibition is sufficient to prevent the PP242-induced increase of GFP-LC3 punctae in HEK293 GFP-LC3 cells

The previous results showed that overnight treatment with LRRK2 inhibitors blocks the PP242-induced increase in GFP-LC3 punctae in HEK293 GFP-LC3 cells. However, the length of this treatment is a potential limitation as longer pharmacological treatments increase the risk that observed results are not directly due to the inhibition of the target, but are caused by effects downstream of target inhibition, potentially including adaptive responses to prolonged target inhibition. Therefore, shorter treatments provide more informative data. The effects of the LRRK2 inhibitors on the PP242-induced increase in GFP-LC3 punctae number were thus measured using a one-hour pre-treatment (Figure 4.8).

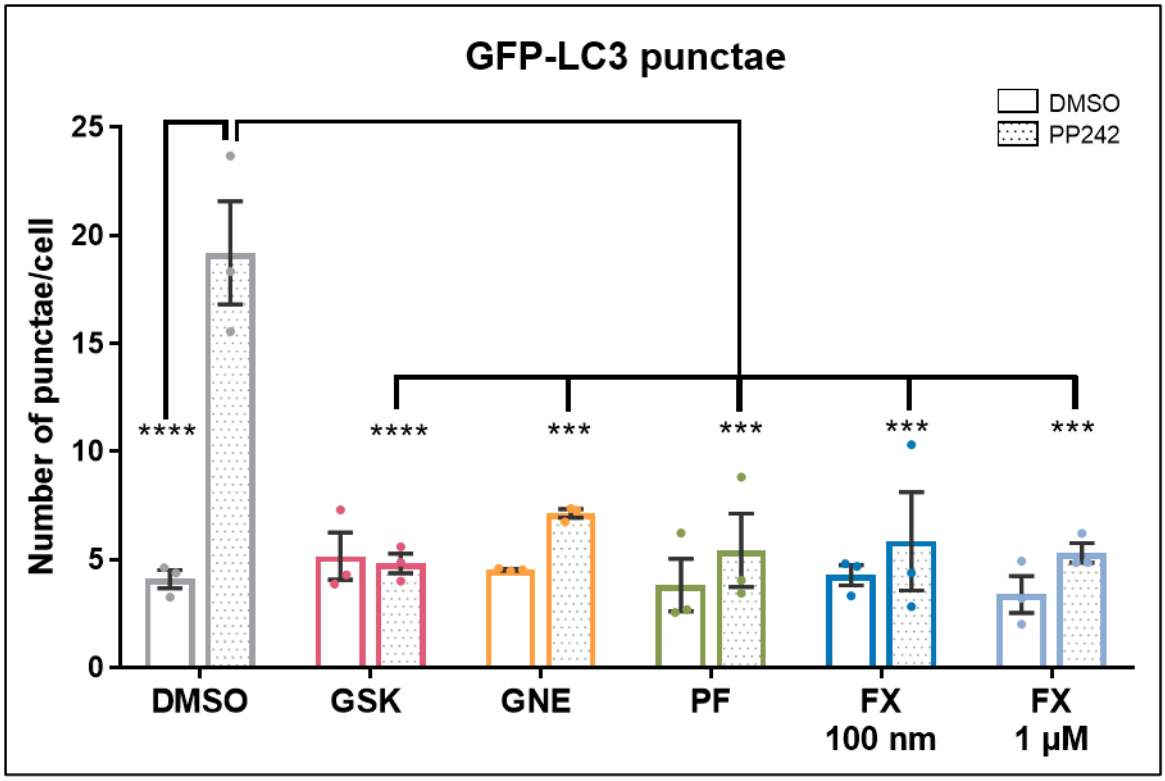

Figure 4.8: One-hour LRRK2 inhibition prevented the PP242-induced increase in GFP-LC3 punctae number in HEK293 GFP-LC3 cells.

HEK293 GFP-LC3 cells were pre-treated with LRRK2 kinase inhibitors (GSK2578215A: GSK; GNE-9605: GNE; PF-06447475: PF; all at 1 µM) or a GTPase inhibitor (FX2149: FX, 100 nM and 1 µM) or DMSO (1:1000 equivalent dilution) for 1 hour, followed by treatment with PP242 (2 µM) or DMSO (1:1000 equivalent dilution) for 1 hour. For each condition, the mean number (± SEM) of GFP-LC3 punctae per cell was calculated, using 50 cells per condition. n=3 repeats (1 coverslip/repeat). Two-way ANOVA (with grouping by experimental repeat), Tukey post-hoc test. PP242 treatment effect: $F(1, 2)=86.98$; $p=0.01$, inhibitors effect: $F(5, 10)=8.962$; $p=0.0019$, interaction: $F(5, 10)=14.35$; $p=0.0003$. On graph: $p<0.0001$ (****), $p<0.001$ (***).

Similar to 16 hours pre-treatment (Figure 4.5), all four LRRK2 inhibitors blocked the PP242-induced accumulation of GFP-LC3 punctae (Figure 4.8). These results suggest that the observed effect of these compounds on PP242-induced GFP-LC3 punctae formation is likely due to LRRK2 acting immediately upon processes involved in autophagy induction, rather than being the consequence of less specific events further downstream of LRRK2 kinase and GTPase inhibition.

4.4 Effects of LRRK2 inhibitors on autophagy at an early stage in HEK293 GFP-LC3 cells

WIPI2 is a protein involved in the early steps of the generation of autophagosomal structures[649], where it not only acts upstream of LC3 but is required for the recruitment of LC3 to autophagic vesicles[650]. Similar to LC3, the induction of autophagy causes WIPI2 to be recruited to membrane structures, allowing its activation to be monitored by fluorescent microscopy as the formation of punctae. Since the previous results in this chapter suggested a role for LRRK2 in PP242-induced autophagy, either at the level of or upstream of the formation of GFP-LC3 punctae, the next step was to investigate the effects of LRRK2 kinase and GTPase inhibition on PP242-induced WIPI2 punctae.

4.4.1 Establishing an assay to quantify endogenous WIPI2 punctae in HEK293 GFP-LC3 cells

Assays to quantify endogenous WIPI2 punctae as a measure of early-stage autophagy had not previously been performed in our laboratory. Thus, before the effect of LRRK2 inhibition on autophagy could be studied by quantification of WIPI2 punctae, the necessary experiment conditions needed to be verified. For consistency with the GFP-LC3 data, the same HEK293 GFP-LC3 cell line was used with an identical PP242 treatment of 2 μM for one hour to induce autophagy via mTORC1 inhibition. The immunocytochemistry conditions chosen were an adaptation of a standard staining protocol used in the Berwick laboratory, with a WIPI2 antibody recommended by Nick Ktistakis (Babraham Institute, Cambridge).

Figure 4.9 shows representative images of endogenous WIPI2 staining from HEK293 GFP-LC3 cells treated with PP242 or DMSO. Although some punctae can be seen in the DMSO-treated cells, the antibody staining is generally diffuse in appearance. However, upon autophagy induction with PP242, a greater number of punctae can be seen within the cells. Indeed, across all experiments performed in HEK293 GFP-LC3 cells in this study, the cells had a mean number of 21 WIPI2 punctae per cell following treatment, compared to 9 punctae per cell without treatment (i.e., basally). As such, when using this

WIPI2 antibody staining protocol, the same PP242 treatment conditions used for GFP-LC3 assays can be utilised to reliably distinguish basal autophagy and autophagy induced by mTORC1 inhibition.

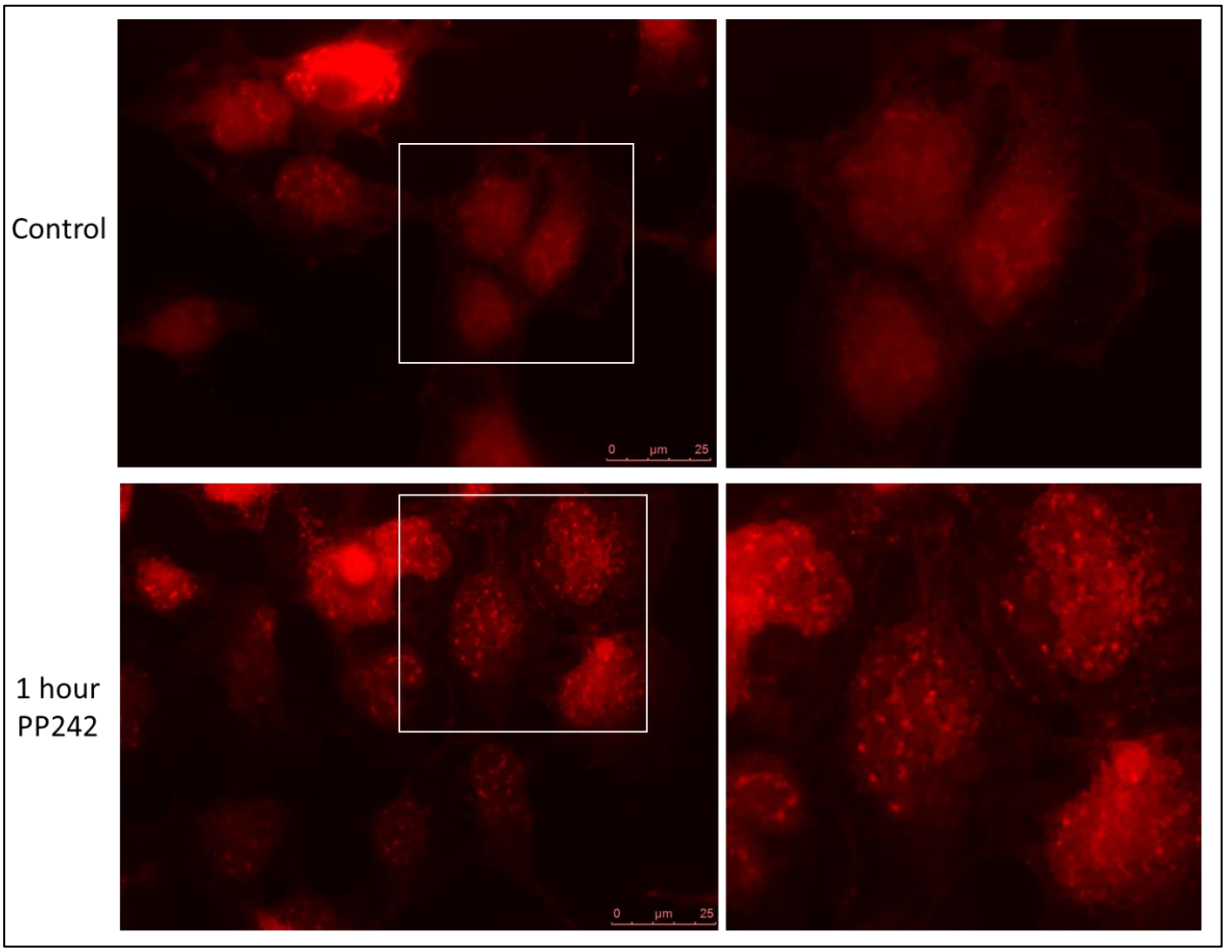

Figure 4.9: Representative images of endogenous WIPI2 punctae in HEK293 GFP LC3 cells.

HEK293 GFP-LC3 cells were stained with an antibody against endogenous WIPI2. The diffuse WIPI2 distribution represents the WIPI2 molecules that are not associated with autophagic vesicles. By contrast, the brighter red punctae represent autophagic vesicles that contain WIPI2. A higher number of punctae are visible in the autophagy-induced condition (PP242 at 2 µM, 1 hour) compared to unstimulated cells with a basal level of autophagy. Images on the left are original images acquired at 63x magnification. Images on the right are enlargements of the indicated areas within the original.

4.4.2 LRRK2 inhibition reduces PP242-induced endogenous WIPI2 punctae formation in HEK293 GFP-LC3 cells

The effect of LRRK2 inhibition on the formation of endogenous WIPI2 punctae was investigated using identical treatment conditions to those used to study GFP-LC3 punctae in Figure 4.8 (one-hour pre-treatment with the kinase inhibitors at 1 µM or GTPase inhibitor at 100 nM, followed by one-hour induction of autophagy with PP242 at 2 µM).

Consistent with all previous GFP-LC3 assays, LRRK2 inhibition had no effect on basal autophagy, but appeared to impair PP242-induced autophagy (Figure 4.10). In particular, when compared to the DMSO-treated cells, three of the four LRRK2 inhibitors (GNE-9605, PF-06447475 and FX2149) elicited statistically significant reductions in the number of PP242-induced WIPI2 punctae, while GSK2578215A appeared to cause a consistent, although non-significant, effect. These results suggest that LRRK2 inhibitors either blocked PP242-induced autophagy upstream of both LC3 and WIPI2, or upstream of LC3 and at the level of WIPI2. Note that since experiments confirmed the efficacy of FX2149 at the lower concentration of 100 nM, this compound was only used at 100 nM in this and subsequent autophagy experiments.

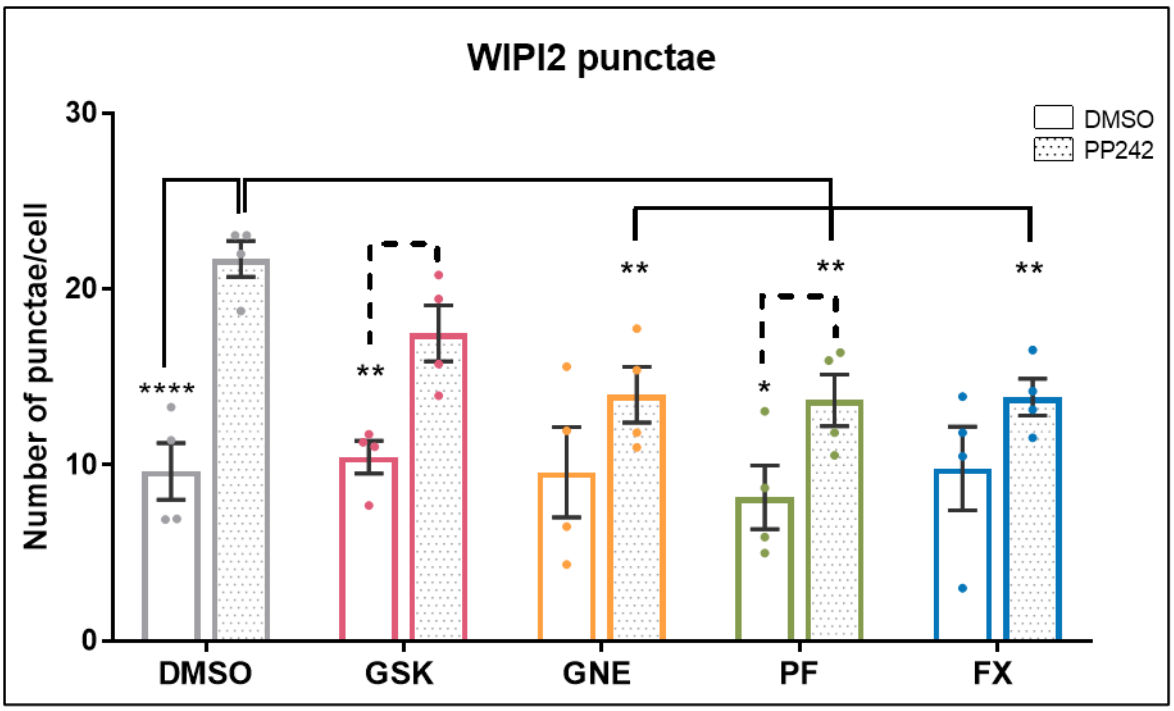

Figure 4.10: One-hour LRRK2 inhibition prevented the PP242-induced increase in endogenous WIPI2 punctae number in HEK293 GFP-LC3 cells.

HEK293 GFP-LC3 cells were pre-treated with LRRK2 kinase inhibitors (GSK2578215A: GSK; GNE-9605: GNE; PF-06447475: PF; all at 1 µM) or a GTPase inhibitor (FX2149: FX, 100 nM) or DMSO (1:1000 equivalent dilution) for 1 hour, followed by treatment with PP242 (2 µM) or DMSO (1:1000 equivalent dilution) for 1 hour. The cells were then fixed and stained with an antibody against the early autophagic marker WIPI2. For each condition, the mean number (± SEM) of WIPI2 punctae per cell was calculated, using 30 cells per condition. n=4 repeats (1 coverslip/repeat). Two-way ANOVA (with grouping by experimental repeat), Tukey post-hoc test. PP242 treatment effect: $F(1, 3)=28.05$; $p=0.013$, inhibitors effect: $F(4, 12)=6.07$; $p=0.0066$, interaction: $F(4, 12)=5.274$; $p=0.01$. On graph: $p<0.0001$ (****), $p<0.01$ (**), $p<0.05$ (*).

It is worth observing that the extent to which LRRK2 kinase and GTPase inhibitors blocked PP242-induced WIPI2 punctae formation was not as strong as was observed for PP242-induced GFP-LC3 punctae

formation (cf. Figure 4.8 and Figure 4.10). In principle, a quantitative comparison between the effect sizes in these two experiments might provide information about the likely sites of action for LRRK2 kinase and GTPase activities within the autophagic pathway, but in this case the comparison is limited by the experiments being performed separately. Nevertheless, since the WIPI2 assays were performed in HEK293 GFP-LC3 cells, the number of GFP-LC3 punctae could also be quantified in the same cells, thereby allowing a direct comparison to be made (Figure 4.11).

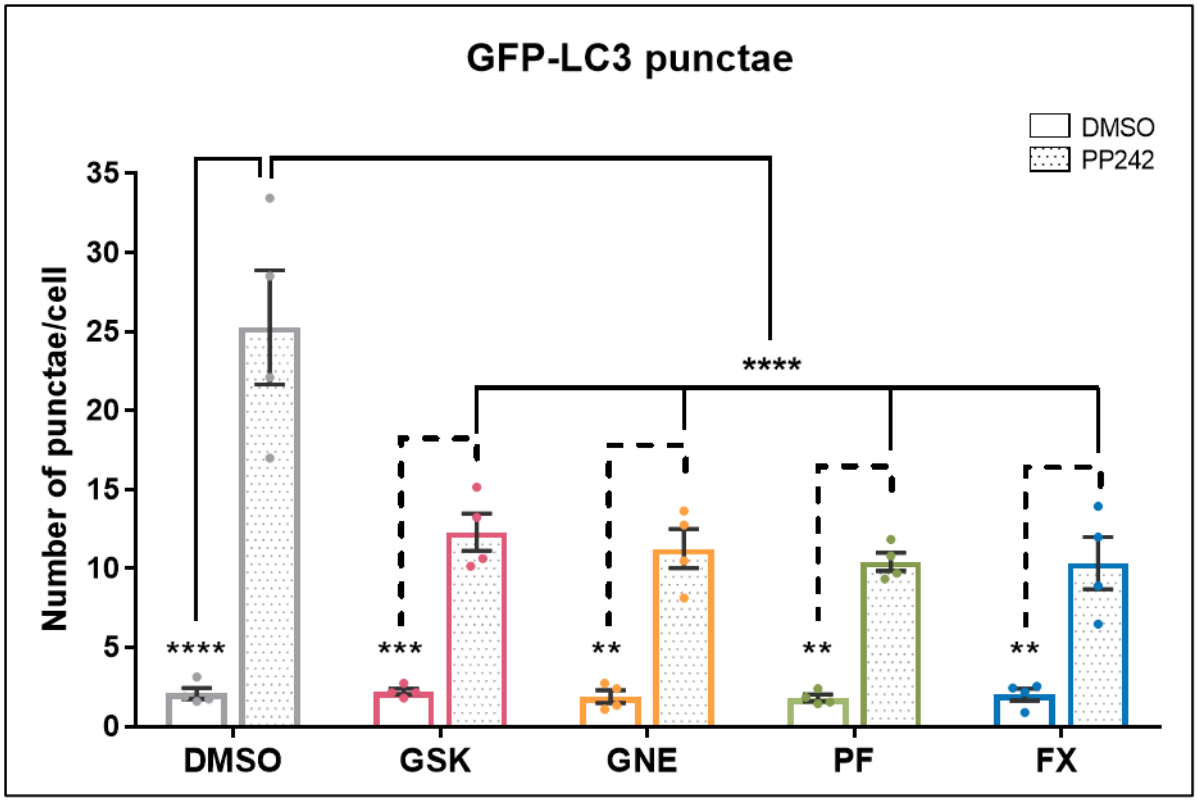

Figure 4.11: One-hour LRRK2 inhibition prevented the PP242-induced increase in GFP-LC3 punctae number in the same HEK293 GFP-LC3 cells used for endogenous WIPI2 assays.

HEK293 GFP-LC3 cells were pre-treated with LRRK2 kinase inhibitors (GSK2578215A: GSK; GNE-9605: GNE; PF-06447475: PF; all at 1 µM) or a GTPase inhibitor (FX2149: FX, 100 nM) or DMSO (1:1000 equivalent dilution) for 1 hour, followed by treatment with PP242 (2 µM) or DMSO (1:1000 equivalent dilution) for 1 hour. The cells were then fixed and stained with an antibody against the early autophagic marker WIPI2. For each condition, the mean number (± SEM) of GFP-LC3 punctae per cell was calculated, using 30 cells per condition. n=4 repeats (1 coverslip/repeat). Two-way ANOVA (with grouping by experimental repeat), Tukey post-hoc test. PP242 treatment effect: $F(1, 3)=68.88$; $p=0.0037$, inhibitor effect: $F(4, 12)=14.08$; $p=0.0002$, interaction: $F(4, 12)=17.73$; $p<0.0001$. On graph: $p<0.0001$ (****), $p<0.001$ (***), $p<0.01$ (**).

Within the same cells used for the WIPI2 assay presented in Figure 4.10, a significant reduction in PP242-induced GFP-LC3 punctae can be observed with all four inhibitors (Figure 4.11). Importantly however, the effects were not as marked as seen previously (cf. Figure 4.8 and Figure 4.11). This indicates that the

different extents to which the inhibitors prevented PP242-induced punctae formation is most likely due to inter-experimental variability, rather than differences between the effect of LRRK2 inhibition on GFP-LC3 and WIPI2 punctae.

For completeness, the number of punctae that appear to be positive for both GFP-LC3 and WIPI2 were quantified (Figure 4.12), although the colocalisation of the two markers cannot be guaranteed as the images were not acquired with confocal microscopy. In theory, GFP-LC3 and WIPI2 double positive punctae represent an intermediary stage in the autophagic pathway, between vesicles containing only WIPI2, and vesicles containing only GFP-LC3. As expected, PP242 treatment induced an increase in these double-positive vesicles, which was partially blocked by all four LRRK2 inhibitors (Figure 4.12).

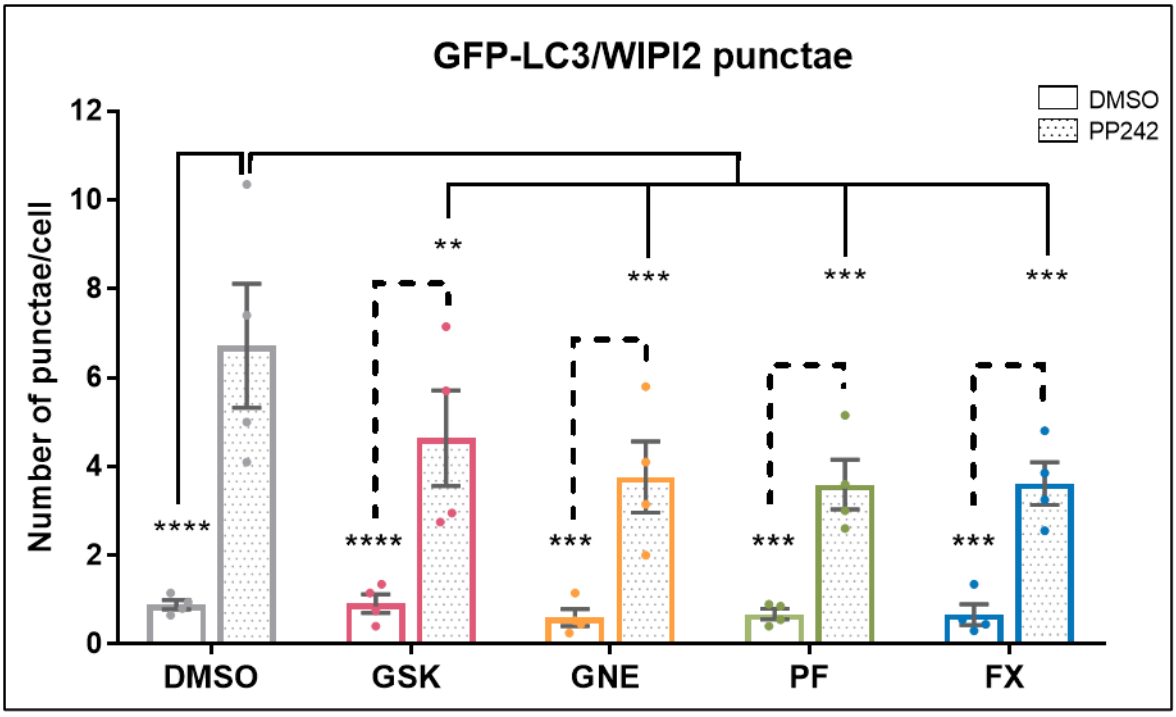

Figure 4.12: One-hour LRRK2 inhibition prevented the PP242-induced increase in GFP-LC3 and WIPI2 double positive punctae number in HEK293 GFP-LC3 cells.

HEK293 GFP-LC3 cells were pre-treated with LRRK2 kinase inhibitors (GSK2578215A: GSK; GNE-9605: GNE; PF-06447475: PF; all at 1 µM) or a GTPase inhibitor (FX2149: FX, 100 nM) or DMSO (1:1000 equivalent dilution) for 1 hour, followed by treatment with PP242 (2 µM) or DMSO (1:1000 equivalent dilution) for 1 hour. The cells were then fixed and stained with an antibody against the early autophagic marker WIPI2. For each condition, the mean number (± SEM) of GFP-LC3/WIPI2 double positive punctae per cell was calculated, using 30 cells per condition. n=4 repeats (1 coverslip/repeat). Two-way ANOVA (with grouping by experimental repeat), Tukey post-hoc test. PP242 treatment effect: $F(1, 3)=18.8$; $p=0.0226$, inhibitors effect: $F(4, 12)=6.191$; $p=0.0061$, interaction: $F(4, 12)=8.064$; $p=0.0021$. On graph: $p<0.0001$ (****), $p<0.001$ (***), $p<0.01$ (**).

To confirm that the LRRK2 kinase and GTPase inhibitors were blocking the PP242-induced increase of the three categories of punctae to the same extent, the percentage of inhibition achieved by each LRRK2 inhibitor was determined. The calculations were performed by first subtracting from each PP242-treated value its corresponding DMSO value, so that the resulting values were measures of the mean number of punctae per cell produced specifically by the PP242 treatment. These numbers were normalised to the DMSO control and expressed as percentages, such that the extent to which each LRRK2 inhibitor affected the PP242-induced increase in the three types of punctae could be calculated.

As depicted in Figure 4.13, this analysis indicated that each LRRK2 inhibitor impaired the PP242-induced increase in endogenous WIPI2 positive punctae, GFP-LC3 positive punctae and GFP-LC3/WIPI2 double positive punctae to similar extents, with no significant differences observed. These data strongly suggest that LRRK2 inhibition is impairing PP242-induced autophagy either at the level of WIPI2 or at a site upstream of this protein in HEK293 GFP-LC3 cells.

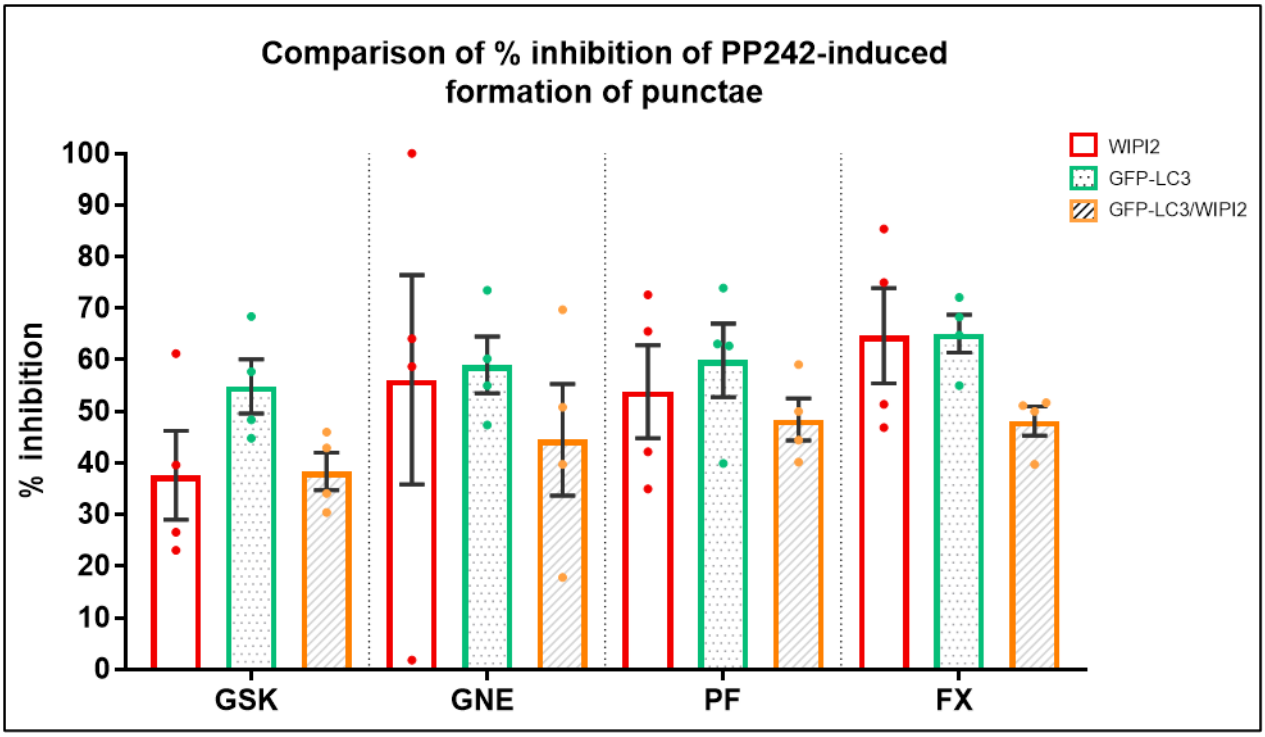

Figure 4.13: LRRK2 inhibition prevented the PP242-induced increase in the three types of punctae number to similar extents in HEK293 GFP-LC3 cells.

The bars represent the percentage of inhibition of the PP242-induced punctae formation associated with each compound (GSK2578215A: GSK; GNE-9605: GNE; PF-06447475: PF; FX2149: FX). The percentage of inhibition was obtained from the data showed in the Figures 4.9, 4.10 and 4.11. n=4 repeats (1 coverslip/repeat). Two-way ANOVA (with grouping by experimental repeat), non-significant. Punctae type effect: $F(2, 6)=1.86$; $p=0.235$, inhibitors effect: $F(3, 9)=2.303$; $p=0.1456$, interaction: $F(6, 18)=0.267$; $p=0.9452$.

4.5 Effects of LRRK2 inhibitors on autophagy in macrophages

As argued in Section 1.6.2 (Chapter 1), the published literature describing effects of modulating LRRK2 enzymatic activities on autophagy are frequently contradictory, which might suggest cell type specific roles for LRRK2. However, few publications study more than one cell line, so differences in the literature can also be attributable to the experimental set-ups used in different laboratories, meaning the explanation of cell type specificity cannot be made with confidence. To address this, RAW264.7 macrophages cells were used to evaluate the effect of LRRK2 inhibitors on endogenous WIPI2 assays, performed under identical conditions to those used in HEK293 GFP-LC3 cells. This immune cell type might seem an unusual choice of cell to study a Parkinson's disease protein, but as stated earlier (Chapter 1, Section 1.6.1.5), neuroinflammation is an important mechanism in the pathology of PD[651]. Moreover, there is an increased activation of the immune response with aging, and immune cells express high levels of LRRK2, with expression increasing when the cells are activated[165,166], which suggests a role for LRRK2 in immune cell response and neuroinflammation. Importantly also, parallel experiments can be performed in isogenically matched RAW264.7 macrophages that are knockout for *Lrrk2*, thereby allowing a comparison between two forms of Lrrk2 loss of function: acute enzymatic inhibition and loss of protein expression.

4.5.1 Establishing conditions to study PP242-induced autophagy in macrophages

Prior to using LRRK2 inhibitors in autophagy assays in the RAW264.7 macrophages cell lines, their potential cytotoxicity was assessed in experiments identical to that described in Section 4.3.2. In both WT and Lrrk2 KO macrophage cell lines, the presence of the inhibitors did not alter the reduction of AB compared to DMSO, indicating that the inhibitors displayed no significant cytotoxicity when applied at 1 µM for 17 hours (Figure 4.14). As such, the treatment conditions used in HEK293 GFP-LC3 cells can be utilised to study autophagy in macrophages as well.

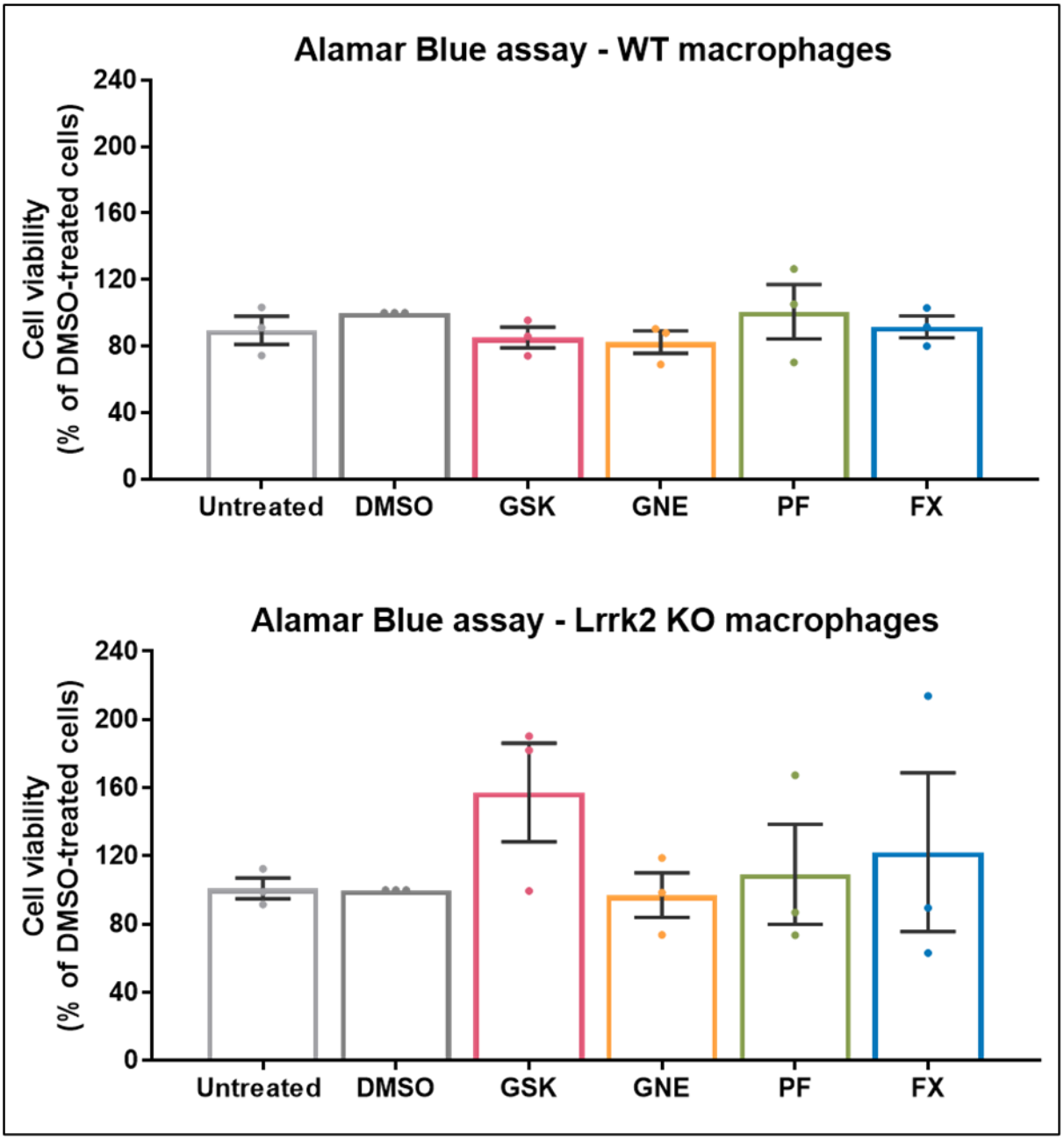

Figure 4.14: The LRRK2 inhibitors did not show cytotoxicity in RAW264.7 macrophages using Alamar Blue assay

RAW264.7 WT or Lrrk2 KO macrophages were incubated overnight (17 hours) with the four LRRK2 inhibitors (GSK2578215A: GSK; GNE-9605: GNE; PF-06447475: PX; FX2149: FX all at 1µM) or DMSO (at an equivalent 1:1000 dilution). The absorbance was measured at 570 nm after 4 hours of incubation in a cell culture incubator. The background (negative control) was subtracted from the values, and the data was normalised to the DMSO values to obtain the percentage of reduction of AB, which corresponds to the viability of the cells. For each condition, 3 replicates were used per experiment. n=3 repeats (triplicates/repeat), One-way ANOVA (with grouping by experimental repeat), Geisser-Greenhouse's correction, non-significant. WT treatment effect: $F(1.067, 2.133)=1.943$; $p=0.29$, KO treatment effect: $F(1.593, 3.186)=1.058$; $p=0.42$.

Since the RAW264.7 macrophages do not express GFP-LC3, the effect of LRRK2 inhibition on autophagy was studied by quantification of endogenous WIPI2 punctae. Thus, the WT and Lrrk2 KO macrophages were subjected to the same treatment and immune staining protocol used in HEK293 GFP-LC3 cells, in a pilot experiment to verify that these conditions would be suitable.

Figure 4.15 shows representative images of WIPI2 staining from WT or Lrrk2 KO macrophages cells treated with PP242 or DMSO. Although some punctae can be seen in the DMSO-treated controls, the antibody staining is generally diffuse in appearance. Upon autophagy induction with PP242 (2 μM, 1 hour), a greater number of punctae can be seen within the cells. Indeed, across all experiments performed in WT or Lrrk2 KO macrophage cells in this study, the cells had a mean of 10 WIPI2 punctae per cell following PP242 treatment, compared to 2 punctae per cell basally.

Thus, this protocol can be used in macrophages to reliably distinguish basal autophagy and induced autophagy via quantification of endogenous WIPI2 punctae.

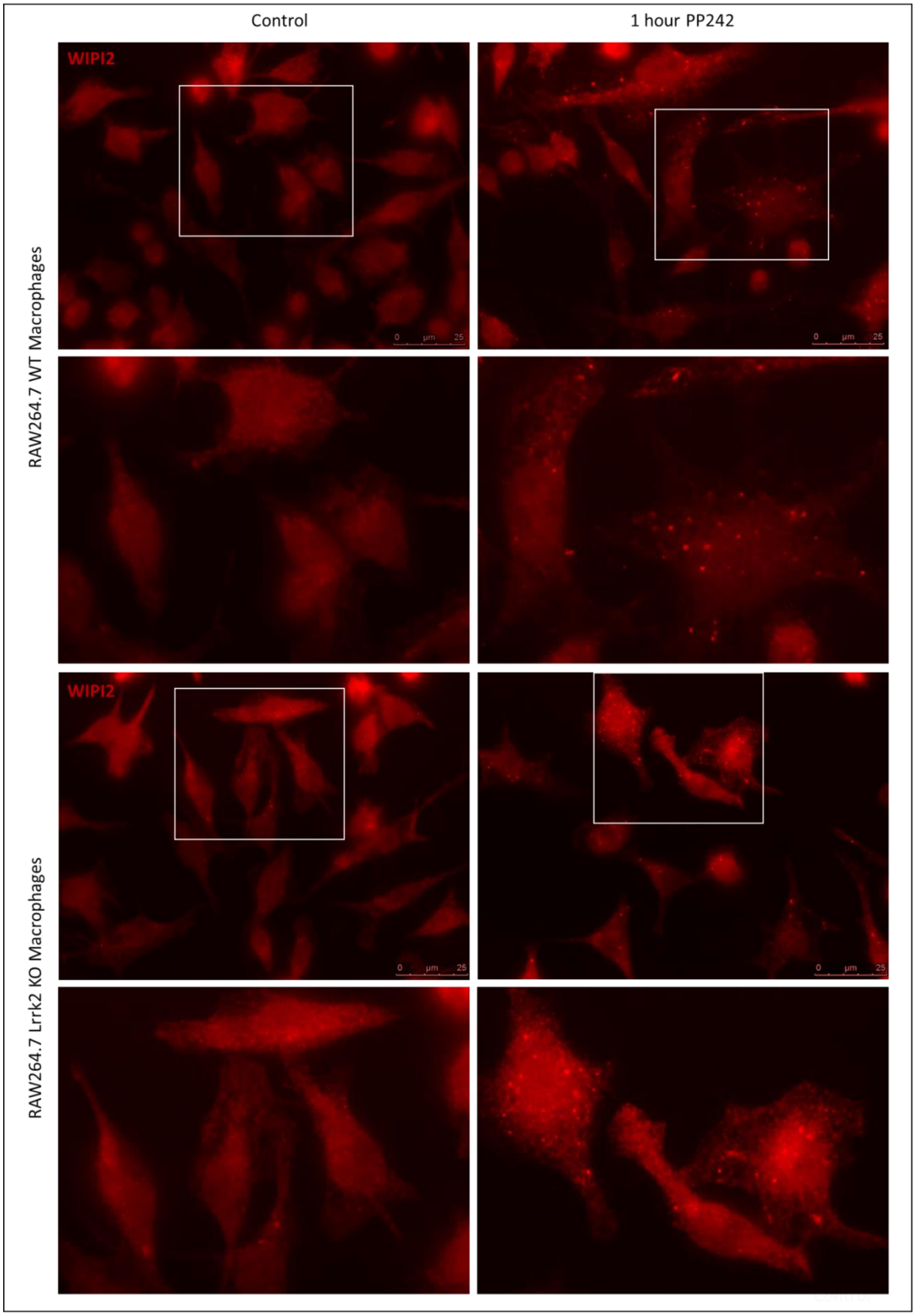

Figure 4.15: Representative images of endogenous WIPI2 punctae in RAW264.7 WT or Lrrk2 KO macrophages.

RAW264.7 WT or Lrrk2 KO macrophages were stained with an antibody against endogenous WIPI2. The diffuse WIPI2 distribution represents the WIPI2 molecules that are not associated with autophagic vesicles. By contrast, the brighter red punctae represent autophagic vesicles that contain WIPI2. A higher number of punctae are visible in the autophagy-induced condition (PP242 2 µM, 1 hour) compared to unstimulated cells with a basal level of autophagy. Images on the top rows are original images acquired at 63x magnification. Images on the bottom rows are enlargements of the indicated areas within the original images.

4.5.2 Loss of LRRK2 does not affect basal or PP242-induced endogenous WIPI2 punctae levels in macrophages

The effect of the loss of Lrrk2 on autophagy in macrophages was analysed using WIPI2 punctae quantification. As expected, PP242 treatment increased the number of WIPI2 punctae compared to control cells treated with the vehicle DMSO (Figure 4.16). Interestingly, there was no difference between the two genotypes, in either basal or PP242-induced WIPI2 punctae numbers.

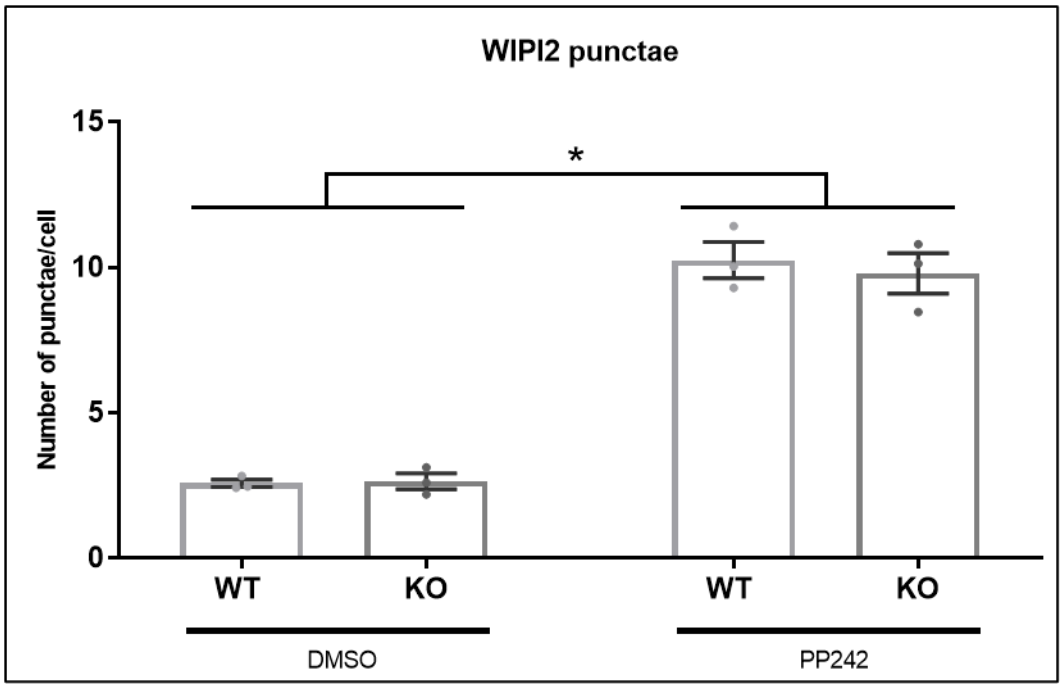

Figure 4.16: The loss of Lrrk2 in macrophages did not affect basal or PP242-induced WIPI2-punctae levels.

WT or Lrrk2 KO macrophages were treated with PP242 (2 μM) or DMSO (1:1000 equivalent dilution) for 1 hour, then fixed and stained with an antibody against endogenous WIPI2. For each condition, the mean number (± SEM) of WIPI2 punctae per cell was calculated, using 30 cells per condition. n=3 repeats (1 coverslip/repeat). Two-way ANOVA (with grouping by experimental repeat), Tukey post-hoc test. Treatment effect: $F(1, 2)=8614$; $p=0.0001$, genotype effect: $F(1, 2)=0.05176$; $p=0.84$, interaction: $F(1, 2)=0.3085$; $p=0.63$. On graph: $p<0.05$ (*).

4.5.3 LRRK2 inhibition does not affect basal or PP242-induced endogenous WIPI2 punctae levels in macrophages

The observation that loss of Lrrk2 does not affect basal or PP242-induced WIPI2 punctae numbers in WT macrophages (Figure 4.16) suggests that Lrrk2 is unlikely to be involved in autophagy in this cell type. However, this result does not exclude the possibility of a requirement for Lrrk2 that is masked by adaptive changes in the Lrrk2 KO cell line. To test this possibility, and also to allow a comparison between

macrophages and HEK293 GFP-LC3 cells, the effect of acute (1 hour) Lrrk2 kinase and GTPase inhibition on basal or PP242-induced WIPI2 punctae levels was examined in WT macrophages.

Consistent with the equivalent experiments performed in HEK293 GFP-LC3 cells (Figure 4.10), inhibition of Lrrk2 kinase or GTPase activities had no effect on basal WIPI2 punctae number (Figure 4.17). In marked contrast however, the four compounds had no effect on the number of PP242-induced WIPI2 punctae (Figure 4.17). The data in this experiment thus support the previous results comparing autophagy in WT and Lrrk2 KO macrophages, and indicate that Lrrk2 is unlikely to be involved in autophagy in this cell type.

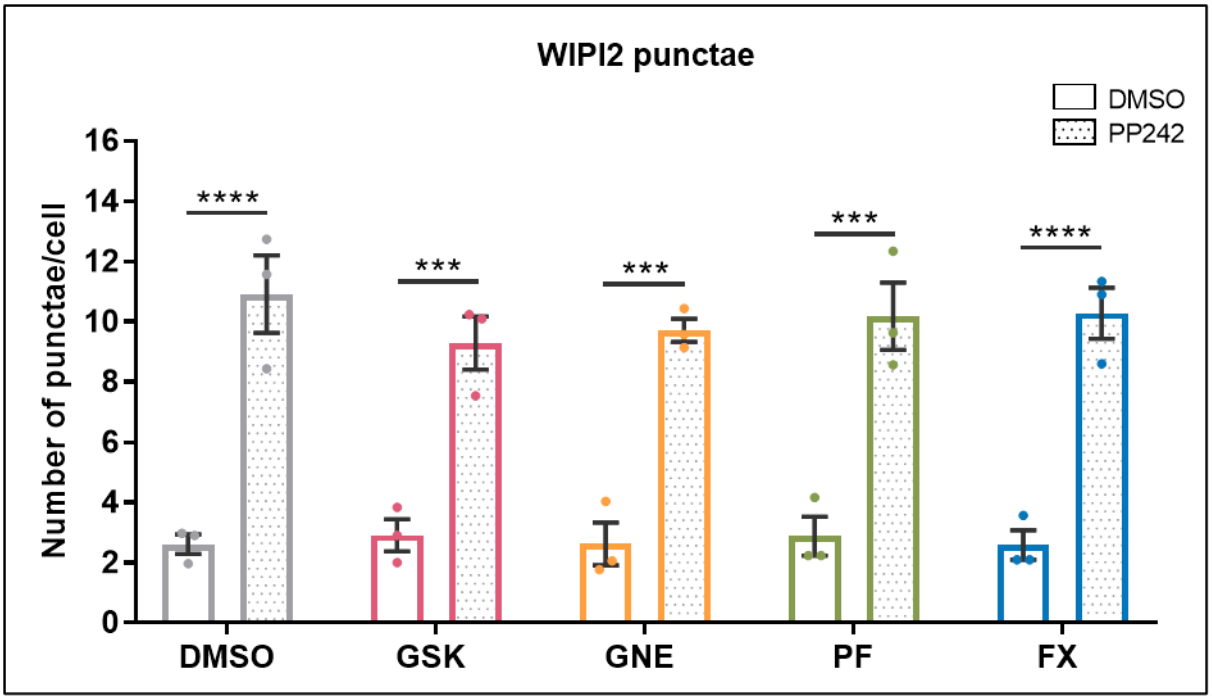

Figure 4.17: One-hour Lrrk2 inhibition had no effect on basal or PP242-induced WIPI2 punctae levels in macrophages.

RAW264.7 WT macrophages were pre-treated with LRRK2 kinase inhibitors (GSK2578215A: GSK; GNE-9605: GNE; PF-06447475: PF; all at 1 µM) or a GTPase inhibitor (FX2149: FX, 100 nM) or DMSO (1:1000 equivalent dilution) for 1 hour, then treated with PP242 (2 µM) or DMSO (1:1000 equivalent dilution) for 1 hour. Cells were then fixed and stained with an antibody against endogenous WIPI2. For each condition, the mean number (± SEM) of WIPI2 punctae per cell was calculated, using 30 cells per condition. n=3 repeats (1 coverslip/repeat). Two-way ANOVA (with grouping by experimental repeat), Tukey post-hoc test. PP242 treatment effect: $F(1, 2)=145.3$; $p=0.0068$, inhibitors effect: $F(4, 8)=1.173$; $p=0.39$, interaction: $F(4, 8)=1.063$; $p=0.43$. On graph: $p<0.0001$ (****), $p<0.001$ (***).

4.6 Effect of LRRK2 inhibition on Ivermectin-induced mitophagy in HEK293 GFP-LC3 cells

Mitochondrial dysfunction has been shown to play an important role in PD pathology. LRRK2 has been implicated in mitochondrial defects[652–655], and a growing number of studies implicate pathogenic LRRK2 mutants in mitochondrial dysfunction, notably affecting mitochondrial morphology and clearance[650,656,657]. Importantly, damaged mitochondria are targeted for degradation via a selective type of autophagy called mitophagy, and numerous studies suggest that autophagy impairment disrupts mitochondrial homeostasis, which can eventually lead to cell death and neurodegeneration.

To support the data obtained in this study, the effects of the LRRK2 inhibitors were tested on mitophagy induced by Ivermectin (IVM). IVM is a compound that is widely used as an anti-parasitic drug[658,659], but can be used as a selective inducer of mitophagy, triggering robust responses within 2 hours of treatment as determined by quantification of LC3 and WIPI2 punctae, among other methods[659]. Importantly, whereas PP242 induces autophagy by acting as an mTORC1 and mTORC2 inhibitor, in HEK293 cells at least, IVM does not appear to rely on mTORC1[659]. Thus, as well as acting as an inducer of a specific type of autophagy that is pertinent to Parkinson's disease, the use of IVM can complement experiments performed using PP242 by allowing the study of a form of autophagy that, in our HEK293 GFP-LC3 cells, is likely independent of mTORC1 inhibition.

Using conditions shown by others to robustly induce mitophagy in HEK293 cells[659], HEK293 GFP-LC3 cells were treated with IVM for two hours at a concentration of 15 µM, before GFP-LC3 punctae were quantified by live-cell imaging. As can be seen in the representative images (Figure 4.18), this treatment induced the formation of GFP-LC3 punctae comparable to the induction observed following one-hour PP242 treatment in previous experiments.

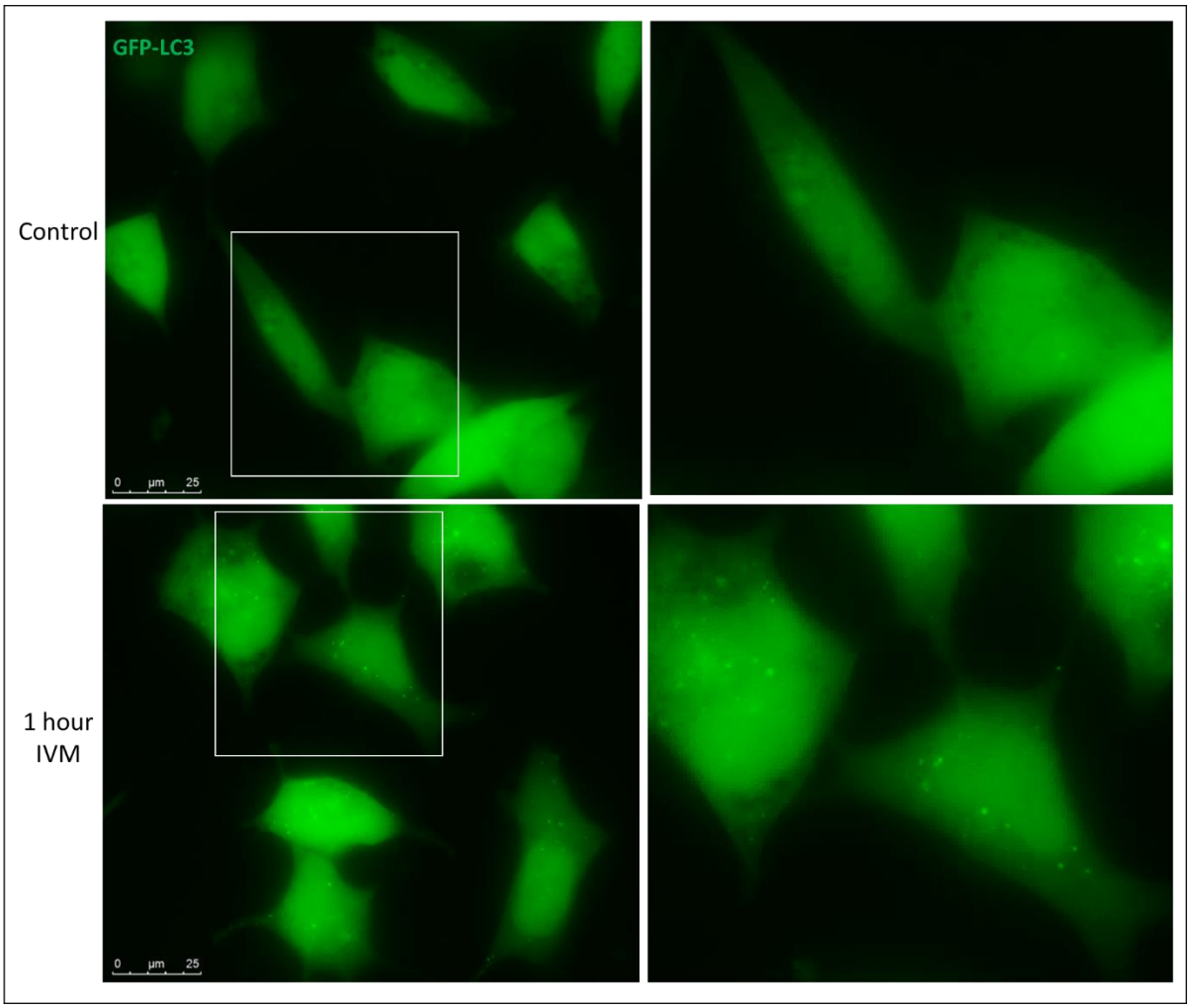

Figure 4.18: Representative images of GFP-LC3 punctae in IVM-treated HEK293 GFP-LC3 cells

Representative images of cells treated with DMSO or IVM at 15 µM for 2 hours. A greater number of GFP-LC3 punctae are visible following IVM treatment. Images on the left are original images acquired at 63x magnification. Images on the right are enlargements of the indicated areas within the original images

To investigate the requirement of LRRK2 kinase and GTPase activities in this process, cells were pre-treated for one hour with the LRRK2 kinase inhibitors (at 1 µM) or GTPase inhibitor (at 100 nM) or with DMSO prior to the IVM treatment (Figure 4.19). As expected, IVM triggered a significant increase in the number of GFP-LC3 punctae in DMSO-treated cells, and consistent with previous experiments, none of the LRRK2 inhibitors affected the basal number of GFP-LC3 punctae (Figure 4.19). Consistent with effects on PP242-induced autophagy in this cell line, LRRK2 inhibition significantly reduced the IVM-induced increase in GFP-LC3 punctae number.

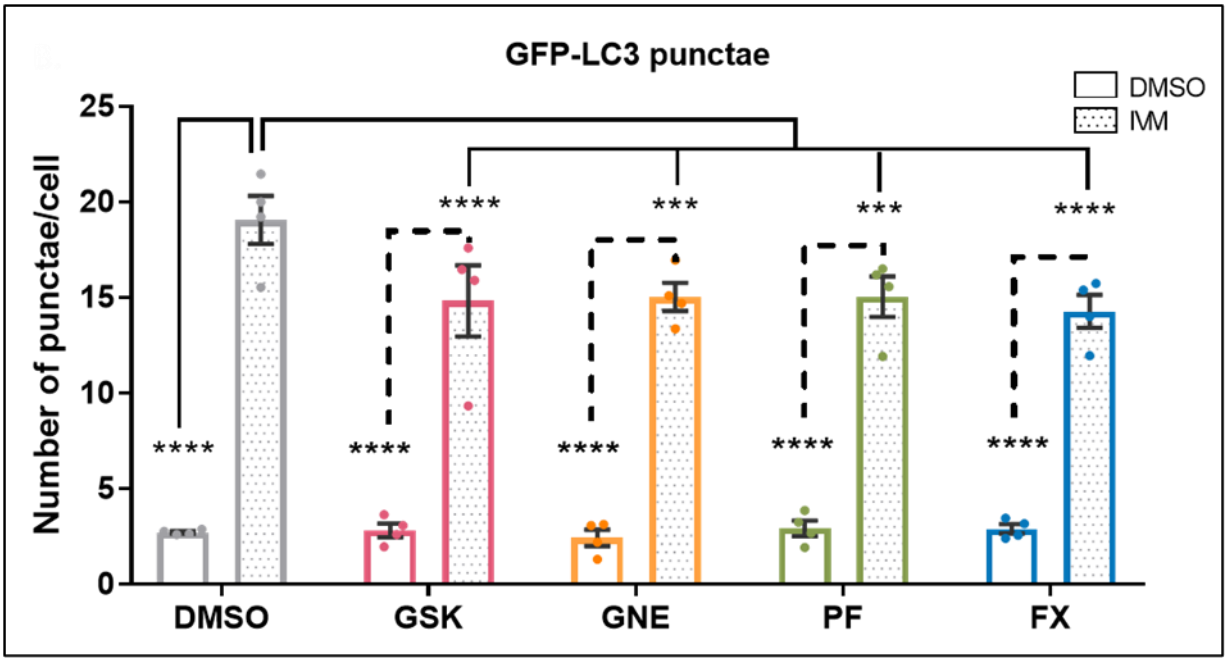

Figure 4.19: One-hour LRRK2 inhibition reduced the IVM-induced increase in GFP-LC3 punctae number in HEK293 GFP-LC3 cells.

HEK293 GFP-LC3 cells were pre-treated with LRRK2 kinase inhibitors (GSK2578215A: GSK; GNE-9605: GNE; PF-06447475: PF; all at 1 µM) or a GTPase inhibitor (FX2149: FX, 100 nM) or DMSO (1:1000 equivalent dilution) for 1 hour, then treated with IVM (15 µM) or DMSO (1:1000 equivalent dilution) for 2 hours. For each condition, the mean number (± SEM) of GFP-LC3 punctae per cell was calculated, using 30 cells per condition. n=4 repeats (1 coverslip/repeat). Two-way ANOVA (with grouping by experimental repeat), Tukey post-hoc test. IVM treatment effect: $F(1, 3)=90.64$; $p=0.0025$, inhibitors effect: $F(4, 12)=8.926$; $p=0.0014$, interaction: $F(4, 12)=14.98$; $p=0.0001$. On graph: $p<0.0001$ (****), $p<0.001$ (***).

These data are consistent with a role for LRRK2 kinase and GTPase activities in mitophagy. Nonetheless, it should be observed that the effect of LRRK2 inhibition was relatively small, as illustrated by the post-hoc pairwise comparisons which revealed significant effects of IVM treatment in each condition, irrespective of the pre-treatment. In particular, the extent with which the LRRK2 inhibitors impaired IVM-induced GFP-LC3 punctae formation compares poorly to equivalent experiments using PP242. Thus, whilst these data support roles for LRRK2 in forms of autophagy that are both dependent and independent of mTORC1 inhibition, the requirement may be greater in the former case.

4.7 Effect of the LRRK2 mutants on autophagy in HEK293 GFP-LC3 cells

Previous experiments in this Chapter indicated a kinase and GTPase activity dependent role for LRRK2 at an early stage of autophagy induced by mTORC1 inhibition in HEK293 GFP-LC3 cells, but not in RAW264.7 macrophages. Given the importance of LRRK2 to Parkinson's disease, the next step was to determine whether pathogenic and protective *LRRK2* mutations might also influence PP242-induced autophagy in HEK293 GFP-LC3 cells.

4.7.1 mApple can be used as a live-cell marker for LRRK2 expression in HEK293 GFP-LC3 cells

Since the use of the CRISPR technique to generate LRRK2 mutant cell lines was unsuccessful, the effects of *LRRK2* mutations on autophagy were investigated using transient overexpression of wild-type and mutant forms of LRRK2 in HEK293 GFP-LC3 cells. To take full advantage of this experimental model, these assays were performed on live cells, but this created a technical challenge of being able to identify which cells have been transfected with myc-tagged LRRK2 constructs. To solve this issue, the LRRK2 plasmids were co-transfected with a plasmid expressing the red fluorescent protein "mApple"[660]. In theory, the presence of a red label would identify the cells likely to overexpress LRRK2, such that only these cells are included in the experiment, while the excitation/emission spectra of mApple would not affect the ability to image and quantify green GFP-LC3 punctae.

To have confidence that mApple can be used as reliable proxy for co-transfected LRRK2, the frequency with which these constructs co-express within individual cells when transfected together was determined. HEK293 GFP-LC3 cells were co-transfected with an mApple plasmid and one of five myc-tagged LRRK2 constructs (wild-type, R1398H, R1441G, G2019S and the R1398H/R1441G double mutant) at a 70:30 by weight ratio of LRRK2 plasmid to mApple plasmid. Cells were subsequently fixed and co-transfection determined by fluorescence microscopy, with exogenous LRRK2 labelled by immunocytochemistry, using the combination of an anti-myc primary antibody and a secondary antibody

conjugated with the far-red fluorophore Alexa-633. An example of a field of HEK293 GFP-LC3 cells co-transfected with mApple (red) and myc-tagged wild-type LRRK2 (cyan) is shown in Figure 4.20.

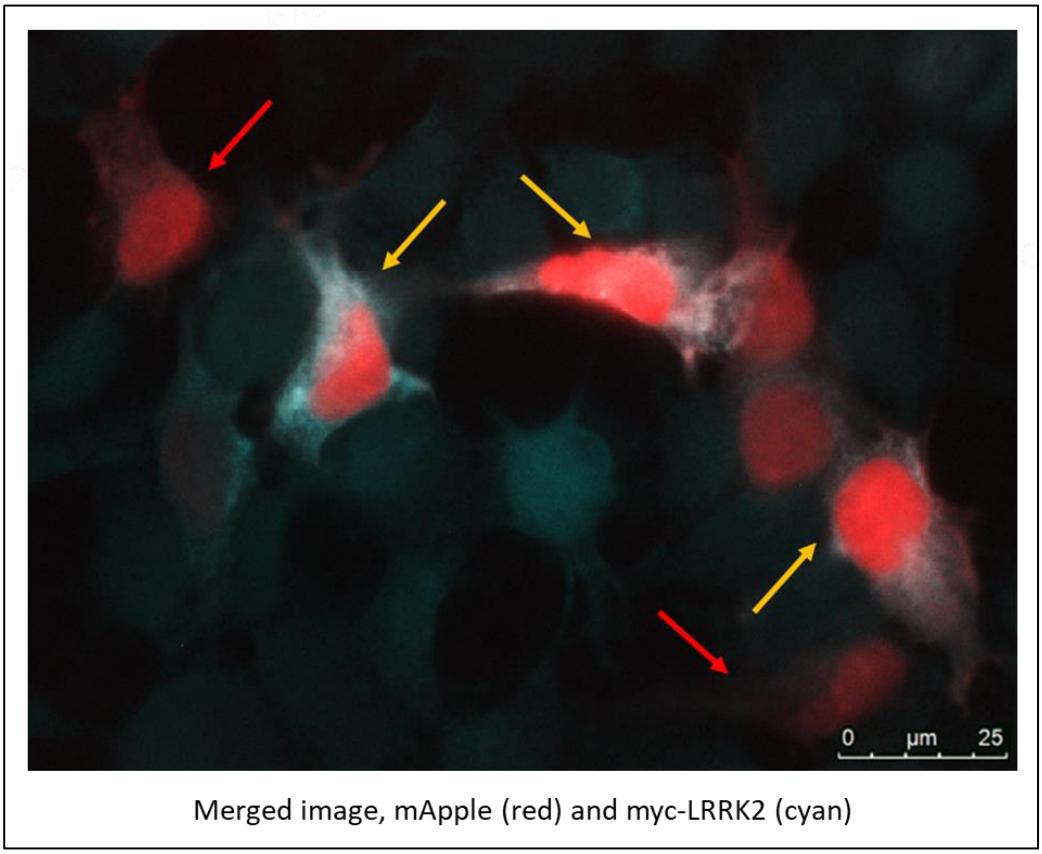

Figure 4.20: HEK293 GFP-LC3 cells expressing mApple and/or myc-LRRK2

HEK293 GFP-LC3 cells were co-transfected with the mApple plasmid and LRRK2 plasmids carrying various mutations of interest. The cells were then fixed and stained with an antibody against the myc-tag of the LRRK2 plasmid. The images represent transfected cells appearing red (expressing mApple) or cyan (expressing LRRK2 WT) via fluorescence microscopy. Cells expressing mApple only are shown with a red arrow, cells co-expressing mApple and LRRK2 WT are shown with a yellow arrow. The other cells that appear cyan are part of the background staining. Images were acquired at 63x magnification.

The proportion of transfected cells expressing one or both types of plasmids was quantified and is shown in Figure 4.21 A. In all cases, 68-82% of transfected cells expressed both constructs, with 12-20% expressing only mApple, and 3-13% expressing LRRK2 alone. Importantly, the different mycLRRK2 constructs used have no significant effects on these ratios, indicating that there are unlikely to be any cytotoxic effects associated with any of the constructs under the conditions used.

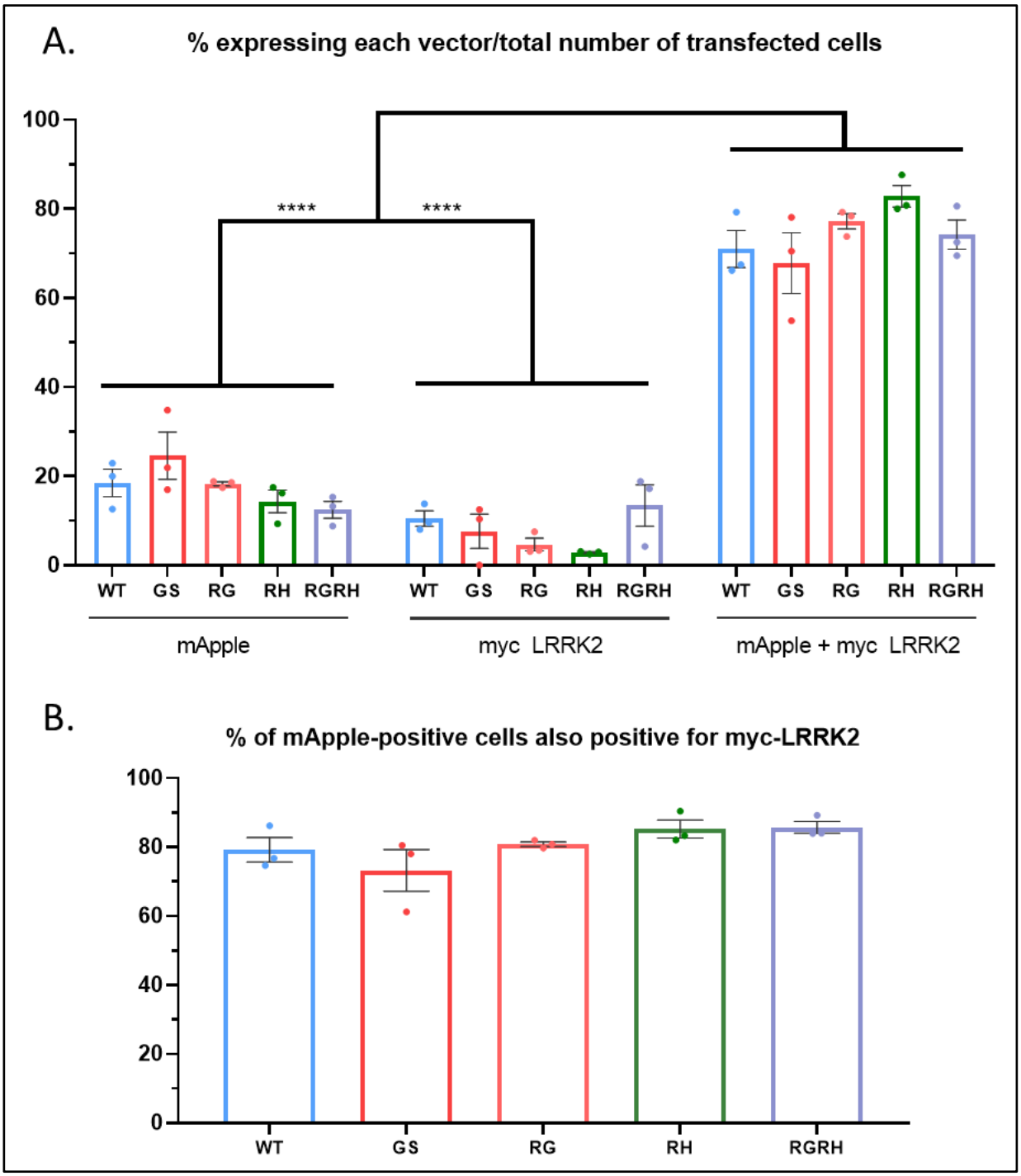

Figure 4.21: Efficiency of mApple and LRRK2 co-transfection in HEK293 GFP-LC3 cells

HEK293 GFP-LC3 cells were co-transfected with mApple and plasmids expressing wild-type LRRK2 (WT) or different LRRK2 mutants (GS (G2019S), RG (R1441G), RH (R1398H protective variant) or RGRH (contains both R1441G and R1398H variants)). Cells were fixed and stained with an antibody against the myc-tag of the LRRK2 proteins. For each condition the number of cells that appeared red (mApple) and/or cyan (myc-LRRK2, Alexa-633) were quantified, using 15 images per condition. **(A)** Quantitative analysis of the transfection efficiency for each plasmid. The percentage corresponds to the proportion of cells expressing LRRK2 and/or mApple compared to the total number of transfected cells. For example, in the WT condition, out of all the transfected cells: ≈ 70% expressed mApple and LRRK2, ≈ 20% expressed mApple alone, and ≈ 10% expressed LRRK2 only. n=3 repeats (1 coverslip/repeat). Two-way ANOVA (with grouping by experimental repeat), Tukey post-hoc test. Transfection type effect: $F(2, 4)=218.9$; $p<0.0001$, LRRK2 variant effect: $F(4, 8)=0.7429$; $p=0.59$, interaction: $F(8, 16)=2.577$; $p=0.051$. On graph: $p<0.0001$ (****). **(B)** Quantitative analysis of cells expressing mApple. The percentage corresponds to the proportion of cells expressing mApple that also co-express LRRK2. n=3 repeats (1 coverslip/repeat). One-way ANOVA (with grouping by experimental repeat), Geisser-Greenhouse's correction, non-significant. LRRK2 variant effect: $F(1.648, 3.297)=1.986$; $p=0.266$.

Importantly, in live-cell GFP-LC3 assays that count GFP-LC3 punctae only in mApple positive cells, cells expressing myc-tagged LRRK2 alone would not be selected for quantification. Thus, to obtain an estimate of the proportion of transfected cells that co-express LRRK2 that is more relevant to the intended use, the fraction of cells expressing LRRK2 alone were removed from the data presented in Figure 4.21 A, and the proportion of LRRK2 and mApple double-positive cells was re-calculated as a percentage of all mApple-positive cells (Figure 4.21 B). This secondary analysis revealed that for all LRRK2 plasmids, co-transfection with mApple at the same 70:30 ratio will allow mApple to be used as a proxy for myc-LRRK2 co-transfection with a confidence of approximately 80%. In other words, in experiment where GFP-LC3 punctae are quantified in all mApple-positive cells, this can be done with the assumption that four out of every five cells will overexpress the relevant LRRK2 construct. Although this ratio could have been higher it was considered sufficient for any robust effects of mutation to be detected.

4.7.2 LRRK2 mutants do not affect basal or PP242-induced GFP-LC3 punctae levels in HEK293 GFP-LC3 cells

To investigate the effects of the LRRK2 mutants on basal or PP242-induced autophagy, HEK293 GFP-LC3 cells were co-transfected with the combination of mApple and myc-LRRK2 plasmids or empty vector using the conditions established previously, with GFP-LC3 punctae only quantified in cells expressing mApple.

Surprisingly, PP242 treatment (2 μM, 1 hour) induced a smaller increase in GFP-LC3 punctae number than was observed in comparable experiments (Figure 4.22; cf. Figure 4.5, Figure **4.8** and Figure 4.11), only rising to 12 punctae per cell in control cells that overexpress mApple but not LRRK2. However, similar results were observed in all six conditions, such that the overall effect of PP242 treatment was statistically significant (ANOVA, $p<0.05$), but only two of the post-hoc pairwise comparisons (those for cells transfected with WT LRRK2 and LRRK2 RGRH) reached significance (Tukey's test, $p<0.05$). Despite this lower induction of autophagy, which is discussed later in this Chapter, statistical analysis indicated that none of the mutant forms of LRRK2 affected basal or induced GFP-LC3 punctae numbers relative to

wild-type LRRK2, whilst over-expression of wild-type LRRK2 also caused no significant effects relative to the empty vector control.

Taken together, these data indicate that pathogenic or protective *LRRK2* mutations either have no effect on PP242-induced autophagy, or have too small an influence to be detectable under these experimental conditions.

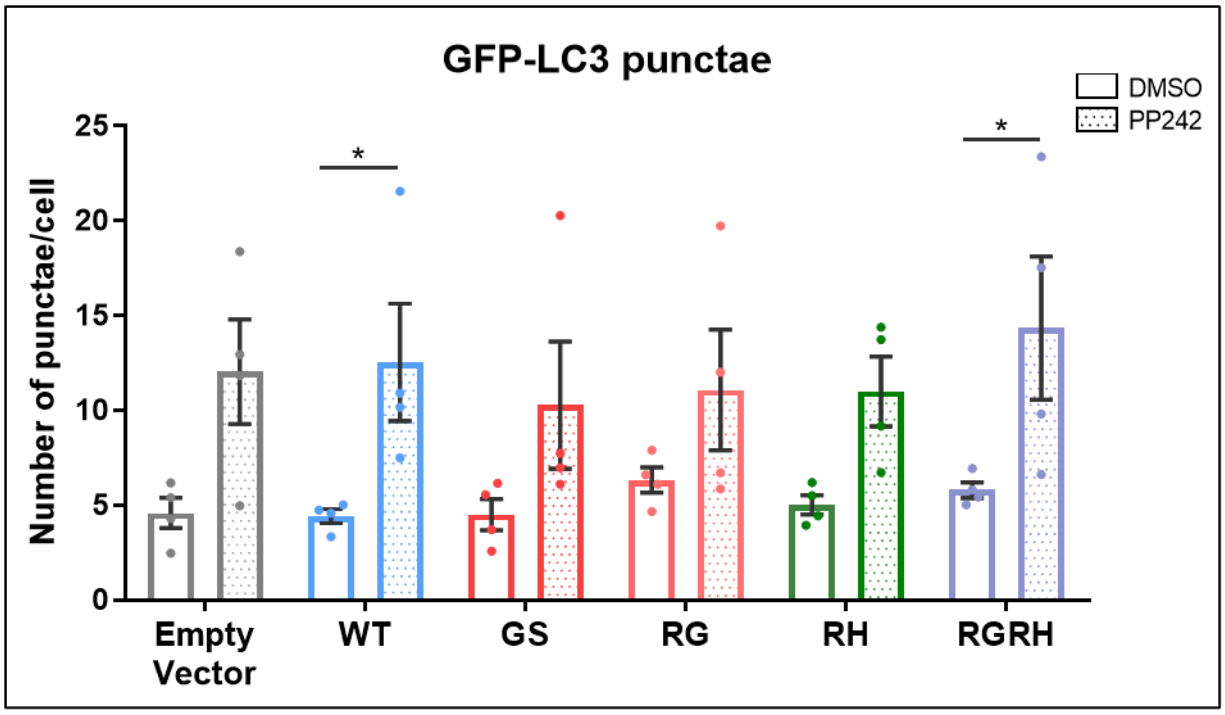

Figure 4.22: LRRK2 mutants do not affect basal or PP242-induced GFP-LC3 punctae levels in HEK293 GFP-LC3 cells.

HEK293 GFP-LC3 cells were co-transfected with the mApple plasmid and plasmids carrying wild-type LRRK2 (WT) or different forms of mutated LRRK2 (GS (G2019S pathogenic variant), RG (R1441G pathogenic variant), RH (R1398H protective variant) or RGRH (contains both R1441G and R1398H variants)), then treated with PP242 (2 µM) or DMSO (1:1000 equivalent dilution) for 1 hour. For each condition, the mean number (± SEM) of GFP-LC3 punctae per cell was calculated, using 50 cells per condition. Relevant cells were selected on the basis of expressing mApple. n=4 repeats (1 coverslip/repeat). Two-way ANOVA (with grouping by experimental repeat), Tukey post-hoc test. PP242 treatment effect: $F(1, 3)=10.74$; $p=0.0465$, LRRK2 variant effect: $F(5, 15)=0.5082$; $p=0.766$, interaction: $F(5, 15)=0.4968$; $p=0.774$. On graph: $p<0.05$ (*).

4.8 Exploring the role of LRRK2 using transmission electron microscopy

The results obtained in this Chapter using fluorescence microscopy assays strongly implicated the enzymatic activities of LRRK2 in the induction of autophagy in HEK293 GFP-LC3 cells but not in macrophages. We thus sought to use a complementary technique to support our data.

As discussed in Section 1.3.6 (Chapter 1), different tools can be used to measure autophagy. Fluorescence microscopy has the advantage that it enables the investigation of autophagy in live cells, but has its own limitations, as discussed later in this Chapter. Commonly, fluorescence microscopy assays can be complemented with transmission electron microscopy, which was the first method largely involved in autophagy research[329]. Electron microscopy is notably adapted to study ultrastructures within cells with subcellular resolution, and has been used in numerous studies to establish the presence, luminal content, number, and morphology of autophagic vesicles[329,337].

New experiments were therefore undertaken to explore whether electron microscopy could reveal changes in the appearance of autophagic vesicles in HEK293 GFP-LC3 cells treated or not with PP242 following LRRK2 inhibition, or in comparison between wildtype and Lrrk2 KO macrophages (data not shown). Unfortunately, it quickly became apparent that this approach was not feasible within the available time. Structures likely to be autophagic in nature varied tremendously within individual cells and their appearance was also influenced by where they were positioned relative to the plane in which the sections were cut. In brief, although a more exhaustive study may yet reveal important insights, there were no obvious gross morphological differences between conditions.

This approach was therefore abandoned. Nonetheless, it was hypothesised that the large increase in autophagic vesicle number elicited by PP242 treatment might be reflected by a corresponding increase in the number of vacuoles visible in electron microscopy samples. By extension, the effects of LRRK2 inhibition or of Lrrk2 knockout might also be reflected in vacuole numbers. Such quantifications would be unlikely to provide any additional mechanistic insight into the role of LRRK2 in autophagy, but would at least provide data in support of the GFP-LC3 and WIPI2 assays. Thus, an assay to quantify the number of vacuoles per cell in transmission electron microscope sections was developed.

4.8.1 Establishing an electron microscopy assay to quantify vacuoles in HEK293 GFP-LC3 cells

As depicted in Figure 4.23, which shows an example field of DMSO-treated HEK293 GFP-LC3 cells, vacuoles can be identified within cells using low magnification (2500-3000x) electron microscopy images. In both HEK293 GFP-LC3 cells and RAW264.7 macrophages vacuoles are easily identifiable as round, electron lucent structures, although they are heterogeneous in terms of their size and content.

The number of vacuoles per cell was calculated using the cell counter plug-in within ImageJ. First, the number of cells that were entirely visible within the area of each image were counted (Figure 4.23, labelled with a blue number 1). Second, vacuoles of any size that were present in the counted cells were counted (labelled with a red number 2). The mean total number of vacuoles per cell in each condition was then calculated from these two values. It should be noted that on a cell-by-cell basis, the total number of vacuoles varied markedly; it was thus decided that calculations of the means for each condition should use values from a minimum of 100 cells.

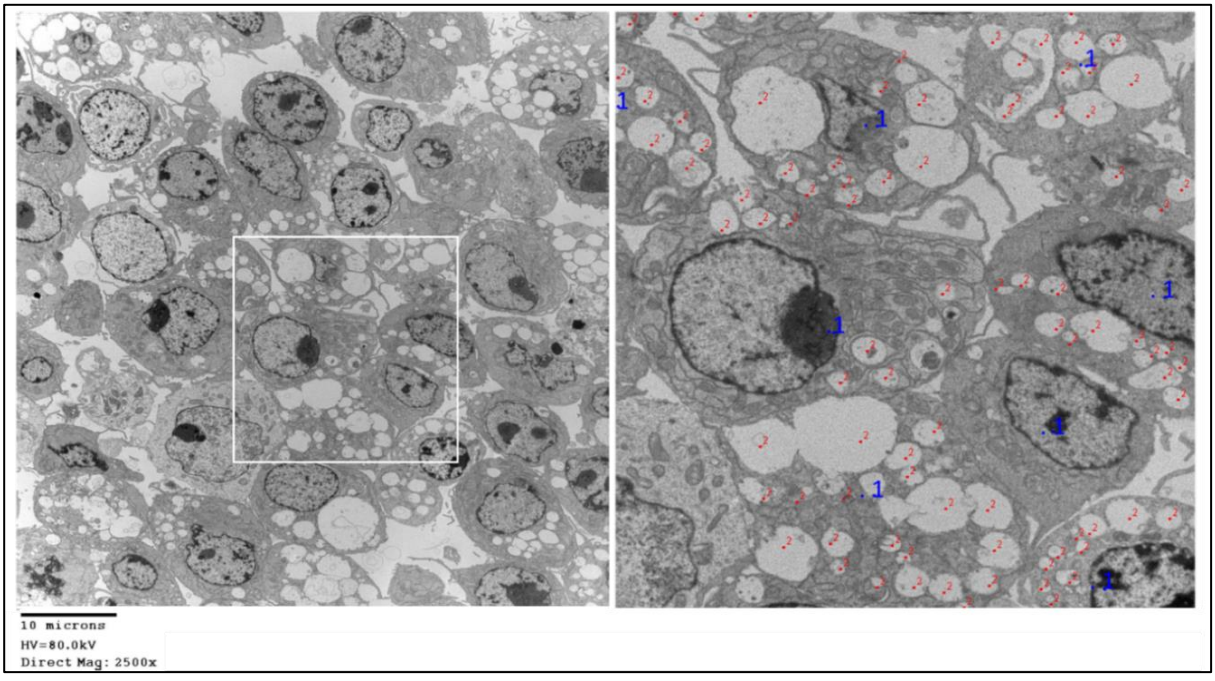

Figure 4.23: Detection of autophagic vesicles in HEK293 GFP-LC3 cells using electron microscopy.

Electron micrographs showing HEK293 GFP-LC3 cells treated 1 hour with a 1:1000 dilution of DMSO before being fixed and processed for electron microscopy. The image on the left is the original image acquired at 2500x magnification. The image on the right is an enlargement of the indicated cropped area within the original to show the quantification method. The number of cells that are entirely visible within the area (labelled with a blue number) and the number of vacuoles of any size that are present in the counted cells (labelled with a red number) were quantified in each image using the cell counter plugin for ImageJ, before calculating the mean number of vacuoles per cell.

4.8.2 Effect of LRRK2 inhibition on PP242-induced vacuole number in HEK293 GFP-LC3 cells

For consistency with the fluorescence microscopy data, the effect of LRRK2 inhibition on the number of vacuoles was investigated using HEK293 GFP-LC3 cells under identical treatment conditions to those used to study GFP-LC3 and WIPI2 punctae throughout this Chapter. Since no effects of LRRK2 inhibitors were found on basal GFP-LC3 or WIPI2 punctae levels, this experiment only explored whether LRRK2 inhibition might affect PP242-induced autophagy. Following treatment, the cells were fixed and processed for observation by electron microscopy (Chapter 2, Section 2.4.7.2), and the vacuoles were quantified using the method described in the previous Section.

As expected, one-hour treatment with PP242 induced a significant increase in the number of vacuoles compared to control cells (Figure 4.24), with vacuole number increasing from a mean of 7 to 12 vacuoles per cell.

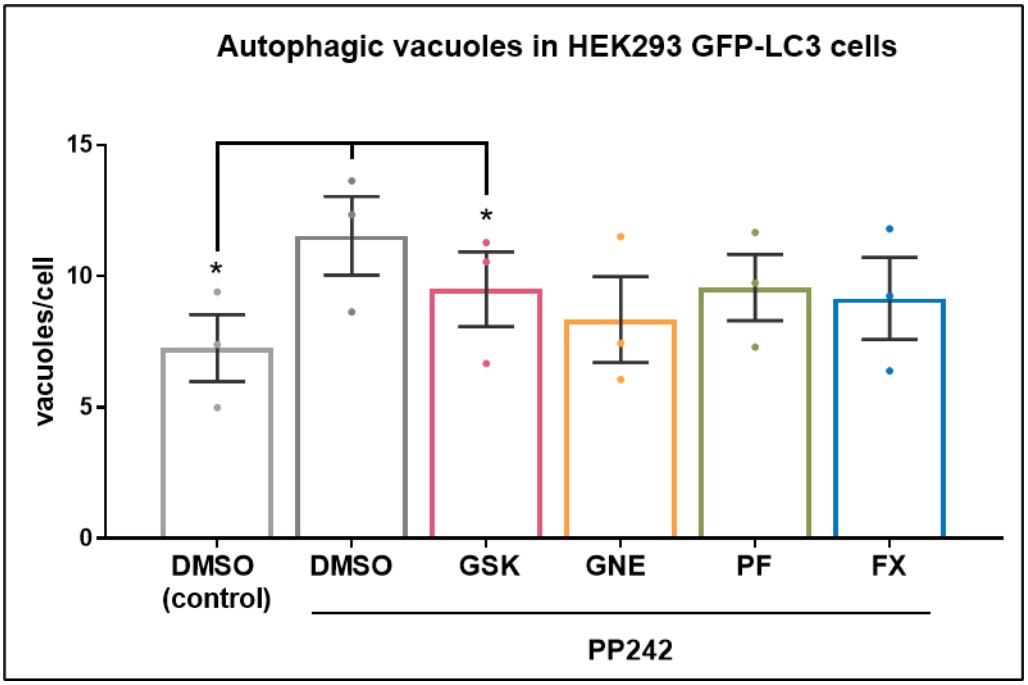

Figure 4.24: One-hour LRRK2 inhibition reduced the PP242-induced increase in vacuole number in HEK293 GFP-LC3 cells.

HEK293 GFP-LC3 cells were pre-treated with LRRK2 kinase inhibitors (GSK2578215A: GSK; GNE-9605: GNE; PF-06447475: PF; all at 1 µM) or a GTPase inhibitor (FX2149: FX, 100 nM) or DMSO (1:1000 equivalent dilution) for 1 hour, then treated with PP242 (2 µM) or DMSO (1:1000 equivalent dilution) for 1 hour. Cells were then processed for electron microscopy. For each condition, the mean number (± SEM) of vacuoles per cell was quantified using the cell counter plugin for ImageJ, from a minimum of 5 images using >100 cells per condition. n=3 repeats, One-way ANOVA (with grouping by experimental repeat), Geisser-Greenhouse ‘s correction, Dunnett’s post-hoc test with comparison to DMSO+PP242. $F(1.231, 2.462)=15.23$; $p=0.042$. On graph: $p<0.05$ (*).

Pre-treatment with LRRK2 inhibitors appeared to globally, but moderately, reduce the PP242-induced increase in vacuoles, with similar results observed with all four inhibitors. The only post-hoc pairwise comparison to reach significance was for cells treated with GSK2578215A, (Dunnett's test, $p<0.05$), but it is worth noting that the pairwise comparisons for PF-06447475 and FX2149 would have reached significance if the experimental design had featured one-tailed post-hoc analysis. One-tailed analysis could legitimately have been performed in this case, since the objective of the experiment was to replicate GFP-LC3 and WIPI2 data, and it was therefore assumed that the effect of LRRK2 inhibition would be to decrease, rather than to increase or decrease, PP242-induced vacuole numbers.

In any case, despite the weak statistics, these electron microscopy data are in general agreement with the fluorescence data obtained using GFP-LC3 and WIPI2 punctae quantification in HEK293 GFP-LC3 cells, which showed an increased autophagy using PP242 that was largely blocked by any of the four LRRK2 inhibitors.

4.8.3 Effect of loss of Lrrk2 on basal and PP242-induced autophagy in RAW264.7 macrophages

To confirm the WIPI2 assay data obtained in wildtype and Lrrk2 KO macrophages suggesting that Lrrk2 was not involved in autophagy in RAW264.7 macrophages (Section 4.5), transmission electron microscopy was used to quantify the number of vacuoles in these cell lines following treatment with PP242 or DMSO.

Similar to HEK293 GFP-LC3 cells, vacuoles could be identified within cells (images not shown), and generally appeared electron light. WT macrophages were found to have a mean of 9 vacuoles per cell basally and a mean of 12 vacuoles per cell when autophagy was induced, whereas Lrrk2 KO macrophages had a mean of 10 vacuoles per cell basally and a mean of 13 vacuoles per cell following PP242 treatment.

Unsurprisingly, statistical analysis found no effect of loss of Lrrk2, which is consistent with WIPI2 assays (Figure 4.25). However, in contrast to the WIPI2 experiments, the effect of PP242 treatment on total vacuole number was not significant. Taken together, these observations support the idea that Lrrk2 is

not involved in PP242-induced autophagy in RAW264.7 macrophages, while also illustrating the limitations of this assay, which are discussed further in Section 4.10.4.3.

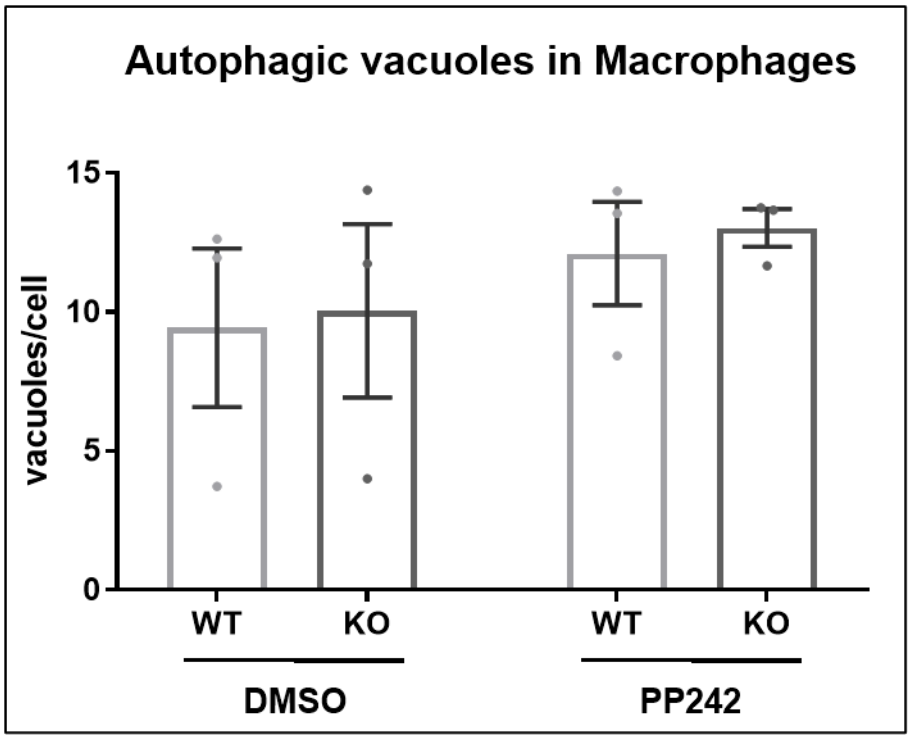

Figure 4.25: The loss of Lrrk2 in RAW264.7 macrophages did not affect basal or PP242-induced vacuole numbers

WT or Lrrk2 KO macrophages were treated with PP242 (2 μM) or DMSO (1:1000 equivalent dilution) for 1 hour. Cells were then processed for electron microscopy. For each condition, the mean number (± SEM) of vacuoles per cell was quantified using the cell counter plugin for ImageJ, from a minimum of 5 images using >100 cells per condition. n=3 repeats, Two-way ANOVA (with grouping by experimental repeat), non-significant. PP242 treatment effect: $F(1, 2)=2.537$; $p=0.252$, genotype effect: $F(1, 2)=1.397$; $p=0.359$, interaction: $F(1, 2)=0.05267$; $p=0.84$.

4.9 Summary of results

The work described in this chapter investigated the function of LRRK2 in autophagy using LRRK2 kinase and GTPase inhibitors in HEK293 GFP-LC3 cells and macrophages, the overexpression of LRRK2 mutants in HEK293 GFP-LC3 cells, and comparisons between wild-type and Lrrk2 KO macrophages. The chosen readouts for the induction of autophagy were measurements of GFP-LC3 and WIPI2 punctae numbers in live and fixed cells, and quantification of endogenous WIPI2 punctae and total vacuole number in fixed cells. Measurements were taken basally and following exposure to autophagy modulators.

The key findings are:

- Exposure to the LRRK2 inhibitors is not cytotoxic for the cell lines used in this study (Figure 4.3 and Figure 4.14).
- Basal autophagy in HEK293 GFP-LC3 cells was not affected by the inhibition of LRRK2 kinase or GTPase activities (Figure 4.4).
- LRRK2 inhibition prevented the PP242-induced increase in GFP-LC3 punctae number in HEK293 GFP-LC3 cells (Figure 4.5, Figure 4.8 and Figure 4.11), but did not block the degradation of autophagosomes (Figure 4.7).
- All four LRRK2 inhibitors prevented the PP242-induced increase in GFP-LC3 punctae number and endogenous WIPI2 punctae number to similar extents in HEK293 GFP-LC3 cells (Figure 4.13).
- Comparison of the number of basal and PP242-induced WIPI2 punctae in RAW264.7 macrophages revealed no effect of loss of Lrrk2 in this cell line (Figure 4.16).
- LRRK2 inhibition had no effect on basal or PP242-induced WIPI2 punctae in wild-type macrophages (Figure 4.17).
- LRRK2 inhibition leads to a partial reduction in the number of IVM-induced GFP-LC3 punctae in HEK293 GFP-LC3 cells (Figure 4.19).

- Overexpression of wild-type LRRK2, pathogenic LRRK2 mutants, or the protective R1398H variant had no effect on basal or PP242-induced GFP-LC3 punctae levels in HEK293 GFP-LC3 cells. (Figure 4.22)
- Quantification of vacuoles from images acquired using transmission electron microscopy supported evidence of an inhibitory effect of LRRK2 inhibitors on PP242-induced autophagy in HEK293 GFP-LC3 cells (Figure 4.24), and similarly supported conclusions that Lrrk2 is not involved in autophagy in macrophages (Figure 4.25).

4.10 Discussion

4.10.1 LRRK2 in autophagy in HEK293 GFP-LC3 cells

4.10.1.1 LRRK2 Inhibitors

In this study, no effects of the inhibitors were observed on basal autophagy in HEK293 GFP-LC3 cells in no fewer than 7 experiments (Figure 4.4, Figure 4.5, Figure 4.7, Figure 4.8, Figure 4.10, Figure 4.11, and Figure 4.19). LRRK2 enzymatic activities are also unlikely to be involved in the later stages of autophagy in this cell line (Figure 4.7) but by contrast, all four inhibitors suppressed PP242-induced autophagy (Figure 4.5, Figure 4.8, Figure 4.10, Figure 4.11 and Figure 4.24), and reduced the formation of WIPI2 and GFP-LC3 punctae to a similar extent (Figure 4.13). Given the different structures of these compounds and the different mechanism of action of FX2149 compared to the kinase inhibitors, these are convincing observations, although it would be interesting to investigate the effect of treatment with vitamin B12, which has been reported to inhibit LRRK2 kinase activity via an alternative, allosteric mechanism[62]. These data strongly indicate that LRRK2 is required for PP242-induced autophagy at an early stage, upstream of LC3 punctae formation, and between inhibition of mTORC1 complex and the recruitment of WIPI2 to autophagic vesicles.

The observation that LRRK2 inhibitors suppressed the induction of autophagy is in disagreement with previous studies[175,176,233,598,617], which described increased autophagy following LRRK2 kinase inhibition. In theory, many differences between the experimental set ups could account for this discrepancy, not least the cell type used. Nonetheless, it should be noted that some of these publications used 1st generation kinase inhibitors which suggests a greater chance of off-target effects.

Intriguingly, similar effects of the kinase inhibitors and the GTPase inhibitor were observed throughout the experiments. This suggests that the GTPase activity of LRRK2 is as important as its kinase activity in this aspect of LRRK2 function, and is perhaps consistent with previous studies suggesting a complex functional relationship between LRRK2 kinase and its GTPase activities[112,164].

4.10.1.2 LRRK2 Mutants

In this study, all of the overexpressed mutant forms of LRRK2 tested (WT LRRK2, R1398H, R1441G, G2019S and the R1398H/R1441G double mutant) had no significant effect on basal or PP242-induced autophagy (Figure 4.22). This is mostly inconsistent with the literature, which would predict an increase in GFP-LC3 punctae in presence of the pathogenic mutants G2019S and R1441G, both in the basal state and following treatment with PP242[108,479]. By extension, since the protective R1398H mutation has been shown to reverse the effects of R1441G in neurite outgrowth assays[108], one might expect a similar opposite effect on autophagy with this variant.

There are a number of explanations that might account for this disagreement. For example, the result obtained may be correct for the HEK293 GFP-LC3 cell type used, while it is also possible that the LRRK2 mutants had too small an influence on autophagy to be detectable under the experimental conditions used. Nonetheless, it is interesting to note that GFP-LC3 punctae were notably fewer in number in this experiment (Figure 4.22) than in other experiments that used this cell line. Thus, it may be the case that transfection of HEK293 GFP-LC3 cells with mApple and/or LRRK2 plasmids prevents the expression of GFP-LC3, causing GFP-LC3 punctae to be harder to observe. This is a plausible hypothesis, since GFP-LC3 expression is driven by a CMV promoter similar to those present in the transfected plasmids, making competition for transcriptional machinery a distinct possibility. A solution to this issue could be to assess the effect of wildtype and mutant LRRK2 constructs on endogenous WIPI2 punctae. Such assays would be performed on a read-out that is less likely to be affected by the exogenous promoters, and the experiment would be further simplified by the omission of mApple, since transfected cells could be identified with an anti-myc antibody targeting myc-LRRK2

4.10.1.3 Comparison between the effects of LRRK2 inhibition and LRRK2 mutations on autophagy

It is now well established that the pathogenic *LRRK2* G2019S mutation causes hyperactivation of LRRK2 kinase activity, whilst the R1441G mutation also appears to exert a similar effect, if not at the level of

kinase activity, then at least at the level of substrate phosphorylation. As such, these mutations can be assumed to affect LRRK2 kinase activity in an opposing manner to LRRK2 kinase inhibitors. The relationship between the LRRK2 GTPase inhibitor FX2149 and the corresponding LRRK2 RocCOR domain mutants R1441G and R1398H is less clear however, since FX2149 prevents guanine nucleotide binding, whereas R1441G and R1398H, by impairing and enhancing GTPase activity respectively, have the effect of shifting LRRK2 towards GTP- and GDP-bound states, respectively. Nonetheless, by analogy with other GTPases, the assumption is that preventing all guanine nucleotide binding and increasing binding specifically to GDP both constitute losses of function, so at a functional level FX2149 is most likely to behave similarly to the protective R1398H mutation, and oppositely to R1441G. Taking all this together, these observations predict a model where both types of inhibitor exert effects in the same direction as R1398H, but in the opposite direction to R1441G and G2019S.

Here, acute inhibition of LRRK2 kinase and GTPase activities caused a marked inhibition of PP242-induced autophagy, yet the overexpression of LRRK2 mutants did not elicit the anticipated effects. A number of factors might account for this. For instance, at the concentrations used the LRRK2 inhibitors can be assumed to abolish the enzymatic activities of LRRK2[177,642–644], whilst the mutant forms of LRRK2 merely modulate these activities. Furthermore, there is a potential problem with endogenous LRRK2. Whilst the inhibitors inactivate the endogenous protein, the overexpressed LRRK2 mutants may not be able to outcompete and replace endogenous LRRK2 sufficiently well to exert a measurable effect on autophagy. As such, it is unfortunate that the CRISPR project was unsuccessful, since the use of cell lines with genomic modifications in *LRRK2* would have circumvented potential interference from endogenous wild-type LRRK2. In addition, it is worth repeating the possibility mentioned in the last section, that overexpression of LRRK2 plasmids and/or mApple might supress GFP-LC3 expression, thereby preventing effects of *LRRK2* mutations from being seen. The proposed experiment examining the effect of overexpressed LRRK2 mutants in HEK293 GFP-LC3 cells using endogenous WIPI2 assays might alone be sufficient to allow the expected effects of mutations to be seen, thereby reconciling the differences between LRRK2 inhibitors and LRRK2 mutants data.

4.10.1.4 IVM-induced autophagy

LRRK2 inhibition in HEK293 GFP-LC3 cells reduced IVM-induced mitophagy (Figure 4.19), albeit seemingly to a lesser extent than the same compounds impair PP242-induced autophagy. Whilst there are some reports that IVM can inhibit mTORC1 in certain cancer lines[661–663] , these compounds appear to induce autophagy via different mechanisms in HEK293 cells, with the induction of autophagy by IVM apparently not relying on the inactivation of mTORC1[659]. These observations suggest that, at least in HEK293 cells and HEK293-derived cell lines like HEK293 GFP-LC3, LRRK2 might be acting at a step shared by both canonical and non-canonical forms of autophagy.

Thus, the next step in studying the role of LRRK2 in IVM-induced autophagy would be to determine at what point LRRK2 might be acting. A key step in canonical autophagy induction is dephosphorylation of the kinase ULK1. In the basal state, the mTORC1-dependent phosphorylation of ULK1 at serine-758 inhibits ULK1 kinase activity, preventing the formation of autophagosomes and blocking autophagy. Inhibition of mTORC1 relieves this repression, thereby inducing the production of autophagic vesicles. However, mTORC1-independent phosphorylation of ULK1 at serine-758 has been reported by Manzoni and colleagues using astrocytic cell lines[616], so in principle, ULK1 is a candidate site of action for LRRK2 in our system. Furthermore, the Manzoni study reported that prolonged (18 hours) treatment with relatively high doses of the LRRK2 inhibitors LRRK2-IN-1, GSK2578215A or MLi-2 increased phosphorylation of ULK1 at the same inhibitory serine-758 phosphorylation site targeted by mTORC1[616]. It should be noted that the authors also reported that, in contrast to our data, the net effect of LRRK2 inhibition was increased autophagy as evidenced by LC3-II levels, but increased phosphorylation of ULK1 at serine-758 *per se* is more consistent with our observation of a repression of autophagy. Importantly, Manzoni and colleagues attributed this apparent disagreement in their data to the plausible possibility that LRRK2 may have both positive and negative effects on autophagy[616], and thus it may be the case that the differing net effect of LRRK2 inhibition on autophagy in different cell types is a function of the strength with which these pro- and anti-autophagic mechanisms operate.

Arguing against ULK1 phosphorylation as the site of action of LRRK2 inhibition in our system is the observation made by Zachari and colleagues that activation of mitophagy by IVM is unaffected in ULK1/ULK2 knockout MEFs, even though PP242-induced autophagy was entirely abrogated in this cell line[659]. However, this same paper reported that the ULK complex components FIP200 and ATG13 were required for IVM-induced mitophagy, and the experimental design used by Zachari and colleagues did not exclude the possibility of a partial requirement for ULK1/2, only an absolute requirement[659]. Importantly, the LRRK2 inhibitors only elicited a small reduction in mitophagy (Figure 4.19) when compared to their effects on PP242-induced autophagy. Therefore, the effect of LRRK2 inhibition on ULK1 phosphorylation, or perhaps more generally at the level of the ULK complex, needs further investigation (see Section 4.10.5 for additional experiments).

Alternatively, further work investigating whether LRRK2 inhibition is able to rectify mitophagy defects, as recently reported in the literature[176], for example using the pH-dependent probe mito-rosella, might help understand the involvement of LRRK2 in this selective type of autophagy.

4.10.2 LRRK2 in autophagy in macrophages

In this study, neither the loss of Lrrk2 (Figure 4.16) or Lrrk2 inhibition (Figure 4.17) affected basal or PP242-induced autophagy in RAW264.7 macrophages. This result is surprising, since the experimental design was identical to that used for HEK293 GFP-LC3 cells, whilst the published literature predict that both LRRK2 inhibition and knockout should disrupt autophagy[233]. Indeed, in various monocytes including the RAW264.7 cell line, the silencing of endogenous Lrrk2 or inhibition of Lrrk2 kinase activity using the GSK2578215A inhibitor led to impaired autophagy, with decreased LC3-II levels[233], suggesting an important role for Lrrk2 kinase function in autophagy in these cell lines. In principle, the absence of effect of *Lrrk2* knockout on autophagy in this study can be explained by the existence of compensatory mechanisms in this cell line. Indeed, cell survival relies on autophagy, so it would not be surprising if there is some redundancy in its regulation[664]. However, the observation that acute loss of function via

enzymatic inhibition has similar effects suggests that a more likely explanation is simply that Lrrk2 is not involved in the early stages of mTORC1-dependent induction of autophagy in macrophages.

Irrespective of whether a role for Lrrk2 in autophagy in macrophages can be entirely excluded or not, the comparison between results obtained in macrophages and HEK293 GFP-LC3 cells provides solid evidence that the function of LRRK2 in autophagy is cell-type specific. There are many differences between the two cell types, but it is interesting to note that immune cells express high levels of LRRK2, and expression levels increase further when the cells are activated[142,17,18]. Whether the effect of LRRK2 on autophagy varies between cell lines depending on expression levels remains to be established, but this unambiguous evidence of cell-type specificity does at least explain the apparent discrepancies in the literature.

4.10.3 Transmission Electron Microscopy assays

Additional transmission electron microscopy (TEM) assays were used in this study to monitor autophagy using vacuole quantification, and provided supporting data. In the case of experiments performed in HEK93 GFP-LC3 cells (Figure 4.24), the results corroborated data from GFP-LC3 and endogenous WIPI2 assays indicating that LRRK2 inhibition prevents the induction of autophagy by PP242, although the effects of LRRK2 inhibition were not as marked and within a smaller range (cf. Figure 4.24 and Figure 4.8, Figure 4.10 and Figure 4.11).

In the case of experiments performed in RAW 264.7 macrophages, although the average number of vacuoles increased following PP242 treatment in both genotypes, the effect of PP242 treatment was surprisingly non-significant (Figure 4.25), which is inconsistent with its effect on autophagic vesicles reported in these cell lines (see Figure 4.16 and Figure 4.17), and throughout this Chapter. However, loss of Lrrk2 had no effect on basal or PP242-induced number of vacuoles (Figure 4.25), which replicates the results obtained with endogenous WIPI2 assays (Figure 4.16) and further support a cell specific role for Lrrk2 in autophagy.

Taken together, the electron microscopy data concur with the fluorescence microscopy data obtained in both HEK293 GFP-LC3 and RAW264.7 macrophage cells in this Chapter, and are thus supportive of a role for LRRK2 in PP242-induced autophagy in HEK293 GFP-LC3 cells, but not in RAW264.7 macrophages.

4.10.4 Limitations of the assays used in this study

4.10.4.1 GFP-LC3 assays

GFP-LC3 assays are widely used but are not without limitations. One important concern is the expression of a relatively large GFP tag, which may to some extent alter the behaviour of the LC3 moiety. It has been shown that GFP-LC3 can be found in aggregates different from autophagic vesicles[268,665], as well as on autophagosomes generated from late endosomes and trans-Golgi[666]. In principle, these structures could be interpreted as punctae and mistakenly counted in GFP-LC3 assays. Moreover, LC3 can be coupled to endosomal membranes, so some of the quantified vesicles could be endocytic vesicles[328]. Data generated by GFP-LC3 assays therefore require supporting evidence obtained using other techniques. The reliability of GFP-LC3 assays can nonetheless be improved by staining samples for other proteins involved in the generation of autophagic vesicles or associated with the membrane of autophagosomes, which can also provide more information about the type of autophagic vesicle being examined. One example is the GABARAP family of proteins that localise on phagophores and are involved in cargo sequestration[667]. Assessing GABARAP lipidation levels[668] can be used as a complementary technique to account for fluctuations in the autophagic flux.

4.10.4.2 WIPI2 assays

Assays of endogenous WIPI2 were used in this study to quantify autophagy upstream of LC3. In the case of experiments performed in HEK293 GFP-LC3 cells, these assays corroborated data from GFP-LC3 quantification, so the WIPI2 data provided important supporting data. Nonetheless, WIPI2 punctae assays have their own limitations. In particular, WIPI2 punctae were quantified on antibody-stained fixed

cells, which can be challenging, as the quality of the images and the intensity of fluorescence can vary. It is worth mentioning that at basal levels, WIPI2 punctae seemed more numerous than GFP-LC3 punctae. This could be a true observation, but it is also possible that non-specific punctae caused by background staining create an overestimation of the number of WIPI2 punctae. In addition, similarly to LC3, WIPI2 could potentially associate with structures that are not autophagic vesicles but could be interpreted as such in WIPI2 assays. Arguing against this, WIPI2 is an endogenous protein, so it cannot be mistargeted as a result of overexpression and/or the addition of a GFP tag. However, endogenous WIPI2 may have as yet undescribed physiological roles on structures that appear similar to, but are not, autophagic vesicles.

4.10.4.3 Quantification of vacuoles observed in TEM images as a proxy measure of autophagy

As outlined, the approach of indirectly measuring changes in autophagic vesicle number by quantifying the total number of vacuoles visible per cell when imaged by low magnification electron microscopy is not an established technique to study autophagy, and is undoubtedly crude in its design. The approach was nonetheless successful, replicating observations made using other techniques, albeit with a relatively small dynamic range and correspondingly weaker statistics (fewer significant differences).

The major limitation with this assay is both obvious and inherent to the experimental design, namely that autophagic vesicles are only likely to represent a fraction of the total number of vacuoles visible. Nevertheless, since the number of vacuoles increased following PP242 treatment in HEK293 GFP-LC3 cells, and PP242 specifically induces an increase in autophagic vesicle number, it is evident that some of the vacuoles quantified must have been autophagic vesicles. But in any case, this method cannot be used with complete confidence that variations in vacuole numbers correspond to variations in autophagosome numbers.

Consistent with many of the observed vacuoles not being related to autophagy, in both HEK293 GFP-LC3 and macrophage cell lines, the number of vacuoles per cell varied considerably, with differences between mean vacuole number apparent only after quantification. For example, an individual cell might

have over fifty vacuoles visible basally, whereas another cell might have no discernible vacuoles even after PP242 treatment. This combination of relatively small differences in mean vacuole numbers between treatment groups and wide variation between cells within treatment groups meant that images of fields of cells that visually reflect the quantification of each treatment group were not possible. Lack of usable images is undoubtedly a limitation for any microscopy-based technique.

Besides this, an additional limitation when compared to other approaches to study autophagy is the length of time taken to generate data, with cells from each treatment group needing to be fixed and stained, and then images laboriously acquired with electron microscopy. The requirement for fixation and staining is itself a limitation, since, similar to WIPI2 assays, this led to some variation in staining intensity between experiments.

Finally, it should be emphasised that statistically significant results were principally obtained for the effect of PP242, which is a potent autophagy inducer. More subtle modulators of autophagy would be unlikely to provide enough stimulus for changes in autophagic vesicle number to be manifest at the level of total number of vacuoles per cell. Thus, whilst this technique undoubtedly works, its use is very limited. In the vast majority of cases, other more established techniques are undoubtedly superior.

4.10.4.4 Verification of LRRK2 inhibitors efficacy

To ensure effective target engagement of the LRRK2 inhibitors at the doses (100 nM or 1µM) and treatment durations (1 hour or 16 hours) employed in this thesis, several experiments could have been performed, in particular assays designed for the quantitative detection of phosphorylation levels on specific phosphosites. Indeed, there are several measures of endogenous LRRK2 activity that could be used as markers of target engagement.

The most obvious marker is the direct estimation of LRRK2 Ser1292 phosphorylation levels, which is a *bona fide* autophosphorylation site, in the presence of LRRK2 inhibitors. In principle, inhibition of LRRK2 kinase activity would likely reduce the levels of phospho-Ser1292-LRRK2, which can be measured using

Western immunoblotting or ELISA-based methods[669], with levels normalised to total LRRK2. Of note, ELISA-based methods are generally more sensitive than Western Blot-based assays to assess LRRK2 kinase activity or the efficiency of LRRK2 inhibitors[669]. Another possibility could be to assess the loss of phosphorylation of other LRRK2 residues that are phosphorylated by other kinases in a LRRK2-dependent manner, such as Ser910, 935, 955 or 973. Typically, LRRK2 inhibition would either prevent upstream phosphorylation of these sites, or might sensitise LRRK2 to dephosphorylation. Indeed, studies have shown dephosphorylation at Ser935 following treatment with LRRK2 inhibitors, mediated by the Protein Phosphatase 1[170,670,671]. As such, LRRK2 phosphorylation of these residues has been used as reliable markers of LRRK2 activity, and research on their use as clinical biomarkers is ongoing[669].

Additionally, phosphorylation of downstream substrates of LRRK2, in particular Rab proteins, represents another interesting readout to measure endogenous LRRK2 kinase activation in our system. A number of phospho-specific antibodies to Rab proteins are available (e.g., phospho-Thr73-Rab10, phospho-Ser106-Rab12 and phospho-Thr72-Rab8a) and can be used as markers of target engagement by Western immunoblotting assays[672]. Indeed, reduced levels of phosphorylated targets (normalised to the total levels of Rab proteins) would reflect LRRK2 inhibition, indicating that pharmacological inhibition of LRRK2 kinase is efficient. Alternatively, a mass spectrometry-based approach could be used to monitor phosphorylation on each target protein.

With regard to LRRK2 GTPase inhibition using FX2149, GTP-binding assays could be used to measure the reduction of LRRK2-GTP binding in presence of FX2149[177]. In principle, this method is based on GTP-agarose pull downs of LRRK2 from the lysates of cells incubated with or without FX2149, followed by Western immunoblotting using antibodies targeting LRRK2[177]. Furthermore, LRRK2 GTPase activity can regulate LRRK2 activation, as mentioned in Section 1.2.2.2. Thus, the same assays of kinase function mentioned above[177] could be another readout for LRRK2 GTPase activity inhibition. As such, Li and colleagues[177] reported that FX2149 reduced LRRK2 GTP-binding activity by approximately 90% when used at a concentration of 10 nM, and reduced phosphorylation at Ser935 by approximately 90% in cells expressing G2019S-LRRK2 when used at 100 nM for 1 hour.

4.10.5 Additional techniques that could be used to support these data

Since LRRK2 inhibition was found to suppress the induction of autophagy in HEK293 GFP-LC3 cells throughout this Chapter, these data strongly suggest that LRRK2 acts as a positive regulator in the activation of autophagy. Thus, the goal of future experimentation will be to determine the site(s) of action of LRRK2 in the mechanisms leading to the induction of autophagy.

To do so, it is possible to investigate and delineate the signalling events through which LRRK2 might act using a set of tailored experiments, which are described below. The experiments would predominantly use Western blotting, although further fluorescent microscopy experiments to monitor the subcellular localisation of autophagic proteins other than LC3 and WIPI2 could be performed. Western blotting allows an extra level of mechanistic detail to be uncovered, by permitting the quantification of protein expression levels and their phosphorylation states in various experimental conditions. Having established the conditions to study the effects of LRRK2 kinase and GTPase inhibitors and LRRK2 mutants on basal and PP242-induced autophagy in HEK293 GFP-LC3 cells in this Chapter, Western blot assays would likely be performed using identical treatment conditions.

An overview of the autophagic pathway is depicted in Figure 1.6, Figure 1.7 and Figure 1.8 (Chapter 1), and the potential experiments detailed below will focus on three protein complexes involved in the initiation of autophagy: ULK1, PI3K class III and ATG9. In brief, the ULK1 complex is central in the induction of autophagy, and acts with the PI3K class III complex and ATG9-containing vesicles to initiate the formation of autophagosomes. Since all these events occur prior to the recruitment of WIPI2 by the PI3K class III complex, LRRK2 may act at one or multiple levels somewhere along this pathway.

4.10.5.1.1 Confirmation of the effect of LRRK2 loss-of-function in HEK293 GFP-LC3 cells using knockout or knockdown

The results obtained with LRRK2 inhibitors in HEK293 GFP-LC3 cells support studying of the effects of LRRK2 knockout/knockdown on autophagy in identical experiments in this cell line. This strategy would thus complement the existing pharmacological approach (i.e., LRRK2 inhibitors) with a molecular

approach (CRISPR-mediated knockout or siRNA-mediated knockdown), and allow a comparison between these approaches in the same cell line. In theory, one would predict that the knockout of LRRK2 would also disrupt the induction of autophagy, and thereby reproduce the effects of LRRK2 inhibition.

However, it is worth mentioning that the molecular approach may not replicate or equate to the pharmacological method, since the former removes the whole LRRK2 protein, which could have cellular consequences that differ from those resulting from the inhibition of LRRK2 enzymatic activities. Furthermore, in the case of LRRK2 knockout rather than knockdown, the treatment is chronic, which would allow cells time to adapt to loss of LRRK2.

4.10.5.1.2 Confirmation that IVM-induced autophagy is mTORC1-independent in our system

As described in Section 4.10.1.4, Zachari and colleagues reported that IVM appears to induce autophagy in HEK293 cells independently of the inactivation of mTORC1 and dephosphorylation of ULK1 at Ser758[659]. It is necessary to assess whether this is also the case using identical experimental conditions to those used in this Chapter. A simple approach to do so would be by monitoring the phosphorylation status of downstream substrates of mTORC1 following IVM treatment. Such substrates could be ULK1 phosphorylation at Ser758, but also the phosphorylation of the P70S6 kinase at Thr389, commonly used as a marker of mTORC1 activity and for monitoring mTORC1 inhibition[673].

Inhibition of mTORC1 using PP242 is associated with loss of phosphorylation of ULK1 at Ser758, which would subsequently induce autophagy, and decreased phosphorylation of P70S6 kinase. Comparison of the phosphorylation status of these proteins in cells treated with IVM or PP242, or left untreated, would provide strong evidence about the effect of IVM on mTORC1 activity. Hypothetically, in the case where the levels of phosphorylated ULK1 or P70S6 kinase are similar between untreated cells and IVM-treated cells, but different to those treated with PP242, these data would suggest that the induction of autophagy using IVM might not involve the inhibition of mTORC1 and dephosphorylation of ULK1 at Ser758. This observation would be consistent with data from the Zachari paper[659]. On the other hand,

should there be a decrease in the levels of phosphorylation of ULK1 at Ser758 and P70S6 kinase at Thr389 following IVM treatment, this result would suggest that IVM action might involve mTORC1 inactivation.

4.10.5.1.3 Assessment of the effects of LRRK2 inhibition on components of the mTORC1/ULK1 pathway

Assessing the effects of LRRK2 inhibition on the activity of mTORC1 and the levels of phosphorylated ULK1 at Ser758 in our system would help reveal whether ULK1 inactivation by mTORC1 is involved in the blockage of autophagy following LRRK2 inhibition, and by extension, whether these proteins are involved in LRRK2-mediated autophagy. In principle, LRRK2 might act in a pathway that is parallel to the mTORC1/ULK1 pathway and independent of these proteins.

As such, a similar experiment to the one described in the previous section could be performed, but monitoring the phosphorylation status of ULK1 at Ser758 and P70S6 kinase at Thr389 following pre-treatment with the LRRK2 inhibitors. For consistency with the previous experiments described in this Chapter, the inhibitors would be used at the same concentration and incubation times used in autophagy assays. The longer 16-hour inhibitor treatment may help see differences, and might replicate the work of Manzoni et al., who reported an increased phosphorylation of ULK at Ser758 as a result of an 18-hour LRRK2 inhibition in H4 cells (neuroglioma)[616].

In theory, LRRK2 inhibition might be sufficient to induce an increase in phosphorylated ULK1 at Ser758 independently of mTORC1 activation, which would explain the subsequent inhibition of autophagy, and would indicate that the effects of LRRK2 inhibition are at least in part ULK1-dependent. In contrast, an absence of alterations in ULK1 phosphorylation at Ser758 following LRRK2 inhibition would suggest that the effects of LRRK2 inhibition on autophagy are likely ULK1-independent. In addition, if LRRK2 inhibition does not induce changes in P70S6 kinase phosphorylation at Thr389, this observation would mean that LRRK2 inhibition does not induce alterations in mTORC1 activity and the effects of LRRK2 inhibition is likely mTORC1-independent.

Nevertheless, further experiments would be needed to confirm a role for mTORC1 and ULK1 in LRRK2-mediated autophagy, for instance performing autophagy assays in HEK293 GFP-LC3 cells in which

components of the mTORC1/ULK1 pathway have been knocked-down using siRNAs. The assays would be those established in this Chapter, such as the translocation of GFP-LC3 and WIPI2 to punctae, following treatment with IVM or PP242. Should ULK1 knockdown prevent the suppression of autophagy resulting from LRRK2 inhibition, ULK1 would therefore likely be involved in the effects of LRRK2 on autophagy.

However, whilst the siRNA approach is informative, it would require caution in the interpretation of the results; in essence, a knockdown of a protein to study a particular process might have an impact on other cellular mechanisms, and mTORC1 is involved in numerous other cellular pathways. Furthermore, since PP242 induces autophagy via the inhibition of mTORC1 and requires the activation of ULK1, knockdown of mTORC1 or ULK1 may have an impact on the activation of autophagy by PP242 and the PP242-induced increase in WIPI2 and GFP-LC3 punctae, which could complicate the analysis of the results.

Another interesting approach to test the involvement of ULK1 in the effects of LRRK2 inhibition on autophagy would be the use of the pharmacological tool BL-918, which is a potent activator of ULK1[674]. Similar to a knockdown of ULK1, if the addition of BL-918 is able to prevent the effects of LRRK2 inhibition and rescue the phenotype in HEK293 GFP-LC3 cells, it would suggest that ULK1 is involved in the effects of LRRK2 inhibition and therefore, ULK1 might be one of the sites where LRRK2 acts to influence macroautophagy.

4.10.5.1.4 Effect of LRRK2 inhibition on the phosphorylation of additional components of the ULK1 complex

Aside from the inhibitory phosphorylation of ULK1 relieved by inactivation of mTORC1, the complexes involved in the induction of autophagy are regulated through phosphorylation and dephosphorylation events that are coordinated by numerous signals inducing or repressing autophagy, such as stress or amino acid depletion (see Chapter 1, Section 1.3.4). Some of the phosphorylation events involved in the induction of autophagy are depicted in Figure 1.7. Putatively, the phosphorylation of ULK1 substrates may vary according to the nature of the signals. Many components of the ULK1 complex, including

ATG101, ATG13, FIP200 and ULK1 itself, are phosphorylated by ULK1 once assembled in complex[251], and their activating phosphorylation is a requirement for the induction of autophagy[328]. ULK1 and ATG13 are also phosphorylated by mTORC1 in nutrient-rich conditions to prevent autophagy induction. Furthermore, since it has been reported that mitophagy requires ATG13 and FIP200 but not ULK1/2, it is likely that additional regulatory mechanisms can be involved in the initiation of autophagy[659].

LRRK2 is a kinase, so it is plausible that LRRK2 might directly phosphorylate proteins acting at early steps in the autophagic pathway. In support of this is evidence that EndoA, which regulates the membrane curvature and autophagosome nucleation at pre-synaptic terminals, can be phosphorylated by LRRK2[610]. Thus, experiments could be performed in HEK293 GFP-LC3 cells to further assess whether LRRK2 is involved in the phosphorylation of ULK1 complex subunits, and if so whether these phosphorylation events mediate the effects of LRRK2 on autophagy.

Importantly, a literature review would be needed to choose the phosphorylation sites of interest on FIP200, ATG13 and ATG101, since studies have suggested multiple potential activation sites over the years[675–678] (Table 4.1). The availability of existing phosphospecific antibodies would also determine the phosphorylation sites that will be studied on these proteins. Alternatively, a mass spectrometry-based approach could be used to monitor phosphorylation on each protein more globally.

Whether by a targeted phosphospecific antibody approach or mass spectrometry, if pharmacological inhibition of LRRK2 enzymatic activities is sufficient to decrease or prevent the phosphorylation of one or more of these subunits following treatment to induce autophagy, this result would be consistent with LRRK2 phosphorylating these proteins as a necessary early step in autophagy induction. Such experiments could be supported with analogous studies using LRRK2 knockdown. Finally, if the experiments performed in cells pointed towards LRRK2 phosphorylating one of more of these proteins, it would be necessary to confirm if LRRK2 can phosphorylate the substrate directly. This would be determined using *in vitro* phosphorylation assays, using recombinant LRRK2 and recombinant substrate protein.

Table 4.1: Reported serine/threonine phosphorylation sites within autophagy initiation complexes.

Numbers of phosphorylation sites relates to human protein and does not include phosphorylation sites identified in other species that may be conserved. Information obtained from PhosphoSitePlus® by Cell Signalling Technology[678].

Complex	Subunit	Number of phosphorylation sites (serine/threonine)
ULK1	ULK1	62
	ULK2	17
	FIP200	46
	ATG13	10
	ATG101	2
PI3K class III	Beclin1	16
	VPS34	20
	AMBRA1	23
	ATG14	7
ATG9	ATG9A	18
	ATG9B	1

4.10.5.1.5 The effect of LRRK2 inhibition on the phosphorylation events of PI3K class III complex components

Another key complex involved in the initiation of autophagy is the PI3K class III nucleation complex, which contains Beclin1, VPS34 and AMBRA1, and produces phosphatidylinositol 3-phosphate (PI3P) via the activity of the lipid kinase VPS34. Synthesis of PIP3 is crucial for the recruitment of WIPI2 to nascent autophagosomes, and various signalling pathways converge on the modulation of this complex to induce or supress autophagy, as described in Chapter 1 Section 1.3.3. ULK1 has been reported to phosphorylate all three of these PI3K class III nucleation complex subunits, and phosphorylation of Beclin1 at Ser14 is required for the activation of the complex and autophagy induction. In principle, LRRK2 inhibition might prevent the phosphorylation of one or more of these subunits and lead to inhibition of autophagy in an analogous manner to that proposed for phosphorylation of ULK1 complex components.

Supporting this idea, it has been shown that LRRK2 can influence the phosphorylation of Beclin1. In particular, membrane-associated LRRK2 is reported to inhibit autophagy by inducing the phosphorylation of Beclin1 at Ser295, a residue also known to be targeted by Akt[679]. However, this observation is not in agreement with our data, which suggest a positive role for LRRK2 in the induction

of autophagy. Nevertheless, the role of LRRK2 in the phosphorylation status of the PI3K class III subunits can be explored using similar experimental designs as described in the previous sections.

Interestingly, instances of Beclin1-independent autophagy have been reported[680,681]. Therefore, it may be informative to delineate if LRRK2-mediated autophagy is Beclin-1 dependent. To do so, the effects of LRRK2 inhibition on autophagy in HEK293 GFP-LC3 cells could be investigated using 3-methyladenine (3-MA). 3-MA is a compound that is commonly used to inhibit autophagy, and is especially relevant here because it only blocks Beclin1-dependent autophagy[328]. However, there is a caveat associated with the use of this compound; some studies also report that 3-MA was ineffective in preventing LRRK2-activated autophagy[141,479].

4.10.5.1.6 The effect of LRRK2 inhibition on ATG9 protein phosphorylation

ATG9 proteins are transmembrane proteins essential for the nucleation and formation of the phagophore. ULK1 can phosphorylate ATG9 at Ser14, which promotes its relocation to sites of phagophore assembly, where ATG9-containing vesicles are a likely source of membrane material[682]. As such, LRRK2 might be involved at the level of ATG9 proteins, with LRRK2 inhibition preventing both the phosphorylation of ATG9 at Ser14 and ATG9 trafficking, thus blocking autophagy. Similar experiments to the ones detailed in the previous sections could be performed to investigate this idea.

4.10.5.1.7 The effect of LRRK2 inhibition on the interaction between LRRK2 and autophagic proteins

Finally, it is reasonable to suppose that LRRK2 might affect autophagy independently of substrate phosphorylation, but in a manner that is nonetheless sensitive to both kinase and GTPase inhibitors. This would likely be via protein-protein interactions, where LRRK2 might have a necessary scaffolding function in one or more of the initiation complexes. As such, LRRK2 inhibitors may affect the stability or structural integrity of LRRK2, which in turn might destabilise or prevent the assembly of the initiation complexes. Since LRRK2 is a dynamic protein, studies suggest that LRRK2 might be involved in numerous cellular pathways depending on the formation of complexes following specific cues or stimuli[683]. Indeed,

LRRK2 has been shown to play important roles in the recruitment of substrates and regulatory partners, notably in the Wnt signalling pathway[112,116], where LRRK2 acts as a central scaffolding subunit[180,684].

Thus, reciprocal co-immunoprecipitation experiments could be performed to test for physical interactions between LRRK2 and candidate interacting proteins that are involved in the early steps of autophagy. Beclin1 within the PI3K class III complex is a likely candidate to explore. An argument supporting this hypothesis is linked to Bcl-2, an anti-apoptotic protein. It has been reported that mitochondria degradation via macroautophagy is mediated by LRRK2, following its binding to Bcl-2[597]. Bcl-2 has also been reported to bind and inhibit Beclin1, and the release of Beclin1 from Bcl-2 appears to be essential for the initiation of the autophagic response[685]. Interestingly, Beclin1 has the capacity to form different functional complexes[686], allowing it to regulate autophagy depending on the stimulus.

4.10.6 Conclusions

The findings presented in this Chapter suggest a cell-type specific action of LRRK2 in autophagy. In HEK293 GFP-LC3 cells, results strongly support the involvement of LRRK2 in the early stages of canonical mTORC1-dependent and perhaps also mTOR-independent autophagy. By contrast, data from RAW264.7 macrophages do not support a role for Lrrk2 in this cell line. Evidence that in HEK293 GFP-LC3 cells LRRK2 kinase or GTPase inhibition blocks autophagy is supported by three distinct techniques. As such, the role of LRRK2 in the early stages of autophagy in this cell line merits more exploration.

5

Investigations into the role of LRRK2 in calcium signalling

5.1 Introduction

Alterations in intracellular calcium homeostasis have been described and linked to neurodegeneration in PD, including impairments in ER, lysosomal and mitochondrial calcium homeostasis[112,479,507,587–590,687]. Importantly, there is evidence for a broad regulatory role for LRRK2 in calcium signalling, with data suggesting that LRRK2 pathogenic mutants may, at least in part, induce cellular defects through impaired calcium homeostasis. In particular, LRRK2 is intimately associated with lysosomal calcium homeostasis[391,479], which, when deregulated in presence of pathogenic LRRK2 mutants, impairs lysosomal function and autophagy[142,479]. Nevertheless, the precise role of LRRK2 in the regulation of calcium signalling remains to be established.

Importantly, the reported effects on global calcium regulation associated with LRRK2 were generally described or extrapolated in the context of other mechanisms or not direct results of LRRK2 modulation, for example in the context of neurite outgrowth[587] or autophagy[479]. It is for instance possible that the described increased ER or lysosomal releases were due to excessive calcium signalling or were secondary to increased pH and not necessarily direct consequences of *LRRK2* mutations[216,479], which has not been examined. Furthermore, the effects of LRRK2 on total ER and lysosomal calcium levels have not been extensively examined either. Therefore, there is a need to undertake a systematic and thorough investigation of the role of LRRK2 in calcium signalling.

The work described in this Chapter investigates the impact of LRRK2 enzymatic activities and LRRK2 pathogenic and protective variants on calcium signalling, with the aim of gaining insight into the involvement of LRRK2 in global and lysosomal calcium signals. To this end, the LRRK2 kinase and GTPase activities were modulated with pharmacological inhibitors, and the effects of *LRRK2* mutations were investigated by transient overexpression of wild-type and mutant LRRK2 constructs. For consistency with the experimental designs used in Chapter 4, the same three cell lines were used, namely HEK293 GFP-LC3 cells, wildtype RAW264.7 macrophages and isogenically matched Lrrk2-knockout RAW264.7 macrophages.

The main experimental approached used in this Chapter was to monitor cytosolic calcium signals with fluorescence microscopy, using cells loaded with the fluorescent calcium dye Fura-2 (see Chapter 1 Section 1.4.3 and Chapter 2 Section 2.5.1 for further details). In principle, Fura-2 signals directly relate to the amount of cytosolic calcium, allowing calcium quantification; as the concentration of cytosolic calcium increases, the 340/380 fluorescence ratio of Fura-2 increases. Changes in calcium signals were assessed by measuring several parameters, described in the next sections.

5.1.1 Calcium signalling parameters measured in this study: spontaneous activity

Certain cell types can display calcium activity in absence of an exogenous stimulation or trigger, i.e., when cells are at rest and maintained in imaging buffer without any stimulation by a calcium mobilising agent. This is called “spontaneous activity”. Calcium release events that occur in spontaneous activity can be sporadic in nature, or follow an oscillatory and periodic pattern.

Spontaneous calcium release events can be recorded from cells loaded with Fura-2. Figure 5.1 depicts an example of a spontaneous activity trace obtained from a single cell, where the calcium signals were recorded over a period of 5 minutes. Each calcium release event corresponds to a “peak”, representing an increase in cytosolic calcium concentration.

For each recording of spontaneous activity, 20 cells were selected, and the calcium signals of each individual cell was measured as single-cell traces. Once the number of peaks was quantified for each cell to obtain the number of peaks per minute, the values were averaged to obtain a single value for the repeat.

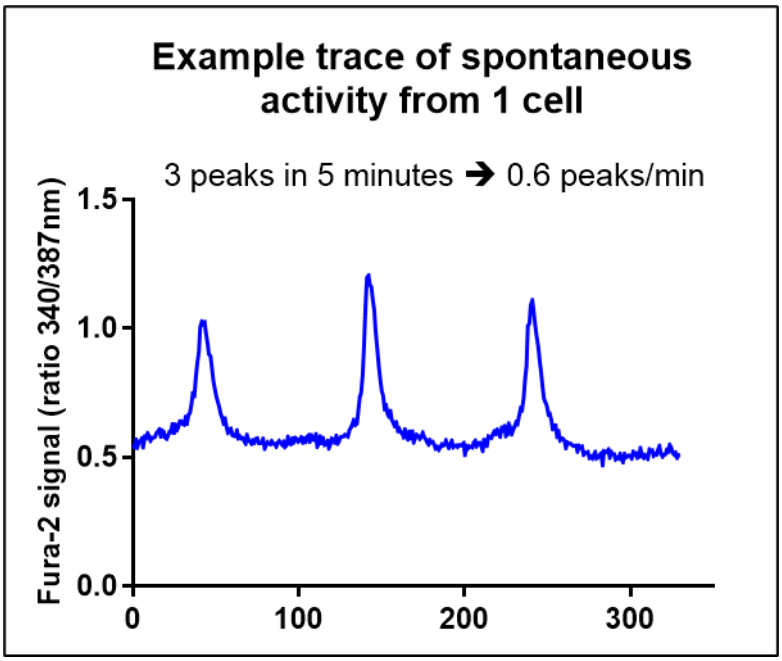

Figure 5.1: Representative spontaneous activity trace from an individual WT RAW264.7 macrophage.

RAW264.7 WT macrophages were loaded with Fura-2 AM (2 µM) in imaging buffer and the calcium signals were recorded for 5 minutes to measure the spontaneous release of calcium. The trace represents the individual calcium signals and peaks from 1 region of interest (ROI) corresponding to 1 individual cell.

5.1.2 Calcium signalling parameters measured in this study: evoked calcium signals

Calcium signals occurring in response to the stimulation of the cells with an agonist are called evoked calcium signals. For example, extracellular application of ATP, a natural agonist of P2Y receptors, to cells leads to the production of IP_3 and increased cytosolic calcium levels resulting from the release of the ER calcium store. Typically, stimulation of cells with ATP will trigger a global calcium response that is larger than the calcium signal observed following a spontaneous calcium release.

Figure 5.2 shows a representative profile of cytosolic calcium signals obtained from WT RAW264.7 macrophages that were superfused with imaging buffer supplemented with ATP. At the start of the recording, 20 cells were selected, and the calcium signals were measured individually, which generated

20 single-cell traces (Figure 5.2 A). These traces were then averaged over time to obtain a single curve with averaged data suitable for analysis (Figure 5.2 B). As such, except for the measure of spontaneous activity, all the calcium traces obtained in this Chapter were averaged over time. In this example (Figure 5.2), cells were stimulated three times with ATP (100 µM) which generated three peaks, each peak corresponding to an increase in cytosolic calcium resulting from a triggered ER calcium release event.

The general protocol followed for the calcium signalling assays described in Section 5.2 is detailed in the legend of Figure 5.2. First, as mentioned in Section 5.2.1, calcium signals were recorded for 5 minutes prior to any stimulation in order to use this data for spontaneous activity analysis. Then, cells were stimulated with ATP (100 µM) and a peak was generated. Upon termination of the signal, cells were washed and allowed to rest for 10 minutes to allow for the intracellular reuptake of calcium, and for the calcium signals to return to baseline. ATP stimulations were repeated two more times, with recordings started 1 minute before the addition of ATP, in order to obtain a baseline for later calculations.

To assess changes in evoked calcium signalling, three parameters were measured in all the experiments performed in this Chapter: the amplitude, the area under the curve (AUC), and the decay. These parameters were measured for each peak using averaged data, and are described in Figure 5.3 using a representative curve as an example:

- **amplitude** (height of the peak) was used as a measure of the rate of calcium release (e.g., faster or sharper if the amplitude is higher in an experimental condition compared to control),
- **AUC** is a measure of the total increase in cytosolic calcium, and reflects the total amount of calcium released
- **decay** represents how quickly the cells return to baseline, which is the termination of the signal (e.g., a smaller decay in an experimental condition compared to control reflects a faster return to baseline, which means that cytosolic calcium has been cleared and re-stored).

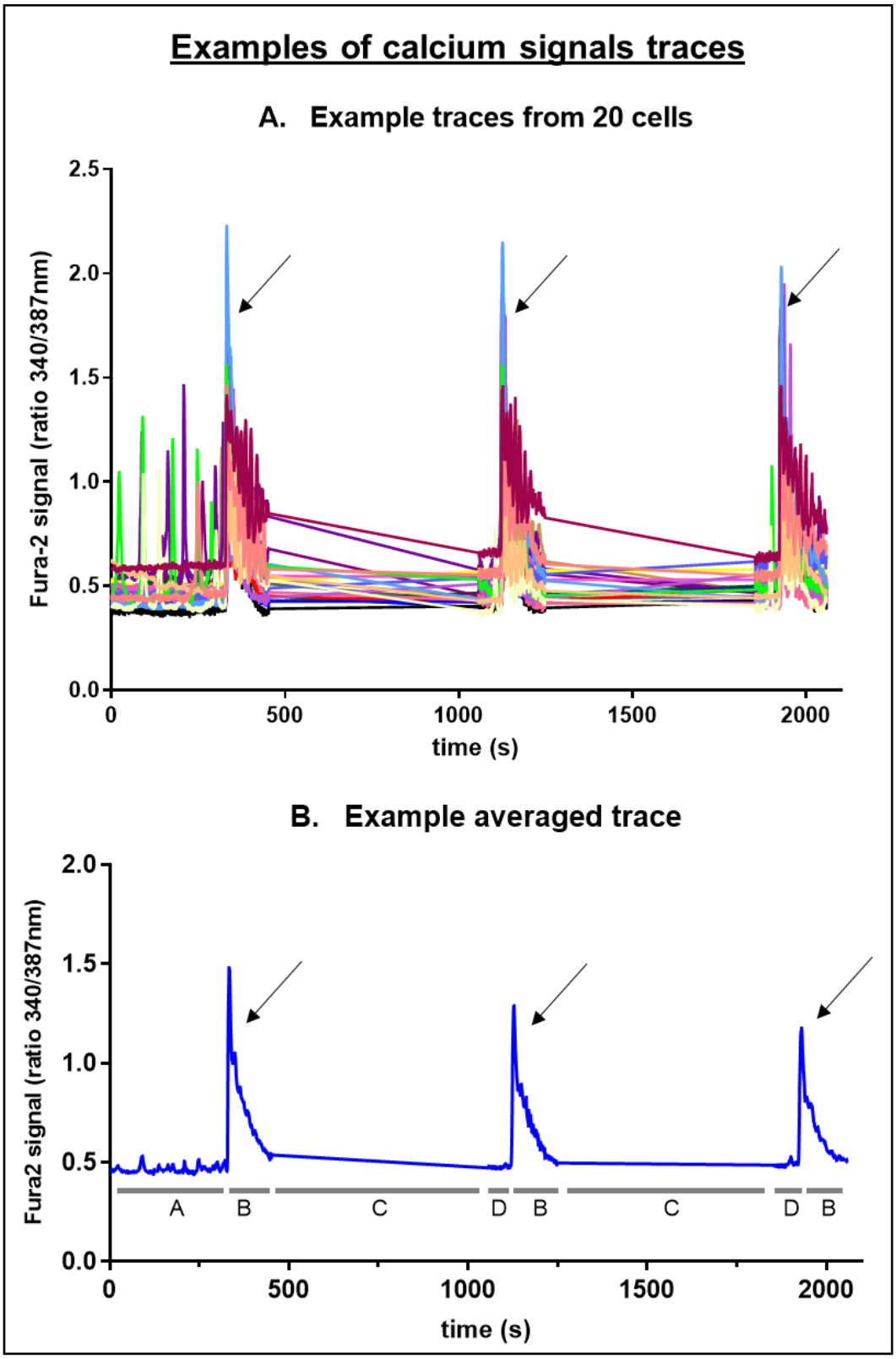

Figure 5.2: Traces representing calcium signals recordings.

RAW264.7 WT macrophages were loaded with Fura-2 (2 µM) and the calcium signals were recorded over time. The arrows show the peaks following an ATP-evoked release of calcium. Panel A shows the calcium signals recorded from 20 regions of interest (ROI) corresponding to 20 individual cells. Panel B shows the averaged calcium signal of the 20 cells. The general protocol followed is depicted in Panel B. The calcium signals were recorded for 5 minutes to obtain the spontaneous cell activity and basal calcium signals (A), then stimulated with the agonist ATP (B). Once the response ended, the recordings were paused for 10 minutes, the cells were washed 4 to 8 times and allowed to rest (C). The recordings were resumed for 1 minute prior to the addition of ATP to obtain the basal levels (D).

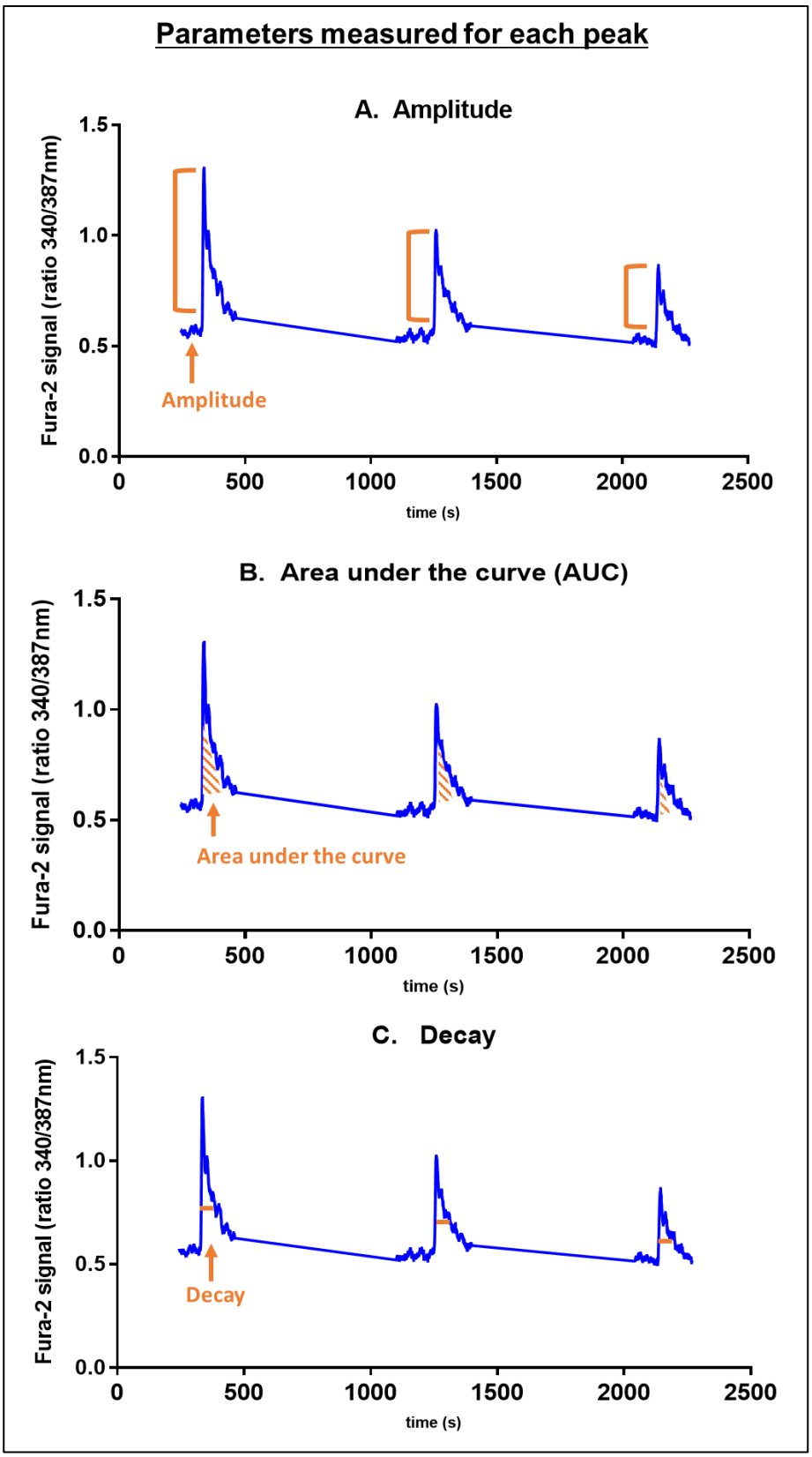

Figure 5.3: Parameters measured for each peak in this Chapter.

Following the protocol described in Figure 5.2: calcium signals were recorded in cells and were evoked by addition of 100 µM ATP. The graphs show the different parameters (depicted in orange) measured for all the calcium experiments performed in this Chapter. A: amplitude, rate of calcium release, B: area under the curve, total calcium release, C: decay, termination of the signal. See Chapter 2, section 2.5.4 for more details.

5.2 Effect of loss of Lrrk2 on cytosolic calcium signals in RAW264.7 macrophages

Prior to investigating the effects of LRRK2 inhibition in calcium assays, the first step was to explore the impact of the loss of Lrrk2 on calcium signals using WT RAW264.7 macrophages and Lrrk2 KO RAW264.7 macrophages. For this purpose, the calcium release patterns, including the spontaneous activity and triggered calcium responses, were studied in both cell lines. The results are described in the next Sections.

5.2.1 Loss of LRRK2 does not affect spontaneous activity in macrophages

To examine how loss of Lrrk2 affects the spontaneous calcium activity in RAW264.7 macrophages, wild-type RAW264.7 or Lrrk2 KO macrophages were loaded with Fura-2, and spontaneous calcium release events were recorded for 5 minutes. The spontaneous activity data presented in Figure 5.4 combines the data obtained from the experiments described in Figure 5.5, Figure 5.7 and Figure 5.9, which all started with a recording of the spontaneous calcium release events prior to any stimulation. This analysis revealed no significant difference in the number of peaks per minute between the two genotypes, suggesting that loss of Lrrk2 did not affect spontaneous activity in WT macrophages.

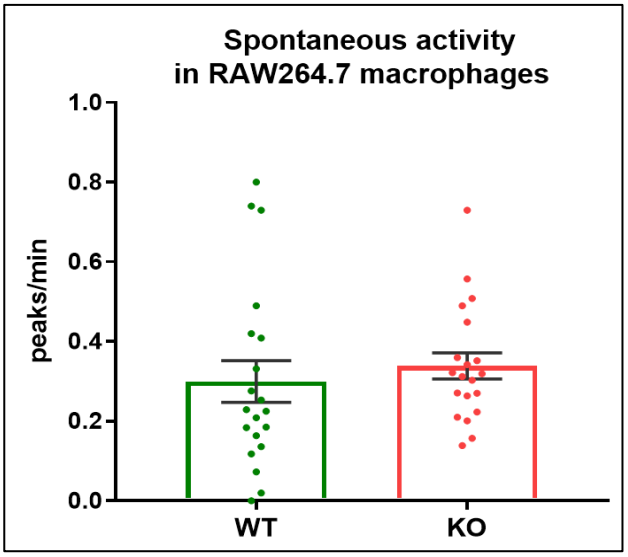

Figure 5.4: Measure of the spontaneous calcium release in RAW264.7 WT or Lrrk2 KO macrophages.

RAW264.7 WT or Lrrk2 KO macrophages were loaded with Fura-2 AM (2 µM) in imaging buffer and the calcium signals were recorded for 5 minutes to measure the spontaneous release of calcium. The number of peaks were quantified for each cell (20 cells/repeat) and averaged to peaks/minute. The bars represent the mean ± SEM peaks/minutes of 20 repeats. This data combines the data obtained from the experiments described in Figure 5.5, Figure 5.7 and Figure 5.9, which all started with a recording of the spontaneous calcium release events prior to any stimulation. n=20, Unpaired T-test, non-significant; t=0.6377, df=38, p=0.52.

5.2.2 Exploring the effect of loss of Lrrk2 on the calcium release pattern in macrophages using ATP

Since the loss of Lrrk2 did not appear to affect the spontaneous activity in RAW264.7 macrophages, the next step was to explore the effect of loss of Lrrk2 on calcium signals occurring in response to the stimulation of the cells with an agonist, i.e., evoked calcium signals.

5.2.2.1 Effect of loss of Lrrk2 on evoked calcium signals in RAW264.7 macrophages

Having established the conditions to monitor calcium signals in Section 5.1.2, the effect of loss of Lrrk2 in WT RAW264.7 macrophages was studied. To do so, Fura-2 loaded WT RAW264.7 macrophages or Lrrk2 KO macrophages were stimulated three times with ATP at a concentration of 100 µM, following a one-minute baseline recording. (*This experiment corresponds to Assay n°1 in Chapter 2 Section 2.5.3.1*). The main reason why cells were stimulated several times was to ensure that any potential effect can be seen, since it is possible that the effects of Lrrk2 knockout would not be visible after a single stimulation, but only after a reset period and the second stimulation. Using averaged data, the amplitude, AUC and decay were analysed for each peak, and the results are shown in Figure 5.5.

As expected, the amplitude (Figure 5.5 A) and the AUC (Figure 5.5 B) data showed a significant decrease between the first ATP stimulation and the third ATP stimulation in both the WT macrophages and the Lrrk2 KO macrophages. This is indicative of a desensitisation to ATP, with less calcium released and at a slower rate. In addition, the amplitude results showed a significant difference between the genotypes in the second and third ATP stimulations (Figure 5.5 A), with the Lrrk2 KO macrophages displaying a higher amplitude than WT macrophages. This indicates that ATP induced a faster calcium release in Lrrk2 KO macrophages.

Furthermore, the decay data showed a significant difference between the two genotypes (Figure 5.5 C), with significantly smaller decay values in Lrrk2 KO macrophages after the second and third ATP stimulations. This suggests that the calcium signals in Lrrk2 KO macrophages needed less time to return

to baseline, i.e., the cytosolic calcium was cleared and re-stored in organelles faster in Lrrk2 KO macrophages than WT macrophages. Altogether, these results suggest that both ATP-stimulated calcium release and calcium reuptake following ATP-stimulated calcium release occur more rapidly in Lrrk2 KO macrophages.

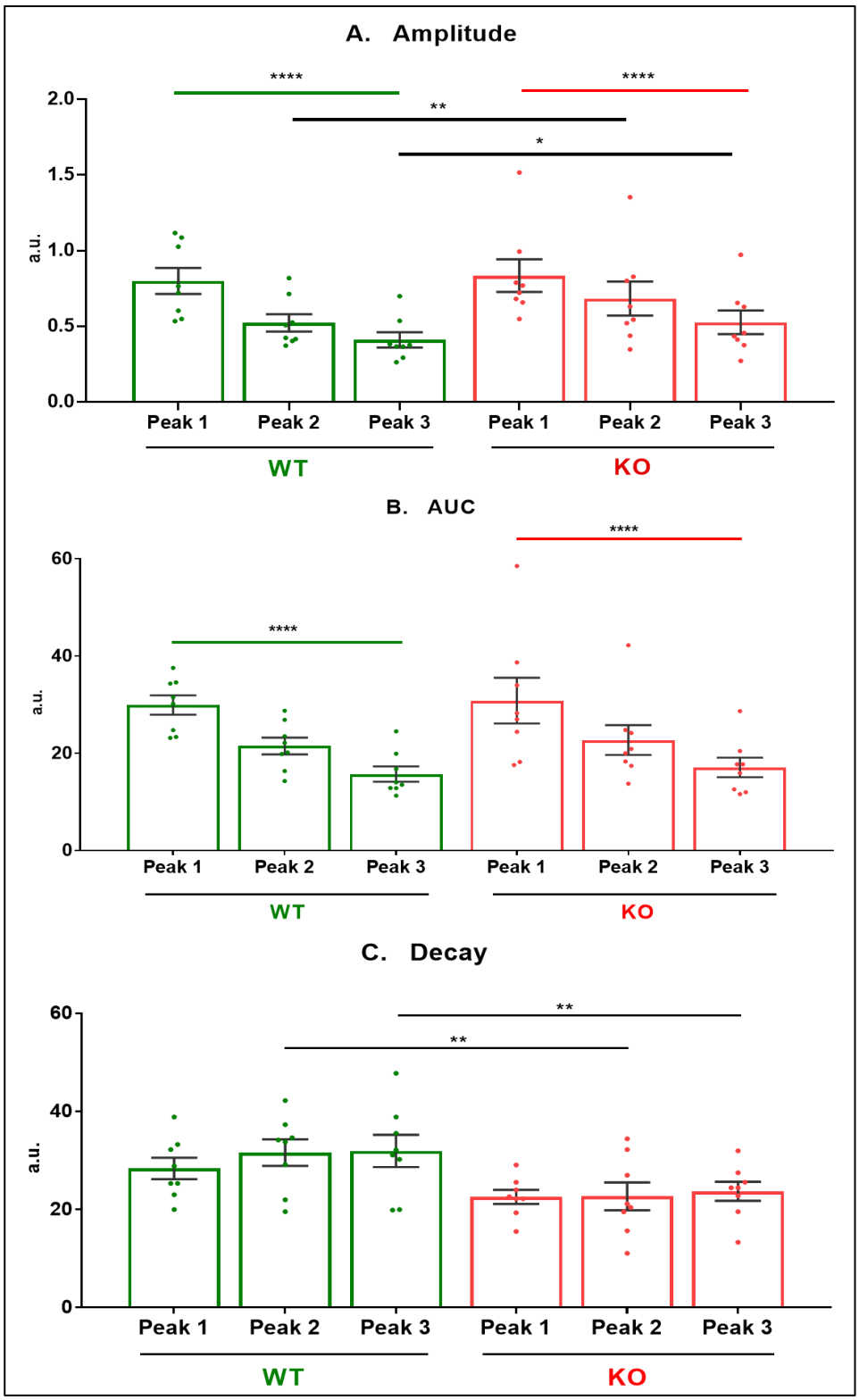

Figure 5.5: Measure of calcium signals in response to ATP in RAW264.7 macrophages.

RAW264.7 WT or Lrrk2 KO macrophages were loaded with Fura-2 AM (2 µM) in imaging buffer and the calcium signals were recorded. After 5 minutes of recording (for the spontaneous activity, used in Figure 5.4), cells were stimulated with ATP (100 µM) to evoke a calcium signal, followed by 8 washes with imaging buffer and 10 minutes of rest. These steps were repeated two more times, and the baseline calcium signals were recorded for 1 minute before each stimulation (Assay 1 in Chapter 2 Section 2.5.3.1). For each peak, each repeat is an average of 20 cells, and the data are the mean ± SEM. n=8 (2 coverslips/4 repeats). Two-way mixed ANOVA (with grouping by experimental repeat), Tukey post-hoc. (A) peak effect: $F(2, 14)= 45.81$, $p<0.0001$; genotype effect: $F(1,7)= 1.305$, $p=0.291$, interaction: $F(2, 14)= 4.222$, $p=0.0367$. (B) peak effect: $F(2, 14)= 33.78$, $p<0.0001$, genotype effect: $F(1, 7)= 0.135$, $p=0.7241$, interaction: $F(2, 14)= 0.03043$, $p=0.9701$. (C) peak effect: $F(2, 14)= 1.625$, $p=0.232$, genotype effect: $F(1, 7)= 5.692$, $p=0.0485$, interaction: $F(2, 14)= 0.7919$, $p=0.4723$. On graphs: $p<0.0001$ (****), $p<0.01$ (**), $p<0.05$ (*).

5.2.2.2 *Effect of loss of Lrrk2 on evoked calcium signals in RAW264.7 macrophages using a range of ATP concentrations*

The differences between genotypes shown in Figure 5.5 were only observed after the second and third stimulations. This indicates that these differences were only detectable after desensitisation when using ATP at 100 µM, which implies that this ATP concentration is saturating for the first stimulation in this experiment. This observation suggests that lower doses of ATP might allow differences between genotypes to be detected more easily, thereby increasing the sensitivity of the assay. Consequently, a submaximal range of ATP concentrations was also tested (0.5 µM, 1 µM, 10 µM or 100 µM).

The effect of loss of Lrrk2 on calcium signals in WT RAW264.7 macrophages was therefore assessed under conditions where WT and Lrrk2 KO macrophages were stimulated with a gradual increase in the concentration of ATP (Figure 5.6), following a similar timeline as detailed in Section 5.2.2.1. (*This experiment corresponds to the Assay n°2 in Chapter 2 Section 2.5.3.1*)

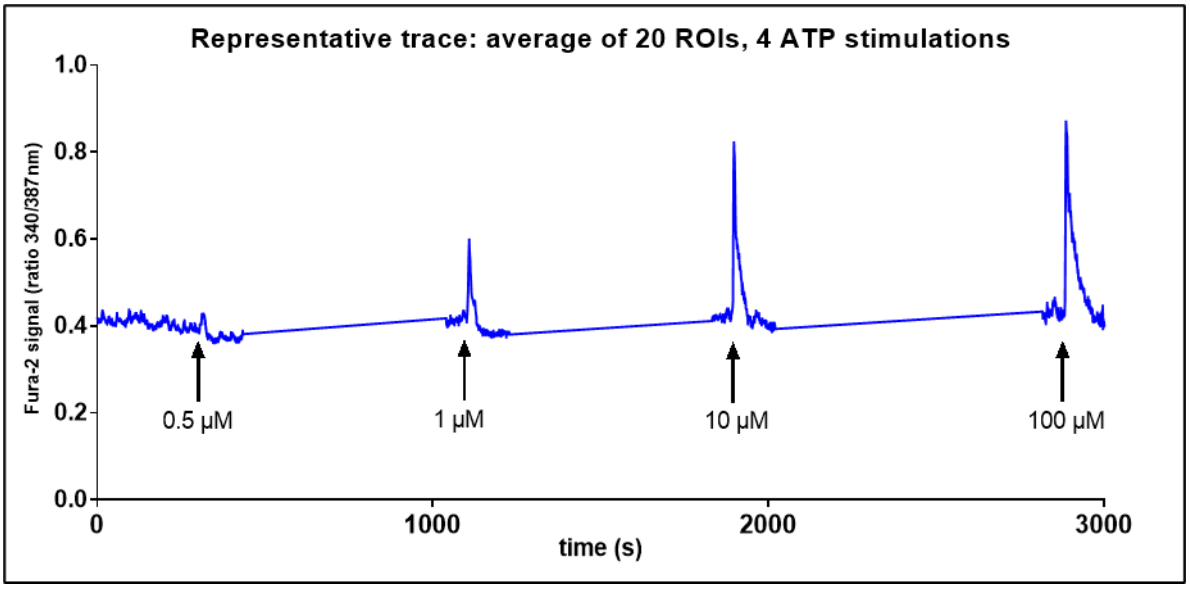

Figure 5.6: Representative trace following the stimulation of WT RAW264.7 macrophages with a range of ATP concentrations.

RAW264.7 WT macrophages were loaded with Fura-2 (2 µM) and the calcium signals were recorded over time, and were evoked by addition of ATP at 0.5 µM, 1 µM, 10 µM or 100 µM (arrows). The trace represents the averaged calcium signal of 20 cells.

The results are shown in Figure 5.7, with the analysis of the same parameters as described in the previous sections.

Predictably, increasing ATP concentrations causes corresponding increases in the size of the ATP response in both genotypes, with significant differences seen between the two lower and two higher doses for both the amplitude and AUC measurements (Figure 5.7 A and B). In addition, the AUC data showed that the calcium release using ATP at 100 µM was significantly larger than using ATP at 10 µM in both genotypes. Importantly also, these results indicate that stimulation with 10 µM ATP was sufficient to elicit a response similar to the response observed with 100 µM. For this reason, ATP was used at a 10 µM concentration in experiments from this point.

Interestingly, both the AUC and the amplitude of the responses recorded in Lrrk2 KO macrophages were significantly larger than the same parameters in WT macrophages (Figure 5.7 A and B), and this was the case following stimulation with ATP at either 10 µM or 100 µM. This result suggests that the calcium release was both faster and greater in the Lrrk2 KO macrophages, which is consistent with the data shown in Figure 5.5. However, there was no significant difference in the decay data between the genotypes in this experiment.

To summarise the findings on the effect of loss of Lrrk2 on the calcium release pattern in WT RAW264.7 macrophages, although no significant difference was detected regarding the spontaneous activity, the significant changes in AUC (Figure 5.7), amplitude (Figure 5.5 and Figure 5.7) and decay (Figure 5.5) data point towards a faster and greater calcium release in the Lrrk2 KO macrophages, perhaps with a faster return to the baseline in this cell line. As such, these data support a potential role for Lrrk2 in the regulation of calcium release in RAW264.7 macrophages.

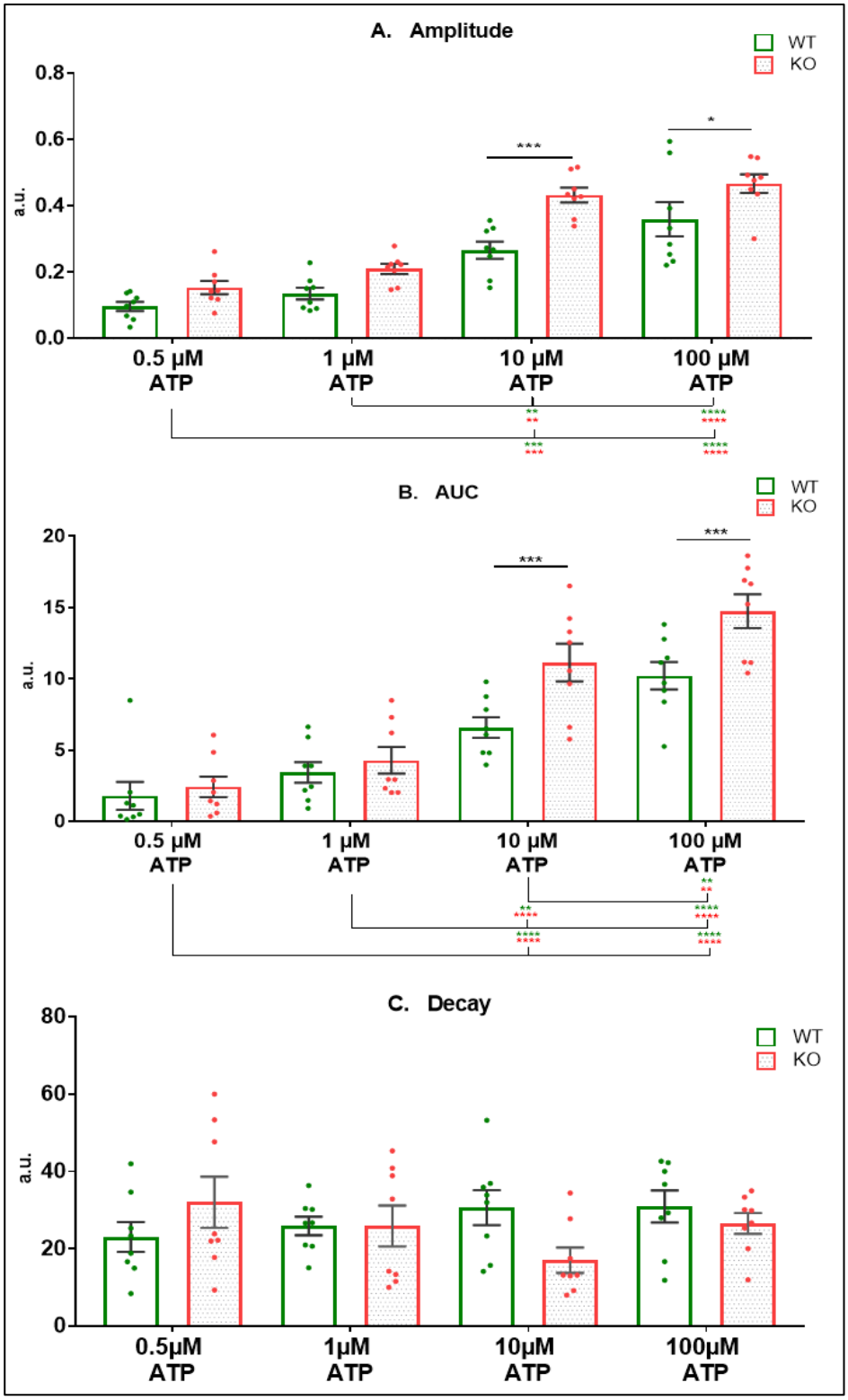

Figure 5.7: Calcium signals evoked using different ATP concentrations.

RAW264.7 WT or Lrrk2 KO macrophages were loaded with Fura-2 AM (2 µM) in imaging buffer and the calcium signals were recorded. Basal signals were recorded for 5 minutes (for the spontaneous activity, used in Figure 5.4), then cells were stimulated with ATP at 0.5 µM, 1 µM, 10 µM or 100 µM to evoke calcium signals, with 8 washes with imaging buffer and 10 minutes of rest in between each stimulation. For each peak, each repeat is an average of 20 cells, and the data are the mean ± SEM. Each panel represents a parameter measured. n=8 (2 coverslips/4 repeats). Two-way mixed ANOVA (with grouping by experimental repeat), Tukey post-hoc test. (A) ATP concentration effect: $F(3,21)= 40.4$; $p<0.0001$, genotype effect: $F(1,7)= 23.74$; $p=0.0018$, interaction: $F(3,21)= 2.88$; $p=0.059$. (B) ATP concentration effect: $F(3,21)= 58.56$; $p<0.0001$, genotype effect: $F(1,7)= 8.28$; $p=0.023$, interaction: $F(3,21)= 8.13$; $p=0.0009$ (C) ATP concentration effect: $F(3,21)= 0.57$; $p=0.63$, genotype effect: $F(1,7)= 0.28$; $p=0.61$, interaction: $F(3,21)= 3.75$; $p=0.0265$. On graphs: $p<0.0001$ (****), $p<0.001$ (***), $p<0.01$ (**), $p<0.05$ (*). Black stars represent the difference between genotypes, red stars represent the differences within KO, and green stars within WT.

5.3 Effect of Lrrk2 inhibition on global calcium release in RAW264.7 macrophages

The observation that loss of Lrrk2 affects the ATP-induced calcium responses in WT macrophages (Figure 5.5 and Figure 5.7) indicates that Lrrk2 is likely involved in calcium signalling in this cell type. To test this possibility further and assess the requirement of the Lrrk2 enzymatic activities in the effects of Lrrk2, the following experiments investigated the role of Lrrk2 kinase and GTPase activities on ATP-evoked calcium responses in RAW264.7 macrophages using the same Lrrk2 inhibitors used in Chapter 4. This approach also allows a comparison between two forms of Lrrk2 loss of function: enzymatic inhibition and loss of protein expression.

5.3.1 DMSO has no effect on calcium release in macrophages

Prior to using the inhibitors in calcium signalling assays, it was considered necessary to verify whether DMSO, the solvent for the inhibitors, had an effect on calcium release, to ensure that any effect observed following Lrrk2 inhibition is directly due to the inhibitors. Thus, an additional control experiment was carried out where WT RAW264.7 macrophages were pre-treated 1 hour with DMSO (1:1000 equivalent dilution) or untreated, and then stimulated three times with ATP (at 2 µM, 10 µM or 100 µM). (*This experiment corresponds to the Assay n°8 detailed in Chapter 2 Section 2.5.3.2*)

The results are shown in Figure 5.8, and revealed no effect of DMSO on calcium release under the experimental conditions of our system.

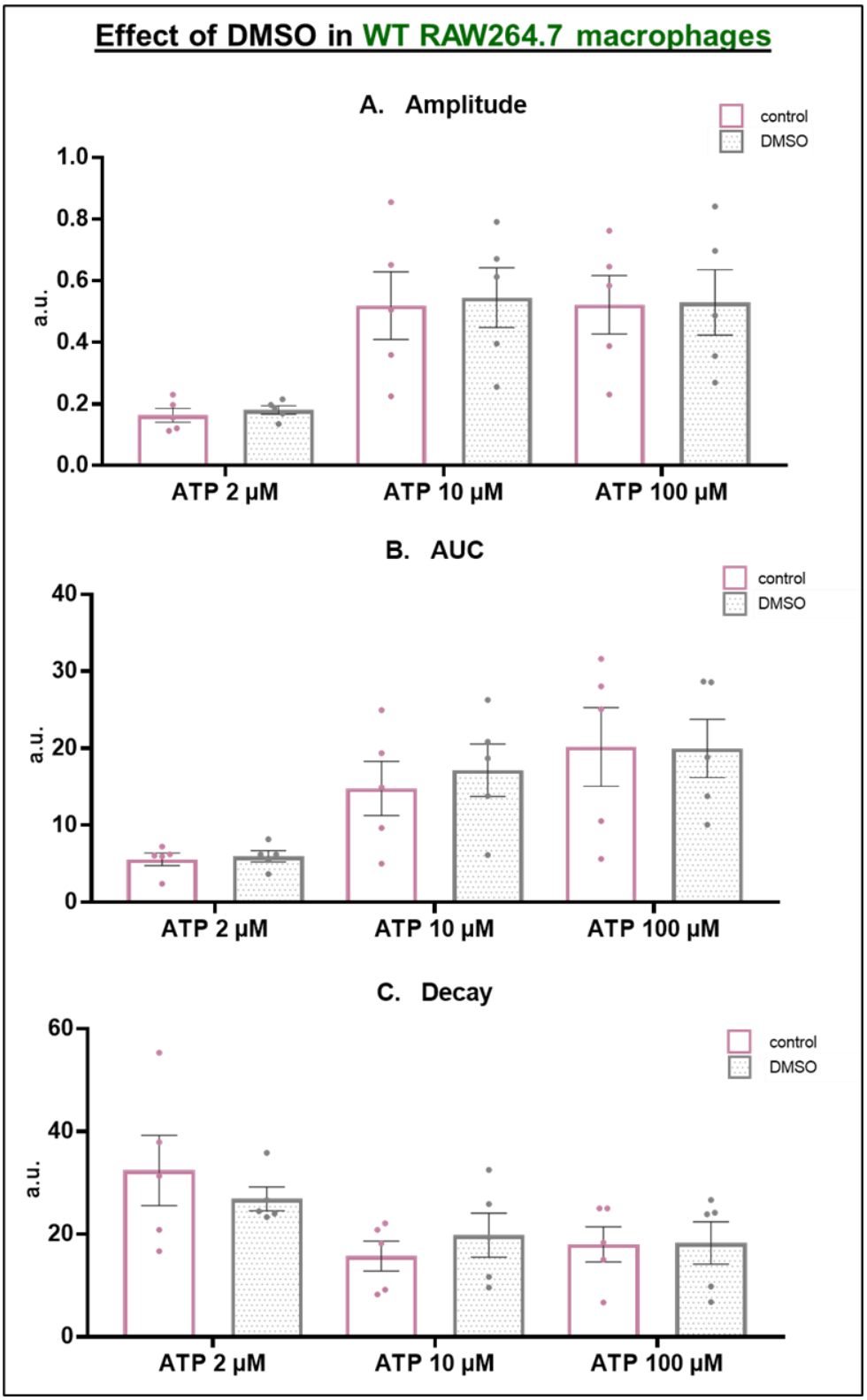

Figure 5.8: DMSO does not affect calcium release in WT RAW264.7 macrophages.

RAW264.7 WT macrophages were pre-treated with DMSO (1:1000 equivalent dilution) for 1 hour, then loaded with Fura-2 AM (2 µM) in imaging buffer, and the calcium signals were recorded. Basal calcium signals were recorded for 1 minute before addition of ATP at 2 µM, 10 µM or 100 µM to evoke calcium signals, with 8 washes with imaging buffer and 10 minutes of rest in between each stimulation. For each peak, each repeat is an average of 20 cells, and the data are the mean ± SEM. Each panel represents a parameter measured. n=5 repeats (1 coverslip/repeat). Two-way mixed ANOVA (with grouping by experimental repeat), non-significant. (A) ATP concentration effect: $F(2, 8)= 18.48$; $p=0.0010$, genotype effect: $F(1, 4)= 0.16$; $p=0.71$, interaction: $F(2, 8)= 0.025$; $p=0.97$. (B) ATP concentration effect: $F(2, 8)= 15.9$; $p=0.0016$, genotype effect: : $F(1, 4)= 0.237$; $p=0.65$, interaction: $F(2, 8)= 0.432$; $p=0.66$ (C) ATP concentration effect: $F(2, 8)= 6.42$; $p=0.0217$, genotype effect: $F(1, 4)= 0.0084$; $p=0.793$, interaction: $F(2, 8)= 1.1$; $p=0.377$.

5.3.2 Effect of Lrrk2 inhibition on calcium release in macrophages

Having confirmed that DMSO does not affect calcium signals in WT RAW264.7 macrophages, the effects of Lrrk2 inhibition on ATP-evoked calcium responses were examined in WT RAW264.7 macrophages and Lrrk2 KO macrophages. Although Lrrk2 is not expressed in the Lrrk2 KO macrophages, this cell line was used in parallel to monitor for potential off-target effects of the inhibitors.

For consistency with the autophagy assays (Chapter 4), the effects of Lrrk2 inhibitors were investigated using identical treatment conditions to those used to study the role of Lrrk2 in autophagy, which correspond to a 1- or 16-hours treatment with the LRRK2 kinase inhibitors at 1 µM or with the GTPase inhibitor at 100 nM. Furthermore, in some experiments, an additional condition combining the use of a LRRK2 kinase inhibitor (GSK2578215A) and the LRRK2 GTPase inhibitor (FX2149) was explored.

5.3.2.1 Lrrk2 inhibition has no effect on spontaneous activity in RAW264.7 macrophages

The effect of acute (1 hour) Lrrk2 inhibition on the spontaneous activity is shown in Figure 5.9. Interestingly, neither the Lrrk2 kinase inhibitors (1 µM) nor the GTPase inhibitor (100 nM) induced significant changes compared to the DMSO-treated control cells. This observation suggests that Lrrk2 enzymatic activities are unlikely to be involved in the spontaneous activity of WT RAW264.7 macrophages, which is consistent with the absence of effect of Lrrk2 KO on the spontaneous activity in this cell line (Figure 5.4).

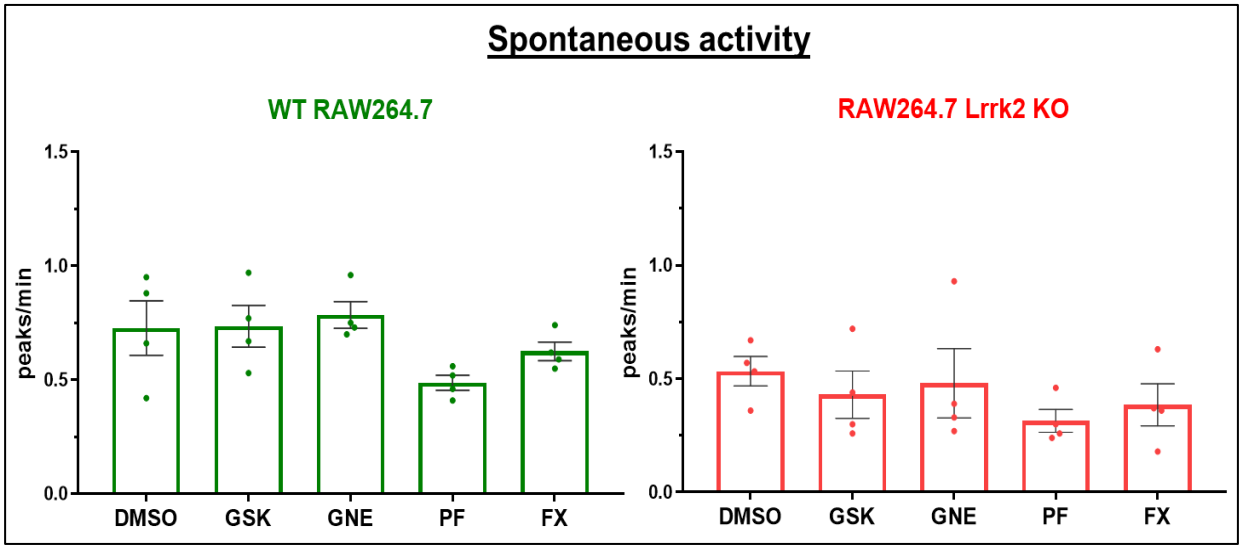

Figure 5.9: No effect of Lrrk2 inhibition on spontaneous activity in macrophage cells.

RAW264.7 WT or Lrrk2 KO macrophages were pre-treated with various Lrrk2 kinase inhibitors (GSK2578215A: GSK; GNE-9605: GNE; PF-06447475: PF; all at 1 µM) or a GTPase inhibitor (FX2149: FX, 100 nM) or DMSO (1:1000 equivalent dilution) for 1 hour, and loaded with Fura-2 AM (2 µM) in imaging buffer. The calcium signals were recorded for 5 minutes to measure the spontaneous release of calcium. Each repeat is an average of 20 cells, peaks were quantified for each cell and averaged to peaks/minute, and the data are mean ± SEM. n=4 repeats (1 coverslip/repeat), One-way ANOVA (with grouping by experimental repeat), Geisser-Greenhouse's correction, non-significant. (WT) Treatment effect: F(1.917, 5.752)= 2.042; p= 0.213 (KO) Treatment effect: F(1.707, 5.12)= 0.7075; p= 0.514.

5.3.2.2 Lrrk2 inhibition has no effect on ATP-evoked calcium responses in RAW264.7 macrophages

In this assay, cells were pre-treated with Lrrk2 inhibitors and calcium release was triggered twice with 10 µM ATP. Two peaks were therefore obtained, and each was analysed separately as "Peak 1" and "Peak 2", as indicated in the relevant graph titles (traces not shown). The effects of acute (1 hour) Lrrk2 inhibition on the ATP-evoked calcium responses are shown below in Figure 5.10 and Figure 5.11, and the effects of 16 hours Lrrk2 inhibition are shown in the Figure 5.12 and Figure 5.13. (*This assay corresponds to Assay n°6 in Chapter 2 Section 2.5.3.3*)

In these experiments, neither 1 hour (Figure 5.10 and Figure 5.11) nor 16 hours (Figure 5.12 and Figure 5.13) pre-treatment with the Lrrk2 kinase and GTPase inhibitors elicited a significant effect on the ATP-induced calcium responses in either genotypes compared to the relevant DMSO-treated control. However, it is important to note a variability in some of the data which might explain, at least to some extent, the lack of effects observed here.

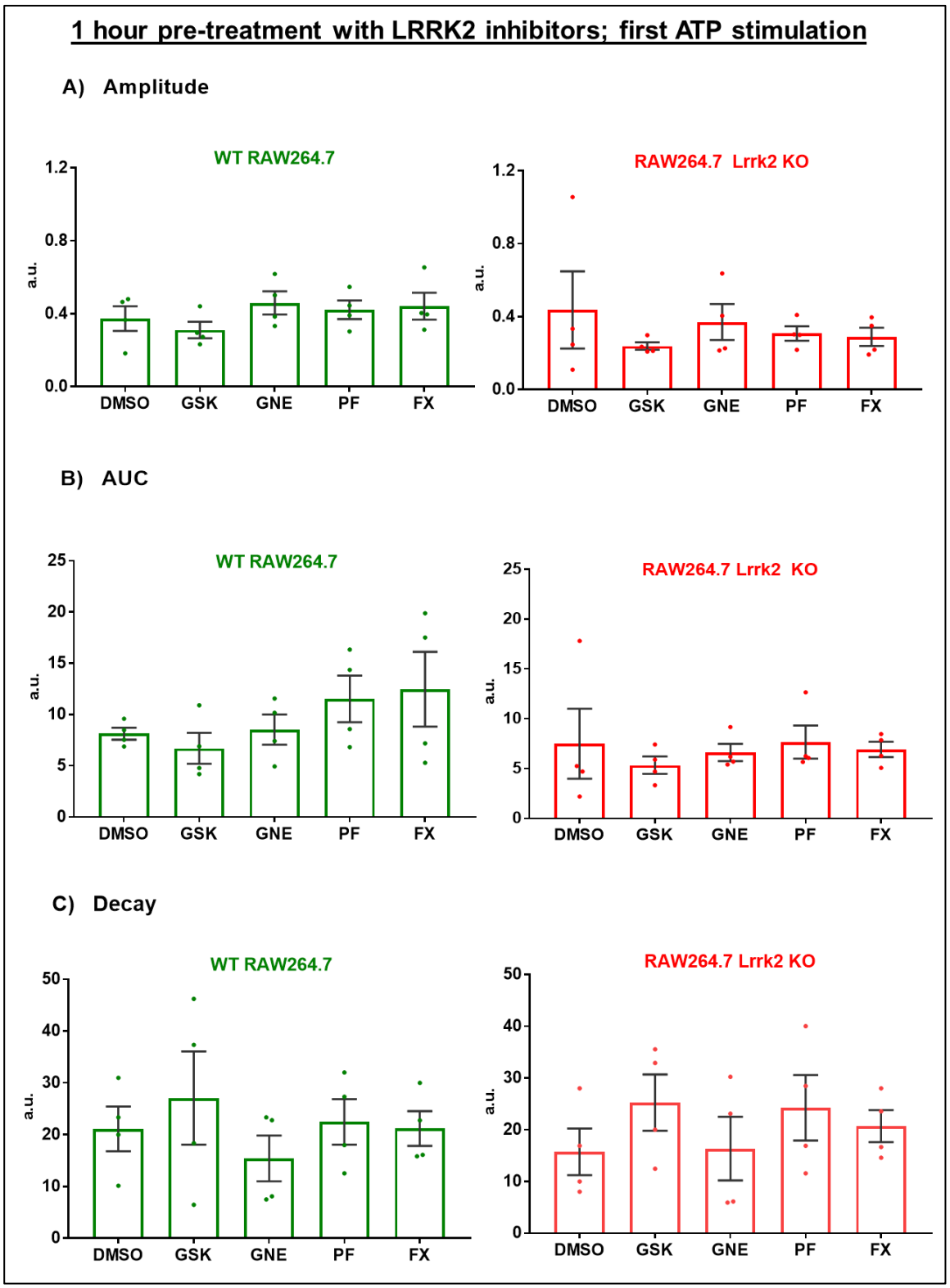

Figure 5.10: No effect of one-hour Lrrk2 inhibition on ATP-evoked calcium release (first stimulation)

RAW264.7 WT or Lrrk2 KO macrophages were pre-treated with various Lrrk2 kinase inhibitors (GSK2578215A: GSK; GNE-9605: GNE; PF-06447475: PF; all at 1 µM) or a GTPase inhibitor (FX2149: FX, 100 nM) or DMSO (1:1000 equivalent dilution) for 1 hour, and loaded with Fura-2 AM (2 µM) in imaging buffer. Basal calcium signals were recorded for 1 minute before addition of 10 µM ATP to evoke calcium signals, with 8 washes with imaging buffer and 10 minutes of rest between two stimulations. Each repeat is an average of 20 cells, and the data are mean ± SEM. n=4 repeats (1 coverslip/repeat), One-way ANOVA (with grouping by experimental repeat), Geisser-Greenhouse's correction, non-significant. (A) WT treatment effect: $F(1.621, 4.863)= 1.31$; $p=0.337$, KO treatment effect: $F(1.223, 3.669)= 0.5427$; $p=0.54$, (B) WT treatment effect: $F(1.356, 4.068)= 1.403$; $p=0.32$, KO treatment effect: $F(1.284, 3.851)= 0.355$; $p=0.64$ (C) WT treatment effect: $F(1.131, 3.393)= 1.83$; $p=0.26$, KO treatment effect: $F(1.294, 3.881)= 1.269$; $p=0.34$.

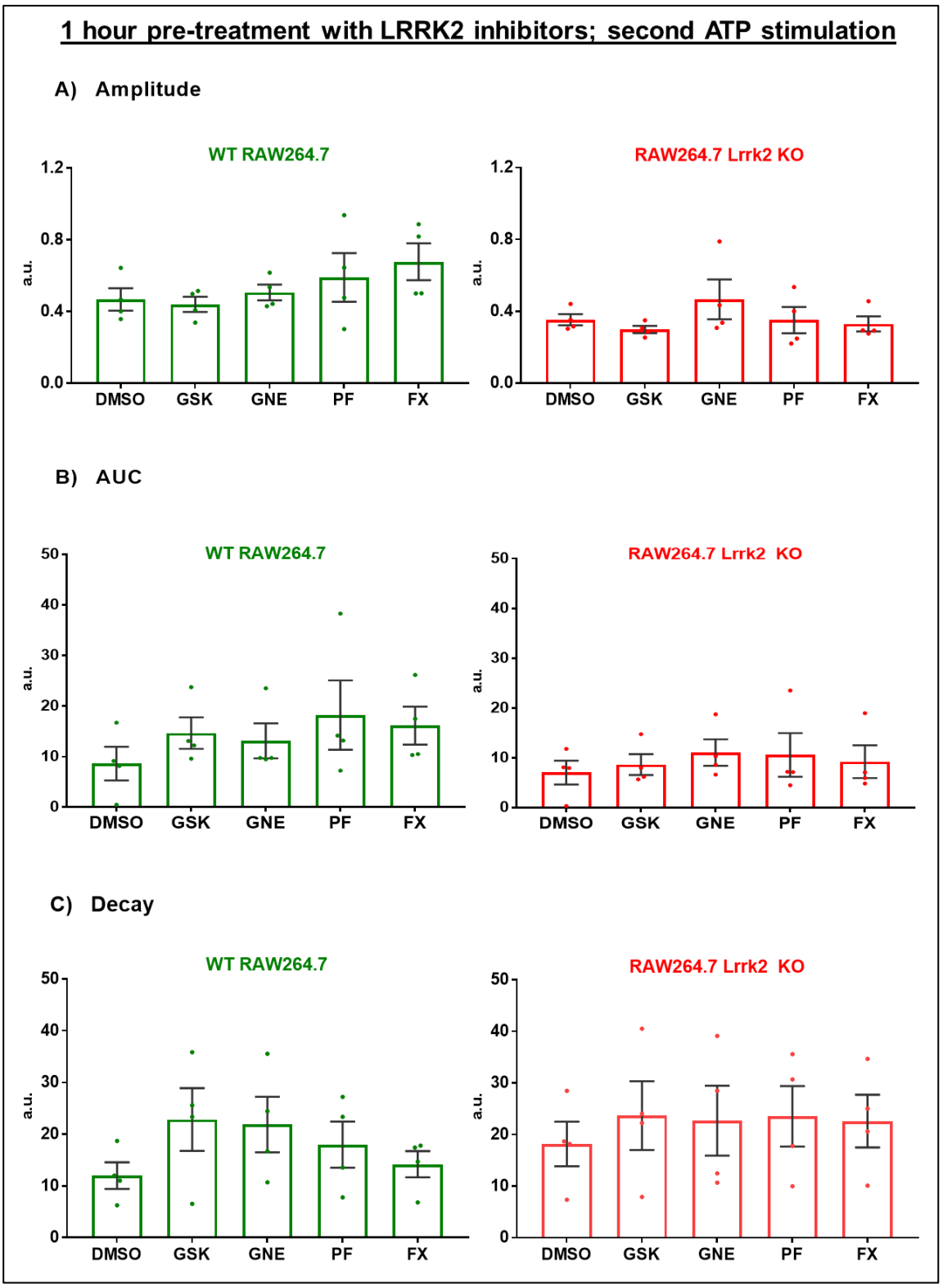

Figure 5.11: No effect of one-hour Lrrk2 inhibition on ATP-evoked calcium release (second stimulation).

RAW264.7 WT or Lrrk2 KO macrophages were pre-treated with various Lrrk2 kinase inhibitors (GSK2578215A: GSK; GNE-9605: GNE; PF-06447475: PF; all at 1 µM) or a GTPase inhibitor (FX2149: FX, 100 nM) or DMSO (1:1000 equivalent dilution) for 1 hour, and loaded with Fura-2 AM (2 µM) in imaging buffer. Basal calcium signals were recorded for 1 minute before addition of 10 µM ATP to evoke calcium signals, with 8 washes with imaging buffer and 10 minutes of rest between two stimulations. Each repeat is an average of 20 cells, and the data are mean ± SEM. n=4 repeats (1 coverslip/repeat), One-way ANOVA (with grouping by experimental repeat), Geisser-Greenhouse's correction, non-significant. (A) WT treatment effect: F(1.606, 4.819)= 1.774; p=0.26, KO treatment effect: F(1.616, 4.848)= 0.8667; p=0.45 (B) WT treatment effect: F(1.235, 3.704)= 0.9669; p=0.41, KO treatment effect: F(1.138, 3.413)= 0.3767; p=0.6 (C) WT treatment effect: F(2.33, 6.989)= 1.657; p=0.26, KO treatment effect: F(1.918, 5.754)= 0.266; p=0.77.

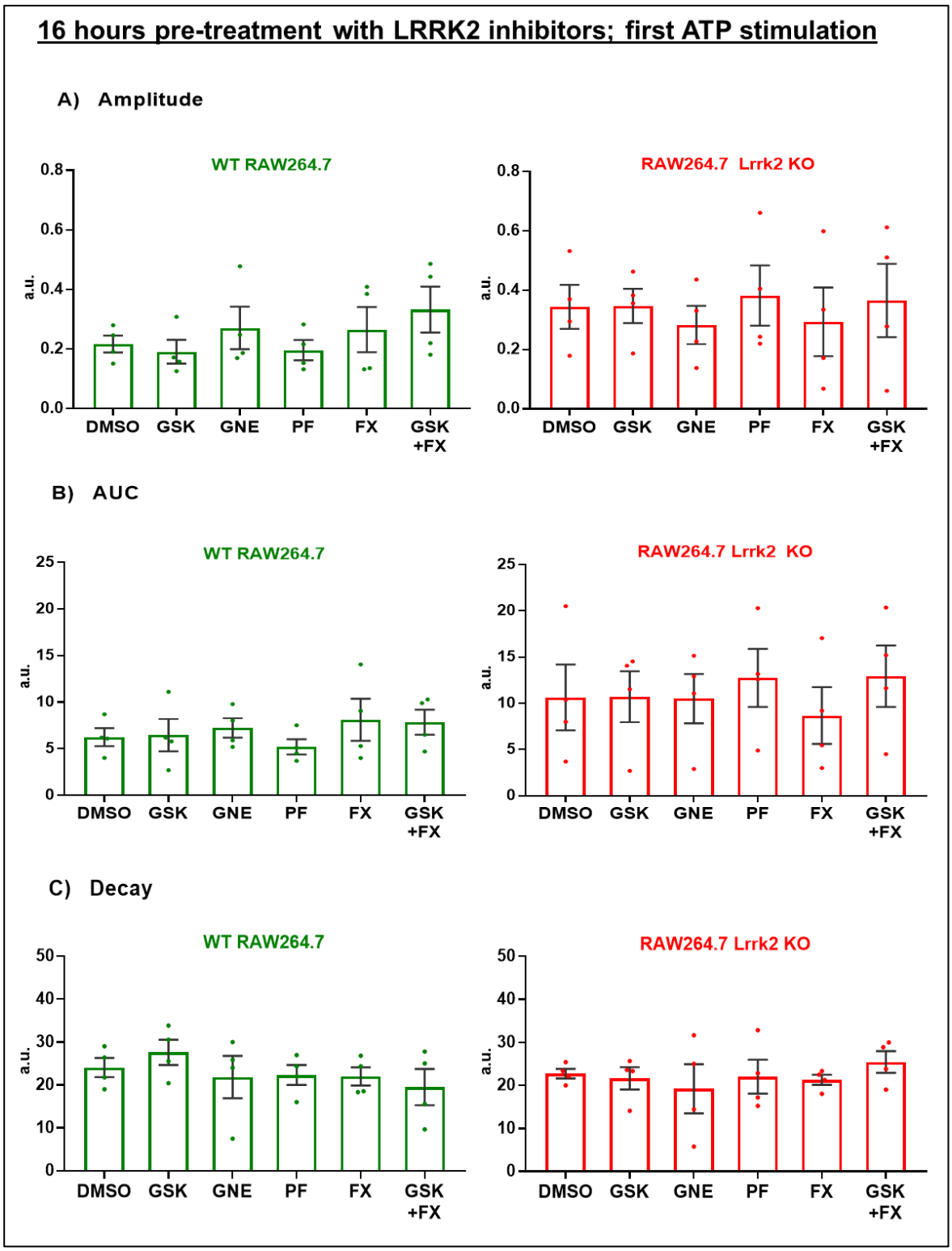

Figure 5.12: No effect of 16 hours Lrrk2 inhibition on ATP-evoked calcium release (first stimulation)

RAW264.7 WT or Lrrk2 KO macrophages were pre-treated with various Lrrk2 kinase inhibitors (GSK2578215A: GSK; GNE-9605: GNE; PF-06447475: PF; all at 1 µM) or a GTPase inhibitor (FX2149: FX, 100 nM) or DMSO (1:1000 equivalent dilution) for 16 hours, and loaded with Fura-2 AM (2 µM) in imaging buffer. Basal calcium signals were recorded for 1 minute before addition of 10 µM ATP to evoke calcium signals, with 8 washes with imaging buffer and 10 minutes of rest between two stimulations. Each repeat is an average of 20 cells, and the data are mean ± SEM. n=4 repeats (1 coverslip/repeat), One-way ANOVA (with grouping by experimental repeat), Geisser-Greenhouse's correction, non-significant. (A) WT treatment effect: $F(2.342, 7.027)= 1.149$; $p=0.38$, KO treatment effect: $F(1.584, 4.753)= 0.4648$; $p=0.61$ (B) WT treatment effect: $F(2.121, 6.364)= 0.627$; $p=0.57$, KO treatment effect: $F(1.32, 3.959)= 0.7144$; $p=0.48$ (C) WT treatment effect: $F(1.271, 3.812)= 1.492$; $p=0.31$, KO treatment effect: $F(1.47, 4.41)= 0.6297$; $p=0.53$.

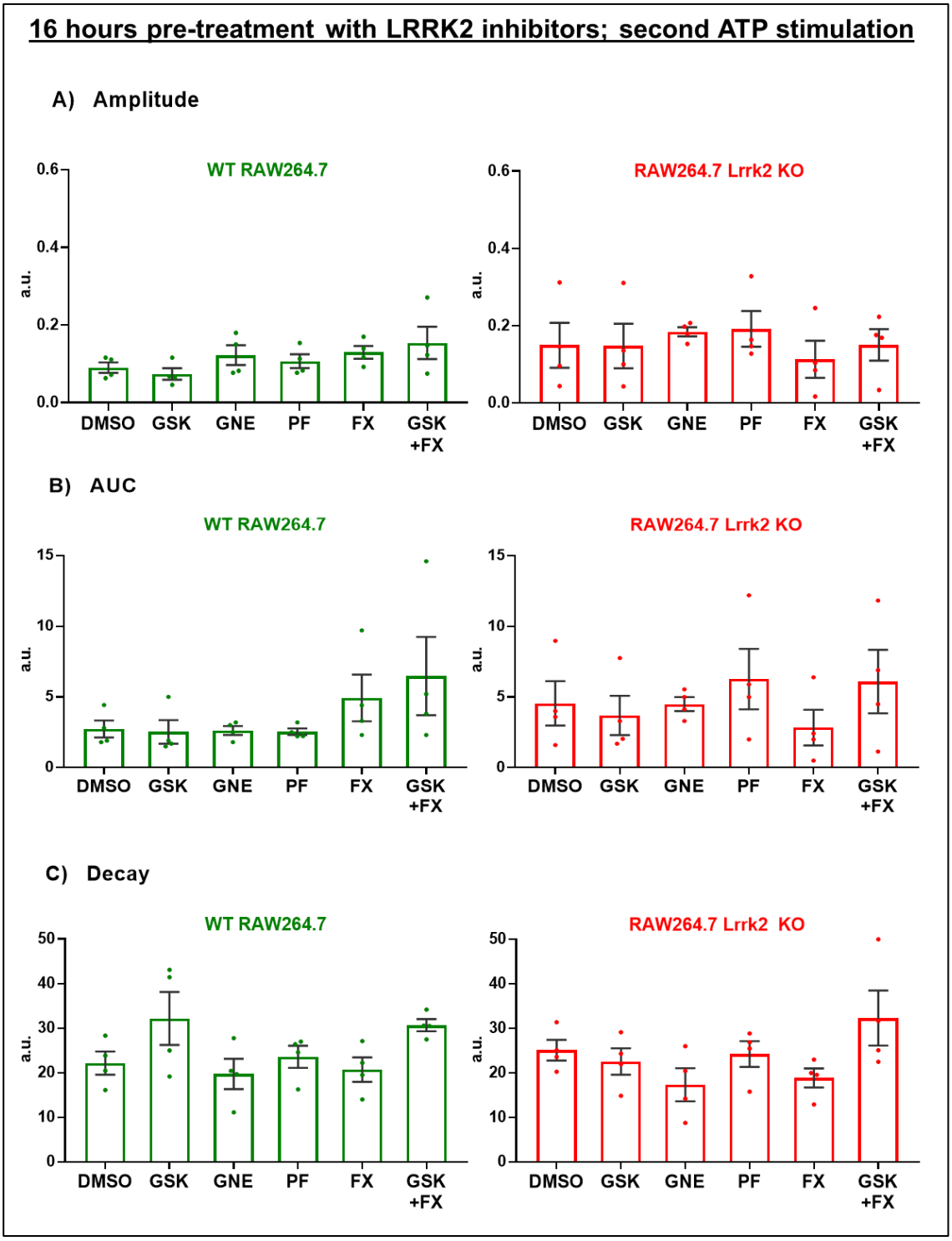

Figure 5.13: No effect of 16 hours Lrrk2 inhibition on ATP-evoked calcium release (second stimulation)

RAW264.7 WT or Lrrk2 KO macrophages were pre-treated with various LRRK2 kinase inhibitors (GSK2578215A: GSK; GNE-9605: GNE; PF-06447475: PF; all at 1 µM) or a GTPase inhibitor (FX2149: FX, 100 nM) or DMSO (1:1000 equivalent dilution) for 16 hours, and loaded with Fura-2 AM (2 µM) in imaging buffer. Basal calcium signals were recorded for 1 minute before addition of 10 µM ATP to evoke calcium signals, with 8 washes with imaging buffer and 10 minutes of rest between two stimulations. Each repeat is an average of 20 cells, and the data are mean ± SEM. n=4 repeats (1 coverslip/repeat), One-way ANOVA (with grouping by experimental repeat), Geisser-Greenhouse's correction, non-significant. (A) WT treatment effect: $F(1.843, 5.53)= 1.665$; $p=0.27$, KO treatment effect: $F(1.58, 4.739)= 0.4879$; $p=0.60$ (B) WT treatment effect: $F(1.232, 3.695)= 1.463$; $p=0.31$, KO treatment effect: $F(1.398, 4.194)= 0.9836$; $p=0.41$ (C) WT treatment effect: $F(2.477, 7.432)= 2.612$; $p=0.13$, KO treatment effect: $F(1.484, 4.452)= 2.614$; $p=0.18$.

Taken together, the data described so far in this Chapter so far suggest that whilst loss of Lrrk2 in RAW264.7 macrophages leads to a significantly faster and larger ATP-evoked calcium release, Lrrk2 kinase and GTPase inhibition has no effect on ATP-evoked calcium signals. These observations are discussed later in this Chapter.

5.4 Effect of LRRK2 inhibition on global calcium release in HEK293 GFP-LC3 cells

To test the role of LRRK2 enzymatic activities in calcium signalling further, the effects of LRRK2 inhibition on ATP-evoked calcium signals were also evaluated in HEK293 GFP-LC3 cells under identical treatment conditions to those used in RAW264.7 macrophages, i.e., pre-treatment with LRRK2 inhibitors for 1 hour or 16 hours, and calcium release triggered twice with ATP at 10 µM. This would allow for a comparison between macrophages and HEK293 GFP-LC3 cells, and would help assess whether the role of LRRK2 is cell-specific, as the data obtained from autophagy assays in Chapter 4 suggested that it was the case. (*This assay corresponds to the Assay n°6 in Chapter 2 Section 2.5.3.3*). Of note, HEK293 GFP-LC3 cells do not display spontaneous calcium activity, so recordings were only made following stimulation.

Similar to the WT RAW264.7 macrophages, neither 1 hour (Figure 5.14 and Figure 5.15) nor 16 hours (Figure 5.16 and Figure 5.17) pre-treatment with the Lrrk2 kinase and GTPase inhibitors elicited any consistent effects on the ATP-induced calcium responses in HEK293 GFP-LC3 cells compared to DMSO-treated cells. Indeed, the only statistically significant pairwise comparison was that one-hour pre-treatment with GSK2578215A elicited an increase in AUC following the second ATP stimulation (Figure 5.15 B). This effect was not observed after the first ATP stimulation (Figure 5.14 B), after 16 hours pre-treatment with the same compound (Figure 5.16 B and Figure 5.17 B), or with any of the other LRRK2 inhibitors when applied in parallel (Figure 5.15 B).

As such, it is most likely that this result is an outlier. Nonetheless, it is also possible that the experiment is underpowered and in need of additional repeats. With this in mind, it is interesting to note that all mean AUC values obtained following one-hour LRRK2 inhibition, for both the first and second stimulations, are greater than their corresponding DMSO controls (Figure 5.14 B and Figure 5.15 B), and this may be underpinned by corresponding increases in decay (Figure 5.14 C and Figure 5.15 C). Interestingly, similar non-significant patterns may be present in the WT RAW264.7 macrophage data, in particular for the second ATP-evoked calcium peak, where all mean values for AUC and decay are greater than DMSO control (Figure 5.11 B and C).

In any case, based on the statistically significant GSK2578215A result alone, these results indicate that one-hour LRRK2 inhibition may have a greater effect on calcium signals in HEK293 GFP-LC3 cells than overnight inhibition. Since calcium signals are tightly regulated in space and in time, it is plausible that long-term inhibition of LRRK2 did not cause any effects due to compensatory mechanisms.

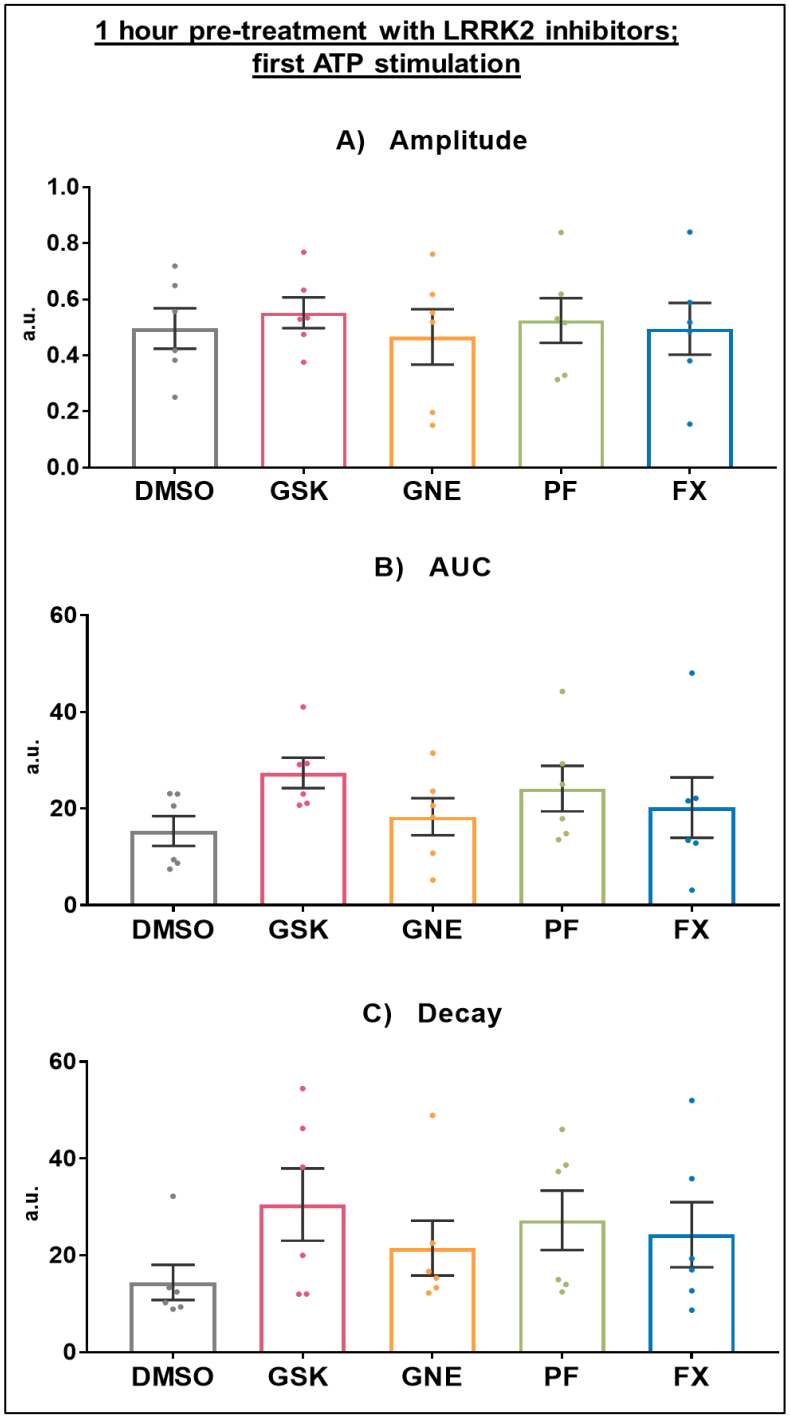

Figure 5.14: No effect of one-hour LRRK2 inhibition on ATP-evoked calcium release in HEK293 GFP-LC3 cells (first stimulation)

HEK293 GFP-LC3 cells were pre-treated with various LRRK2 kinase inhibitors (GSK2578215A: GSK; GNE-9605: GNE; PF-06447475: PF; all at 1 µM) or a GTPase inhibitor (FX2149: FX, 100 nM) or DMSO (1:1000 equivalent dilution) for 1 hour, and

loaded with Fura-2 AM (2 µM) in imaging buffer. Basal calcium signals were recorded for 1 minute before addition of 10 µM ATP to evoke calcium signals, with 8 washes with imaging buffer and 10 minutes of rest between two stimulations. Each repeat is an average of 20 cells, and the data are mean ± SEM. n=6 repeats (1 coverslip/repeat), One-way ANOVA (with grouping by experimental repeat), Geisser-Greenhouse's correction, non-significant. (A) treatment effect: F(2.728, 13.64)= 0.3589; p=0.76 (B) treatment effect: F(2.07, 10.35)= 1.696; p=0.23 (C) treatment effect: F(2.367, 11.83)= 2.081; p=0.16.

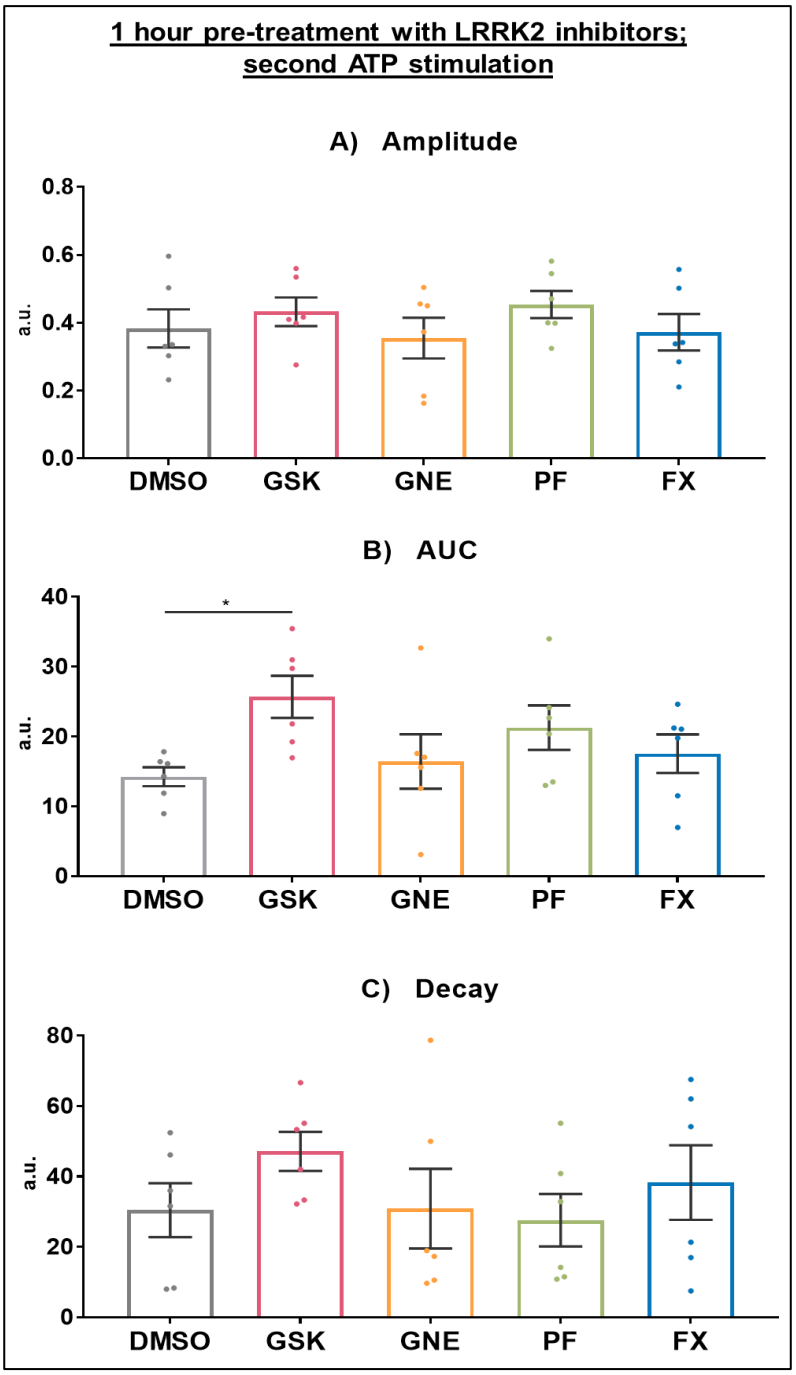

Figure 5.15: Effect of one-hour LRRK2 inhibition on ATP-evoked calcium release in HEK293 GFP-LC3 cells (second stimulation)

HEK293 GFP-LC3 cells were pre-treated with various LRRK2 kinase inhibitors (GSK2578215A: GSK; GNE-9605: GNE; PF-06447475: PF; all at 1 µM) or a GTPase inhibitor (FX2149: FX, 100 nM) or DMSO (1:1000 equivalent dilution) for 1 hour, and loaded with Fura-2 AM (2 µM) in imaging buffer. Basal calcium signals were recorded for 1 minute before addition of 10 µM ATP to evoke calcium signals, with 8 washes with imaging buffer and 10 minutes of rest between two stimulations. Each repeat is an average of 20 cells, and the data are mean ± SEM. n=6 repeats (1 coverslip/repeat), One-way ANOVA (with grouping by experimental repeat), Geisser-Greenhouse's correction, Dunnett post-hoc (comparison to DMSO). (A) treatment effect: F(1.786, 8.931)= 1.492; p=0.27 (B) treatment effect: F(2.309, 11.55)= 4.276; p=0.04 (C) treatment effect: F(1.969, 9.843)= 1.724; p=0.23. On graphs: p<0.05 (*).

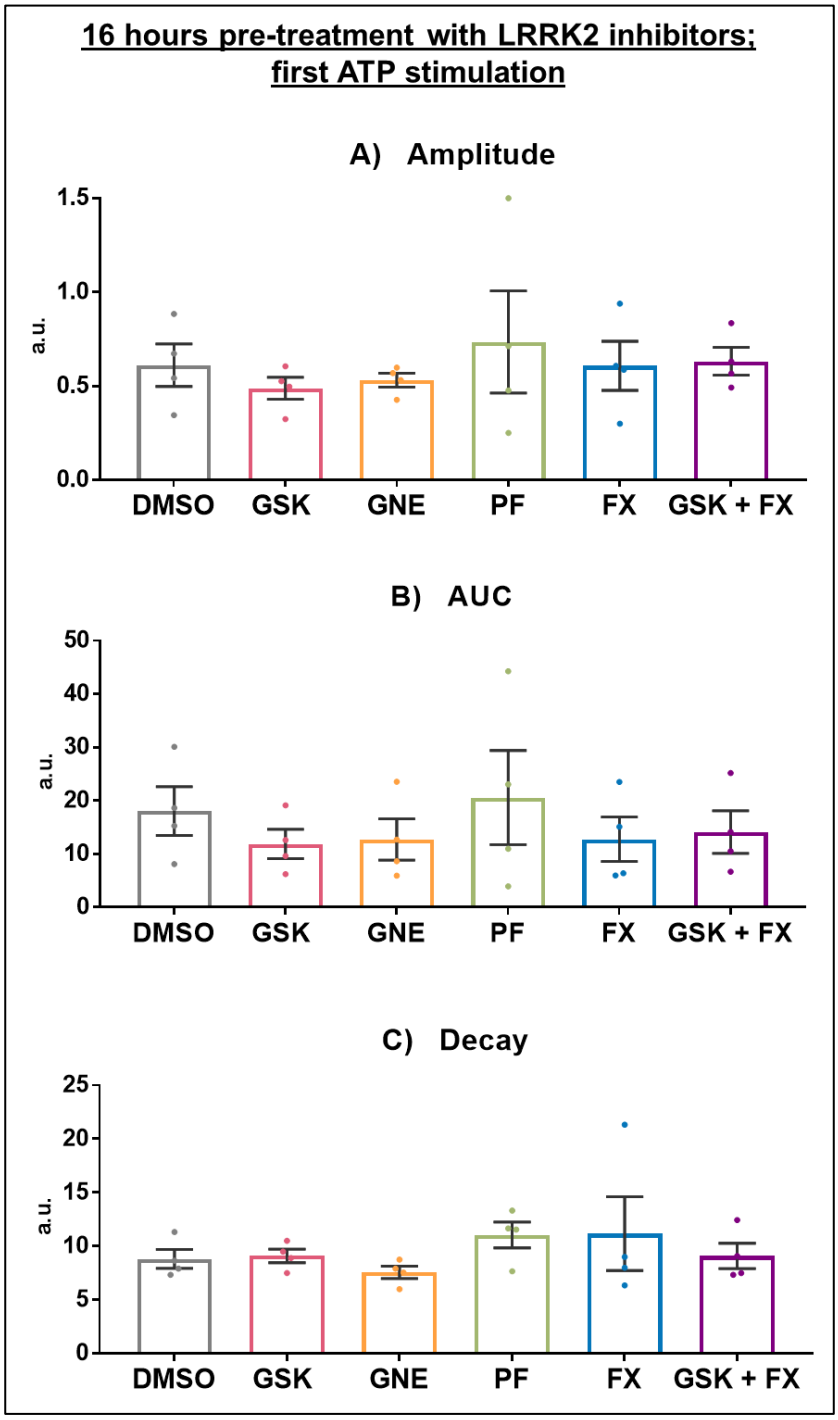

Figure 5.16: No effect of 16 hours LRRK2 inhibition on ATP-evoked calcium release in HEK293 GFP-LC3 cells (first stimulation)

HEK293 GFP-LC3 cells were pre-treated with various LRRK2 kinase inhibitors (GSK2578215A: GSK; GNE-9605: GNE; PF-06447475: PF; all at 1 µM) or a GTPase inhibitor (FX2149: FX, 100 nM) or DMSO (1:1000 equivalent dilution) for 16 hours, and loaded with Fura-2 AM (2 µM) in imaging buffer. Basal calcium signals were recorded for 1 minute before addition of 10 µM ATP to evoke calcium signals, with 8 washes with imaging buffer and 10 minutes of rest between two stimulations. Each repeat is an average of 20 cells, and the data are mean ± SEM. n=4 repeats (1 coverslip/repeat), One-way ANOVA (with grouping by experimental repeat), Geisser-Greenhouse's correction, non-significant. (A) treatment effect: $F(1.886, 5.657)= 0.4554$; $p=0.65$ (B) treatment effect: $F(2.155, 6.466)= 0.6371$; $p=0.57$ (C) treatment effect: $F(1.13, 3.391)= 0.7248$; $p=0.47$.

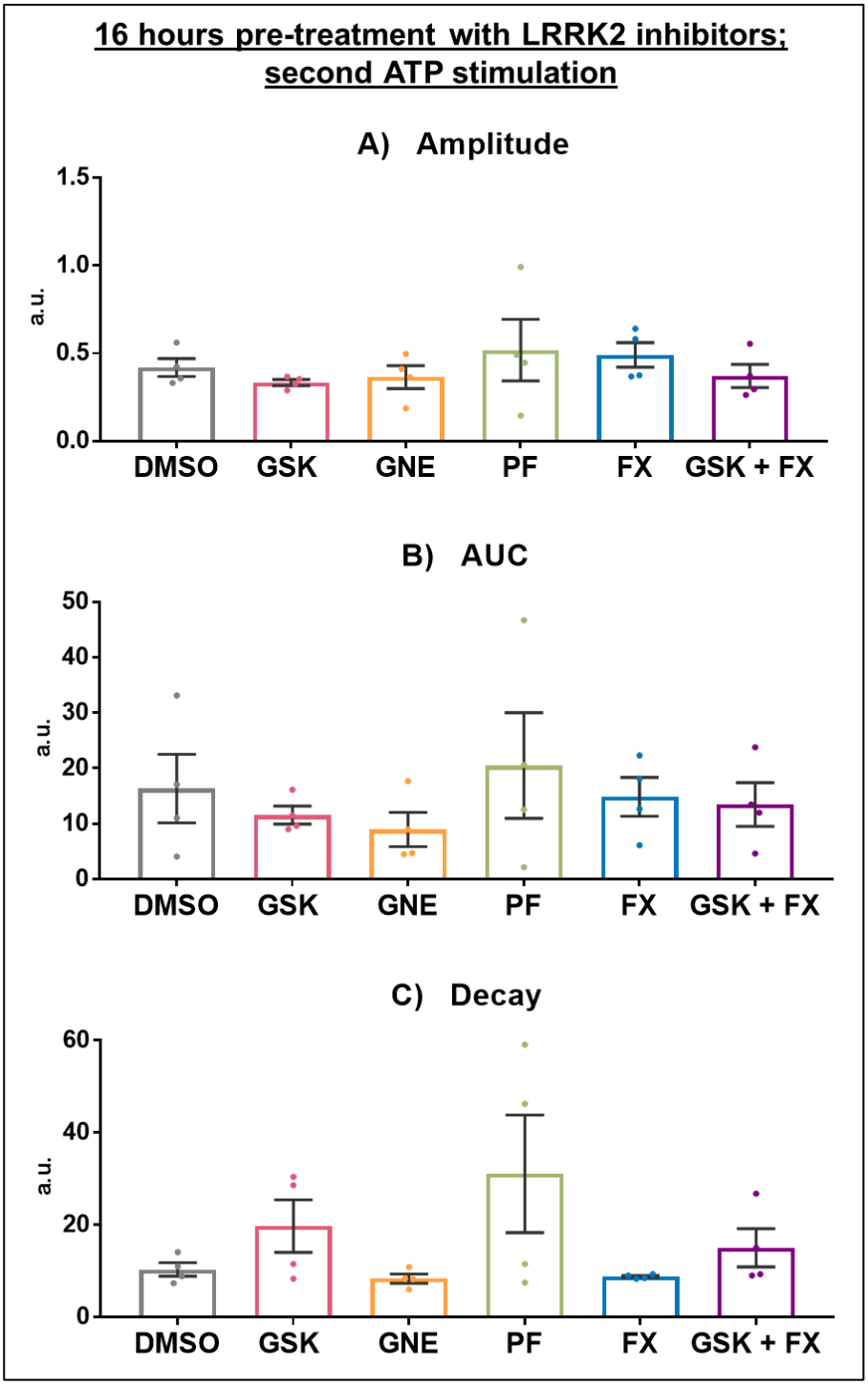

Figure 5.17: No effect of 16 hours LRRK2 inhibition on ATP-evoked calcium release in HEK293 GFP-LC3 cells (second stimulation)

HEK293 GFP-LC3 cells were pre-treated with various LRRK2 kinase inhibitors (GSK2578215A: GSK; GNE-9605: GNE; PF-06447475: PF; all at 1 µM) or a GTPase inhibitor (FX2149: FX, 100 nM) or DMSO (1:1000 equivalent dilution) for 16 hours, and loaded with Fura-2 AM (2 µM) in imaging buffer. Basal calcium signals were recorded for 1 minute before addition of 10 µM ATP to evoke calcium signals, with 8 washes with imaging buffer and 10 minutes of rest between two stimulations. Each repeat is an average of 20 cells, and the data are mean ± SEM. n=4 repeats (1 coverslip/repeat), One-way ANOVA (with grouping by experimental repeat), Geisser-Greenhouse's correction, non-significant. (A) treatment effect: $F(1.743, 5.23)= 0.8569$; $p=0.46$ (B) treatment effect: $F(1.939, 5.816)= 0.8288$; $p=0.48$ (C) treatment effect: $F(1.163, 3.49)= 2.747$; $p=0.18$.

5.5 Effect of LRRK2 inhibition on lysosomal calcium in RAW264.7 macrophages

Overall, the previous assays described in this Chapter do not support any robust effects of LRRK2 enzymatic inhibition on ATP-evoked calcium responses, although, when applied acutely, the data possibly hint at subtle effects that may be beyond the sensitivity of the assays used. Regardless, these assays investigated the global increase in the concentration of cytosolic calcium, since stimulation of cells with extracellular ATP leads to release of ER calcium stores. Importantly however, certain studies support a specific role for LRRK2 in lysosomal calcium homeostasis. Given this and the known relevance of lysosomal calcium homeostasis to the autophagic pathway, another experimental approach was designed specifically to explore the role of LRRK2 in lysosomal calcium storage.

5.5.1 Establishing the parameters to study lysosomal calcium responses

To determine whether LRRK2 is involved in lysosomal calcium storage in RAW264.7 macrophages and HEK293 GFP-LC3 cells, a two-step experiment to measure calcium signal profiles was designed. These steps refer to two distinct stimulations that will each trigger an increase in cytosolic calcium levels and a corresponding “peak”, but through different mechanisms. An example trace is shown in Figure 5.18.

The strategy is to first stimulate cells with cyclopiazonic acid (CPA), a compound that blocks the SERCA pumps, thereby preventing ER calcium replenishment, but also leading to a gradual elevation of cytosolic calcium due to natural leakage from stores[688]. Once the CPA response ends and ER stores are presumed to be exhausted, cells are stimulated a second time using Ionomycin. Ionomycin is a membrane permeant calcium ionophore which binds calcium ions and facilitates their transport directly across the membrane of acidic stores, in particular lysosomes[414,688]. Importantly, pre-treatment with CPA will prevent any calcium released from lysosomes from triggering a much larger “calcium-induced calcium release” from the ER, meaning the initial release of lysosomal calcium can be measured without being swamped by a bigger signal. In other words, Fura-2 signals recorded in response to ionomycin in cells pre-treated with CPA will reflect only lysosomal calcium release. Importantly, during all these recordings,

all measurements were carried out in calcium-free imaging buffer, to prevent any calcium influx from the extracellular environment into the cytosol.

In theory, since the mechanism through which Ionomycin acts is passive and diffusion-based, unlike ATP, it is only limited by the amount and concentration of calcium stored in the target organelles and in the cytosol, which eventually reaches equilibrium. As such, the AUC data that would be obtained from the analysis of the Ionomycin-evoked peak would be reflective of the total amount of calcium stored in lysosomes. Similarly, AUC data from the CPA-evoked peak would reflect the total amount of calcium stored in the ER.

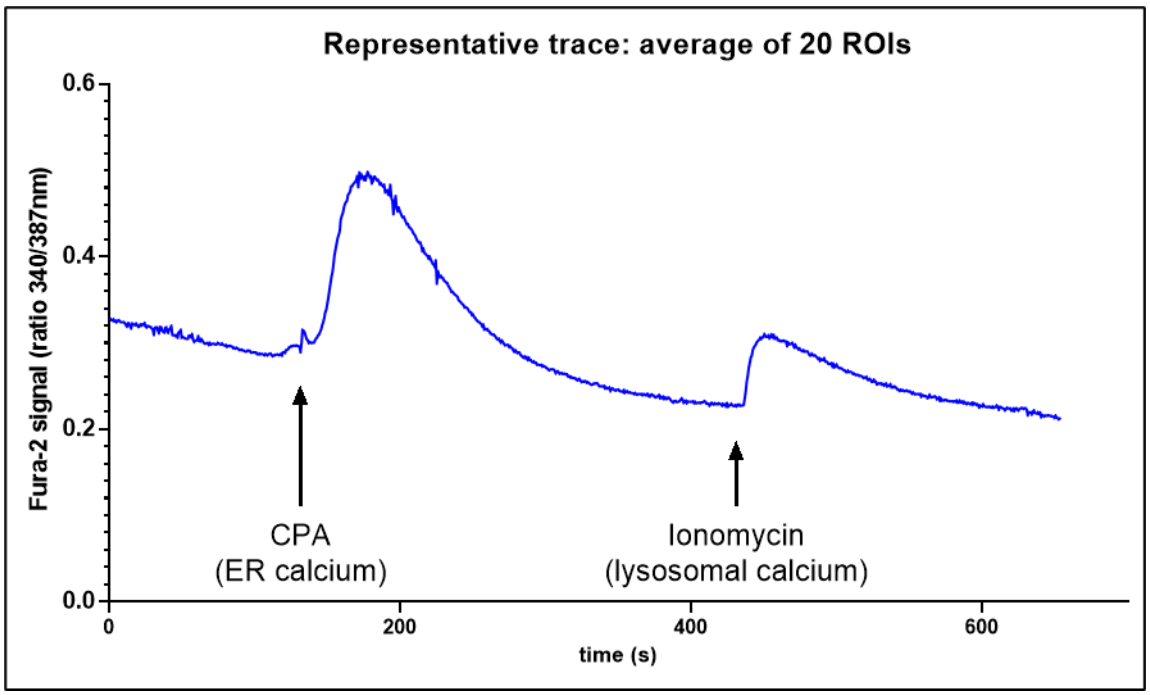

Figure 5.18: Representative trace of calcium signals following CPA and Ionomycin stimulations in RAW264.7 macrophages.

Calcium signals were recorded in cells, and evoked by addition of CPA and Ionomycin (both at 10 μM) in calcium-free buffer. This trace is an average overtime of 20 traces obtained from 20 cells.

5.5.2 Loss of Lrrk2 has no effect on CPA- and Ionomycin-evoked calcium signals in RAW264.7 macrophages

The first aim was to examine whether loss of Lrrk2 in macrophages had an effect on the total amount of calcium stored in the ER or in lysosomes. To do so, the effect of loss of Lrrk2 on the CPA- and Ionomycin-evoked calcium responses was determined in WT RAW264.7 or Lrrk2 KO macrophages. Cells were superfused with calcium-free imaging buffer supplemented with CPA followed by a combination of CPA and Ionomycin (to maintain the SERCA blockade).

The results presented in Figure 5.19 correspond to the DMSO control data obtained from both genotypes in the experiments described in Figure 5.20 A (where cells were pre-treated with DMSO at 1:1000 equivalent dilution for 1 hour prior to recordings). This analysis revealed that there was no significant difference in both the CPA and Ionomycin responses between the two genotypes, suggesting that loss of Lrrk2 did not affect the amount of calcium stored in the ER or in lysosomes in WT macrophages.

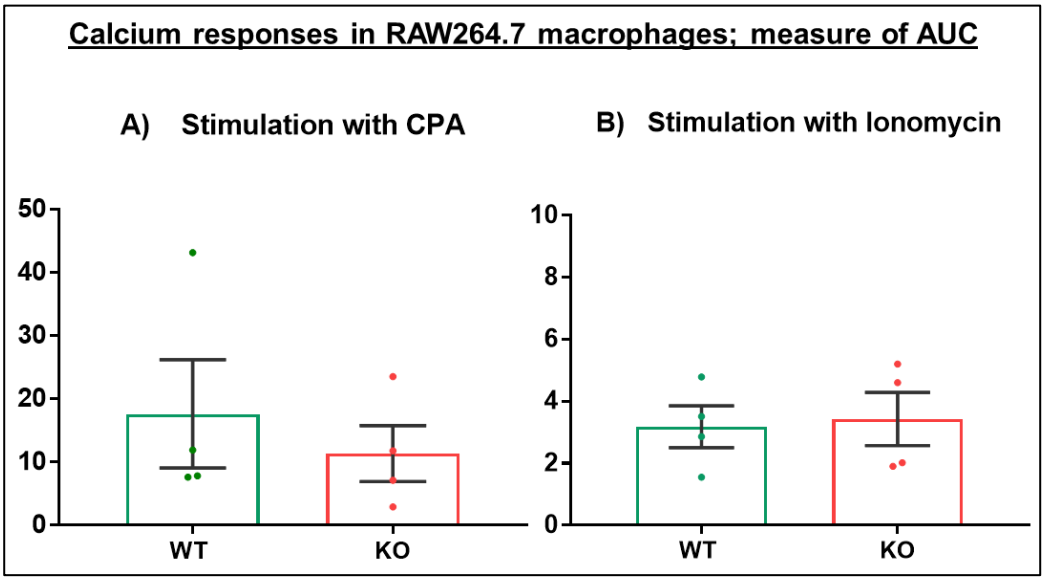

Figure 5.19: Measure of calcium signals in response to CPA and Ionomycin in RAW264.7 macrophages.

RAW264.7 WT or Lrrk2 KO macrophages were pre-treated with DMSO (1:1000 equivalent dilution) for 1 hour, and loaded with Fura-2 AM (2 µM) in imaging buffer. Basal calcium signals were recorded for 1 minute before addition of CPA (10 µM) followed by CPA (10 µM) + Ionomycin (10 µM) to evoke calcium signals, with 1 wash with imaging buffer between the stimulations. The stimulations and washes were performed in calcium-free buffer. Each repeat is an average of 20 cells, and the data are mean ± SEM. The data presented here are extracted from the DMSO data obtained in the experiments described in Figure 5.20. n=4 repeats (1 coverslip/repeat), Unpaired T-test, non-significant. (A) t=0.651, df=6, p=0.54 (B) t=0.2314, df=6, p=0.82.

5.5.3 LRRK2 inhibition has no effect on CPA- and Ionomycin-evoked calcium signals in RAW264.7 macrophages

Since the loss of Lrrk2 did not appear to affect the CPA- or Ionomycin-induced calcium responses in WT RAW264.7 macrophages, the next step was to explore the effect of LRRK2 inhibition on the CPA- or Ionomycin-evoked calcium signals in WT RAW264.7 and Lrrk2 KO macrophages in parallel, under identical treatment conditions to those used in the previous assays in this Chapter (i.e., pre-treatment with LRRK2 inhibitors for 1 hour or 16 hours). Cells were then superfused with calcium-free imaging buffer supplemented with CPA followed by a combination of CPA and Ionomycin to trigger an elevation in cytosolic calcium levels. (*This assay corresponds to Assay n°7 in Chapter 2 Section 2.5.3.3*).

Neither 1-hour (Figure 5.20) nor 16 hours (Figure 5.21) pre-treatment with the Lrrk2 kinase and GTPase inhibitors elicited any effects on the CPA- or Ionomycin evoked calcium responses in RAW264.7 macrophages, compared to DMSO-treated cells. This observation suggests that inhibition of Lrrk2 enzymatic activities has no effect on the amount of calcium stored in lysosomes.

Taken together, the data presented in this Section indicate that neither loss of Lrrk2 nor inhibition of Lrrk2 kinase and GTPase activities has an effect on the CPA- or Ionomycin-evoked calcium signals. These observations are discussed later in this Chapter.

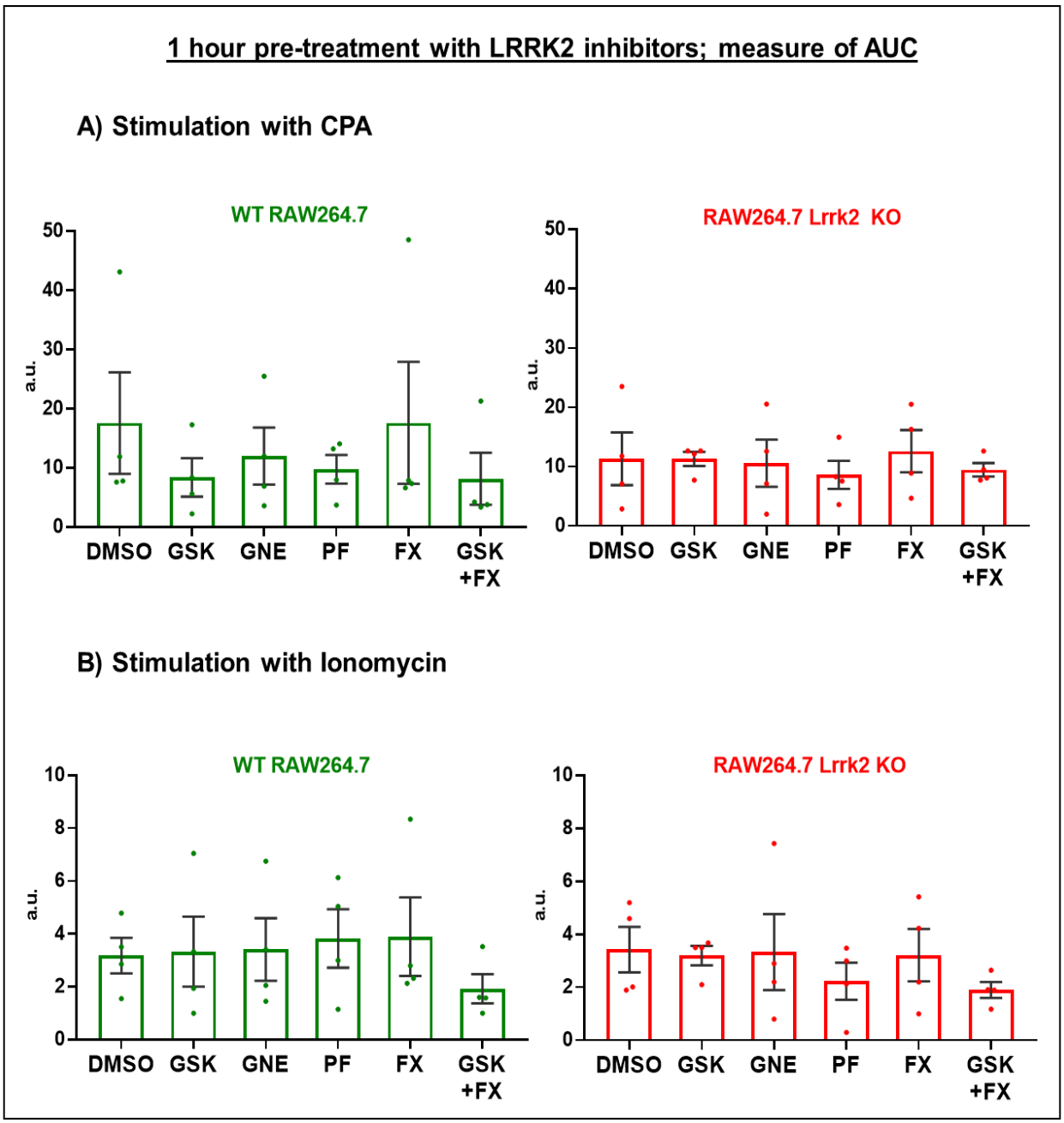

Figure 5.20: No effect of one-hour Lrrk2 inhibition on CPA- or Ionomycin-evoked calcium signals.

RAW264.7 WT or Lrrk2 KO macrophages were pre-treated with various Lrrk2 kinase inhibitors (GSK2578215A: GSK; GNE-9605: GNE; PF-06447475: PF; all at 1 µM) or a GTPase inhibitor (FX2149: FX, 100 nM) or DMSO (1:1000 equivalent dilution) for 16 hours, and loaded with Fura-2 AM (2 µM) in imaging buffer. Basal calcium signals were recorded for 1 minute before addition of CPA (10 µM) followed by CPA (10 µM) + Ionomycin (10 µM) to evoke calcium signals, with 1 wash between the stimulations. The stimulations and wash were performed in calcium-free buffer. Each repeat is an average of 20 cells, and the data are mean ± SEM. n=4 repeats (1 coverslip/repeat). One-way ANOVA (with grouping by experimental repeat), Geisser-Greenhouse's correction, non-significant. (A) WT treatment effect: $F(1.22, 3.659)= 1.461$; $p=0.31$, KO treatment effect: $F(1.645, 4.936)= 0.2412$; $p=0.75$ (B) WT treatment effect: $F(1.676, 5.028)= 1.106$; $p=0.39$, KO treatment effect: $F(1.557, 4.672)= 1.159$; $p=0.37$.

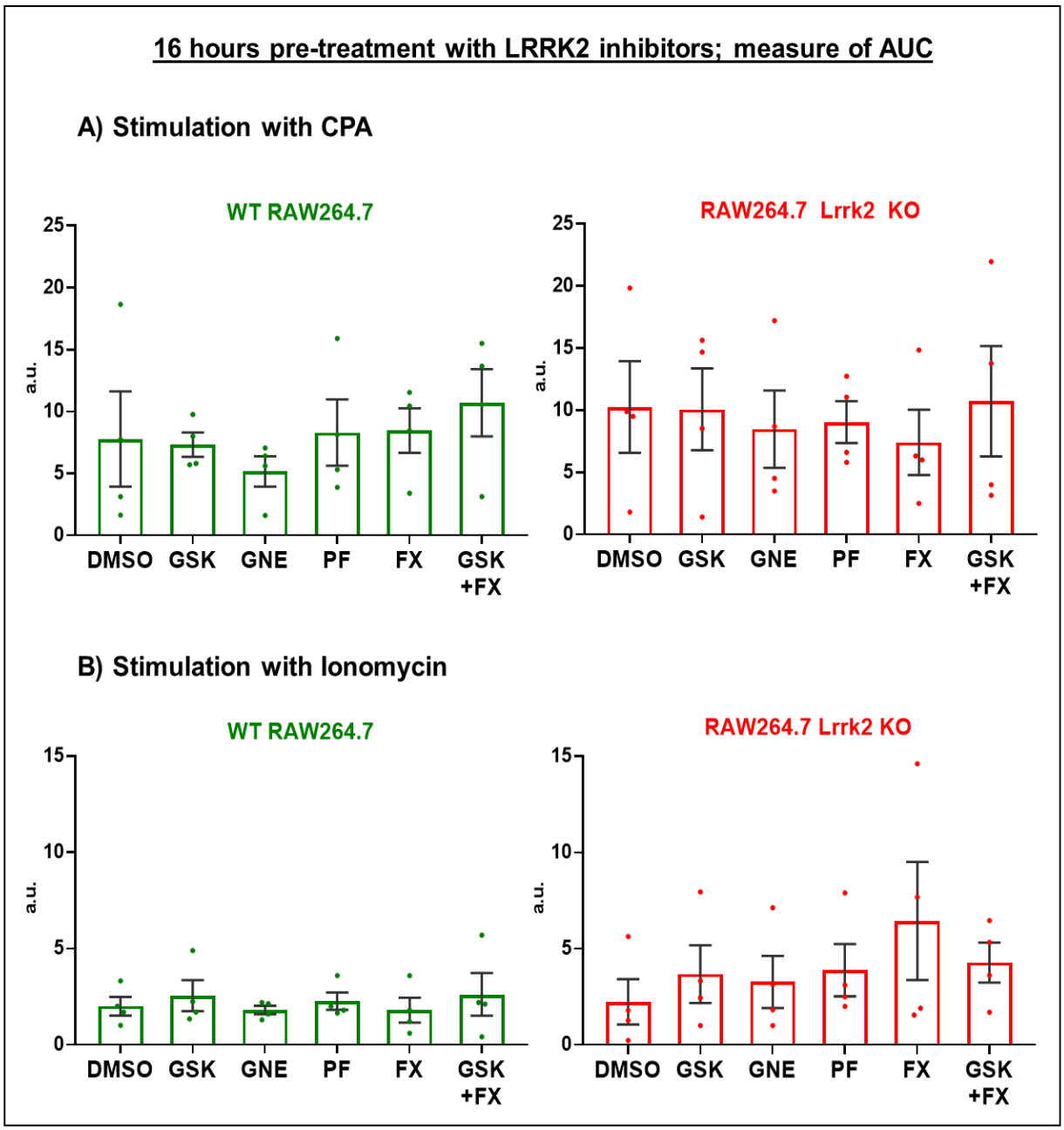

Figure 5.21: No effect of 16 hours Lrrk2 inhibition on CPA- or Ionomycin-evoked calcium signals.

RAW264.7 WT or Lrrk2 KO macrophages were pre-treated with various Lrrk2 kinase inhibitors (GSK2578215A: GSK; GNE-9605: GNE; PF-06447475: PF; all at 1 µM) or a GTPase inhibitor (FX2149: FX, 100 nM) or DMSO (1:1000 equivalent dilution) for 16 hours, and loaded with Fura-2 AM (2 µM) in imaging buffer. Basal calcium signals were recorded for 1 minute before addition of CPA (10 µM) followed by CPA (10 µM) + Ionomycin (10 µM) to evoke calcium signals, with 1 wash between the stimulations. The stimulations and washes were performed in calcium-free buffer. Each repeat is an average of 20 cells, and the data are mean ± SEM. n=4 repeats (1 coverslip/repeat). One-way ANOVA (with grouping by experimental repeat), Geisser-Greenhouse's correction, non-significant. (A) WT treatment effect: $F(1.471, 4.414)= 1.139$; $p=0.37$, KO treatment effect: $F(1.905, 5.715)= 0.2138$; $p=0.80$ (B) WT treatment effect: $F(1.396, 4.187)= 1.012$; $p=0.40$, KO treatment effect: $F(1.114, 3.342)= 1.335$ $p=0.33$.

5.5.4 Verification of the effect of CPA in RAW264.7 macrophages

To make sure that the responses that were observed in response to the combination of CPA and Ionomycin were indeed lysosomal calcium responses, an additional control experiment was carried out to determine the efficiency of prior CPA treatment. (*This experiment corresponds to Assay n°3 in Chapter 2 Section 2.5.3.1*). The example trace is shown in Figure 5.22 and the results are shown in Figure 5.23. In theory, if the CPA stimulation emptied the ER calcium store and blocked the reuptake of calcium via the SERCA pumps, a stimulation with ATP should not trigger a calcium response.

Consistent with this, whilst 10 µM CPA elicited a calcium response (Figure 5.22 and Figure 5.23), the subsequent stimulation with 10 µM ATP had no effect on cytosolic calcium levels. This indicates that the ATP-evoked calcium release was abrogated, which confirms that the calcium responses following Ionomycin stimulation were indeed corresponding to lysosomal calcium.

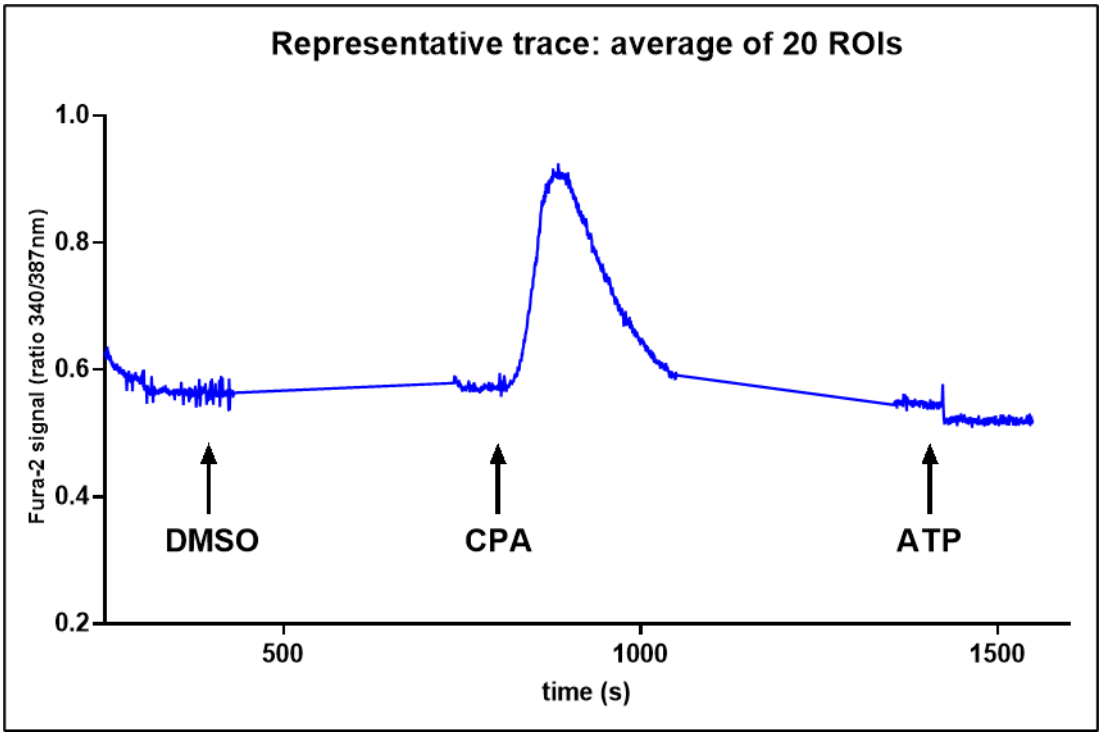

Figure 5.22: Representative trace showing that CPA prevents the ATP-mediated calcium release from the ER.
Representative trace obtained using WT RAW264.7 macrophages stimulated with DMSO (1:1000 equivalent dilution), CPA (10 µM) or ATP (10 µM) (arrows).

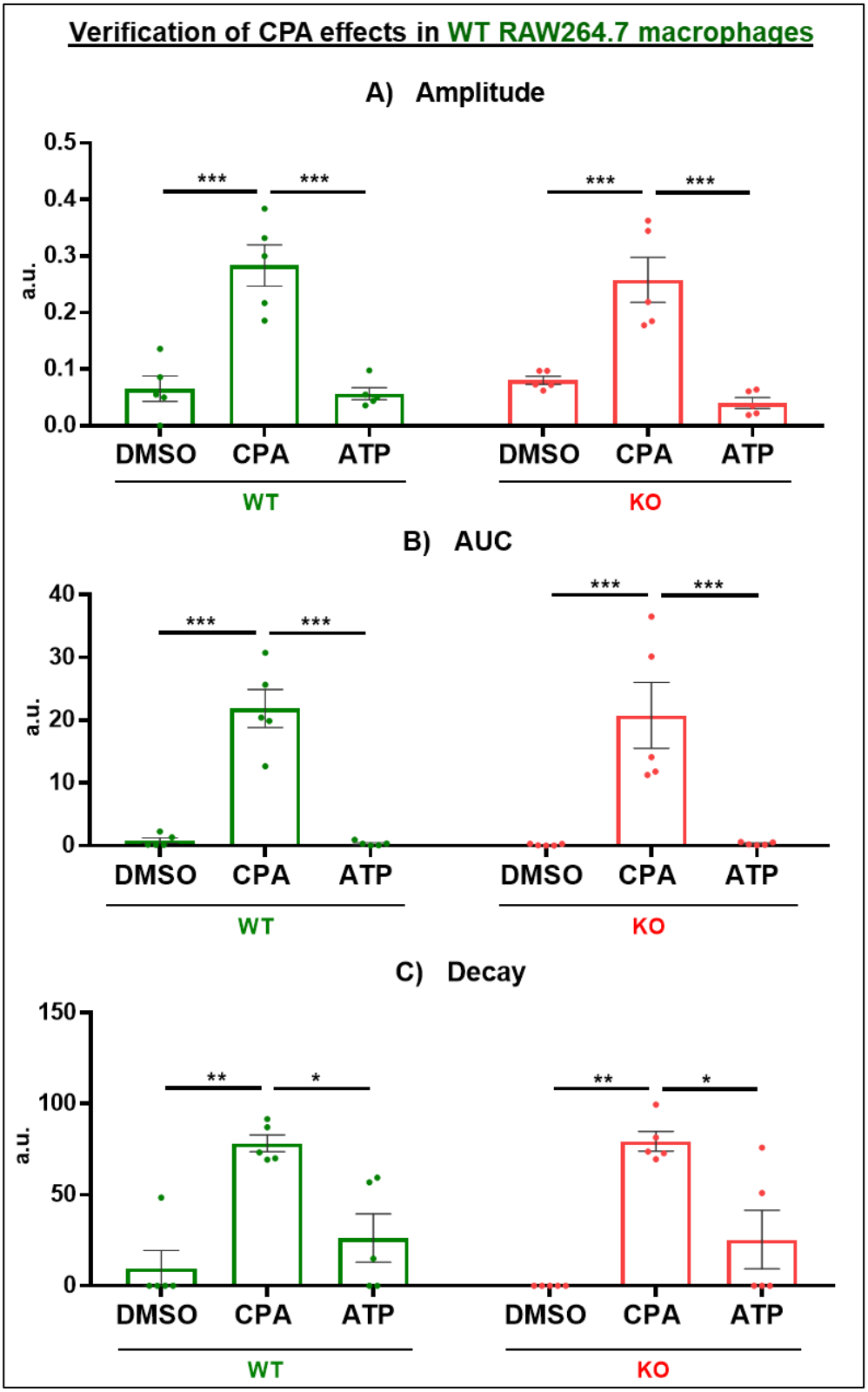

Figure 5.23: CPA empties the ER calcium store and prevents the ATP-mediated calcium release from the ER.

RAW264.7 WT or Lrrk2 KO macrophages were loaded with Fura-2 AM (2 µM) in imaging buffer. Basal calcium signals were recorded for 1 minute before addition of DMSO (1:1000 equivalent dilution), followed by the agonists CPA (10 µM) and ATP (10 µM) to evoke calcium signals, with 8 washes and 10 minutes of rest between the stimulations. The stimulations and washes were performed in calcium-free buffer. Each repeat is an average of 20 cells, and the data are mean ± SEM. n=5 repeats (1 coverslip/repeat). Two-way ANOVA (with grouping by experimental repeat), Tukey post-hoc test. (A) peak effect: $F(2, 8)= 52.08$; $p<0.0001$, genotype effect: $F(1, 4)= 0.4809$; $p=0.53$, interaction: $F(2, 8)= 0.7707$; $p=0.49$ (B) peak effect: $F(2, 8)= 32.07$; $p=0.0002$, genotype effect: $F(1, 4)= 0.1839$; $p=0.69$, interaction: $F(2, 8)= 0.04719$; $p=0.95$ (C) peak effect: $F(2, 8)= 26.98$; $p=0.0003$, genotype effect: $F(1, 4)= 0.12$; $p=0.75$, interaction: $F(2, 8)= 0.2019$; $p=0.82$. On graphs: $p<0.001$ (***), $p<0.01$ (**), $p<0.05$ (*).

5.6 Effect of LRRK2 inhibition on lysosomal calcium in HEK293 GFP-LC3 cells

The effects of LRRK2 inhibition on CPA- and Ionomycin-evoked calcium signals were also assessed in HEK293 GFP-LC3 cells under identical treatment conditions to those used in RAW264.7 macrophages, i.e., pre-treatment with LRRK2 inhibitors for 1 hour or 16 hours and calcium release triggered twice with calcium-free imaging buffer supplemented with CPA followed by the combination of CPA and Ionomycin. (*This assay corresponds to Assay n°7 in Chapter 2 Section 2.5.3.3*).

Similar to the results obtained in macrophages, none of the four LRRK2 inhibitors elicited any significant difference in the CPA- or Ionomycin-evoked calcium signals compared to the DMSO-treated control, both after 1 hour (Figure 5.24) or 16 hours of inhibition (Figure 5.25).

It is worth mentioning that a potential pattern can be seen in the CPA data following 16 hours inhibition (Figure 5.25 A), where the AUC data obtained with the LRRK2 kinase inhibitors (GSK2578215A, GNE-9605, PF-06447475) appear to be higher than the DMSO control. If true, this would suggest that prolonged LRRK2 kinase inhibition leads to increased ER calcium storage. However, given the variability within these data, this interpretation is only speculative.

Taken together, the results presented so far suggest that LRRK2 enzymatic activities are unlikely to be involved in calcium storage in the ER or lysosomes in HEK293 GFP-LC3 cells.

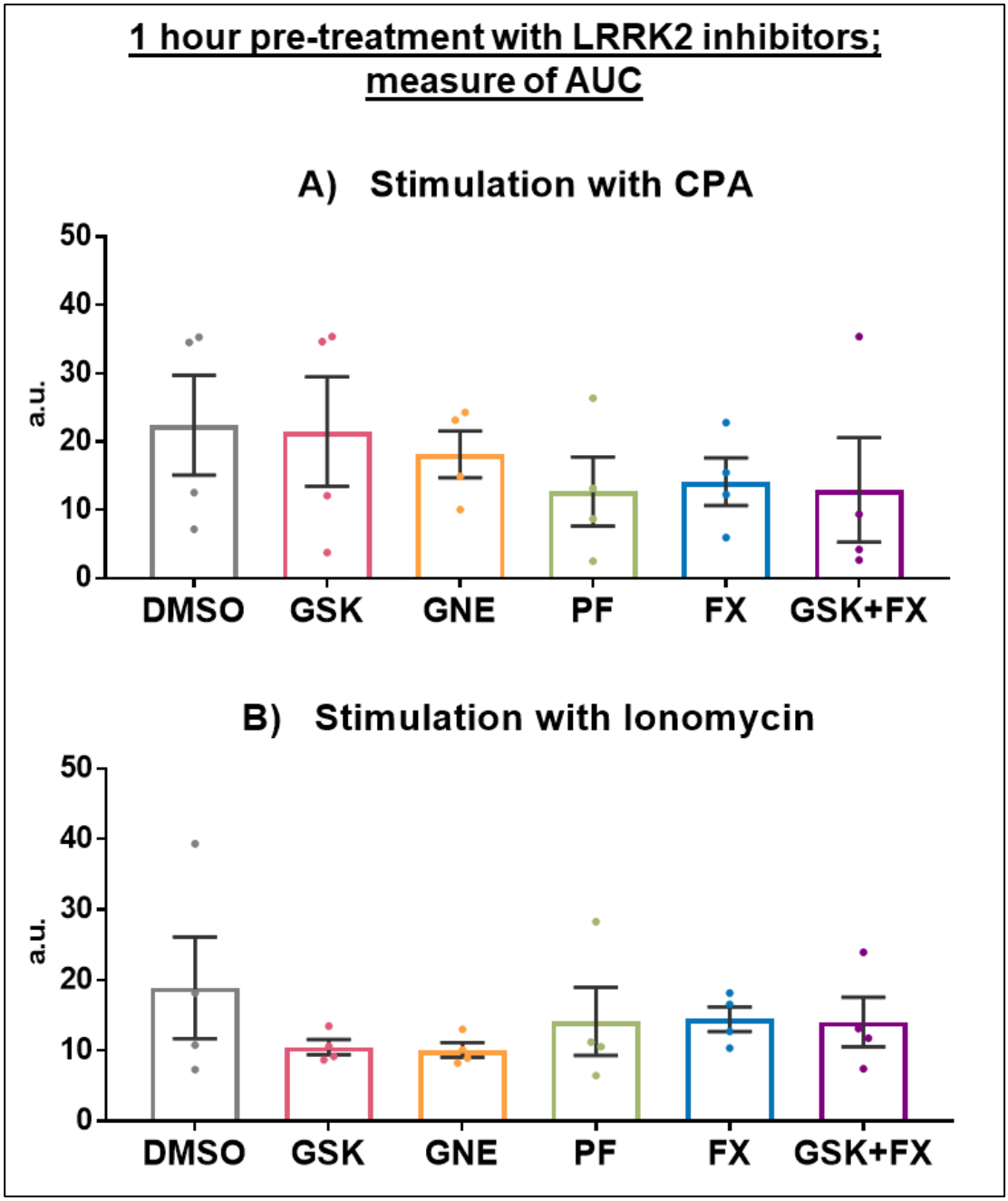

Figure 5.24: No effect of one-hour LRRK2 inhibition on CPA- or Ionomycin-evoked calcium signals.

HEK293 GFP-LC3 cells were pre-treated with various LRRK2 kinase inhibitors (GSK2578215A: GSK; GNE-9605: GNE; PF-06447475: PF; all at 1 µM) or a GTPase inhibitor (FX2149: FX, 100 nM) or DMSO (1:1000 equivalent dilution) for 1 hour, and loaded with Fura-2 AM (2 µM) in imaging buffer. Basal calcium signals were recorded for 1 minute before addition of 10 µM CPA followed by 10 µM CPA + 10 µM Ionomycin to evoke calcium signals, with 1 wash between the stimulations. The stimulations and wash were performed in calcium-free buffer. Each repeat is an average of 20 cells, and the data are mean ± SEM. n=4 repeats (1 coverslip/repeat). One-way ANOVA (with grouping by experimental repeat), Geisser-Greenhouse's correction, non-significant. (A) treatment effect: $F(2.035, 6.105)= 1.153$; $p=0.38$ (B) treatment effect: $F(1.687, 5.061)= 0.6989$; $p=0.52$.

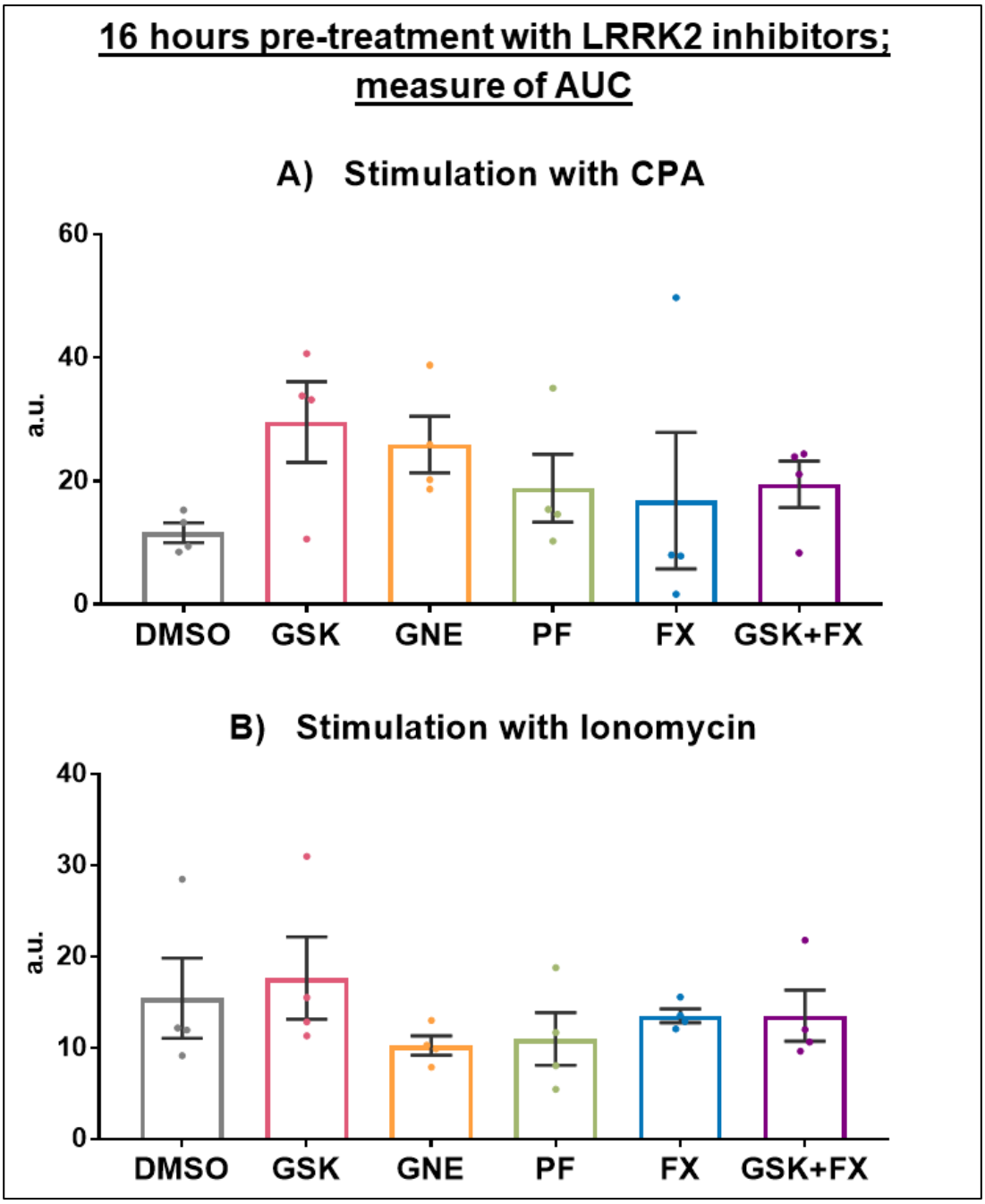

Figure 5.25: No effect of 16 hours LRRK2 inhibition on CPA- or Ionomycin-evoked calcium signals.

HEK293 GFP-LC3 cells were pre-treated with various LRRK2 kinase inhibitors (GSK2578215A: GSK; GNE-9605: GNE; PF-06447475: PF; all at 1 µM) or a GTPase inhibitor (FX2149: FX, 100 nM) for 16 hours, and loaded with Fura-2 AM (2 µM) in imaging buffer. Basal calcium signals were recorded for 1 minute before addition of 10 µM CPA followed by 10 µM CPA + 10 µM Ionomycin to evoke calcium signals, with 1 wash between the stimulations. The stimulations and wash were performed in calcium-free buffer. Each repeat is an average of 20 cells, and the data are mean ± SEM. n=4 repeats (1 coverslip/repeat). One-way ANOVA (with grouping by experimental repeat), Geisser-Greenhouse's correction, non-significant. (A) treatment effect: $F(1.939, 5.816) = 1.211$; $p=0.36$ (B) treatment effect: $F(1.346, 4.037) = 1.428$; $p=0.32$.

5.7 Effect of LRRK2 mutants on calcium release in HEK293 GFP-LC3 cells

The next step was to determine whether pathogenic and protective *LRRK2* mutations might influence ATP-evoked calcium release and calcium storage in the ER and lysosomes in HEK293 GFP-LC3 cells. To do so, the effects of *LRRK2* mutations on calcium signalling were investigated using transient overexpression of wild-type and mutant forms of LRRK2 in HEK293 GP-LC3. Cells were thus co-transfected with the combination of mApple and myc-LRRK2 plasmids (or empty vector) using the transfection conditions established in the previous Chapter (Chapter 4 Section 4.7.1).

5.7.1 LRRK2 mutants have no effect on global calcium release

Firstly, the effects of LRRK2 mutants on ATP-evoked calcium signals were explored under similar conditions to those used throughout this Chapter, monitoring calcium signals triggered twice with 10 µM ATP. (*This assay corresponds to Assay n°4 in Chapter 2 Section 2.5.3.2*)

The results are depicted in Figure 5.26 and Figure 5.27. Statistical analysis indicated that neither of the pathogenic mutant forms of LRRK2 affected the ATP-evoked calcium responses relative to wild-type LRRK2, whilst overexpression of wild-type LRRK2 also caused no significant effects relative to the empty vector control. It is worth mentioning that the protective R1398H mutant appears to display higher amplitude and AUC values than wild-type LRRK2 for both peaks (Figure 5.26 and Figure 5.27, A and B), although these also fail to reach statistical significance. Whether an effect of this mutant can be shown will require further repeats of the experiment.

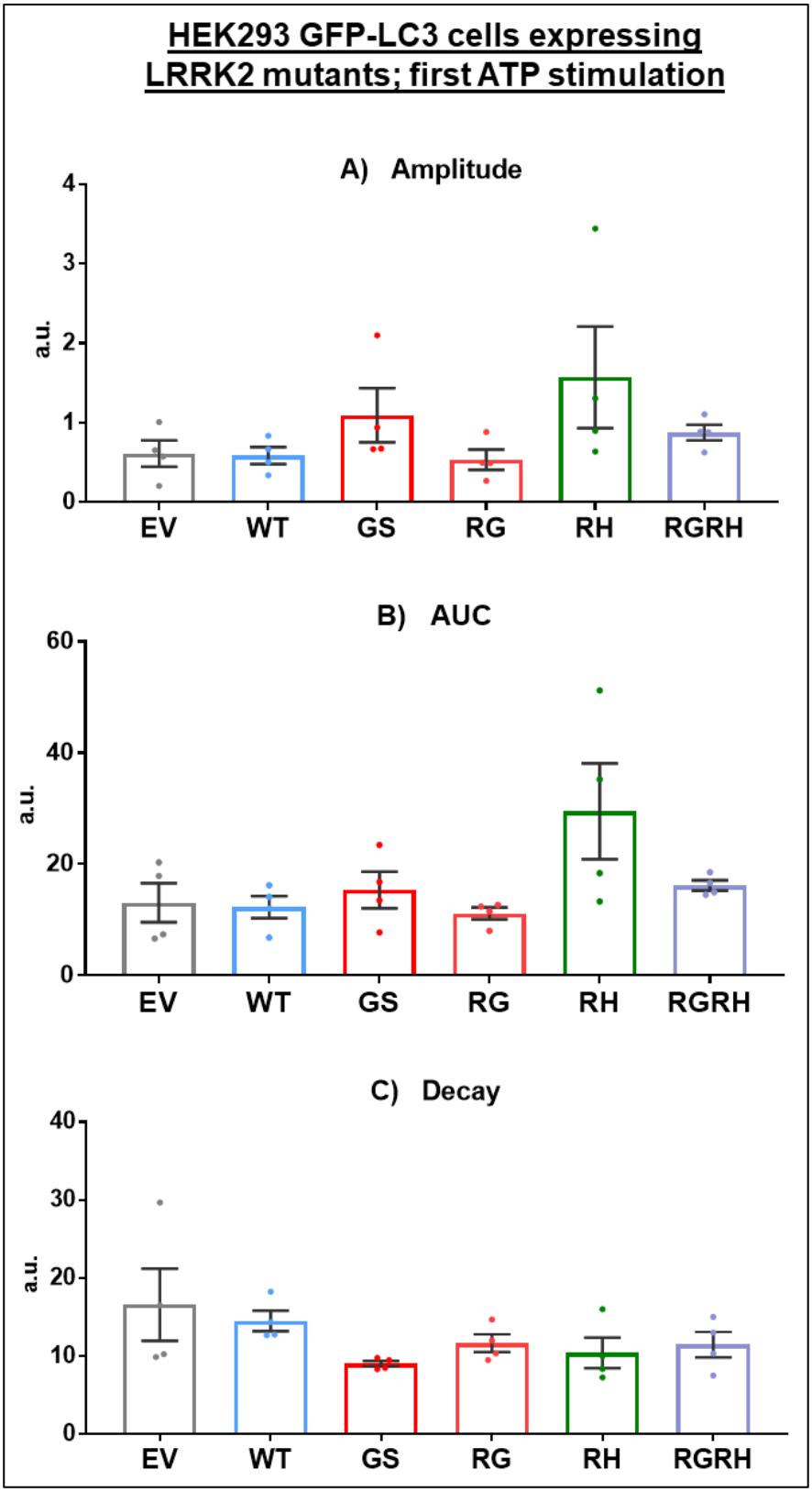

Figure 5.26: No effect of LRRK2 mutants on ATP-evoked calcium release (first stimulation).

HEK293 GFP-LC3 cells were co-transfected with the mApple plasmid and plasmids carrying wild-type LRRK2 (WT) or different forms of mutated LRRK2 (RG (pathogenic variant), RH (protective variant) or RGRH (contains both variants), GS (pathogenic variant)), and loaded with Fura-2 AM (2 µM) in imaging buffer. Basal calcium signals were recorded for 1 minute before addition of 10 µM ATP to evoke calcium signals, with 8 washes with imaging buffer and 10 minutes rest between the two stimulations. Each repeat is an average of 20 cells, and the data are mean ± SEM. n=4 repeats (1 coverslip/repeat). One-way ANOVA (with grouping by experimental repeat), Geisser-Greenhouse's correction, non-significant. (A) LRRK2 variant effect: $F(1.296, 3.887)= 1.513$; $p=0.30$ (B) LRRK2 variant effect: $F(1.559, 4.676)= 2.378$; $p=0.19$. (C) LRRK2 variant effect: $F(1.246, 3.738)= 1.456$; $p=0.31$.

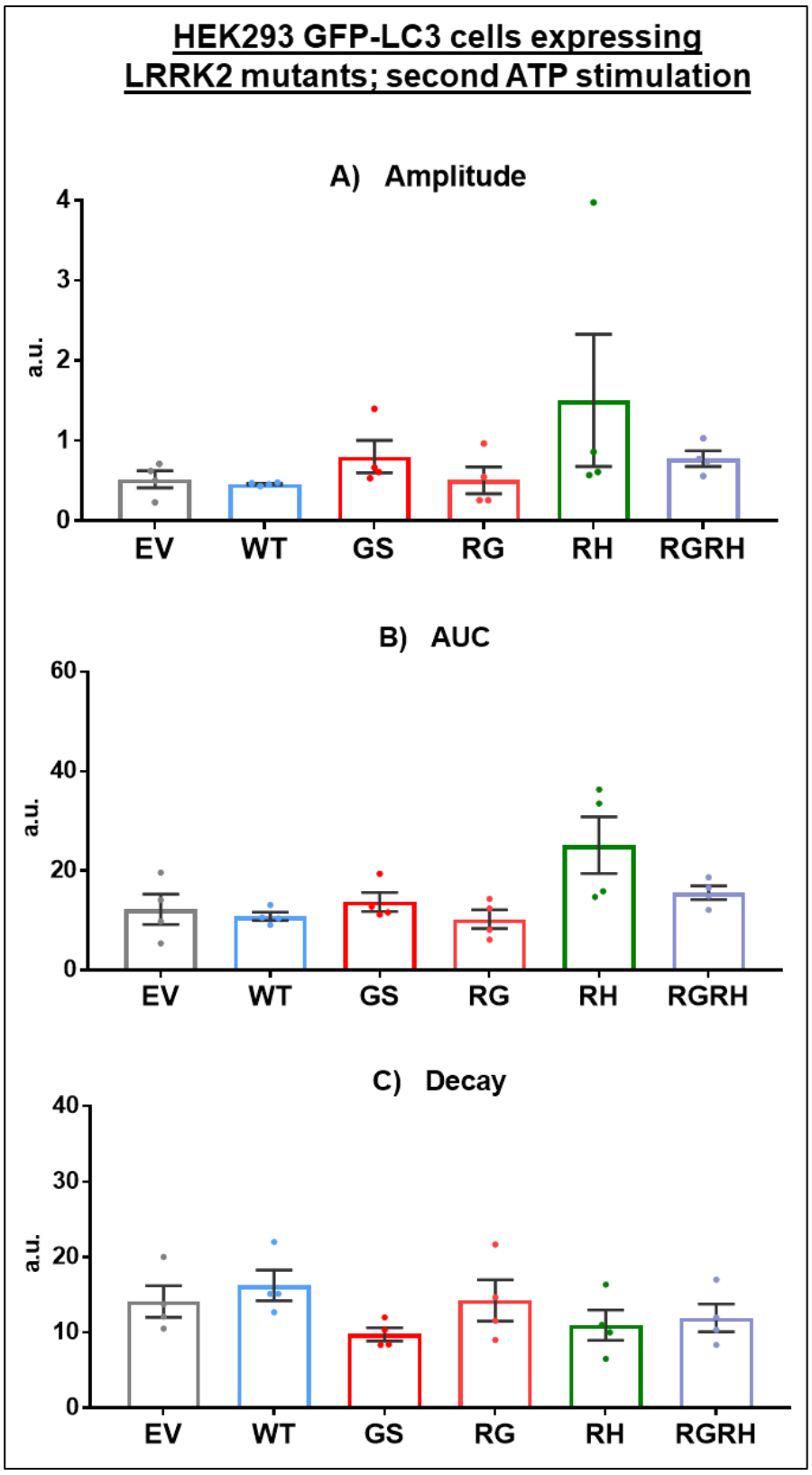

Figure 5.27: No effect of LRRK2 mutants on ATP-evoked calcium release (second stimulation).

HEK293 GFP-LC3 cells were co-transfected with the mApple plasmid and plasmids carrying wild-type LRRK2 (WT) or different forms of mutated LRRK2 (RG (pathogenic variant), RH (protective variant) or RGRH (contains both variants), GS (pathogenic variant)), and loaded with Fura-2 AM (2 µM) in imaging buffer. Basal calcium signals were recorded for 1 minute before addition of 10 µM ATP to evoke calcium signals, with 8 washes with imaging buffer and 10 minutes rest between the two stimulations. Each repeat is an average of 20 cells, and the data are mean ± SEM. n=4 repeats (1 coverslip/repeat). One-way ANOVA (with grouping by experimental repeat), Geisser-Greenhouse's correction, non-significant. (A) LRRK2 variant effect: $F(1.116, 3.348)= 1.194$; $p=0.36$ (B) LRRK2 variant effect: $F(1.704, 5.112)= 3.651$; $p=0.11$. (C) LRRK2 variant effect: $F(1.147, 3.441)= 1.421$; $p=0.32$.

5.7.2 LRRK2 mutants have no effect on lysosomal calcium storage

The effects of LRRK2 mutants on calcium signalling were further tested on CPA- and Ionomycin-evoked calcium signals in HEK293 GFP-LC3 cells, shown in Figure 5.28. (*This experiment corresponds to Assay n°5 in Chapter 2 Section 2.5.3.2*)

Similar to the findings obtained with ATP-evoked calcium signals, statistical analysis indicated that none of the mutant forms of LRRK2 affected the Ionomycin-evoked calcium responses (Figure 5.28 B) relative to wild-type LRRK2, whilst overexpression of wild-type LRRK2 also caused no significant effects relative to the empty vector control. Comparable results were found for CPA-evoked calcium responses (Figure 5.28 A).

Taken together, the data indicate that over-expression of wildtype or pathogenic or protective LRRK2 mutants in HEK293 GFP-LC3 cells either have no effect on ATP, CPA or Ionomycin-induced calcium signals, or have too small an impact to be detectable under these experimental conditions.

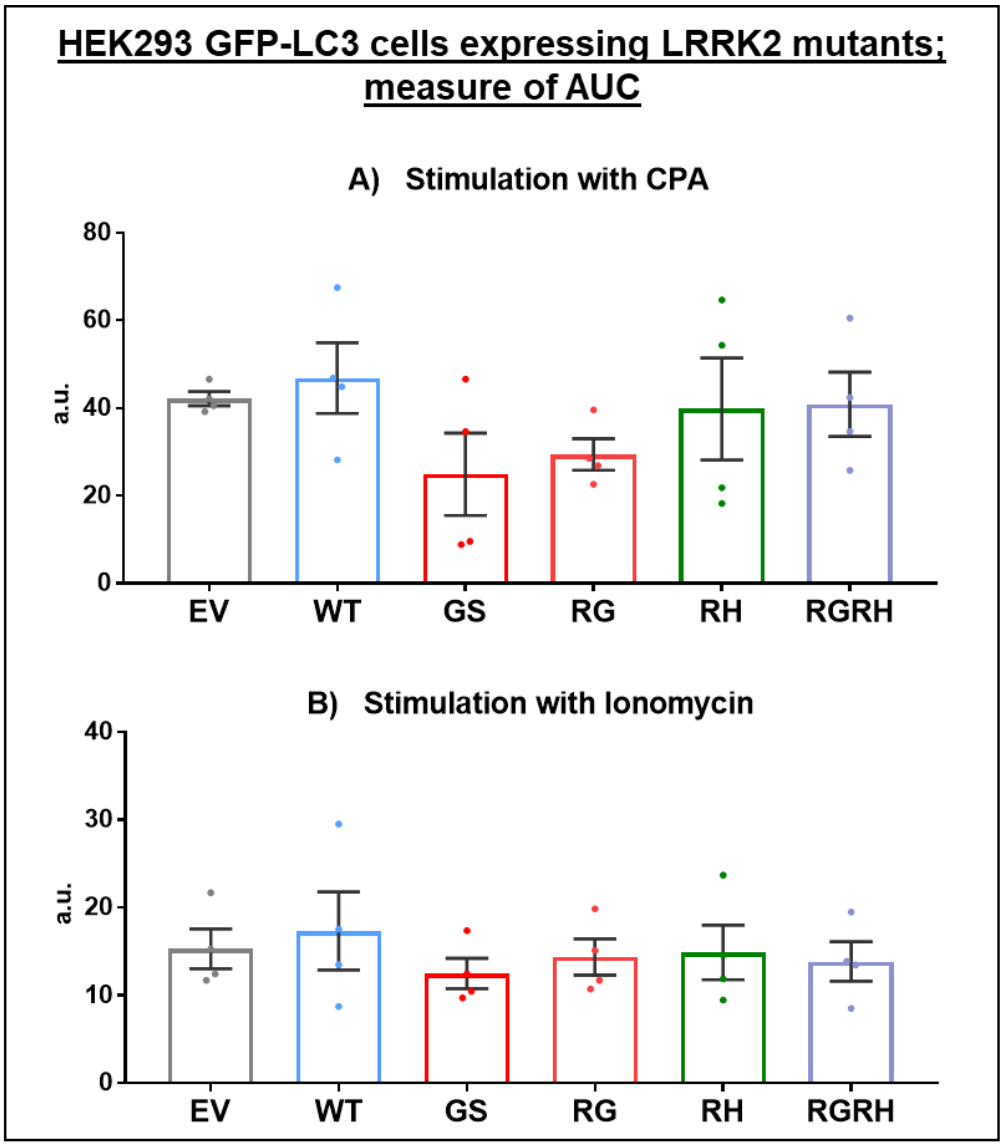

Figure 5.28: No effect of the LRRK2 mutants on CPA- or Ionomycin-evoked calcium signals.

HEK293 GFP-LC3 cells were co-transfected with the mApple plasmid and plasmids carrying wild-type LRRK2 (WT) or different forms of mutated LRRK2 (RG (pathogenic variant), RH (protective variant) or RGRH (contains both variants), GS (pathogenic variant)), and loaded with Fura-2 AM (2 µM) in imaging buffer. Basal calcium signals were recorded for 1 minute before addition of 10 µM CPA followed by 10 µM CPA + 10 µM Ionomycin to evoke calcium signals, with 1 wash between the stimulations. The stimulations and wash were performed in calcium-free buffer. Each repeat is an average of 20 cells, and the data are mean ± SEM. n=4 repeats (1 coverslip/repeat). One-way ANOVA (with grouping by experimental repeat), Geisser-Greenhouse's correction, non-significant. (A) LRRK2 variant effect: $F(2.624, 7.873)= 1.427$; $p=0.30$ (B) LRRK2 variant effect: $F(2.524, 7.571)= 0.5555$; $p=0.63$.

5.8 Exploring the effects of BAPTA and calcium indicators on autophagy and calcium signals in HEK293 GFP-LC3 cells

The data presented so far in this Chapter provide more-convincing evidence of a role for LRRK2 in calcium signalling in macrophages than in HEK293 GFP-LC3 cells. However, it should be noted that an equivalent experiment to those that yielded the strongest data – experiments studying the effects of LRRK2 knockout on ATP-evoked calcium signalling – have not been performed in HEK293 GFP-LC3 cells. This potential cell type specificity is especially interesting in the context of the data presented in the previous Chapter, which found strong evidence of a role for LRRK2 in autophagy in HEK293 GFP-LC3 cells, but not in macrophages. If true, these observations would suggest that the effect of LRRK2 inhibition on PP242-induced autophagy in HEK293 GFP-LC3 cells is unlikely to be mediated by alterations in calcium signalling. In principle, it would be useful to conclude the work in this thesis by formally testing the non-involvement of calcium signalling on the effects of LRRK2 inhibition on PP242-induced autophagy. However, several important factors make studies assessing calcium signals concomitantly with using LRRK2 inhibitors and autophagy modulators technically challenging.

For example, it has been shown that 3-methyladenine (3-MA), a commonly used compound that blocks autophagy, did not prevent LRRK2-activated autophagy[141,449,479]. In addition, BafA1, which blocks autophagy by preventing the acidification of lysosomes and inhibiting the degradation stages, has been shown to also inhibit the SERCA calcium pumps[449] localised on intracellular membranes. As such, BafA1 impairs both lysosomal function and calcium signalling.

Perhaps more problematic, most studies reporting an involvement of calcium in autophagy are dependent on the use of the high-affinity calcium chelator BAPTA to buffer intracellular calcium[433,435,449], but recent findings have shown that BAPTA has significant off-target effects independently of calcium[433]. In particular, BAPTA and several calcium indicators have been found to inhibit the cellular enzyme Na^+,K^+/ATPase, which is involved in numerous processes including the regulation of calcium signalling[433,689]. Importantly, many commonly used calcium indicators dyes (including Fura-2) are also structurally related to BAPTA, so these compounds may also alter the state of the cell by inhibiting the

Na^+,K^+/ATPase[433,689].

Since BAPTA and structural analogues of BAPTA have not been tested side-by-side for off-target effects on autophagy, it was considered useful for the wider scientific community to conclude this study by formally examining this. Two BAPTA analogues, di-bromo-BAPTA and di-fluoro-BAPTA, that do not buffer calcium to the same extent as BAPTA (BAPTA: Kd = 160 nM, di-bromo-BAPTA: Kd = 1.6 µM, di-fluoro-BAPTA: Kd = 65 µM) were thus used as complementary controls. Since these calcium chelators have a lower affinity for calcium, they should not phenocopy the effects of BAPTA in inhibiting processes that are genuinely calcium-dependent, but can be expected to behave similarly if the effect of BAPTA does not involve calcium chelation[433].

5.8.1 Effects of BAPTA and BAPTA analogues on autophagy and calcium signalling in HEK293 GFP-LC3 cells

First, additional experiments were performed in HEK293 GFP-LC3 cells to determine the effects of BAPTA and its two analogues on autophagy (quantification of GFP-LC3 punctae) and on calcium signalling (ATP-evoked calcium signals). The goal was to determine whether the BAPTA analogues exert a similar effect to BAPTA on autophagy while buffering calcium to a smaller extent to BAPTA. The analogues di-bromo-BAPTA-AM and di-fluoro-BAPTA-AM are referred to as BAPTA-DB and BAPTA-FF respectively in the figures of this section.

5.8.1.1 Treatment with BAPTA or BAPTA analogues blocks the PP242-mediated induction of autophagy in HEK293 GFP-LC3 cells

For consistency with the autophagy assays described in Chapter 4, the effects of BAPTA and its analogues on autophagy were investigated using the quantification of GFP-LC3 punctae in HEK293 GFP-LC3 cells under conditions where the numbers of autophagic vesicles are elevated, i.e., following a one-hour induction of autophagy with PP242 treatment (at 2 µM). Prior to PP242 treatment, cells were pre-treated for 1 hour with BAPTA (10 µM), di-bromo-BAPTA (10 µM), di-fluoro-BAPTA (10 µM), 3-MA (5 mM) or

DMSO (1:1000 equivalent dilution), where 3-MA was used as a positive control for the inhibition of autophagy. (*This assay corresponds to Protocol G in Chapter 2 Section 2.6.1*). The results are shown in Figure 5.29.

As expected, one-hour treatment with PP242 induced a significant increase in the number of GFP-LC3 punctae compared to DMSO-treated cells (Figure 5.29). However, all the conditions tested (pre-treatment with BAPTA, di-bromo-BAPTA or di-fluoro-BAPTA) abolished the PP242-induced induction of autophagy to a similar extent as 3-MA. These results show that treatment with both high-affinity (BAPTA) and low-affinity calcium buffers (di-bromo-BAPTA and di-fluoro-BAPTA) were sufficient to block the induction of autophagy. Thus, these BAPTA analogues phenocopy the effect of BAPTA, which is consistent with BAPTA inhibiting autophagy independently of calcium chelation.

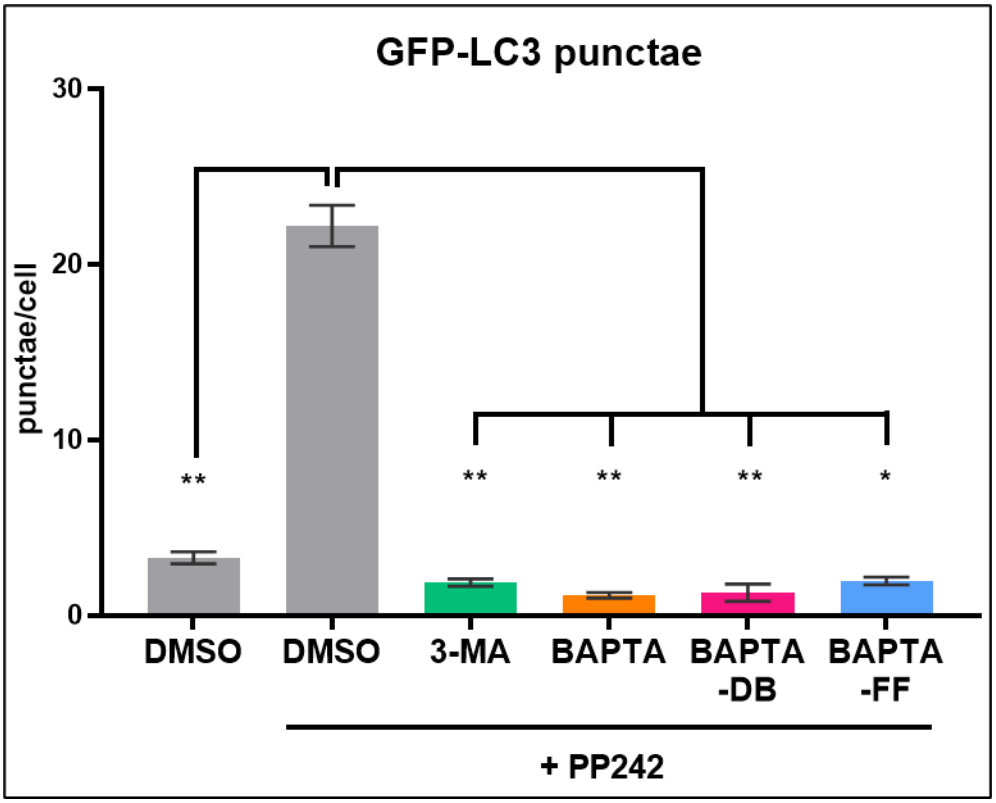

Figure 5.29: Di-bromo-BAPTA and di-fluoro-BAPTA abolish the PP242-induced increase of GFP-LC3 punctae to a similar extent as BAPTA and 3-MA.

HEK293 GFP-LC3 cells were pre-treated with various compounds (3-MA 5 mM, BAPTA 10 µM, di-bromo-BAPTA: BAPTA-DB 10 µM, di-fluoro-BAPTA: BAPTA-FF 10 µM) or DMSO (1:1000 equivalent dilution) for 1 hour then stimulated with PP242 (2 µM) for 1 hour. For each condition the mean number (± SEM) of GFP-LC3 punctae was calculated, using 30 cells per condition. n=3 repeats (1 coverslip/repeat). One-way ANOVA (with grouping by experimental repeat), Geisser-Greenhouse's correction, Dunnett post-hoc test with comparison to DMSO+PP242. Treatment effect: $F(1.241, 2.483) = 230.4$; $p=0.0016$. On graphs: $p<0.01$ (**), $p<0.05$ (*).

5.8.1.2 Treatment with BAPTA analogues does not abolish calcium signals in HEK293 GFP-LC3 cells

An additional calcium assay was carried out to confirm that the three BAPTA compounds were affecting calcium signalling as expected under the conditions used in the previous GFP-LC3 assay. To do so, ATP-evoked calcium signals were analysed in HEK293 GFP-LC3 cells pre-treated for 1 hour with PP242 at 2 µM or one of the three calcium chelators (BAPTA, di-bromo-BAPTA or di-fluoro-BAPTA) at 10 µM. Here, PP242 treatment was included as a control, to verify that this compound does not affect calcium signalling. (*This assay corresponds to Protocol H in Chapter 2 Section 2.6.2*). Cells were only stimulated once with ATP (10 µM), and the results are depicted in Figure 5.30.

Induction of autophagy with PP242 treatment did not induce significant changes in the calcium response compared to DMSO-treated cells. Also as expected, pre-treatment with BAPTA at a concentration of 10 µM abolished the ATP-evoked calcium response (Figure 5.30 A and B), whilst pre-treatment with 10 µM di-fluoro-BAPTA had no significant effect. Maybe consistent with its intermediate Kd, pre-treatment with 10 µM di-bromo-BAPTA produced a partial effect, markedly reducing the amplitude of the calcium response compared to DMSO-treated cells (Figure 5.30 A), but not affecting the AUC.

As such, these data indicate that the relative effects of BAPTA, di-bromo-BAPTA and di-fluoro-BAPTA on autophagy do not correlate with their effects on calcium signalling, which is consistent with all three compounds inhibiting autophagy independently of calcium chelation.

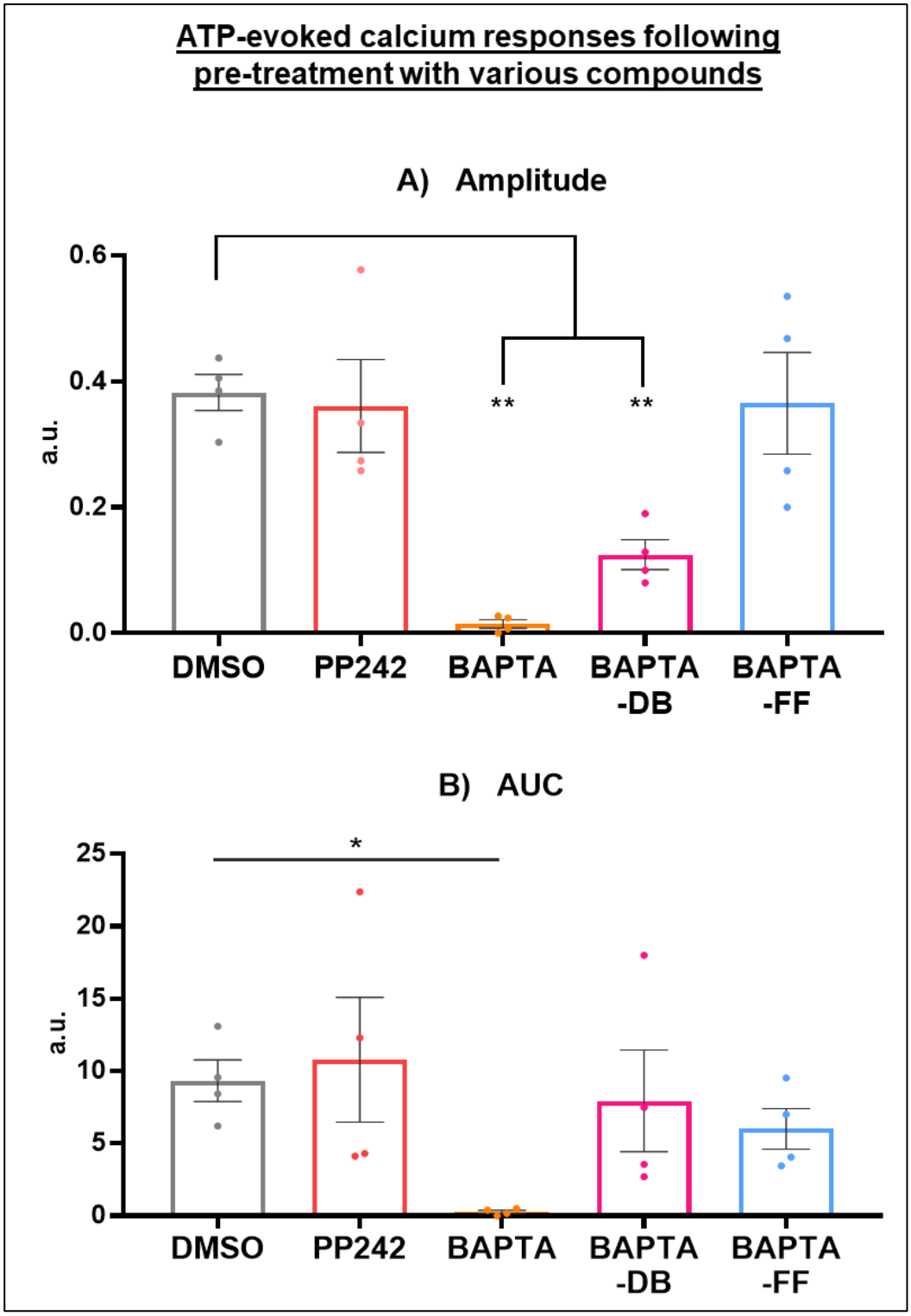

Figure 5.30: The low-affinity BAPTA analogues do not completely block calcium signals in HEK293 GFP-LC3 cells

HEK293 GFP-LC3 cells were pre-treated with various compounds (2 µM PP242, 10 µM BAPTA, 10 µM di-bromo-BAPTA: BAPTA-DB, 10 µM di-fluoro-BAPTA: BAPTA-FF) or DMSO (1:1000 equivalent dilution) for 1 hour then loaded with Fura-2 AM (2 µM) in imaging buffer. Basal calcium signals were recorded for 1 minute before addition of agonist ATP (10 µM) to evoke calcium signals. Each repeat is an average of 25 cells, and the data are mean ± SEM. n=4 repeats (1 coverslip/repeat). One-way ANOVA (with grouping by experimental repeat), Geisser-Greenhouse's correction, Dunnett post-hoc test with comparison to DMSO. (A) treatment effect: $F(1.609, 4.826)= 20.02$; $p=0.0053$ (B) treatment effect: $F(1.174, 3.522)= 4.337$; $p=0.12$. On graphs: $p<0.01$ (**), $p<0.05$ (*).

5.8.2 Effects of calcium indicators on autophagy

Given that BAPTA and two BAPTA analogues were shown to block the induction of autophagy, it is worth exploring whether calcium indicators, which possess a similar chemical structure to BAPTA, can also affect this process. Indeed, in assays studying both autophagy and calcium signalling, any off-target effect of calcium indicators on autophagy would be an important issue. Thus, to complete this investigation on the effects of BAPTA and BAPTA-related compounds on autophagy, an experiment was performed to evaluate the effects of calcium indicators on autophagy in HEK293 GFP-LC3 cells. This experiment was carried out under conditions where autophagy was stimulated, i.e., following a one-hour induction of autophagy with PP242 treatment (at 2 μM), and GFP-LC3 punctae were quantified. (*This assay corresponds to Protocol I in Chapter 2 Section 2.6.3*)

Two calcium indicators were tested: Fura-2 which has been used throughout this Chapter, and Cal-590. Cal-590 has a different spectral wavelength to Fura-2 (excitation: 574 nm/red emission: 588 nm), which allows this compound to be imaged simultaneously with GFP in combined GFP-LC3 and calcium assays. Furthermore, Fura-2 and Cal-590 were used at two different concentrations and durations of treatment. These compounds were either loaded in cells at 2 μM for 30 minutes, which corresponds to their normal loading conditions, or at 10 μM for 1 hour, which matches the loading conditions used for the BAPTA treatment of 1 hour at 10 μM.

Consistent with the results depicted in Figure 5.29, PP242 treatment induced a significant increase in GFP-LC3 punctae compared to DMSO control cells, while BAPTA significantly suppressed this increase (Figure 5.31). Surprisingly, incubation with either Fura-2 or Cal-590 also reduced the PP242-induced increase in GFP-LC3 punctae, at both loading conditions tested. However, although the overall mean number of GFP-LC3 punctae associated with the normal loading conditions for Fura-2 is noticeably lower than the DMSO control, the post-hoc pairwise comparison only approached statistical significance (Dunnett's test, $p=0.08$), while all the other comparisons were significant.

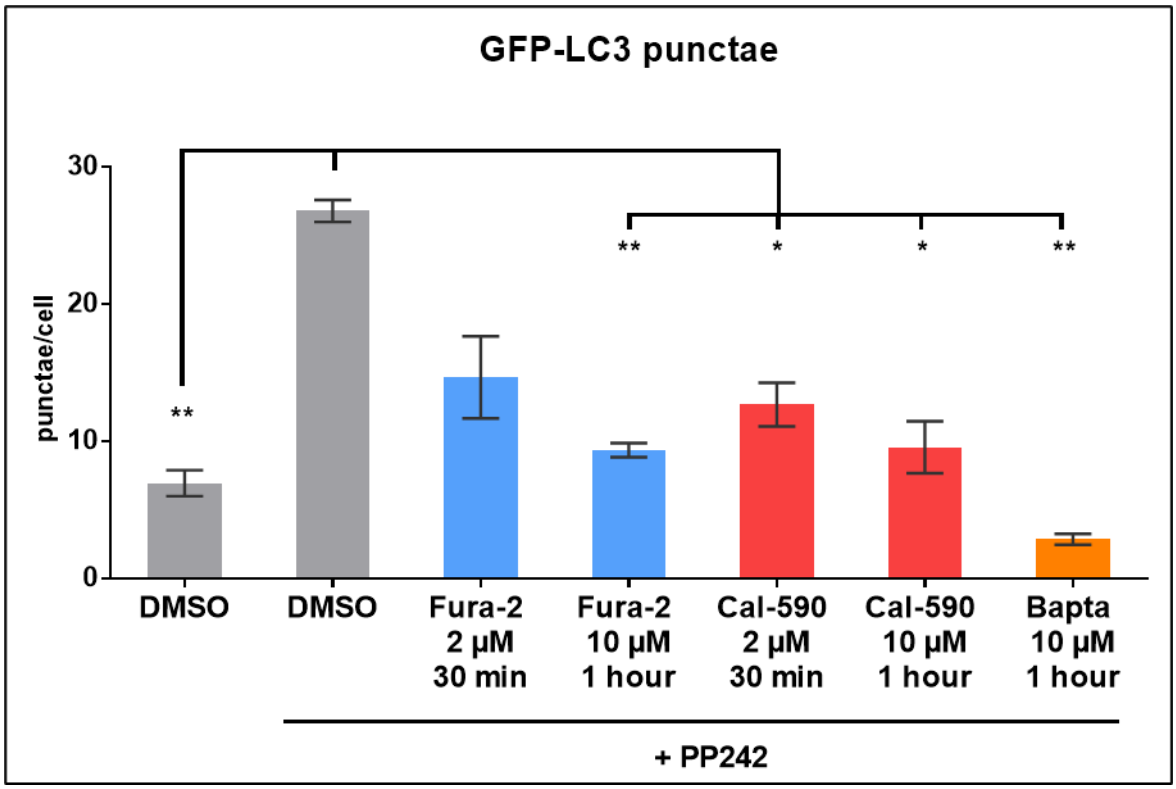

Figure 5.31: Fura-2 and Cal-590 decrease the PP242-induced autophagy.

HEK293 GFP-LC3 cells were pre-treated with various compounds (DMSO + 20% (w/v) PA at 1 µl/ml, Fura-2 at 2 or 10 µM, Cal-590 at 2 or 10 µM, BAPTA 10 µM) for 30 minutes or 1 hour, then stimulated with PP242 (2 µM) for 1 hour. For each condition, the mean number (± SEM) of GFP-LC3 punctae was calculated, using 30 cells per condition. n=3 repeats (1 coverslip/repeat). One-way ANOVA (with grouping by experimental repeat), Geisser-Greenhouse's correction, Dunnett post-hoc with comparison to DMSO+PP242. Treatment effect: $F(1.199, 2.398)= 56.14$; $p=0.01$. On graph: $p<0.01$ (**), $p<0.05$ (*).

Taken together, both BAPTA analogues and calcium indicators that have a chemical structure related to BAPTA, display a similar effect to BAPTA on autophagy, i.e., repressing the induction of this process. Thus, the data suggest that this repression might occur via a mechanism independent of calcium, and implicate the chemical structure shared by these compounds in their off-target effect on autophagy.

5.9 Summary of results

The work described in this chapter investigated the function of LRRK2 in calcium signalling using LRRK2 kinase and GTPase inhibitors in HEK293 GFP-LC3 cells and RAW264.7 macrophages; the overexpression of LRRK2 mutants in HEK293 GFP-LC3 cells; and comparisons between wild-type RAW264.7 and Lrrk2 KO macrophages. Calcium signals were triggered in response to agonist stimulation, i.e., ATP for global calcium, CPA and ionomycin to target lysosomal calcium. In addition, the effects of two BAPTA analogues and two calcium indicators on autophagy and calcium signals were tested in HEK293 GFP-LC3 cells. The findings are summarised in Table 5.1 and Table 5.2, and are discussed in the next Sections.

Table 5.1: Summary of the results from the LRRK2-related calcium assays described in this Chapter.

↑: increase; ↓: decrease; ns: no significant effect; (?): possible trends/patterns in the data. Statistically significant results are indicated in bold font.

Parameter:	**Spontaneous activity in RAW264.7 macrophages**	
WT vs KO	ns	Figure 5.4
LRRK2 inhibitors 1 hour	ns	Figure 5.9

Stimulation:	**ATP**			**CPA**	**Ionomycin**
Parameter:	**Amplitude**	**AUC**	**Decay**	**AUC**	**AUC**
RAW264.7 macrophages					
WT vs KO	**↑ in Lrrk2 KO** Figure 5.5 A / Figure 5.7 A	**↑ in Lrrk2 KO** Figure 5.7 B	**↓ in Lrrk2 KO** Figure 5.5 C	ns Figure 5.19 A	ns Figure 5.19 B
LRRK2 inhibitors 16 hours	ns	ns	ns	ns	ns
	Figure 5.12 and Figure 5.13			Figure 5.21 A	Figure 5.21 B
LRRK2 inhibitors 1 hour	ns	ns (↑ with kinase inhibitors after 2nd stimulation in WT?)	ns (↑ with kinase inhibitors after 2nd stimulation in WT?)	ns	ns
	Figure 5.10 and Figure 5.11			Figure 5.20 A	Figure 5.20 B
HEK293 GFP-LC3 cells					
LRRK2 inhibitors 16 hours	ns	ns	ns	ns (↑ with kinase inhibitors?)	ns
	Figure 5.16 and Figure 5.17			Figure 5.25 A	Figure 5.25 B
LRRK2 inhibitors 1 hour	ns	**↑ with GSK2578215A** (↑ with kinase inhibitors?)	ns	ns	ns
	Figure 5.14 and Figure 5.15			Figure 5.24 A	Figure 5.24 B
Pathogenic LRRK2 mutants vs WT LRRK2	ns	ns	ns	ns	ns
	Figure 5.26 and Figure 5.27			Figure 5.28 A	Figure 5.28 B
R398H variant vs WT LRRK2	ns (↑?)	ns (↑?)	ns	ns	ns
	Figure 5.26 and Figure 5.27			Figure 5.28 A	Figure 5.28 B

Table 5.2: Summary of the BAPTA-related results presented in this Chapter.

↓: decrease; ↓↓: abolish; ns: no significant effect. Statistically significant results are indicated in bold font.

HEK293 GFP-LC3 cells	**Autophagy assay - GFP-LC3 punctae**
BAPTA vs PP242	↓↓ Figure 5.29
di-bromo-BAPTA and di-fluoro-BAPTA vs PP242	↓↓ Figure 5.29
Calcium indicators vs PP242	↓ Figure 5.31

HEK293 GFP-LC3 cells	**Calcium assay – ATP response**	
Parameter:	**AUC**	**Amplitude**
BAPTA vs DMSO	↓↓ Figure 5.30	↓↓
di-bromo-BAPTA vs DMSO	ns Figure 5.30	↓
di-fluoro-BAPTA vs DMSO	ns Figure 5.30	ns

5.10 Discussion

5.10.1 RAW264.7 macrophages

5.10.1.1 Global calcium signals

Although loss of Lrrk2 had no effect on spontaneous calcium activity (Figure 5.1 B), Lrrk2 KO macrophages displayed a significantly faster increase in cytosolic calcium concentration following ATP stimulation (amplitude; Figure 5.5 A, Figure 5.7 A). Other less reproducible data indicated that these responses to ATP were also larger (AUC; Figure 5.7 B) and were accompanied with a faster cytosolic calcium clearance (decay; Figure 5.5 C). Potentially, a larger amount of calcium ions initially stored in the ER of Lrrk2 KO macrophages compared to WT macrophages could have caused these ATP-induced responses to be larger. However, the CPA data (Figure 5.19 A) indicated that this was not the case, which suggest that there is an actual effect observed in these ATP data. As such, since stimulation with ATP leads to the IP_3-R-mediated release of calcium by the ER, these results support a role for Lrrk2 regulating the size, speed and duration of cytosolic calcium levels dependent on IP_3-R in WT RAW264.7 macrophages.

Importantly, loss of Lrrk2 function via enzymatic inhibition had no consistent significant effects on ATP-evoked calcium release under similar conditions (one-hour inhibition: Figure 5.10 and Figure 5.11; 16 hours inhibition: Figure 5.12 and Figure 5.13). However, there may be some interesting underlying patterns in the Lrrk2 inhibitors data from WT (but not Lrrk2 KO) macrophages (Table 5.1). In particular, the tendency towards increased second peak AUC values following one-hour Lrrk2 inhibition (Figure 5.11 B) is potentially consistent with KO data, and also appears to mirror patterns seen in equivalent HEK293 GFP-LC3 cell experiments (Peak 1, Figure 5.14 B and Peak 2, Figure 5.15 B). But in any case, irrespective of whether these patterns turn out to be true, the comparison between effects of Lrrk2 knockout and Lrrk2 enzymatic inhibition certainly suggests a greater importance for Lrrk2 protein than Lrrk2 kinase or GTPase activities in ATP-evoked calcium signalling in macrophages.

As such, Lrrk2 may exert its function in the regulation of ER-mediated calcium release through its scaffolding ability. In principle, this could be via protein-protein interactions with any of a number of proteins involved in ER calcium release, including the IP_3-R itself. Possibly consistent with a role as a regulatory scaffolding but not kinase or GTPase role, Lrrk2 inhibition also had no effect on calcium released from ER stores following stimulation with the SERCA pump inhibitor CPA (Figure 5.20 A and Figure 5.21 A).

5.10.1.2 Lysosomal calcium signals

In regards to lysosomal calcium signals, neither loss of Lrrk2 (Figure 5.19 B), nor inhibition of Lrrk2 enzymatic activities (Figure 5.20 B and Figure 5.21 B) elicited changes in Ionomycin-induced calcium responses in RAW264.7 macrophages. These results revealed that Lrrk2 enzymatic activities are unlikely to be involved in the regulation of lysosomal calcium concentration in this cell line. However, given the mode of action of Ionomycin (i.e., passive transfer of calcium ions across the lysosomal membrane), these data do not exclude a role for Lrrk2 in the active release of calcium from this organelle, for example via TPC2. This observation is particularly interesting, since TPC2 has been reported to be a LRRK2 target[479]. As such, future work might focus on determining whether LRRK2 regulates lysosomal calcium release via TPC2, and whether these calcium signals are involved in LRRK2-mediated regulation of autophagy through the CaMKKβ/AMPK pathway, as suggested by the work of Gómez-Suaga and colleagues[479].

5.10.2 HEK293 GFP-LC3 cells

5.10.2.1 LRRK2 inhibitors

In this study, LRRK2 inhibition in HEK293 GFP-LC3 cells only had one statistically significant effect on the calcium responses triggered with ATP: an increased AUC for the second ATP stimulation following acute inhibition with GSK2578215A (Figure 5.15 B). At face value, this result suggests that LRRK2 kinase activity

is involved in the regulation of ER-mediated calcium release in this cell line. As noted, a consistent underlying tendency may be present for the other inhibitors (Figure 5.14 and Figure 5.15, B and C), and a similar qualitative pattern appears to be present in the equivalent WT RAW264.7 macrophage (but not Lrrk2 KO) data (Figure 5.11 B and C). While these non-significant observations give some confidence, further repeats will be necessary to determine if the tendency is robust. Furthermore, if the effect does turn out to be unique to a single inhibitor, then the most likely interpretation would be that this is an off-target effect of GSK2578215A. As such, great caution should be taken in the interpretation of this result.

Similar to the results obtained in macrophages, LRRK2 inhibition had no effect on the CPA- or Ionomycin-evoked calcium responses in HEK293 GFP-LC3 cells (Figure 5.24 and Figure 5.25). As mentioned, an underlying tendency may be present in the CPA data following 16 hours inhibition with each of the three kinase inhibitors (Figure 5.25 A), further supporting a role for LRRK2 kinase activity in ER calcium storage, although additional repeats will be necessary to determine if this finding is robust. Nevertheless, these results indicate that LRRK2 enzymatic activities are unlikely to be involved in the regulation of lysosomal calcium concentration in HEK293 GFP-LC3 cells.

5.10.2.2 LRRK2 mutants

Here, neither the overexpression of wildtype or pathogenic mutant forms of LRRK2 had any significant effects on the calcium responses evoked by ATP (Figure 5.26 and Figure 5.27), CPA (Figure 5.28 A) or Ionomycin (Figure 5.28 B). However, the protective R1398H mutant generated data suggestive of an increased size and rate of calcium release following ATP stimulation (both peaks), and encouragingly this tendency is not present with the R1441G/R1398H double mutant (Figure 5.26 and Figure 5.27). More repeats, as well as a statistically significant difference between R1398H and WT, are needed before this observation can be considered a robust effect

The lack of effect of pathogenic mutants is mostly inconsistent with the literature, which would predict impaired ER calcium signalling in presence of the pathogenic LRRK2 mutants[587–590], and studies have

shown lysosomal calcium deregulations associated with overexpression of wild-type LRRK2 and pathogenic LRRK2 G2019S[175,216], in particular larger lysosomal calcium release[216,479]. In addition, overexpression of the pathogenic LRRK2 R1441C mutant (similar to R1441G) has been shown to induce a decrease in lysosomal calcium release that is secondary to an increase in lysosomal pH[391]. As such, the link between LRRK2 and calcium signalling reported in the literature[175,218,479] was not reproduced in the two cell types (HEK293 GFP-LC3 cells and RAW264.7 macrophages) used in this study.

Nevertheless, the absence of effects of the LRRK2 mutants is in agreement with the calcium data obtained using LRRK2 inhibitors presented in this study. Although it is possible that technical limitations prevented more subtle effects from being detected, the data described in this Chapter point towards pathogenic LRRK2 mutants having no effect on calcium signalling in this cell line.

Interestingly however, it has been shown that LRRK2 participates in the maintenance of lysosomal homeostasis in RAW264.7 macrophages and HEK293 cells, especially in conditions of stressed lysosomes[218]. In addition, LRRK2 is involved in the regulation of lysosomal acidification[175], likely via the v-H^+-ATPase pump[391]. Importantly, lysosomal pH controls lysosomal calcium content, as well as lysosomal calcium-dependent fusion events in the autophagic pathway. With this in mind, a role for mutated LRRK2 in lysosomal calcium homeostasis via maintenance of lysosomal pH cannot be excluded, and will be important to further investigate in the future.

As a closing remark on the LRRK2 calcium signalling data, it is fascinating to speculate that there may be a consistent pattern across the different loss of LRRK2 function ATP-evoked calcium signalling experiments performed in this study, including Lrrk2 knockout in RAW264.7 macrophages, LRRK2 enzymatic inhibition in both HEK293 GFP-LC3 cells and RAW264.7 macrophages, and the expression of the R1398H variant in HEK293 GFP-LC3 cells. In all of these experiments, AUC values were either unchanged or displayed a tendency to increase, but never to decrease (Table 5.1, Figure 5.5, Figure 5.7, Figure 5.10, Figure 5.11, Figure 5.14, Figure 5.15, Figure 5.26 and Figure 5.27). Although it must be stressed that this general tendency is only speculative, it is nonetheless intriguing, and merits further

exploration to understand the role of LRRK2 in the regulation of ER calcium storage and release in these cell lines.

5.10.3 Perspectives on the measurement of calcium signals

Acidic calcium stores not only refer to lysosomes, but also to lysosome-related organelles and other acidic compartments. In fact, the Golgi apparatus is an acidic store. As a result, it is possible that calcium released from these compartments interferes with the lysosomal signals monitored in this study. Although NAADP could have been used to stimulate calcium release from the lysosomes, NAADP target receptors can be located elsewhere other than the lysosomes, for example on endosomes[690]. In addition, NAADP can induce the release of H^+ into the cytosol, which could be mistaken for a calcium signal[414]. Alternatively, another calcium indicator, Fura-Dextran, which is able to enter the lysosomes following a pulse/chase, could have been used. Fura-Dextran can detect lysosomal calcium changes, but requires that the lysosomal pH is maintained constant[414], which can constitute a drawback. Another control that could have been performed to ensure that the Ionomycin-evoked calcium signals were lysosomal was to use Antimycin and Oligomycin, mitochondrial depolarising agents that would empty the mitochondrial calcium store, or to use Rhod2, which is a mitochondrial calcium indicator that would allow the visualisation of potential mitochondrial calcium signals.

Of note, it is possible that a more sensitive approach will be necessary to see small variations that cannot be observed in the conditions and set-up used in this study. Furthermore, it could be challenging to compare the cell lines used, since their inherent function and the role of LRRK2 might be different and have an impact on the results. For example, the HEK293 GFP-LC3 cells did not display any spontaneous activity in this study.

5.10.4 BAPTA and calcium indicators

Additional autophagy and calcium assays were performed in this study to assess the effects on autophagy and calcium signalling of BAPTA, two BAPTA analogues (di-bromo-BAPTA and di-fluoro-BAPTA), and two calcium indicators with structures related to BAPTA (Fura-2 and Cal-590). These experiments provided very interesting data. The results showed that pre-treatment with 10 µM BAPTA is sufficient to abolish both the PP242-induced induction of autophagy (Figure 5.29) and the ATP-induced calcium response (Figure 5.30). This is consistent with the effects of this calcium chelator reported in the literature[435]. In contrast, pre-treatment with the BAPTA analogues had only a partial effect (di-bromo-BAPTA) or no effect (di-fluoro-BAPTA) on the ATP-induced calcium response (Figure 5.30), but these analogues blocked autophagy similarly to BAPTA when used at the same concentrations (Figure 5.29).

As such, these results imply that the common repressing effect of these three compounds on autophagy was unlikely to occur through calcium chelation, but likely via a mechanism that is calcium-independent, and strongly support a potential involvement of the chemical structure shared by these compounds. This hypothesis is supported by the fact that these anti-autophagic effects were mirrored, although to a smaller extent, by the two calcium indicators, which share part of their structure with BAPTA (Figure 5.31). As mentioned, inhibition of Na^+,K^+/ATPase has been reported as a calcium-independent target of BAPTA[433,689], and it would undoubtedly be interesting to test this possibility in our system.

In any case, the data presented in Figure 5.29, Figure 5.30 and Figure 5.31 not only indicate that BAPTA is an inappropriate tool to investigate the role of calcium signals in the autophagic pathway, but also draw into question its standard use as a calcium buffering agent due to off-target effects on cellular physiology[433,689]. As a minimum, low-affinity BAPTA analogues like di-bromo-BAPTA and di-fluoro-BAPTA must be used alongside BAPTA as additional controls to monitor for calcium-independent effects, since these compounds can be expected to have similar off-target effects[433,689]. But in any case, further work is undoubtedly required to establish better tools to study calcium signalling.

Although potential off-target effects always need to be assessed, alternative methods could be used instead of BAPTA to study the involvement of calcium signalling in cellular processes. In the case where a specific calcium process is targeted, pharmacological reagents have proven efficient to explore mitochondrial calcium entry or IP_3-mediated calcium signals, such as xestospongin B, mitoxantrone, or the novel 'IP_3 sponge'[433,691]. In addition, EGTA is another calcium chelator that could be used instead of BAPTA in autophagy assays, although the absence of an inhibitory effect of EGTA on autophagy would first need to be robustly shown. EGTA has a similar affinity to calcium compared to BATPA but slower calcium-binding kinetics, so this compound will take longer than BAPTA to buffer calcium and reach equilibrium. Although this feature could be a drawback, it can be useful since EGTA is able to prevent more distal events following calcium signals while BAPTA would block proximal ones as well as the whole calcium signalling process, and can help distinguish calcium buffering from rapid and transient calcium signals. For example, BAPTA is able to dissipate local calcium gradients in microdomains, whilst EGTA would dissipate diffused calcium gradients[423]. However, a caveat might be the pH-sensitivity of EGTA compared to BAPTA, which might limit its application.

In regards to the use of calcium indicators, the data presented here indicate that it is best to keep the loading of these compounds to a minimum to prevent any adverse effects on the mechanism studied. Indeed, a number of previous studies have suggested caution in the use of BAPTA analogues and calcium indicators, and have presented off-target effects associated with these compounds[433,689]. As an alternative, experiments monitoring intracellular calcium experiments could consider alternative reporters that are not derived from BAPTA. One example of this would be the expression of fluorescent genetically encoded calcium indicators (GECIs), which are hybrid fusion proteins made of a calcium-binding protein (such as calmodulin) attached to a fluorophore (such as GFP). GECI probes can be used to target a specific cellular compartment and in long-term recordings, and the large number of GECIs available with different properties to suit various experimental requirements is an advantage. However, whilst they do not require cell loading, GECIs need to be introduced in the target cell to be expressed, for example through transfection in a transient or stable manner, which might have adverse effects. In

addition, reports have described potential off-targets effects, as well as low expression levels[692], and GECIs might be less efficient than chemical indicators[693].

5.11 Conclusions

The findings presented in this Chapter support a role for Lrrk2 in IP_3-R mediated calcium signals in WT RAW264.7 macrophages, but provide only weak evidence of a similar function in HEK293 GFP-LC3 cells. In addition, the data suggest that LRRK2 is not involved in the regulation of lysosomal calcium storage in either cell line, although a role in regulating lysosomal calcium *release*, for example by modulating calcium channels, cannot be excluded. As such, the role of LRRK2 in calcium signalling in both cell lines merits more exploration.

Furthermore, our data indicate that BAPTA is an inappropriate tool to investigate the role of calcium in the autophagic pathway, thereby questioning the veracity of previous BAPTA-related data in the literature that support the involvement of calcium in autophagy. In addition, caution should be taken in using Fura-2 and Cal-590 due to their potential off-target effects in cells, in particular their repressing effect on autophagy described in this study.

6

General Discussion and Perspectives

6.1 Summary of results and conclusions

The work presented in this thesis sought to understand the role of LRRK2 in the regulation of calcium signalling and autophagy to provide insight into the early impairments involved in PD pathogenesis. In particular, this project aimed to develop new cellular models containing pathogenic and protective *LRRK2* mutations to explore the role of LRRK2 and LRRK2 enzymatic activities in these processes. The key findings of this project are summarised below and in Table 6.1 and Table 6.2.

The work in Chapter 3 aimed at developing isogenically matched cell lines using the CRISPR/Cas9 gene-editing technique to investigate the effects of *LRRK2* mutations. Despite numerous attempts following thorough optimisation, the sequencing results revealed that the designed CRISPR/Cas9 plasmids were not able to elicit double-strand DNA breaks in *LRRK2* in HEK239T cells. Since this approach was unsuccessful, alternative strategies to study *LRRK2* mutations were pursued in Chapter 4 and Chapter 5.

Chapter 4 investigated the impact of LRRK2 enzymatic activities and *LRRK2* pathogenic and protective variants on autophagy, with the aim of gaining insight into the steps at which LRRK2 acts (Table 6.1). The findings revealed a cell-type specific action of LRRK2 in autophagy, where LRRK2 appears to be pro-autophagic and is involved in the early stages of this process in HEK293 GFP-LC3 cells, but does not appear to be involved in autophagy in RAW264.7 macrophages. These results have been thoroughly discussed in Chapter 4, in particular proposed future studies to determine the site(s) of action of LRRK2 in the mechanisms leading to the induction of autophagy (Section 4.10.5).

The work reported in Chapter 5 explored the role of LRRK2 enzymatic activities and *LRRK2* pathogenic and protective variants on global and lysosomal calcium signals (Table 6.2). The results indicated that Lrrk2 is involved in IP_3-R mediated calcium signals in WT RAW264.7 macrophages, although results from inhibitor treatment do not convincingly replicate the effect of knockout, which suggests this role for Lrrk2 may be as a scaffolding protein. An equivalent loss of LRRK2 expression experiment was not performed in HEK293 GFP-LC3 cells, although experiments using LRRK2 inhibitors gave similar results to macrophages. LRRK2 was not shown to be involved in the regulation of lysosomal calcium storage in either cell line. When taken with the results in Chapter 4, these data indicate that the role of LRRK2 in autophagy induction in HEK293 GFP-LC3 cells is unlikely to involve intracellular calcium. Potential future studies have been discussed in the Discussion Section of Chapter 5 (Section 5.10). Additional findings revealed that the calcium indicators Fura-2 and Cal-590, as well as BAPTA and two BAPTA analogues, displayed significant off-target effects on autophagy, and indicated that BAPTA is an unsuitable tool to explore the role of calcium signals in autophagy.

The remainder of this Chapter discusses three talking points that arise from these results and conclusions and are not covered within the Discussion Sections of individual Results Chapters. Firstly, in light of the failure of CRISPR/Cas9, the potential challenges associated to this technique are discussed, and alternative genome editing techniques that have evolved during the course of this work are summarised. Secondly, since the data presented in this thesis provide direct evidence that the role for LRRK2 in autophagy is cell-type specific, the potential causes for this cell-type specificity are discussed. Thirdly, the implications of calcium-independent effects of BAPTA on autophagy are discussed further in the context of previous studies implicating LRRK2 in autophagy.

Table 6.1: Summary of the key Autophagy-related findings described in Chapter 4.

HEK293 GFP-LC3 cells	
Results	**Corresponding figures**
GFP-LC3 assays	
LRRK2 inhibition prevented the PP242-induced increase in GFP-LC3 punctae number.	Figure 4.5, Figure 4.8 and Figure 4.11
LRRK2 inhibition did not block the degradation of autophagosomes.	Figure 4.7
No effect of LRRK2 pathogenic mutants or protective variant on GFP-LC3 punctae number	Figure 4.22
WIPI2 assays	
LRRK2 inhibition prevented the PP242-induced increase in endogenous WIPI2 punctae number, to a similar extent as GFP-LC3 punctae number.	Figure 4.10 and Figure 4.13
IVM assay	
LRRK2 inhibition reduced the number of IVM-induced GFP-LC3 punctae.	Figure 4.19
Electron microscopy	
LRRK2 inhibition prevented the PP242-induced increase in autophagic vesicle number.	Figure 4.24
RAW264.7 macrophages	
Results	**Corresponding figures**
WIPI2 assays	
No effect of loss of Lrrk2 on WIPI2 punctae number.	Figure 4.16
No effect of Lrrk2 inhibition on WIPI2 punctae number.	Figure 4.17
Electron microscopy	
No effect of loss of Lrrk2 on autophagic vesicle number.	Figure 4.25

Table 6.2: Summary of the key Calcium signalling-related findings described in Chapter 5.

HEK293 GFP-LC3 cells	
Results	**Corresponding figures**
Assay: ATP, CPA, Ionomycin stimulations	
No effect of LRRK2 inhibition (1 or 16 hours).	- ATP: Figure 5.14, Figure 5.15, Figure 5.16 and Figure 5.17 - CPA, Ionomycin: Figure 5.24 and Figure 5.25
No effect of LRRK2 pathogenic mutants or protective variant.	- ATP: Figure 5.26 and Figure 5.27 - CPA, Ionomycin: Figure 5.28
Assay: ATP stimulations	
BAPTA and BAPTA-DB markedly reduced the response.	Figure 5.30
Assay: GFP-LC3 punctae quantification	
BAPTA, BAPTA-DB and BAPTA-FF prevented the PP242-induced increase in GFP-LC3 punctae number.	Figure 5.29
Fura-2 and Cal590 reduced the PP242-induced increase in GFP-LC3 punctae number.	Figure 5.31
RAW264.7 macrophages	
Results	**Corresponding figures**
Assay: ATP stimulations	
Lrrk2 KO macrophages displayed faster + larger increase in cytosolic calcium, and faster calcium clearance.	Figure 5.5 and Figure 5.7
No effect of Lrrk2 inhibition (1 or 16 hours).	Figure 5.10, Figure 5.11, Figure 5.12 and Figure 5.13
Assay: CPA, Ionomycin stimulations	
No effect of loss of Lrrk2.	Figure 5.19
No effect of Lrrk2 inhibition (1 or 16 hours).	Figure 5.20 and Figure 5.21
Assay: Spontaneous activity	
No effect of loss of Lrrk2.	Figure 5.4
No effect of Lrrk2 inhibition (1 or 16 hours).	Figure 5.9

6.2 Perspectives on the CRISPR/Cas9 technology

6.2.1 Potential challenges in targeting *LRRK2* with CRISPR/Cas9

Whilst our attempt at using CRISPR/Cas9 technique was unsuccessful, recent published work demonstrated the use of this technique to create LRRK2 knockout[694] or LRRK2 G2019S knock-in[695] in human iPS cells. Thus, the *LRRK2* gene is not entirely refractory to genome editing. Nonetheless, it is worth observing that publications reporting the successful use of CRISPR technology to modify *LRRK2* are relatively few and far between, which points towards difficulties in targeting this gene.

The reasons why certain genes or regions of the genome may be more or less amenable to genome editing are not fully understood, but likely relate to the chromosomal architecture and presence of DNA-binding proteins that may influence the availability of that region of DNA to Cas9. At this time, it is not yet known whether or how chromatin critically influences Cas9 targeting in eukaryotes.

Interestingly, a recent study has revealed that nucleosomes hindered Cas9 access to DNA[696], suggesting that the Cas9 system might not be able to effectively target the DNA in nucleosomes. Since the balance of histone acetylation and deacetylation regulates chromatin remodelling, we could speculate that the use of histone modifiers in combination with Cas9, such as histone deacetylation inhibitors, might potentially enhance the accessibility of DNA to Cas9, and help overcome the limitation of chromosome compaction, thereby improving CRISPR/Cas9 efficiency. Consistent with this hypothesis, Liu and colleagues[697] have recently reported that histone deacetylation inhibitors were able to increase CRISPR/Cas9 gene editing frequencies, whilst Li and colleagues[698] described an increase of CRISPR/Cas9-mediated HDR DNA repair.

Fascinatingly, another hypothesis is that the slow off-rate of Cas9, i.e. the persistence of Cas9 binding to the DNA strand, might prevent the DNA repair enzymes from initiating the DSB repair process[699], thereby affecting the efficiency of the Cas9 system. Although this has not been investigated in mammalian cells, it suggests that promoting Cas9 dissociation from the DNA may improve CRISPR/Cas9 genome editing[699].

Thus, these possibilities might all be responsible for the challenge in targeting *LRRK2* with CRISPR/Cas9, and represent further avenues to explore.

6.2.2 Alternative genome editing technologies to create new cell lines

Importantly, the CRISPR/Cas9 technique is not without limitations, and off-target effects have been reported[700]. Therefore, newer genome editing approaches have been developed, including the recently discovered CRISPR type Cas12a, which has the potential to improve on-target editing efficiency compared to Cas9[701]. More recently, base editing[702] is a genome editing technology that allows the generation of point mutations at specific sites in DNA or RNA. To do so, base editing mediates the conversion of a target base pair into another, without the need to generate and repair a double-stranded break. Indeed, base editors are created from the fusion of a base-modification enzyme (nucleobase deaminase) and a partially active Cas endonuclease (a nickase) that can induce a single-strand cut on each strand, where the nicked and non-edited strand is repaired using the edited strand. One of the main advantages is the reduction of unwanted off-target editing by-products, as well as increased precision on-target gene editing efficiency. However, recent findings have also reported off-target effects for base editors[703,704].

The latest developed technology is called prime editor[705]. Defined as a “search and replace” genome editing approach, prime editing is based on the use of a partially active Cas9 nickase combined with a reverse transcriptase and a prime editing guide RNA, which contains both the complementary sequence to the target site, and the genetic information with the desired edit[705]. Since this approach requires a 3-steps checkpoint, it improves the precision and on-target efficiency whilst reducing the off-target editing compared to the other techniques mentioned above.

As such, these gene editing methods are promising tools to explore as alternatives to the CRISPR/Cas9 technique to generate isogenic cell lines carrying point mutations in the *LRRK2* gene. Gene editing methods are continuously optimised, but also tested in a range of different cell types and models, which will help provide a better understanding of their respective limitations and benefits in the future.

6.3 Cell-type specificity for LRRK2 in autophagy

As mentioned in Chapter 1 Section 1.6.2, the published literature is controversial in regards to the role of LRRK2 in the autophagy-lysosomal pathway, describing opposite effects of LRRK2 activity in different cell types and experimental systems. In principle, these contradictory results can be explained by numerous variables in protocols used (e.g., model, method to monitor autophagy, LRRK2 protein levels). Of note, some of the inconsistencies might also be explained by the plausible possibility that LRRK2 inhibition has an impact on LRRK2 protein levels, or may even lead to protein degradation[706]. Thus, LRRK2 kinase activity might be required to maintain steady-state levels of LRRK2 aside from regulating LRRK2 function and correct subcellular localisation. Other potential contributions to a cell-type specificity for the role of LRRK2 are explored in the next sections.

6.3.1 LRRK2 interactome

Importantly, it is likely that the relationship between LRRK2 and autophagy is more complex and cell-type specific, with potential time-dependent effects of LRRK2. Since LRRK2 possesses enzymatic activities as well as domains conferring protein-protein interaction abilities, the interaction network of LRRK2 is likely to be large. Described as a "hub protein", LRRK2 might have distinct roles in various cellular pathways and cell types[112,180–182]. Indeed, the LRRK2 interactome is also likely to vary depending on the cell-type specific expression of LRRK2 partners and on their own interactomes, resulting in the formation of different protein complexes in a cell type-specific context[180]. Interestingly, this might give an explanation for the myriad of diseases LRRK2 is associated with. This hypothesis is further supported by the inconsistent findings yielded in studies investigating the effect of the LRRK2 kinase inhibitors on autophagy (see Chapter 1, Section 1.6.2.3 for more details). Importantly, our calcium and autophagy data obtained using various assays in HEK293 GFP-LC3 cells and RAW264.7 macrophages are also in line with a cell-type specific role of LRRK2 hypothesis. As such, the diverse interactome of LRRK2 might contribute to the cell-type specific difference reported in this thesis.

Of note, although the link between autophagy and LRRK2 has been extensively explored, studies carried out in immune cells only represent a small percentage, despite the important role of autophagy and lysosomes in these cells. As such, how the role of LRRK2 in the autophagy-endolysosomal pathways impact immune cells remains unknown, which merits further exploration.

6.3.2 LRRK2 and LRRK1

Additionally, it is worth mentioning that *LRRK2* has a paralog, *LRRK1*, which has not been associated with PD[592]. *LRRK1* encodes a protein with similar domains and structure to that of LRRK2, although LRRK1 does not have the ARM domain. This might indicate different functions for these proteins, which is supported by their respective interactome[707]. However, LRRK2 and LRRK1 have common interactors which suggest some signalling cross-talk between these proteins. With this in mind, the available data suggest that LRRK1 and LRRK2 may have redundant functions, and LRRK1 has been shown to be involved in autophagy-endolysosomal pathways[479,592,707–710]. Thus, LRRK1 may compensate for the loss of LRRK2 function in the context of autophagy. Indeed, a recent study showed that brains of LRRK2 and LRRK1 double-knockout mice displayed an altered autophagy-lysosome pathway and neuronal death, which was not the case when only one of LRRK2 or LRRK1 was knockout[592]. In any case, it would be interesting to further explore the possibility of a redundancy in the function of LRRK1 and LRRK2 in the autophagic pathway. As such, these observations might, in part, explain some of the discrepancies and the cell-type specific effects of LRRK2 observed in the literature.

6.3.3 Potential modifications to the *LRRK2* sequence

Furthermore, potential genetic, developmental or environmental factors inducing modifications to the LRRK2 sequence might be responsible for, at least in part, some of the cell-type specificities associated with LRRK2 function in the literature and reported in this thesis. This might also explain the reduced penetrance of LRRK2, where such factors might provide the toxic input leading to PD, or influence other risk genes converging to pathways involving LRRK2.

With regard to epigenetics, Fernandez-Santiago and colleagues revealed a PD-associated hypermethylation solely occurring in differentiated dopaminergic neurons from LRRK2-PD patients but not in the non-reprogrammed somatic skin cells, nor in dopaminergic neurons from healthy controls[711]. Thus, cell-specific epigenetic modifications might play an important role in the development of PD. Furthermore, a number of studies have reported that microRNAs and post-translational modification are involved in the regulation of *LRRK2* gene expression and protein expression[712–714]. In particular, miR-205 has been shown to suppress LRRK2 protein expression by binding to the 3'-UTR of the *LRRK2* gene[712] without affecting LRRK2 mRNA levels, whilst pathogenic elevation of LRRK2 protein in patients with sporadic PD was accompanied with a downregulation of miR-205 expression[712]. Thus, these findings suggest that overexpression of miR-205 might have neuroprotective effects in PD, and miR-205 levels might influence LRRK2-PD risk.

Another mechanism regulating gene expression is alternative splicing, which increases the coding potential of the genome. Generally, large genes, such as *LRRK2,* can be expected to produce multiple transcripts following splicing, and research groups have explored LRRK2 splicing variants as well as LRRK2 RNA expression in several tissues[713,715]. Recently, studies have identified the presence of several LRRK2 spliced transcripts in the human brain with regional differences, in particular in the substantia nigra[713], and a differential expression of LRRK2 splice variants in mice[715] as well. Given this, it is likely that LRRK2 mRNA transcript variability also exists in other cell types. Since these splicing events occurred within the Roc and COR domains of LRRK2, as well as in the protein-protein interaction domain WD40, it would not be surprising that this alternative splicing has important consequences on LRRK2 enzymatic activities, LRRK2 dimer formation and binding partners. Therefore, further studies are currently underway to explore the involvement of these LRRK2 splice variants in PD[713].

6.4 LRRK2 and calcium in the context of autophagy

Since its development, BAPTA has been considered one of the most definitive ways to establish the involvement of calcium in a cellular process. In the context of the LRRK2-mediated regulation of autophagy, recent findings challenge the use of BAPTA and strongly indicate the need to reassess the now compromised BAPTA-related findings linking LRRK2 and autophagy through calcium signals. For example, Gómez-Suaga and colleagues[479] reported that BAPTA prevented the increase in autophagosome formation upon overexpression of WT LRRK2 or of its pathogenic G2019S mutant. Similarly, Cherra and colleagues[590] used BAPTA to demonstrate the contribution of LRRK2 mutant-mediated deregulations in calcium homeostasis on mitophagy, whilst Hockey and colleagues[216] suggested that lysosomal morphology defects found in LRRK2 G2019S fibroblasts were caused by the disruption of local calcium signals since they were inhibited by BAPTA. In addition, Verma and colleagues[588] reasoned that mitochondrial calcium uptake through the mitochondrial uniporter was necessary for the induction of mitophagy by mutant LRRK2 based on results obtained with BAPTA treatment. In each case, it is difficult to determine whether these results were caused by calcium chelation by BAPTA or by off-target effects (or a combination of the two). Therefore, it is clear that these experiments need to be repeated using BAPTA analogues with decreased affinity for calcium (e.g., di-bromo-BAPTA and di-fluoro-BAPTA) as additional controls. If these compounds replicate the effect of BAPTA then it can be assumed that the effect of BAPTA is independent of calcium binding. Alternatively, other potential tools to explore specific calcium processes, for example mitochondrial calcium entry or IP_3-mediated calcium signals, have also been alluded to in the Discussion of Chapter 5 (Section 5.10.4).

Importantly, these observations do not necessarily imply that all evidence linking LRRK2 with autophagy via calcium signalling in these papers must be discarded. Indeed, some conclusions were reached using other strategies that did not rely on the use of BAPTA. Indeed, Cherra and colleagues[590] generated evidence of the involvement of L-type calcium channels in the LRRK2 mutant-mediated increase in mitophagy without using BAPTA. Furthermore, using a range of pharmacological and genetic approaches, Gómez-Suaga and colleagues[479] revealed a molecular mechanism where LRRK2-mediated

calcium release via TCP2/NAADP receptors was involved in the effects of LRRK2 on autophagy induction, in particular through the activation of the CaMMKβ/AMPK pathway. Of note, it is also possible that LRRK2 had an effect on the upstream production of NAADP. In line with these findings, Hockey and colleagues[216] demonstrated that LRRK2 mutant-mediated lysosomal defects were both NAADP- and PI(3,5)P_2-dependent and involved TPC2 receptors, and also reported the involvement of NAADP-regulated global calcium signalling. Taken together, these data still make a convincing case of a role for lysosomal calcium signals in the LRRK2-mediated regulation of autophagy, although follow-up studies using BAPTA analogues are avidly awaited.

Bibliography

1. Gan-Or Z, Dion PA, Rouleau GA. Genetic perspective on the role of the autophagy-lysosome pathway in Parkinson disease. *Autophagy*. 2015;11(9):1443-1457. doi:10.1080/15548627.2015.1067364
2. Elbaz A, Bower JH, Maraganore DM, et al. Risk tables for parkinsonism and Parkinson ' s disease. *J Clin Epidemiol*. 2002;55:25-31.
3. Yang YX, Wood NW, Latchman DS. Molecular basis of Parkinson's disease. *Neuroreport*. 2009;20(2):150-156. doi:10.1097/WNR.0b013e32831c50df
4. Jost WH, Reichmann H. An essay on the shaking palsy_remasterised. *J Neural Transm*. 2017:1-2. doi:10.1007/s00702-017-1684-0
5. Postuma RB, Berg D, Stern M, et al. MDS clinical diagnostic criteria for Parkinson's disease. *Mov Disord*. 2015;30(12):1591-1601. doi:10.1002/mds.26424
6. Poewe W. Non-motor symptoms in Parkinson's disease. *Eur J Neurol*. 2008;15(SUPPL. 1):14-20. doi:10.1111/j.1468-1331.2008.02056.x
7. Pfeiffer RF. Non-motor symptoms in Parkinson's disease. *Park Relat Disord*. 2016;22:S119-S122. doi:10.1016/j.parkreldis.2015.09.004
8. Jankovic J. Parkinson's disease: Clinical features and diagnosis. *J Neurol Neurosurg Psychiatry*. 2008;79(4):368-376. doi:10.1136/jnnp.2007.131045
9. Chaudhuri KR, Schapira AH. Non-motor symptoms of Parkinson's disease: dopaminergic pathophysiology and treatment. *Lancet Neurol*. 2009;8(5):464-474. doi:10.1016/S1474-4422(09)70068-7
10. Duty S, Jenner P. Animal models of Parkinson's disease: A source of novel treatments and clues to the cause of the disease. *Br J Pharmacol*. 2011;164(4):1357-1391. doi:10.1111/j.1476-5381.2011.01426.x
11. AlDakheel A, Kalia L V., Lang AE. Pathogenesis-Targeted, Disease-Modifying Therapies in Parkinson Disease. *Neurotherapeutics*. 2014;11(1):6-23. doi:10.1007/s13311-013-0218-1
12. Armstrong MJ, Okun MS. Diagnosis and Treatment of Parkinson Disease: A Review. *JAMA - J Am Med Assoc*. 2020;323(6):548-560. doi:10.1001/jama.2019.22360
13. Antony PMA, Diederich NJ, Krüger R, Balling R. The hallmarks of Parkinson's disease. *FEBS J*. 2013;280(23):5981-5993. doi:10.1111/febs.12335
14. Gerfen CR, Surmeier DJ. Modulation of Striatal Projection Systems by Dopamine. *Annu Rev Neurosci*. 2011;34(1):441-466. doi:10.1146/annurev-neuro-061010-113641
15. D'Ardenne K, Eshel N, Luka J, Lenartowicz A, Nystrom LE, Cohen JD. Role of prefrontal cortex and the midbrain dopamine system in working memory updating. *Proc Natl Acad Sci U S A*. 2012;109(49):19900-19909. doi:10.1073/pnas.1116727109
16. Pignatelli M, Bonci A. Role of Dopamine Neurons in Reward and Aversion: A Synaptic Plasticity Perspective. *Neuron*. 2015;86(5):1145-1157. doi:10.1016/j.neuron.2015.04.015
17. Love TM. Oxytocin, motivation and the role of dopamine. *Pharmacol Biochem Behav*. 2014;119:49-60. doi:10.1016/j.pbb.2013.06.011
18. Simonyan K. Recent advances in understanding the role of the basal ganglia. *F1000Research*. 2019;8(0):122. doi:10.12688/f1000research.16524.1
19. Damier P, Hirsch EC, Agid Y, Graybiel AM. The substantia nigra of the human brain: II. Patterns of loss of dopamine-containing neurons in Parkinson's disease. *Brain*. 1999;122(8):1437-1448. doi:10.1093/brain/122.8.1437
20. Giráldez-Pérez R, Antolín-Vallespín M, Muñoz M, Sánchez-Capelo A. Models of α-synuclein aggregation in Parkinson's disease. *Acta Neuropathol Commun*. 2014;2:176. doi:10.1186/s40478-014-0176-9
21. McCann H, Stevens CH, Cartwright H, Halliday GM. α-Synucleinopathy phenotypes. *Park Relat Disord*. 2014;20(SUPPL.1). doi:10.1016/S1353-8020(13)70017-8
22. Wang T, Hay JC. Alpha-synuclein toxicity in the early secretory pathway: How it drives neurodegeneration in parkinsons disease. *Front Neurosci*. 2015;9(NOV):1-8. doi:10.3389/fnins.2015.00433
23. Cookson MR. α-Synuclein and neuronal cell death. *Mol Neurodegener*. 2009;4:9. doi:10.1186/1750-1326-4-9
24. Surmeier DJ, Obeso JA, Halliday GM. Selective neuronal vulnerability in Parkinson disease. *Nat Rev Neurosci*. 2017;18(2):101-113. doi:10.1038/nrn.2016.178

25. Kalia L V., Lang AE, Hazrati L-NN, et al. Clinical correlations with lewy body pathology in LRRK2-related Parkinson disease. *JAMA Neurol*. 2015;72(1):100-105. doi:10.1001/jamaneurol.2014.2704
26. Villar-Piqué A, Lopes da Fonseca T, Outeiro TF. Structure, function and toxicity of alpha-synuclein: the Bermuda triangle in synucleinopathies. *J Neurochem*. 2016;139:240-255. doi:10.1111/jnc.13249
27. Burré J, Sharma M, Südhof TC. Cell Biology and Pathophysiology of α-Synuclein. *Cold Spring Harb Perspect Med*. 2017:a024091. doi:10.1101/cshperspect.a024091
28. Ferreira M, Massano J. An updated review of Parkinson's disease genetics and clinicopathological correlations. *Acta Neurol Scand*. 2017;135(3):273-284. doi:10.1111/ane.12616
29. Ingelsson M. Alpha-synuclein oligomers-neurotoxic molecules in Parkinson's disease and other lewy body disorders. *Front Neurosci*. 2016;10(SEP):1-10. doi:10.3389/fnins.2016.00408
30. Kalia L V., Kalia SK, McLean PJ, Lozano AM, Lang AE. α-Synuclein oligomers and clinical implications for Parkinson disease. *Ann Neurol*. 2013;73(2):155-169. doi:10.1002/ana.23746
31. Reeve A, Simcox E, Turnbull D. Ageing and Parkinson's disease: Why is advancing age the biggest risk factor? *Ageing Res Rev*. 2014;14(1):19-30. doi:10.1016/j.arr.2014.01.004
32. Jiang T, Sun Q, Chen S. Oxidative stress: A major pathogenesis and potential therapeutic target of antioxidative agents in Parkinson's disease and Alzheimer's disease. *Prog Neurobiol*. 2016;147:1-19. doi:10.1016/j.pneurobio.2016.07.005
33. Hwang O. Role of Oxidative Stress in Parkinson's Disease. *Exp Neurobiol*. 2013;22(1):11-17. doi:10.5607/en.2013.22.1.11
34. Thomas B. Molecular insights into Parkinson's disease. *F1000 Med Rep*. 2011;3(April):1-8. doi:10.3410/M3-7
35. Dawson TM. Molecular Pathways of Neurodegeneration in Parkinson's Disease. *Science (80-)*. 2003;302(5646):819-822. doi:10.1126/science.1087753
36. Guzman JN, Sanchez-Padilla J, Wokosin D, et al. Oxidant stress evoked by pacemaking in dopaminergic neurons is attenuated by DJ-1. *Nature*. 2010;468(7324):696-700. doi:10.1038/nature09536
37. Pacelli C, Giguère N, Bourque MJ, Lévesque M, Slack RS, Trudeau LÉ. Elevated Mitochondrial Bioenergetics and Axonal Arborization Size Are Key Contributors to the Vulnerability of Dopamine Neurons. *Curr Biol*. 2015;25(18):2349-2360. doi:10.1016/j.cub.2015.07.050
38. Dexter DT, Jenner P. Parkinson disease: from pathology to molecular disease mechanisms. *Free Radic Biol Med*. 2013;62:132-144. doi:10.1016/j.freeradbiomed.2013.01.018
39. Wickremaratchi MM, Ben-Shlomo Y, Morris HR. The effect of onset age on the clinical features of Parkinson's disease. *Eur J Neurol*. 2009;16(4):450-456. doi:10.1111/j.1468-1331.2008.02514.x
40. Corti O, Brice A. Mitochondrial quality control turns out to be the principal suspect in parkin and PINK1-related autosomal recessive Parkinson's disease. *Curr Opin Neurobiol*. 2013;23(1):100-108. doi:10.1016/j.conb.2012.11.002
41. Valente EM. Hereditary Early-Onset Parkinson's Disease Caused by Mutations in PINK1. *Science (80-)*. 2004;304(5674):1158-1160. doi:10.1126/science.1096284
42. Zimprich A, Biskup S, Leitner P, et al. Mutations in LRRK2 cause autosomal-dominant parkinsonism with pleomorphic pathology. *Neuron*. 2004;44(4):601-607. doi:10.1016/j.neuron.2004.11.005
43. Boland B, Yu WH, Corti O, et al. Promoting the clearance of neurotoxic proteins in neurodegenerative disorders of ageing. *Nat Rev Drug Discov*. 2018;17(9):660-688. doi:10.1038/nrd.2018.109
44. Henriques CM, Ferreira MG. Consequences of telomere shortening during lifespan. *Curr Opin Cell Biol*. 2012;24(6):804-808. doi:10.1016/j.ceb.2012.09.007
45. López-Otín C, Blasco MA, Partridge L, Serrano M, Kroemer G. The hallmarks of aging. *Cell*. 2013;153(6):1194. doi:10.1016/j.cell.2013.05.039
46. Sun Y, Coppé JP, Lam EWF. Cellular Senescence: The Sought or the Unwanted? *Trends Mol Med*. 2018;24(10):871-885. doi:10.1016/j.molmed.2018.08.002
47. Tran J, Anastacio H, Bardy C. Genetic predispositions of Parkinson's disease revealed in patient-derived brain cells. *npj Park Dis*. 2020;6(1). doi:10.1038/s41531-020-0110-8
48. Baldi I, Cantagrel A, Lebailly P, et al. Association between Parkinson's disease and exposure to pesticides in southwestern France. *Neuroepidemiology*. 2003;22(5):305-310. doi:10.1159/000071194
49. Elbaz A, Clavel J, Rathouz PJ, et al. Professional exposure to pesticides and Parkinson disease. *Ann Neurol*. 2009;66(4):494-504. doi:10.1002/ana.21717
50. Breckenridge CB, Berry C, Chang ET, Sielken RL, Mandel JS. Association between Parkinson's disease and cigarette smoking, rural living, well-water consumption, farming and pesticide use: Systematic review and meta-analysis. *PLoS One*. 2016;11(4):1-42. doi:10.1371/journal.pone.0151841

51. Dutheil F, Beaune P, Tzourio C, Loriot M-A, Elbaz A. Interaction Between ABCB1 and Professional Exposure to Organochlorine Insecticides in Parkinson Disease. *Arch Neurol*. 2010;67(6):296-299. doi:10.1001/archneurol.2010.101
52. Delamarre A, Meissner WG. Epidemiology, environmental risk factors and genetics of Parkinson's disease. *Presse Med*. 2017;46(2):175-181. doi:10.1016/j.lpm.2017.01.001
53. Narayan S, Liew Z, Paul K, et al. Household organophosphorus pesticide use and parkinson's disease. *Int J Epidemiol*. 2013;42(5):1476-1485. doi:10.1093/ije/dyt170
54. Ungerstedt U. 6-Hydroxy-Dopamine Induced Degeneration of Central Monoamine Neurons. *Eur J Pharmacol*. 1968;5(1):107-110. doi:10.1016/0014-2999(68)90164-7
55. Hamadjida A, Frouni I, Kwan C, Huot P. Classic animal models of Parkinson's disease: A historical perspective. *Behav Pharmacol*. 2019;30(4):291-310. doi:10.1097/FBP.0000000000000441
56. Langston JW, Ballard P, Tetrud JW, Irwin I. Chronic Parkinsonism in humans due to a product of meperidine-analog synthesis. *Science*. 1983;219(4587):979-980. doi:10.1126/science.6823561
57. González-Polo RA, Rodríguez-Martín A, Morán JM, Niso M, Soler G, Fuentes JM. Paraquat-induced apoptotic cell death in cerebellar granule cells. *Brain Res*. 2004;1011(2):170-176. doi:10.1016/j.brainres.2004.02.078
58. González-Polo RA, Niso-Santano M, Ortíz-Ortíz MA, et al. Inhibition of paraquat-induced autophagy accelerates the apoptotic cell death in neuroblastoma SH-SY5Y cells. *Toxicol Sci*. 2007;97(2):448-458. doi:10.1093/toxsci/kfm040
59. Sulzer D, Surmeier DJ. Neuronal vulnerability, pathogenesis, and Parkinson's disease. *Mov Disord*. 2013;28(1):41-50. doi:10.1002/mds.25095
60. Jackson-Lewis V, Blesa J, Przedborski S. Animal models of Parkinson's disease. *Parkinsonism Relat Disord*. 2012;18:S183-S185. doi:10.1016/S1353-8020(11)70057-8
61. Tamilselvam K, Braidy N, Manivasagam T, et al. Neuroprotective effects of hesperidin, a plant flavanone, on rotenone-induced oxidative stress and apoptosis in a cellular model for Parkinson's disease. *Oxid Med Cell Longev*. 2013;2013. doi:10.1155/2013/102741
62. Miyazaki I, Isooka N, Imafuku F, et al. Chronic systemic exposure to low-dose rotenone induced central and peripheral neuropathology and motor deficits in mice: reproducible animal model of parkinson's disease. *Int J Mol Sci*. 2020;21(9). doi:10.3390/ijms21093254
63. Nandipati S, Litvan I. Environmental exposures and Parkinson's disease. *Int J Environ Res Public Health*. 2016;13(9). doi:10.3390/ijerph13090881
64. Jellinger KA. *The Relevance of Metals in the Pathophysiology of Neurodegeneration, Pathological Considerations*. Vol 110. 1st ed. Elsevier Inc.; 2013. doi:10.1016/B978-0-12-410502-7.00002-8
65. Ngwa HA, Kanthasamy A, Jin H, Anantharam V, Kanthasamy AG. Vanadium exposure induces olfactory dysfunction in an animal model of metal neurotoxicity. *Neurotoxicology*. 2014;43:73-81. doi:10.1016/j.neuro.2013.12.004
66. Winneke G. Developmental aspects of environmental neurotoxicology: Lessons from lead and polychlorinated biphenyls. *J Neurol Sci*. 2011;308(1-2):9-15. doi:10.1016/j.jns.2011.05.020
67. Hu CY, Fang Y, Li FL, et al. Association between ambient air pollution and Parkinson's disease: Systematic review and meta-analysis. *Environ Res*. 2019;168:448-459. doi:10.1016/j.envres.2018.10.008
68. Costa J, Lunet N, Santos C, Santos J, Vaz-Carneiro A. Caffeine exposure and the risk of Parkinson's disease: A systematic review and meta-analysis of observational studiess. *J Alzheimer's Dis*. 2010;20(SUPPL.1). doi:10.3233/JAD-2010-091525
69. Jafari S, Etminan M, Aminzadeh F, Samii A. Head injury and risk of Parkinson disease: A systematic review and meta-analysis. *Mov Disord*. 2013;28(9):1222-1229. doi:10.1002/mds.25458
70. Shen CH, Chou CH, Liu FC, et al. Association between tuberculosis and Parkinson disease a nationwide, population-based cohort study. *Med (United States)*. 2016;95(8):1-8. doi:10.1097/MD.0000000000002883
71. Zhu F, Li C, Gong J, Zhu W, Gu L, Li N. The risk of Parkinson's disease in inflammatory bowel disease: A systematic review and meta-analysis. *Dig Liver Dis*. 2019;51(1):38-42. doi:10.1016/j.dld.2018.09.017
72. Gasser T. Mendelian forms of Parkinson's disease. *Biochim Biophys Acta - Mol Basis Dis*. 2009;1792(7):587-596. doi:10.1016/j.bbadis.2008.12.007
73. Shulman JM, De Jager PL, Feany MB. Parkinson's Disease: Genetics and Pathogenesis. *Annu Rev Pathol Mech Dis*. 2011;6(1):193-222. doi:10.1146/annurev-pathol-011110-130242
74. Chang D, Nalls MA, Hallgrímsdóttir IB, et al. A meta-analysis of genome-wide association studies identifies 17 new Parkinson's disease risk loci. *Nat Genet*. 2017;49(10):1511-1516. doi:10.1038/ng.3955
75. Klein C, Westenberger A. Genetics of Parkinson's Disease. *Cold Spring Harb Perspect Med*.

2012;2(1):a008888-a008888. doi:10.1101/cshperspect.a008888

76. Nalls MA, Pankratz N, Lill CM, et al. Large-scale meta-analysis of genome-wide association data identifies six new risk loci for Parkinson's disease. *Nat Genet*. 2014;46(9):989-993. doi:10.1038/ng.3043
77. Singleton AB, Farrer MJ, Bonifati V. The genetics of Parkinson's disease: Progress and therapeutic implications. *Mov Disord*. 2013;28(1):14-23. doi:10.1002/mds.25249
78. Polymeropoulos MH, Lavedan C, Leroy E, et al. Mutation in the α-synuclein gene identified in families with Parkinson's disease. *Science (80-)*. 1997;276(5321):2045-2047. doi:10.1126/science.276.5321.2045
79. Kitada T, Asakawa S, Hattori N, et al. Mutations in the parkin gene cause autosomal recessive juvenile parkinsonism. *Nature*. 1998;392(6676):605-608. doi:10.1038/33416
80. Bonifati V, Rizzu P, Van Baren MJ, et al. Mutations in the DJ-1 gene associated with autosomal recessive early-onset parkinsonism. *Science (80-)*. 2003;299(5604):256-259. doi:10.1126/science.1077209
81. Van der Merwe C, Jalali Sefid Dashti Z, Christoffels A, Loos B, Bardien S. Evidence for a common biological pathway linking three Parkinson's disease-causing genes: Parkin, PINK1 and DJ-1. *Eur J Neurosci*. 2015;41(9):1113-1125. doi:10.1111/ejn.12872
82. Celardo I, Martins LM, Gandhi S. Unravelling mitochondrial pathways to Parkinson's disease. *Br J Pharmacol*. 2014;171(8):1943-1957. doi:10.1111/bph.12433
83. Gasser T. Molecular pathogenesis of Parkinson disease: Insights from genetic studies. *Expert Rev Mol Med*. 2009;11(July):1-20. doi:10.1017/S1462399409001148
84. Stockman JA. Multicenter Analysis of Glucocerebrosidase Mutations in Parkinson's Disease. *Yearb Pediatr*. 2011;2011:419-420. doi:10.1016/S0084-3954(10)79717-7
85. Maiti P, Manna J, Dunbar GL. Current understanding of the molecular mechanisms in Parkinson's disease: Targets for potential treatments. *Transl Neurodegener*. 2017;6(1):28. doi:10.1186/s40035-017-0099-z
86. Yilmaz R, Hopfner F, van Eimeren T, Berg D. Biomarkers of Parkinson's disease: 20 years later. *J Neural Transm*. 2019;126(7):803-813. doi:10.1007/s00702-019-02001-3
87. Emamzadeh FN, Surguchov A. Parkinson's Disease: Biomarkers, Treatment, and Risk Factors. *Front Neurosci*. 2018;12(August):612. doi:10.3389/fnins.2018.00612
88. Gubellini P, Kachidian P. Animal models of Parkinson's disease: An updated overview. *Rev Neurol (Paris)*. 2015;171(11):750-761. doi:10.1016/j.neurol.2015.07.011
89. Zeng X-S, Geng W-S, Jia J-J. Neurotoxin-Induced Animal Models of Parkinson Disease: Pathogenic Mechanism and Assessment. *ASN Neuro*. 2018;10:175909141877743. doi:10.1177/1759091418777438
90. Blesa J, Przedborski S. Parkinson's disease: animal models and dopaminergic cell vulnerability. *Front Neuroanat*. 2014;8(December):155. doi:10.3389/fnana.2014.00155
91. Konnova EA, Swanberg M. Animal Models of Parkinson's Disease. In: Stoker TB GJ, ed. *Parkinson's Disease: Pathogenesis and Clinical Aspects*. Codon Publications; 2018:83-106. doi:10.15586/codonpublications.parkinsonsdisease.2018.ch5
92. Dawson TM, Ko HS, Dawson VL. Genetic Animal Models of Parkinson's Disease. *Neuron*. 2010;66(5):646-661. doi:10.1016/j.neuron.2010.04.034
93. Goldberg MS, Fleming SM, Palacino JJ, et al. Parkin-deficient Mice Exhibit Nigrostriatal Deficits but Not Loss of Dopaminergic Neurons. *J Biol Chem*. 2003;278(44):43628-43635. doi:10.1074/jbc.M308947200
94. Kitada T, Pisani A, Porter DR, et al. Impaired dopamine release and synaptic plasticity in the striatum of PINK1-deficient mice. *Proc Natl Acad Sci*. 2007;104(27):11441-11446. doi:10.1073/pnas.0702717104
95. Manzoni C, Lewis PA. LRRK2 and Autophagy. In: *Leucine-Rich Repeat Kinase 2 (LRRK2)*. Vol 5. ; 2017:89-105. doi:10.1007/978-3-319-49969-7_5
96. Falkenburger BH, Saridaki T, Dinter E. Cellular models for Parkinson's disease. *J Neurochem*. 2016;139:121-130. doi:10.1111/jnc.13618
97. Hargus G, Ehrlich M, Hallmann A-LA, Kuhlmann T. Human stem cell models of neurodegeneration: a novel approach to study mechanisms of disease development. *Acta Neuropathol*. 2014;127(2):151-173. doi:10.1007/s00401-013-1222-6
98. Lázaro DF, Pavlou MAS, Outeiro TF. Cellular models as tools for the study of the role of alpha-synuclein in Parkinson's disease. *Exp Neurol*. 2017;298(5):162-171. doi:10.1016/j.expneurol.2017.05.007
99. Roessler R, Smallwood SA, Veenvliet J V, et al. Detailed analysis of the genetic and epigenetic signatures of iPSC-derived mesodiencephalic dopaminergic neurons. *Stem Cell Reports*. 2014;2(4):520-533. doi:10.1016/j.stemcr.2014.03.001
100. Ross CA, Akimov SS. Human-induced pluripotent stem cells: Potential for neurodegenerative diseases. *Hum Mol Genet*. 2014;23(R1):17-26. doi:10.1093/hmg/ddu204
101. Musunuru K. Genome editing of human pluripotent stem cells to generate human cellular disease models.

Dis Model Mech. 2013;6(4):896-904. doi:10.1242/dmm.012054

102. Kumari U, Tan EK. LRRK2 in Parkinson's disease: Genetic and clinical studies from patients. *FEBS J*. 2009;276(22):6455-6463. doi:10.1111/j.1742-4658.2009.07344.x
103. Kluss JH, Mamais A, Cookson MR. LRRK2 links genetic and sporadic Parkinson's disease. *Biochem Soc Trans*. 2019;47(2):651-661. doi:10.1042/BST20180462
104. Paisán-Ruíz C, Lang AE, Kawarai T, et al. LRRK2 gene in Parkinson disease: Mutation analysis and case control association study. *Neurology*. 2005;65(5):696-700. doi:10.1212/01.WNL.0000167552.79769.b3
105. Smith WW, Pei Z, Jiang H, et al. Leucine-rich repeat kinase 2 (LRRK2) interacts with parkin, and mutant LRRK2 induces neuronal degeneration. *Proc Natl Acad Sci U S A*. 2005;102(51):18676-18681. doi:10.1073/pnas.0508052102
106. Paisán-Ruiz C, Lewis PA, Singleton AB. LRRK2: Cause, Risk, and Mechanism. *J Parkinsons Dis*. 2013;3(2):85-103. doi:10.3233/JPD-130192
107. Marras C. Phenotype in parkinsonian and nonparkinsonian LRRK2 G2019S mutation carriers. *Neurology*. 2011;77(15):1501-1501. doi:10.1212/wnl.0b013e3182306ab3
108. Nixon-Abell J, Berwick DC, Grannó S, Spain VA, Blackstone C, Harvey K. Protective LRRK2 R1398H Variant Enhances GTPase and Wnt Signaling Activity. *Front Mol Neurosci*. 2016;9(March):18. doi:10.3389/fnmol.2016.00018
109. Hui KY, Fernandez-Hernandez H, Hu J, et al. Functional variants in the LRRK2 gene confer shared effects on risk for Crohn's disease and Parkinson's disease. *Sci Transl Med*. 2018;10(423):eaai7795. doi:10.1126/scitranslmed.aai7795
110. Mata IF, Wedemeyer WJ, Farrer MJ, Taylor JP, Gallo KA. LRRK2 in Parkinson's disease: protein domains and functional insights. *Trends Neurosci*. 2006;29(5):286-293. doi:10.1016/j.tins.2006.03.006
111. Bosgraaf L, Van Haastert PJM. Roc, a Ras/GTPase domain in complex proteins. *Biochim Biophys Acta - Mol Cell Res*. 2003;1643(1-3):5-10. doi:10.1016/j.bbamcr.2003.08.008
112. Berwick DC, Heaton GR, Azeggagh S, Harvey K. LRRK2 Biology from structure to dysfunction: research progresses, but the themes remain the same. *Mol Neurodegener*. 2019;14(1):49. doi:10.1186/s13024-019-0344-2
113. Outeiro TF, Harvey K, Dominguez-Meijide A, Gerhardt E. LRRK2, alpha-synuclein, and tau: Partners in crime or unfortunate bystanders? *Biochem Soc Trans*. 2019;47(3):827-838. doi:10.1042/BST20180466
114. Paisán-Ruíz C, Jain S, Evans EW, et al. Cloning of the gene containing mutations that cause PARK8-linked Parkinson's disease. *Neuron*. 2004;44(4):595-600. doi:10.1016/j.neuron.2004.10.023
115. Law BMH, Spain VA, Leinster VHL, et al. A direct interaction between leucine-rich repeat kinase 2 and specific β-Tubulin isoforms regulates tubulin acetylation. *J Biol Chem*. 2014;289(2):895-908. doi:10.1074/jbc.M113.507913
116. Berwick DC, Harvey K. LRRK2 functions as a wnt signaling scaffold, bridging cytosolic proteins and membrane-localized LRP6. *Hum Mol Genet*. 2012;21(22):4966-4979. doi:10.1093/hmg/dds342
117. Arranz AM, Delbroek L, Van Kolen K, et al. LRRK2 functions in synaptic vesicle endocytosis through a kinase-dependent mechanism. *J Cell Sci*. 2015;128(3):541-552. doi:10.1242/jcs.158196
118. Nichols RJ, Dzamko N, Morrice NA, et al. 14-3-3 binding to LRRK2 is disrupted by multiple Parkinson's disease-associated mutations and regulates cytoplasmic localization. *Biochem J*. 2010;430(3):393-404. doi:10.1042/BJ20100483
119. Li X, Wang QJ, Pan N, et al. Phosphorylation-dependent 14-3-3 binding to LRRK2 is impaired by common mutations of familial parkinson's disease. *PLoS One*. 2011;6(3):1-13. doi:10.1371/journal.pone.0017153
120. Orenstein SJ, Kuo SH, Tasset I, et al. Interplay of LRRK2 with chaperone-mediated autophagy. *Nat Neurosci*. 2013;16(4):394-406. doi:10.1038/nn.3350
121. Ho DH, Je AR, Lee H, et al. LRRK2 Kinase Activity Induces Mitochondrial Fission in Microglia via Drp1 and Modulates Neuroinflammation. *Exp Neurobiol*. 2018;27(3):171. doi:10.5607/en.2018.27.3.171
122. Alegre-Abarrategui J, Christian H, Lufino MMP, et al. LRRK2 regulates autophagic activity and localizes to specific membrane microdomains in a novel human genomic reporter cellular model. *Hum Mol Genet*. 2009;18(21):4022-4034. doi:10.1093/hmg/ddp346
123. Guaitoli G, Gilsbach BK, Raimondi F, Gloeckner CJ. First model of dimeric LRRK2: The challenge of unrevealing the structure of a multidomain Parkinson's-associated protein. *Biochem Soc Trans*. 2016;44(6):1635-1641. doi:10.1042/BST20160226
124. Berger Z, Smith KA, Lavoie MJ. Membrane localization of LRRK2 is associated with increased formation of the highly active lrrk2 dimer and changes in its phosphorylation. *Biochemistry*. 2010;49(26):5511-5523. doi:10.1021/bi100157u

125. Sen S, Webber PJ, West AB. Dependence of leucine-rich repeat kinase 2 (LRRK2) kinase activity on dimerization. *J Biol Chem*. 2009;284(52):36346-36356. doi:10.1074/jbc.M109.025437
126. Civiero L, Russo I, Bubacco L, Greggio E. Molecular Insights and Functional Implication of LRRK2 Dimerization. In: *Leucine-Rich Repeat Kinase 2 (LRRK2)*. Vol 14. ; 2017:107-121. doi:10.1007/978-3-319-49969-7_6
127. Islam MS, Moore DJ. Mechanisms of LRRK2-dependent neurodegeneration: Role of enzymatic activity and protein aggregation. *Biochem Soc Trans*. 2017;45(1):163-172. doi:10.1042/BST20160264
128. Berwick DC, Javaheri B, Wetzel A, et al. Pathogenic LRRK2 variants are gain-of-function mutations that enhance LRRK2-mediated repression of β-catenin signaling. *Mol Neurodegener*. 2017;12(1):9. doi:10.1186/s13024-017-0153-4
129. Lin CH, Tsai PI, Wu RM, Chien CT. LRRK2 G2019S mutation induces dendrite degeneration through mislocalization and phosphorylation of tau by recruiting autoactivated GSK3β. *J Neurosci*. 2010;30(39):13138-13149. doi:10.1523/JNEUROSCI.1737-10.2010
130. Okubadejo NU, Rizig M, Ojo OO, et al. Leucine rich repeat kinase 2 (LRRK2) GLY2019SER mutation is absent in a second cohort of Nigerian Africans with Parkinson disease. *PLoS One*. 2018;13(12):1-7. doi:10.1371/journal.pone.0207984
131. Cookson M. The role of leucine-rich repeat kinase 2 (LRRK2) in Parkinson's disease. *Nat Rev Neurosci*. 2010;11(12):791-797. doi:10.1038/nrn2935.The
132. West AB, Moore DJ, Biskup S, et al. Parkinson's disease-associated mutations in leucine-rich repeat kinase 2 augment kinase activity. *Proc Natl Acad Sci U S A*. 2005;102(46):16842-16847. doi:10.1073/pnas.0507360102
133. Lewis PA, Greggio E, Beilina A, Jain S, Baker A, Cookson MR. The R1441C mutation of LRRK2 disrupts GTP hydrolysis. *Biochem Biophys Res Commun*. 2007;357(3):668-671. doi:10.1016/j.bbrc.2007.04.006
134. West AB. Achieving neuroprotection with LRRK2 kinase inhibitors in Parkinson disease. *Exp Neurol*. 2017;298:236-245. doi:10.1016/j.expneurol.2017.07.019
135. Blauwendraat C, Reed X, Kia DA, et al. Frequency of loss of function variants in LRRK2 in Parkinson disease. *JAMA Neurol*. 2018;75(11):1416-1422. doi:10.1001/jamaneurol.2018.1885
136. Steger M, Tonelli F, Ito G, et al. Phosphoproteomics reveals that Parkinson's disease kinase LRRK2 regulates a subset of Rab GTPases. *Elife*. 2016;5(JANUARY2016):1-28. doi:10.7554/eLife.12813.001
137. Sheng Z, Zhang S, Bustos D, et al. Ser1292 autophosphorylation is an indicator of LRRK2 kinase activity and contributes to the cellular effects of PD mutations. *Sci Transl Med*. 2012;4(164). doi:10.1126/scitranslmed.3004485
138. Civiero L, Cogo S, Biosa A, Greggio E. The role of LRRK2 in cytoskeletal dynamics. *Biochem Soc Trans*. 2018;46(6):1653-1663. doi:10.1042/BST20180469
139. Zhao Y, Dzamko N. Recent Developments in LRRK2-Targeted Therapy for Parkinson's Disease. *Drugs*. 2019;79(10):1037-1051. doi:10.1007/s40265-019-01139-4
140. Greggio E, Jain S, Kingsbury A, et al. Kinase activity is required for the toxic effects of mutant LRRK2/dardarin. *Neurobiol Dis*. 2006;23(2):329-341. doi:10.1016/j.nbd.2006.04.001
141. Plowey ED, Cherra SJ, Liu YJ, Chu CT. Role of autophagy in G2019S-LRRK2-associated neurite shortening in differentiated SH-SY5Y cells. *J Neurochem*. 2008;105(3):1048-1056. doi:10.1111/j.1471-4159.2008.05217.x
142. Albanese F, Novello S, Morari M. Autophagy and LRRK2 in the Aging Brain. *Front Neurosci*. 2019;13(December):1-23. doi:10.3389/fnins.2019.01352
143. Atashrazm F, Dzamko N. LRRK2 inhibitors and their potential in the treatment of Parkinson's disease: current perspectives. *Clin Pharmacol*. 2016;8:177-189. doi:10.2147/CPAA.S102191
144. Harvey K, Outeiro TF. The role of LRRK2 in cell signalling. *Biochem Soc Trans*. 2018;47(1):197-207. doi:10.1042/BST20180464
145. Greggio E, Zambrano I, Kaganovich A, et al. The Parkinson disease-associated leucine-rich repeat kinase 2 (LRRK2) is a dimer that undergoes intramolecular autophosphorylation. *J Biol Chem*. 2008;283(24):16906-16914. doi:10.1074/jbc.M708718200
146. Li X, Moore DJ, Xiong Y, Dawson TM, Dawson VL. Reevaluation of phosphorylation sites in the parkinson disease-associated leucine-rich repeat kinase 2. *J Biol Chem*. 2010;285(38):29569-29576. doi:10.1074/jbc.M110.127639
147. De Wit T, Baekelandt V, Lobbestael E. LRRK2 Phosphorylation: Behind the Scenes. *Neuroscientist*. 2018;24(5):486-500. doi:10.1177/1073858418756309
148. Athanasopoulos PS, Heumann R, Kortholt A. The role of (auto)-phosphorylation in the complex activation mechanism of LRRK2. *Biol Chem*. 2018;399(7):643-647. doi:10.1515/hsz-2017-0332

149. Hutagalung AH, Novick PJ. Role of Rab GTPases in membrane traffic and cell physiology. *Physiol Rev*. 2011;91(1):119-149. doi:10.1152/physrev.00059.2009
150. Stenmark H. Rab GTPases as coordinators of vesicle traffic. *Nat Rev Mol Cell Biol*. 2009;10(8):513-525. doi:10.1038/nrm2728
151. Madero-Pérez J, Fdez E, Fernández B, et al. Cellular effects mediated by pathogenic LRRK2: Homing in on Rab-mediated processes. *Biochem Soc Trans*. 2017;45(1):147-154. doi:10.1042/BST20160392
152. MacLeod DA, Rhinn H, Kuwahara T, et al. RAB7L1 Interacts with LRRK2 to Modify Intraneuronal Protein Sorting and Parkinson's Disease Risk. *Neuron*. 2013;77(3):425-439. doi:10.1016/j.neuron.2012.11.033
153. Manzoni C, Mamais A, Dihanich S, et al. Pathogenic parkinson's disease mutations across the functional domains of LRRK2 alter the autophagic/lysosomal response to starvation. *Biochem Biophys Res Commun*. 2013;441(4):862-866. doi:10.1016/j.bbrc.2013.10.159
154. Roosen DA, Cookson MR. LRRK2 at the interface of autophagosomes, endosomes and lysosomes. *Mol Neurodegener*. 2016;11(1):1-10. doi:10.1186/s13024-016-0140-1
155. Purlyte E, Dhekne HS, Sarhan AR, et al. Rab29 activation of the Parkinson's disease-associated LRRK 2 kinase. *EMBO J*. 2019;38(2):101237. doi:10.15252/embj.2018101237
156. Steger M, Diez F, Dhekne HS, et al. Systematic proteomic analysis of LRRK2-mediated rab GTPase phosphorylation establishes a connection to ciliogenesis. *Elife*. 2017;6(i):1-22. doi:10.7554/eLife.31012
157. Pfeffer SR. LRRK2 and Rab GTPases. *Biochem Soc Trans*. 2018;46(6):1707-1712. doi:10.1042/BST20180470
158. Feldmann A, Bekbulat F, Huesmann H, et al. The RAB GTPase RAB18 modulates macroautophagy and proteostasis. *Biochem Biophys Res Commun*. 2017;486(3):738-743. doi:10.1016/j.bbrc.2017.03.112
159. Langemeyer L, Fröhlich F, Ungermann C. Rab GTPase Function in Endosome and Lysosome Biogenesis. *Trends Cell Biol*. 2018;28(11):957-970. doi:10.1016/j.tcb.2018.06.007
160. Ao X, Zou L, Wu Y. Regulation of autophagy by the Rab GTPase network. *Cell Death Differ*. 2014;21(3):348-358. doi:10.1038/cdd.2013.187
161. Nixon-Abell J, Berwick DC, Harvey K. L'RRK de Triomphe: A solution for LRRK2 GTPase activity? *Biochem Soc Trans*. 2016;44(6):1625-1634. doi:10.1042/BST20160240
162. Deyaert E, Wauters L, Guaitoli G, et al. A homologue of the Parkinson's disease-associated protein LRRK2 undergoes a monomer-dimer transition during GTP turnover. *Nat Commun*. 2017;8(1):1-12. doi:10.1038/s41467-017-01103-4
163. Liu Z, Bryant N, Kumaran R, et al. LRRK2 phosphorylates membrane-bound Rabs and is activated by GTP-bound Rab7L1 to promote recruitment to the trans-Golgi network. *Hum Mol Genet*. 2018;27(2):385-395. doi:10.1093/hmg/ddx410
164. Chen J, Chen Y, Pu J. Leucine-Rich Repeat Kinase 2 in Parkinson's Disease: Updated from Pathogenesis to Potential Therapeutic Target. *Eur Neurol*. 2018;79(5-6):256-265. doi:10.1159/000488938
165. Hakimi M, Selvanantham T, Swinton E, et al. Parkinson's disease-linked LRRK2 is expressed in circulating and tissue immune cells and upregulated following recognition of microbial structures. *J Neural Transm*. 2011;118(5):795-808. doi:10.1007/s00702-011-0653-2
166. Thévenet J, Gobert R, van Huijsduijnen RH, Wiessner C, Sagot YJ. Regulation of LRRK2 expression points to a functional role in human monocyte maturation. *PLoS One*. 2011;6(6). doi:10.1371/journal.pone.0021519
167. Dzamko N, Inesta-Vaquera F, Zhang J, et al. The IkappaB kinase family phosphorylates the Parkinson's disease kinase LRRK2 at Ser935 and Ser910 during Toll-Like Receptor signaling. *PLoS One*. 2012;7(6). doi:10.1371/journal.pone.0039132
168. Pennington K, Chan T, Torres M, Andersen J. The dynamic and stress-adaptive signaling hub of 14-3-3: emerging mechanisms of regulation and context-dependent protein–protein interactions. *Oncogene*. 2018;37(42):5587-5604. doi:10.1038/s41388-018-0348-3
169. Muda K, Bertinetti D, Gesellchen F, et al. Parkinson-related LRRK2 mutation R1441C/G/H impairs PKA phosphorylation of LRRK2 and disrupts its interaction with 14-3-3. *Proc Natl Acad Sci U S A*. 2014;111(1). doi:10.1073/pnas.1312701111
170. Dzamko N, Deak M, Hentati F, et al. Inhibition of LRRK2 kinase activity leads to dephosphorylation of Ser 910/Ser935, disruption of 14-3-3 binding and altered cytoplasmic localization. *Biochem J*. 2010;430(3):405-413. doi:10.1042/BJ20100784
171. Lavalley NJ, Slone SR, Ding H, West AB, Yacoubian TA. 14-3-3 Proteins regulate mutant LRRK2 kinase activity and neurite shortening. *Hum Mol Genet*. 2016;25(1):109-122. doi:10.1093/hmg/ddv453
172. Di Maio R, Hoffman EK, Rocha EM, et al. LRRK2 activation in idiopathic Parkinson's disease (PLA). *Sci Transl Med*. 2018;10(451):eaar5429. doi:10.1126/scitranslmed.aar5429
173. Cogo S, Greggio E, Lewis PA. Leucine Rich Repeat Kinase 2: beyond Parkinson's and beyond kinase

inhibitors. *Expert Opin Ther Targets*. 2017;21(8):751-753. doi:10.1080/14728222.2017.1342968

174. Hatcher JM, Choi HG, Alessi DR, Gray NS. Small-Molecule Inhibitors of LRRK2. In: Vol 14. ; 2017:241-264. doi:10.1007/978-3-319-49969-7_13
175. Schapansky J, Khasnavis S, DeAndrade MP, et al. Familial knockin mutation of LRRK2 causes lysosomal dysfunction and accumulation of endogenous insoluble α-synuclein in neurons. *Neurobiol Dis*. 2018;111(December 2017):26-35. doi:10.1016/j.nbd.2017.12.005
176. Bonello F, Hassoun SM, Mouton-Liger F, et al. LRRK2 impairs PINK1/Parkin-dependent mitophagy via its kinase activity: Pathologic insights into Parkinson's disease. *Hum Mol Genet*. 2019;28(10):1645-1660. doi:10.1093/hmg/ddz004
177. Li T, He X, Thomas JM, et al. A novel GTP-binding inhibitor, FX2149, attenuates LRRK2 toxicity in Parkinson's disease models. *PLoS One*. 2015;10(3):1-15. doi:10.1371/journal.pone.0122461
178. Thomas JM, Li T, Yang W, Xue F, Fishman PS, Smith WW. 68 and FX2149 attenuate mutant LRRK2-R1441C-induced neural transport impairment. *Front Aging Neurosci*. 2017;8(JAN):1-11. doi:10.3389/fnagi.2016.00337
179. Li T, Yang D, Zhong S, et al. Novel LRRK2 GTP-binding inhibitors reduced degeneration in Parkinson's disease cell and mouse models. *Hum Mol Genet*. 2014;23(23):6212-6222. doi:10.1093/hmg/ddu341
180. Lewis P a, Manzoni C. LRRK2 and human disease: a complicated question or a question of complexes? *Sci Signal*. 2012;5(207):pe2. doi:10.1126/scisignal.2002680
181. Wallings R, Manzoni C, Bandopadhyay R. Cellular processes associated with LRRK2 function and dysfunction. *FEBS J*. 2015;282(15):2806-2826. doi:10.1111/febs.13305
182. Cookson MR, Hardy J, Lewis PA. Genetic neuropathology of Parkinson's disease. *Int J Clin Exp Pathol*. 2008;1(3):217-231.
183. Salašová A, Yokota C, Potěšil D, Zdráhal Z, Bryja V, Arenas E. A proteomic analysis of LRRK2 binding partners reveals interactions with multiple signaling components of the WNT/PCP pathway. *Mol Neurodegener*. 2017;12(1):54. doi:10.1186/s13024-017-0193-9
184. Kawakami F, Shimada N, Ohta E, et al. Leucine-rich repeat kinase 2 regulates tau phosphorylation through direct activation of glycogen synthase kinase-3β. *FEBS J*. 2014;281(1):3-13. doi:10.1111/febs.12579
185. Sato A, Yamamoto H, Sakane H, Koyama H, Kikuchi A. Wnt5a regulates distinct signalling pathways by binding to Frizzled2. *EMBO J*. 2010;29(1):41-54. doi:10.1038/emboj.2009.322
186. Berwick DC, Harvey K. The regulation and deregulation of Wnt signaling by PARK genes in health and disease. *J Mol Cell Biol*. 2014;6(1):3-12. doi:10.1093/jmcb/mjt037
187. Berwick DC, Harvey K. The importance of Wnt signalling for neurodegeneration in Parkinson's disease. *Biochem Soc Trans*. 2012;40(5):1123-1128. doi:10.1042/BST20120122
188. Alves dos Santos MTM, Smidt MP. En1 and Wnt signaling in midbrain dopaminergic neuronal development. *Neural Dev*. 2011;6(1):23. doi:10.1186/1749-8104-6-23
189. Sancho RM, Law BMH, Harvey K. Mutations in the LRRK2 Roc-COR tandem domain link Parkinson's disease to Wnt signalling pathways. *Hum Mol Genet*. 2009;18(20):3955-3968. doi:10.1093/hmg/ddp337
190. Pellegrini L, Wetzel A, Grannó S, Heaton G, Harvey K. Back to the tubule: microtubule dynamics in Parkinson's disease. *Cell Mol Life Sci*. 2017;74(3):409-434. doi:10.1007/s00018-016-2351-6
191. Godena VK, Brookes-Hocking N, Moller A, et al. Increasing microtubule acetylation rescues axonal transport and locomotor deficits caused by LRRK2 Roc-COR domain mutations. *Nat Commun*. 2014;5:1-11. doi:10.1038/ncomms6245
192. Ramírez MB, Lara Ordóñez AJ, Fdez E, Hilfiker S. LRRK2: From kinase to GTPase to microtubules and back. *Biochem Soc Trans*. 2017;45(1):141-146. doi:10.1042/BST20160333
193. Dhekne HS, Yanatori I, Gomez RC, et al. A pathway for parkinson's disease LRRK2 kinase to block primary cilia and sonic hedgehog signaling in the brain. *Elife*. 2018;7:1-26. doi:10.7554/eLife.40202
194. Madero-Pérez J, Fdez E, Fernández B, et al. Parkinson disease-associated mutations in LRRK2 cause centrosomal defects via Rab8a phosphorylation. *Mol Neurodegener*. 2018;13(1):3. doi:10.1186/s13024-018-0235-y
195. Fdez E, Fernández B, Lobbestael E, et al. RAB7L1-Mediated Relocalization of LRRK2 to the Golgi Complex Causes Centrosomal Deficits via RAB8A. *Front Mol Neurosci*. 2018;11(November):1-19. doi:10.3389/fnmol.2018.00417
196. Schraen-Maschke S, Sergeant N, Dhaenens CM, et al. Tau as a biomarker of neurodegenerative diseases. *Biomark Med*. 2008;2(4):363-384. doi:10.2217/17520363.2.4.363
197. Iqbal K, Liu F, Gong C-X, Grundke-Iqbal I. Tau in Alzheimer disease and related tauopathies. *Curr Alzheimer Res*. 2010;7(8):656-664. doi:10.2174/156720510793611592

198. Houlden H, Singleton AB. The genetics and neuropathology of Parkinson's disease. *Acta Neuropathol*. 2012;124(3):325-338. doi:10.1007/s00401-012-1013-5
199. Khan NL, Jain S, Lynch JM, et al. Mutations in the gene LRRK2 encoding dardarin (PARK8) cause familial Parkinson's disease: Clinical, pathological, olfactory and functional imaging and genetic data. *Brain*. 2005;128(12):2786-2796. doi:10.1093/brain/awh667
200. Melrose HL, Dächsel JC, Behrouz B, et al. Impaired dopaminergic neurotransmission and microtubule-associated protein tau alterations in human LRRK2 transgenic mice. *Neurobiol Dis*. 2010;40(3):503-517. doi:10.1016/j.nbd.2010.07.010
201. Kawakami F, Yabata T, Ohta E, et al. LRRK2 phosphorylates tubulin-associated tau but not the free molecule: LRRK2-mediated regulation of the tau-tubulin association and neurite outgrowth. *PLoS One*. 2012;7(1):1-9. doi:10.1371/journal.pone.0030834
202. Li Y, Liu W, Oo TF, et al. Mutant LRRK2 R1441G BAC transgenic mice recapitulate cardinal features of Parkinson's disease. *Nat Neurosci*. 2009;12(7):826-828. doi:10.1038/nn.2349
203. Tapia-Rojas C, Inestrosa NC. Loss of canonical Wnt signaling is involved in the pathogenesis of Alzheimer's disease. *Neural Regen Res*. 2018;13(10):1705-1710. doi:10.4103/1673-5374.238606
204. Guerreiro PS, Gerhardt E, Lopes da Fonseca T, Bähr M, Outeiro TF, Eckermann K. LRRK2 Promotes Tau Accumulation, Aggregation and Release. *Mol Neurobiol*. 2016;53(5):3124-3135. doi:10.1007/s12035-015-9209-z
205. Hsieh CH, Shaltouki A, Gonzalez AE, et al. Functional Impairment in Miro Degradation and Mitophagy Is a Shared Feature in Familial and Sporadic Parkinson's Disease. *Cell Stem Cell*. 2016;19(6):709-724. doi:10.1016/j.stem.2016.08.002
206. Angeles DC, Gan BH, Onstead L, et al. Mutations in LRRK2 increase phosphorylation of peroxiredoxin 3 exacerbating oxidative stress-induced neuronal death. *Hum Mutat*. 2011;32(12):1390-1397. doi:10.1002/humu.21582
207. Angeles DC, Ho P, Chua LL, et al. Thiol peroxidases ameliorate LRRK2 mutant-induced mitochondrial and dopaminergic neuronal degeneration in Drosophila. *Hum Mol Genet*. 2014;23(12):3157-3165. doi:10.1093/hmg/ddu026
208. Karuppagounder SS, Xiong Y, Lee Y, et al. LRRK2 G2019S transgenic mice display increased susceptibility to 1-methyl-4-phenyl-1,2,3,6-tetrahydropyridine (MPTP)-mediated neurotoxicity. *J Chem Neuroanat*. 2016;76(2015):90-97. doi:10.1016/j.jchemneu.2016.01.007
209. Cooper O, Seo H, Andrabi S, et al. Pharmacological rescue of mitochondrial deficits in iPSC-derived neural cells from patients with familial Parkinson's disease. *Sci Transl Med*. 2012;4(141). doi:10.1126/scitranslmed.3003985
210. Nguyen HN, Byers B, Cord B, et al. LRRK2 mutant iPSC-derived da neurons demonstrate increased susceptibility to oxidative stress. *Cell Stem Cell*. 2011;8(3):267-280. doi:10.1016/j.stem.2011.01.013
211. Schwarz DS, Blower MD. The endoplasmic reticulum: Structure, function and response to cellular signaling. *Cell Mol Life Sci*. 2016;73(1):79-94. doi:10.1007/s00018-015-2052-6
212. Tsujii S, Ishisaka M, Hara H. Modulation of endoplasmic reticulum stress in Parkinson's disease. *Eur J Pharmacol*. 2015;765:154-156. doi:10.1016/j.ejphar.2015.08.033
213. Vitte J, Traver S, Maués De Paula A, et al. Leucine-rich repeat kinase 2 is associated with the endoplasmic reticulum in dopaminergic neurons and accumulates in the core of Lewy bodies in Parkinson disease. *J Neuropathol Exp Neurol*. 2010;69(9):959-972. doi:10.1097/NEN.0b013e3181efc01c
214. Klein AD, Mazzulli JR. Is Parkinson's disease a lysosomal disorder? *Brain*. 2018;141(8):2255-2262. doi:10.1093/brain/awy147
215. Henry AG, Aghamohammadzadeh S, Samaroo H, et al. Pathogenic LRRK2 mutations, through increased kinase activity, produce enlarged lysosomes with reduced degradative capacity and increase ATP13A2 expression. *Hum Mol Genet*. 2015;24(21):6013-6028. doi:10.1093/hmg/ddv314
216. Hockey LN, Kilpatrick BS, Eden ER, et al. Dysregulation of lysosomal morphology by pathogenic LRRK2 is corrected by TPC2 inhibition. *J Cell Sci*. 2015;128(2):232-238. doi:10.1242/jcs.164152
217. Tong Y, Yamaguchi H, Giaime E, et al. Loss of leucine-rich repeat kinase 2 causes impairment of protein degradation pathways, accumulation of α-synuclein, and apoptotic cell death in aged mice. *Proc Natl Acad Sci U S A*. 2010;107(21):9879-9884. doi:10.1073/pnas.1004676107
218. Eguchi T, Kuwahara T, Sakurai M, et al. LRRK2 and its substrate Rab GTPases are sequentially targeted onto stressed lysosomes and maintain their homeostasis. *Proc Natl Acad Sci*. 2018;115(39):E9115-E9124. doi:10.1073/pnas.1812196115
219. Herbst S, Campbell P, Harvey J, et al. LRRK 2 activation controls the repair of damaged endomembranes in

macrophages . *EMBO J*. 2020;39(18):1-14. doi:10.15252/embj.2020104494

220. Bonet-Ponce L, Beilina A, Williamson CD, et al. LRRK2 mediates tubulation and vesicle sorting from lysosomes. *Sci Adv*. 2020;6(46):1-15. doi:10.1126/sciadv.abb2454
221. Piccoli G, Condliffe SB, Bauer M, et al. LRRK2 controls synaptic vesicle storage and mobilization within the recycling pool. *J Neurosci*. 2011;31(6):2225-2237. doi:10.1523/JNEUROSCI.3730-10.2011
222. Belluzzi E, Gonnelli A, Cirnaru MD, et al. LRRK2 phosphorylates pre-synaptic N-ethylmaleimide sensitive fusion (NSF) protein enhancing its ATPase activity and SNARE complex disassembling rate. *Mol Neurodegener*. 2016;11(1):1-16. doi:10.1186/s13024-015-0066-z
223. Migheli R, Del Giudice MG, Spissu Y, et al. LRRK2 Affects Vesicle Trafficking, Neurotransmitter Extracellular Level and Membrane Receptor Localization. *PLoS One*. 2013;8(10). doi:10.1371/journal.pone.0077198
224. Beccano-Kelly DA, Kuhlmann N, Tatarnikov I, et al. Synaptic function is modulated by LRRK2 and glutamate release is increased in cortical neurons of G2019S LRRK2 knock-in mice. *Front Cell Neurosci*. 2014;8(SEP):1-11. doi:10.3389/fncel.2014.00301
225. Piccoli G, Onofri F, Cirnaru MD, et al. Leucine-Rich Repeat Kinase 2 Binds to Neuronal Vesicles through Protein Interactions Mediated by Its C-Terminal WD40 Domain. *Mol Cell Biol*. 2014;34(12):2147-2161. doi:10.1128/mcb.00914-13
226. Cirnaru MD, Marte A, Belluzzi E, et al. LRRK2 kinase activity regulates synaptic vesicle trafficking and neurotransmitter release through modulation of LRRK2 macro-molecular complex. *Front Mol Neurosci*. 2014;7(MAY):1-12. doi:10.3389/fnmol.2014.00049
227. Matta S, Van Kolen K, da Cunha R, et al. LRRK2 Controls an EndoA Phosphorylation Cycle in Synaptic Endocytosis. *Neuron*. 2012;75(6):1-15. doi:10.1016/j.neuron.2012.08.022
228. Bedford C, Sears C, Perez-Carrion M, Piccoli G, Condliffe SB. LRRK2 Regulates Voltage-Gated Calcium Channel Function. *Front Mol Neurosci*. 2016;9(May):1-16. doi:10.3389/fnmol.2016.00035
229. Rassu M, Del Giudice MG, Sanna S, et al. Role of LRRK2 in the regulation of dopamine receptor trafficking. *PLoS One*. 2017;12(6):1-22. doi:10.1371/journal.pone.0179082
230. Parisiadou L, Yu J, Sgobio C, et al. LRRK2 regulates synaptogenesis and dopamine receptor activation through modulation of PKA activity. *Nat Neurosci*. 2014;17(3):367-376. doi:10.1038/nn.3636
231. Wallings RL, Tansey MG. LRRK2 regulation of immune-pathways and inflammatory disease. *Biochem Soc Trans*. 2019;47(6):1581-1595. doi:10.1042/BST20180463
232. Gardet A, Benita Y, Li C, et al. LRRK2 Is Involved in the IFN-γ Response and Host Response to Pathogens. *J Immunol*. 2010;185(9):5577-5585. doi:10.4049/jimmunol.1000548
233. Schapansky J, Nardozzi JD, Felizia F, LaVoie MJ. Membrane recruitment of endogenous LRRK2 precedes its potent regulation of autophagy. *Hum Mol Genet*. 2014;23(16):4201-4214. doi:10.1093/hmg/ddu138
234. Wang D, Xu L, Lv L, et al. Association of the LRRK2 genetic polymorphisms with leprosy in Han Chinese from Southwest China. *Genes Immun*. 2015;16(2):112-119. doi:10.1038/gene.2014.72
235. Wang Z, Arat S, Magid-Slav M, Brown JR. Meta-analysis of human gene expression in response to Mycobacterium tuberculosis infection reveals potential therapeutic targets. *BMC Syst Biol*. 2018;12(1):1-18. doi:10.1186/s12918-017-0524-z
236. Zhang F-R, Huang W, Chen S-M, et al. Genomewide Association Study of Leprosy. *N Engl J Med*. 2009;361(27):2609-2618. doi:10.1056/NEJMoa0903753
237. Russo I, Berti G, Plotegher N, et al. Leucine-rich repeat kinase 2 positively regulates inflammation and down-regulates NF-κB p50 signaling in cultured microglia cells. *J Neuroinflammation*. 2015;12(1):1-13. doi:10.1186/s12974-015-0449-7
238. Lopez de Maturana R, Aguila JC, Sousa A, et al. Leucine-rich repeat kinase 2 modulates cyclooxygenase 2 and the inflammatory response in idiopathic and genetic Parkinson's disease. *Neurobiol Aging*. 2014;35(5):1116-1124. doi:10.1016/j.neurobiolaging.2013.11.018
239. López de Maturana R, Lang V, Zubiarrain A, et al. Mutations in LRRK2 impair NF-KB pathway in iPSC-derived neurons. *J Neuroinflammation*. 2016;13(1):1-15. doi:10.1186/s12974-016-0761-x
240. Kim B, Yang MS, Choi D, et al. Impaired inflammatory responses in murine lrrk2-knockdown brain microglia. *PLoS One*. 2012;7(4):1-12. doi:10.1371/journal.pone.0034693
241. Liu Z, Lee J, Krummey S, Lu W, Cai H, Lenardo MJ. The kinase LRRK2 is a regulator of the transcription factor NFAT that modulates the severity of inflammatory bowel disease. *Nat Immunol*. 2011;12(11):1063-1070. doi:10.1038/ni.2113
242. Moore DL, Goldberg JL. Multiple transcription factor families regulate axon growth and regeneration. *Dev Neurobiol*. 2011;71(12):1186-1211. doi:10.1002/dneu.20934
243. Moehle MS, Webber PJ, Tse T, et al. LRRK2 inhibition attenuates microglial inflammatory responses. *J*

Neurosci. 2012;32(5):1602-1611. doi:10.1523/JNEUROSCI.5601-11.2012

244. Cabezudo D, Baekelandt V, Lobbestael E. Multiple-Hit Hypothesis in Parkinson's Disease: LRRK2 and Inflammation. *Front Neurosci*. 2020;14(April). doi:10.3389/fnins.2020.00376
245. Yang Z, Klionsky DJ. Mammalian autophagy: Core molecular machinery and signaling regulation. *Curr Opin Cell Biol*. 2010;22(2):124-131. doi:10.1016/j.ceb.2009.11.014
246. Rabinowitz JD, White E. Autophagy and metabolism. *Science (80-)*. 2010;330(6009):1344-1348. doi:10.1126/science.1193497
247. Mizushima N, Komatsu M. Autophagy: Renovation of cells and tissues. *Cell*. 2011;147(4):728-741. doi:10.1016/j.cell.2011.10.026
248. Mizushima N, Levine B, Cuervo AM, Klionsky DJ. Autophagy fights disease through cellular self-digestion. *Nature*. 2008;451(7182):1069-1075. doi:10.1038/nature06639
249. Rubinsztein DC, Codogno P, Levine B. Autophagy modulation as a potential therapeutic target for diverse diseases. *Nat Rev Drug Discov*. 2012;11(9):709-730. doi:10.1038/nrd3802
250. Fraldi A, Klein AD, Medina DL, Settembre C. Brain Disorders Due to Lysosomal Dysfunction. *Annu Rev Neurosci*. 2016;39(1):277-295. doi:10.1146/annurev-neuro-070815-014031
251. Dikic I, Elazar Z. Mechanism and medical implications of mammalian autophagy. *Nat Rev Mol Cell Biol*. 2018;19(6):349-364. doi:10.1038/s41580-018-0003-4
252. Cheon SY, Kim H, Rubinsztein DC, Lee JE. Autophagy, Cellular Aging and Age-related Human Diseases. *Exp Neurobiol*. 2019;28(6):643-657. doi:10.5607/en.2019.28.6.643
253. Li WW, Li J, Bao JK. Microautophagy: Lesser-known self-eating. *Cell Mol Life Sci*. 2012;69(7):1125-1136. doi:10.1007/s00018-011-0865-5
254. Kaushik S, Bandyopadhyay U, Sridhar S, et al. Chaperone-mediated autophagy at a glance. *J Cell Sci*. 2011;124(4):495-499. doi:10.1242/jcs.073874
255. Feng Y, He D, Yao Z, Klionsky DJ. The machinery of macroautophagy. *Cell Res*. 2014;24(1):24-41. doi:10.1038/cr.2013.168
256. Klionsky DJ, Eskelinen EL. The vacuole versus the lysosome: When size matters. *Autophagy*. 2014;10(2):185-187. doi:10.4161/auto.27367
257. Komatsu M, Waguri S, Chiba T, et al. Loss of autophagy in the central nervous system causes neurodegeneration in mice. *Nature*. 2006;441(7095):880-884. doi:10.1038/nature04723
258. Webb JL, Ravikumar B, Atkins J, Skepper JN, Rubinsztein DC. α-synuclein Is Degraded by Both Autophagy and the Proteasome. *J Biol Chem*. 2003;278(27):25009-25013. doi:10.1074/jbc.M300227200
259. Stolz A, Ernst A, Dikic I. Cargo recognition and trafficking in selective autophagy. *Nat Cell Biol*. 2014;16(6):495-501. doi:10.1038/ncb2979
260. Itakura E, Mizushima N. Characterization of autophagosome formation site by a hierarchical analysis of mammalian Atg proteins. *Autophagy*. 2010;6(6):764-776. doi:10.4161/auto.6.6.12709
261. Bento CF, Renna M, Ghislat G, et al. Mammalian Autophagy: How Does It Work? *Annu Rev Biochem*. 2016;85(1):685-713. doi:10.1146/annurev-biochem-060815-014556
262. Axe EL, Walker SA, Manifava M, et al. Autophagosome formation from membrane compartments enriched in phosphatidylinositol 3-phosphate and dynamically connected to the endoplasmic reticulum. *J Cell Biol*. 2008;182(4):685-701. doi:10.1083/jcb.200803137
263. Mizushima N, Yoshimori T, Ohsumi Y. The Role of Atg Proteins in Autophagosome Formation. *Annu Rev Cell Dev Biol*. 2011;27(1):107-132. doi:10.1146/annurev-cellbio-092910-154005
264. Kabeya Y. LC3, a mammalian homologue of yeast Apg8p, is localized in autophagosome membranes after processing. *EMBO J*. 2000;19(21):5720-5728. doi:10.1093/emboj/19.21.5720
265. Polson HEJ, De Lartigue J, Rigden DJ, et al. Mammalian Atg18 (WIPI2) localizes to omegasome-anchored phagophores and positively regulates LC3 lipidation. *Autophagy*. 2010;6(4):506-522. doi:10.4161/auto.6.4.11863
266. Dooley HC, Razi M, Polson HEJ, Girardin SE, Wilson MI, Tooze SA. WIPI2 Links LC3 Conjugation with PI3P, Autophagosome Formation, and Pathogen Clearance by Recruiting Atg12-5-16L1. *Mol Cell*. 2014;55(2):238-252. doi:10.1016/j.molcel.2014.05.021
267. Tsuboyama K, Koyama-Honda I, Sakamaki Y, Koike M, Morishita H, Mizushima N. The ATG conjugation systems are important for degradation of the inner autophagosomal membrane. *Science (80-)*. 2016;354(6315):1036-1041. doi:10.1126/science.aaf6136
268. Pankiv S, Clausen TH, Lamark T, et al. p62/SQSTM1 binds directly to Atg8/LC3 to facilitate degradation of ubiquitinated protein aggregates by autophagy. *J Biol Chem*. 2007;282(33):24131-24145. doi:10.1074/jbc.M702824200

269. Fimia GM, Kroemer G, Piacentini M. Molecular mechanisms of selective autophagy. *Cell Death Differ*. 2013;20(1):1-2. doi:10.1038/cdd.2012.97
270. Nguyen TN, Padman BS, Usher J, Oorschot V, Ramm G, Lazarou M. Atg8 family LC3/GABARAP proteins are crucial for autophagosome-lysosome fusion but not autophagosome formation during PINK1/Parkin mitophagy and starvation. *J Cell Biol*. 2016;215(6):857-874. doi:10.1083/jcb.201607039
271. Itakura E, Kishi-Itakura C, Mizushima N. The hairpin-type tail-anchored SNARE syntaxin 17 targets to autophagosomes for fusion with endosomes/lysosomes. *Cell*. 2012;151(6):1256-1269. doi:10.1016/j.cell.2012.11.001
272. Han J, Pluhackova K, Böckmann RA. The multifaceted role of SNARE proteins in membrane fusion. *Front Physiol*. 2017;8(JAN). doi:10.3389/fphys.2017.00005
273. Jiang P, Nishimura T, Sakamaki Y, et al. The HOPS complex mediates autophagosome-lysosome fusion through interaction with syntaxin 17. *Mol Biol Cell*. 2014;25(8):1327-1337. doi:10.1091/mbc.E13-08-0447
274. McEwan DG, Popovic D, Gubas A, et al. PLEKHM1 regulates autophagosome-lysosome fusion through HOPS complex and LC3/GABARAP proteins. *Mol Cell*. 2015;57(1):39-54. doi:10.1016/j.molcel.2014.11.006
275. Lawrence RE, Zoncu R. The lysosome as a cellular centre for signalling, metabolism and quality control. *Nat Cell Biol*. 2019;21(2):133-142. doi:10.1038/s41556-018-0244-7
276. Saleeb RS, Kavanagh DM, Dun AR, Dalgarno PA, Duncan RR. A VPS33A-binding motif on syntaxin 17 controls autophagy completion in mammalian cells. *J Biol Chem*. 2019;294(11):4188-4201. doi:10.1074/jbc.RA118.005947
277. Schröder BA, Wrocklage C, Hasilik A, Saftig P. The proteome of lysosomes. *Proteomics*. 2010;10(22):4053-4076. doi:10.1002/pmic.201000196
278. Yu L, McPhee CK, Zheng L, et al. Termination of autophagy and reformation of lysosomes regulated by mTOR. *Nature*. 2010;465(7300):942-946. doi:10.1038/nature09076
279. Munson MJ, Allen GF, Toth R, Campbell DG, Lucocq JM, Ganley IG. mTOR activates the VPS 34– UVRAG complex to regulate autolysosomal tubulation and cell survival. *EMBO J*. 2015;34(17):2272-2290. doi:10.15252/embj.201590992
280. Chévrier M, Brakch N, Lesueur C, et al. Autophagosome maturation is impaired in Fabry disease. *Autophagy*. 2010;6(5):589-599. doi:10.4161/auto.6.5.11943
281. Kishi-Itakura C, Koyama-Honda I, Itakura E, Mizushima N. Correction to Ultrastructural analysis of autophagosome organization using mammalian autophagy-deficient cells [Journal of Cell Science, 2014, 127, 4089-4102]. *J Cell Sci*. 2014;127(22):4984. doi:10.1242/jcs.164293
282. Liang CC, Wang C, Peng X, Gan B, Guan JL. Neural-specific deletion of FIP200 leads to cerebellar degeneration caused by increased neuronal death and axon degeneration. *J Biol Chem*. 2010;285(5):3499-3509. doi:10.1074/jbc.M109.072389
283. Hara T, Nakamura K, Matsui M, et al. Suppression of basal autophagy in neural cells causes neurodegenerative disease in mice. *Nature*. 2006;441(7095):885-889. doi:10.1038/nature04724
284. Saxton RA, Sabatini DM. mTOR Signaling in Growth, Metabolism, and Disease. *Cell*. 2017;168(6):960-976. doi:10.1016/j.cell.2017.02.004
285. Sarbassov DD, Ali SM, Sabatini DM. Growing roles for the mTOR pathway. *Curr Opin Cell Biol*. 2005;17(6):596-603. doi:10.1016/j.ceb.2005.09.009
286. Wong M. Mammalian Target of Rapamycin (mTOR) Pathways in Neurological Diseases. *Biomed J*. 2013;36(2):40. doi:10.4103/2319-4170.110365
287. Meijer AJ, Lorin S, Blommaart EF, Codogno P. Regulation of autophagy by amino acids and MTOR-dependent signal transduction. *Amino Acids*. 2015;47(10):2037-2063. doi:10.1007/s00726-014-1765-4
288. Kim YC, Guan K. mTOR: a pharmacologic target for autophagy regulation. *J Clin Invest*. 2015;125(1):25-32. doi:10.1172/JCI73939
289. Korolchuk VI, Saiki S, Lichtenberg M, et al. Lysosomal positioning coordinates cellular nutrient responses. *Nat Cell Biol*. 2011;13(4):453-462. doi:10.1038/ncb2204
290. Sancak Y, Bar-Peled L, Zoncu R, Markhard AL, Nada S, Sabatini DM. Ragulator-rag complex targets mTORC1 to the lysosomal surface and is necessary for its activation by amino acids. *Cell*. 2010;141(2):290-303. doi:10.1016/j.cell.2010.02.024
291. Zachari M, Ganley IG. The mammalian ULK1 complex and autophagy initiation. *Essays Biochem*. 2017;61(6):585-596. doi:10.1042/ebc20170021
292. Yuan HX, Russell RC, Guan KL. Regulation of PIK3C3/VPS34 complexes by MTOR in nutrient stress-induced autophagy. *Autophagy*. 2013;9(12):1983-1995. doi:10.4161/auto.26058
293. Sardiello M, Palmieri M, Ronza A Di, et al. A gene network regulating lysosomal biogenesis and function.

Science (80-). 2009;325(5939):473-477. doi:10.1126/science.1174447

294. Scotto Rosato A, Montefusco S, Soldati C, et al. TRPML1 links lysosomal calcium to autophagosome biogenesis through the activation of the CaMKKβ/VPS34 pathway. *Nat Commun*. 2019;10(1):5630. doi:10.1038/s41467-019-13572-w
295. Settembre C, Zoncu R, Medina DL, et al. A lysosome-to-nucleus signalling mechanism senses and regulates the lysosome via mTOR and TFEB. *EMBO J*. 2012;31(5):1095-1108. doi:10.1038/emboj.2012.32
296. Napolitano G, Esposito A, Choi H, et al. mTOR-dependent phosphorylation controls TFEB nuclear export. *Nat Commun*. 2018;9(1). doi:10.1038/s41467-018-05862-6
297. Kim J, Kundu M, Viollet B, Guan K-L. AMPK and mTOR regulate autophagy through direct phosphorylation of Ulk1. *Nat Cell Biol*. 2011;13(2):132-141. doi:10.1038/ncb2152
298. Hawley SA, Selbert MA, Goldstein EG, Edelman AM, Carling D, Hardie DG. 5'-AMP activates the AMP-activated protein kinase cascade, and Ca2+/calmodulin activates the calmodulin-dependent protein kinase I cascade, via three independent mechanisms. *J Biol Chem*. 1995;270(45):27186-27191. doi:10.1074/jbc.270.45.27186
299. Egan D, Kim J, Shaw RJ, Guan K-L. The autophagy initiating kinase ULK1 is regulated via opposing phosphorylation by AMPK and mTOR. *Autophagy*. 2011;7(6):643-644. doi:10.4161/auto.7.6.15123
300. Maday S, Holzbaur ELF. Autophagosome biogenesis in primary neurons follows an ordered and spatially regulated pathway. *Dev Cell*. 2014;30(1):71-85. doi:10.1016/j.devcel.2014.06.001
301. Shehata M, Matsumura H, Okubo-Suzuki R, Ohkawa N, Inokuchi K. Neuronal stimulation induces autophagy in hippocampal neurons that is involved in AMPA receptor degradation after chemical long-term depression. *J Neurosci*. 2012;32(30):10413-10422. doi:10.1523/JNEUROSCI.4533-11.2012
302. Okerlund ND, Schneider K, Leal-Ortiz S, et al. Erratum: Bassoon Controls Presynaptic Autophagy through Atg5 (Neuron (2017) 93(4) (897–913.e7)(S0896627317300508)(10.1016/j.neuron.2017.01.026)). *Neuron*. 2018;97(3):727. doi:10.1016/j.neuron.2018.01.010
303. Hernandez D, Torres CA, Setlik W, et al. Regulation of Presynaptic Neurotransmission by Macroautophagy. *Neuron*. 2012;74(2):277-284. doi:10.1016/j.neuron.2012.02.020
304. Shen W, Ganetzky B. Autophagy promotes synapse development in Drosophila. *J Cell Biol*. 2009;187(1):71-79. doi:10.1083/jcb.200907109
305. Ban B-K, Jun M-H, Ryu H-H, Jang D-J, Ahmad ST, Lee J-A. Autophagy Negatively Regulates Early Axon Growth in Cortical Neurons. *Mol Cell Biol*. 2013;33(19):3907-3919. doi:10.1128/mcb.00627-13
306. Gomez-Sanchez JA, Carty L, Iruarrizaga-Lejarreta M, et al. Schwann cell autophagy, myelinophagy, initiates myelin clearance from injured nerves. *J Cell Biol*. 2015;210(1):153-168. doi:10.1083/jcb.201503019
307. Jang SY, Shin YK, Park SY, et al. Autophagic myelin destruction by schwann cells during wallerian degeneration and segmental demyelination. *Glia*. 2016;64(5):730-742. doi:10.1002/glia.22957
308. Friedman LG, Lachenmayer ML, Wang J, et al. Disrupted autophagy leads to dopaminergic axon and dendrite degeneration and promotes presynaptic accumulation of α-synuclein and LRRK2 in the brain. *J Neurosci*. 2012;32(22):7585-7593. doi:10.1523/JNEUROSCI.5809-11.2012
309. Tsvetkov AS, Arrasate M, Barmada S, et al. Proteostasis of polyglutamine varies among neurons and predicts neurodegeneration. *Nat Chem Biol*. 2013;9(9):586-594. doi:10.1038/nchembio.1308
310. Fekadu J, Rami A. Beclin-1 Deficiency Alters Autophagosome Formation, Lysosome Biogenesis and Enhances Neuronal Vulnerability of HT22 Hippocampal Cells. *Mol Neurobiol*. 2016;53(8):5500-5509. doi:10.1007/s12035-015-9453-2
311. Lipinski MM, Zheng B, Lu T, et al. Genome-wide analysis reveals mechanisms modulating autophagy in normal brain aging and in Alzheimer's disease. *Proc Natl Acad Sci U S A*. 2010;107(32):14164-14169. doi:10.1073/pnas.1009485107
312. Cuervo AM, Bergamini E, Brunk UT, Dröge W, Ffrench M, Terman A. Autophagy and aging: the importance of maintaining "clean" cells. *Autophagy*. 2005;1(3):131-140. doi:10.4161/auto.1.3.2017
313. Boland B, Nixon RA. Neuronal macroautophagy: From development to degeneration. *Mol Aspects Med*. 2006;27(5-6):503-519. doi:10.1016/j.mam.2006.08.009
314. Bingol B. Autophagy and lysosomal pathways in nervous system disorders. *Mol Cell Neurosci*. 2018;91(December 2017):167-208. doi:10.1016/j.mcn.2018.04.009
315. Sun N, Youle RJ, Finkel T. The Mitochondrial Basis of Aging. *Mol Cell*. 2016;61(5):654-666. doi:10.1016/j.molcel.2016.01.028
316. Rezzani R, Stacchiotti A, Rodella LF. Morphological and biochemical studies on aging and autophagy. *Ageing Res Rev*. 2012;11(1):10-31. doi:10.1016/j.arr.2011.09.001
317. Vellai T. Autophagy genes and ageing. *Cell Death Differ*. 2009;16(1):94-102. doi:10.1038/cdd.2008.126

318. Cuervo AM, Dice JF. Age-related decline in chaperone-mediated autophagy. *J Biol Chem*. 2000;275(40):31505-31513. doi:10.1074/jbc.M002102200
319. Cuervo AM. Autophagy and aging: keeping that old broom working. *Trends Genet*. 2008;24(12):604-612. doi:10.1016/j.tig.2008.10.002
320. Petiot A, Pattingre S, Arico S, Meley D, Codogno P. Diversity of signaling controls of macroautophagy in mammalian cells. *Cell Struct Funct*. 2002;27(6):431-441. doi:10.1247/csf.27.431
321. Tanik SA, Schultheiss CE, Volpicelli-Daley LA, Brunden KR, Lee VMY. Lewy body-like α-synuclein aggregates resist degradation and impair macroautophagy. *J Biol Chem*. 2013;288(21):15194-15210. doi:10.1074/jbc.M113.457408
322. Rubinsztein DC, Mariño G, Kroemer G. Autophagy and aging. *Cell*. 2011;146(5):682-695. doi:10.1016/j.cell.2011.07.030
323. Hansen M, Rubinsztein DC, Walker DW. Autophagy as a promoter of longevity: insights from model organisms. *Nat Rev Mol Cell Biol*. 2018;19(9):579-593. doi:10.1038/s41580-018-0033-y
324. Bergamini E. Autophagy: A cell repair mechanism that retards ageing and age-associated diseases and can be intensified pharmacologically. *Mol Aspects Med*. 2006;27(5-6):403-410. doi:10.1016/j.mam.2006.08.001
325. Simonsen A, Cumming RC, Brech A, Isakson P, Schubert DR, Finley KD. Promoting basal levels of autophagy in the nervous system enhances longevity and oxidant resistance in adult Drosophila. *Autophagy*. 2008;4(2):176-184. doi:10.4161/auto.5269
326. Sepe S, Milanese C, Gabriels S, et al. Inefficient DNA Repair Is an Aging-Related Modifier of Parkinson's Disease. *Cell Rep*. 2016;15(9):1866-1875. doi:10.1016/j.celrep.2016.04.071
327. Menzies FM, Fleming A, Rubinsztein DC. Compromised autophagy and neurodegenerative diseases. *Nat Rev Neurosci*. 2015;16(6):345-357. doi:10.1038/nrn3961
328. Klionsky DJ, Abdelmohsen K, Abe A, et al. Guidelines for the use and interpretation of assays for monitoring autophagy (3rd edition). *Autophagy*. 2016;12(1):1-222. doi:10.1080/15548627.2015.1100356
329. Mizushima N, Yoshimori T, Levine B. Methods in Mammalian Autophagy Research. *Cell*. 2010;140(3):313-326. doi:10.1016/j.cell.2010.01.028
330. Cadwell K, Debnath J. Beyond self-eating: The control of nonautophagic functions and signaling pathways by autophagyrelated proteins. *J Cell Biol*. 2018;217(3):813-822. doi:10.1083/jcb.201706157
331. Jiang P, Mizushima N. LC3- and p62-based biochemical methods for the analysis of autophagy progression in mammalian cells. *Methods*. 2015;75:13-18. doi:10.1016/j.ymeth.2014.11.021
332. Wu YT, Tan HL, Shui G, et al. Dual role of 3-methyladenine in modulation of autophagy via different temporal patterns of inhibition on class I and III phosphoinositide 3-kinase. *J Biol Chem*. 2010;285(14):10850-10861. doi:10.1074/jbc.M109.080796
333. Mauthe M, Orhon I, Rocchi C, et al. Chloroquine inhibits autophagic flux by decreasing autophagosome-lysosome fusion. *Autophagy*. 2018;14(8):1435-1455. doi:10.1080/15548627.2018.1474314
334. Mauvezin C, Neufeld TP. Bafilomycin A1 disrupts autophagic flux by inhibiting both V-ATPase-dependent acidification and Ca-P60A/SERCA-dependent autophagosome-lysosome fusion. *Autophagy*. 2015;11(8):1437-1438. doi:10.1080/15548627.2015.1066957
335. L. Hebron M. Tyrosine Kinase Inhibition Regulates Early Systemic Immune Changes and Modulates the Neuroimmune Response in α-Synucleinopathy. *J Clin Cell Immunol*. 2014;05(05):30-33. doi:10.4172/2155-9899.1000259
336. Sarkar S, Davies JE, Huang Z, Tunnacliffe A, Rubinsztein DC. Trehalose, a novel mTOR-independent autophagy enhancer, accelerates the clearance of mutant huntingtin and α-synuclein. *J Biol Chem*. 2007;282(8):5641-5652. doi:10.1074/jbc.M609532200
337. Ylä-Anttila P, Vihinen H, Jokitalo E, Eskelinen EL. *Monitoring Autophagy by Electron Microscopy in Mammalian Cells*. Vol 451. 1st ed. Elsevier Inc.; 2009. doi:10.1016/S0076-6879(08)03610-0
338. Eskelinen EL. To be or not to be? Examples of incorrect identification of autophagic compartments in conventional transmission electron microscopy of mammalian cells. *Autophagy*. 2008;4(2):257-260. doi:10.4161/auto.5179
339. Eskelinen EL. Fine structure of the autophagosome. *Methods Mol Biol*. 2008;445(11):11-28. doi:10.1007/978-1-59745-157-4_2
340. Rai S, Manjithaya R. Fluorescence microscopy: A tool to study autophagy. *AIP Adv*. 2015;5(8):0-8. doi:10.1063/1.4928185
341. Yang KC, Sathiyaseelan P, Ho C, Gorski SM. Evolution of tools and methods for monitoring autophagic flux in mammalian cells. *Biochem Soc Trans*. 2018;46(1):97-110. doi:10.1042/BST20170102

342. Seglen PO, Luhr M, Mills IG, Sætre F, Szalai P, Engedal N. Macroautophagic cargo sequestration assays. *Methods*. 2015;75:25-36. doi:10.1016/j.ymeth.2014.12.021
343. Luhr M, Szalai P, Engedal N. The lactate dehydrogenase sequestration assay — A simple and reliable method to determine bulk autophagic sequestration activity in mammalian cells. *J Vis Exp*. 2018;2018(137):1-10. doi:10.3791/57971
344. Sammels E, Parys JB, Missiaen L, De Smedt H, Bultynck G. Intracellular Ca2+ storage in health and disease: A dynamic equilibrium. *Cell Calcium*. 2010;47(4):297-314. doi:10.1016/j.ceca.2010.02.001
345. Pinton P, Giorgi C, Siviero R, Zecchini E, Rizzuto R. Calcium and apoptosis: ER-mitochondria Ca2+ transfer in the control of apoptosis. *Oncogene*. 2008;27(50):6407-6418. doi:10.1038/onc.2008.308
346. Harr MW, Distelhorst CW. Apoptosis and autophagy: decoding calcium signals that mediate life or death. *Cold Spring Harb Perspect Biol*. 2010;2(10). doi:10.1101/cshperspect.a005579
347. Ringer S. A third contribution regarding the Influence of the Inorganic Constituents of the Blood on the Ventricular Contraction. *J Physiol*. 1883;4(2-3):222-225. doi:10.1113/jphysiol.1883.sp000127
348. Raffaello A, Mammucari C, Gherardi G, Rizzuto R. Calcium at the Center of Cell Signaling: Interplay between Endoplasmic Reticulum, Mitochondria, and Lysosomes. *Trends Biochem Sci*. 2016;41(12):1035-1049. doi:10.1016/j.tibs.2016.09.001
349. Berridge MJ, Lipp P, Bootman MD. The versatility and universality of calcium signalling. *Nat Rev Mol Cell Biol*. 2000;1(1):11-21. doi:10.1038/35036035
350. Parekh AB. Decoding cytosolic Ca2+ oscillations. *Trends Biochem Sci*. 2011;36(2):78-87. doi:10.1016/j.tibs.2010.07.013
351. Berridge MJ, Bootman MD, Roderick HL. Calcium signalling: dynamics, homeostasis and remodelling. *Nat Rev Mol Cell Biol*. 2003;4(7):517-529. doi:10.1038/nrm1155
352. Parekh AB. Calcium signalling in health and disease. *Semin Cell Dev Biol*. 2019;94(June):1-2. doi:10.1016/j.semcdb.2019.05.030
353. Bootman M. The endoplasmic reticulum is a focal point for co-ordination of cellular activity. *Cell Calcium*. 2002;32:231-234. doi:10.1016/s0143-4160(02)00200-2
354. Burgoyne T, Patel S, Eden ER. Calcium signaling at ER membrane contact sites. *Biochim Biophys Acta - Mol Cell Res*. 2014;1853(9):2012-2017. doi:10.1016/j.bbamcr.2015.01.022
355. Samtleben S, Jaepel J, Fecher C, Andreska T, Rehberg M, Blum R. Direct imaging of ER calcium with targeted-esterase induced dye loading (TED). *J Vis Exp*. 2013;(75):1-17. doi:10.3791/50317
356. Berridge MJ. The endoplasmic reticulum: A multifunctional signaling organelle. *Cell Calcium*. 2002;32(5-6):235-249. doi:10.1016/S0143416002001823
357. Munaron L. Shuffling the cards in signal transduction: Calcium, arachidonic acid and mechanosensitivity. *World J Biol Chem*. 2011;2(4):59. doi:10.4331/wjbc.v2.i4.59
358. Clapham DE. Calcium Signaling. *Cell*. 2007;131(6):1047-1058. doi:10.1016/j.cell.2007.11.028
359. Rizzuto R, Marchi S, Bonora M, et al. Ca2+ transfer from the ER to mitochondria: When, how and why. *Biochim Biophys Acta - Bioenerg*. 2009;1787(11):1342-1351. doi:10.1016/j.bbabio.2009.03.015
360. Santulli G, Nakashima R, Yuan Q, Marks AR. Intracellular calcium release channels: an update. *J Physiol*. 2017;595(10):3041-3051. doi:10.1113/JP272781
361. Elíes J, Yáñez M, Pereira TMC, Gil-Longo J, MacDougall DA, Campos-Toimil M. *Calcium Signaling (Book)*. Vol 1131. (Islam MS, ed.). Cham: Springer International Publishing; 2020. doi:10.1007/978-3-030-12457-1
362. Smyth JT, Hwang SY, Tomita T, DeHaven WI, Mercer JC, Putney JW. Activation and regulation of store-operated calcium entry. *J Cell Mol Med*. 2010;14(10):2337-2349. doi:10.1111/j.1582-4934.2010.01168.x
363. Prakriya M, Lewis RS. Store-operated calcium channels. *Physiol Rev*. 2015;95(4):1383-1436. doi:10.1152/physrev.00020.2014
364. Stathopulos PB, Ikura M. Store operated calcium entry: From concept to structural mechanisms. *Cell Calcium*. 2017;63:3-7. doi:10.1016/j.ceca.2016.11.005
365. Groschner K., Graier W.F., Romanin C. *Store-Operated Ca2+ Entry (SOCE) Pathways*. (Groschner K, Graier WF, Romanin C, eds.). Vienna: Springer Vienna; 2012. doi:10.1007/978-3-7091-0962-5
366. Brini M, Cali T, Ottolini D, Carafoli E. Calcium pumps: Why So many? *Compr Physiol*. 2012;2(2):1045-1060. doi:10.1002/cphy.c110034
367. Brini M, Carafoli E. The Plasma Membrane Ca2+ ATPase and the plasma membrane Sodium Calcium exchanger cooperate in the regulation of cell Calcium. *Cold Spring Harb Perspect Biol*. 2011;3(2):1-15. doi:10.1101/cshperspect.a004168
368. Cárdenas C, Miller RA, Smith I, et al. Essential Regulation of Cell Bioenergetics by Constitutive InsP3 Receptor Ca2+ Transfer to Mitochondria. *Cell*. 2010;142(2):270-283. doi:10.1016/j.cell.2010.06.007

369. Gellerich FN, Gizatullina Z, Trumbeckaite S, et al. The regulation of OXPHOS by extramitochondrial calcium. *Biochim Biophys Acta - Bioenerg*. 2010;1797(6-7):1018-1027. doi:10.1016/j.bbabio.2010.02.005
370. Hoppins S. The regulation of mitochondrial dynamics. *Curr Opin Cell Biol*. 2014;29(1):46-52. doi:10.1016/j.ceb.2014.03.005
371. Hansford RG, Zorov D. Role of mitochondrial calcium transport in the control of substrate oxidation. *Mol Cell Biochem*. 1998. doi:10.1007/978-1-4615-5653-4_23
372. Marchi S, Patergnani S, Pinton P. The endoplasmic reticulum–mitochondria connection: One touch, multiple functions. *Biochim Biophys Acta - Bioenerg*. 2014;1837(4):461-469. doi:10.1016/j.bbabio.2013.10.015
373. De Stefani D, Rizzuto R, Pozzan T. Enjoy the Trip: Calcium in Mitochondria Back and Forth. *Annu Rev Biochem*. 2016;85(1):161-192. doi:10.1146/annurev-biochem-060614-034216
374. Bravo R, Vicencio JM, Parra V, et al. Increased ER-mitochondrial coupling promotes mitochondrial respiration and bioenergetics during early phases of ER stress. *J Cell Sci*. 2011;124(14):2511. doi:10.1242/jcs.095455
375. Verfaillie T, Rubio N, Garg AD, et al. PERK is required at the ER-mitochondrial contact sites to convey apoptosis after ROS-based ER stress. *Cell Death Differ*. 2012;19(11):1880-1891. doi:10.1038/cdd.2012.74
376. Szabadkai G, Rizzuto R. how mitochondrial beauty translates into biological virtue. *Curr Opin Cell Biol*. 2013;25(4):477-482. doi:10.1016/j.ceb.2013.03.006
377. Gomes DA, Thompson M, Souto NC, et al. The type III inositol 1,4,5-trisphosphate receptor preferentially transmits apoptotic Ca2+ signals into mitochondria. *J Biol Chem*. 2005;280(49):40892-40900. doi:10.1074/jbc.M506623200
378. Friedman JR, Lackner LL, West M, DiBenedetto JR, Nunnari J, Voeltz GK. ER tubules mark sites of mitochondrial division. *Science (80-)*. 2011;334(6054):358-362. doi:10.1126/science.1207385
379. Hamasaki M, Furuta N, Matsuda A, et al. Autophagosomes form at ER-mitochondria contact sites. *Nature*. 2013;495(7441):389-393. doi:10.1038/nature11910
380. Ashrafi G, Schwarz TL. The pathways of mitophagy for quality control and clearance of mitochondria. *Cell Death Differ*. 2013;20(1):31-42. doi:10.1038/cdd.2012.81
381. Patel S, Docampo R. Acidic calcium stores open for business: expanding the potential for intracellular Ca2+ signaling. *Trends Cell Biol*. 2010;20(5):277-286. doi:10.1016/j.tcb.2010.02.003
382. Scott CC, Gruenberg J. Ion flux and the function of endosomes and lysosomes: pH is just the start. *BioEssays*. 2011;33(2):103-110. doi:10.1002/bies.201000108
383. Patel S, Muallem S. Acidic Ca2+ stores come to the fore. *Cell Calcium*. 2011;50(2):109-112. doi:10.1016/j.ceca.2011.03.009
384. Luzio JP, Pryor PR, Bright NA. Lysosomes: fusion and function. *Nat Rev Mol Cell Biol*. 2007;8(8):622-632. doi:10.1038/nrm2217
385. Galione A. A primer of NAADP-mediated Ca2+ signalling: From sea urchin eggs to mammalian cells. *Cell Calcium*. 2015;58(1):27-47. doi:10.1016/j.ceca.2014.09.010
386. Morgan AJ, Platt FM, Lloyd-Evans E, Galione A. Molecular mechanisms of endolysosomal Ca2+ signalling in health and disease. *Biochem J*. 2011;439(3):349-378. doi:10.1042/BJ20110949
387. Patel S, Ramakrishnan L, Rahman T, et al. The endo-lysosomal system as an NAADP-sensitive acidic Ca2+ store: Role for the two-pore channels. *Cell Calcium*. 2011;50(2):157-167. doi:10.1016/j.ceca.2011.03.011
388. Appelqvist H, Wäster P, Kågedal K, Öllinger K. The lysosome: From waste bag to potential therapeutic target. *J Mol Cell Biol*. 2013;5(4):214-226. doi:10.1093/jmcb/mjt022
389. Lloyd-Evans E. Acidic Ca 2 + Stores in Neurodegeneration. *Messenger*. 2016;5(1):37-55. doi:10.1166/msr.2016.1054
390. Pryor PR, Mullock BM, Bright NA, Gray SR, Luzio JP. The Role of Intraorganellar Ca2+In Late Endosome–Lysosome Heterotypic Fusion and in the Reformation of Lysosomes from Hybrid Organelles. *J Cell Biol*. 2000;149(5):1053-1062. doi:10.1083/jcb.149.5.1053
391. Wallings R, Connor-Robson N, Wade-Martins R. LRRK2 interacts with the vacuolar-type H+-ATPase pump a1 subunit to regulate lysosomal function. *Hum Mol Genet*. 2019;28(16):2696-2710. doi:10.1093/hmg/ddz088
392. Lu Y, Hao BX, Graeff R, Wong CWM, Wu WT, Yue J. Two pore channel 2 (TPC2) inhibits autophagosomal-lysosomal fusion by alkalinizing lysosomal pH. *J Biol Chem*. 2013;288(33):24247-24263. doi:10.1074/jbc.M113.484253
393. Lin PH, Duann P, Komazaki S, et al. Lysosomal two-pore channel subtype 2 (TPC2) regulates skeletal muscle autophagic signaling. *J Biol Chem*. 2015;290(6):3377-3389. doi:10.1074/jbc.M114.608471

394. Lloyd-Evans E, Morgan AJ, He X, et al. Niemann-Pick disease type C1 is a sphingosine storage disease that causes deregulation of lysosomal calcium. *Nat Med*. 2008;14(11):1247-1255. doi:10.1038/nm.1876
395. Gerasimenko J V., Lur G, Sherwood MW, et al. Pancreatic protease activation by alcohol metabolite depends on Ca 2+ release via acid store IP3 receptors. *Proc Natl Acad Sci U S A*. 2009;106(26):10758-10763. doi:10.1073/pnas.0904818106
396. Guse AH, Lee HC. NAADP: A Universal Ca2+ Trigger. *Sci Signal*. 2008;1(44):re10-re10. doi:10.1126/scisignal.144re10
397. Calcraft PJ, Ruas M, Pan Z, et al. NAADP mobilizes calcium from acidic organelles through two-pore channels. *Nature*. 2009;459(7246):596-600. doi:10.1038/nature08030
398. Lin-Moshier Y, Walseth TF, Churamani D, et al. Photoaffinity labeling of nicotinic acid adenine dinucleotide phosphate (NAADP) targets in mammalian cells. *J Biol Chem*. 2012;287(4):2296-2307. doi:10.1074/jbc.M111.305813
399. Marchant JS, Lin-Moshier Y, Walseth TF, Patel S. The Molecular Basis for Ca2+ Signalling by NAADP: Two-Pore Channels in a Complex? *Messenger*. 2012;1(1):63-76. doi:10.1166/msr.2012.1003
400. Zhu MX, Ma J, Parrington J, Galione A, Mark Evans A. TPCs: Endolysosomal channels for Ca2+ mobilization from acidic organelles triggered by NAADP. *FEBS Lett*. 2010;584(10):1966-1974. doi:10.1016/j.febslet.2010.02.028
401. Kintzer AF, Stroud RM. On the structure and mechanism of two-pore channels. *FEBS J*. 2018;285(2):233-243. doi:10.1111/febs.14154
402. Pitt SJ, Funnell TM, Sitsapesan M, et al. TPC2 is a novel NAADP-sensitive Ca2+ release channel, operating as a dual sensor of luminal pH and Ca2+. *J Biol Chem*. 2010;285(45):35039-35046. doi:10.1074/jbc.M110.156927
403. Pitt SJ, Lam AKM, Rietdorf K, Galione A, Sitsapesan R. Reconstituted Human TPC1 is a proton-permeable ion channel and is activated by NAADP or Ca2+. *Sci Signal*. 2014;7(326):1-12. doi:10.1126/scisignal.2004854
404. Wang X, Zhang X, Dong XP, et al. TPC proteins are phosphoinositide- Activated sodium-selective ion channels in endosomes and lysosomes. *Cell*. 2012;151(2):372-383. doi:10.1016/j.cell.2012.08.036
405. Morgan AJ, Galione A. Two-pore channels (TPCs): Current controversies. *BioEssays*. 2014;36(2):173-183. doi:10.1002/bies.201300118
406. Jha A, Ahuja M, Patel S, Brailoiu E, Muallem S. Convergent regulation of the lysosomal two-pore channel-2 by Mg 2+, NAADP, PI(3,5)P2 and multiple protein kinases. *EMBO J*. 2014;33(5):501-511. doi:10.1002/embj.201387035
407. Feng X, Huang Y, Lu Y, et al. Drosophila TRPML forms PI(3,5)P2-activated cation channels in both endolysosomes and plasma Membrane. *J Biol Chem*. 2014;289(7):4262-4272. doi:10.1074/jbc.M113.506501
408. Xiong J, Zhu MX. Regulation of lysosomal ion homeostasis by channels and transporters. *Sci China Life Sci*. 2016;59(8):777-791. doi:10.1007/s11427-016-5090-x
409. Cheng X, Shen D, Samie M, Xu H. Mucolipins: Intracellular TRPML1-3 channels. *FEBS Lett*. 2010;584(10):2013-2021. doi:10.1016/j.febslet.2009.12.056
410. Zhang F, Jin S, Yi F, Li PL. TRP-ML1 functions as a lysosomal NAADP-sensitive Ca 2+ release channel in coronary arterial myocytes. *J Cell Mol Med*. 2009;13(9 B):3174-3185. doi:10.1111/j.1582-4934.2008.00486.x
411. Yamaguchi S, Jha A, Li Q, et al. Transient receptor potential mucolipin 1 (TRPML1) and two-pore channels are functionally independent organellar ion channels. *J Biol Chem*. 2011;286(26):22934-22942. doi:10.1074/jbc.M110.210930
412. Onyenwoke RU, Sexton JZ, Yan F, et al. The mucolipidosis IV Ca2+ channel TRPML1 (MCOLN1) is regulated by the TOR kinase. *Biochem J*. 2015;470(3):331-342. doi:10.1042/BJ20150219
413. Christensen KA, Myers JT, Swanson JA. pH-dependent regulation of lysosomal calcium in macrophages. *J Cell Sci*. 2002;115(3):599-607.
414. Garrity AG, Wang W, Collier CMD, Levey SA, Gao Q, Xu H. The endoplasmic reticulum, not the pH gradient, drives calcium refilling of lysosomes. *Elife*. 2016;5(MAY2016). doi:10.7554/eLife.15887
415. Wang W, Zhang X, Gao Q, et al. A voltage-dependent K+ channel in the lysosome is required for refilling lysosomal Ca2+ stores. *J Cell Biol*. 2017;216(6):1715-1730. doi:10.1083/jcb.201612123
416. Yang J, Zhao Z, Gu M, Feng X, Xu H. Release and uptake mechanisms of vesicular Ca2+ stores. *Protein Cell*. 2018;10(1):8-19. doi:10.1007/s13238-018-0523-x
417. Patel S, Brailoiu E. Triggering of Ca 2+ signals by NAADP-gated two-pore channels: A role for membrane contact sites? *Biochem Soc Trans*. 2012;40(1):153-157. doi:10.1042/BST20110693

418. Phillips MJ, Voeltz GK. Structure and function of ER membrane contact sites with other organelles. *Nat Rev Mol Cell Biol*. 2016;17(2):69-82. doi:10.1038/nrm.2015.8
419. Allison R, Edgar JR, Pearson G, et al. Defects in ER-endosome contacts impact lysosome function in hereditary spastic paraplegia. *J Cell Biol*. 2017;216(5):1337-1355. doi:10.1083/jcb.201609033
420. Penny CJ, Kilpatrick BS, Eden ER, Patel S. Coupling acidic organelles with the ER through Ca2+ microdomains at membrane contact sites. *Cell Calcium*. 2015;58(4):387-396. doi:10.1016/j.ceca.2015.03.006
421. Galione A, Ruas M. NAADP receptors. *Cell Calcium*. 2005;38(3-4 SPEC. ISS.):273-280. doi:10.1016/j.ceca.2005.06.031
422. Atakpa P, Thillaiappan NB, Mataragka S, Prole DL, Taylor CW. IP3 Receptors Preferentially Associate with ER-Lysosome Contact Sites and Selectively Deliver Ca2+ to Lysosomes. *Cell Rep*. 2018;25(11):3180-3193.e7. doi:10.1016/j.celrep.2018.11.064
423. Morgan AJ, Davis LC, Wagner SKTY, et al. Bidirectional Ca2+ signaling occurs between the endoplasmic reticulum and acidic organelles. *J Cell Biol*. 2013;200(6):789-805. doi:10.1083/jcb.201204078
424. Ronco V, Potenza DM, Denti F, et al. A novel Ca2+-mediated cross-talk between endoplasmic reticulum and acidic organelles: Implications for NAADP-dependent Ca2+ signalling. *Cell Calcium*. 2015;57(2):89-100. doi:10.1016/j.ceca.2015.01.001
425. López-Sanjurjo CI, Tovey SC, Prole DL, Taylor CW. Lysosomes shape Ins(1,4,5)P3-evoked Ca2+ signals by selectively sequestering Ca2+ released from the endoplasmic reticulum. *J Cell Sci*. 2013;126(1):289-300. doi:10.1242/jcs.116103
426. Vingtdeux V, Giliberto L, Zhao H, et al. AMP-activated protein kinase signaling activation by resveratrol modulates amyloid-β peptide metabolism. *J Biol Chem*. 2010;285(12):9100-9113. doi:10.1074/jbc.M109.060061
427. Seidler NW, Jona I, Vegh M, Martonosi A. Cyclopiazonic acid is a specific inhibitor of the Ca2+-ATPase of sarcoplasmic reticulum. *J Biol Chem*. 1989;264(30):17816-17823.
428. Moncoq K, Trieber CA, Young HS. The molecular basis for cyclopiazonic acid inhibition of the sarcoplasmic reticulum calcium pump. *J Biol Chem*. 2007;282(13):9748-9757. doi:10.1074/jbc.M611653200
429. Hove-Madsen L, Baudet S, Bers DM. *Making and Using Calcium-Selective Mini- and Microelectrodes*. Vol 99. Elsevier Inc.; 2010. doi:10.1016/B978-0-12-374841-6.00003-7
430. Tsien R. New calcium indicators and buffers with high selectivity against magnesium and protons: design, syn. *Biochemistry*. 1980;19(1966):2396-2404. http://scholar.google.com/scholar?hl=en&btnG=Search&q=intitle:new+calcium+indicators+and+buffers+with+high+selectivity+against+magnesium+and+protons#4.
431. Bootman MD, Rietdorf K, Collins T, Walker S, Sanderson M. Ca2+-sensitive fluorescent dyes and intracellular Ca2+ imaging. *Cold Spring Harb Protoc*. 2013;8(2):83-99. doi:10.1101/pdb.top066050
432. Zanin S, Lidron E, Rizzuto R, Pallafacchina G. Methods to Measure Intracellular Ca2+ Concentration Using Ca2+-Sensitive Dyes. In: Raffaello A, Vecellio Reane D, eds. *Methods in Molecular Biology*. Vol 1925. Methods in Molecular Biology. New York, NY: Springer New York; 2019:43-58. doi:10.1007/978-1-4939-9018-4_4
433. Bootman MD, Allman S, Rietdorf K, Bultynck G. Deleterious effects of calcium indicators within cells; an inconvenient truth. *Cell Calcium*. 2018;73(March):82-87. doi:10.1016/j.ceca.2018.04.005
434. Ghislat G, Patrons M, Rizzutos R, Knecht E. Withdrawal of essential amino acids increases autophagy by a pathway involving Ca2+/calmodulin-dependent kinase kinase-β (CaMKK-β). *J Biol Chem*. 2012;287(46):38625-38636. doi:10.1074/jbc.M112.365767
435. Engedal N, Torgersen ML, Guldvik IJ, et al. Modulation of intracellular calcium homeostasis blocks autophagosome formation. *Autophagy*. 2013;9(10):1475-1490. doi:10.4161/auto.25900
436. Choi S, Kim HJ. The Ca2+ channel TRPML3 specifically interacts with the mammalian ATG8 homologue GATE16 to regulate autophagy. *Biochem Biophys Res Commun*. 2014;443(1):56-61. doi:10.1016/j.bbrc.2013.11.044
437. Høyer-Hansen M, Bastholm L, Szyniarowski P, et al. Control of Macroautophagy by Calcium, Calmodulin-Dependent Kinase Kinase-β, and Bcl-2. *Mol Cell*. 2007;25(2):193-205. doi:10.1016/j.molcel.2006.12.009
438. Sarkar S, Floto RA, Berger Z, et al. Lithium induces autophagy by inhibiting inositol monophosphatase. *J Cell Biol*. 2005;170(7):1101-1111. doi:10.1083/jcb.200504035
439. Wang SH, Shih YL, Ko WC, Wei YH, Shih CM. Cadmium-induced autophagy and apoptosis are mediated by a calcium signaling pathway. *Cell Mol Life Sci*. 2008;65(22):3640-3652. doi:10.1007/s00018-008-8383-9
440. Decuypere JP, Bultynck G, Parys JB. A dual role for Ca2+ in autophagy regulation. *Cell Calcium*. 2011;50(3):242-250. doi:10.1016/j.ceca.2011.04.001

441. Decuypere JP, Monaco G, Bultynck G, Missiaen L, De Smedt H, Parys JB. The IP3 receptor-mitochondria connection in apoptosis and autophagy. *Biochim Biophys Acta - Mol Cell Res*. 2011;1813(5):1003-1013. doi:10.1016/j.bbamcr.2010.11.023
442. Høyer-Hansen M, Jäättelä M. Connecting endoplasmic reticulum stress to autophagy by unfolded protein response and calcium. *Cell Death Differ*. 2007;14(9):1576-1582. doi:10.1038/sj.cdd.4402200
443. Ogata M, Hino S, Saito A, et al. Autophagy Is Activated for Cell Survival after Endoplasmic ReticulumStress. *Mol Cell Biol*. 2006;26(24):9220-9231. doi:10.1128/mcb.01453-06
444. Bialik S, Kimchi A. Lethal weapons: DAP-kinase, autophagy and cell death. DAP-kinase regulates autophagy. *Curr Opin Cell Biol*. 2010;22(2):199-205. doi:10.1016/j.ceb.2009.11.004
445. Høyer-Hansen M, Jäättelä M. AMP-activated protein kinase: A universal regulator of autophagy? *Autophagy*. 2007;3(4):381-383. doi:10.4161/auto.4240
446. Decuypere JP, Welkenhuyzen K, Luyten T, et al. Ins(1,4,5)P3 receptor-mediated Ca2+ signaling and autophagy induction are interrelated. *Autophagy*. 2011;7(12):1472-1489. doi:10.4161/auto.7.12.17909
447. Decuypere JP, Kindt D, Luyten T, et al. mTOR-Controlled Autophagy Requires Intracellular Ca2+ Signaling. *PLoS One*. 2013;8(4). doi:10.1371/journal.pone.0061020
448. Grotemeier A, Alers S, Pfisterer SG, et al. AMPK-independent induction of autophagy by cytosolic Ca2+ increase. *Cell Signal*. 2010;22(6):914-925. doi:10.1016/j.cellsig.2010.01.015
449. Bootman MD, Chehab T, Bultynck G, Parys JB, Rietdorf K. The regulation of autophagy by calcium signals: Do we have a consensus? *Cell Calcium*. 2018;70(October):32-46. doi:10.1016/j.ceca.2017.08.005
450. Luzio JP, Gray SR, Bright NA. Endosome-lysosome fusion. *Biochem Soc Trans*. 2010;38(6):1413-1416. doi:10.1042/BST0381413
451. Kim HJ, Soyombo AA, Tjon-Kon-Sang S, So I, Muallem S. The Ca2+ channel TRPML3 regulates membrane trafficking and autophagy. *Traffic*. 2009;10(8):1157-1167. doi:10.1111/j.1600-0854.2009.00924.x
452. Kilpatrick BS, Yates E, Grimm C, Schapira AH, Patel S. Endo-lysosomal TRP mucolipin-1 channels trigger global ER Ca2+ release and Ca2+ influx. *J Cell Sci*. 2016;129(20):3859-3867. doi:10.1242/jcs.190322
453. Medina DL, Di Paola S, Peluso I, et al. Lysosomal calcium signalling regulates autophagy through calcineurin and TFEB. *Nat Cell Biol*. 2015;17(3):288-299. doi:10.1038/ncb3114
454. Medina DL, Ballabio A. Lysosomal calcium regulates autophagy. *Autophagy*. 2015;11(6):970-971. doi:10.1080/15548627.2015.1047130
455. Zhang X, Yu L, Xu H. Lysosome calcium in ROS regulation of autophagy. *Autophagy*. 2016;12(10):1954-1955. doi:10.1080/15548627.2016.1212787
456. Zhang X, Cheng X, Yu L, et al. MCOLN1 is a ROS sensor in lysosomes that regulates autophagy. *Nat Commun*. 2016;7(May). doi:10.1038/ncomms12109
457. Li RJ, Xu J, Fu C, et al. Regulation of mTORC1 by lysosomal calcium and calmodulin. *Elife*. 2016;5:1-16. doi:10.7554/eLife.19360
458. Williams A, Sarkar S, Cuddon P, et al. Novel targets for Huntington's disease in an mTOR-independent autophagy pathway. *Nat Chem Biol*. 2008;4(5):295-305. doi:10.1038/nchembio.79
459. Xia HG, Zhang L, Chen G, et al. Control of basal autophagy by calpain1 mediated cleavage of ATG5. *Autophagy*. 2010;6(1):61-66. doi:10.4161/auto.6.1.10326
460. Criollo A, Maiuri MC, Tasdemir E, et al. Regulation of autophagy by the inositol trisphosphate receptor. *Cell Death Differ*. 2007;14(5):1029-1039. doi:10.1038/sj.cdd.4402099
461. Vicencio JM, Ortiz C, Criollo A, et al. The inositol 1,4,5-trisphosphate receptor regulates autophagy through its interaction with Beclin 1. *Cell Death Differ*. 2009;16(7):1006-1017. doi:10.1038/cdd.2009.34
462. Salido GM, Sage SO, Rosado JA. TRPC channels and store-operated Ca2+ entry. *Biochim Biophys Acta - Mol Cell Res*. 2009;1793(2):223-230. doi:10.1016/j.bbamcr.2008.11.001
463. Criollo A, Vicencio JM, Tasdemir E, Maiuri MC, Lavandero S, Kroemer G. The inositol trisphosphate receptor in the control of autophagy. *Autophagy*. 2007;3(4):350-353. doi:10.4161/auto.4077
464. Decuypere J-P, Parys JB, Bultynck G. Regulation of the Autophagic Bcl-2/Beclin 1 Interaction. *Cells*. 2012;1(3):284-312. doi:10.3390/cells1030284
465. Moldoveanu T, Hosfield CM, Lim D, Elce JS, Jia Z, Davies PL. A Ca2+ switch aligns the active site of calpain. *Cell*. 2002;108(5):649-660. doi:10.1016/S0092-8674(02)00659-1
466. Arthur JSC, Elce JS, Hegadorn C, Williams K, Greer PA. Disruption of the Murine Calpain Small Subunit Gene, Capn4: Calpain Is Essential for Embryonic Development but Not for Cell Growth and Division. *Mol Cell Biol*. 2000;20(12):4474-4481. doi:10.1128/mcb.20.12.4474-4481.2000
467. Yousefi S, Perozzo R, Schmid I, et al. Calpain-mediated cleavage of Atg5 switches autophagy to apoptosis. *Nat Cell Biol*. 2006;8(10):1124-1132. doi:10.1038/ncb1482

468. Russo R, Berliocchi L, Adornetto A, et al. Calpain-mediated cleavage of Beclin-1 and autophagy deregulation following retinal ischemic injury in vivo. *Cell Death Dis*. 2011;2(4):e144-9. doi:10.1038/cddis.2011.29
469. Bano D, Young KW, Guerin CJ, et al. Cleavage of the plasma membrane Na+/Ca2+ exchanger in excitotoxicity. *Cell*. 2005;120(2):275-285. doi:10.1016/j.cell.2004.11.049
470. Demarchi F, Bertoli C, Copetti T, et al. Calpain is required for macroautophagy in mammalian cells. *J Cell Biol*. 2006;175(4):595-605. doi:10.1083/jcb.200601024
471. Ravikumar B, Vacher C, Berger Z, et al. Inhibition of mTOR induces autophagy and reduces toxicity of polyglutamine expansions in fly and mouse models of Huntington disease. *Nat Genet*. 2004;36(6):585-595. doi:10.1038/ng1362
472. Nixon RA, Yang DS. Autophagy and neuronal cell death in neurological disorders. *Cold Spring Harb Perspect Biol*. 2012;4(10):1-23. doi:10.1101/cshperspect.a008839
473. Vellai T, Tóth ML, Kovács AL. Janus-Faced Autophagy: A Dual Role of Cellular Self-Eating in Neurodegeneration? *Autophagy*. 2007;3(5):461-463. doi:10.4161/auto.4282
474. Liou B, Peng Y, Li R, et al. Modulating ryanodine receptors with dantrolene attenuates neuronopathic phenotype in Gaucher disease mice. *Hum Mol Genet*. September 2016:ddw322. doi:10.1093/hmg/ddw322
475. Chung KM, Jeong EJ, Park H, An HK, Yu SW. Mediation of autophagic cell death by type 3 ryanodine receptor (RyR3) in adult hippocampal neural stem cells. *Front Cell Neurosci*. 2016;10(MAY):1-15. doi:10.3389/fncel.2016.00116
476. Vervliet T, Pintelon I, Welkenhuyzen K, et al. Basal ryanodine receptor activity suppresses autophagic flux. *Biochem Pharmacol*. 2017;132:133-142. doi:10.1016/j.bcp.2017.03.011
477. Pereira GJS, Hirata H, Fimia GM, et al. Nicotinic Acid Adenine Dinucleotide Phosphate (NAADP) regulates autophagy in cultured astrocytes. *J Biol Chem*. 2011;286(32):27875-27881. doi:10.1074/jbc.C110.216580
478. Lu Y, Hao B, Graeff R, Yue J. NAADP/TPC2/Ca2+ signaling inhibits autophagy. *Commun Integr Biol*. 2013;6(6). doi:10.4161/cib.27595
479. Gómez-Suaga P, Luzón-Toro B, Churamani D, et al. Leucine-rich repeat kinase 2 regulates autophagy through a calcium-dependent pathway involving NAADP. *Hum Mol Genet*. 2012;21(3):511-525. doi:10.1093/hmg/ddr481
480. Collier TJ, Kanaan NM, Kordower JH. Ageing as a primary risk factor for Parkinson's disease: Evidence from studies of non-human primates. *Nat Rev Neurosci*. 2011;12(6):359-366. doi:10.1038/nrn3039
481. Hindle J V. Ageing, neurodegeneration and Parkinson's disease. *Age Ageing*. 2010;39(2):156-161. doi:10.1093/ageing/afp223
482. Surmeier DJ. Calcium, ageing, and neuronal vulnerability in Parkinson's disease. *Lancet Neurol*. 2007;6(10):933-938. doi:10.1016/S1474-4422(07)70246-6
483. Finkel T, Holbrook NJ. Oxidants, oxidative stress and the biology of ageing. *Nature*. 2000;408(6809):239-247. doi:10.1038/35041687
484. Indo HP, Yen H-C, Nakanishi I, et al. A mitochondrial superoxide theory for oxidative stress diseases and aging. *J Clin Biochem Nutr*. 2015;56(1):1-7. doi:10.3164/jcbn.14-42
485. Balaban RS, Nemoto S, Finkel T. Mitochondria, oxidants, and aging. *Cell*. 2005;120(4):483-495. doi:10.1016/j.cell.2005.02.001
486. Zhang J, Wang X, Vikash V, et al. ROS and ROS-Mediated Cellular Signaling. *Oxid Med Cell Longev*. 2016;2016(Figure 1). doi:10.1155/2016/4350965
487. Brieger K, Schiavone S, Miller FJ, Krause KH. Reactive oxygen species: From health to disease. *Swiss Med Wkly*. 2012;142. doi:10.4414/smw.2012.13659
488. Kauppila TES, Kauppila JHK, Larsson NG. Mammalian Mitochondria and Aging: An Update. *Cell Metab*. 2017;25(1):57-71. doi:10.1016/j.cmet.2016.09.017
489. Henle ES, Linn S. Formation, prevention, and repair of DNA damage by iron/hydrogen peroxide. *J Biol Chem*. 1997;272(31):19095-19098. doi:10.1074/jbc.272.31.19095
490. Kumar H, Lim HW, More SV, et al. The role of free radicals in the aging brain and Parkinson's disease: Convergence and parallelism. *Int J Mol Sci*. 2012;13(8):10478-10504. doi:10.3390/ijms130810478
491. Lee DH, Gold R, Linker RA. Mechanisms of oxidative damage in multiple sclerosis and neurodegenerative diseases: Therapeutic modulation via fumaric acid esters. *Int J Mol Sci*. 2012;13(9):11783-11803. doi:10.3390/ijms130911783
492. Danielson SR, Andersen JK. Oxidative and nitrative protein modifications in Parkinson's disease. *Free Radic Biol Med*. 2008;44(10):1787-1794. doi:10.1016/j.freeradbiomed.2008.03.005
493. Seet RCS, Lee CYJ, Lim ECH, et al. Oxidative damage in Parkinson disease: Measurement using accurate biomarkers. *Free Radic Biol Med*. 2010;48(4):560-566. doi:10.1016/j.freeradbiomed.2009.11.026

494. Vila M, Bové J, Dehay B, Rodríguez-Muela N, Boya P. Lysosomal membrane permeabilization in Parkinson disease. *Autophagy*. 2011;7(1):98-100. doi:10.4161/auto.7.1.13933
495. Matsuda W, Furuta T, Nakamura KC, et al. Single nigrostriatal dopaminergic neurons form widely spread and highly dense axonal arborizations in the neostriatum. *J Neurosci*. 2009;29(2):444-453. doi:10.1523/JNEUROSCI.4029-08.2009
496. Wong E, Cuervo AM. Autophagy gone awry in neurodegenerative diseases. *Nat Neurosci*. 2010;13(7):805-811. doi:10.1038/nn.2575
497. Martinez-vicente M, Sulzer D, Cuervo AM, et al. Dopamine-modified α-synuclein blocks chaperone-mediated autophagy. 2008;118(2):777-788. doi:10.1172/JCI32806.somal
498. Son JH, Shim JH, Kim KH, Ha JY, Han JY. Neuronal autophagy and neurodegenerative diseases. *Exp Mol Med*. 2012;44(2):89-98. doi:10.3858/emm.2012.44.2.031
499. Guzman JN, Sánchez-Padilla J, Chan CS, Surmeier DJ. Robust pacemaking in substantia nigra dopaminergic neurons. *J Neurosci*. 2009;29(35):11011-11019. doi:10.1523/JNEUROSCI.2519-09.2009
500. Hage TA, Khaliq ZM. Tonic firing rate controls dendritic Ca2+ signaling and synaptic gain in substantia nigra dopamine neurons. *J Neurosci*. 2015;35(14):5823-5836. doi:10.1523/JNEUROSCI.3904-14.2015
501. Dragicevic E, Schiemann J, Liss B. Dopamine midbrain neurons in health and Parkinson's disease: Emerging roles of voltage-gated calcium channels and ATP-sensitive potassium channels. *Neuroscience*. 2015;284:798-814. doi:10.1016/j.neuroscience.2014.10.037
502. Puopolo M, Raviola E, Bean BP. Roles of subthreshold calcium current and sodium current in spontaneous firing of mouse midbrain dopamine neurons. *J Neurosci*. 2007;27(3):645-656. doi:10.1523/JNEUROSCI.4341-06.2007
503. Putzier I, Kullmann PHM, Horn JP, Levitan ES. Cav1.3 channel voltage dependence, not Ca2+ selectivity, drives pacemaker activity and amplifies bursts in nigral dopamine neurons. *J Neurosci*. 2009;29(49):15414-15419. doi:10.1523/JNEUROSCI.4742-09.2009
504. Burgoyne RD, Haynes LP. Sense and specificity in neuronal calcium signalling. *Biochim Biophys Acta - Mol Cell Res*. 2015;1853(9):1921-1932. doi:10.1016/j.bbamcr.2014.10.029
505. Brini M, Calì T, Ottolini D, Carafoli E. Neuronal calcium signaling: Function and dysfunction. *Cell Mol Life Sci*. 2014;71(15):2787-2814. doi:10.1007/s00018-013-1550-7
506. Foehring RC, Zhang XF, Lee JCF, Callaway JC. Endogenous calcium buffering capacity of substantia nigral dopamine neurons. *J Neurophysiol*. 2009;102(4):2326-2333. doi:10.1152/jn.00038.2009
507. Hurley MJ, Brandon B, Gentleman SM, Dexter DT. Parkinson's disease is associated with altered expression of Ca V1 channels and calcium-binding proteins. *Brain*. 2013;136(7):2077-2097. doi:10.1093/brain/awt134
508. Park J-S, Davis RL, Sue CM. Mitochondrial Dysfunction in Parkinson's Disease: New Mechanistic Insights and Therapeutic Perspectives. *Curr Neurol Neurosci Rep*. 2018;18(5):21. doi:10.1007/s11910-018-0829-3
509. Keeney PM, Xie J, Capaldi RA, Bennett JP. Parkinson's disease brain mitochondrial complex I has oxidatively damaged subunits and is functionally impaired and misassembled. *J Neurosci*. 2006;26(19):5256-5264. doi:10.1523/JNEUROSCI.0984-06.2006
510. Perier C, Bové J, Dehay B, et al. Apoptosis-inducing factor deficiency sensitizes dopaminergic neurons to parkinsonian neurotoxins. *Ann Neurol*. 2010;68(2):184-192. doi:10.1002/ana.22034
511. Schapira AH, Jenner P. Etiology and pathogenesis of Parkinson's disease. *Mov Disord*. 2011;26(6):1049-1055. doi:10.1002/mds.23732
512. Cadenas E, Davies KJA. Mitochondrial free radical generation, oxidative stress, and aging. *Free Radic Biol Med*. 2000;29(3-4):222-230. doi:10.1016/S0891-5849(00)00317-8
513. Gahl RF, Dwivedi P, Tjandra N. Bcl-2 proteins bid and bax form a network to permeabilize the mitochondria at the onset of apoptosis. *Cell Death Dis*. 2016;7(10):e2424-11. doi:10.1038/cddis.2016.320
514. Brookes PS, Yoon Y, Robotham JL, Anders MW, Sheu SS. Calcium, ATP, and ROS: A mitochondrial love-hate triangle. *Am J Physiol - Cell Physiol*. 2004;287(4 56-4). doi:10.1152/ajpcell.00139.2004
515. Graef M, Nunnari J. Mitochondria regulate autophagy by conserved signalling pathways. *EMBO J*. 2011;30(11):2101-2114. doi:10.1038/emboj.2011.104
516. Lee J, Giordano S, Zhang J. Autophagy, mitochondria and oxidative stress: cross-talk and redox signalling. *Biochem J*. 2012;441(2):523-540. doi:10.1042/BJ20111451
517. Raturi A, Simmen T. Where the endoplasmic reticulum and the mitochondrion tie the knot: The mitochondria-associated membrane (MAM). *Biochim Biophys Acta - Mol Cell Res*. 2013;1833(1):213-224. doi:10.1016/j.bbamcr.2012.04.013
518. Chen Y, Azad MB, Gibson SB. Superoxide is the major reactive oxygen species regulating autophagy. *Cell Death Differ*. 2009;16(7):1040-1052. doi:10.1038/cdd.2009.49

519. Scherz-Shouval R, Elazar Z. Regulation of autophagy by ROS: Physiology and pathology. *Trends Biochem Sci*. 2011;36(1):30-38. doi:10.1016/j.tibs.2010.07.007
520. Li L, Chen Y, Gibson SB. Starvation-induced autophagy is regulated by mitochondrial reactive oxygen species leading to AMPK activation. *Cell Signal*. 2013;25(1):50-65. doi:10.1016/j.cellsig.2012.09.020
521. Chakraborty D, Felzen V, Hiebel C, et al. Enhanced autophagic-lysosomal activity and increased BAG3-mediated selective macroautophagy as adaptive response of neuronal cells to chronic oxidative stress. *Redox Biol*. 2019;24(March):101181. doi:10.1016/j.redox.2019.101181
522. Surmeier DJ, Guzman JN, Sanchez-Padilla J, Goldberg JA. *What Causes the Death of Dopaminergic Neurons in Parkinson's Disease?* Vol 183. Elsevier B.V.; 2010. doi:10.1016/S0079-6123(10)83004-3
523. Ramirez-Moreno MJ, Duarte-Jurado AP, Gopar-Cuevas Y, et al. Autophagy Stimulation Decreases Dopaminergic Neuronal Death Mediated by Oxidative Stress. *Mol Neurobiol*. 2019;56(12):8136-8156. doi:10.1007/s12035-019-01654-1
524. Angelova PR, Ludtmann MHR, Horrocks MH, et al. Ca 2+ is a key factor in α-synuclein-induced neurotoxicity. *J Cell Sci*. 2016;129(9):1792-1801. doi:10.1242/jcs.180737
525. Danzer KM, Haasen D, Karow AR, et al. Different species of α-synuclein oligomers induce calcium influx and seeding. *J Neurosci*. 2007;27(34):9220-9232. doi:10.1523/JNEUROSCI.2617-07.2007
526. Schöndorf DC, Ivanyuk D, Baden P, et al. The NAD+ Precursor Nicotinamide Riboside Rescues Mitochondrial Defects and Neuronal Loss in iPSC and Fly Models of Parkinson's Disease. *Cell Rep*. 2018;23(10):2976-2988. doi:10.1016/j.celrep.2018.05.009
527. Nah J, Yuan J, Jung YK. Autophagy in neurodegenerative diseases: From mechanism to therapeutic approach. *Mol Cells*. 2015;38(5):381-389. doi:10.14348/molcells.2015.0034
528. Jungverdorben J, Till A, Brüstle O. Induced pluripotent stem cell-based modeling of neurodegenerative diseases: a focus on autophagy. *J Mol Med*. 2017;95(7):705-718. doi:10.1007/s00109-017-1533-5
529. Lynch-day MA, Mao K, Wang K, Zhao M, Klionsky DJ. The Role of Autophagy in Parkinson ' s Disease. *Cold Spring Harb Lab Press*. 2015:1-14. doi:10.1101/cshperspect.a009357
530. Gómez-Suaga P, Fdez E, Blanca Ramírez M, Hilfiker S. A link between autophagy and the pathophysiology of LRRK2 in Parkinson's disease. *Parkinsons Dis*. 2012;2012:324521. doi:10.1155/2012/324521
531. Karabiyik C, Lee MJ, Rubinsztein DC. Autophagy impairment in Parkinson's disease. Lane JD, Korolchuk VI, Murray JT, eds. *Essays Biochem*. 2017;61(6):711-720. doi:10.1042/EBC20170023
532. Surmeier DJ, Schumacker PT, Guzman JD, Ilijic E, Yang B, Zampese E. Calcium and Parkinson's disease. *Biochem Biophys Res Commun*. 2017;483(4):1013-1019. doi:10.1016/j.bbrc.2016.08.168
533. Schapira AHV. Calcium dysregulation in Parkinson's disease. *Brain*. 2013;136(7):2015-2016. doi:10.1093/brain/awt180
534. Bose A, Beal MF. Mitochondrial dysfunction and oxidative stress in induced pluripotent stem cell models of Parkinson's disease. *Eur J Neurosci*. 2019;49(4):525-532. doi:10.1111/ejn.14264
535. Lin MT, Beal MF. Mitochondrial dysfunction and oxidative stress in neurodegenerative diseases. *Nature*. 2006;443(7113):787-795. doi:10.1038/nature05292
536. Lie PPY, Nixon RA. Lysosome trafficking and signaling in health and neurodegenerative diseases. *Neurobiol Dis*. 2019;122:94-105. doi:10.1016/j.nbd.2018.05.015
537. Rajawat YS, Hilioti Z, Bossis I. Aging: Central role for autophagy and the lysosomal degradative system. *Ageing Res Rev*. 2009;8(3):199-213. doi:10.1016/j.arr.2009.05.001
538. Crews L, Spencer B, Desplats P, et al. Selective molecular alterations in the autophagy pathway in patients with lewy body disease and in models of α-synucleinopathy. *PLoS One*. 2010;5(2). doi:10.1371/journal.pone.0009313
539. Decressac M, Mattsson B, Weikop P, Lundblad M, Jakobsson J, Björklund A. TFEB-mediated autophagy rescues midbrain dopamine neurons from α-synuclein toxicity. *Proc Natl Acad Sci U S A*. 2013;110(19). doi:10.1073/pnas.1305623110
540. Cuervo AM, Stafanis L, Fredenburg R, Lansbury PT, Sulzer D. Impaired degradation of mutant α-synuclein by chaperone-mediated autophagy. *Science (80-)*. 2004;305(5688):1292-1295. doi:10.1126/science.1101738
541. Sala G, Marinig D, Riva C, et al. Rotenone down-regulates HSPA8/hsc70 chaperone protein in vitro: A new possible toxic mechanism contributing to Parkinson's disease. *Neurotoxicology*. 2016;54:161-169. doi:10.1016/j.neuro.2016.04.018
542. Xilouri M, Brekk OR, Polissidis A, Chrysanthou-Piterou M, Kloukina I, Stefanis L. Impairment of chaperone-mediated autophagy induces dopaminergic neurodegeneration in rats. *Autophagy*. 2016;12(11):2230-2247. doi:10.1080/15548627.2016.1214777

543. Sato S, Uchihara T, Fukuda T, et al. Loss of autophagy in dopaminergic neurons causes Lewy pathology and motor dysfunction in aged mice. *Sci Rep*. 2018;8(1):1-10. doi:10.1038/s41598-018-21325-w
544. Watanabe Y, Tatebe H, Taguchi K, et al. p62/SQSTM1-Dependent Autophagy of Lewy Body-Like α-Synuclein Inclusions. *PLoS One*. 2012;7(12):1-12. doi:10.1371/journal.pone.0052868
545. Winslow AR, Chen CW, Corrochano S, et al. α-Synuclein impairs macroautophagy: Implications for Parkinson's disease. *J Cell Biol*. 2010;190(6):1023-1037. doi:10.1083/jcb.201003122
546. Volpicelli-Daley LA, Gamble KL, Schultheiss CE, Riddle DM, West AB, Lee VM-Y. Formation of α-synuclein Lewy neurite–like aggregates in axons impedes the transport of distinct endosomes. Martin TFJ, ed. *Mol Biol Cell*. 2014;25(25):4010-4023. doi:10.1091/mbc.e14-02-0741
547. Hessvik NP, Llorente A. Current knowledge on exosome biogenesis and release. *Cell Mol Life Sci*. 2018;75(2):193-208. doi:10.1007/s00018-017-2595-9
548. Borland H, Vilhardt F. Prelysosomal compartments in the unconventional secretion of amyloidogenic seeds. *Int J Mol Sci*. 2017;18(1):1-40. doi:10.3390/ijms18010227
549. Lee HJ, Patel S, Lee SJ. Intravesicular localization and exocytosis of α-synuclein and its aggregates. *J Neurosci*. 2005;25(25):6016-6024. doi:10.1523/JNEUROSCI.0692-05.2005
550. Jang A, Lee HJ, Suk JE, Jung JW, Kim KP, Lee SJ. Non-classical exocytosis of α-synuclein is sensitive to folding states and promoted under stress conditions. *J Neurochem*. 2010;113(5):1263-1274. doi:10.1111/j.1471-4159.2010.06695.x
551. Jucker M, Walker LC. Self-propagation of pathogenic protein aggregates in neurodegenerative diseases. *Nature*. 2013;501(7465):45-51. doi:10.1038/nature12481
552. Lee HJ, Cho ED, Lee KW, Kim JH, Cho SG, Lee SJ. Autophagic failure promotes the exocytosis and intercellular transfer of α-synuclein. *Exp Mol Med*. 2013;45(5):e22-9. doi:10.1038/emm.2013.45
553. Bisaglia M, Greggio E, Beltramini M, Bubacco L. Dysfunction of dopamine homeostasis: Clues in the hunt for novel Parkinson's disease therapies. *FASEB J*. 2013;27(6):2101-2110. doi:10.1096/fj.12-226852
554. Bisaglia M, Filograna R, Beltramini M, Bubacco L. Are dopamine derivatives implicated in the pathogenesis of Parkinson's disease? *Ageing Res Rev*. 2014;13(1):107-114. doi:10.1016/j.arr.2013.12.009
555. Henchcliffe C, Beal FM. Mitochondrial biology and oxidative stress in Parkinson disease pathogenesis. *Nat Clin Pract Neurol*. 2008;4(11):600-609. doi:10.1038/ncpneuro0924
556. Conway KA, Rochet JC, Bieganski RM, Lansbury J. Kinetic stabilization of the α-synuclein protofibril by a dopamine-α-synuclein adduct. *Science (80-)*. 2001;294(5545):1346-1349. doi:10.1126/science.1063522
557. Lotharius J. Impaired dopamine storage resulting from alpha-synuclein mutations may contribute to the pathogenesis of Parkinson's disease. *Hum Mol Genet*. 2002;11(20):2395-2407. doi:10.1093/hmg/11.20.2395
558. Missiroli S, Genovese I, Perrone M, Vezzani B, Vitto VAM, Giorgi C. The Role of Mitochondria in Inflammation: From Cancer to Neurodegenerative Disorders. *J Clin Med*. 2020;9(3):740. doi:10.3390/jcm9030740
559. Mathew A, Lindsley TA, Sheridan A, et al. Degraded mitochondrial dna is a newly identified subtype of the damage associated molecular pattern (DAMP) family and possible trigger of neurodegeneration. *J Alzheimer's Dis*. 2012;30(3):617-627. doi:10.3233/JAD-2012-120145
560. Park S, Won JH, Hwang I, Hong S, Lee HK, Yu JW. Defective mitochondrial fission augments NLRP3 inflammasome activation. *Sci Rep*. 2015;5:1-14. doi:10.1038/srep15489
561. Perry VH. Innate inflammation in Parkinson's disease. *Cold Spring Harb Perspect Med*. 2012;2(9):1-12. doi:10.1101/cshperspect.a009373
562. Yang TT, Lin C, Hsu CT, Wang TF, Ke FY, Kuo YM. Differential distribution and activation of microglia in the brain of male C57BL/6J mice. *Brain Struct Funct*. 2013;218(4):1051-1060. doi:10.1007/s00429-012-0446-x
563. Schapansky J, Nardozzi JD, Lavoie MJ. The complex relationships between microglia, alpha-synuclein, and LRRK2 in Parkinson's disease. *Neuroscience*. 2015;302:74-88. doi:10.1016/j.neuroscience.2014.09.049
564. Zucca FA, Segura-Aguilar J, Ferrari E, et al. Interactions of iron, dopamine and neuromelanin pathways in brain aging and Parkinson's disease. *Prog Neurobiol*. 2017;155:96-119. doi:10.1016/j.pneurobio.2015.09.012
565. Wilms H, Rosenstiel P, Sievers J, Deuschl G, Zecca L, Lucius R. Activation of microglia by human neuromelanin is NF-kappaB dependent and involves p38 mitogen-activated protein kinase: implications for Parkinson's disease. *FASEB J*. 2003;17(3):500-502. doi:10.1096/fj.02-0314fje
566. Zhang W, Phillips K, Wielgus AR, et al. Neuromelanin activates microglia and induces degeneration of dopaminergic neurons: Implications for progression of parkinson's disease. *Neurotox Res*. 2011;19(1):63-72. doi:10.1007/s12640-009-9140-z

567. Garaschuk O, Verkhratsky A. Physiology of Microglia. *Methods Mol Biol*. 2019;2034:27-40. doi:10.1007/978-1-4939-9658-2_3
568. Nayernia Z, Jaquet V, Krause KH. New insights on NOX enzymes in the central nervous system. *Antioxidants Redox Signal*. 2014;20(17):2815-2837. doi:10.1089/ars.2013.5703
569. Zhang W, Wang T, Pei Z, et al. Aggregated α-synuclein activates microglia: a process leading to disease progression in Parkinson's disease. *FASEB J*. 2005;19(6):533-542. doi:10.1096/fj.04-2751com
570. Gao HM, Zhang F, Zhou H, Kam W, Wilson B, Hong JS. Neuroinflammation and α-synuclein dysfunction potentiate each other, driving chronic progression of neurodegeneration in a mouse model of Parkinson's disease. *Environ Health Perspect*. 2011;119(6):807-814. doi:10.1289/ehp.1003013
571. Rocha EM, De Miranda B, Sanders LH. Alpha-synuclein: Pathology, mitochondrial dysfunction and neuroinflammation in Parkinson's disease. *Neurobiol Dis*. 2018;109:249-257. doi:10.1016/j.nbd.2017.04.004
572. Shams R, Banik NL, Haque A. *Calpain in the Cleavage of Alpha-Synuclein and the Pathogenesis of Parkinson's Disease*. Vol 167. 1st ed. Elsevier Inc.; 2019. doi:10.1016/bs.pmbts.2019.06.007
573. Mosharov E V., Larsen KE, Kanter E, et al. Interplay between Cytosolic Dopamine, Calcium, and α-Synuclein Causes Selective Death of Substantia Nigra Neurons. *Neuron*. 2009;62(2):218-229. doi:10.1016/j.neuron.2009.01.033
574. Duda J, Pötschke C, Liss B. Converging roles of ion channels, calcium, metabolic stress, and activity pattern of Substantia nigra dopaminergic neurons in health and Parkinson's disease. *J Neurochem*. 2016;139:156-178. doi:10.1111/jnc.13572
575. Lin X, Parisiadou L, Gu X, et al. Leucine-rich repeat kinase 2 regulates the progression of neuropathology induced by Parkinson's disease-related mutant α-synuclein. *Neuron*. 2009;64(6):807-827. doi:10.1016/j.neuron.2009.11.006.Leucine-Rich
576. Qing H, Wong W, McGeer EG, McGeer PL. Lrrk2 phosphorylates alpha synuclein at serine 129: Parkinson disease implications. *Biochem Biophys Res Commun*. 2009;387(1):149-152. doi:10.1016/j.bbrc.2009.06.142
577. Guerreiro PS, Huang Y, Gysbers A, et al. LRRK2 interactions with α-synuclein in Parkinson's disease brains and in cell models. *J Mol Med*. 2013;91(4):513-522. doi:10.1007/s00109-012-0984-y
578. Skibinski G, Nakamura K, Cookson MR, Finkbeiner S. Mutant LRRK2 toxicity in neurons depends on LRRK2 levels and synuclein but not kinase activity or inclusion bodies. *J Neurosci*. 2014;34(2):418-433. doi:10.1523/JNEUROSCI.2712-13.2014
579. Alegre-Abarrategui J, Ansorge O, Esiri M, Wade-Martins R. LRRK2 is a component of granular alpha-synuclein pathology in the brainstem of Parkinson's disease. *Neuropathol Appl Neurobiol*. 2008;34(3):272-283. doi:10.1111/j.1365-2990.2007.00888.x
580. Bieri G, Brahic M, Bousset L, et al. LRRK2 modifies α-syn pathology and spread in mouse models and human neurons. *Acta Neuropathol*. 2019;(0123456789). doi:10.1007/s00401-019-01995-0
581. Volpicelli-Daley LA, Abdelmotilib H, Liu Z, et al. G2019s-LRRK2 expression augments α-synuclein sequestration into inclusions in neurons. *J Neurosci*. 2016;36(28):7415-7427. doi:10.1523/JNEUROSCI.3642-15.2016
582. Novello S, Arcuri L, Dovero S, et al. G2019S LRRK2 mutation facilitates α-synuclein neuropathology in aged mice. *Neurobiol Dis*. 2018;120:21-33. doi:10.1016/j.nbd.2018.08.018
583. Maekawa T, Sasaoka T, Azuma S, et al. Leucine-rich repeat kinase 2 (LRRK2) regulates α-synuclein clearance in microglia. *BMC Neurosci*. 2016;17(1):1-12. doi:10.1186/s12868-016-0315-2
584. Tanji K, Odagiri S, Miki Y, et al. P62 deficiency enhances α-synuclein pathology in mice. *Brain Pathol*. 2015;25(5):552-564. doi:10.1111/bpa.12214
585. Kalogeropulou AF, Zhao J, Bolliger MF, et al. P62/SQSTM1 is a novel leucine-rich repeat kinase 2 (LRRK2) substrate that enhances neuronal toxicity. *Biochem J*. 2018;475(7):1271-1293. doi:10.1042/BCJ20170699
586. Park S, Han S, Choi I, et al. Interplay between leucine-rich repeat kinase 2 (LRRK2) and p62/SQSTM-1 in Selective Autophagy. *PLoS One*. 2016;11(9):1-14. doi:10.1371/journal.pone.0163029
587. Korecka JA, Talbot S, Osborn TM, et al. Neurite Collapse and Altered ER Ca 2+ Control in Human Parkinson Disease Patient iPSC-Derived Neurons with LRRK2 G2019S Mutation. *Stem Cell Reports*. 2019;12(1):29-41. doi:10.1016/j.stemcr.2018.11.021
588. Verma M, Callio J, Otero PA, Sekler I, Wills ZP. Mitochondrial calcium dysregulation contributes to dendrite degeneration mediated by PD/LBD-associated LRRK2 mutants. *J Neurosci*. 2017;37(46):3791-16. doi:10.1523/JNEUROSCI.3791-16.2017
589. Schwab AJ, Ebert AD. Neurite Aggregation and Calcium Dysfunction in iPSC-Derived Sensory Neurons with Parkinson's Disease-Related LRRK2 G2019S Mutation. *Stem Cell Reports*. 2015;5(6):1039-1052.

doi:10.1016/j.stemcr.2015.11.004

590. Cherra SJ, Steer E, Gusdon AM, Kiselyov K, Chu CT. Mutant LRRK2 elicits calcium imbalance and depletion of dendritic mitochondria in neurons. *Am J Pathol*. 2013;182(2):474-484. doi:10.1016/j.ajpath.2012.10.027
591. Yan J, Almilaji A, Schmid E, et al. Leucine-rich repeat kinase 2-sensitive Na+/Ca2+ exchanger activity in dendritic cells. *FASEB J*. 2015;29(5):1701-1710. doi:10.1096/fj.14-264028
592. Giaime E, Tong Y, Wagner LK, Yuan Y, Huang G, Shen J. Age-Dependent Dopaminergic Neurodegeneration and Impairment of the Autophagy-Lysosomal Pathway in LRRK-Deficient Mice. *Neuron*. 2017;96(4):796-807.e6. doi:10.1016/j.neuron.2017.09.036
593. Manzoni C, Mamais A, Roosen DA, et al. MTOR independent regulation of macroautophagy by Leucine Rich Repeat Kinase 2 via Beclin-1. *Sci Rep*. 2016;6(May):1-10. doi:10.1038/srep35106
594. Su YC, Qi X. Inhibition of excessive mitochondrial fission reduced aberrant autophagy and neuronal damage caused by LRRK2 G2019S mutation. *Hum Mol Genet*. 2013;22(22):4545-4561. doi:10.1093/hmg/ddt301
595. Bravo-San Pedro JM, Niso-Santano M, Gómez-Sánchez R, et al. The LRRK2 G2019S mutant exacerbates basal autophagy through activation of the MEK/ERK pathway. *Cell Mol Life Sci*. 2013;70(1):121-136. doi:10.1007/s00018-012-1061-y
596. Yakhine-Diop SMS, Bravo-San Pedro JM, Gómez-Sánchez R, et al. G2019S LRRK2 mutant fibroblasts from Parkinson's disease patients show increased sensitivity to neurotoxin 1-methyl-4-phenylpyridinium dependent of autophagy. *Toxicology*. 2014;324:1-9. doi:10.1016/j.tox.2014.07.001
597. Su YC, Guo X, Qi X. Threonine 56 phosphorylation of Bcl-2 is required for LRRK2 G2019S-induced mitochondrial depolarization and autophagy. *Biochim Biophys Acta - Mol Basis Dis*. 2015;1852(1):12-21. doi:10.1016/j.bbadis.2014.11.009
598. Manzoni C, Mamais A, Dihanich S, et al. Inhibition of LRRK2 kinase activity stimulates macroautophagy 2013a. *Biochim Biophys Acta - Mol Cell Res*. 2013;1833(12):2900-2910. doi:10.1016/j.bbamcr.2013.07.020
599. Sánchez-Danés A, Richaud-Patin Y, Carballo-Carbajal I, et al. Disease-specific phenotypes in dopamine neurons from human iPS-based models of genetic and sporadic Parkinson's disease. *EMBO Mol Med*. 2012;4(5):380-395. doi:10.1002/emmm.201200215
600. Gómez-Suaga P, Hilfiker S. LRRK2 as a modulator of lysosomal calcium homeostasis with downstream effects on autophagy. *Autophagy*. 2012;8(4):692-693. doi:10.4161/auto.19305
601. Gómez-Suaga P, Churchill GC, Patel S, Hilfiker S. A link between LRRK2, autophagy and NAADP-mediated endolysosomal calcium signalling. *Biochem Soc Trans*. 2012;40(5):1140-1146. doi:10.1042/BST20120138
602. Pungaliya PP, Bai Y, Lipinski K, et al. Identification and characterization of a leucine-rich repeat kinase 2 (LRRK2) consensus phosphorylation motif. *PLoS One*. 2010;5(10):1-13. doi:10.1371/journal.pone.0013672
603. Cho HJ, Yu J, Xie C, et al. Leucine-rich repeat kinase 2 regulates Sec16A at ER exit sites to allow ER –Golgi export. *EMBO J*. 2014;33(20):2314-2331. doi:10.15252/embj.201487807
604. Higashi S, Biskup S, West AB, et al. Localization of Parkinson's disease-associated LRRK2 in normal and pathological human brain. *Brain Res*. 2007;1155(1):208-219. doi:10.1016/j.brainres.2007.04.034
605. Connor-Robson N, Booth H, Martin JG, et al. An integrated transcriptomics and proteomics analysis reveals functional endocytic dysregulation caused by mutations in LRRK2. *Neurobiol Dis*. 2019;127(March):512-526. doi:10.1016/j.nbd.2019.04.005
606. Shin N, Jeong H, Kwon J, et al. LRRK2 regulates synaptic vesicle endocytosis. *Exp Cell Res*. 2008;314(10):2055-2065. doi:10.1016/j.yexcr.2008.02.015
607. Pan PY, Li X, Wang J, et al. Parkinson's disease-associated LRRK2 hyperactive kinase mutant disrupts synaptic vesicle trafficking in ventral midbrain neurons. *J Neurosci*. 2017;37(47):11366-11376. doi:10.1523/JNEUROSCI.0964-17.2017
608. Longo F, Mercatelli D, Novello S, et al. Age-dependent dopamine transporter dysfunction and Serine129 phospho-α-synuclein overload in G2019S LRRK2 mice. *Acta Neuropathol Commun*. 2017;5(1):22. doi:10.1186/s40478-017-0426-8
609. Nguyen M, Krainc D. LRRK2 phosphorylation of auxilin mediates synaptic defects in dopaminergic neurons from patients with Parkinson's disease. *Proc Natl Acad Sci U S A*. 2018;115(21):5576-5581. doi:10.1073/pnas.1717590115
610. Soukup SF, Kuenen S, Vanhauwaert R, et al. A LRRK2-Dependent EndophilinA Phosphoswitch Is Critical for Macroautophagy at Presynaptic Terminals. *Neuron*. 2016;92(4):829-844. doi:10.1016/j.neuron.2016.09.037
611. Zoppino FCM, Militello RD, Slavin I, Álvarez C, Colombo MI. Autophagosome formation depends on the small GTPase rab1 and functional ER exit sites. *Traffic*. 2010;11(9):1246-1261. doi:10.1111/j.1600-0854.2010.01086.x

612. Dou Z, Pan JA, Dbouk HA, et al. Class IA PI3K p110β Subunit Promotes Autophagy through Rab5 Small GTPase in Response to Growth Factor Limitation. *Mol Cell*. 2013;50(1):29-42. doi:10.1016/j.molcel.2013.01.022
613. Jeong GR, Jang EH, Bae JR, et al. Dysregulated phosphorylation of Rab GTPases by LRRK2 induces neurodegeneration. *Mol Neurodegener*. 2018;13(1):1-17. doi:10.1186/s13024-018-0240-1
614. Vilariño-Güell C, Wider C, Ross OA, et al. VPS35 mutations in parkinson disease. *Am J Hum Genet*. 2011;89(1):162-167. doi:10.1016/j.ajhg.2011.06.001
615. Vogiatzi T, Xilouri M, Vekrellis K, Stefanis L. Wild type α-synuclein is degraded by chaperone-mediated autophagy and macroautophagy in neuronal cells. *J Biol Chem*. 2008;283(35):23542-23556. doi:10.1074/jbc.M801992200
616. Manzoni C, Mamais A, Dihanich S, et al. mTOR independent alteration in ULK1 Ser758 phosphorylation following chronic LRRK2 kinase inhibition. *Biosci Rep*. 2018;0(March):BSR20171669. doi:10.1042/BSR20171669
617. Härtlova A, Herbst S, Peltier J, et al. LRRK2 is a negative regulator of Mycobacterium tuberculosis phagosome maturation in macrophages. *EMBO J*. 2018;37(12):e98694. doi:10.15252/embj.201798694
618. Saez-Atienzar S, Bonet-Ponce L, Blesa JR, et al. The LRRK2 inhibitor GSK2578215A induces protective autophagy in SH-SY5Y cells: involvement of Drp-1-mediated mitochondrial fission and mitochondrial-derived ROS signaling. *Cell Death Dis*. 2014;5(8):e1368. doi:10.1038/cddis.2014.320
619. Mendivil-Perez M, Velez-Pardo C, Jimenez-Del-Rio M. Neuroprotective Effect of the LRRK2 Kinase Inhibitor PF-06447475 in Human Nerve-Like Differentiated Cells Exposed to Oxidative Stress Stimuli: Implications for Parkinson's Disease. *Neurochem Res*. 2016;41(10):2675-2692. doi:10.1007/s11064-016-1982-1
620. Blanca Ramírez M, Lara Ordóñez AJ, Fdez E, et al. GTP binding regulates cellular localization of Parkinson's disease-associated LRRK2. *Hum Mol Genet*. 2017;26(14):2747-2767. doi:10.1093/hmg/ddx161
621. Daniel Harris, BA, Lynn McNicoll, MD, Gary Epstein-Lubow, MD, and Kali S. Thomas P. Phosphorylation of LRRK2 by casein kinase 1α regulates trans-Golgi clustering via differential interaction with ARHGEF7. *Physiol Behav*. 2017;176(1):139-148. doi:10.1016/j.physbeh.2017.03.040
622. Luerman GC, Nguyen C, Samaroo H, et al. Phosphoproteomic evaluation of pharmacological inhibition of leucine-rich repeat kinase 2 reveals significant off-target effects of LRRK-2-IN-1. *J Neurochem*. 2014;128(4):561-576. doi:10.1111/jnc.12483
623. Thomas JM, Wang X, Guo G, et al. GTP-binding inhibitors increase LRRK2-linked ubiquitination and Lewy body-like inclusions. *J Cell Physiol*. 2020;235(10):7309-7320. doi:10.1002/jcp.29632
624. Kovalevich J, Langford D. Considerations for the use of SH-SY5Y neuroblastoma cells in neurobiology. *Methods Mol Biol - Neuronal Cell Cult Methods Protoc*. 2013;1078(January 2016):9-21. doi:10.1007/978-1-62703-640-5
625. Donato R, Miljan EA, Hines SJ, et al. Differential development of neuronal physiological responsiveness in two human neural stem cell lines. *BMC Neurosci*. 2007;8:36. doi:10.1186/1471-2202-8-36
626. Ran FA, Hsu PPD, Wright J, Agarwala V, Scott D a, Zhang F. Genome engineering using the CRISPR-Cas9 system. *Nat Protoc*. 2013;8(11):2281-2308. doi:10.1038/nprot.2013.143
627. Badger JL, Cordero-Llana O, Hartfield EM, Wade-Martins R. Parkinson's disease in a dish - Using stem cells as a molecular tool. *Neuropharmacology*. 2014;76(PART A):88-96. doi:10.1016/j.neuropharm.2013.08.035
628. Borgs L, Peyre E, Alix P, et al. Dopaminergic neurons differentiating from LRRK2 G2019S induced pluripotent stem cells show early neuritic branching defects. *Sci Rep*. 2016;6(August):33377. doi:10.1038/srep33377
629. Ciccia A, Elledge SJ. The DNA Damage Response: Making It Safe to Play with Knives. *Mol Cell*. 2010;40(2):179-204. doi:10.1016/j.molcel.2010.09.019
630. Liu M, Rehman S, Tang X, et al. Methodologies for improving HDR efficiency. *Front Genet*. 2019;10(JAN):1-9. doi:10.3389/fgene.2018.00691
631. Barman HK, Rasal KD, Chakrapani V, et al. Gene editing tools: state-of-the-art and the road ahead for the model and non-model fishes. *Transgenic Res*. 2017;(Fao 2015). doi:10.1007/s11248-017-0030-5
632. Horii T, Tamura D, Morita S, Kimura M, Hatada I. Generation of an ICF syndrome model by efficient genome editing of human induced pluripotent stem cells using the CRISPR system. *Int J Mol Sci*. 2013;14(10):19774-19781. doi:10.3390/ijms141019774
633. Paquet D, Kwart D, Chen A, et al. Efficient introduction of specific homozygous and heterozygous mutations using CRISPR/Cas9. *Nature*. 2016;533(7601):1-18. doi:10.1038/nature17664
634. Gaj T, Gersbach CA, Barbas CF. ZFN, TALEN, and CRISPR/Cas-based methods for genome engineering. *Trends Biotechnol*. 2013;31(7):397-405. doi:10.1016/j.tibtech.2013.04.004
635. Liang P, Zhang X, Chen Y, Huang J. Developmental history and application of CRISPR in human disease. *J*

Gene Med. 2017:e2963. doi:10.1002/jgm.2963

636. Redman M, King A, Watson C, King D. What is CRISPR/Cas9? *Arch Dis Child - Educ Pract Ed*. 2016;101(4):213-215. doi:10.1136/archdischild-2016-310459
637. Kim EJ, Kang KH, Ju JH. CRISPR-Cas9: a promising tool for gene editing on induced pluripotent stem cells. *Korean J Intern Med*. 2017;32(1):42-61. doi:10.3904/kjim.2016.198
638. Singh V, Gohil N, García RR, Braddick D, Fofié CK. Recent Advances of CRISPR-Cas9 Genome Editing Technologies for Biological and Biomedical Investigations. *J Cell Biochem*. 2017;(May). doi:10.1002/jcb.26165
639. Qiu P, Shandilya H, D'Alessio JM, O'Connor K, Durocher J, Gerard GF. Mutation detection using Surveyor™ nuclease. *Biotechniques*. 2004;36(4):702-707. doi:10.2144/04364PF01
640. Johnson ME, Stecher B, Labrie V, Brundin L, Brundin P. Triggers, Facilitators, and Aggravators: Redefining Parkinson's Disease Pathogenesis. *Trends Neurosci*. 2019;42(1):4-13. doi:10.1016/j.tins.2018.09.007
641. Janes MR, Limon JJ, So L, et al. Effective and selective targeting of leukemia cells using a TORC1/2 kinase inhibitor. *Nat Med*. 2010;16(2):205-213. doi:10.1038/nm.2091
642. Reith AD, Bamborough P, Jandu K, et al. GSK2578215A; A potent and highly selective 2-arylmethyloxy-5-substitutent- N-arylbenzamide LRRK2 kinase inhibitor. *Bioorganic Med Chem Lett*. 2012;22(17):5625-5629. doi:10.1016/j.bmcl.2012.06.104
643. Estrada AA, Chan BK, Baker-Glenn C, et al. Discovery of highly potent, selective, and brain-penetrant aminopyrazole Leucine-rich repeat kinase 2 (LRRK2) small molecule inhibitors. *J Med Chem*. 2014;57(3):921-936. doi:10.1021/jm401654j
644. Henderson JL, Kormos BL, Hayward MM, et al. Discovery and preclinical profiling of 3-[4-(morpholin-4-yl)-7H-pyrrolo[2,3-d]pyrimidin-5-yl]benzonitrile (PF-06447475), a highly potent, selective, brain penetrant, and in vivo active LRRK2 kinase inhibitor. *J Med Chem*. 2015;58(1):419-432. doi:10.1021/jm5014055
645. Sakurai H, Nishi A, Sato N, Mizukami J, Miyoshi H, Sugita T. TAK1-TAB1 fusion protein: A novel constitutively active mitogen-activated protein kinase kinase kinase that stimulates AP-1 and NF-κB signaling pathways. *Biochem Biophys Res Commun*. 2002;297(5):1277-1281. doi:10.1016/S0006-291X(02)02379-3
646. Karaman MW, Herrgard S, Treiber DK, et al. A quantitative analysis of kinase inhibitor selectivity. *Nat Biotechnol*. 2008;26(1):127-132. doi:10.1038/nbt1358
647. Manning G, Whyte DB, Martinez R, Hunter T, Sudarsanam S. The protein kinase complement of the human genome. *Science (80-)*. 2002;298(5600):1912-1934. doi:10.1126/science.1075762
648. Zhou J, Tan SH, Nicolas V, et al. Activation of lysosomal function in the course of autophagy via mTORC1 suppression and autophagosome-lysosome fusion. *Cell Res*. 2013;23(4):508-523. doi:10.1038/cr.2013.11
649. Proikas-Cezanne T, Robenek H. Freeze-fracture replica immunolabelling reveals human WIPI-1 and WIPI-2 as membrane proteins of autophagosomes. *J Cell Mol Med*. 2011;15(9):2007-2010. doi:10.1111/j.1582-4934.2011.01339.x
650. Smith GA, Jansson J, Rocha EM, Osborn T, Hallett PJ, Isacson O. Fibroblast Biomarkers of Sporadic Parkinson's Disease and LRRK2 Kinase Inhibition. *Mol Neurobiol*. 2016;53(8):5161-5177. doi:10.1007/s12035-015-9435-4
651. Russo I, Bubacco L, Greggio E. LRRK2 and neuroinflammation: Partners in crime in Parkinson's disease? *J Neuroinflammation*. 2014;11:1-9. doi:10.1186/1742-2094-11-52
652. Mortiboys H, Johansen KK, Aasly JO, Bandmann O. Mitochondrial impairment in patients with Parkinson disease with the G2019S mutation in LRRK2. *Neurology*. 2010;75(22):2017-2020. doi:10.1212/WNL.0b013e3181ff9685
653. Wang X, Yan MH, Fujioka H, et al. LRRK2 regulates mitochondrial dynamics and function through direct interaction with DLP1. *Hum Mol Genet*. 2012;21(9):1931-1944. doi:10.1093/hmg/dds003
654. Papkovskaia TD, Chau KY, Inesta-vaquera F, et al. G2019s leucine-rich repeat kinase 2 causes uncoupling protein-mediated mitochondrial depolarization. *Hum Mol Genet*. 2012;21(19):4201-4213. doi:10.1093/hmg/dds244
655. Niu J, Yu M, Wang C, Xu Z. Leucine-rich repeat kinase 2 disturbs mitochondrial dynamics via dynamin-like protein. *J Neurochem*. 2012;122(3):650-658. doi:10.1111/j.1471-4159.2012.07809.x
656. Sanderson MJ, Smith I, Parker I, Bootman MD. Fluorescence Microscopy. *Cold Spring Harb Protoc*. 2014;2014(10):pdb.top071795-pdb.top071795. doi:10.1101/pdb.top071795
657. Grünewald A, Arns B, Meier B, Brockmann K, Tadic V, Klein C. Does uncoupling protein 2 expression qualify as marker of disease status in LRRK2-associated parkinson's disease? *Antioxidants Redox Signal*. 2014;20(13):1955-1960. doi:10.1089/ars.2013.5737
658. Crump A, Omura S. Ivermectin, "Wonder drug" from Japan: The human use perspective. *Proc Japan Acad*

Ser B Phys Biol Sci. 2011;87(2):13-28. doi:10.2183/pjab.87.13

659. Zachari M, Gudmundsson SR, Li Z, et al. Selective Autophagy of Mitochondria on a Ubiquitin-Endoplasmic-Reticulum Platform. *Dev Cell*. 2019;50(5):627-643.e5. doi:10.1016/j.devcel.2019.06.016
660. Shaner NC, Lin MZ, McKeown MR, et al. Improving the photostability of bright monomeric orange and red fluorescent proteins. *Nat Methods*. 2008;5(6):545-551. doi:10.1038/nmeth.1209
661. Liu J, Liang H, Chen C, et al. Ivermectin induces autophagy-mediated cell death through the AKT/mTOR signaling pathway in glioma cells. *Biosci Rep*. 2019;39(12):1-13. doi:10.1042/BSR20192489
662. Juarez M, Schcolnik-Cabrera A, Dueñas-Gonzalez A. The multitargeted drug ivermectin: from an antiparasitic agent to a repositioned cancer drug. *Am J Cancer Res*. 2018;8(2):317-331. http://www.ncbi.nlm.nih.gov/pubmed/29511601%0Ahttp://www.pubmedcentral.nih.gov/articlerender.fcgi?artid=PMC5835698.
663. Liu Y, Fang S, Sun Q, Liu B. Anthelmintic drug ivermectin inhibits angiogenesis, growth and survival of glioblastoma through inducing mitochondrial dysfunction and oxidative stress. *Biochem Biophys Res Commun*. 2016;480(3):415-421. doi:10.1016/j.bbrc.2016.10.064
664. He C, Klionsky DJ. Regulation Mechanisms and Signaling Pathways of Autophagy. *Annu Rev Genet*. 2009;43(1):67-93. doi:10.1146/annurev-genet-102808-114910
665. Barth S, Glick D, Macleod KF. Autophagy: assays and artifacts. *J Pathol*. 2010;221(2):117-124. doi:10.1002/path.2694
666. Davis S, Wang J, Ferro-Novick S. Crosstalk between the Secretory and Autophagy Pathways Regulates Autophagosome Formation. *Dev Cell*. 2017;41(1):23-32. doi:10.1016/j.devcel.2017.03.015
667. Szalai P, Hagen LK, Sætre F, et al. Autophagic bulk sequestration of cytosolic cargo is independent of LC3, but requires GABARAPs. *Exp Cell Res*. 2015;333(1):21-38. doi:10.1016/j.yexcr.2015.02.003
668. Shpilka T, Weidberg H, Pietrokovski S, Elazar Z. Atg8: An autophagy-related ubiquitin-like protein family. *Genome Biol*. 2011;12(7). doi:10.1186/gb-2011-12-7-226
669. Rideout HJ, Chartier-Harlin MC, Fell MJ, et al. The Current State-of-the Art of LRRK2-Based Biomarker Assay Development in Parkinson's Disease. *Front Neurosci*. 2020;14(August):1-17. doi:10.3389/fnins.2020.00865
670. Vancraenenbroeck R, De Raeymaecker J, Lobbestael E, et al. In silico, in vitro and cellular analysis with a kinome-wide inhibitor panel correlates cellular LRRK2 dephosphorylation to inhibitor activity on LRRK2. *Front Mol Neurosci*. 2014;7(JUNE). doi:10.3389/fnmol.2014.00051
671. Lobbestael E, Zhao J, Rudenko IN, et al. Identification of protein phosphatase 1 as a regulator of the LRRK2 phosphorylation cycle. *Biochem J*. 2013;456(1):119-128. doi:10.1042/BJ20121772
672. Lis P, Burel S, Steger M, et al. Development of phospho-specific Rab protein antibodies to monitor in vivo activity of the LRRK2 Parkinson's disease kinase. *Biochem J*. 2018;475(1):1-22. doi:10.1042/BCJ20170802
673. Hartmann B. P70S6 kinase phosphorylation for pharmacodynamic monitoring. *Clin Chim Acta*. 2012;413(17-18):1387-1390. doi:10.1016/j.cca.2012.03.023
674. Ouyang L, Zhang L, Zhang S, et al. Small-Molecule Activator of UNC-51-Like Kinase 1 (ULK1) That Induces Cytoprotective Autophagy for Parkinson's Disease Treatment. *J Med Chem*. 2018;61(7):2776-2792. doi:10.1021/acs.jmedchem.7b01575
675. Papinski D, Kraft C. Regulation of Autophagy by Signaling Through the Atg1/ULK1 Complex. *J Mol Biol*. 2016;428(9):1725-1741. doi:10.1016/j.jmb.2016.03.030
676. Egan DF, Chun MGH, Vamos M, et al. Small Molecule Inhibition of the Autophagy Kinase ULK1 and Identification of ULK1 Substrates. *Mol Cell*. 2015;59(2):285-297. doi:10.1016/j.molcel.2015.05.031
677. Sophie Mokas JRM, Cristina Garreau M-J, Fournier ´e, et al. ULK-Atg13-FIP200 Complexes Mediate mTOR Signaling to the Autophagy Machinery. *Mol Biol Cell*. 2009;20:2673-2683. doi:10.1091/mbc.E08-12-1249
678. Hornbeck P V., Zhang B, Murray B, Kornhauser JM, Latham V, Skrzypek E. PhosphoSitePlus, 2014: mutations, PTMs and recalibrations. *Nucleic Acids Res*. 2015;43(D1):D512-D520. doi:10.1093/nar/gku1267
679. Takagawa T, Kitani A, Fuss I, et al. An increase in LRRK2 suppresses autophagy and enhances dectin-1–induced immunity in a mouse model of colitis. *Sci Transl Med*. 2018;10(444):1-13. doi:10.1126/scitranslmed.aan8162
680. Grishchuk Y, Ginet V, Truttmann AC, Clarke PGH, Puyal J. Beclin 1-independent autophagy contributes to apoptosis in cortical neurons. *Autophagy*. 2011;7(10):1115-1131. doi:10.4161/auto.7.10.16608
681. Tian S, Lin J, Zhou J, et al. Beclin 1-independent autophagy induced by a Bcl-XL/Bcl-2 targeting compound, Z18. *Autophagy*. 2010;6(8):1032-1041. doi:10.4161/auto.6.8.13336
682. Zhou C, Ma K, Gao R, et al. Regulation of mATG9 trafficking by Src- and ULK1-mediated phosphorylation in basal and starvation-induced autophagy. *Cell Res*. 2017;27(2):184-201. doi:10.1038/cr.2016.146
683. Manzoni C. The LRRK2-macroautophagy axis and its relevance to Parkinson's disease. *Biochem Soc Trans*.

2017;45(1):155-162. doi:10.1042/BST20160265

684. Berwick DC, Harvey K. LRRK2 signaling pathways: The key to unlocking neurodegeneration? *Trends Cell Biol*. 2011;21(5):257-265. doi:10.1016/j.tcb.2011.01.001
685. Yang Q, Wang R, Zhu L. Beclin 1, Bcl-2 and Autophagy. In: Qin Z-H, ed. *Autophagy: Biology and Diseases*. Vol 1206. Advances in Experimental Medicine and Biology. Singapore: Springer Nature Singapore; 2019:435-452. doi:10.1007/978-981-15-0602-4_5
686. He C, Levine B. The Beclin 1 interactome. *Curr Opin Cell Biol*. 2010;22(2):140-149. doi:10.1016/j.ceb.2010.01.001
687. Kilpatrick BS. Connecting Ca2+ and Lysosomes to Parkinson Disease. *Messenger*. 2016;5(1):76-86. doi:10.1166/msr.2016.1059
688. Morgan AJ, Jacob R. Ionomycin enhances Ca2+ influx by stimulating store-regulated cation entry and not by a direct action at the plasma membrane. *Biochem J*. 1994;300(3):665-672. doi:10.1042/bj3000665
689. Smith NA, Kress BT, Lu Y, Chandler-Militello D, Benraiss A, Nedergaard M. Fluorescent Ca2+ indicators directly inhibit the Na,K-ATPase and disrupt cellular functions. *Sci Signal*. 2018;11(515). doi:10.1126/scisignal.aal2039
690. Patel S, Cai X. Evolution of acidic Ca2+ stores and their resident Ca2+-permeable channels. *Cell Calcium*. 2015;57(3):222-230. doi:10.1016/j.ceca.2014.12.005
691. Uchiyama T, Yoshikawa F, Hishida A, Furuichi T, Mikoshiba K. A novel recombinant hyperaffinity inositol 1,4,5-trisphosphate (IP3) absorbent traps IP3, resulting in specific inhibition of IP3-mediated calcium signaling. *J Biol Chem*. 2002;277(10):8106-8113. doi:10.1074/jbc.M108337200
692. Rose T, Goltstein PM, Portugues R, Griesbeck O. Putting a finishing touch on GECIs. *Front Mol Neurosci*. 2014;7(November):1-15. doi:10.3389/fnmol.2014.00088
693. Lock JT, Parker I, Smith IF. A comparison of fluorescent Ca2+ indicators for imaging local Ca2+ signals in cultured cells. *Cell Calcium*. 2015;58(6):638-648. doi:10.1016/j.ceca.2015.10.003
694. Chen S, Luo Z, Ward C, et al. Generation of two LRRK2 homozygous knockout human induced pluripotent stem cell lines using CRISPR/Cas9. *Stem Cell Res*. 2020;45(March):101804. doi:10.1016/j.scr.2020.101804
695. Qing X, Walter J, Jarazo J, Arias-Fuenzalida J, Hillje AL, Schwamborn JC. CRISPR/Cas9 and piggyBac-mediated footprint-free LRRK2-G2019S knock-in reveals neuronal complexity phenotypes and α-Synuclein modulation in dopaminergic neurons. *Stem Cell Res*. 2017;24:44-50. doi:10.1016/j.scr.2017.08.013
696. Horlbeck MA, Witkowsky LB, Guglielmi B, et al. Nucleosomes impede cas9 access to DNA in vivo and in vitro. *Elife*. 2016;5(MARCH2016):1-21. doi:10.7554/eLife.12677
697. Liu B, Chen S, Rose A La, et al. Inhibition of histone deacetylase 1 (HDAC1) and HDAC2 enhances CRISPR/Cas9 genome editing. *Nucleic Acids Res*. 2020;48(2):517-532. doi:10.1093/nar/gkz1136
698. Li G, Zhang X, Wang H, et al. Increasing CRISPR/Cas9-mediated homology-directed DNA repair by histone deacetylase inhibitors. *Int J Biochem Cell Biol*. 2020;125(February):105790. doi:10.1016/j.biocel.2020.105790
699. Clarke R, Heler R, MacDougall MS, et al. Enhanced Bacterial Immunity and Mammalian Genome Editing via RNA-Polymerase-Mediated Dislodging of Cas9 from Double-Strand DNA Breaks. *Mol Cell*. 2018;71(1):42-55.e8. doi:10.1016/j.molcel.2018.06.005
700. Safari F, Hatam G, Behbahani AB, et al. CRISPR System: A High-throughput Toolbox for Research and Treatment of Parkinson's Disease. *Cell Mol Neurobiol*. 2020;40(4):477-493. doi:10.1007/s10571-019-00761-w
701. Liu R, Liang L, Freed EF, Gill RT. Directed Evolution of CRISPR/Cas Systems for Precise Gene Editing. *Trends Biotechnol*. 2020:1-12. doi:10.1016/j.tibtech.2020.07.005
702. Rees HA, Liu DR. Base editing: precision chemistry on the genome and transcriptome of living cells. *Nat Rev Genet*. 2018;19(12):770-788. doi:10.1038/s41576-018-0059-1
703. Zuo E, Sun Y, Wei W, et al. Cytosine base editor generates substantial off-target single-nucleotide variants in mouse embryos. *Science (80-)*. 2019;364(6437):289-292. doi:10.1126/science.aav9973
704. Liang P, Xie X, Zhi S, et al. Genome-wide profiling of adenine base editor specificity by EndoV-seq. *Nat Commun*. 2019;10(1):1-9. doi:10.1038/s41467-018-07988-z
705. Anzalone A V., Randolph PB, Davis JR, et al. Search-and-replace genome editing without double-strand breaks or donor DNA. *Nature*. 2019;576(7785):149-157. doi:10.1038/s41586-019-1711-4
706. Kelly K, West AB. Pharmacodynamic Biomarkers for Emerging LRRK2 Therapeutics. *Front Neurosci*. 2020;14(August):1-11. doi:10.3389/fnins.2020.00807
707. Reyniers L, Del Giudice MG, Civiero L, et al. Differential protein protein interactions of LRRK1 and LRRK2 indicate roles in distinct cellular signaling pathways. *J Neurochem*. 2014;131(2):239-250.

doi:10.1111/jnc.12798

708. Toyofuku T, Morimoto K, Sasawatari S, Kumanogoh A. Leucine-Rich Repeat Kinase 1 Regulates Autophagy through Turning On TBC1D2-Dependent Rab7 Inactivation. *Mol Cell Biol*. 2015;35(17):3044-3058. doi:10.1128/mcb.00085-15
709. Kania E, Parys JB. The emerging interrelation between ROCO and related kinases, intracellular Ca 2+ signaling, and autophagy. *Biochim Biophys Acta - Mol Cell Res*. 2019;1866(7):1054-1067. doi:10.1016/j.bbamcr.2018.12.008
710. Rivero-Ríos P, Romo-Lozano M, Fernández B, Fdez E, Hilfiker S. Distinct Roles for RAB10 and RAB29 in Pathogenic LRRK2-Mediated Endolysosomal Trafficking Alterations. *Cells*. 2020;9(7). doi:10.3390/cells9071719
711. Fernández-Santiago R, Carballo-Carbajal I, Castellano G, et al. Aberrant epigenome in iPSC -derived dopaminergic neurons from Parkinson's disease patients . *EMBO Mol Med*. 2015;7(12):1529-1546. doi:10.15252/emmm.201505439
712. Cho HJ, Liu G, Jin SM, et al. Microrna-205 regulates the expression of parkinson's disease-related leucine-rich repeat kinase 2 protein. *Hum Mol Genet*. 2013;22(3):608-620. doi:10.1093/hmg/dds470
713. Vlachakis D, Labrou NE, Iliopoulos C, et al. Insights into the influence of specific splicing events on the structural organization of LRRK2. *Int J Mol Sci*. 2018;19(9):1-13. doi:10.3390/ijms19092784
714. Labbé C, Lorenzo-Betancor O, Ross OA. Epigenetic regulation in Parkinson's disease. *Acta Neuropathol*. 2016;132(4):515-530. doi:10.1007/s00401-016-1590-9
715. Giesert F, Hofmann A, Bürger A, et al. Expression Analysis of Lrrk1, Lrrk2 and Lrrk2 Splice Variants in Mice. *PLoS One*. 2013;8(5). doi:10.1371/journal.pone.0063778

Appendices

Appendix 1: Animal models of PD[90].

Appendix 2: Cellular models of PD[90,96,98]

Appendix 3: CRISPR/Cas9 Plasmid map.

Appendix 4: PCR programs and conditions used for the experiments.

Appendix 1: Animal models of PD[90]

Type of animal model (rodent)		Mechanisms	Pathology			Main limitations	Use				
			LB toxicity	Motor symptoms	Dopaminergic degeneration		Investigating molecular mechanisms	Study LB formation	Drug screening, Testing disease-modifying therapy	Study of motor symptoms	Study of non-motor symptoms
Genetic (mutations)	α-synuclein	- Accumulation of α-synuclein - Oxidative stress	+	-	+	- Low level of dopaminergic degeneration - Mild to moderate deficits in PD pathological processes and motor symptoms - Inconsistency	+	+	+	-	+
	PINK1	Mitochondrial dysfunction	No LB, no obvious phenotype				+	-	-	-	-
	Parkin						+	-	-	-	-
	LRRK2	Overexpression mutant					+	-	-	-	-
	DJ-1	Mitochondrial dysfunction	-	+	-		+	-	-	-	-
Neurotoxin	6-OHDA	- Mitochondrial defects - Oxidative stress	-	+	+	No LB	-	+	-	+	-
	MPTP		-	+	+		-	+	-	+	+
	Rotenone		+	+	+	Inconsistency	+	+	-	+	-
	Paraquat		+	+	+	- Inconsistency - No rotenone-induced PD in humans	+	+	-	+	-

Appendix 2: Cellular models of PD[90,96,98]

Type of cellular model			Mechanisms and pathology	Main limitations	Use		
					Investigating molecular mechanisms	Study LB formation	Testing disease-modifying therapy, drug screening
Genetic	iPSc	α-synuclein	- Accumulation of α-synuclein - Oxidative stress	- Patient-specific phenotype - Variability in cell lines and differentiation techniques	+	+	+
		PINK1 or Parkin	- Oxidative stress - Mitochondrial dysfunction - Calcium deregulations		+	-	+
		LRRK2	- Altered neuronal morphology - Accumulation of α-synuclein - Oxidative stress		+	+	+
		GBA	- Accumulation of α-synuclein - Calcium deregulations		+	-	+
	SH-SY5Y	α-synuclein	- Accumulation of α-synuclein - Oxidative stress	- Variability in data - Reproducibility - Overexpression, mutations, or siRNA strategies	+	+	+
		PINK1 or Parkin	- Oxidative stress - Mitochondrial dysfunction - Calcium deregulations		+	-	+
		LRRK2	- Altered neuronal morphology - Accumulation of α-synuclein - Oxidative stress		+	-	+
		GBA	- Accumulation of α-synuclein - Calcium deregulations		+	-	+
Neurotoxin	ReN VM	OHDA	- Mitochondrial defects - Oxidative stress	- Variability in data - Reproducibility	+	-	+
		MPP+			+	-	+
	SH-SY5Y	Rotenone			+	-	+
		OHDA			+	-	+
		MPP+			+	-	+

Appendix 3: CRISPR/Cas9 Plasmid map.

All CRISPR/Cas9 plasmids were derived from the Zhang Lab CRISPR plasmid *pSpCas9(BB)-2A-GFP* (PX458) available from Addgene[626] (plasmid #48138, source: https://www.addgene.org/48138/). The sequence coding for Cas9 can be seen in purple. The gRNA sequence is in blue. The GFP cassette is in green. Cas9 will cut a DNA target site according to the sequence targeted by the gRNA.

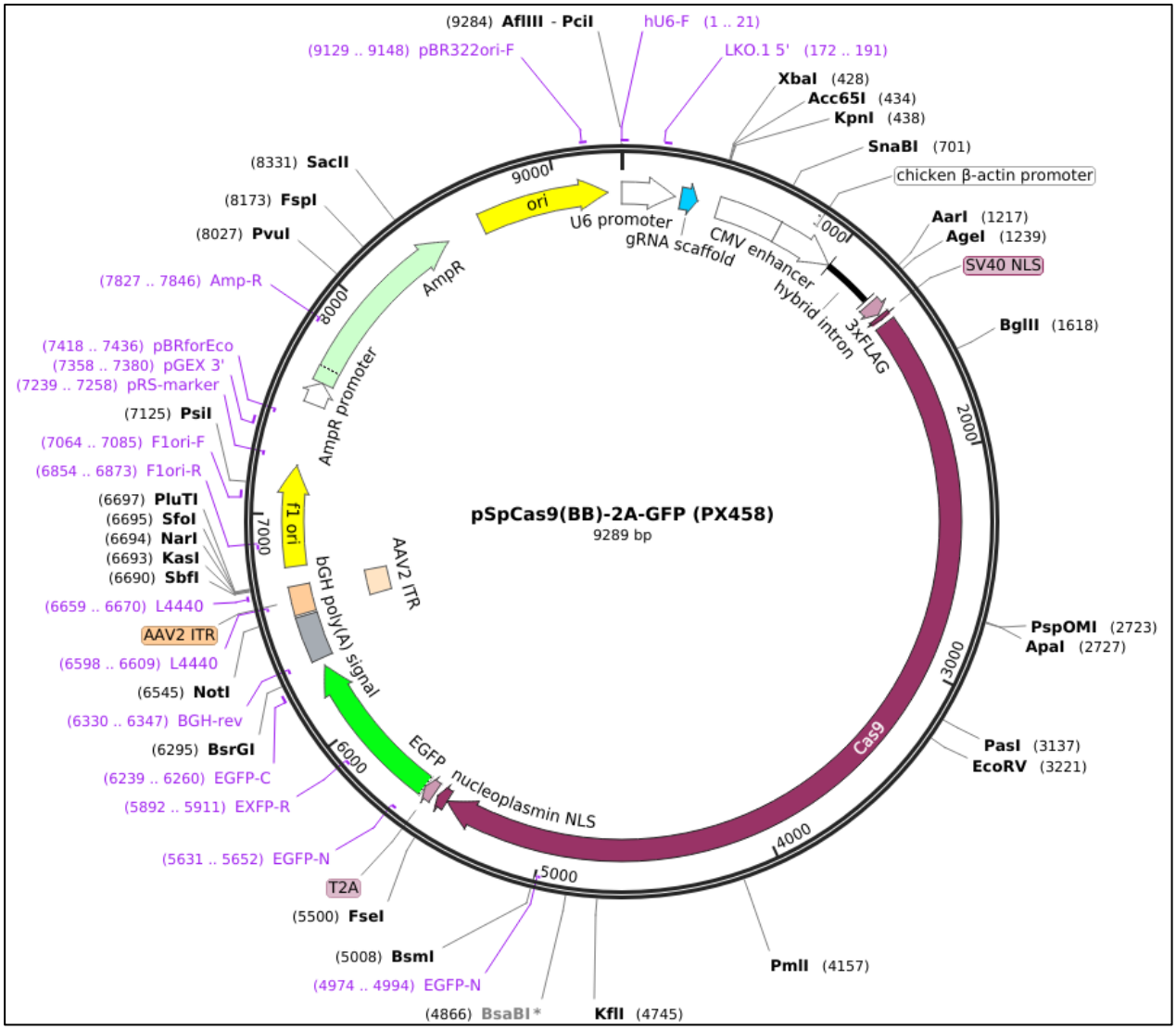

Appendix 4: PCR programs and conditions used for the experiments.

Each change of parameter compared to the initial parameters is highlighted in grey. The annealing temperature was one of the main focuses. Several gradient PCRs were also performed for each set of primers. A gradient PCR has a range of annealing temperatures determined by the experimenter, where each row in the PCR thermocycler corresponds to a specific temperature. Another interesting feature is the touchdown PCR, which allows the thermocycler to use a specific annealing temperature for a chosen number of cycles, and to then decrease the temperature to reach another specific annealing temperature with a determined decrement. The two chosen conditions were n°9 and n°11.

	PCR program						
Condition	**Initial denaturation 5min**	**Denaturation 20s**	**Annealing 15s**	**Elongation 30s**	**Number of cycles**	**Final elongation 5min**	**Hold forever**
1	95°C	98°C	60°C	72°C	34	72°C	20°C
2	95°C	98°C	60°C	72°C, 15s	34		
3	95°C	98°C	gradient 50-70°C	72°C	40		
4	95°C	98°C	gradient 60-66°C	72°C	40		
5	98°C	98°C	gradient 60-66°C	72°C	40		
6	95°C	98°C	60°C 20s	72°C	40		
7	95°C	98°C	66°C 20s	72°C	40		
8	98°C	98°C	66°C 20s	72°C	40		
9	98°C	98°C	66°C 20s	72°C	34		
10	98°C	98°C	61.5°C 20s	72°C	40		
11	98°C	98°C	60°C 20s	72°C	34		
12	95°C	98°C	touchdown (15s each temperature)	72°C			
13	95°C	98°C	touchdown (30s each temperature)	72°C			
14	98°C	98°C	gradient 60-62°C 20s	72°C	40		
15	98°C	98°C	gradient 58-63°C 20s	72°C	34		